Bisphosphazen-Protonenschwämme und Metall-Perfluoranilide:

Liganddesign für BRØNSTED-Superbasen und LEWIS-Supersäuren

Kumulative Dissertation

zur Erlangung des Doktorgrades der Naturwissenschaften

(Dr. rer. nat.)

dem Fachbereich Chemie

der Philipps-Universität Marburg

vorgelegt von

Julius Kögel

aus Hanau

Marburg 2014

Die vorliegende Arbeit wurde in der Zeit von Februar 2011 bis April 2014 unter Leitung von Herrn Prof. Dr. Jörg Sundermeyer am Fachbereich Chemie der Philipps-Universität Marburg angefertigt.

Vom Fachbereich Chemie der Philipps-Universität Marburg (Hochschulkennziffer: 1180)
als Dissertation angenommen am: 15.04.2014

Erstgutachter: Prof. Dr. Jörg Sundermeyer
Zweitgutachter: Prof. Dr. Carsten von Hänisch

Tag der mündlichen Prüfung: 15.05.2014

Erklärung

Ich erkläre, dass eine Promotion noch an keiner anderen Hochschule als der Philipps-Universität Marburg, Fachbereich Chemie, versucht wurde.

Ich versichere, dass ich die vorgelegte Dissertation mit dem Titel

Bisphosphazen-Protonenschwämme und Metall-Perfluoranilide:
Liganddesign für BRØNSTED-Superbasen und LEWIS-Supersäuren

selbst und ohne fremde Hilfe verfasst, nicht andere als die in ihr angegebenen Quellen oder Hilfsmittel benutzt und alle vollständig oder sinngemäß übernommenen Zitate als solche gekennzeichnet habe.
Diese Dissertation wurde in der vorliegenden oder einer ähnlichen Form noch bei keiner anderen in- oder ausländischen Hochschule anlässlich eines Promotionsgesuches oder zu anderen Prüfungszwecken eingereicht.

Marburg, den

Unterschrift

Danksagung

Zunächst möchte ich mich bei Prof. Dr. Jörg Sundermeyer für die Möglichkeit bedanken, meine Doktorarbeit unter seiner Betreuung anfertigen zu dürfen und dabei zum einen viele eigene Ideen selbstständig umsetzen zu können, zum anderen aber auch Unterstützung und Rat zu erhalten, wenn es nötig war.

Ich bedanke mich bei Prof. Dr. Carsten von Hänisch für die Übernahme des Zweitgutachtens sowie bei den Mitgliedern der Prüfungskommission Prof. Dr. Eric Meggers und Prof Dr. Norbert Hampp.

Ein ganz großes Dankeschön geht an meine Familie, meine Freundin Sara und meine Freunde, die mich immer unterstützt und mir den Rücken freigehalten haben. Danke an meinen alten Mitbewohner David „Herrn Schorch“ Grosse-Hagenbrock für inzwischen mehr als acht ereignisreiche gemeinsame Jahre in Marburg. Eduard Baal, Silas Böttger, Lars Hendrik Finger, David Grosse-Hagenbrock, Sara Siegemeyer und Wolf Schorn gilt ein besonderer Dank für das fleißige Korrekturlesen. Der nächste Dank geht an alle Mitglieder des Arbeitskreises 44 Eduard Baal, Malcolm Bartlett, Silas Böttger, Axel Braam, Lars Hendrik Finger, Timo Gneuß, David Grosse-Hagenbrock, Manuel Hartweg**,** Jasmin Heinzer, Marius Hoffmann, Ahmed Ibrahim, Paul Kübler, Martin Liebold, Christina Poggel, Christian Prinzisky, Susanne Pulz, Nicholas Rau, Katrin Schlechter, Fabian Schröder, Wolf Schorn und Alexander Venker sowie an die „Ehemaligen“ Michael Elfferding, Noa Klara Hangaly, Marcus Harrer, Nina Hillesheim, Benjamin Oelkers, Elisabeth Seikel, Marion Stricker und Oliver Thomas für die gute Atmosphäre in der Gruppe. Danke, dass ihr immer ein offenes Ohr für meine chemischen Probleme hattet und mir ausgeholfen habt, wenn es mal wieder an einer Schliffkappe oder trockenem THF-d_8 gefehlt hat. Ich habe auch die Zeit außerhalb des Labors mit euch sehr genossen und werde unsere Kanutour, die leider letztlich erfolglosen Chemiker-Fußballturniere und natürlich die unterhaltsamen Runden im Kaffeeraum immer in guter Erinnerung behalten. Irene Barth möchte ich dafür danken, dass sie als gute Seele des Arbeitskreises immer für uns da ist und ein reibungsloses Arbeiten möglich macht.

Ein besonderer Dank geht an Eduard Baal, Donatas Gesevicius, Martin Scott und Felicia Weber, deren Bachelorarbeiten ich betreuen durfte, für aufopferungsvollen Einsatz im Labor und gute Ideen. Ohne euch wäre diese Arbeit nicht in dieser Form möglich gewesen! Gleiches gilt für die Vertiefungsstudenten Carl Philipp Rosenau, Nicolas Frank, Alexander Gese, Felicia Weber, Nis-Julian Kneusels und Sebastian Ullrich, die diese Arbeit ebenfalls sehr bereichert haben. Wichtige Synthesearbeiten wurden zudem von den AC-MPR-Praktikanten Johannes Jammer, Kornelius Neue, Wei Zou, Donatas Gesevicius, Nis-Julian Kneusels und Patrick Szabo sowie einer Vielzahl von Studenten des AC-FPRs durchgeführt.

Ich möchte mich bei den Mitarbeitern der NMR-Abteilung Dr. Xiulan Xie, Klaus Pützger, Gert Häde, Cornelia Mischke für eine Vielzahl von Auftragsmessungen bedanken und natürlich dafür, dass sie uns auch dann mit ^{31}P-NMR-Spektren versorgt hat, wenn das Praktikumsgerät mal gestreikt hat. Besonderer Dank geht an Frau Xie für die Durchführung der aufwändigen Messungen zur kinetischen

Basizität von Protonenschwämmen. Die im Rahmen dieser Arbeit diskutierten Kristallstrukturen sind den Mitarbeitern der XRD-Abteilung Dr. Klaus Harms, Michael Marsch und Radostan Riedel zu verdanken, die durch ihre Fingerfertigkeit auch den unmöglichsten Proben einen geeigneten Kristall entlocken konnten. In diesem Zusammenhang ist auch die Unterstützung von Fabian Schröder und Lars Finger hervorzuheben, die immer für mich da waren, wenn es beim Lösen und Verfeinern der Strukturen mal etwas kniffliger wurde. Für die Aufnahme von Massenspektren geht der Dank an die Massenabteilung um Dr. Uwe Linne und Jan Bamberger. Des Weiteren möchte ich mich für die Durchführung der Elementaranalysen bei Kristina Milbrat, Heike Mallinger und Yvonne Ullrich bedanken.

Zu großem Dank verpflichtet bin ich Dr. Borislav Kovačević und dem leider zu Beginn dieser Arbeit verstorbenen Prof. Dr. Zvonimir Maksić aus Zagreb, deren theoretische Berechnungen meine Forschungen an Protonenschwämmen seit meiner Diplomarbeit begleiten und unsere experimentellen Ergebnisse sehr bereichert haben. Danke Boris für den regen Austausch und nicht zuletzt für deine Geduld mit uns! Dr. Ivari Kaljurand aus der Gruppe von Prof. Dr. Ivo Leito in Tartu danke ich für die Basizitätsmessungen an Protonenschwämmen in der Gasphase und die Aciditätsmessungen an NH-Säuren in Lösung. Ich bedanke mich bei Dr. Sascha Goll aus der Arbeitsgruppe von Prof. Dr. Ingo Krossing in Freiburg für den fruchtbaren Austausch im Rahmen unserer gemeinsamen Arbeiten an den NH-Säuren. Michael Klues aus der Arbeitsgruppe von Prof. Dr. Gregor Witte in Marburg danke ich für die Zusammenarbeit im Bereich der Diazapentacene. Dr. Davor Margetić aus Zagreb möchte ich für die Durchführung von Berechnungen bezüglich der Basizität von Bisylid-Protonenschwämmen danken.

Für die zweijährige finanzielle Unterstützung meiner Promotion danke ich dem Fonds der Chemischen Industrie.

Vorwort

Die vorliegende kumulative Dissertation beschäftigt sich mit Superbasen, die als Pinzettenliganden für ein Proton agieren, und mit NH-Säuren und deren Potential zur Generierung LEWIS-acider Metallzentren. Die einzelnen Abschnitte der Dissertation sind gemäß der beiden bearbeiteten Themenbereiche unterteilt, wobei das Gebiet der Superbasen jeweils zuerst betrachtet wird. Die *Einleitung* beschreibt zunächst die dieser Arbeit zu Grunde liegenden Konzepte und die bisherigen Entwicklungen in den untersuchten Themengebieten in der Fachliteratur und in vorhergehenden Dissertationen aus der Arbeitsgruppe SUNDERMEYER. Die Zielsetzung dieser Arbeit ist in der *Aufgabenstellung* dargestellt. Es folgen die *Zusammenfassungen* der wichtigsten Ergebnisse in deutscher und englischer Sprache, wobei auch bisher unveröffentlichte Resultate diskutiert werden. Im Abschnitt *Kumulativer Teil* sind die Inhalte der Veröffentlichungen und Manuskripte kurz zusammengefasst und es wird der Anteil der einzelnen Autoren beschrieben. Die verwendeten Quellen sind im Abschnitt *Literatur* aufgeführt. Die bereits erschienenen Publikationen befinden sich zusammen mit den beiden bisher unveröffentlichten Manuskripten im Anhang.

Ein elektronischer Anhang zu dieser Dissertation befindet sich auf einer DVD im Einband der Arbeit. Die DVD enthält Informationen zu den in dieser Dissertation erhaltenen Kristallstrukturen, die jeweiligen *Supporting Information* der Publikationen und einen Experimentalteil. Letzterer beschreibt die Synthesen und spektroskopischen Daten aller im Rahmen dieser Arbeit dargestellten Verbindungen, insbesondere auch die der bisher unveröffentlichten Substanzen im Bereich der Bisylide und chiralen Superbasen mit Cyclohexanrückgrat.

Inhaltsverzeichnis

1. Einleitung

1.1 Organische Superbasen

1.1.1 Einführung

Die Übertragung eines Protons von einer BRØNSTED-Säure auf eine BRØNSTED-Base zählt zu den fundamentalen Prozessen der Chemie und nimmt eine Schlüsselrolle in einer Vielzahl von chemischen Reaktionen ein.[1] Der Einsatz von Protonenakzeptoren ist beispielsweise erforderlich, um aus einer CH-aciden Verbindung ein Carbanion zur Umsetzung mit einem Elektrophil zu generieren oder um in einer Reaktion freigesetzte Protonen abzufangen. Grundsätzlich kann der präparative Chemiker zwischen Basen aus drei unterschiedlichen Kategorien auswählen: Salzartige anorganische Basen wie Metallhydroxide, -amide oder -carbonate sind billig und verfügen über eine vergleichsweise hohe Basizität. Ihr Einsatz in der organischen Synthese ist jedoch durch ihre geringe Löslichkeit in den meisten organischen Lösungsmitteln beschränkt, sodass häufig auf eine heterogene Reaktionsführung zurückgegriffen werden muss. Unter Berücksichtigung von Umweltaspekten ist zu bemerken, dass beim industriellen Einsatz anorganischer Basen große, unter Umständen toxische Salzfrachten anfallen, die eine teure Entsorgung erfordern. Vertreter der Klasse der metallorganischen Basen wie *n*-Butyllithium weisen die höchste Basizität unter den hier diskutierten Verbindungen sowie ein gutes Löslichkeitsverhalten in organischen Lösungsmitteln auf.[2] Die hohe Reaktivität und die nukleophilen Eigenschaften der Metallorganyle gehen jedoch in vielen Fällen mit einer geringen Selektivität und somit der Bildung unerwünschter Nebenprodukte einher. Besonders im Hinblick auf Anwendungen im großen Maßstab kann zudem die Handhabung der teilweise pyrophoren Reagenzien ein Problem darstellen. Der hohe Preis der Metallorganyle ist auf ihre energieintensive Produktion zurückzuführen, was auch unter ökologischen Gesichtspunkten nachteilhaft ist.[3] Neutrale organische Basen stellen die dritte Klasse dar. Ihre einfachsten Vertreter sind organische Amine (Abbildung 1.1), die sich durch eine gute Löslichkeit in organischen Lösungsmitteln auszeichnen und als milde Reagenzien häufig eine selektive Deprotonierung gewährleisten.

Abbildung 1.1: Beispiele für organische Stickstoffbasen.

Ihre Nukleophilie kann durch sterische Abschirmung des Basizitätszentrums herabgesetzt werden. Durch chirale, häufig von Aminosäuren abgeleitete Aminbasen können enantioselektive Reaktionen katalysiert werden (siehe Kapitel 1.1.11). Des Weiteren erlaubt die kovalente Anknüpfung organischer Basen an eine Polymermatrix ihre leichte Abtrennung aus der Reaktionsmischung.[4] Organische Basen sind als nicht pyrophore, metallfreie Reagenzien mit häufig geringer Toxizität auch für den Einsatz im großen Maßstab attraktiv, da sie zudem in vielen Anwendungen recycelt werden können und somit

wichtige Anforderungen nachhaltiger Reaktionsführung im Sinne des Konzeptes von *Green Chemistry* erfüllen.[5] Jedoch bleibt die Basizität einfacher Amine deutlich hinter der von Vertretern der beiden anderen Klassen von Basen zurück, sodass ihr Einsatz auf Substrate mit einer ausreichend hohen Acidität beschränkt ist, die etwa bei vielen CH-aciden Verbindungen nicht gegeben ist. Durch die intensive Forschung an den der BRØNSTED-Basizität zugrunde liegenden Prinzipien durch synthetische, analytische und theoretische Chemiker in den zurückliegenden Jahrzehnten gelang die Darstellung organischer Superbasen, deren Basizität an die anorganischer und metallorganischer Basen heranreicht und die somit die Anwendungsbreite für organische Basen erheblich erweitern.[6]

1.1.2 Eigenschaften von Basen

An dieser Stelle soll kurz auf die wichtigsten thermodynamischen und kinetischen Größen eingegangen werden, die zur Beschreibung der Eigenschaften der im Rahmen dieser Arbeit behandelten Basen herangezogen werden. Die bedeutendste Größe zur Quantifizierung der thermodynamischen Basizität einer Verbindung ist der pK_S-Wert ihrer konjugierten Säure, im Folgenden als pK_{BH^+}-Wert bezeichnet. Dieser entspricht dem negativen dekadischen Logarithmus der Konstante K_s, die aus der Gleichgewichtskonstanten K für die in Schema 1.1 dargestellten Reaktion im Lösungsmittel S hervorgeht.[7] Die Konzentration von S wird hierbei als konstant angenommen.

$$BH^+ + S \rightleftharpoons B + SH^+ \qquad K_S = K \cdot c(S) = \frac{c(B) \cdot c(SH^+)}{c(BH^+)} \qquad pK_{BH^+} = -\lg(K_S)$$

Schema 1.1: Zusammenhang des pK_{BH^+}-Wertes einer Base B mit der Gleichgewichtskonstante K im Lösungsmittel S.

Je basischer eine Verbindung ist, desto höher ist ihr pK_{BH^+}-Wert, wobei ein Unterschied von einer Einheit auf der pK_{BH^+}-Werteskala auf Grund des logarithmischen Zusammenhanges einem Basizitätsunterschied von einer Größenordnung entspricht. Der pK_{BH^+}-Wert einer Verbindung ist stark lösungsmittelabhängig, da er wesentlich von der Basizität des verwendeten Solvens bestimmt wird und zudem die in der Reaktionsgleichung in Schema 1.1 dargestellten Spezies je nach Lösungsmittel unterschiedlich gut stabilisiert werden. In der Literatur ist die Angabe von pK_{BH^+}-Werten in Wasser,[8] THF,[9] DMSO[10] oder Acetonitril[7,11] verbreitet, wobei für Superbasen die Acetonitril-Skala etabliert ist. Für viele Basen kann zwischen den pK_{BH^+}-Werten auf unterschiedlichen Skalen näherungsweise ein linearer Zusammenhang angenommen werden.[11] In der Regel wird bei der experimentellen Bestimmung des pK_{BH^+}-Wertes einer Base mit unbekannter Basizität nicht die Protonierung des Solvens betrachtet, sondern die Base konkurriert mit einer zweiten Base mit bekanntem pK_{BH^+}-Wert um Protonen. Die Gleichgewichtskonzentrationen der beiden Basen und ihrer protonierten Formen werden üblicherweise NMR-[12] oder UV/Vis-spektroskopisch[7] ermittelt.

Gegenstand theoretischer Betrachtungen von Basen sind deren Protonenaffinität, die der Enthalpieänderung (ΔH) im Rahmen der in Schema 1.2 dargestellten Reaktion entspricht, und die

Gasphasen-Basizität, welche die entsprechende Änderung der freien Enthalpie (ΔG) darstellt.[13] Je höher die Beträge dieser Werte sind, desto basischer ist eine Verbindung.

Schema 1.2: Zusammenhang von Gasphasen-Basizität (ΔG) und Protonenaffinität (ΔH) einer Base mit der Gleichgewichtskonstante *K*.[13]

Experimentell können diese Werte für flüchtige Basen über massenspektrometrische Verfahren bestimmt werden.[9b,14] Da die theoretische Berechnung von pK_{BH^+}-Werten in Lösung aus den entsprechenden Gasphasen-Basizitäten die komplizierte Einbeziehung der Wechselwirkungen mit Lösungsmittelmolekülen erfordert, wird hierbei zumeist auf semi-empirische Verfahren zurückgegriffen.[9b,15]

Neben den bisher diskutierten Größen, die die thermodynamische Basizität einer Verbindung charakterisieren, spielt die kinetische Basizität eine wichtige Rolle.[16] Sie wird durch die Protonenselbstaustausch-Geschwindigkeit beschrieben und ist abhängig von der sterischen Abschirmung des Basizitätszentrums. Der effiziente Einsatz einer Base in katalytischen Anwendungen erfordert eine ausreichend hohe kinetische Basizität. Eine weitere wichtige Eigenschaft in Bezug auf den Einsatz einer Base in organischen Synthesen ist ihre Nukleophilie. Diese kann beispielsweise durch die Reaktion mit Halogenalkanen wie Isopropylbromid, Octylbromid[17] oder Ethyliodid[12] getestet werden, die mit Basen entweder in einer Eliminierungsreaktion zu einem Alken reagieren oder im Rahmen einer nukleophilen Substitution das basische Zentrum alkylieren (Schema 1.3).

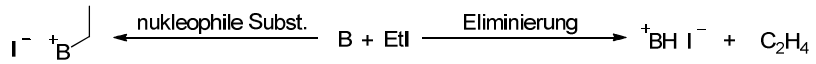

Schema 1.3: Mögliche Reaktionen einer Base mit Ethyliodid.

1.1.3 Klassen organischer Superbasen

In der Literatur existieren keine allgemein gültigen Kriterien, die eine Superbase von einer gewöhnlichen organischen Base abgrenzen. Es erscheint jedoch vernünftig, als Bedingung für Superbasizität einen minimalen pK_{BH^+}-Wert auf der Acetonitril-Skala zu fordern. In diesem Sinne wurde von SUNDERMEYER *et. al* vorgeschlagen, die Schwelle für eine organische Superbase bei einem pK_{BH^+}-Wert von 25 festzusetzen, was etwa einer Gasphasen-Basizität von 1000 kJ/mol entspricht.[18] Nach dieser Definition markiert das Pentamethylguanidin (PMG) die Grenze zur Superbasizität, während die Basizität des Amidins 1,8-Diazabicyclo[5.4.0]undec-7-en (DBU) knapp darunter liegt (Abbildung 1.2).

DBU
pK_{BH^+} (MeCN)
= 24.34

PMG
pK_{BH^+} (MeCN)
= 25.00

Abbildung 1.2: Stabilisierung der positiven Ladung in Amidinium-[11a] und Guanidiniumkationen.[19]

Des Weiteren werden in der Literatur häufig Verbindungen als Superbasen bezeichnet, die nach Protonierung auf Grund mesomerer Grenzstrukturen, sterischer Effekte oder negativer Hyperkonjugation im besonderen Maße zur Stabilisierung einer positiven Ladung in der Lage sind und sich somit von gewöhnlichen organischen Aminbasen abgrenzen. Zu den organischen Superbasen zählen neben den Amidinen und Guanidinen, deren korrespondierende Säuren durch die Ausbildung mesomerer Grenzstrukturen stabilisiert werden (Abbildung 1.2), die Azaphosphatrane, die erstmals von VERKADE *et. al* beschrieben wurden.[20] Diese Käfigverbindungen verfügen über ein basisches Phosphoratom, dessen positive Ladung nach Protonierung durch Wechselwirkung mit einem apikalen Stickstoffdonor stabilisiert wird. Dies geht mit der Kontraktion des Käfigs einher (Schema 1.4).

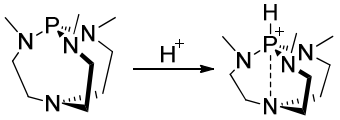

Schema 1.4: Azaphosphatran und dessen Kontraktion nach Protonierung.

Die basischsten Vertreter der organischen Superbasen gehören zur Klasse der seit den 1980er Jahren hauptsächlich von SCHWESINGER *et al.* untersuchten Phosphazenbasen, deren pK_{BH^+}-Werte in Acetonitril einen Bereich von mehr als zwanzig Größenordnungen überstreichen.[17,21] Bereits die simpelste, 1973 von ISSLEIB beschriebene SCHWESINGER-Base (dma)P_1-Me[22] (dma = Dimethylamino) zeigt in Acetonitril einen pK_{BH^+}-Wert von 27.55.[21a] SCHWESINGER *et al.* zeigten, dass die Basizität einfacher P_1-Basen durch die sukzessive Einführung weiterer PN-Einheiten, sogenannten Homologisierungen, auf pK_{BH^+}-Werte von bis zu 46.9 für die verzweigte P_5-Base (pyr)P_5-*t*Bu (pyr = Pyrrolidino) gesteigert werden kann (Abbildung 1.3). Ein Homologisierungsschritt geht mit der Zunahme der möglichen mesomeren Grenzstrukturen für die protonierte Form einer SCHWESINGER-Base einher, sodass die positive Ladung eine bessere Stabilisierung erfährt. Es konnten Phosphazenbasen mit bis zu sieben Phosphoratomen dargestellt werden, wobei ab den P_5-Basen keine weitere Zunahme der Basizität beobachtet wurde. Die genaue Basizität einer SCHWESINGER-Base kann durch die Wahl der Aminosubstituenten und der Alkylgruppe am Iminostickstoffatom eingestellt werden. Für höhere Homologe beeinflusst zudem der Verzweigungsgrad des Phosphazengerüstes den pK_{BH^+}-Wert.

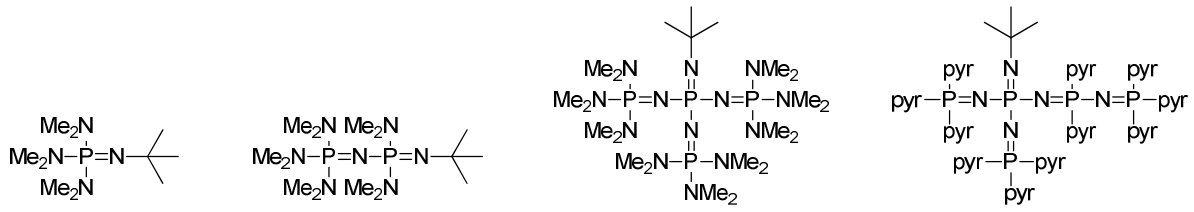

Abbildung 1.3: Erhöhung des pK_{BH}^{+}-Wertes von (dma)P_1-*t*Bu durch Einführung weiterer PN-Einheiten. Die rechts gezeigte SCHWESINGER-Base (pyr)P_5-*t*Bu ist der bisher basischste Vertreter dieser Verbindungsklasse.[21]

1.1.4 Protonenschwämme

Das Phänomen der Protonenschwämme wurde erstmals 1968 von ALDER beschrieben, der die ungewöhnlich hohe Basizität des 1,8-Bis(dimethylamino)naphthalins (DMAN) beobachtete.[23] Während *N*,*N*-Dimethylanilin (pK_{BH}^{+} (H_2O) = 5.06)[24] oder 1,8-Diaminonaphthalin (pK_{BH}^{+} (H_2O) = 4.61)[23] auf Grund des negativen induktiven Effektes der aromatischen Substituenten vergleichsweise wenig basisch sind, weist DMAN einen pK_{BH}^{+}-Wert von 12.34 in Wasser (pK_{BH}^{+} (DMSO) = 7.5,[25] pK_{BH}^{+} (MeCN) = 18.62[11a]) und somit eine um mehr als sieben Größenordnungen höhere Basizität auf. Die Forschungen von ALDER zeigten, dass im Rahmen der sukzessiven Methylierung des 1,8-Diaminonaphthalins nach Einführen der vierten Methylgruppe eine sprunghafte Zunahme des pK_{BH}^{+}-Wertes von 6.43 auf 12.34 zu beobachten ist (Schema 1.5).[23]

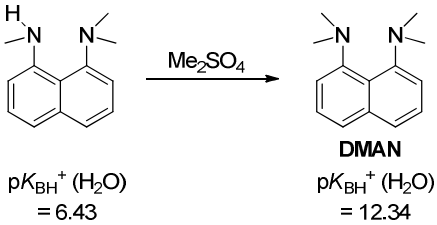

Schema 1.5: Sprunghafte Zunahme der Basizität bei Methylierung von *N*,*N*,*N*'-Trimethyl-1,8-diaminonaphthalin.[23]

Die unerwartet hohe Basizität des DMANs liegt in der erzwungenen räumlichen Nähe der beiden Basizitätszentren in *peri*-Position des Naphthalins begründet. Die Abstoßung der beiden freien Elektronenpaare der basischen Stickstoffatome führt zu einer Verdrillung des aromatischen Rückgrats, sodass keine optimale Überlappung der p-Orbitale des Aromaten gewährleistet ist. Protonierung des DMANs führt nicht nur zur Aufhebung der sterischen Spannung im Naphthalingerüst, sondern auch zur Ausbildung einer energetisch günstigen intramolekularen Wasserstoffbrückenbindung, was mit einer Annäherung der beiden Basizitätszentren verbunden ist. Die N-H···N-Wasserstoffbrücke in protonierten Protonenschwämmen wurde in vielen experimentellen und theoretischen Arbeiten hinsichtlich ihrer Geometrie sowie unter thermodynamischen und kinetischen Gesichtspunkten untersucht, da sie als einfaches Modell für die in biochemischen Systemen auftretenden

Wasserstoffbrückenbindungen dienen kann.[26] Auf Grund der Stabilität der Wasserstoffbrückenbindung kommt es auch durch starke Mineralsäuren wie Perchlorsäure nicht zu einer zweifachen Protonierung des DMANs.[27]

Der Begriff Protonenschwamm geht darauf zurück, dass die meisten Vertreter dieser Klasse über eine vergleichsweise geringe kinetische Basizität verfügen. Dies ist auf die Abschirmung des „aciden" Protons durch hydrophobe Reste sowie die Ausbildung einer stabilen Wasserstoffbrückenbindung zurückzuführen. Dies limitiert die Anwendung von Protonenschwämmen in der BRØNSTED-Basen-Katalyse, macht diese Klasse von Superbasen jedoch für Reaktionen interessant, in denen freigesetzte Protonen nahezu vollständig von anderen Reaktionspartnern abgeschirmt werden müssen.

In den vergangenen Jahrzehnten wurde ALDERs DMAN auf vielfältige Art und Weise modifiziert, um Protonenschwämme mit höheren pK_{BH^+}-Werten darzustellen und das Phänomen ihrer enormen Basizität tiefergehend zu erforschen. So wurden die Methylgruppen an den beiden Basizitätszentren des DMANs durch andere Alkylgruppen substituiert, sodass durch einen höheren sterischen Anspruch und einen stärkeren positiven induktiven Effekt eine weitere Destabilisierung der freien Base und somit eine höhere Basizität erreicht wurden (Abbildung 1.4).[28,29]

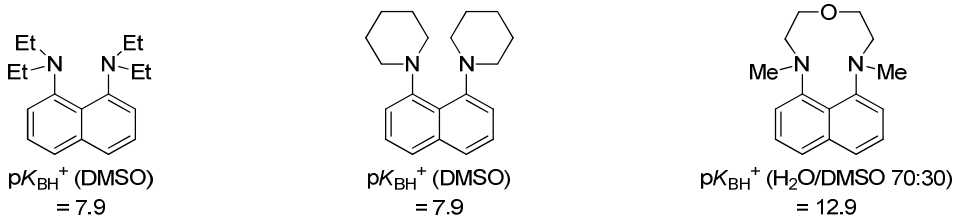

Abbildung 1.4: pK_{BH^+}-Werte von Protonenschwämmen mit Ethyl-[28] und Piperidinyl-Substituenten[28] sowie eines Protonenschwamms, bei dem die Basizitätszentren verbrückt sind.[29]

Des Weiteren wurde das Naphthalinrückgrat substituiert, wobei bevorzugt in 2- und 7-Position des Aromaten sterisch anspruchsvolle und elektronenschiebende Reste eingeführt wurden, die eine weitere Annäherung der beiden basischen Stickstoffatome erzwingen, was als *buttressing effect* bezeichnet wird (Abbildung 1.5).[26f,30]

Abbildung 1.5: Derivate des DMANs mit Methoxy- und Pyrrolidinosubstituenten in 2- und 7-Position des Naphthalins.[26f]

Die räumliche Nähe zweier basischer Stickstoffatome konnte auch durch andere Grundgerüste erreicht werden (Abbildung 1.6): In der Literatur sind Protonenschwämme mit Fluoren-,[31] Heterofluoren-,[32] Phenanthren-,[33] Biphenyl-[34] oder Helicenrückgrat[35] beschrieben. In dem von ZIRNSTEIN *et al.* publizierten Chino[7,8-h]chinolin sind die beiden Stickstoffatome in ein aromatisches System

eingebunden.[36] In der Gruppe von POTÁČEK gelang die Darstellung eines korbartigen Protonenschwamms.[37] Vor Kurzem wurden zudem makrozyklische Verbindungen mit interagierenden Protonenakzeptorfunktionalitäten publiziert.[38]

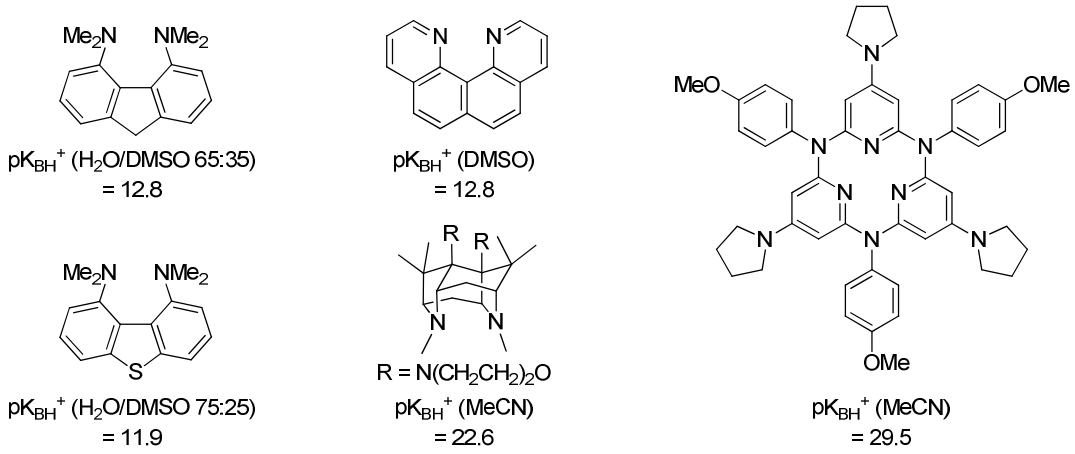

Abbildung 1.6: Protonenschwämme mit alternativen Grundgerüsten.[31,32,36,37b,38c]

Die Entwicklungen im Bereich der Protonenschwämme wurden in Übersichtsartikeln von STAAB,[27] ALDER,[39] LLAMAS-SAIZ,[40] POZHARSKII,[41] NAGASAWA,[42] CHAMBRON,[43] und MAKSIĆ[44] zusammengefasst.

1.1.5 Hybrid-Superbasen

Die im vorangegangenen Abschnitt beschriebenen Modifikationen des ursprünglichen Protonenschwamms DMAN durch Austausch der Substituenten an den Basizitätszentren, Einführung von Substituenten in 2- und 7-Position des Naphthalinrückgrats oder Variation des Grundgerüsts gewährleisten lediglich eine unwesentliche Steigerung der Basizität, wenn die gezeigten makrozyklischen Verbindungen vernachlässigt werden.[45] Die pK_{BH^+}-Werte der beschriebenen Verbindungen liegen deutlich unter denen von simplen P_1-Phosphazenbasen. Eine drastische Erhöhung der Basizität konnte durch Kombination mit anderen superbasischen Elementen erreicht werden, wobei funktionelle Gruppen mit hoher intrinsischer Basizität durch ein geeignetes Gerüst in räumliche Nähe gezwungen werden. In diesem Zusammenhang wurde in der Arbeitsgruppe SUNDERMEYER eine Serie guanidinosubstituierter Protonenschwämme mit Naphthalinrückgrat dargestellt, die über eine bemerkenswerte kinetische Basizität verfügen (Abbildung 1.7).[16,46,47] Im für lange Zeit basischsten Protonenschwamm wird die Interaktion zweier Amidin-Funktionalitäten mit Hilfe eines Vinamidin-Gerüsts erreicht.[48] Diese von SCHWESINGER *et al.* beschriebene Superbase mit hoher kinetischer Basizität weist einen pK_{BH^+}-Wert von 31.94 in Acetonitril auf. Kürzlich wurde von BELDING und DUDDING ein Protonenschwamm mit zwei chelatisierenden Cyclopropeniminyleinheiten publiziert.[49]

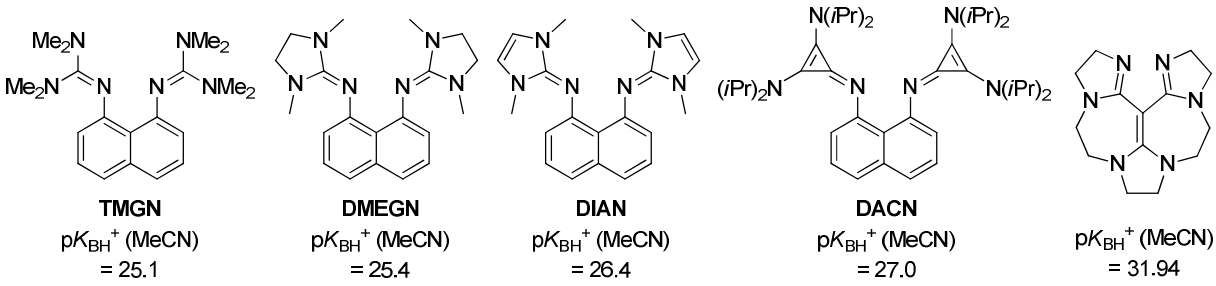

Abbildung 1.7: Drei guanidinosubstituierte Protonenschwämme, ein Protonenschwamm mit Cyclopropeniminyleinheiten und SCHWESINGERs Vinamidin-Schwamm.[16,46-49]

MAKSIĆ und KOVAČEVIĆ berechneten für eine bisher experimentell nicht zugängliche Superbase, in der zwei Guanidinophosphazene über ein Naphthalinrückgrat verknüpft sind, einen pK_{BH}^+-Wert von 44.8 in Acetonitril.[50]

1.1.6 Eigenschaften von Bisphosphazen-Protonenschwämmen

Die ersten naphthalinbasierten Bisphosphazen-Protonenschwämme mit PPh_3- und PPh_2Me-Substituenten wurden bereits Anfang der 1990er Jahre von LLAMAS-SAIZ *et al.* beschrieben, wobei die Verbindungen lediglich in ihrer protonierten Form charakterisiert werden konnten.[51] Für den Protonenschwamm mit Triphenylphosphin-Einheiten wurde eine vergleichsweise geringe Basizität von 15.6 auf der H_2O-Skala gefunden, was auf die elektronenziehende Wirkung der Arylsubstituenten zurückzuführen ist.

In der Arbeitsgruppe SUNDERMEYER wurde 2005 von RAAB *et al.* das 1,8-Bis-(hexamethylaminophosphazenyl)naphthalin (HMPN) dargestellt, in dem zwei SCHWESINGER-Basen über ein 1,8-disubstituiertes Naphthalin-Gerüst verknüpft sind und das mit einem pK_{BH}^+-Wert von 29.9 in Acetonitril um elf Größenordnungen basischer als ALDERs DMAN ist.[12] Eine weitere Basizitätserhöhung konnte im Rahmen der eigenen Diplomarbeit durch Substitution der Dimethylaminogruppen des HMPNs durch Pyrrolidinoeinheiten erreicht werden.[52] Das entsprechende Bisphosphazen 1,8-Bis[tris(pyrrolidino)phosphazenyl]naphthalin (TPPN) ist mit einem pK_{BH}^+-Wert von 32.3 in Acetonitril der bisher basischste experimentell zugängliche Protonenschwamm.

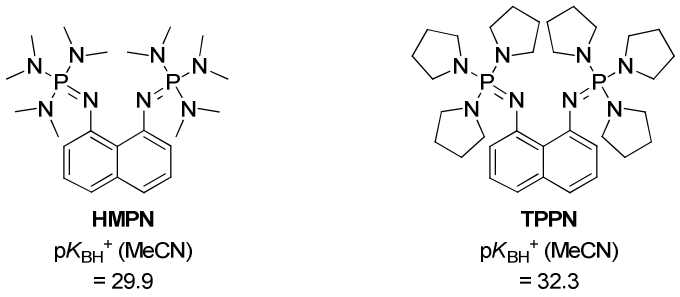

Abbildung 1.8: Bisphosphazen-Protonenschwämme HMPN und TPPN.[12,52]

An dieser Stelle soll am Beispiel des TPPNs kurz auf die strukturellen Eigenschaften der Bisphosphazene eingegangen werden, die die typischen Merkmale von Protonenschwämmen aufweisen: Die Kristallstruktur der freien Base zeigt eine starke Verdrillung des Naphthalins von 8.2(2)° (Abbildung 1.9), die nach Protonierung durch $HN(SO_2CF_3)_2$ für die beiden Formeleinheiten in der asymmetrischen Einheit auf 5.1(4)° bzw. 2.6(4)° vermindert wird. Zudem wird in der Kristallstruktur von TPPN·$HN(SO_2CF_3)_2$ eine starke Annäherung der beiden Basizitätszentren von 2.766(3) Å auf 2.600(6) bzw. 2.625(5) Å beobachtet, wobei die N-H···N-Wasserstoffbrücke eine nicht-lineare, unsymmetrische Geometrie aufweist.

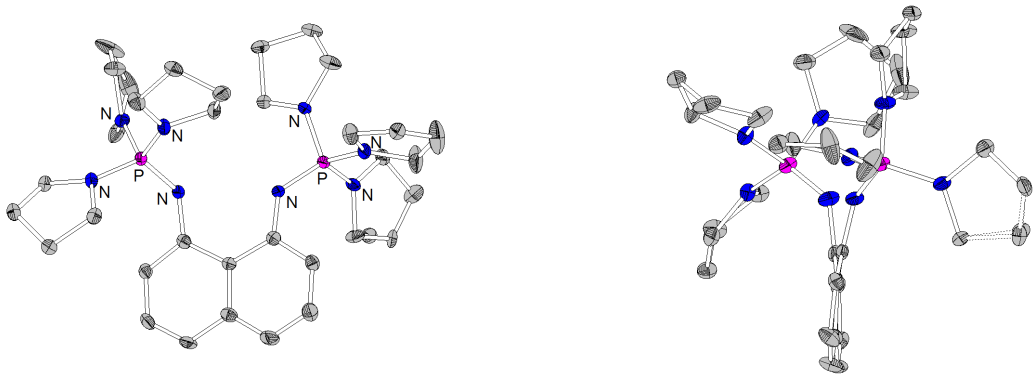

Abbildung 1.9: Molekülstruktur von TPPN (Ellipsoide mit 30% Aufenthaltswahrscheinlichkeit). Die Seitenansicht verdeutlicht die Verzerrung des Naphthalinrückgrats.[52]

Theoretische Berechnungen von MAKSIĆ und KOVAČEVIĆ sagen für eine Homologisierung des TPPNs zu P_2-TPPN eine Erhöhung des pK_{BH}^+-Wertes um nahezu acht Größenordnungen auf 40.2 voraus. In der eigenen Diplomarbeit konnte über eine STAUDINGER-Reaktion das Hydrochlorid des P_2-TPPNs dargestellt und strukturell charakterisiert werden (Abbildung 1.10). Die Isolierung der freien Base und die Bestimmung des pK_{BH}^+-Wertes gelangen bisher nicht.

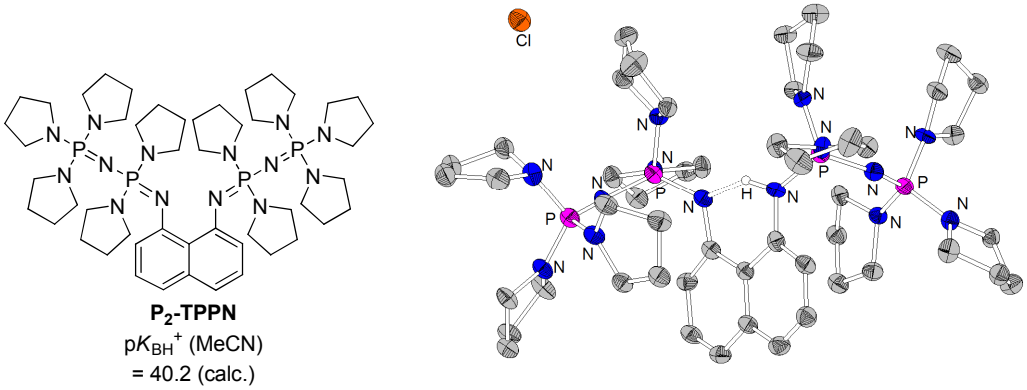

Abbildung 1.10: P_2-TPPN und die Molekülstruktur seines Hydrochlorids (Ellipsoide mit 30% Aufenthaltswahrscheinlichkeit).[52]

1.1.7 Darstellung von Bisphosphazen-Protonenschwämmen

Die Synthese von HMPN erfolgt über eine KIRSANOV-Reaktion,[53] bei der das Bromophosphoniumbromid $[(Me_2N)_3PBr]^+Br^-$ in Gegenwart der Hilfsbase Triethylamin mit 1,8-

Diaminonaphthalin umgesetzt wird. Es wird zunächst das Hydrobromid des Protonenschwamms gebildet, aus dem durch Deprotonierung mit der starken anorganischen Base NaHMDS die freie Base HMPN erhalten wird (Schema 1.6). Die räumliche Nähe der beiden Aminogruppen im 1,8-Diaminonaphthalin erschwert die zweifache KIRSANOV-Reaktion, was in nicht auftrennbaren Gemischen des Protonenschwamms mit dem entsprechenden Monophosphazen resultieren kann. Die sterische Abschirmung des aciden Protons durch hydrophobe Reste kann zudem dazu führen, dass die Deprotonierung unvollständig abläuft und die freie Base mit dem entsprechenden Hydrobromid verunreinigt ist.

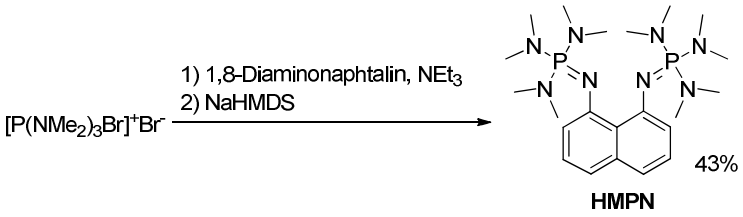

Schema 1.6: Darstellung von HMPN über eine KIRSANOV-Reaktion.[12]

In ersten sondierenden Experimenten konnte während der eigenen Diplomarbeit gezeigt werden, dass die beiden alkylsubstituierten Protonenschwämme TMPN und TBPN (Abbildung 1.11) über eine KIRSANOV-Reaktion in Form ihrer Hydrobromide zugänglich sind, wobei die Salze noch stark mit Triethylammoniumbromid verunreinigt waren. Die Synthese von TBPN über die KIRSANOV-Route und die Kristallstruktur seines Hydrobromids wurden 2012 von XIONG *et al.* publiziert.[54]

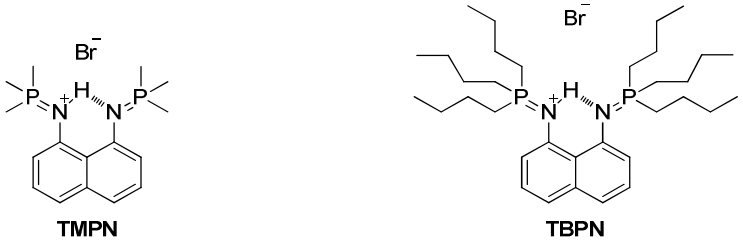

Abbildung 1.11: Hydrobromide der alkylsubstituierten Bisphosphazen-Protonenschwämme TMPN und TBPN.[52]

Eine zweite Strategie zur Darstellung von Bisphosphazen-Protonenschwämmen ist die STAUDINGER-Reaktion,[55] bei der die Verknüpfung des Naphthalin-Gerüsts mit einem Phosphin weiter vom aromatischen Gerüst entfernt vorgenommen wird und die zur erfolgreichen Darstellung von TPPN führte. 1,8-Diazidonaphthalin wird mit einem Phosphin umgesetzt, wobei sich zunächst ein Bisphosphazid bildet, das im Falle von TPPN($2N_2$) bei 90 °C in Toluol innerhalb von 12 h unter Abspaltung von zwei Äquivalenten elementaren Stickstoffs TPPN bildet (Schema 1.7). In diesem Zusammenhang gelang auch die Isolierung des Zwischenproduktes TPPN($1N_2$), das sowohl eine Phosphazen- als auch eine Phosphazideinheit aufweist. Im Gegensatz zur KIRSANOV-Reaktion wird bei der STAUDINGER-Reaktion direkt die freie Base des Protonenschwamms erhalten. Nachteile dieser Route sind die Verwendung des aufwändig herzustellenden und nur in kleinen Mengen zugänglichen

1,8-Diazidonaphthalins, was die Synthese von TPPN im großen Maßstab verhindert, sowie die hohe Stabilität der Bisphosphazide, die zum Teil auch bei hohen Temperaturen keinen elementaren Stickstoff eliminieren. Bisher konnten lediglich HMPN, TPPN und das Hydrochlorid des P_2-TPPNs aus den entsprechenden Bisphosphazid-Vorläufern erhalten werden.

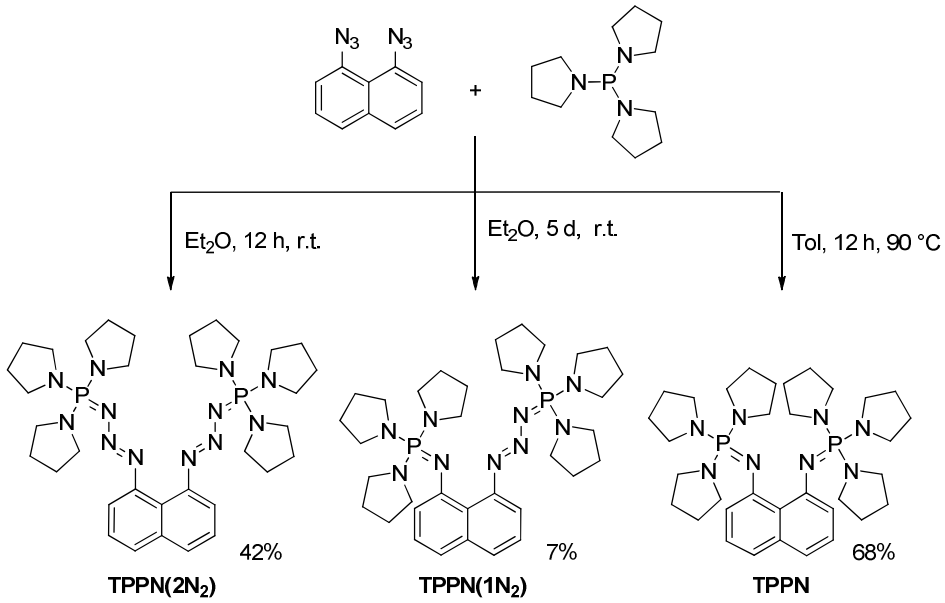

Schema 1.7: Darstellung von TPPN($2N_2$), TPPN($1N_2$) und TPPN über eine STAUDINGER-Reaktion.[52]

1.1.8 Stabile Bisphosphazide

Die STAUDINGER-Reaktion zwischen 1,8-Diazidonaphthalin mit Phosphor(III)-amiden ermöglichte die Isolierung einer Serie von Bisphosphaziden, die zum Teil auch strukturell charakterisiert wurden (Abbildung 1.12).[47,52] Von MAKSIĆ und KOVAČEVIĆ wurde für Bisphosphazide eine den entsprechenden Bisphosphazen-Protonenschwämmen vergleichbare Basizität berechnet, was bisher jedoch noch nicht experimentell untersucht wurde.

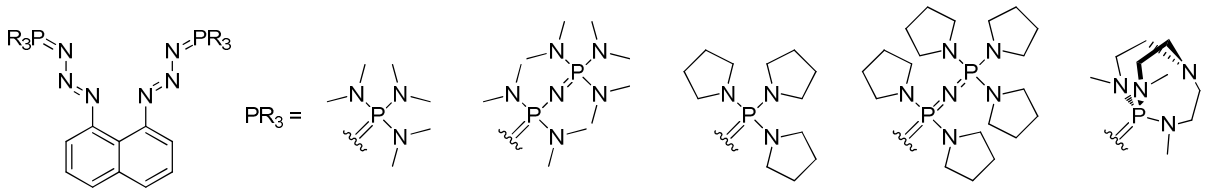

Abbildung 1.12: Stabile Bisphosphazide mit 1,8-disubstituiertem Naphthalinrückgrat.[47,52]

Phosphazide wurden zunächst als instabile Intermediate der STAUDINGER-Reaktion betrachtet, wobei inzwischen eine Vielzahl stabiler Vertreter dieser Verbindungsklasse bekannt ist, was in einem Review-Artikel von BEBBINGTON und BOURISSOU zusammengefasst wurde.[56] Chirale chelatisierende Bisphosphazide wurden in der Literatur bereits von NAKA *et al.* erfolgreich als Organokatalysatoren in asymmetrischen konjugierten Additionen von nukleophilen Enolen an Enone getestet.[57]

1.1.9 Bisylid-Protonenschwämme

Theoretische Arbeiten von KOPPEL *et al.* zeigen, dass Phosphorylide über eine deutlich höhere intrinsische Basizität als die entsprechenden isoelektronischen Phosphazene verfügen (Abbildung 1.13).[58]

Abbildung 1.13: Vergleich der Gasphasen-Protonenaffinität eines Phosphazens mit der eines isoelektronischen Ylids.[58,59]

Eine Zunahme der Basizität wurde gemäß Rechnungen von DAVOR MARGETIĆ auch für die Substitution der basischen Iminstickstoffatome des Bisphosphazen-Protonenschwamms HMPN durch CH-Einheiten vorausgesagt.[60] Der entsprechende Bisylid-Protonenschwamm zeigt mit 283.4 kcal/mol eine dem TPPN (283.2 kcal/mol) vergleichbare theoretische Gasphasen-Protonenaffinität. Ein noch höherer Wert wird für die gemischte Verbindung mit jeweils einer Phosphazen- und Ylideinheit berechnet. Von Interesse ist in diesem Zusammenhang besonders die Position des „aciden" Protons in der einfach protonierten Spezies eines Bisylid-Schwamms.

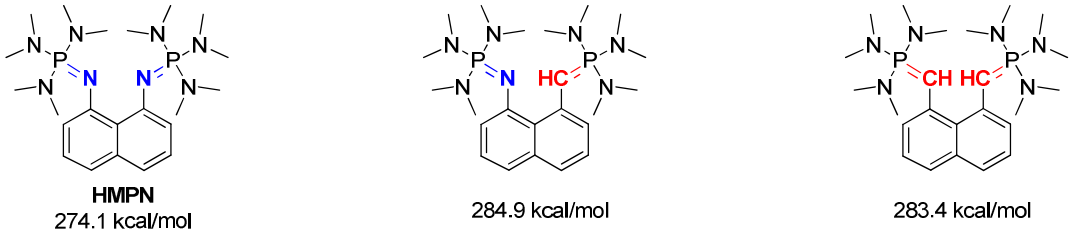

Abbildung 1.14: Vergleich der Gasphasen-Protonenaffinität des Bisphosphazens HMPN mit dem entsprechenden Bisylid-Protonenschwamm und der gemischten Spezies.[60]

Die zweifach protonierte Form einer analogen methylsubstituierten Verbindung wurde bereits 1987 von ENGELHARDT *et al.* durch Umsetzung von 1,8-Bis(chlormethyl)naphthalin mit Trimethylphosphin erhalten.[61] Deprotonierungsversuche mit Kaliumhydrid führten jedoch zur Eliminierung von Methan (Schema 1.8).

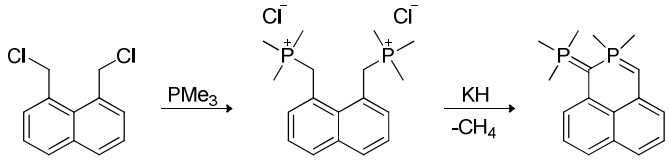

Schema 1.8: Darstellung eines zweifach protonierten Bisylids und dessen Reaktion mit Kaliumhydrid.[61]

1.1.10 Anwendungen organischer Superbasen

Auf Grund ihrer gegenüber klassischen Aminen drastisch erhöhten Basizität sind organische Superbasen zur Deprotonierung einer Vielzahl CH-acider Verbindungen in der Lage, was ihre

vielseitige Anwendung als BRØNSTED-Basen oder Organokatalysatoren in der organischen Synthese gewährleistet. Die präparative Bedeutung organischer Superbasen wurde 2009 in einem Buch von ISHIKAWA zusammengefasst.[6] Besonders die kommerziell erhältlichen Phosphazenbasen können auf Grund ihrer extremen pK_{BH^+}-Werte in Reaktionen eingesetzt werden, die zuvor weitestgehend anorganischen und metallorganischen Basen vorbehalten waren. Hierzu zählen sigmatrope Umlagerungen,[62] MICHAEL-Additionen,[63] PETERSON-[64] und JULIA-KOCIENSKI-Olefinierungen[65] sowie die Generierung von Enolaten[66] und S-Yliden,[67] wobei die Reaktionen zum Teil unter milderen Bedingungen und mit höherer Stereoselektivität ablaufen als mit metallhaltigen Basen.

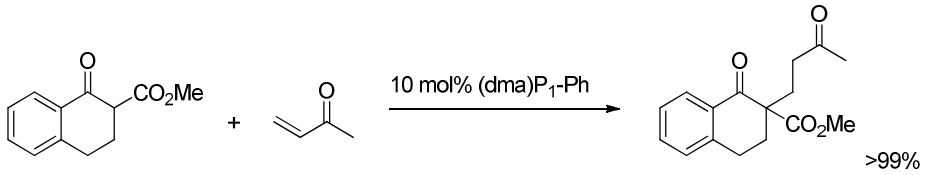

Schema 1.9: Anwendung der SCHWESINGER-Base (dma)P_1-Ph in einer MICHAEL-Addition.[63]

Organische Superbasen, insbesondere die SCHWESINGER-Base (dma)P_4-*t*Bu, wurden hinsichtlich ihrer Eignung als Promotoren in metallfreien anionischen Polymerisationsreaktionen untersucht, sodass auf diesem Gebiet besonders in den letzten Jahren eine rege Publikationstätigkeit verzeichnet werden konnte.[68] Systeme auf Basis von superbasischen Phosphazenen wurden erfolgreich in der Ringöffnungspolymerisation von zyklischen Lactonen,[69] Epoxiden,[70] Cyclopropan-Derivaten[71] und zyklischen Siloxanen[72] eingesetzt. Des Weiteren gelang die anionische Polymerisation von Methylmethacrylat (Schema 1.10).[73]

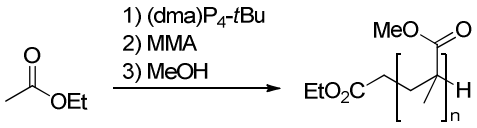

Schema 1.10: Anwendung der SCHWESINGER-Base (dma)P_4-*t*Bu in der anionischen Polymerisation von Methylmethacrylat (MMA).[73a]

Kürzlich wurden diphenylphosphinosubstituierte Derivate des DMANs als Liganden in der ESI-Massenspektrometrie eingesetzt.[74] DMAN und TMGN haben im Bereich der Bioanalytik Verwendung zur Detektion von Biomolekülen wie Lipiden oder Peptiden als Matrix in der MALDI-Massenspektrometrie gefunden.[75]

1.1.11 Chirale organische Superbasen

Chirale Amine spielen eine herausragende Rolle in der asymmetrischen Katalyse - nicht zuletzt im Rahmen der intensiven Forschung im Bereich der Organokatalyse seit der zurückliegenden Dekade.[76] Hierbei ist die Verwendung chiraler Amine als Basen jedoch wie bei ihren achiralen Verwandten auf Grund ihrer relativ geringen Basizität auf vergleichsweise acide Substrate beschränkt. Asymmetrische Reaktionen mit starken metallorganischen Basen konnten unter anderem durch Beigabe chiraler

Amine wie Spartein erreicht werden.[77] BHUNYIA *et al.* beschrieben die enantioselektive Öffnung von Epoxiden mit chiralen Lithiumamiden.[78] Auf Grund der in den vorangegangen Kapiteln bereits beschriebenen Nachteile von Metallorganylen und salzartigen Basen haben in den vergangenen 15 Jahren zunehmend auch chirale organische Superbasen das wissenschaftliche Interesse geweckt, wobei mittlerweile jede Klasse von Superbasen über eine Reihe chiraler Vertreter verfügt.

In diesem Zusammenhang ist die Klasse der chiralen Guanidine hinsichtlich struktureller Vielfalt und präparativer Bedeutung am weitesten entwickelt, was bereits in mehreren Übersichtsartikeln beschrieben wurde.[79,80] Beispielsweise konnte von ISHIKAWA *et al.* erfolgreich gezeigt werden, dass chirale Guanidine asymmetrische MICHAEL-Additionen, nukleophile Epoxidierungen und Cyanierungsreaktionen mittels Trimethylsilylcyanid katalysieren können.[81] Die chiralen Basen wurden zudem stöchiometrisch in kinetischen Racematspaltungen von sekundären Alkoholen eingesetzt. Eine weitere Studie zu chiralen Guanidinen, deren Fokus auf C_3-symmetrischen Guanidiniumsalzen lag, wurde kürzlich von CASTIGLIA *et al.* publiziert.[82] Für die im Vergleich zu den Guanidinen weniger basischen Vertreter der Klasse chiraler Amidine existieren ebenfalls Literaturbeispiele.[83]

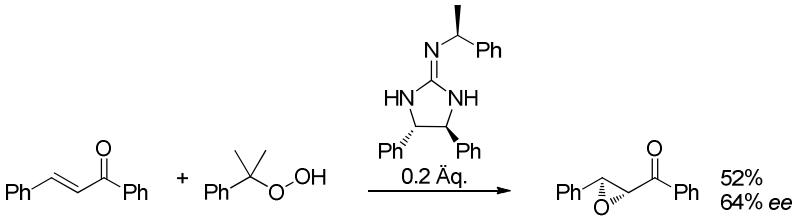

Schema 1.11: Guanidinkatalysierte enantioselektive Epoxidierung.[81a]

ALDER veröffentlichte 2005 eine theoretische Arbeit über C_2-symmetrische Protonenschwämme mit pK_{BH}^{+}-Werten zwischen 30 und 33 auf der Acetonitril-Skala.[84] Eine weitere theoretische Studie von SINGH *et al.* widmet sich chiralen substituierten *cis*-1,3,5,7-Tetraazadecalinen, die Protonenaffinitäten in der Gasphase oberhalb von 1000 kJ/mol aufweisen.[85] Chirale Protonenschwämme mit einem Grundgerüst auf Basis des klassischen 1,8-Diaminonaphthalins konnten durch Substitution einer oder beider Aminofunktionen durch Binaphthyleinheiten erreicht werden.[86] Die Rutheniumkomplexe davon abgeleiteter Verbindungen wurden erfolgreich als Katalysatoren in asymmetrischen allylischen Veretherungsreaktionen getestet.[86b]

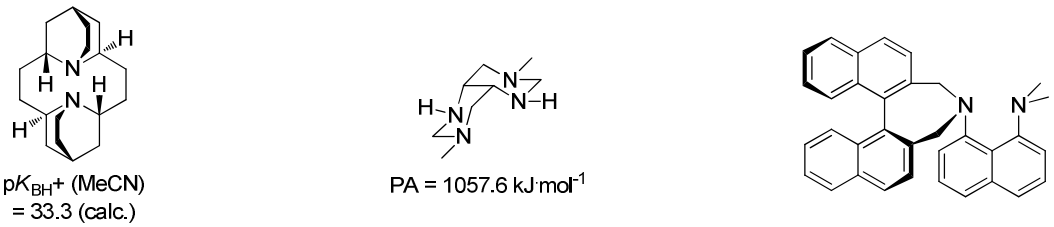

Abbildung 1.15: Chirale Superbasen mit interagierenden Protonenakzeptorfunktionalitäten.[84-86]

In der Literatur sind eine Reihe C_3-symmetrischer Proazaphosphatrane beschrieben, die ihre Stereozentren entweder an den Substituenten der drei dem basischen Phosphorzentrum benachbarten

Aminogruppen oder an den verbrückenden Methylengruppen tragen.[87] LIU *et al.* verwendeten chirale Proazaphosphatrane zur Bestimmung der *ee*-Werte chiraler Azide,[87a] konnten bei der Addition von Trimethylsilylcyanid an Benzaldehyd oder der Öffnung von prochiralen Epoxiden unter katalytischem Einsatz dieser Superbasen jedoch keine Enantiomerenüberschüsse erzielen.[87b] ISHIHARA *et al.* beobachteten einen *ee*-Wert von 15% für die Umsetzung von Benzaldehyd mit Diethylzink in Anwesenheit eines chiralen Proazaphosphatrans.[87c]

Abbildung 1.16: Chirale Proazaphosphatrane.[87]

Bereits 1999 wurde von BRUNEL *et al.* erstmals ein chirales Phosphin in der asymmetrischen Cyclopropanierung von Olefinen eingesetzt.[88] Des Weiteren stellten ALAJARÍN *et al.* makrozyklische C_3-symmetrische Phosphazene über eine STAUDIGNER-Reaktion dar.[89] KÖHN *et al.* publizierten drei chirale, vom Prolin abgeleitete superbasische P_1-Phosphazene, deren in der Literatur angegebene pK_{BH^+}-Werte zwischen 35 und 37 auf der Acetonitril-Skala jedoch im Vergleich mit anderen P_1-Phosphazenen um einige Größenordnungen zu hoch erscheinen.[90]

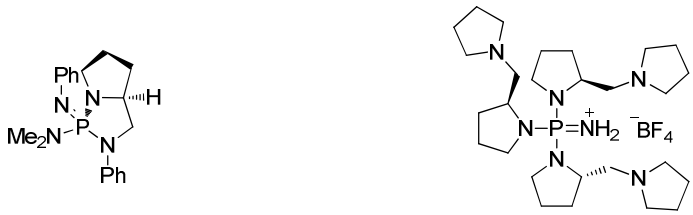

Abbildung 1.17: Chirale P_1-Phosphazene.[88,90]

In der Literatur sind nur wenige chirale Superbasen beschrieben, in denen mehrere superbasische Merkmale in einem Molekül kombiniert sind. Proazaphosphatrane wurden mit chiralen Aziden umgesetzt, die von Weinsäure, einem Zucker oder einem Cinchona-Alkaloid abgeleitet sind, um chirale Iminophosphorane mit Phosphatrankäfigen zu generieren.[91] Die von HIMMEL publizierten C_2-symmetrischen über ein Binaphthylrückgrat verknüpften Bisguanidine stellen keine Protonenschwämme im engeren Sinne dar, weil sich die beiden Basizitätszentren in der freien Base aus dem Weg gehen können.[92] Es ist jedoch wahrscheinlich, dass es nach Protonierung zur Chelatisierung des Protons unter Ausbildung einer intramolekularen Wasserstoffbrückenbindung kommt. Kürzlich wurden von TERADA *et al.* spirozyklische P_3-Phosphazene und eine Reihe chiraler Phosphazene mit Guanidinosubstituenten publiziert.[93] Die hohe Basizität der Guanidinophosphazene ermöglichte asymmetrische elektrophile Aminierungsreaktionen mit einem Azodicarboxylat.

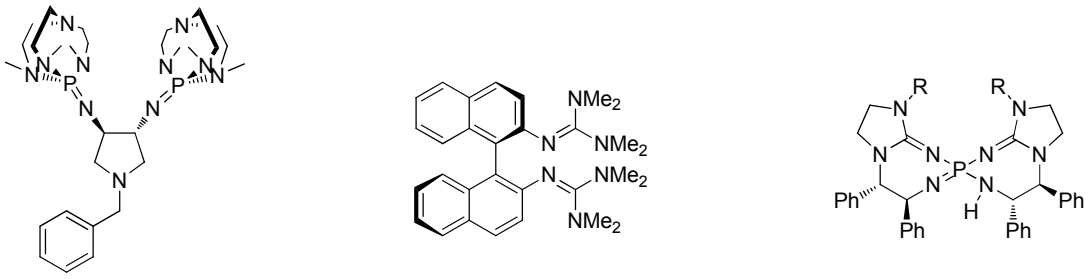

Abbildung 1.18: Chirale Hybridsuperbasen: C_2-symmetrisches Bisphosphazen mit zwei Azaphosphatrankäfigen,[91] C_2-symmetrisches Bisguanidin[92] und chirales Guanidinophosphazen.[93]

1.2 NH-Säuren und LEWIS-Supersäuren

1.2.1 NH-Säuren

Der Begriff NH-Säuren bezeichnet sekundäre Amine oder Amide mit zumeist perfluorierten Substituenten mit hoher Gruppenelektronegativität, die eine Delokalisierung der negativen Ladung in den korrespondierenden Anionen über mesomere oder induktive Effekte gewährleisten.[94] Der wichtigste Vertreter dieser Verbindungsklasse, das Bis(trifluormethylsulfonyl)imid $HN(SO_2CF_3)_2$, hat seit dessen erstmaliger Beschreibung durch DESMARTEAU[95] besonders durch die schwach koordinierenden Eigenschaften seines Anions große Bedeutung im Bereich der ionischen Flüssigkeiten und der Elektrochemie erlangt. Seine geringe Neigung zur Ausbildung gerichteter elektrostatischer Wechselwirkungen macht das Bis(trifluormethylsufonyl)imid-Anion zu einem idealen Bestandteil ionischer Flüssigkeiten mit Pyrrolidinium-,[96] Imidazolium-,[97] Guanidinium-[98] oder Phosphonium-Kationen.[99] Derartige ionische Verbindungen mit Schmelzpunkten unterhalb von 100 °C werden auch als *designer solvents* bezeichnet und haben sich neben ihrer Anwendung als umweltfreundliche Reaktionsmedien[100] oder in Gasabsorptionsprozessen[101] als mögliche Elektrolyte für elektrochemische Anwendungen erwiesen.[102] In diesem Zusammenhang ist besonders das breite elektrochemische Fenster des Bis(trifluormethylsulfonyl)imid-Anions von Bedeutung.

Die herausragende Acidität von $HN(SO_2CF_3)_2$ in der Gasphase sowie in flüssigen Medien wie Dichlorethan oder Acetonitril macht die NH-Säure zudem zum Gegenstand einer Vielzahl theoretischer und experimenteller Arbeiten.[103] Das Bis(trifluormethylsulfonyl)imid verfügt über eine Gasphasen-Acidität[104] von 286.5 kcal/mol[103b] und ist somit eine stärkere BRØNSTED-Säure als einige klassische Mineralsäuren wie Iodwasserstoff (309.2 kcal/mol)[105] oder H_2SO_4 (302.2 kcal/mol).[106] Interessanterweise reagiert $HN(SO_2CF_3)_2$ in wässriger Lösung nicht unter Ausbildung von Hydroxoniumionen, sondern bildet lediglich eine Wasserstoffbrückenbindung zu einem Wassermolekül aus.[107] Derivate des Bis(trifluormethylsulfonyl)imids mit längerkettigen perfluorierten Resten zeigen sogar noch höhere BRØNSTED-Aciditäten in der Gasphase ($HN(SO_2C_2F_5)_2$: 283.7 kcal/mol).[103b] Die hohe Acidität ermöglicht die Anwendung in BRØNSTED-Säure-katalysierten Reaktionen wie Cycloadditionen,[108] Hetero-MICHAEL-Additionen (Schema 1.12),[109] enantioselektiven DIELS-ALDER-Reaktionen[110] oder Cyclisierungen von Siloxyalkinen mit Arenen und Alkenen.[111]

Kürzlich wurde von CHEON und YAMAMOTO ein Review zur Bedeutung superacider BRØNSTED-Säuren in der Katalyse publiziert.[112]

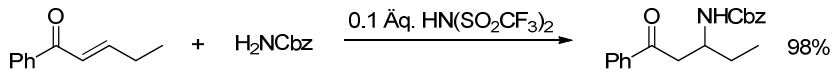

Schema 1.12: Bis(trifluormethylsulfonyl)imid als BRØNSTED-Säure-Katalysator in einer Aza-MICHAEL-Addition.[109]

Auf Grund seiner schlechten Donor-Eigenschaften kann das Bis(trifluormethylsulfonyl)imid als Ligand zur Generierung LEWIS-acider katalytisch aktiver Metallzentren fungieren, was in einem Übersichtsartikel von ANTONIOTTI *et. al* und einem Mini-Review von GAL zusammengefasst wurde.[113]

Das erstmals von BROOKE dargestellte Decafluordiphenylamin $HN(C_6F_5)_2$ kann leicht und in großen Maßstab durch die Reaktion von Hexafluorbenzol mit Lithiumamid erhalten werden (Schema 1.13).[114]

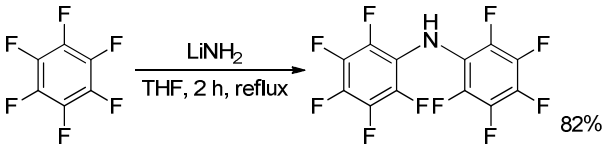

Schema 1.13: Darstellung von Decafluordiphenylamin.[114]

Die Acidität des Decafluordiphenylamins in der Gasphase liegt mit 316.5 kcal/mol[103a] deutlich unter der des Bis(trifluormethylsulfonyl)imids, was in Lösung einem höheren pK_s-Wert von mehreren Größenordnungen entsprechen sollte. Dennoch erwies sich das Anion des Decafluordiphenylamins ebenfalls als geeignet zur Darstellung ionischer Flüssigkeiten[115] und das entsprechende Lithiumsalz ist für elektrochemische Anwendungen im Gespräch.[116] Hervorstechend ist die interessante Koordinationschemie des $[N(C_6F_5)_2]^-$, das nicht wie $[N(SO_2CF_3)_2]^-$ unter Ausbildung von Sechsring-Chelaten an ein Metallzentrum koordinieren kann, sondern neben einem Stickstoffdonor lediglich aromatische Fluoratome zur Ausbildung von hemilabilen Metall-Fluor-Kontakten zur Verfügung stellt. Die Koordination organisch gebundener Fluoratome ermöglicht die Stabilisierung stark LEWIS-acider Metallzentren, wobei das Aufbrechen der Metall-Fluor-Kontakte eine Koordinationsstelle freigeben kann, was Metallkomplexe mit Decafluordiphenylamid-Liganden für katalytische Anwendungen interessant macht. Zur Wechselwirkung zwischen Metallzentren und organisch gebundenen Fluoratomen sind zwei Übersichtsartikel von PLENIO erschienen.[117] Für den Decafluordiphenylamid-Liganden sind in der Literatur neben den Lithiumsalzen $LiN(C_6F_5)_2{\cdot}THF$ und $LiN(C_6F_5)_2{\cdot}\ Et_2O$[118] (Abbildung 1.19) Decafluordiphenylamid-Komplexe des Germaniums[119] und des Neodyms[120] sowie der Übergangsmetalle Titan, Zirconium, Vanadium, Eisen, Cobalt[121] und Wolfram[122] zu finden. Kürzlich wurden von YIN *et al.* die solvatfreien Komplexe $La[N(C_6F_5)_2]_3$ und $Ce[N(C_6F_5)_2]_3$ sowie davon abgeleitete Lösungsmitteladdukte und at-Komplexe publiziert.[123]

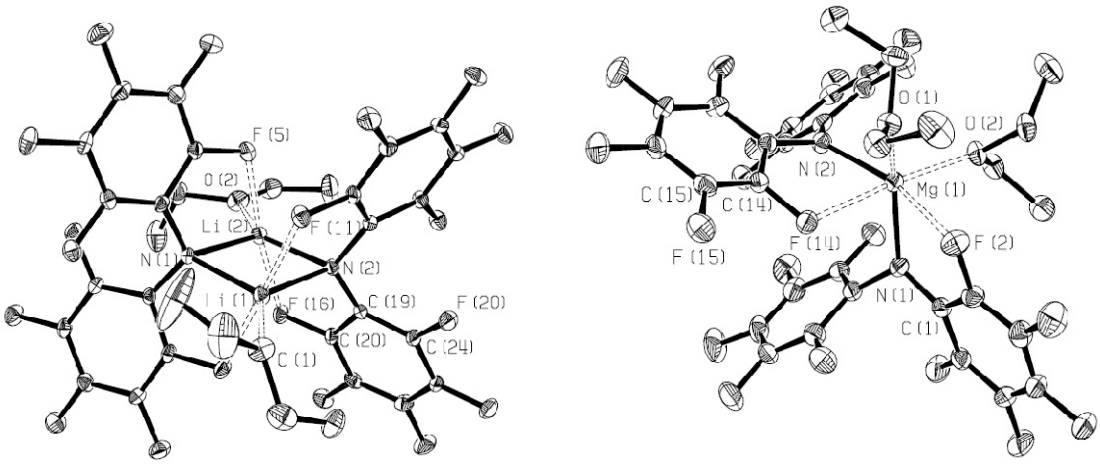

Abbildung 1.19: Metall-Fluor-Kontakte in den Molekülstrukturen von $LiN(C_6F_5)_2 \cdot Et_2O$ und $Mg[N(C_6F_5)_2]_2 \cdot 2Et_2O$.[124]

Zudem wurden in der Arbeitsgruppe SUNDERMEYER weitere Decafluordiphenylamid-Komplexe mit Metallen des s- (Li, Na, K, Mg, Ca, Ba), p- (Al, Sn, Pb), d- (Ti, V, Zn) und f-Blocks (Y, La, Ce, Sm, Eu) dargestellt und größtenteils auch strukturell charakterisiert.[124-126] LINDER testete einige der Erdalkali- und Seltenerdmetallkomplexe in der Ringöffnungspolymerisation von ε-Caprolacton, wobei besonders der Europiumkomplex gute Polymerisationseigenschaften zeigte und bereits bei Raumtemperatur Poly-ε-caprolacton mit einer engen Molmassenverteilung lieferte (Schema 1.14).

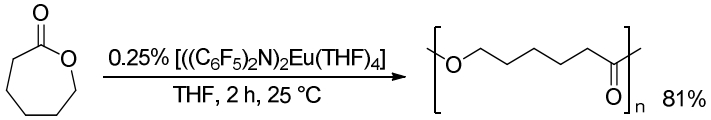

Schema 1.14: Polymerisation von ε-Caprolacton mit $[((C_6F_5)_2N)_2Eu(THF)_4]$.[126]

In der Arbeitsgruppe SUNDERMEYER wurden von THOMAS LINDER mit $HN(C_6F_5)(SO_2CF_3)$ und $HN(C_6F_5)(SO_2C_4F_9)$ zwei unsymmetrisch substituierte Hybride aus Decafluordiphenylamin und einem Bis(perfluoralkylsulfonyl)imid dargestellt.[115] Die Synthese erfolgte durch Deprotonierung von Pentafluoranilin mit NaHMDS und anschließende Umsetzung mit Trifluormethansulfonsäureanhydrid bzw. Nonafluorbutansulfonsäurefluorid, wobei zunächst die entsprechenden Natriumsalze gebildet wurden, die nach Protonierung durch Sublimation gereinigt werden konnten.

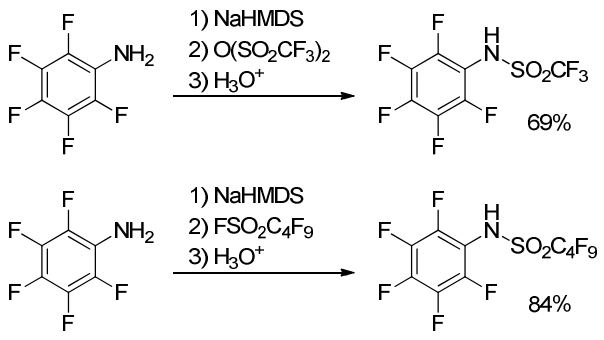

Schema 1.15: Darstellung von $HN(C_6F_5)(SO_2CF_3)$ und $HN(C_6F_5)(SO_2C_4F_9)$ ausgehend von Pentafluoranilin.[115]

In den beiden NH-Säuren ist die hohe Gruppenelektronegativität einer Perfluoralkylsulfonyleinheit mit einer aromatischen Pentafluorphenylfunktionalität mit der Möglichkeit zur Ausbildung von Metall-Fluor-Kontakten kombiniert. Die neuen NH-aciden Amide wurden röntgenkristallographisch charakterisiert ($HN(C_6F_5)(SO_2C_4F_9)$ in Form seines Etherats) und fungierten als Anionen in je drei ionischen Flüssigkeiten mit Imidazolium- und Phosphonium-Kationen.[115] Ihre korrespondierenden Lithiumsalze wurden in der Arbeitsgruppe ROLING bezüglich ihrer elektrochemischen Eigenschaften untersucht.[116]

1.2.2 LEWIS-Supersäuren

Als Maßstab für die LEWIS-Acidität einer Verbindung wurde von der Arbeitsgruppe KROSSING in Anlehnung an Arbeiten von BARTLETT die Fluoridionenaffinität in der Gasphase (FIA, *engl. fluoride ion affinity*) gewählt (Schema 1.16).[127,128] Analog zur Definition für BRØNSTED-Supersäuren, die acider als die stärkste konventionelle BRØNSTED-Säure, 100%ige H_2SO_4, sein müssen, wird für eine LEWIS-Supersäure eine höhere FIA als die von SbF_5 (489 kJ/mol) verlangt. Nach dieser Definition erfüllen beispielsweise die meisten Borane wie etwa das prominente Trispentafluorphenylboran (444 kJ/mol) die Kriterien für LEWIS-Superacidität nicht.

$$A_{(g)} + F^-_{(g)} \longrightarrow AF^-_{(g)} \quad \Delta H = -FIA$$

Schema 1.16: Fluoridionenaffinität (FIA) in der Gasphase.

MÜLLER *et al.* publizierten 2008 die Darstellung des homoleptischen Aluminiumkomplexes des Perfluor-*tert*-butanols $Al[OC(CF_3)_3]_3$ über eine Alkaneliminierungsreaktion, wobei die Verbindung auf Grund ihrer extremen LEWIS-Acidität zunächst nur als Addukt mit dem schwachen Donor Fluorbenzol isoliert werden konnte.[128] Für die freie LEWIS-Säure wurde mit Hilfe von theoretischen Berechnungen eine FIA von 537 kJ/mol ermittelt und DFT-Rechnungen zeigen, dass das Metallzentrum durch Ausbildung zweier Kontakte zu Fluoratomen der *tert*-Butylgruppen stabilisiert wird.

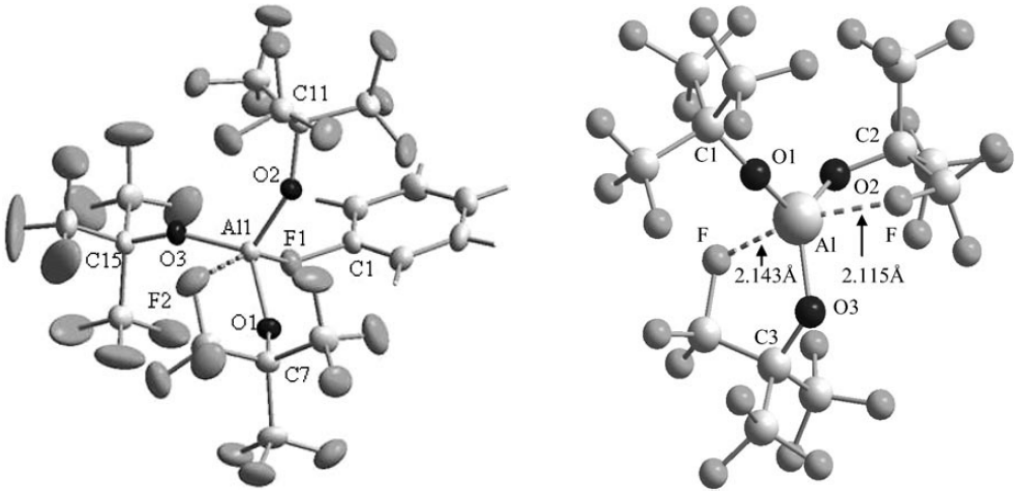

Abbildung 1.20: Kristallstruktur des Fluorbenzol-Adduktes von $Al[OC(CF_3)_3]_3$ (links) sowie die durch DFT-Rechnungen ermittelte Struktur des solvatfreien $Al[OC(CF_3)_3]_3$ (rechts).[128]

Kürzlich wurde ein weiterer LEWIS-superacider Aluminiumkomplex mit einer FIA von 530 kJ/mol publiziert, in dem die $OC(CF_3)_3$-Liganden durch pentafluorphenylsubstituierte Perfluorcyclohexanol-Einheiten ($O(C_6F_{10}(C_6F_5))$) ersetzt wurden.[129] Das Design neuer LEWIS-Supersäuren ist auch Gegenstand theoretischer Untersuchungen.[130] FRENKING zeigte in einer theoretische Studie zu LEWIS-Säuren mit Metallen der Gruppe 13, dass eine Erhöhung der LEWIS-Acidität durch Pyramidalisierung der freien LEWIS-Säure erreicht werden kann.[131]

Im Rahmen der LEWIS-Supersäuren sind auch die entsprechenden schwach koordinierenden Anionen (WCAs, *engl. weakly coordinating anions*) von Interesse, die aus der Bildung von at-Komplexen resultieren. Sie sind in der Lage, nackte, äußerst reaktive Kationen zu stabilisieren, was beispielsweise in der homogenen Polymerisationskatalyse mit Zirconocen-Katalysatoren ausgenutzt werden kann.[132] Ausgehend von dem von BIHLMEIER *et al.* publizierten Silbersalz $Ag^+[Al(OC(CF_3)_3)_4]^-$[133] konnten hochreaktive Metallkationen wie amidosubstituierte Germanium(II)- und Zinn(II)-Monokationen,[134] homoleptische Ethen-Komplexe der Münzmetalle (Abbildung 1.21 links),[135] die tBu$_3$Si$^+$-Quelle [tBu$_3$Si-Ga-SitBu$_3$]$^+$,[136] Gallium(I)-Arenkomplexe (Abbildung 1.21 rechts)[137] oder Phosphankomplexe des einwertigen Galliums und des Indiums[138] stabilisiert werden. Zudem gelang die Darstellung weiterer kationischer Spezies wie zum Beispiel die Isolierung der Carbokationen $[CCl_3]^+$ und $[CBr_3]^+$,[139] des Trityliumkations,[140] eines Radikal-Kations des Benzidins,[141] eines stabilen $[AsBr_4]^+$-Kations[142] oder eines $[Ag_2Se_{12}]^{2+}$-Käfigs.[143]

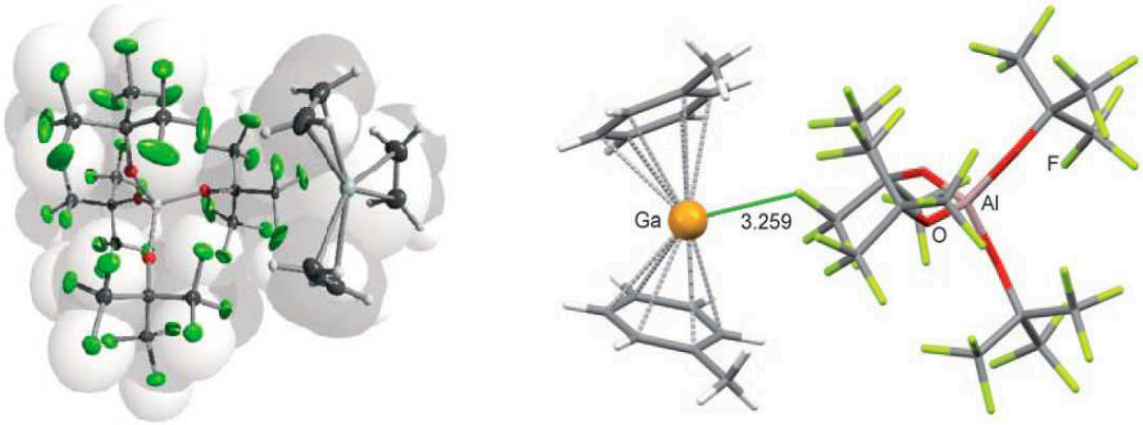

Abbildung 1.21: Molekülstrukturen von $[Ag(C_2H_4)_3]^+[Al(OC(CF_3)_3)_4]^-$[135b] und $[Ga(C_6H_5Me)_2]^+[Al(OC(CF_3)_3)_4]^-$.[137] In der Darstellung des Silber-Ethen-Komplexes ist der sterische Anspruch des WCAs verdeutlicht.

Durch Umsetzung von $Al[OC(CF_3)_3]_3$ mit den Alkoholen (–)-Menthol, Pentafluorphenol und Nonafluor-*tert*-Butanol wurden BRØNSTED-Supersäuren dargestellt, deren *in silico* bestimmte Gasphasen-Aciditäten zwischen 279.7 und 249.0 kcal/mol deutlich unter dem Wert von $HN(SO_2CF_3)_2$ (286.5 kcal/mol)[103b] liegen.[144]

Die Arbeiten von KROSSING *et al.* zeigen wichtige Voraussetzungen, die Liganden erfüllen müssen, um in homoleptischen Komplexen mit einem Metall der Gruppe 13 molekulare LEWIS-Supersäuren zu bilden: Zunächst sollten stark elektronenziehende Substituenten schwach ausgeprägte Donoreigenschaften gewährleisten. Zudem sollten die Liganden über einen hohen sterischen Anspruch verfügen, um die Bildung von Oligomeren zu vermeiden, die für eine Verringerung der LEWIS-Acidität sorgen und die theoretische Berechnung der FIA erschweren. Selbstverständlich muss das Ligandensystem inert gegenüber intramolekularen oder intermolekularen Zersetzungsreaktionen mit dem LEWIS-aciden Zentrum sein. Schließlich sollte das Metallzentrum nicht koordinativ abgesättigt sein, sondern seine hohe positive Ladungsdichte sollte durch hemilabile Kontakte wie beispielsweise zu organisch gebundenen Fluoratomen stabilisiert werden, sodass bei Anwesenheit eines besseren Donors eine Koordinationsstelle freigegeben wird.

Obwohl NH-Säuren mit perfluorierten, stark elektronenziehenden Gruppen in den meisten Fällen eine geringere Acidität und somit bessere Donoreigenschaften als die entsprechenden perfluorierten Alkohole aufweisen, können sie dennoch als vielversprechende Liganden zur Generierung von LEWIS-superaciden Verbindungen mit Metallen der Gruppe 13 angesehen werden. Die Verwendung sekundärer Amine gewährleistet nicht nur eine gute sterische Abschirmung des Metallzentrums, sondern die Verwendung unsymmetrisch substituierter Amine ermöglicht zudem eine große strukturelle Vielfalt sowie die gezielte Abstimmung des Donorcharakters und des sterischen Anspruchs des Liganden.

In der Arbeitsgruppe SUNDERMEYER wurde von ALEXANDER KHVOROST erstmalig der homoleptische Aluminiumkomplex des Decafluordiphenylamins $Al[N(C_6F_5)_2]_3$ über eine Alkaneliminierungsreaktion

dargestellt und röntgenkristallographisch charakterisiert.[124] Die Kristallstruktur zeigt ein fünffach koordiniertes Aluminiumzentrum, das neben drei Al-N-Bindungen zwei Aluminium-Fluor-Kontakte zu *ortho*-Fluoratomen der Pentafluorphenylsubstituenten ausbildet (d(Al-F): 2.084(1) und 2.060(1) Å). Die Synthese wurde von DENIS SOROKIN optimiert, der den Aluminiumkomplex durch Umsetzung von Aluminiumtrichlorid mit $LiN(C_6F_5)_2$ in Toluol unter Abspaltung von Lithiumchlorid erhielt und die Verbindung auf diese Weise im größeren Maßstab zugänglich machte.[125]

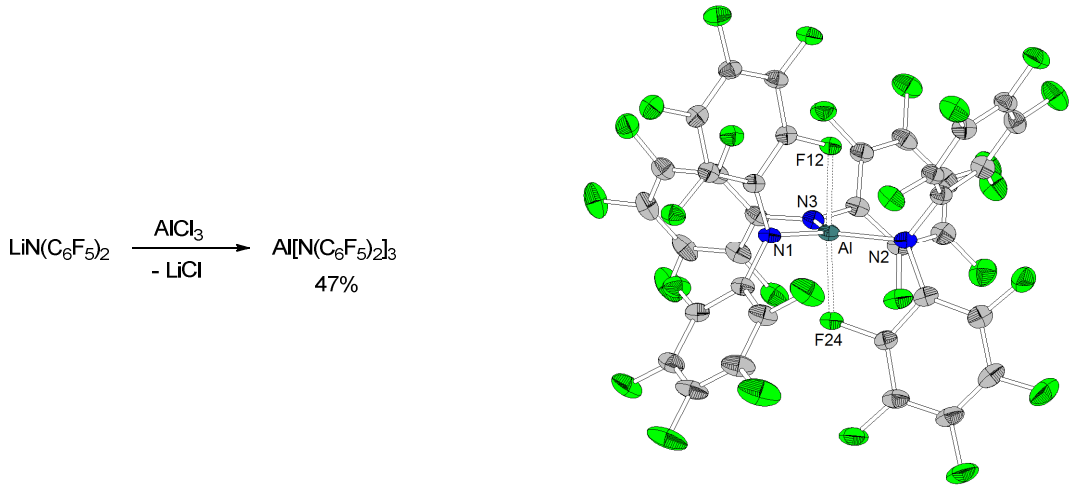

Schema 1.17: Synthese und Molekülstruktur von $Al[N(C_6F_5)_2]_3$ (Ellipsoide mit 30% Aufenthaltswahrscheinlichkeit).[124]

SOROKIN gelang neben der Kristallisation von LEWIS-Säure-Base-Addukten von $Al[N(C_6F_5)_2]_3$ mit Acetonitril und *tert*-Butylisocyanid die Darstellung der Aluminat-Komplexe $[Cs(Tol)_3]^+[Al(N(C_6F_5)_2)_3F]^-$ und $[Ph_3C]^+[((C_6F_5)_2N)_3AlF\text{-}Li\text{-}FAl(N(C_6F_5)_2)_3]^-$ sowie deren röntgenkristallographische Charakterisierung. $Al[N(C_6F_5)_2]_3$ und $[Ph_3C]^+[Al(N(C_6F_5)_2)_3F]^-$ wurden als Aktivatoren von Dimethylzirconocen in der homogenen Ethenpolymerisation getestet, wobei Ersteres unter bestimmten Bedingungen eine dem $B(C_6F_5)_3$ vergleichbare Aktivität zeigte. Die in der Arbeitsgruppe KROSSING durch theoretische Berechnungen ermittelte Fluoridionen-Affinität in der Gasphase von 515 kJ/mol sowie der experimentelle Befund, dass $Al[N(C_6F_5)_2]_3$ zur Abstraktion eines Fluoridions von einem SbF_6^--Anion in der Lage ist, weisen $Al[N(C_6F_5)_2]_3$ als LEWIS-Supersäure aus.

2. Aufgabenstellung

Anknüpfend an die erfolgreiche Synthese des bisher basischsten Protonenschwamms TPPN über eine STAUDINGER-Reaktion im Rahmen der eigenen Diplomarbeit sollte das Potential dieser Syntheseroute zur Darstellung weiterer Bisphosphazene untersucht werden (Schema 2.1). In diesem Zusammenhang sind auch die zunächst gebildeten Bisphosphazide von Interesse, da theoretische Berechnungen für diese Verbindungsklasse ebenfalls eine hohe Basizität vorhersagen.

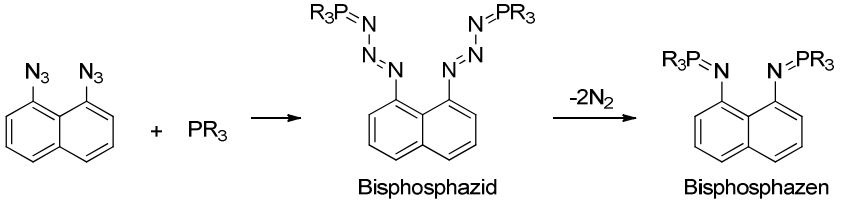

Schema 2.1: Darstellung eines Bisphosphazen-Protonenschwamms über die STAUDINGER-Route.

Über eine STAUDINGER-Reaktion konnte neben TPPN auch das Hydrochlorid von dessen höherem Homologen P_2-TPPN erhalten werden. Ziel der vorliegenden Arbeit ist die erfolgreiche Darstellung von P_2-TPPN in seiner freien Basenform und die Bestimmung seines pK_{BH^+}-Wertes, wobei theoretische Berechnungen eine Basizität im Bereich der stärksten bekannten organischen Superbasen erwarten lassen. Um den Einfluss der Chelatisierung des aciden Protons auf die Basizität zu ermitteln, soll das entsprechende Monophosphazen synthetisiert und hinsichtlich seines pK_{BH^+}-Wertes untersucht werden.

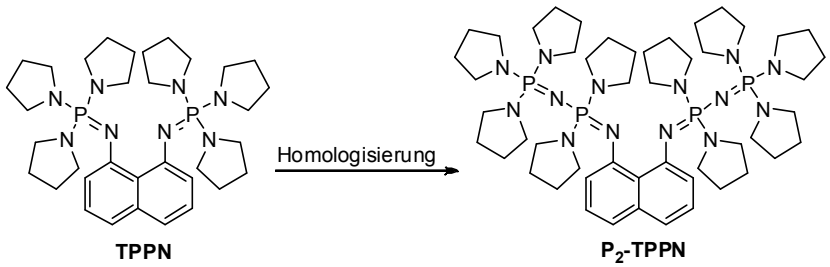

Schema 2.2: Homologisierung von TPPN.

Sondierende Experimente im Rahmen der eigenen Diplomarbeit lieferten erste Erkenntnisse, dass eine KIRSANOV-Reaktion, die ohne das aufwändig und nur in kleinen Mengen darstellbare 1,8-Diazidonaphthalin auskommt, zur Darstellung alkylsubstituierter Bisphosphazen-Protonenschwämme geeignet sein könnte. Diese konnten bisher nur stark verunreinigt in Form ihrer Hydrobromide erhalten werden. Es sollen geeignete Reaktionsbedingungen gefunden werden, um die potentiellen Superbasen in hoher Reinheit zugänglich zu machen und mit ihren aminosubstituierten Analoga zu vergleichen.

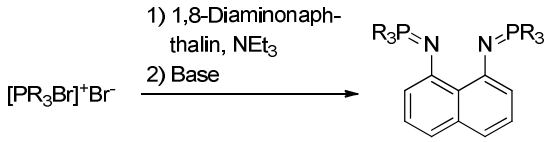

Schema 2.3: Darstellung alkylsubstituierter Bisphosphazen-Protonenschwämme über eine KIRSANOV-Reaktion.

Untersuchungen an neuen Bisphosphazen-Protonenschwämmen beinhalten die Ermittlung ihrer pK_{BH^+}-Werte mittels NMR-Titrationsexperimenten mit einer Vergleichsbase bekannter Basizität sowie die Untersuchung ihrer nukleophilen Eigenschaften und Koordinationschemie. Die Superbasen sollen sowohl als freie Base, als auch in ihrer protonierten Form dargestellt und nach Möglichkeit röntgenkristallographisch charakterisiert werden. Die Kristallstrukturen dienen als Basis für theoretische Berechnungen durch Dr. BORISLAV KOVAČEVIĆ (Ruđer Bošković Institute, Zagreb).
Die von Dr. DAVOR MARGETIĆ (Ruđer Bošković Institute, Zagreb) durchgeführten Berechnungen zur hohen Basizität von chelatisierenden Bisylid-Protonenschwämmen sollen experimentell untersucht werden, wobei zunächst die entsprechenden zweifach protonierten Spezies dargestellt werden, die dann mit einer geeigneten Base deprotoniert werden sollen.
Die Erkenntnisse bezüglich der Synthese superbasischer Phosphazene mit wechselwirkenden Protonenakzeptorfunktionalitäten sollen vom 1,8-disubstituierten Naphthalin auf die chiralen Binaphthyl- und 1,2-Diaminocyclohexangerüste übertragen werden, um chirale organische Superbasen mit bisher unerreichten pK_{BH^+}-Werten zu erhalten (Abbildung 2.1).

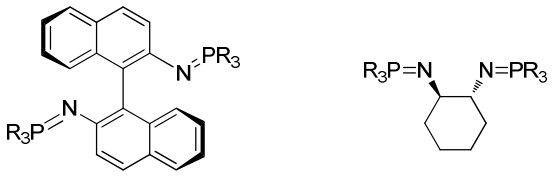

Abbildung 2.1: Chirale Bisphosphazene mit Binaphthyl- und 1,2-Diaminocyclohexanrückgrat.

Der zweite Teil dieser Arbeit beschäftigt sich mit NH-aciden Aminen und Amiden, die über einen Pentafluorphenylsubstituenten und einen zweiten stark elektronenziehenden perfluorierten Rest verfügen. Diese Verbindungsklasse soll um neue Vertreter erweitert werden, wobei zunächst ihren Kristallstrukturen sowie der Darstellung ihrer Lithiumsalze besondere Aufmerksamkeit gelten soll. In Kooperationen sollen die NH-Säuren bezüglich ihrer theoretischen BRØNSTED-Acidität in Lösung und in der Gasphase (Dr. SASCHA GOLL, Arbeitsgruppe KROSSING, Freiburg), ihrer experimentellen pK_S-Werte in Acetonitril (Arbeitsgruppe LEITO, Tartu) sowie hinsichtlich der elektrochemischen Eigenschaften ihrer Lithiumsalze (FABIAN WOHDE, Arbeitsgruppe ROLING, Marburg) untersucht werden.

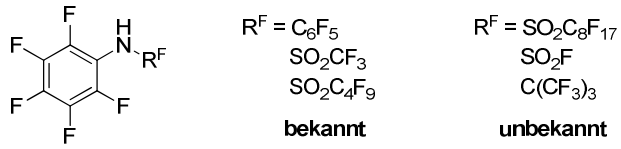

Abbildung 2.2: Pentafluorphenylsubstituierte NH-acide Amine und Amide.

Des Weiteren soll geprüft werden, ob sich pentafluorphenylsubstituierte NH-Säuren auf Grund ihrer schlechten Elektronendonoreigenschaften zur Generierung stark LEWIS-acider Metallzentren eignen. Ziel ist in diesem Zusammenhang zunächst die Darstellung der homoleptischen Aluminiumkomplexe der in der Arbeitsgruppe SUNDERMEYER erstmals von THOMAS LINDER beschriebenen NH-Säuren $HN(C_6F_5)(SO_2CF_3)$ und $HN(C_6F_5)(SO_2C_4F_9)$ über Alkan- oder Salzeliminierungsreaktionen. Von besonderem Interesse ist hierbei die röntgenkristallographische Charakterisierung der Metallkomplexe, die Einblicke in den Koordinationsmodus und mögliche Metall-Fluor-Kontakte ermöglicht (Abbildung 2.3). Für die erhaltenen Metallkomplexe soll die LEWIS-Acidität durch Bildung von Lösungsmittel-Addukten und at-Komplexen nachgewiesen werden.

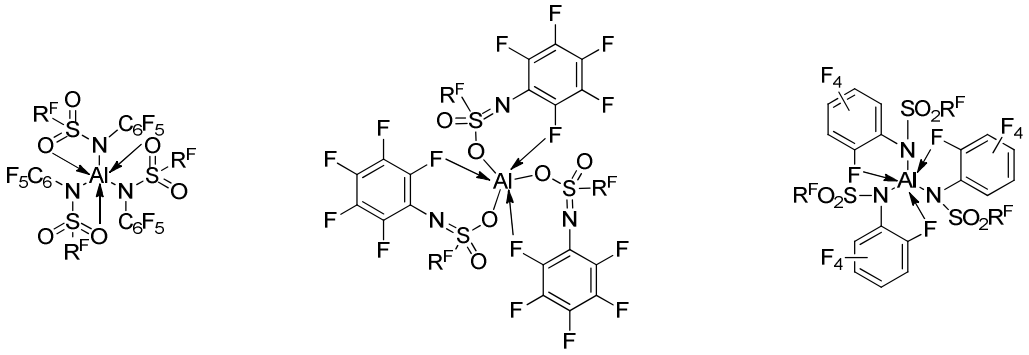

Abbildung 2.3: Denkbare Koordinationsmodi in $Al[N(C_6F_5)(R^F)]_3$ (R^F = CF_3, C_4F_9).

In Anlehnung an die von ALEXANDER KHVOROST und DENIS SOROKIN charakterisierten LEWIS-Supersäure $Al[N(C_6F_5)_2]_3$ soll in der vorliegenden Arbeit die analoge Galliumverbindung $Ga[N(C_6F_5)_2]_3$ dargestellt werden und hinsichtlich ihrer LEWIS-Acidität in Konkurrenzexperimenten mit dem bekannten Aluminiumkomplex verglichen werden.

3. Zusammenfassung

Im ersten Teil der vorliegenden Dissertation wird die Fragestellung behandelt, welche Prinzipien maßgeblich für BRØNSTED-Superbasizität sind. In der Arbeitsgruppe SUNDERMEYER konnte bereits erfolgreich gezeigt werden, dass die Kombination von SCHWESINGERs Phosphazenbasen mit ALDERs Konzept der Protonenschwämme mit interagierenden Protonenakzeptorfunktionalitäten zu neutralen organischen Superbasen mit hohen pK_{BH}^{+}-Werten von ca. 30 (MeCN) führt (Abbildung 3.1). Im ersten Teil dieser Arbeit wurde das Potential der STAUDINGER- und der KIRSANOV-Reaktion zur Darstellung solcher Bisphosphazen-Protonenschwämme untersucht. Hierbei wurde der Einfluss neuer Strukturmotive wie die Substitution der Aminogruppen in den bekannten Verbindungen durch Alkylreste oder die Einführung einer weiteren PN-Einheit auf die Basizität der Protonenschwämme betrachtet. Von besonderem Interesse sind in diesem Zusammenhang stets die strukturellen Merkmale der Verbindungen als freie Basen und in ihrer protonierten Form. Zudem wurden neben der Nukleophilie und der kinetischen Basizität der Hybrid-Superbasen auch ihre Koordinationschemie in neutralen und kationischen Alkylkomplexen von Metallen der Gruppen 12 und 13 erforscht. Des Weiteren wurden die Erfahrungen mit chelatisierenden Phosphazenbasen zur Darstellung chiraler Superbasen genutzt.

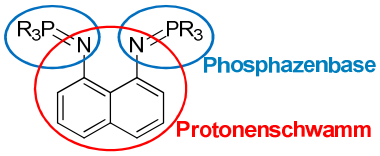

Abbildung 3.1: Verknüpfung zweier Phosphazenbasen über ein 1,8-disubstituiertes Naphthalinrückgrat.

Der zweite Teil dieser Arbeit behandelt die Grundlagen zur gezielten Generierung starker LEWIS-Säuren mit schwach koordinierenden Amidoliganden. Hierbei wurden NH-acide Amine und Amide betrachtet, die über zwei unterschiedliche perfluorierte und somit stark elektronenziehende Substituenten verfügen (Abbildung 3.2). Neben der Synthese neuer Vertreter dieser Verbindungsklasse wurde ihre Koordinationschemie sowie ihr Potential zur Generierung LEWIS-acider Metallzentren mit Metallen der Gruppe 13 untersucht. Erfolgreich dargestellte Komplexe wurden hinsichtlich ihrer LEWIS-aciden Eigenschaften charakterisiert.

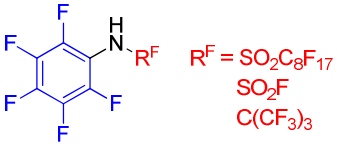

Abbildung 3.2: Neue pentafluorphenylsubstituierte NH-Säuren.

3.1 Die STAUDINGER-Reaktion – Darstellung stabiler Bisphosphazide und eines höheren Homologen des TPPNs

In einer STAUDINGER Reaktion wurden neben Phosphor(III)-amiden $P(NRR')_3$ mit einfachen linearen oder cyclischen Aminogruppen eine *N*-guanidino-substituierte Verbindung, zwei gemischtvalente P(III)-P(V)-Vorläufer und eine vom (*S*)-Prolin abgeleitete chirale Phosphor(III)-Verbindung mit 1,8-Diazidonaphthalin umgesetzt, sodass die Verbindungsklasse der stabilen Bisphosphazide um acht neue Vertreter erweitert werden konnte (Schema 3.1). In Abbildung 3.3 sind die Kristallstrukturen von drei Bisphosphaziden gezeigt, wobei die Struktur der diethylaminosubstituierten Verbindung ein Wassermolekül enthält, das Wasserstoffbrückenbindungen zu den α-Stickstoffatomen ausbildet. Die von theoretischen Rechnungen vorhergesagte hohe Basizität der Bisphosphazide konnte experimentell nicht bestätigt werden, da Protonierungsversuche in der Zersetzung letzterer zu nicht identifizierten Produkten resultierten. Experimentelle Befunde und Rechnungen von BORISLAV KOVAČEVIĆ legen nach Protonierung einen Zerfallsmechanismus über eine Arinspezies nahe. Für keines der in Schema 3.1 gezeigten Bisphosphazide konnte bei hohen Temperaturen die Bildung des entsprechenden Bisphosphazens unter Eliminierung von molekularem Stickstoff erreicht werden. Der synthetische Nutzen der STAUDINGER-Reaktion zur Darstellung von Bisphosphazen-Protonenschwämmen ist somit auf Grund der ungewöhnlichen Stabilität der Bisphosphazid-Vorläufer stark eingeschränkt.

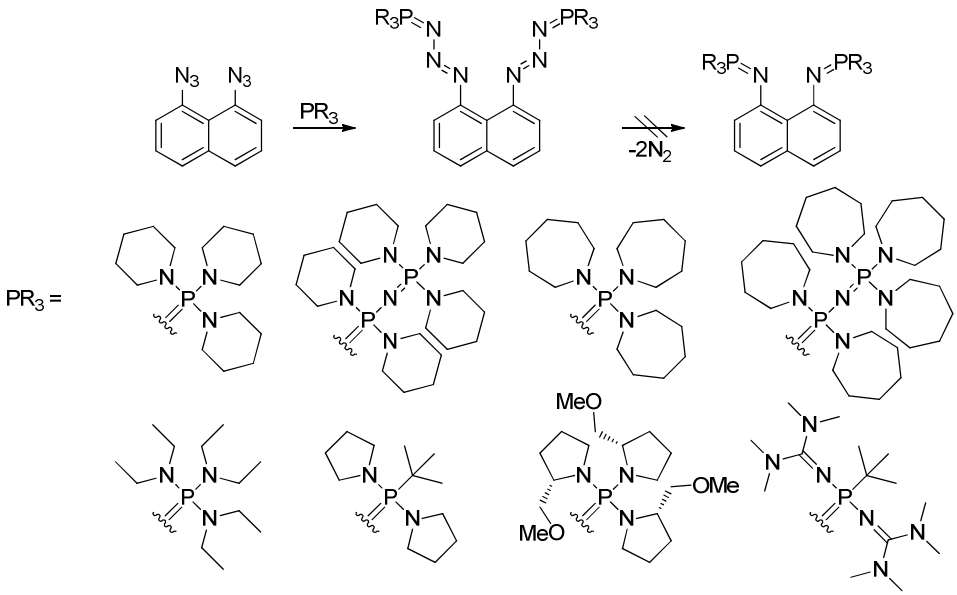

Schema 3.1: Neue Vertreter der Klasse der stabilen Bisphosphazide.

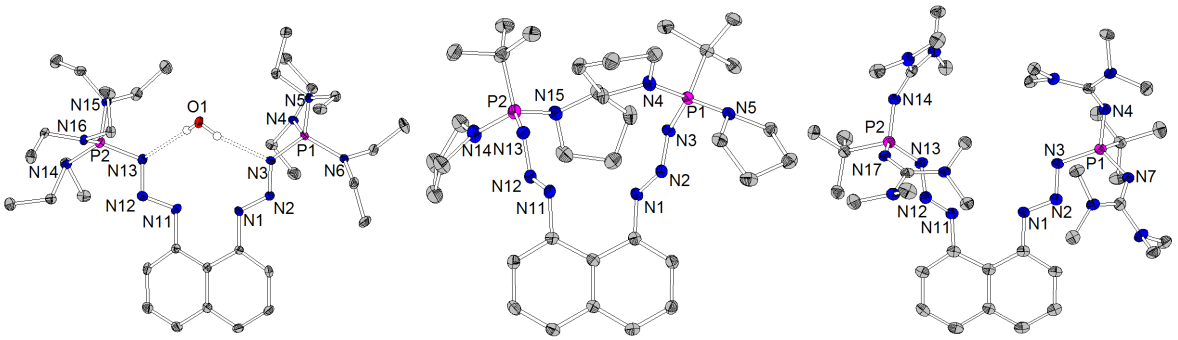

Abbildung 3.3: Molekülstrukturen von Bisphosphaziden mit -$P(NEt_2)_3$, -$P(N(CH_2)_4)_2$*t*Bu und -$P(N{=}C(NMe_2)_2)_2$*t*Bu Substituenten (Ellipsoide mit 30% Aufenthaltswahrscheinlichkeit).

In einer STAUDINGER-Reaktion gelang jedoch erstmals die erfolgreiche Darstellung von P_2-TPPN in seiner freien Basenform (Schema 3.2). Durch Optimierung der Synthese konnte zunächst der entsprechende P(V)-P(III)-Vorläufer $(pyr)_3P{=}N\text{-}P(pyr)_2$ rein dargestellt und mit 1,8-Diazidonaphthalin zum höheren Homologen des TPPNs umgesetzt werden. Die Kristallstrukturen von P_2-TPPN und seines $HN(SO_2CF_3)_2$-Salzes sind in Abbildung 3.4 gegenüber gestellt.

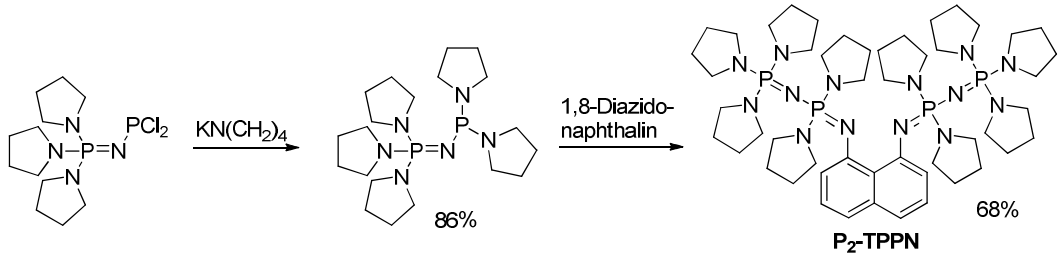

Schema 3.2: Darstellung von P_2-TPPN über eine STAUDINGER-Reaktion.

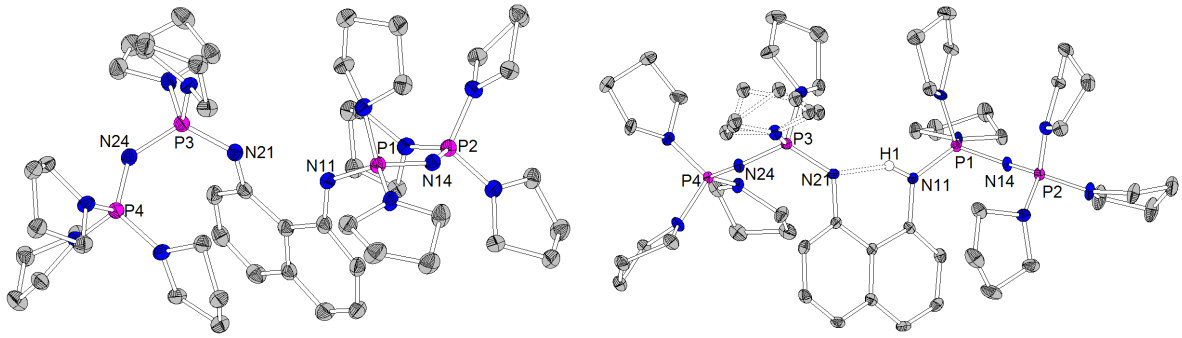

Abbildung 3.4: Molekülstrukturen von P_2-TPPN und P_2-TPPN·$HN(SO_2CF_3)_2$ (Ellipsoide mit 30% Aufenthaltswahrscheinlichkeit, $[N(SO_2CF_3)_2]^-$ nicht dargestellt).

3.2 Die KIRSANOV-Reaktion – Darstellung alkylsubstituierter Bisphosphazen-Protonenschwämme

Vier neue alkylsubstituierte Bisphosphazen-Protonenschwämme konnten in einer KIRSANOV-Reaktion dargestellt werden. Das methylsubstituierte TMPN und das *n*-butylsubstituierte TBPN konnten ausgehend von den jeweiligen Phosphinen in einfachen Eintopfreaktionen in Form ihrer freien Base erhalten werden (Schema 3.3).

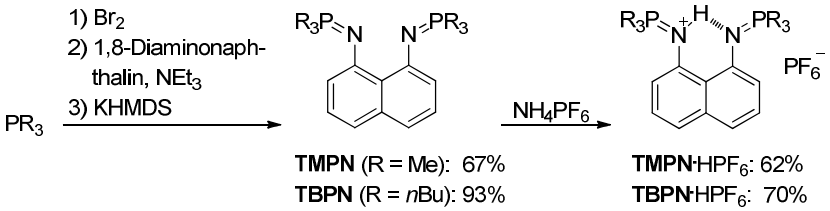

Schema 3.3: Darstellung von TMPN und TBPN über eine Eintopfreaktion ausgehend von den jeweiligen Phosphinen und anschließende Protonierung mit Ammoniumhexafluorophosphat.

Die Synthesen von TiPrPN und TcyPPN (Abbildung 3.5) erwiesen sich auf Grund des höheren sterischen Anspruchs der sekundären Alkylgruppen als schwieriger, weshalb jeweils die entstehenden Zwischenprodukte isoliert wurden.

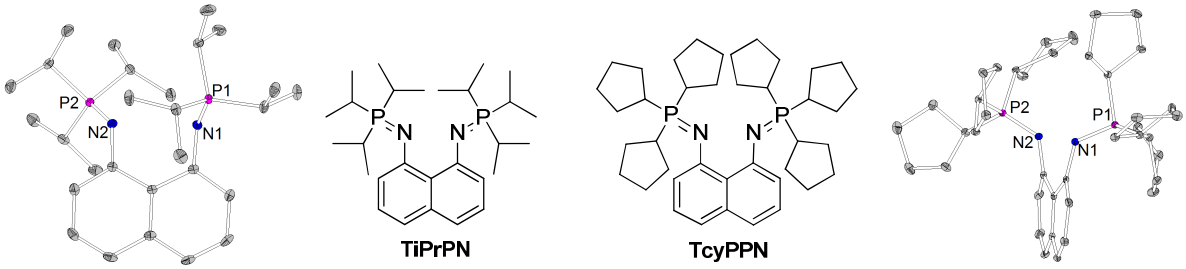

Abbildung 3.5: TiPrPN und TcyPPN sowie deren Molekülstrukturen (Ellipsoide mit 30% Aufenthaltswahrscheinlichkeit).

Die Röntgenstrukturanalysen der Hydrobromide der vier alkylsubstituierten Bisphosphazen-Protonenschwämme zeigten in allen Fällen die Ausbildung von nicht-linearen unsymmetrischen Wasserstoffbrückenbindungen (Abbildung 3.6).

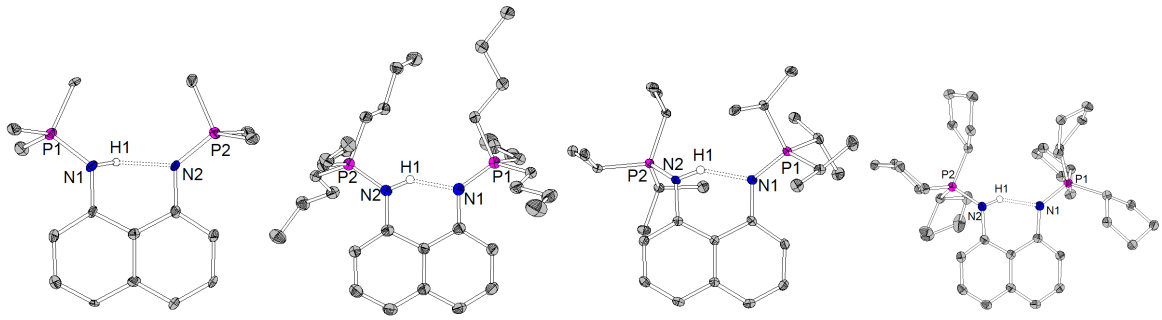

Abbildung 3.6: Molekülstrukturen von TMPN·HBr, TBPN·HBr, TiPrPN·HBr und TcyPPN·HBr (Ellipsoide mit 30% Aufenthaltswahrscheinlichkeit, Anion und Lösungsmittelmoleküle nicht dargestellt).

Das bisher nur über eine STAUDINGER-Reaktion zugängliche pyrrolidinosubstituierte TPPN konnte ebenfalls über die KIRSANOV-Route erhalten werden. Dies ermöglicht dessen Synthese im großen Maßstab (Schema 3.4). Die Darstellung weiterer aminosubstituierter Bisphosphazen-Protonenschwämme mit Hilfe der KIRSANOV-Route gelang jedoch nicht.

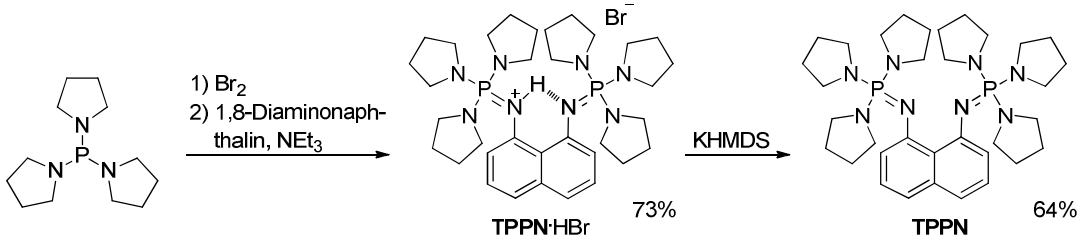

Schema 3.4: Darstellung von TPPN·HBr über eine KIRSANOV-Reaktion und anschließende Deprotonierung mit KHMDS.

3.3 Basizität, Nukleophilie und Koordinationschemie der dargestellten Bisphosphazen-Protonenschwämme

Die pK_{BH^+}-Werte der neuen Bisphosphazen-Protonenschwämme konnten mit Hilfe von NMR-Titrationsexperimenten ermittelt werden. Die alkylsubstituierten Superbasen weisen pK_{BH^+}-Werte zwischen 29.3 für TMPN und 30.9 für TBPN auf der Acetonitril-Skala auf (Tabelle 3.1) und verfügen somit über eine dem NMe_2-substituierten HMPN ähnliche Basizität. Ein neuer Basizitätsrekord für Protonenschwämme wurde für P_2-TPPN ermittelt, das in Konkurrenzexperimenten mit der SCHWESINGER-Base (dma)P_4-*t*Bu in THF einen pK_{BH^+}-Wert von 42.1 auf der Acetonitril-Skala zeigte. Somit konnte der pK_{BH^+}-Wert des bisher basischsten Protonenschwamms TPPN (32.3) durch eine Homologisierung gemäß dem Konzept von SCHWESINGER um nahezu zehn Größenordnungen gesteigert werden. Der enorme Einfluss der Chelatisierung des Protons auf die Basizität konnte durch einen Vergleich von P_2-TPPN mit dem entsprechenden Monophosphazen (pyr)P_2-1-Naph verdeutlicht werden. Die nicht-chelatisierende SCHWESINGER-Base wurde über eine KIRSANOV-Reaktion aus 1-Aminonaphthalin dargestellt und wies einen pK_{BH^+}-Wert zwischen 25 und 26 auf der Acetonitril-Skala auf. Somit bedingt die kooperative Wechselwirkung der beiden Basizitätszentren in P_2-TPPN eine Zunahme des pK_{BH^+}-Wertes um etwa 16 Größenordnungen. Eine Übersicht der pK_{BH^+}-Werte (MeCN) der in dieser Arbeit synthetisierten Bisphosphazen-Protonenschwämme im Vergleich mit anderen Hybrid-Superbasen ist in Abbildung 3.7 dargestellt.

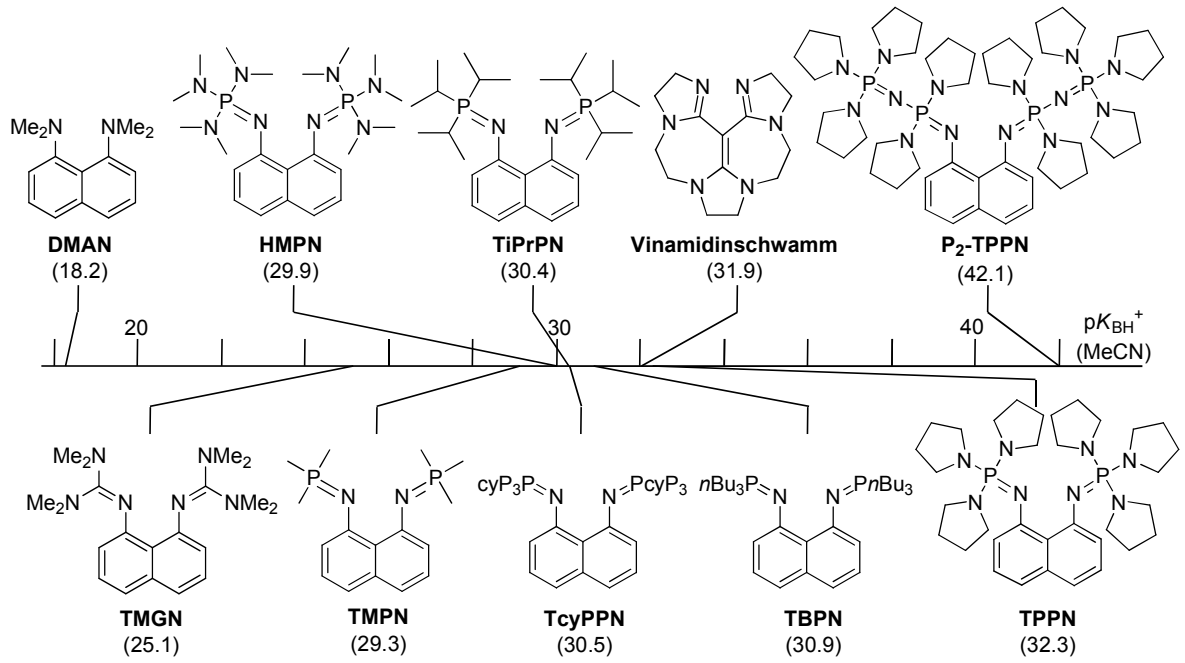

Abbildung 3.7: Die pK_{BH}^{+}-Werte verschiedener Hybrid-Superbasen auf der Acetonitril-Skala.

Des Weiteren führte BORISLAV KOVAČEVIĆ auf Basis von Kristallstrukturdaten Rechnungen zur Basizität der Protonenschwämme in Lösung und in der Gasphase durch. Dr. IVARI KALJURAND (Arbeitsgruppe LEITO, Tartu) bestimmte die Gasphasen-Basizität einiger Verbindungen experimentell (Tabelle 3.1).

Tabelle 3.1: Experimentell und theoretisch bestimmte Basizitäten von Bisphosphazen-Protonenschwämmen in Lösung und in der Gasphase.

	pK_{BH}^{+} (MeCN) (exp.)	**pK_{BH}^{+} (MeCN) (calc.)**	**Gasphasen-Basizität [kcal/mol] (exp.)**	**Gasphasen-Basizität [kcal/mol] (calc.)**	**Protonenaffinität [kcal/mol] (calc.)**
TMPN	29.3	29.7	261.2	262.7	271.8
HMPN	29.9	29.1	268.9	-	274.1
TiPrPN	30.4	30.9	266.0	267.9	275.1
TcyPPN	30.5	32.2	268.3	271.1	279.0
TBPN	30.9	30.0	267.7	269.5	278.8
TPPN	32.3	33.0	-	-	283.2
P_2-TPPN	42.1	40.2	-	-	298.0

Mit pK_{BH}^{+}-Werten in Acetonitril von über 25 und Gasphasen-Basizitäten von mehr als 1000 kJ/mol (238.8 kcal/mol) erfüllen somit alle der dargestellten Bisphosphazen-Protonenschwämme die Kriterien für BRØNSTED-Superbasizität. Die enorme Basizität dieser Verbindungen geht auf die folgenden Ursachen zurück: Die gewählten Phosphazeneinheiten, deren basische Stickstoffatome eine hohe negative Partialladung tragen, verfügen über eine beträchtliche intrinsische Basizität. Während in

Guanidinen eine Delokalisierung der negativen N-Partialladung durch konjugative Effekte erfolgt, tritt in Phosphazenen eine Stabilisierung durch weniger effiziente negative Hyperkonjugation auf. Daher ist eine –N=P(V) Einheit intrinsisch basischer als eine –N=C(IV) Baugruppe. Des Weiteren wird die nach Protonierung auftretende positive Ladung über möglichst viele Phosphoratome mit Alkyl- oder Aminostubstituenten delokalisiert. Schließlich wird eine drastische Erhöhung der Basizität durch eine strukturell erzwungene Wechselwirkung zweier Basizitätszentren erreicht, was sowohl zur Destabilisierung der freien Base als auch zur energetisch günstigen Chelatisierung des Protons führt.

Um die basischen Eigenschaften der Superbasen in Bezug zu ihrer Nukleophilie zu setzen, wurden sie mit Ethyliodid umgesetzt, wobei die Protonenschwämme als Basen oder als Nukleophile reagieren können (Schema 3.5). Für TMPN, TiPrPN und TBPN wurde in Acetonitril keine Eliminierungsreaktion, sondern ausschließlich die N-Alkylierung beobachtet, während im Falle der entsprechenden Reaktion von TcyPPN in THF der protonierte Schwamm zumindest zu 29% gebildet wurde. Lediglich P_2-TPPN reagierte mit Ethyliodid 100% chemoselektiv als Superbase.

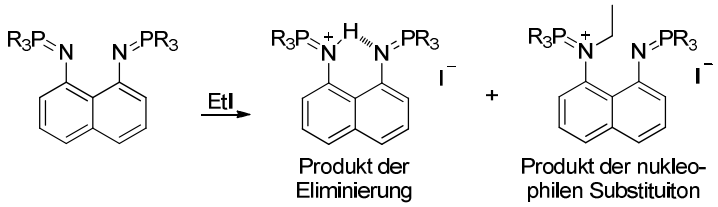

Schema 3.5: Umsetzung eines Bisphosphazen-Protonenschwammes mit Ethyliodid zur Untersuchung seiner nukleophilen Eigenschaften.

TMPN und TPPN wurden mit Hilfe NMR-spektroskopischer Methoden hinsichtlich ihrer kinetischen Basizität untersucht. Erwartungsgemäß wurde für TPPN (66 kJ/mol) bei 300 K eine höhere Aktivierungsenergie für den Protonenselbstaustausch beobachtet als für TMPN (51 kJ/mol). Dies kann auf eine stärkere Abschirmung der Basizitätszentren im aminosubstituierten Protonenschwamm zurückgeführt werden.

Um die Reaktivität der dargestellten Bisphosphazene gegenüber LEWIS-Säuren zu untersuchen, wurde TMPN mit Trimethylaluminium und Trimethylgallium umgesetzt, was zur Bildung kationischer Aluminium- bzw. Galliumkomplexe mit einem Tetramethylmetallatanion als Gegenion führte (Schema 3.6).

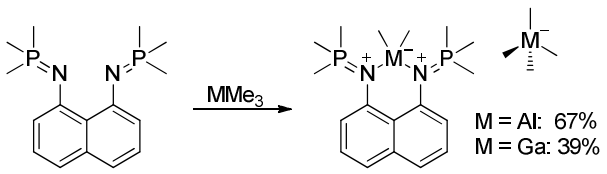

Schema 3.6: Umsetzung von TMPN mit Trimethylaluminium und Trimethylgallium.

Die erhaltenen Verbindungen konnten strukturell charakterisiert werden und wiesen ein von den beiden Stickstoffatomen symmetrisch koordiniertes Metallzentrum auf, das deutlich außerhalb der Naphthalinebene steht (Abbildung 3.8).

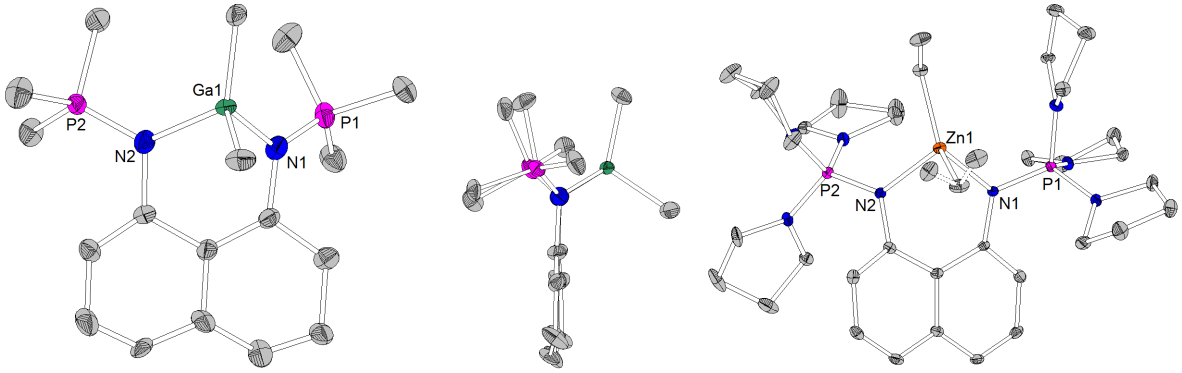

Abbildung 3.8: Molekülstrukturen von $[TMPN\text{-}GaMe_2]^+[GaMe_4]^-$ und $[TPPN\text{-}ZnEt_2]$ (Ellipsoide mit 30% Aufenthaltswahrscheinlichkeit, $[GaMe_4]^-$ und Lösungsmittelmoleküle aus Gründen der Übersichtlichkeit nicht dargestellt).

Des Weiteren gelang die strukturelle Charakterisierung der Verbindung $[TPPN\text{-}AlMe_2]^+[AlCl_2Me_2]^-$. Analog zu den mit TMPN und TPPN durchgeführten Reaktionen konnte auch mit dem piperidinosubstituierten Bisphosphazid (Schema 3.1) ein kationischer Aluminiumkomplex durch Umsetzung mit Trimethylaluminium erhalten werden. Das Metallzentrum wird von den beiden γ-Stickstoffatomen koordiniert. Die Reaktion von TPPN mit Diethylzink lieferte einen neutralen Dialkylzinkkomplex, der ebenfalls röntgenkristallographisch charakterisiert wurde (Abbildung 3.8).

3.4 Versuche zur Darstellung von Bisylid-Protonenschwämmen

Die Umsetzung von l,8-Bis(brommethyl)naphthalin mit Tris(dimethylamino)phosphin, dem entsprechenden homologen P_2-Vorläufer und Tris(pyrrolidino)phosphin führte zur Darstellung der jeweiligen Bisphosphoniumsalze (Schema 3.7).

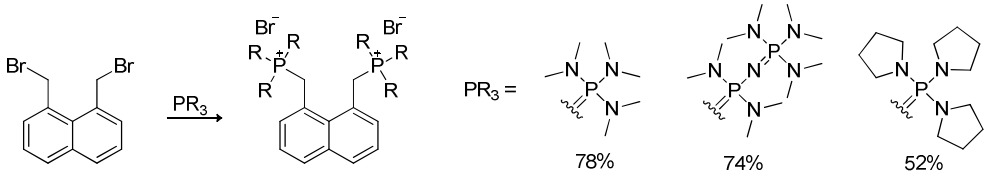

Schema 3.7: Darstellung von drei Bisphosphoniumsalzen.

Von diesen konnten die P_1-Verbindungen röntgenkristallographisch charakterisiert werden (Abbildung 3.9). Die Darstellung der entsprechenden monoprotonierten Spezies und Bisylide im präparativen Maßstab durch Deprotonierung der in Schema 3.7 gezeigten Verbindungen gelang nicht. Es konnten jedoch Einkristalle vom Bisylid der dimethylaminosubstituierten P_1-Verbindung erhalten werden, deren XRD-Strukturanalyse die Existenz eines der Zielmoleküle in kristalliner Phase bestätigt (Abbildung 3.9).

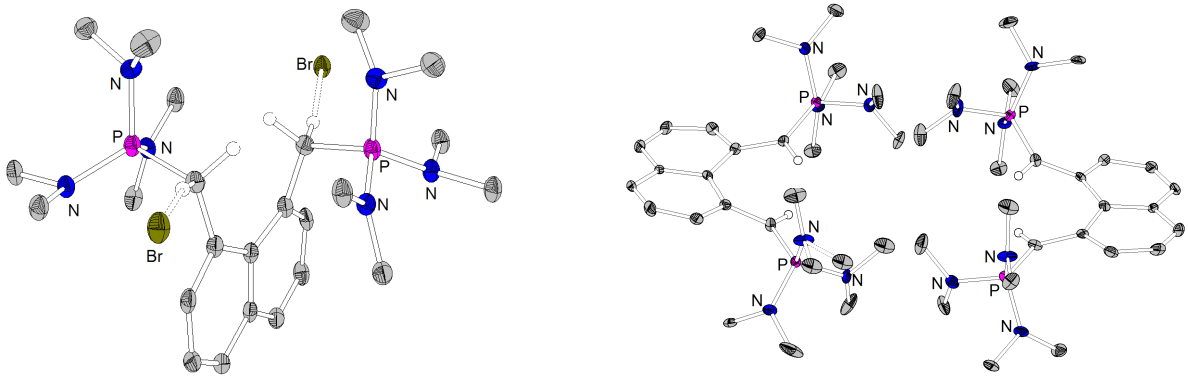

Abbildung 3.9: Molekülstrukturen eines Bisphosphoniumsalzes und des entsprechenden Bisylids (Ellipsoide mit 30% Aufenthaltswahrscheinlichkeit).

3.5 Darstellung chiraler Bisphosphazene mit Binaphthyl- und *trans*-1,2-Diaminocyclohexanrückgrat

Zur Darstellung axial chiraler Superbasen wurde (*S*)-(–)-1,1′-Binaphthyl-2,2′-diamin in einer KIRSANOV-Reaktion mit Bromophosphoniumbromiden in Anwesenheit von Triethylamin umgesetzt, wobei drei neue chirale Basen erhalten wurden, die jeweils als freie Basen und in ihrer protonierten Form charakterisiert wurden (Schema 3.8, Binap-P_1Pyr nicht dargestellt).

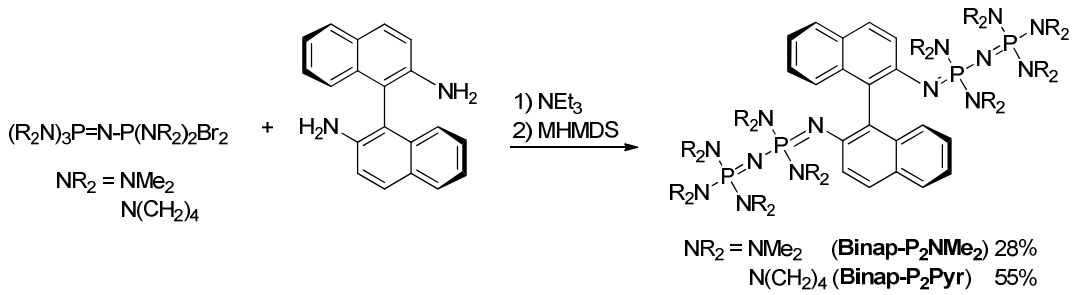

Schema 3.8: Darstellung zweier axial chiraler Superbasen mit Binaphthylrückgrat.

Die Kristallstruktur von Binap-P_2NMe_2 zeigt für die beiden Moleküle in der asymmetrischen Einheit einen großen Abstand der beiden Basizitätszentren von 3.98(1) und 4.11(1) Å, sodass im Gegensatz zu klassischen Protonenschwämmen nicht von einer Destabilisierung der freien Base durch Abstoßung der freien Elektronenpaare der beiden Stickstoffatome ausgegangen werden kann (Abbildung 3.10). Die pK_{BH}^{+}-Werte von Binap-P_2NMe_2 und Binap-P_2Pyr betragen 29.3 bzw. 30.8 auf der Acetonitril-Skala und sind somit deutlich höher als für entsprechende nicht-chelatisierende *N*-Aryl-Phosphazene zu erwarten wäre. Dies deutet auf die Bildung einer stabilen N-H···N-Wasserstoffbrücke hin. Die Umsetzung von Binap-P_2Pyr mit zwei Äquivalenten Trimethylaluminium führte analog zur entsprechenden Reaktion des TMPNs zur Bildung eines kationischen Dimethylaluminium-Komplexes (Abbildung 3.10).

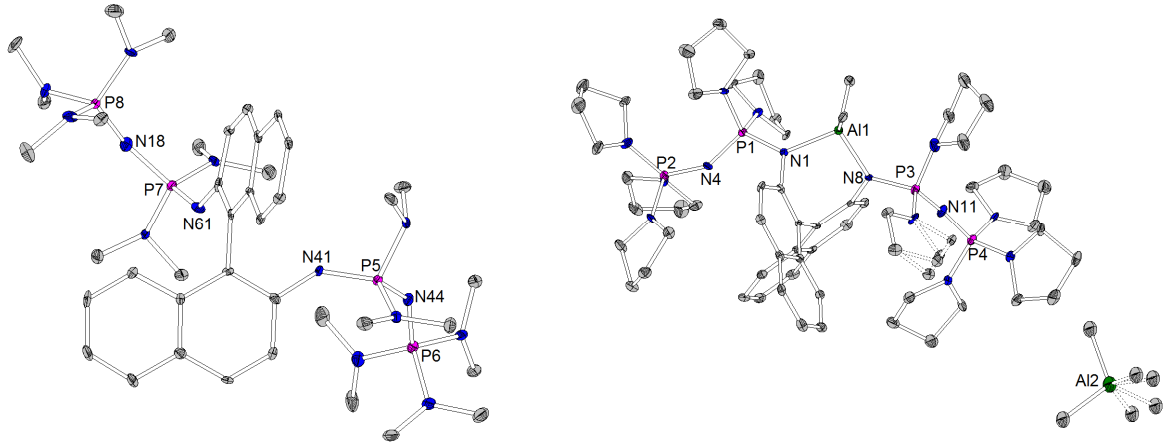

Abbildung 3.10: Molekülstrukturen der chiralen Superbase Binap-P_2NMe_2 (Darstellung eines Moleküls aus der asymmetrischen Einheit) und eines kationischen Dimethylaluminium-Komplexes von Binap-P_2Pyr (Ellipsoide mit 30% Aufenthaltswahrscheinlichkeit).

Ausgehend von (*R*,*R*)-1,2-Diaminocyclohexan wurden auf einer analogen Syntheseroute zwei weitere chirale Superbasen dargestellt (Schema 3.9), die nach Umsetzung mit *p*-Toluolsulfonsäure auch in ihrer monoprotonierten Form charakterisiert werden konnten.

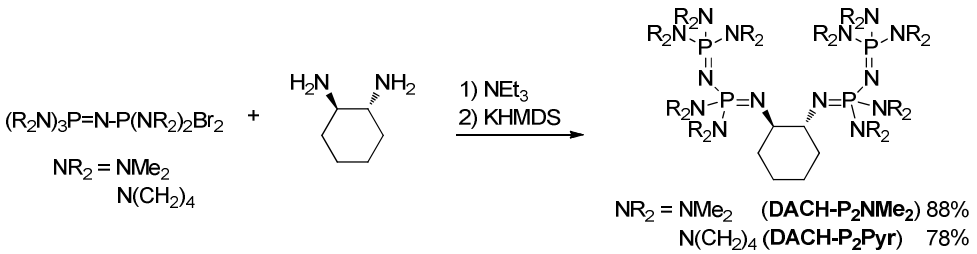

Schema 3.9: Von (*R*,*R*)-1,2-Diaminocyclohexan ausgehende Darstellung zweier C_2-symmetrischer Superbasen.

In der Kristallstruktur der freien Base DACH-P_2NMe_2 befinden sich die beiden Phosphazeneinheiten jeweils in axialer Position, sodass es nicht zur Abstoßung der freien Elektronenpaare der beiden basischsten Stickstoffatome kommt. Theoretische Berechnungen von BORISLAV KOVAČEVIĆ legen jedoch nahe, dass nach Protonierung eine Konformationsänderung auftritt, die die Chelatisierung des aciden Protons erlaubt (Abbildung 3.11).

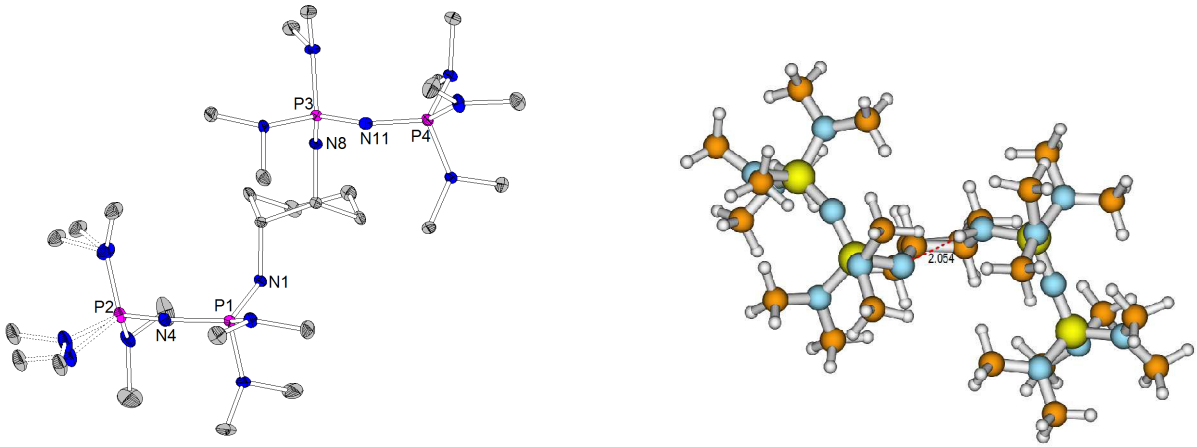

Abbildung 3.11: Kristallstruktur der chiralen Superbase DACH-P_2NMe_2 (Ellipsoide mit 30% Aufenthaltswahrscheinlichkeit) und von BORISLAV KOVAČEVIĆ theoretisch ermittelte Struktur der entsprechenden einfach protonierten Spezies.

Die energetisch günstige Ausbildung einer intramolekularen Wasserstoffbrückenbindung führt gemäß der Rechnungen zu außerordentlich hohen pK_{BH}^+-Werten im Bereich von SCHWESINGER-P_3-Basen (38.1 für DACH-P_2NMe_2 und 40.3 für DACH-P_2Pyr in Acetonitril), sodass DACH-P_2Pyr die bisher stärkste chirale organische Superbase wäre. Auf Grund fehlender Vergleichsbasen konnte der pK_{BH}^+-Wert (MeCN) von DACH-P_2Pyr experimentell bisher lediglich etwa auf einen Wert zwischen 37 und 41 eingegrenzt werden. Die Kristallstruktur von DACH-P_2Pyr·2HBr zeigt (Abbildung 3.12), dass eine zweifache Protonierung der Bisphosphazene mit Diaminocyclohexanrückgrat möglich ist.

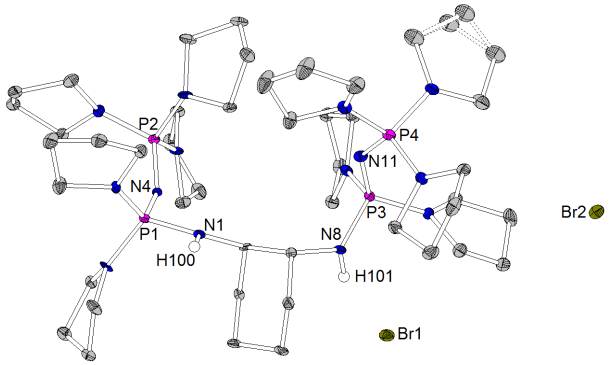

Abbildung 3.12: Molekülstruktur von DACH-P_2Pyr·2HBr (Ellipsoide mit 30% Aufenthaltswahrscheinlichkeit).

3.6 Darstellung pentafluorphenylsubstituierter NH-Säuren

Die Klasse unsymmetrisch substituierter NH-Säuren wurde um $HN(C_6F_5)(SO_2C_8F_{17})$, $HN(C_6F_5)(SO_2F)$ und $HN(C_6F_5)(C(CF_3)_3)$ erweitert. Die Synthesen gingen jeweils von Pentafluoranilin aus, wobei in allen Fällen zunächst ein Alkalimetallsalz der entsprechenden NH-Säure gebildet wurde, das unter stark sauren Bedingungen protoniert wurde.

Die Darstellung von $HN(C_6F_5)(SO_2C_8F_{17})$ erfolgte nach der durch THOMAS LINDER in der eigenen Arbeitsgruppe etablierten Methode über die Reaktion von durch NaHMDS deprotoniertem Pentafluoranilin mit Perfluoroctylsulfonylfluorid. Im Rahmen der Synthese von $HN(C_6F_5)(SO_2F)$

wurde zunächst das von W. SUNDERMEYER publizierte *N*-Pentafluorphenylsulfamoylchlorid dargestellt. Der Fluor-Chlor-Austausch erfolgte durch Kaliumfluorid in Anwesenheit von [18]-Krone-6. Die Umsetzung von Pentafluoranilin mit Hexafluoraceton und anschließende Dehydratisierung des zunächst gebildeten Halbaminals mit Phosphorylchlorid lieferte das Imin $C_6F_5N{=}C(CF_3)_2$, auf das mit Trifluormethyltrimethylsilan und Cäsiumfluorid eine CF_3-Gruppe übertragen wurde.

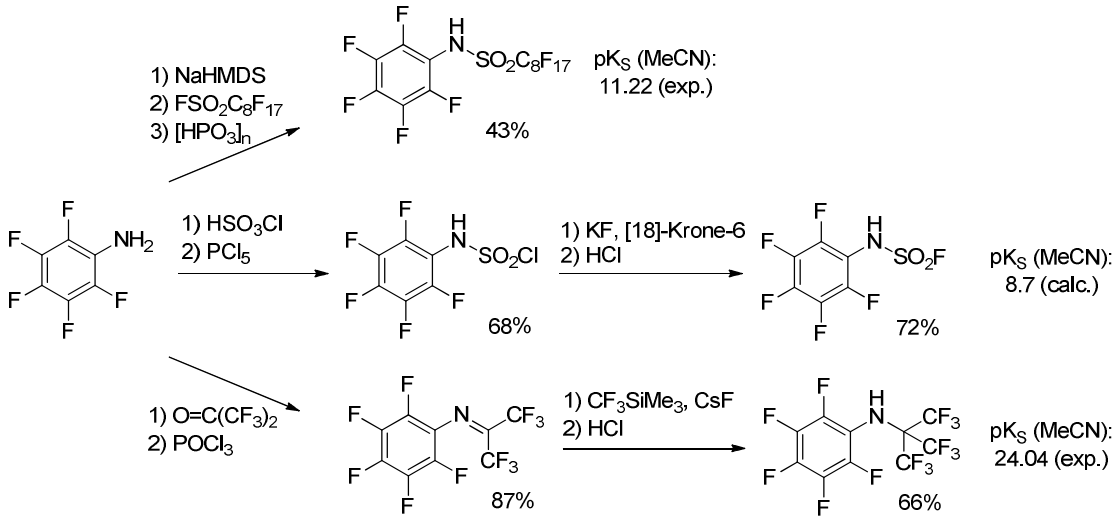

Schema 3.10: Synthese von drei neuen NH-Säuren ausgehend von Pentafluoranilin.

Es gelang die röntgenkristallographische Charakterisierung der sublimierbaren Feststoffe $HN(C_6F_5)(SO_2C_8F_{17})$ und $HN(C_6F_5)(SO_2F)$, wobei die Ausbildung ausgedehnter Wasserstoffbrückennetzwerke beobachtet wurde (Abbildung 3.13). Zudem konnte erstmalig eine etherfreie Kristallstruktur des bekannten $HN(C_6F_5)(SO_2C_4F_9)$ erhalten werden.

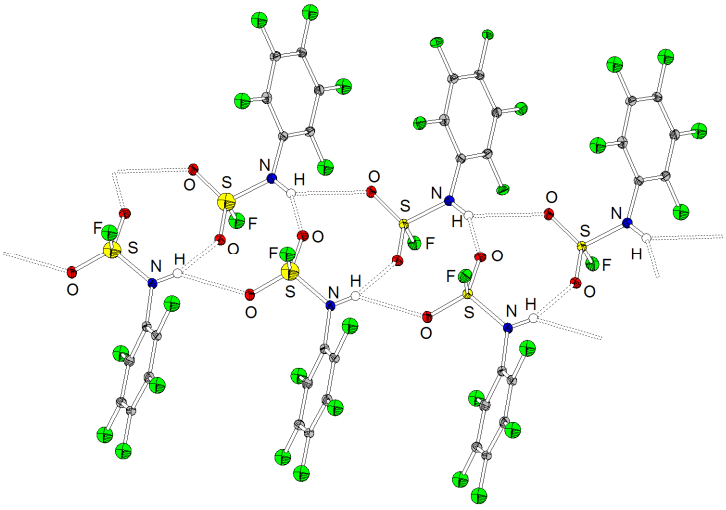

Abbildung 3.13: Ausbildung von Doppelsträngen in der Kristallstruktur von $HN(C_6F_5)(SO_2F)$ (Ellipsoide mit 30% Aufenthaltswahrscheinlichkeit).

Die neuen NH-Säuren wurden von SASCHA GOLL (Arbeitsgruppe KROSSING, Freiburg) und in der Arbeitsgruppe LEITO hinsichtlich ihrer theoretischen und experimentellen BRØNSTED-Acidität

untersucht (Schema 3.10). $LiN(C_6F_5)(SO_2C_8F_{17})$ und $LiN(C_6F_5)(C(CF_3)_3)$ wurden durch Deprotonierung der entsprechenden NH-Säuren mit LiHMDS dargestellt. Ihre elektrochemische Charakterisierung durch FABIAN WOHDE (Arbeitsgruppe ROLING, Marburg) zeigte jedoch keine vorteilhaften Eigenschaften im Vergleich zu aktuell in Lithiumbatterien verwendeten Leitsalzen wie $LiN(SO_2CF_3)_2$. Die erfolgreiche Darstellung des Lithiumsalzes von $HN(C_6F_5)(SO_2F)$ wurde auf Grund der Labilität der S-F-Bindung verhindert, wobei das durch eine nukleophile Substitution entstehende Produkt $HN(C_6F_5)(SO_2N(SO_2F)(C_6F_5))$ mittels Kristallstrukturanalyse und (-)-ESI-Massenspektrometrie identifiziert werden konnte.

3.7 Darstellung von Metallkomplexen der NH-Säuren

Als Synthesestrategien für homoleptische Komplexe von NH-Säuren mit Metallen der Gruppe 13 wurden Alkan-, Salz- oder Amineliminierungsreaktionen in Betracht gezogen. Die Umsetzung der Sulfonamide $HN(C_6F_5)(SO_2CF_3)$ und $HN(C_6F_5)(SO_2C_4F_9)$ mit Trimethylaluminium lieferte die entsprechenden Aluminiumkomplexe unter Abspaltung von Methan (Schema 3.11). Es konnte keine Bildung von LEWIS-Säure-Base-Addukten mit Diethylether oder DMAP nachgewiesen werden, sodass die beiden Metallkomplexe trotz der hohen BRØNSTED-Acidität von $HN(C_6F_5)(SO_2CF_3)$ und $HN(C_6F_5)(SO_2C_4F_9)$ nicht als LEWIS-Säuren betrachtet werden können. Dies kann auf die koordinative Absättigung des Aluminiums durch je drei Stickstoff- und drei Sauerstoffdonoren in drei Vierring-Chelaten zurückgeführt werden, was durch Kristallstrukturanalyse belegt wurde.

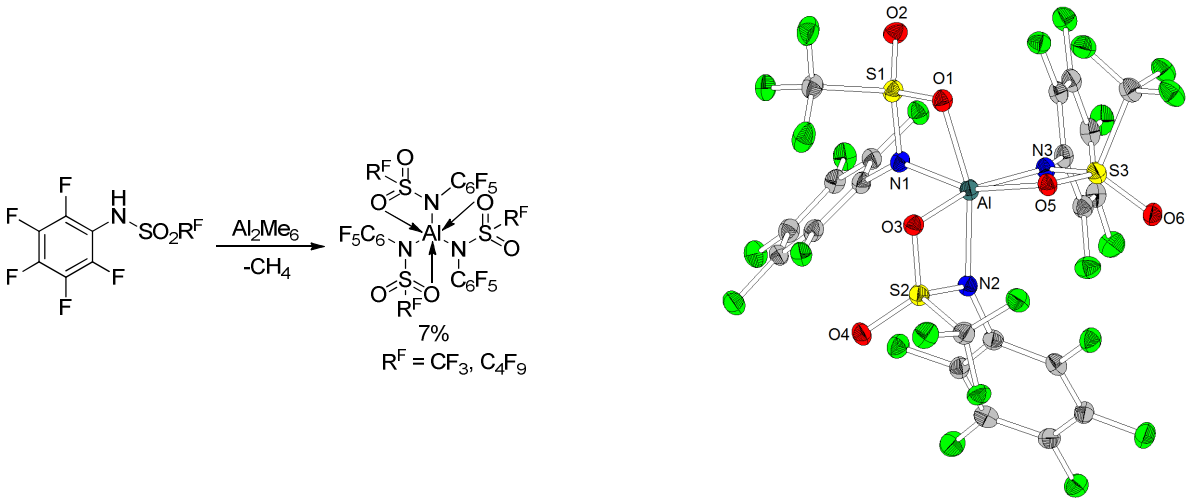

Schema 3.11: Darstellung von $Al[N(C_6F_5)(SO_2CF_3)]_3$ und $Al[N(C_6F_5)(SO_2C_4F_9)]_3$ über Alkaneliminierungsreaktionen und Molekülstruktur von $Al[N(C_6F_5)(SO_2CF_3)]_3$ (Ellipsoide mit 30% Aufenthaltswahrscheinlichkeit).

Für das verwandte $Al[N(C_6F_5)(SO_2C_8F_{17})]_3$ wurde ein analoger Koordinationsmodus erwartet, sodass auf dessen Synthese verzichtet wurde. Die Umsetzung von $HN(C_6F_5)(SO_2F)$ mit Trimethylaluminium führte lediglich zur Bildung von $HN(C_6F_5)(SO_2Me)$, welches röntgenkristallographisch charakterisiert wurde. Darstellungsversuche von Aluminium- und Galliumkomplexen des $HN(C_6F_5)(C(CF_3)_3)$ über

die oben genannten Synthesestrategien erwiesen sich vermutlich auf Grund des hohen sterischen Anspruchs der Nonafluor-*tert*-butylgruppe als ebenfalls nicht erfolgreich.

Durch Umsetzung von $HN(C_6F_5)(C(CF_3)_3)$ mit Metallbistrimethylsilylamiden M(HMDS) (M = Li, Na, K) bzw. $M(HMDS)_2$ (M = Ca, Ba) und Di-*n*-butylmagnesium wurden homoleptische Komplexe der neuen NH-Säure mit Metallen des s-Blocks erhalten. Von diesen konnten das Lithium- (Abbildung 3.14), Natrium-, Kalium-, Cäsium- und Magnesiumsalz (Abbildung 3.14) röntgenkristallographisch charakterisiert werden, wobei im kristallinen Zustand eine Vielzahl von Metall-Fluor-Kontakten beobachtet wurde. Dies deutet auf eine Delokalisierung der negativen Ladung im $[N(C_6F_5)(C(CF_3)_3)]^-$-Liganden über die Fluoratome hin. Es ist zudem erwähnenswert, dass die Einkristalle der Salze $LiN(C_6F_5)(C(CF_3)_3)$ und $Mg[N(C_6F_5)(C(CF_3)_3)]_2$ durch Sublimation gewonnen wurden. Eine derart hohe Flüchtigkeit von Verbindungen hohen ionischen Anteils, die nicht von einer thermischen M-F Abspaltung begleitet ist, ist bislang einzigartig in der Chemie von Fluororganometallamiden.

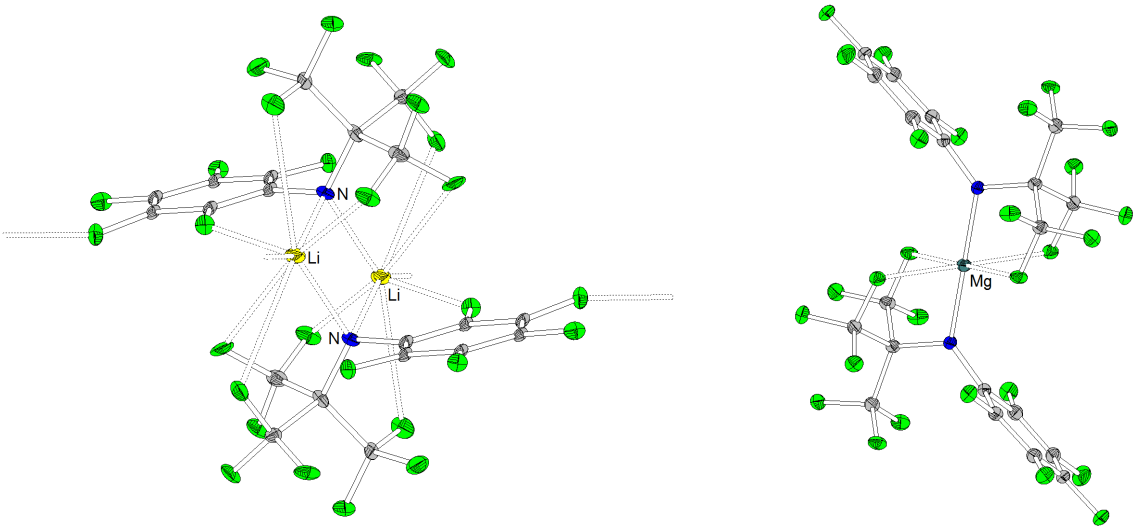

Abbildung 3.14: Kristallstrukturen von $LiN(C_6F_5)(C(CF_3)_3)$ und $Mg[N(C_6F_5)(C(CF_3)_3)]_2$ (Ellipsoide mit 30% Aufenthaltswahrscheinlichkeit).

In Anlehnung an das von ALEXANDER KHVOROST und DENIS SOROKIN beschriebene LEWIS-superacide $Al[N(C_6F_5)_2]_3$ wurde die entsprechende Galliumverbindung $Ga[N(C_6F_5)_2]_3$ über eine Salzeliminierungsreaktion dargestellt (Schema 3.12). Die Molekülstruktur von $Ga[N(C_6F_5)_2]_3$ zeigt ein trigonal-planar durch drei Stickstoffdonoren koordiniertes Galliumzentrum, das zusätzlich durch die Ausbildung von sechs Metall-Fluor-Kontakten zu *ortho*-Fluoratomen der perfluorierten Phenylringe stabilisiert wird.

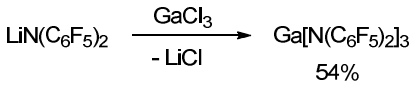

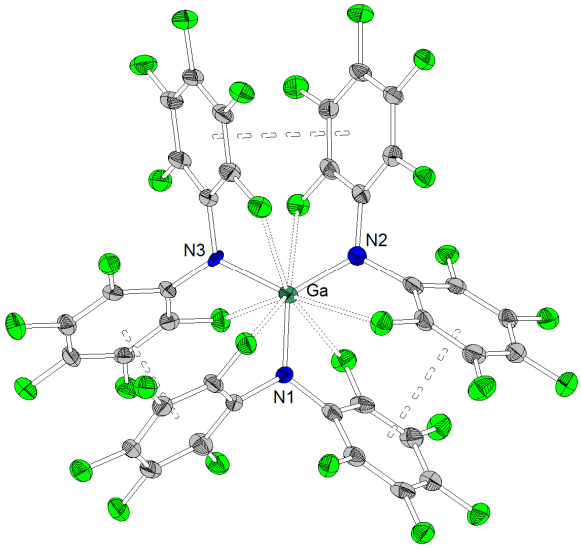

Schema 3.12: Darstellung von $Ga[N(C_6F_5)_2]_3$ und dessen Molekülstruktur (Ellipsoide mit 30% Aufenthaltswahrscheinlichkeit).

Die LEWIS-Acidität der Verbindung wurde zunächst durch Kristallisation von LEWIS-Säure-Base-Addukten mit THF (Abbildung 3.15), Acetonitril, *tert*-Butylisonitril und Trimethylphosphin nachgewiesen. Die Adduktbildung bewirkt jeweils das Aufbrechen der Gallium-Fluor-Kontakte, eine Verlängerung der Gallium-Stickstoff-Bindungen sowie eine Pyramidalisierung des Galliums. Der Gallat-Komplex $[AsPh_4]^+[ClGa(N(C_6F_5)_2)_3]^-$ wurde durch Reaktion mit Tetraphenylarsoniumchlorid dargestellt und ebenfalls röntgenkristallographisch charakterisiert (Abbildung 3.15).

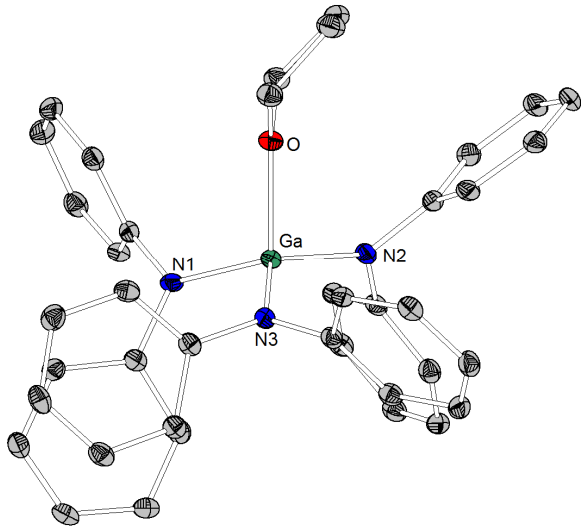

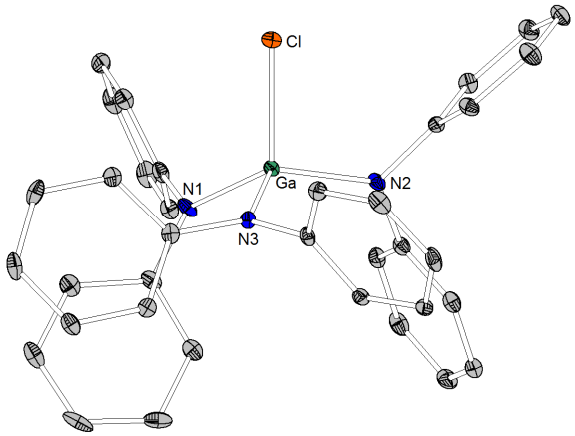

Abbildung 3.15: Molekülstrukturen von $Ga[(N(C_6F_5)_2)_3]_3 \cdot THF$ und $[AsPh_4]^+[ClGa(N(C_6F_5)_2)_3]^-$ (Ellipsoide mit 30% Aufenthaltswahrscheinlichkeit, Fluoratome und $[AsPh_4]^+$ aus Gründen der Übersichtlichkeit nicht dargestellt).

Zur Bestimmung der LEWIS-Acidität von $Al[N(C_6F_5)_2]_3$ und $Ga[N(C_6F_5)_2]_3$ wurden Experimente im NMR-Maßstab durchgeführt, in denen die LEWIS-Säuren untereinander oder mit $B(C_6F_5)_3$ in

Dichlormethan um Chloridionen konkurrieren (Schema 3.13). Die Lage des Gleichgewichts wurde jeweils mittels ^{19}F-NMR-Spektroskopie detektiert. Für die Chloridionenaffinität in Dichlormethan wurde folgende Reihenfolge erhalten: $B(C_6F_5)_3$ < $Ga[N(C_6F_5)_2]_3$ < $Al[N(C_6F_5)_2]_3$. Im Rahmen der Messgenauigkeit fand jeweils eine quantitative Übertragung der Chloridionen auf die stärkere LEWIS-Säure statt. Mit Hilfe von theoretischen Rechnungen von Dr. DANIEL HIMMEL aus der Arbeitsgruppe KROSSING wurde für $Ga[N(C_6F_5)_2]_3$ eine Fluoridionenaffinität in der Gasphase (FIA) von 476 kJ/mol ermittelt. Dieser Wert liegt knapp unter der FIA von SbF_5 (489 kJ/mol), die als Schwelle zur LEWIS-Superacidität betrachtet wird. $Al[N(C_6F_5)_2]_3$ hingegen ist mit einer FIA von 517 kJ/mol eine LEWIS-Supersäure stärker als SbF_5.

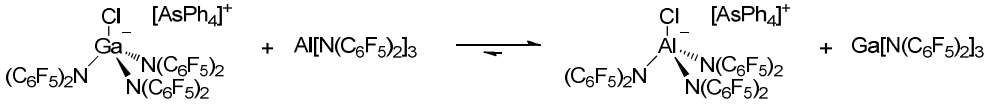

Schema 3.13: Qualitative Konkurrenzexperimente zur Bestimmung der Chloridionenaffinität von $Al[N(C_6F_5)_2]_3$ und $Ga[N(C_6F_5)_2]_3$.

Im Rahmen des zweiten Teils dieser Dissertation wurden die grundlegenden Prinzipien zur Generierung extrem acider Metall-LEWIS-Säuren beleuchtet: Die hohe Ladung der kleinen Metallkationen Al^{3+} und Ga^{3+} kann durch schwach koordinierende Liganden kompensiert werden, wobei auf Grund von deren geringer Donorstärke eine hohe positive Partialladung auf dem Metallatom verbleibt. Die hierbei verwendeten Amidoliganden mit zwei perfluorierten, stark elektronenziehende Gruppen gewährleisten eine Delokalisierung der negativen Ladung des Liganden über eine Vielzahl von elektronegativen O-, N- und F-Atomen. Das LEWIS-acide Metallzentrum wird zudem durch die Ausbildung hemilabiler Metall-Fluor-Kontakte mit Fluoratomen im Ligandenrückgrat stabilisiert. Während $HN(C_6F_5)_2$ die beiden starken LEWIS-Säuren $Al[N(C_6F_5)_2]_3$ und $Ga[N(C_6F_5)_2]_3$ bildet, konnte für das vom mehr als zehn Größenordnungen acideren $HN(C_6F_5)(SO_2CF_3)$ abgeleitete $Al[N(C_6F_5)(SO_2CF_3)]_3$ keine LEWIS-aciden Eigenschaften nachgewiesen werden. Dies zeigt, dass nicht die BRØNSTED-Acidität einer NH-Säure, sondern die Ladungsdelokalisierung im korrespondierenden Anion maßgeblich für die LEWIS-Acidität eines Metallkomplexes ist. Verteilt sich die negative Ladung auf nur wenige, dafür starke Ligand-Donoratome, führt dies nicht zur Ausbildung hemilabiler M···F bzw. M···O Kontakte, sondern zu starken Chelatbindungen, die dem Angriff einer externen LEWIS-Base widerstehen.

Abschließend sollen die wichtigsten Resultate dieser Arbeit kurz zusammengefasst werden.
Im Bereich der chelatisierenden Bisphosphazen-Superbasen wurden folgende Ergebnisse erhalten:

- Mit der Synthese des Bisphosphazen-Protonenschwammes P_2-TPPN gelang die Homologisierung von TPPN, wobei ein neuer Basizitätsrekord für Protonenschwämme aufgestellt wurde.

- Vier neue alkylsubstituierte Bisphosphazen-Protonenschwämme sowie das bekannte TPPN wurden über eine KIRSANOV-Reaktion dargestellt. Somit gelang die Synthese dieser Verbindungsklasse auch im großen Maßstab, sodass sie der Science Community für Untersuchungen zur Anwendung in der organischen Synthese und Katalyse zugänglich gemacht ist.
- Die Klasse der stabilen Bisphosphazide wurde um acht Vertreter erweitert. Einkristallstrukturanalysen erlauben einen interessanten Einblick in die spezifische Anbindung von Wassermolekülen an die konformativ starren stickstoffreichen π-Bindungssysteme, die über zwei unterschiedliche Bindungsstellen verfügen.
- Es konnte bewiesen werden, dass die hier vorgestellten Protonenschwämme nicht nur perfekte Chelatliganden für das Proton, sondern auch Ligandpinzetten für LEWIS-acide Metallalkyle darstellen.
- Durch Kombination eines konfigurativ stabilen, C_2-symmetrischen Binaphthyl- bzw. *trans*-1,2-Diaminocyclohexan-Rückgrats mit zwei P_2-Bisphosphazen-Funktionalitäten konnte in den Bereich der stärksten bekannten chiralen Superbasen vorgestoßen werden.

Im Rahmen der Untersuchungen NH-acider Amine und Amide sowie LEWIS-acider Metallkomplexe auf Basis dieser anorganischen Liganden können die folgenden Resultate als die wichtigsten gelten:

- Es wurden die drei neuen unsymmetrisch substituierten NH-Säuren $HN(C_6F_5)(SO_2C_8F_{17})$, $HN(C_6F_5)(SO_2F)$ und $HN(C_6F_5)(C(CF_3)_3)$ dargestellt.
- Die Koordinationschemie des sterisch anspruchsvollen sekundären Amins $HN(C_6F_5)(C(CF_3)_3)$ wurde in homoleptischen Amiden mit Metallen des s-Blocks untersucht. Die Lithium- und Magnesiumsalze entpuppten sich überraschend als unzersetzt sublimierbar.
- Es gelang die Darstellung von $Al[N(C_6F_5)(SO_2CF_3)]_3$ und $Al[N(C_6F_5)(SO_2C_4F_9)]_3$, wobei für die beiden Aluminiumkomplexe keine LEWIS-aciden Eigenschaften nachgewiesen werden konnten.
- Der Galliumkomplex $Ga[N(C_6F_5)_2]_3$ wurde erstmalig dargestellt und durch Bildung von Lösungsmittel-Addukten und eines Gallat-Komplexes sowie mit Hilfe von Konkurrenzexperimenten mit anderen LEWIS-Säuren hinsichtlich seiner qualitativen LEWIS-Acidität charakterisiert. $Ga[N(C_6F_5)_2]_3$ besitzt eine höhere Fluoridionen-Affinität in der Gasphase (FIA) als die berühmte und vielfach angewendete LEWIS-Säure $B(C_6F_5)_3$ (BCF).

4. Summary

The first part of this dissertation treats the fundamental principles of BRØNSTED superbasicity. It has been successfully demonstrated in the SUNDERMEYER group that the combination of SCHWESINGER's phosphazene bases with ALDER's concept of proton sponges with two interacting proton acceptor functionalities leads to neutral organic superbases with high pK_{BH^+} values in the range of 30 on the acetonitrile scale (Figure 4.1). In the first part of this thesis, the potential of the STAUDINGER and the KIRSANOV reaction for the preparation of such bisphosphazene proton sponges was investigated. It was studied how new structure motives like the substitution of the amino substituents in known bisphosphazenes for alkyl groups or the insertion of another PN unit affects the basicity of the proton sponges. A focus was on the structural characterization of the bisphosphazenes as free bases as well as in their protonated forms. Furthermore, the hybrid superbases were studied concerning their nucleophilic properties, kinetic basicity and coordination chemistry in neutral and cationic group 12 and 13 metal alkyl complexes. The experience with chelating phosphazene bases was also applied to the preparation of chelating superbases.

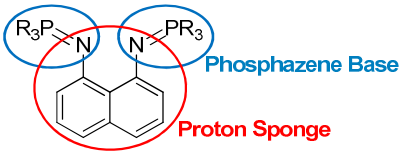

Figure 4.1: The connection of two phosphazene bases *via* a 1,8-disubstituted naphthalene backbone.

The second part of this work is concerned with the principles of strong LEWIS acids with weakly coordinating amido ligands. In this context, NH-acidic amines and amides with two different perfluorinated strongly electron-withdrawing substituents were considered (Figure 4.2). New representatives of this compound class were prepared and characterized with respect to their coordination chemistry and their potential to generate highly LEWIS acidic group 13 metal complexes. The latter were extensively studied with reference to their LEWIS acidic properties.

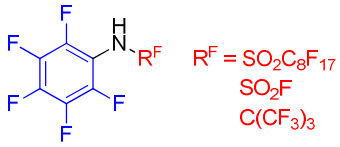

Figure 4.2: New pentafluorophenyl-substituted NH-acids.

4.1 The STAUDINGER Reaction – Preparation of Stable Bisphosphazides and a Higher Homolog of TPPN

P(III) amides bearing simple linear or cyclic amino substituents, guanidino groups or chiral moieties derived from (*S*)-proline as well as mixed-valent P(III)-P(V)-amides were reacted with 1,8-diazidonaphthalene in a STAUDINGER reaction to give a series of eight new stable bisphosphazides (Scheme 4.1). The molecular structures of three bisphosphazides are shown in Figure 4.1. The structure of the diethylamino-substituted species contains a water molecule forming hydrogen bonds to the two α-nitrogen atoms of the bisphosphazide. The theoretically predicted high basicity of that compound class could not be verified experimentally because protonation experiments resulted in the decomposition of the bisphosphazides to unidentified products. Theoretical calculations by BORISLAV KOVAČEVIĆ suggest a decay mechanism *via* an aryne species. The clean elimination of two equivalents of molecular nitrogen at high temperatures under the formation of the desired bisphosphazenes was observed for none of the compounds shown in Scheme 4.1. Thus, the synthetic scope of the STAUDINGER reaction for the preparation of bisphosphazene proton sponges turned out to be strongly limited.

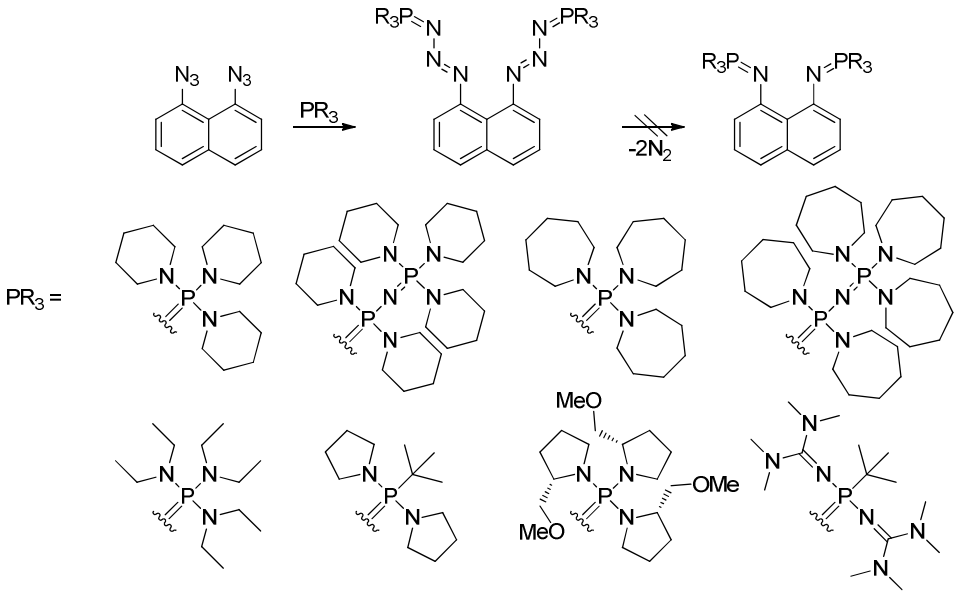

Scheme 4.1: New representatives of the compound class of stable bisphosphazides.

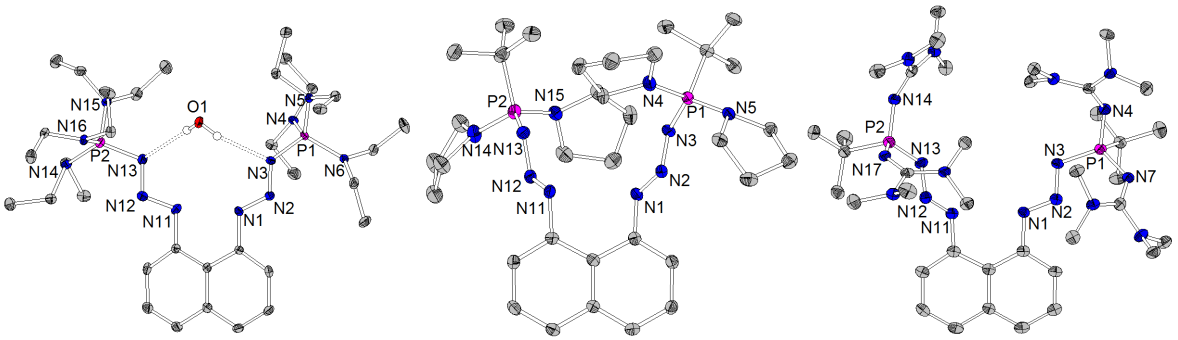

Figure 4.3: Molecular structures of bisphosphazides with -P(NEt$_2$)$_3$, -P(N(CH$_2$)$_4$)$_2$*t*Bu and -P(N=C(NMe$_2$)$_2$)$_2$*t*Bu substituents (ellipsoids with 30% probability).

The STAUDINGER reaction allowed the preparation of P$_2$-TPPN in its free base form after the corresponding P(V)-P(III)-precursor (pyr)$_3$P=N-P(pyr)$_2$ could be prepared in high purity by optimization of its preparation procedure (Scheme 4.2). Thus, a successful homologization of TPPN could be performed for the first time. The molecular structures of P$_2$-TPPN and its HN(SO$_2$CF$_3$)$_2$ salt are shown in Figure 4.4.

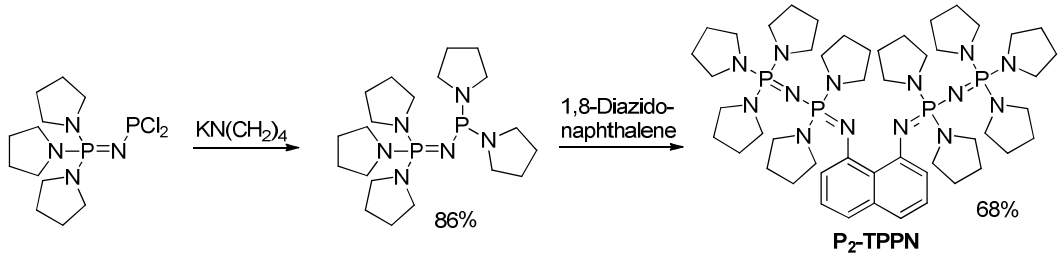

Scheme 4.2: Preparation of P$_2$-TPPN *via* the STAUDINGER reaction.

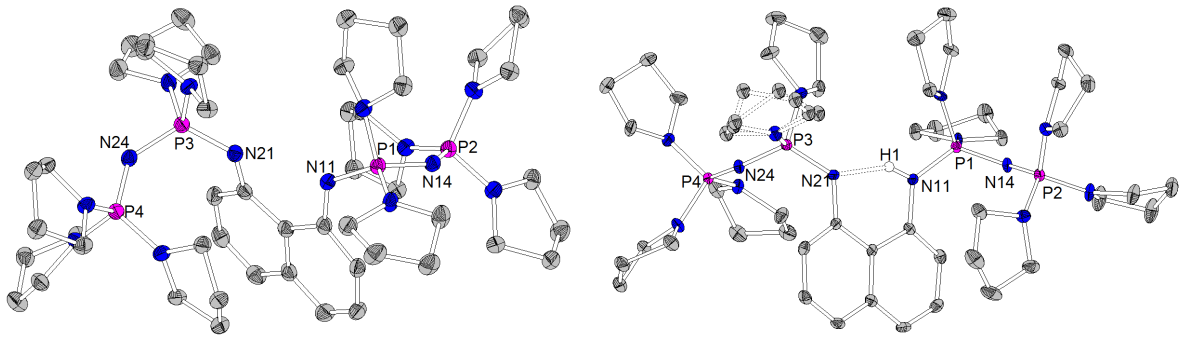

Figure 4.4: Molecular structures of P$_2$-TPPN and P$_2$-TPPN·HN(SO$_2$CF$_3$)$_2$ (ellipsoids with 30% probability, [N(SO$_2$CF$_3$)$_2$]$^-$ omitted for clarity).

4.2 The KIRSANOV Reaction – Synthesis of Alkyl-Substituted Bisphosphazene Proton Sponges

Four new alkyl-substituted bisphosphazene proton sponges were prepared *via* the KIRSANOV reaction. The methyl-substituted TMPN and the *n*-butyl-substituted TBPN could be obtained in their free base forms from simple one-pot procedures starting from the corresponding phosphanes (Scheme 4.3)

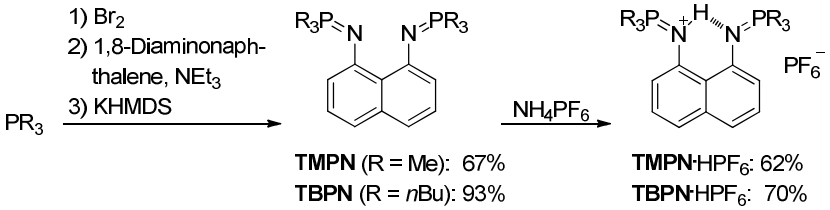

Scheme 4.3: One-pot syntheses of TMPN and TBPN starting from the corresponding phosphanes and subsequent protonation with ammonium hexafluorophosphate.

Since the preparation of TiPrPN and TcyPPN (Figure 4.5) was more difficult due to the higher sterical demand of the secondary alkyl substituents, their syntheses were performed stepwise.

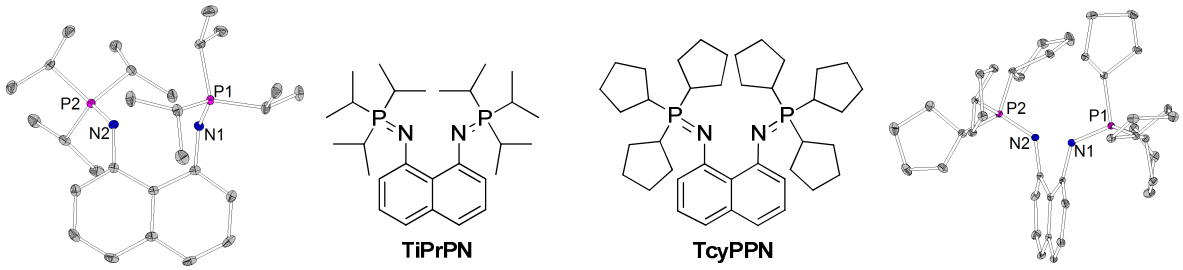

Figure 4.5: TiPrPN and TcyPPN and their molecular structures (ellipsoids with 30% probability).

X-ray diffraction analyses of the hydrobromides of the four alkyl-substituted bisphosphazene proton sponges revealed the formation of non-linear unsymmetrical N-H···N hydrogen bonds (Figure 4.6).

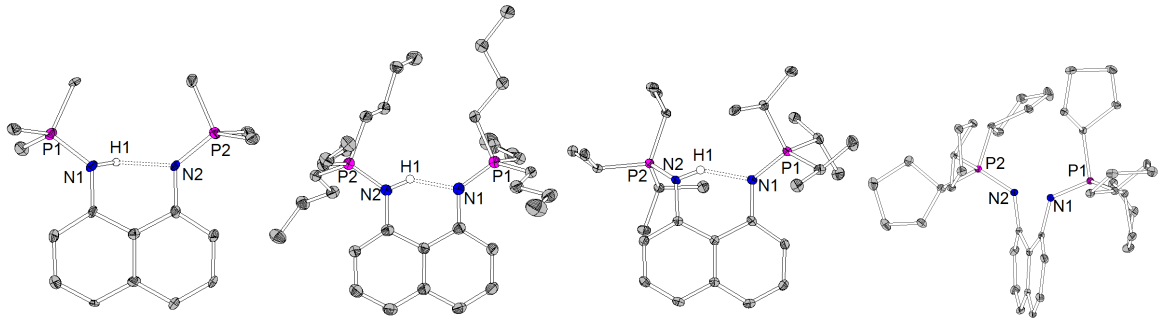

Figure 4.6: Molecular structures of TMPN·HBr, TBPN·HBr, TiPrPN·HBr and TcyPPN·HBr (ellipsoids with 30% probability, anions and solvent molecules omitted for clarity).

TPPN which used to be prepared *via* the STAUDINGER reaction could also be obtained from a KIRSANOV procedure allowing its synthesis in large scale (Scheme 4.4). However, the KIRSANOV reaction proved unsuitable for the preparation of further amino-substituted bisphosphazene proton sponges apart from TPPN.

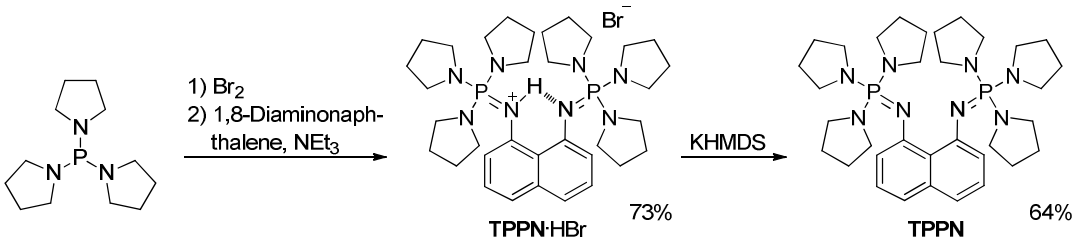

Scheme 4.4: Synthesis of TPPN·HBr *via* the KIRSANOV reaction and subsequent deprotonation by KHMDS.

4.3 Basicity, Nucleophilicity and Coordination Chemistry of Bisphosphazene Proton Sponges

The pK_{BH}^+ values of the new bisphosphazene proton sponges were determined by means of NMR titration experiments. The alkyl-substituted superbases exhibit pK_{BH}^+ values between 29.3 for TMPN and 30.9 for TBPN in acetonitrile and therefore show a similar basicity to the NMe_2-substituted HMPN. A new basicity record for proton sponges was observed for P_2-TPPN which exhibits a pK_{BH}^+ value of 42.1 on the MeCN scale. Thus, the homologization of the hitherto most basic proton sponge TPPN (32.3) lead to an increase in its pK_{BH}^+ value by nearly ten orders of magnitude. The enormous influence of proton chelation on the basicity could be demonstrated by the comparison of P_2-TPPN with the corresponding monophosphazene (pyr)P_2-1-Naph. This non-chelating SCHWESINGER base was prepared from 1-naphthylamine *via* a KIRSANOV reaction and shows a pK_{BH}^+ value between 25 and 26 on the acetonitrile scale. Hence, the cooperative interaction of the basicity centers of two phosphazene bases in P_2-TPPN leads to an increase in the pK_{BH}^+ value by the factor 10^{16} compared to the non-chelating analog. A compilation of the pK_{BH}^+ values of hybrid superbases is shown in Figure 4.7.

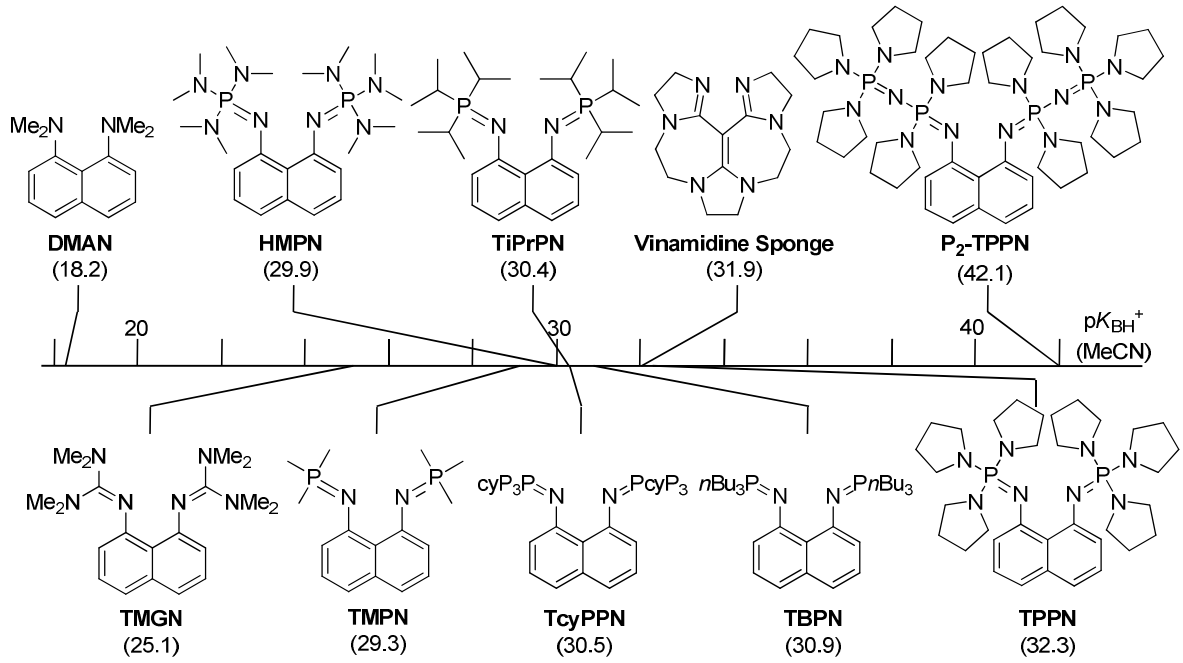

Figure 4.7: Compilation of hybrid superbases and their pK_{BH}^+ values on the acetonitrile scale.

Theoretical calculations concerning the basic properties of proton sponges in the gas phase and in solution were performed by BORISLAV KOVAČEVIĆ on the basis of the bisphosphazenes' crystal structures. Furthermore, Dr. IVARI KALJURAND (LEITO group, Tartu) determined the experimental gas phase basicity of some proton sponges experimentally (Table 4.1).

Table 4.1: Experimentally and theoretically determined basicities of bisphosphazene proton sponges in solution and in the gas phase.

	pK_{BH}^+ (MeCN) (exp.)	pK_{BH}^+ (MeCN) (calc.)	Gas phase basicity [kcal/mol] (exp.)	Gas phase basicity [kcal/mol] (calc.)	Proton affinity [kcal/mol] (calc.)
TMPN	29.3	29.7	261.2	262.7	271.8
HMPN	29.9	29.1	268.9	-	274.1
TiPrPN	30.4	30.9	266.0	267.9	275.1
TcyPPN	30.5	32.2	268.3	271.1	279.0
TBPN	30.9	30.0	267.7	269.5	278.8
TPPN	32.3	33.0	-	-	283.2
P_2-TPPN	42.1	40.2	-	-	298.0

All presented bisphosphazene proton sponges fulfill the criteria for BRØNSTED superbases with pK_{BH}^+ values above 25 in acetonitrile and a gas phase basicity higher than 1000 kJ/mol (238.8 kcal/mol). The enormous basicity of the bisphosphazenes can be referred to the following reasons: The chosen phosphazene units exhibit a high negative partial charge on their basic nitrogen atoms. Whereas the negative partial charge is delocalized in guanidines by conjugative effects, it is only stabilized by negative hyperconjugation in phosphazenes. Thus, a -N=P(V) unit possesses a higher intrinsic basicity than a -N=C(IV) building block. The positive charge occurring after protonation is delocalized over alkyl- or amino-substituted phosphorous atoms. Finally, a drastic basicity enhancement is achieved by the spatial proximity of two basicity centers leading to a destabilization of the free base and the energetically favorable chelation of the proton after protonation.

The reaction with ethyl iodide was used as a benchmark to examine the nucleophilic properties of the superbases studied herein. The bisphosphazenes can either react as bases or as N-nucleophiles as shown in Scheme 4.5. TMPN, TiPrPN and TBPN are exclusively alkylated by ethyl iodide in acetonitrile. In case of the corresponding reaction of TcyPPN in THF, a 71:29 ratio in favor of the alkylated product is observed. P_2-TPPN is the only superbase in this series revealing a perfect chemoselectivity for the HI elimination reaction.

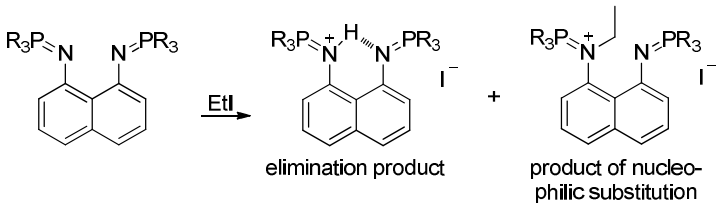

Scheme 4.5: Conversion of a bisphosphazene proton sponge with ethyl iodide to determine the nucleophilic properties.

The kinetic basicity of TMPN and TPPN was studied by means of NMR spectroscopic methods. As expected, TPPN (66 kJ/mol) showed a higher activation energy for the proton self exchange at 300 K than TMPN (51 kJ/mol) which can be referred to the stronger sterical shielding of the basicity centers in the amino-substituted compound.

To investigate the reactivity of bisphosphazene proton sponges towards LEWIS acids, TMPN was reacted with trimethylaluminum and trimethylgallium leading to the formation of cationic dialkylmetal complexes with $[MMe_4]^-$ counteranions (Scheme 4.6).

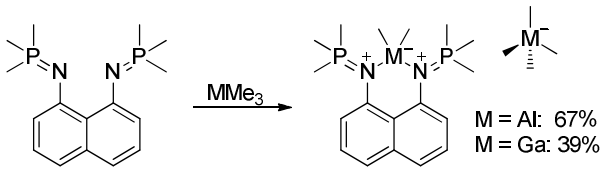

Scheme 4.6: Reactions of TMPN with trimethylaluminum and trimethylgallium.

The obtained metal complexes were characterized by means of x-ray diffraction analysis revealing the coordination of the metal center by the two basic nitrogen atoms. In contrast to the acidic protons in the protonated sponges, the metal atoms are located outside the naphthalene plane (Figure 4.8).

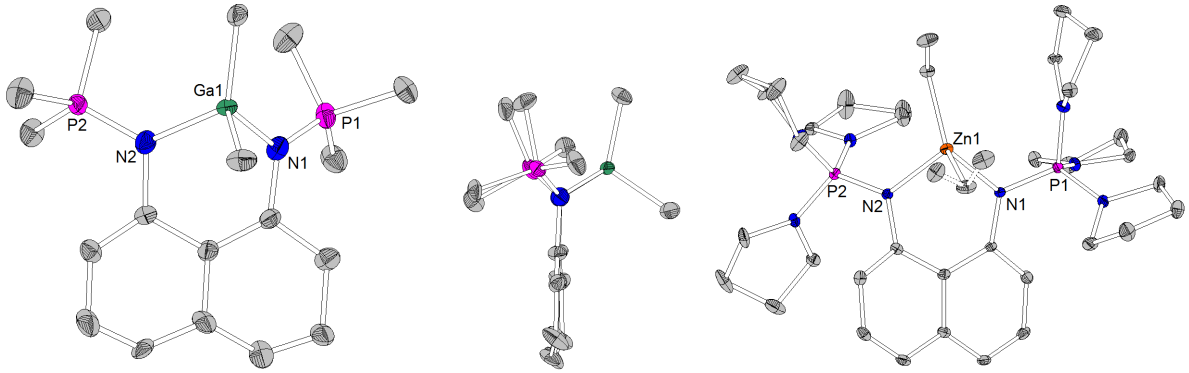

Figure 4.8: Molecular structures of $[TMPN\text{-}GaMe_2]^+[GaMe_4]^-$ and $[TPPN\text{-}ZnEt_2]$ (ellipsoids with 30% probability, $[GaMe_4]^-$ and solvent molecules omitted for clarity).

The related $[TPPN\text{-}AlMe_2]^+[AlCl_2Me_2]^-$ could be structurally characterized as well. An analogous reactivity towards trimethylaluminum was observed for the piperidino-substituted bisphosphazide (Scheme 4.1). The bisphosphazide forms a cationic dimethylaluminum complex whose crystal structure revealed the coordination of the metal center by the two γ-nitrogen atoms. The reaction of

TPPN with diethylzinc yielded a neutral dialkylzinc complex which was analyzed by x-ray diffraction analysis (Figure 4.8).

4.4 Attempts to prepare Bisylid Proton Sponges

The conversion of 1,8-bis(bromomethyl)naphthalene with tris(dimethylamino)phosphane, the homologous mixed-valent P(III)-P(V) precursor and tris(pyrrolidino)phosphane yielded three bisphosphonium salts (Scheme 4.7).

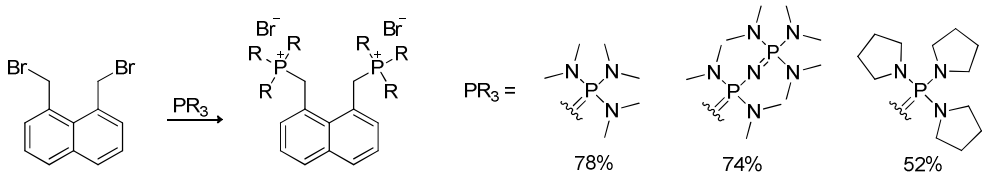

Scheme 4.7: Preparation of three bisphosphonium salts.

The two P_1 compounds were structurally characterized (Figure 4.9). Attempts to synthesize the monoprotonated or bisylid species by deprotonation of the bisphosphonium salts in preparative scale remained unsuccessful. However, singe crystals of the $P(NMe_2)_3$-substituted bisylid suitable for XRD-analysis could be obtained proving the existence of the target compound (Figure 4.9).

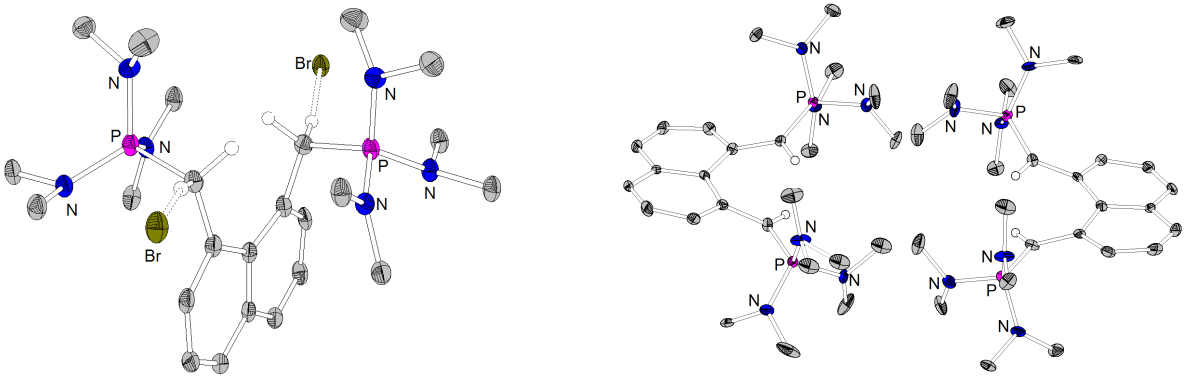

Figure 4.9: Molecular structures of a bisphosphonium salt and the corresponding bisylid (ellipsoids with 30% probability).

4.5 Chiral Bisphosphazenes with a Binaphthyl and a *trans*-1,2-Diaminocyclohexane Backbone

Three axial chiral superbases could be obtained from the KIRSANOV reaction of (*S*)-(–)-1,1′-binaphthyl-2,2′-diamine with bromophosphonium bromides in the presence of triethylamine. The bisphosphazenes were characterized as free bases and in their protonated forms (Scheme 4.8, Binap-P_1Pyr is not shown).

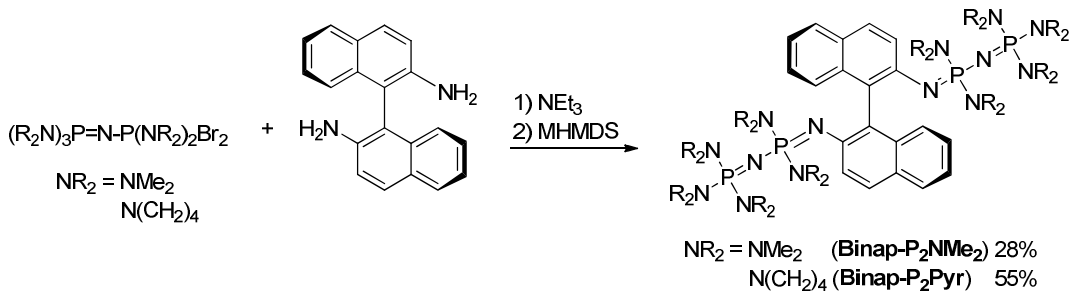

Scheme 4.8: Preparation of two axial chiral superbases with a binaphthyl backbone.

The two molecules found in the asymmetric unit of the molecular structure of Binap-P_2NMe_2 exhibit a large distance between the two basicity centers of 3.98(1) and 4.11(1) Å. Thus, a destabilization of the free base form by repulsion of the two basicity centers' lone pairs is not found in contrast to classical proton sponges. The pK_{BH}^{+} values of Binap-P_2NMe_2 and Binap-P_2Pyr are 29.3 and 30.8 on the acetonitrile scale and therefore considerably higher than it would be expected for the corresponding non-chelating *N*-arylphosphazenes. This indicates the formation of a stable intramolecular N-H···N hydrogen bond in the monoprotonated form which is also suggested by theoretical calculations by BORISLAV KOVAČEVIĆ. As observed for naphthalene-substituted bisphosphazenes, the reaction of Binap-P_2Pyr with two equivalents of trimethylaluminum yielded a cationic dimethylaluminum complex (Figure 4.10).

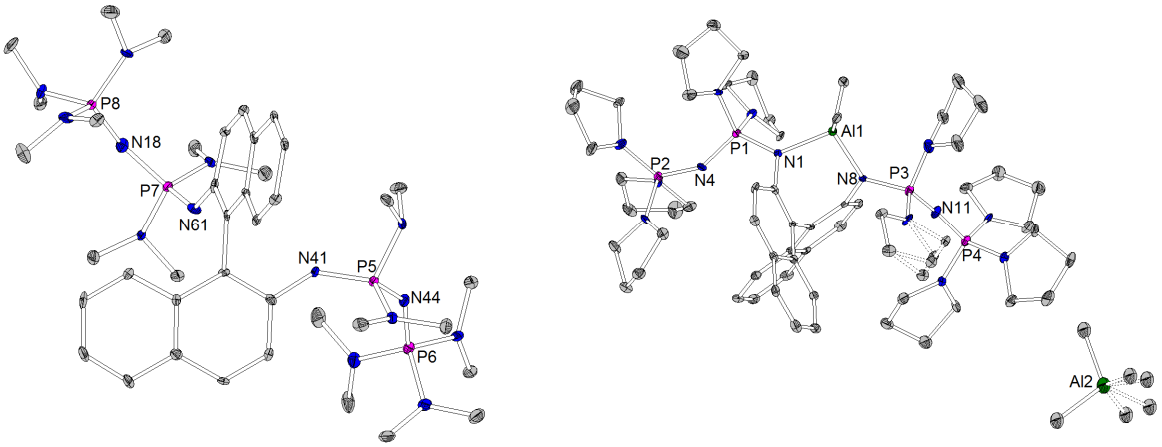

Figure 4.10: Molecular structures of the chiral superbase Binap-P_2NMe_2 (only one molecule of the asymmetric unit is shown) and a cationic dimethylaluminum complex of Binap-P_2Pyr (ellipsoids with 30% probability).

An analogous procedure to the preparation of the binaphthyl-substituted bisphosphazenes yielded the two chiral superbases DACH-P_2NMe_2 and DACH-P_2Pyr which originate from (*R*,*R*)-1,2-diaminocyclohexane (Scheme 4.9). The corresponding monoprotonated species were accessible by the reaction of the free bases with *p*-toluenesulfonic acid.

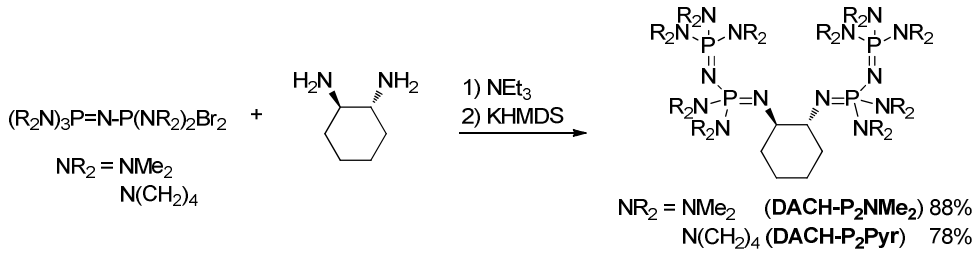

Scheme 4.9: Preparation of two chiral superbases on the basis of (*R*,*R*)-1,2-diaminocyclohexane.

The molecular structure of DACH-P_2NMe_2 reveals that the two phosphazene substituents are located in axial positions of the cyclohexane ring (Figure 4.11). As observed for the binaphthyl-based superbases, there is no repulsion of the two basicity centers' lone pairs in the free base form. Theoretical calculations by BORISLAV KOVAČEVIĆ suggest that a conformation change occurs after protonation resulting in a stable N-H···N hydrogen bond (Figure 4.11).

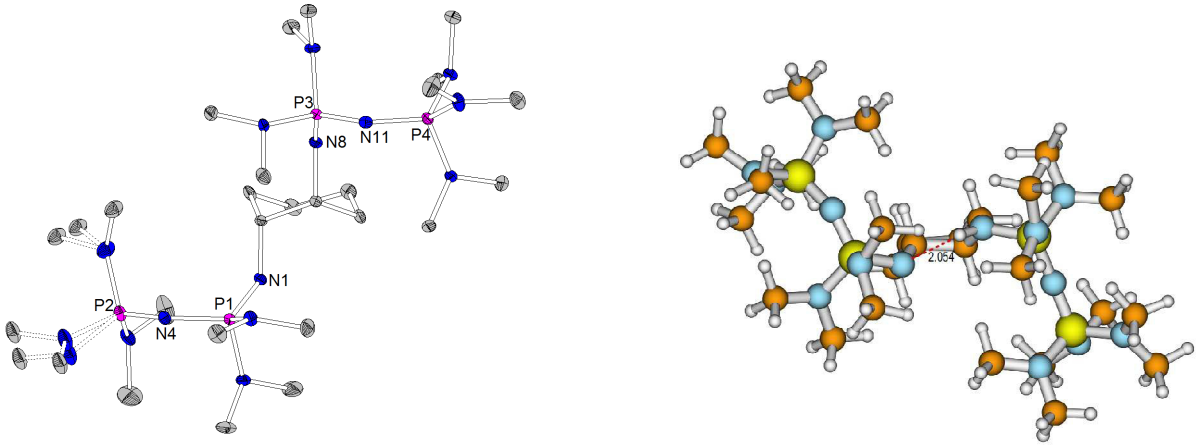

Figure 4.11: Crystal structure of the chiral superbase DACH-P_2NMe_2 (ellipsoids with 30% probability) and theoretically obtained structure of the corresponding monoprotonated species (calculations by BORISLAV KOVAČEVIĆ).

According to theoretical calculations, the energetically favorable formation of an intramolecular hydrogen bond after protonation leads to very high pK_{BH}^+ values in the range of SCHWESINGER-P_3 bases (38.1 for DACH-P_2NMe_2 and 40.3 for DACH-P_2Pyr on the MeCN scale). Thus, DACH-P_2Pyr can be considered the strongest nonionic chiral superbase. NMR titration experiments show a pK_{BH}^+ value between 37 and 41 for DACH-P_2Pyr, but the exact pK_{BH}^+ values could not be determined due to lack of suitable commercially available bases with a similar basicity. The molecular structure of DACH-P_2Pyr·2HBr demonstrates (Figure 4.12) that bisprotonation of the presented bisphosphazenes is possible.

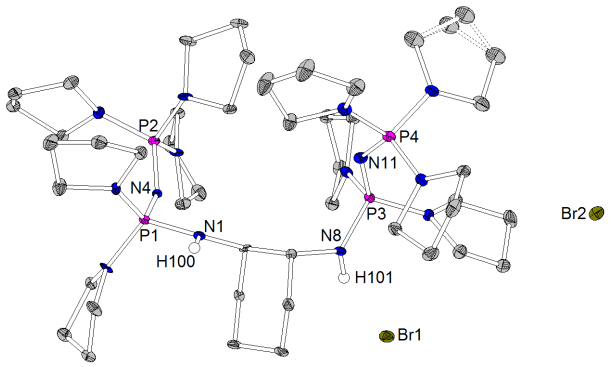

Figure 4.12: Molecular structure of DACH-P_2Pyr·2HBr (ellipsoids with 30% probability).

4.6 Synthesis of Pentafluorophenyl-Substituted NH-Acids

The class of unsymmetrically substituted NH-acids was extended by the three new representatives $HN(C_6F_5)(SO_2C_8F_{17})$, $HN(C_6F_5)(SO_2F)$ and $HN(C_6F_5)(C(CF_3)_3)$. All synthesis routes started from pentafluoroaniline and initially yielded the alkaline metal salts of the desired products which were protonated under highly acidic conditions to give the free NH-acids.

$HN(C_6F_5)(SO_2C_8F_{17})$ was prepared on the basis of a procedure developed by THOMAS LINDER in the SUNDERMEYER group *via* the reaction of *in situ* deprotonated pentafluoroaniline with perfluorooctylsulfonyl fluoride. The synthesis of $HN(C_6F_5)(SO_2F)$ required the preparation of literature-known *N*-pentafluorophenylsulfamoyl chloride which was converted to the target compound by a fluorine-chlorine exchange reaction with potassium fluoride in the presence of 18-crown-6. The conversion of pentafluoroaniline with hexafluoroacetone and subsequent dehydration of the initially formed hemiaminal by phosphoryl chloride yielded $C_6F_5N{=}C(CF_3)_2$. Finally, the imine was trifluoromethylated by trifluoromethyltrimethylsilane and cesium fluoride.

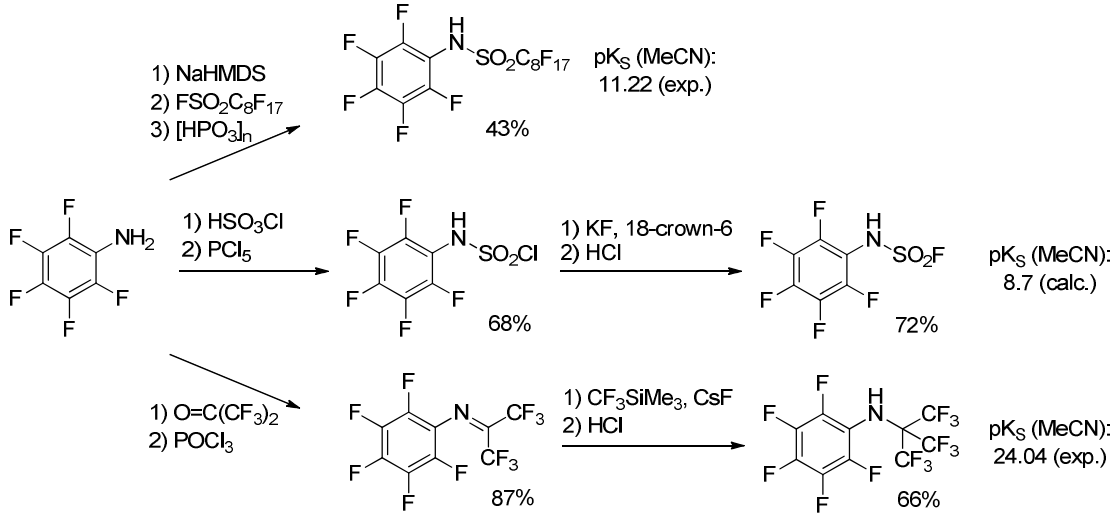

Schema 4.10: Syntheses of three new pentafluorophenyl-substituted NH-acids.

The x-ray diffraction analyses of the volatile solids $HN(C_6F_5)(SO_2C_8F_{17})$ and $HN(C_6F_5)(SO_2F)$ revealed the formation of extended hydrogen bond networks (Figure 4.13). Furthermore, an ether free crystal structure of the known $HN(C_6F_5)(SO_2C_4F_9)$ could be obtained for the first time.

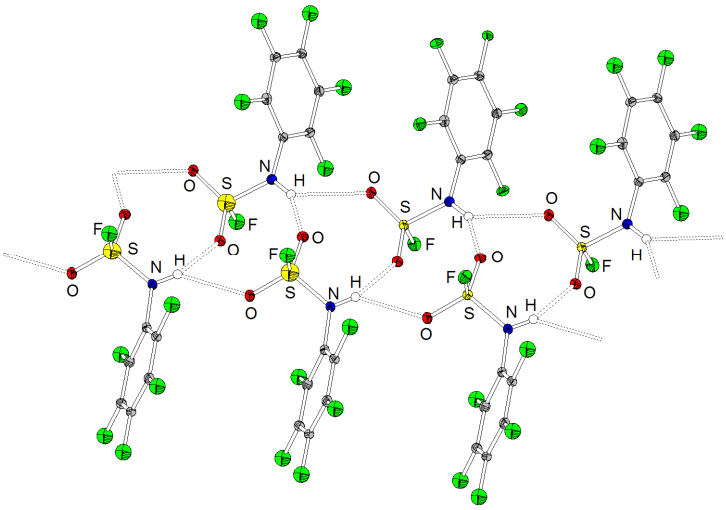

Figure 4.13: Formation of double strands in the crystal structure of $HN(C_6F_5)(SO_2F)$ (ellipsoids with 30% probability).

The new NH-acids were investigated by SASCHA GOLL (KROSSING group, Freiburg) and in the group of Ivo LEITO concerning their theoretical and experimental BRØNSTED-acidity (Scheme 4.10). $LiN(C_6F_5)(SO_2C_8F_{17})$ and $LiN(C_6F_5)(C(CF_3)_3)$ were prepared by the deprotonation of the corresponding NH-acids by LiHMDS. However, their electrochemical characterization by FABIAN WOHDE (ROLING group, Marburg) did not reveal advantageous properties in comparison to conducting salts like $LiN(SO_2CF_3)_2$ that are commonly used in lithium batteries. The preparation of the lithium salt of $HN(C_6F_5)(SO_2F)$ was prevented by the lability of the S-F bond. Deprotonation attempts led to a nucleophilic substitution reaction forming $HN(C_6F_5)(SO_2N(SO_2F)(C_6F_5))$ which was characterized by x-ray diffraction analysis and ESI mass spectrometry.

4.7 Preparation of Metal Complexes of NH-acidic Amines and Amides

Alkane, salt and amine elimination reactions were considered as possible synthetic strategies for the preparation of homoleptic group 13 metal complexes of NH-acids. The reactions of $HN(C_6F_5)(SO_2CF_3)$ and $HN(C_6F_5)(SO_2C_4F_9)$ with trimehylaluminum yielded the two desired metal complexes *via* methane elimination reactions (Scheme 4.11). The formation of LEWIS acid-base adducts with diethylether or DMAP could not be observed which can be referred to the coordinative saturation of the aluminum center by three oxygen and three nitrogen donors forming three stable four-membered ring chelates. Thus, the two metal complexes cannot be considered LEWIS acids.

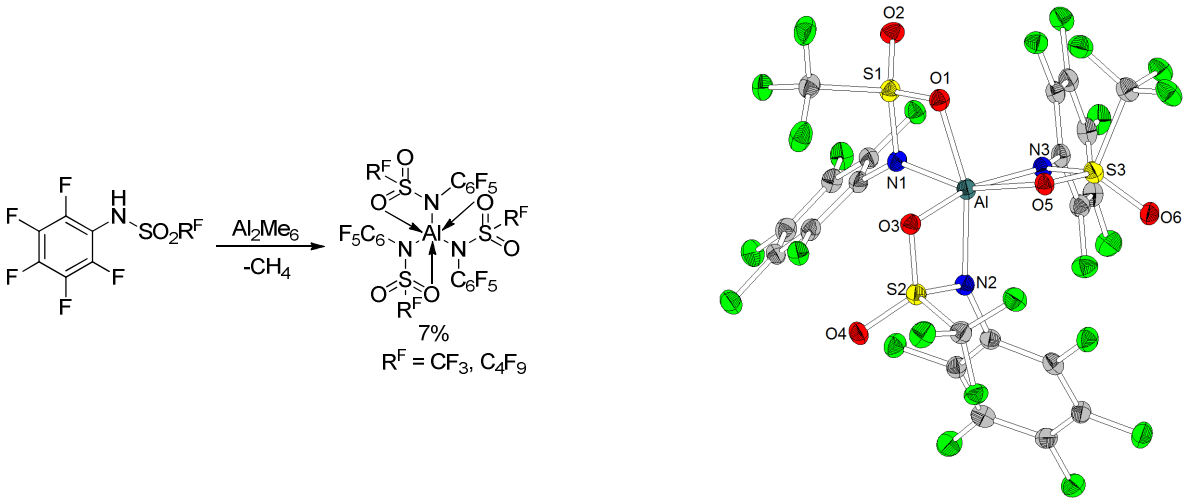

Scheme 4.11: Preparation of $Al[N(C_6F_5)(SO_2CF_3)]_3$ and $Al[N(C_6F_5)(SO_2C_4F_9)]_3$ *via* alkane elimination reactions and the molecular structure of $Al[N(C_6F_5)(SO_2CF_3)]_3$ (ellipsoids with 30% probability).

An analogous coordination mode was expected for the related $Al[N(C_6F_5)(SO_2C_8F_{17})]_3$ which was therefore not prepared. The reaction of $HN(C_6F_5)(SO_2F)$ with trimethylaluminum resulted in the formation of the structurally characterized $HN(C_6F_5)(SO_2Me)$. Attempts to prepare aluminum and gallium complexes of $HN(C_6F_5)(C(CF_3)_3)$ *via* the synthesis strategies mentioned above were not successful which might be a result of the high sterical demand of the perfluorinated *tert*-butyl group.
The conversion of $HN(C_6F_5)(C(CF_3)_3)$ with metal bis(trimethylsilyl)amides M(HMDS) (M = Li, Na, K) and $M(HMDS)_2$ (M = Ca, Ba) and dibutylmagnesium yielded a series of homoleptic s-block metal complexes of the NH-acid. The lithium, sodium, potassium, cesium and magnesium salts (Figure 4.14) were characterized by x-ray diffraction analysis revealing manifold secondary metal fluorine interactions in the crystalline state. This indicates the delocalization of the negative charge in the $[N(C_6F_5)(C(CF_3)_3)]^-$ ligand to the fluorine atoms. Interestingly, the single crystals of $LiN(C_6F_5)(C(CF_3)_3)$ and $Mg[N(C_6F_5)(C(CF_3)_3)]_2$ were obtained by sublimation. Such high volatility without thermal M-F elimination is unique in the chemistry of mainly ionic perfluorinated metal amides.

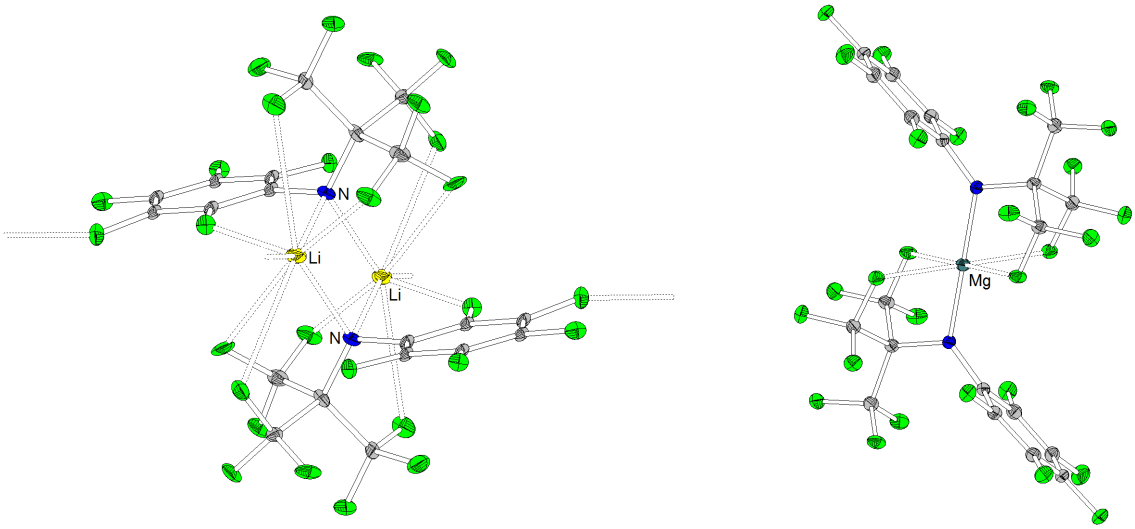

Figure 4.14: Crystal structures of $LiN(C_6F_5)(C(CF_3)_3)$ and $Mg[N(C_6F_5)(C(CF_3)_3)]_2$ (ellipsoids with 30% probability).

A salt elimination reaction yielded the gallium compound $Ga[N(C_6F_5)_2]_3$ (Scheme 4.12) which is derived from the LEWIS superacidic aluminum complex $Al[N(C_6F_5)_2]_3$ described by ALEXANDER KHVOROST and DENIS SOROKIN. The gallium atom is coordinated by three nitrogen donors in a trigonal planar fashion and is further stabilized by six secondary metal fluorine interactions to *ortho*-fluorine atoms of C_6F_5 moieties.

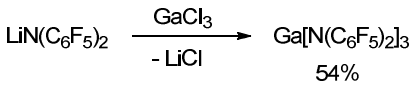

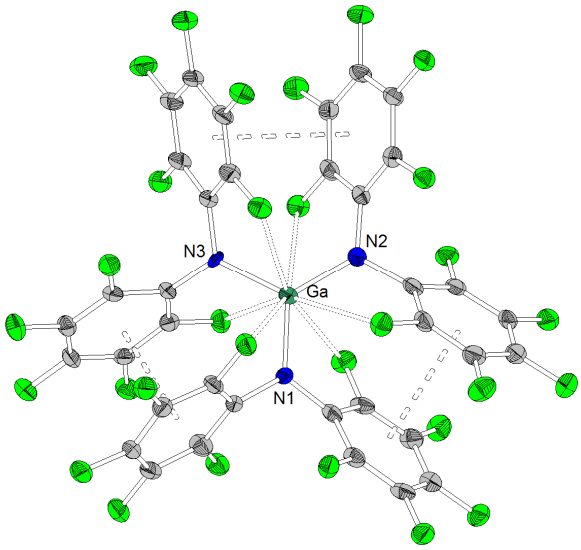

Scheme 4.12: Preparation of $Ga[N(C_6F_5)_2]_3$ and its molecular structure (ellipsoids with 30% probability).

The LEWIS acidity of $Ga[N(C_6F_5)_2]_3$ was proved by the crystallization of LEWIS acid-base adducts with THF (Figure 4.15), acetonitrile, *tert*-butylisonitrile and trimethylphosphane. The adduct formation led to the breakup of the metal fluorine interactions, the elongation of the Ga-N bonds and the pyramidalization of the gallium atom. The reaction of $Ga[N(C_6F_5)_2]_3$ with tetraphenylarsonium chloride yielded the ate complex $[AsPh_4]^+[ClGa(N(C_6F_5)_2)_3]^-$ which was also structurally characterized (Figure 4.14).

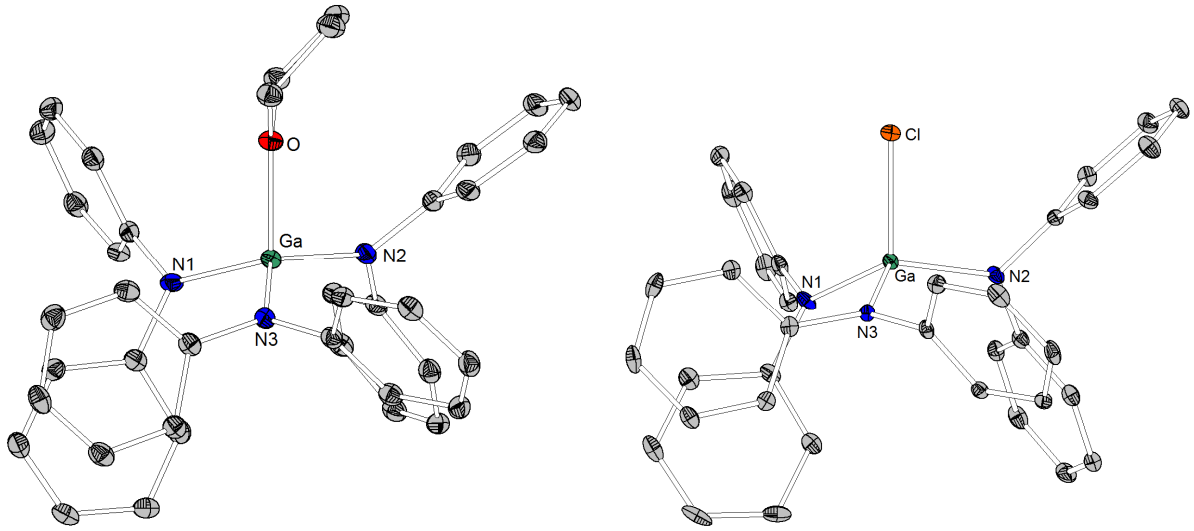

Figure 4.15: Molecular structures of $Ga[(N(C_6F_5)_2)_3]_3 \cdot THF$ and $[AsPh_4]^+[ClGa(N(C_6F_5)_2)_3]^-$ (ellipsoids with 30% probability, fluorine atoms and $[AsPh_4]^+$ omitted for clarity).

The qualitative LEWIS acidity of $Al[N(C_6F_5)_2]_3$ and $Ga[N(C_6F_5)_2]_3$ was investigated by competition experiments for chloride ions in dichloromethane among themselves and with $B(C_6F_5)_3$ (Scheme 4.13). The state of equilibrium was detected by means of ^{19}F NMR spectroscopy. The following order was found for the chloride ion affinity in dichloromethane: $B(C_6F_5)_3 < Ga[N(C_6F_5)_2]_3 < Al[N(C_6F_5)_2]_3$. The chloride ion transfer to the stronger LEWIS acid was quantitative within the measurement accuracy in each case. Dr. DANIEL HIMMEL from the KROSSING group calculated a fluoride ion affinity in the gas phase (FIA) of 476 kJ/mol for $Ga[N(C_6F_5)_2]_3$. This value lies slightly below the FIA of SbF_5 (489 kJ/mol) which is the threshold for LEWIS superacidity. $Al[N(C_6F_5)_2]_3$ exhibits a calculated FIA of 517 kJ/mol and therefore is a LEWIS superacid.

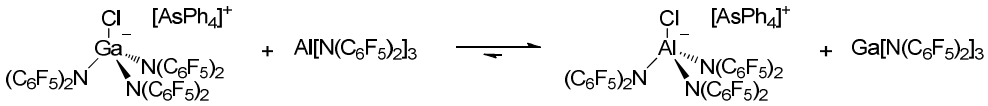

Scheme 4.13: A qualitative competition experiment for the determination of the chloride ion affinity of $Al[N(C_6F_5)_2]_3$ and $Ga[N(C_6F_5)_2]_3$.

The second part of this dissertation sheds light on the fundamental principles for the generation of extremely LEWIS acidic metal complexes: The high charge of the small metal cations Al^{3+} and Ga^{3+} can be compensated by weakly coordinating anions with a weak donor character leading to a high positive partial charge on the metal atom. Two perfluorinated substituents at amido ligands provide delocalization of the negative charge over a large number of electronegative O-, N- and F-atoms. The metal center is further stabilized by the formation of hemilabile metal fluorine interactions. Whereas $HN(C_6F_5)_2$ formed the strong LEWIS acids $Al[N(C_6F_5)_2]_3$ and $Ga[N(C_6F_5)_2]_3$, $Al[N(C_6F_5)(SO_2CF_3)]_3$ derived from the by more than ten orders of magnitude more acidic $HN(C_6F_5)(SO_2CF_3)$ did not show LEWIS acidic behavior. This observation demonstrates that the LEWIS acidity of a metal complex is not

determined by the BRØNSTED acidity of an NH-acid but by the charge distribution in its corresponding anion. The distribution of the negative charge over only a few but strong ligand donor atoms does not lead to hemilabile M···F or M···O contacts, but to strong chelates that are not broken up by external LEWIS bases.

The subsequent part contains a brief summary of the most important achievements of this thesis.
The following results were obtained in the field of chelating bisphosphazene superbases:

- A new basicity record for proton sponges was achieved by P_2-TPPN (pK_{BH^+} (MeCN) = 42.1). The higher homolog of TPPN could be synthesized *via* the STAUDINGER reaction.
- Four new alkyl-substituted bisphosphazene proton sponges and the known TPPN were prepared *via* the KIRSANOV reaction. This makes this compound class accessible for preparation in large scale allowing its application to organic synthesis and catalysis.
- The compound class of stable bisphosphazides was extended by eight representatives. X-ray diffraction analyses gave interesting insights into the coordination of water molecules by these constrained geometry ligands with two different binding sites.
- It could be shown that the presented proton sponges are not only perfect chelate ligands for the proton, but also pincer ligands for LEWIS acidic metal alkyls.
- The combination of configuratively stable C_2-symmetric binaphthyl and *trans*-1,2-diaminocyclohexane backbones with two P_2-phosphazene functionalities yielded chiral superbases which are among the most basic representatives of that compound class.

Among the results in the area of NH-acids and LEWIS acidic metal complexes based on these inorganic ligands, the following can be considered the most important:

- The three new unsymmetrically substituted NH-acids $HN(C_6F_5)(SO_2C_8F_{17})$, $HN(C_6F_5)(SO_2F)$ and $HN(C_6F_5)(C(CF_3)_3)$ were prepared.
- The coordination chemistry of the sterically demanding secondary amine $HN(C_6F_5)(C(CF_3)_3)$ was investigated in homoleptic s-block metal complexes. The lithium and magnesium salts sowed a unexpectedly high volatility.
- $Al[N(C_6F_5)(SO_2CF_3)]_3$ and $Al[N(C_6F_5)(SO_2C_4F_9)]_3$ were obtained, but did not show LEWIS acidic behavior.
- The gallium complex $Ga[N(C_6F_5)_2]_3$ was synthesized and its LEWIS acidic properties were investigated in competition experiments for chloride anions and by the preparation of LEWIS acid-base adducts and a gallate complex. $Ga[N(C_6F_5)_2]_3$ exhibits a higher fluoride ion affinity in the gas phase (FIA) than the prominent and widely used LEWIS acid $B(C_6F_5)_3$ (BCF).

5. Kumulativer Teil

5.1 Eine neue Synthesestrategie für superbasische Bisphosphazen-Protonenschwämme der zweiten und dritten Generation: Die Suche nach dem besten Chelatliganden für das Proton

Journal of the American Chemical Society **2013**, *135*(*47*), 17768-17774

A New Synthetic Pathway to the Second and Third Generation of Superbasic Bisphosphazene Proton Sponges: The Run for the Best Chelating Ligand for a Proton

Julius F. Kögel, Benjamin Oelkers, Borislav Kovačević, Jörg Sundermeyer

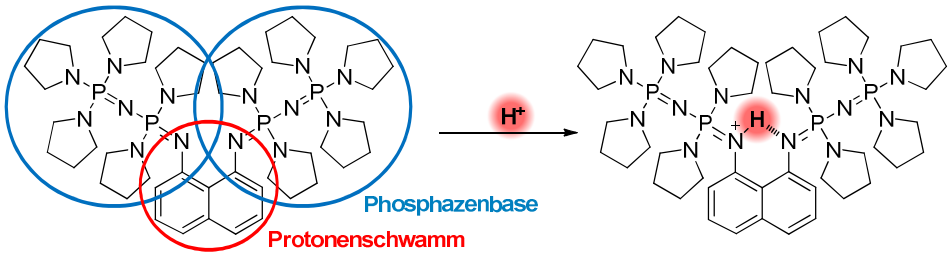

In Anlehnung an das bereits 2005 von SUNDERMEYER *et al.* publizierte NMe_2-substituierte HMPN (pK_{BH}^+ (MeCN) = 29.9) wurden durch Verknüpfung zweier Phosphazene über ein 1,8-disubstituiertes Naphthalingerüst die beiden bisher basischsten Bisphosphazen-Protonenschwämme TPPN und P_2-TPPN synthetisiert. Ausgehend von 1,8-Diazidonaphthalin wurde in einer STAUDINGER-Reaktion als neuer Synthesestrategie zur Darstellung dieser Verbindungsklasse zunächst TPPN erhalten, welches als pyrrolidinosubstituiertes Analogon des HMPNs einen pK_{BH}^+-Wert von 32.3 in Acetonitril aufweist. Des Weiteren wurde Tris(pyrrolidino)phosphin in drei Synthesestufen zu einem Vorläufer für P_2-TPPN umgesetzt, das ebenfalls über eine STAUDINGER-Reaktion erhalten werden konnte. Das Einführen einer weiteren Phosphazeneinheit in TPPN wird gemäß dem Konzept von SCHWESINGERs Phosphazenbasen als Homologisierung bezeichnet und führt zu einer drastischen Erhöhung des pK_{BH}^+-Wertes um mehrere Größenordnungen. P_2-TPPN verfügt über einen pK_{BH}^+-Wert von 42.1 auf der Acetonitril-Skala und ist somit um mehr als zehn Größenordnungen basischer als der bisher basischste Protonenschwamm. Auf Basis von Kristallstrukturen der beiden neuen Protonenschwämme als freie Basen sowie in ihrer protonierten Form wurde ihre Basizität in Lösung und in der Gasphase auch mit Hilfe theoretischer Berechnungen untersucht. Durch einen Vergleich der Basizität von TPPN und P_2-

TPPN mit den entsprechenden nicht-chelatisierenden Phosphazenen konnte theoretisch und experimentell gezeigt werden, dass der Einfluss der Chelatisierung des Protons im Falle des P_2-TPPNs zu einer Zunahme des pK_{BH^+}-Wertes um 16 Größenordnungen führt.

In der vorliegenden Arbeit konnte nicht nur ein neuer Basizitätsrekord für Protonenschwämme aufgestellt werden, sondern es wurden auch die der hohen Basizität zu Grunde liegenden Prinzipien eingehend beleuchtet und somit wichtige Grundlagen für das gezielte Design von chelatisierenden Superbasen geliefert.

Erklärung der Eigenleistung

Das Manuskript wurde mit Ausnahme des Abschnitts *Theoretical Section* von mir verfasst und alle wissenschaftlichen Arbeiten im Zusammenhang mit der Synthese und Charakterisierung der vorgestellten Verbindungen wurden von mir durchgeführt. Die Untersuchungen an TPPN sowie Vorversuche zur Darstellung von P_2-TPPN erfolgten zum Teil bereits im Rahmen der eigenen Diplomarbeit.[52] Dr. Benjamin Oelkers löste die Kristallstrukturen von TPPN·$HN(SO_2CF_3)_2$ und P_2-TPPN. Dr. Borislav Kovačević vom Rudjer Bošković Institute in Zagreb führte die theoretischen Berechnungen durch und verfasste den Abschnitt *Theoretical Section*. Prof. Dr. Jörg Sundermeyer war als Betreuer meiner Dissertation wichtiger Ideengeber und Diskussionspartner.

5.2 Superbasische alkylsubstituierte Bisphosphazen-Protonenschwämme – Synthese, strukturelle Eigenschaften, thermodynamische und kinetische Basizität und Koordinationschemie

Chemistry - A European Journal **2014**, *20*(*25*), 7670-7685

Superbasic Alkyl-Substituted Bisphosphazene Proton Sponges - Synthesis, Structural Features, Thermodynamic and Kinetic Basicity, Nucleophilicity and Coordination Chemistry

Julius F. Kögel, Xiulan Xie, Eduard Baal, Donatas Gesevicius, Benjamin Oelkers, Borislav Kovačević, Jörg Sundermeyer

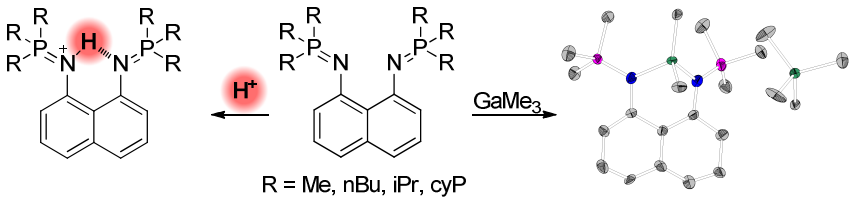

Vier neue alkylsubstituierte Bisphosphazen-Protonenschwämme mit Methyl- (TMPN), Isopropyl- (TiPrPN), Cyclopentyl- (TcyPPN) und *n*-Butylsubstituenten (TBPN) wurden über eine KIRSANOV-Route dargestellt und hinsichtlich ihrer strukturellen Eigenschaften, ihrer thermodynamischen und kinetischen Basizität, ihrer Nukleophilie und ihrer Koordinationschemie untersucht. TBPN und TMPN sind durch einfache Eintopfsynthesen aus kommerziell erhältlichen oder leicht zugänglichen Ausgangsverbindungen darstellbar, was ihre Synthese im großen Maßstab ermöglicht. Ebenfalls stark vereinfacht wurde die Darstellung des zuvor nur in einer STAUDINGER-Reaktion zugänglichen pyrrolidinosubstituierten TPPN. Die Kristallstrukturen der Hydrobromide der vier neuen Bisphosphazene zeigten jeweils das Vorliegen einer nicht-linearen unsymmetrischen Wasserstoffbrückenbindung. Für TiPrPN und TcyPPN konnten zudem zur Röntgenstrukturanalyse geeignete Kristalle der freien Basen erhalten werden, in denen die für Protonenschwämme charakteristische Verdrillung des Naphthalingerüstes zu beobachten ist. Die alkylsubstituierten Bisphosphazene weisen mit pK_{BH}^{+}-Werten in Acetonitril im Bereich von 29.3 (TMPN) und 30.9 (TBPN) dem NMe_2-substituierten HMPN (pK_{BH}^{+} (MeCN) = 29.9) ähnliche Basizitäten auf, wobei die thermodynamische Basizität in Lösung und in der Gasphase auch Gegenstand theoretischer Berechnungen war. Die Protonen-Selbstaustauschgeschwindigkeit wurde mittels NMR-spektroskopischer Verfahren exemplarisch für TMPN und TPPN ermittelt. Das sterisch wenig abgeschirmte TMPN wies in diesen Experimenten im Gegensatz zu TPPN eine hohe kinetische

Basizität auf. In der Reaktion mit Ethyliodid zeigten alle vier alkylsubstituierten Bisphosphazen-Protonenschwämme eine hohe Nukleophilie, was für die Anwendung in der BRØNSTED-Basenkatalyse nachteilig sein könnte. Die strukturell charakterisierten Metallkomplexe der Form [TMPN-MMe_2]$^+$[MMe_4]$^-$ (M = Al, Ga) konnten durch Reaktion von TMPN mit Trimethylaluminium bzw. Trimethylgallium erhalten werden und geben einen Einblick in die Koordinationschemie der Protonenschwämme.

Erklärung der Eigenleistung

Das Manuskript wurde mit Ausnahme der Abschnitte *Kinetic Basicity* und *Theoretical Section* von mir verfasst und die synthetischen und analytischen Arbeiten wurden im Rahmen meiner Doktorarbeit durchgeführt. Letztere erfolgten zum Teil innerhalb der von mir betreuten Bachelorarbeiten von Eduard Baal (Darstellung von TMPN und TBPN)[145] und Donatas Gesevicius (TiPrPN).[146] Dr. Xiulan Xie führte die NMR-spektroskopischen Messungen zur Bestimmung der kinetischen Basizität durch, wertete die Spektren aus und verfasste den Abschnitt *Kinetic Basicity*. Die Lösung der Kristallstruktur von TMPN·HBr erfolgte durch Dr. Benjamin Oelkers. Die theoretischen Berechnungen und der Abschnitt *Theoretical Section* gehen auf Dr. Borislav Kovačević zurück. Prof. Dr. Jörg Sundermeyer begleitete die Forschungen als Betreuer meiner Dissertation, sodass die Ergebnisse stets mit ihm diskutiert wurden.

5.3 Stabile vom 1,8-Diazidonaphthalin abgeleitete Bisphosphazide – Synthese, spektroskopische und strukturelle Eigenschaften und theoretische Untersuchungen

Chemistry - A European Journal **2014**, *20*(*20*), 5994-6009

Constrained Geometry Bisphosphazides derived from 1,8-Diazidonaphthalene – Synthesis, Spectroscopic Characteristics, Structural Features and Theoretical Investigations

Julius F. Kögel, Nuri C. Abacılar, Felicia Weber, Benjamin Oelkers, Klaus Harms, Borislav Kovačević, Jörg Sundermeyer

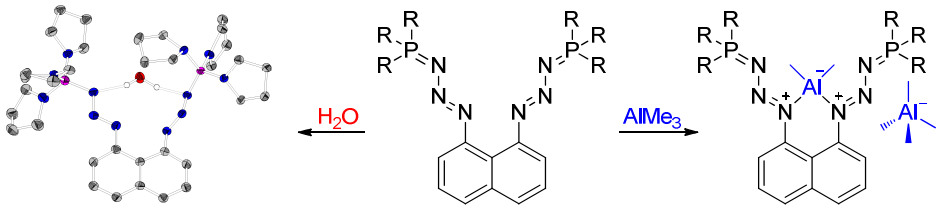

Durch eine STAUDINGER-Reaktion von 1,8-Diazidonaphthalin mit verschiedenen Phosphor(III)-Vorläufern konnte eine Serie von elf Bisphosphaziden mit einer für diese Verbindungsklasse ungewöhnlich hohen Stabilität dargestellt werden. Neben Bisphosphaziden mit einfachen offenkettigen und cyclischen Aminoresten wurden auch Verbindungen mit P_2-Einheiten, Azaphosphatrankäfigen, Guanidinsubstituenten und chiralen, vom L-Prolin abgeleiteten Aminogruppen erhalten. Für sechs der Bisphosphazide konnten zur Röntgenstrukturanalyse geeignete Einkristalle erhalten werden, wobei in drei Fällen die Wechselwirkung mit einem Wassermolekül beobachtet wurde, das Wasserstoffbrückenbindungen zu den beiden α-Stickstoffatomen ausbildet. Der synthetische Nutzen der STAUDINGER-Route zur Darstellung von Bisphosphazen-Protonenschwämmen erwies sich als sehr eingeschränkt, da die gezielte Eliminierung zweier Äquivalente N_2 in hochsiedenden Lösungsmitteln auf Grund der außergewöhnlichen Stabilität der zunächst gebildeten Bisphosphazide lediglich in drei Fällen erreicht werden konnte. Das Energieprofil der Reaktion von 1,8-Diazidonaphthalin mit Trispyrrolidinophosphin sowie die darauffolgende Eliminierung von zwei Äquivalenten molekularen Stickstoffs aus dem zunächst entstehenden Bisphosphazid wurde mit Hilfe theoretischer Berechnungen untersucht. In diesem Zusammenhang gelang die Isolierung und strukturelle Charakterisierung des Zwischenproduktes, das sowohl eine Phosphazen- als auch eine Phosphazideinheit aufweist. Die chromophoren Eigenschaften der Bisphosphazide, die im Gegensatz zu ihren nahezu farblosen Bisphosphazenanaloga eine hell- bis

tiefgrüne Farbe aufweisen, wurden an Hand der pyrrolidinosubstituierten Spezies exemplarisch mittels UV/Vis-Spektroskopie sowie auf Basis theoretischer Berechnungen untersucht.

Theoretische Berechnungen gehen für chelatisierende Bisphosphazide auf Basis des 1,8-Diazidonaphthalins von einer hohen Basizität im Bereich der entsprechenden Bisphosphazene aus. Ihre Umsetzung mit BRØNSTED-Säuren resultierte jedoch in ihrem Zerfall, wobei *in silico* ein möglicher Zerfallsmechanismus über eine hochreaktive Arinspezies postuliert wurde. Während sich die hier vorgestellten Verbindungen gegenüber BRØNSTED-Säuren als instabil erwiesen, wurde bei Reaktion des piperidinosubstituierten Bisphosphazides mit der LEWIS-Säure Trimethylaluminium ein kationischer Dimethylaluminium-Komplex mit einem Tetramethylaluminatgegenion gebildet, in dem das $[AlMe_2]^+$-Fragment durch die beiden γ-Stickstoffatome koordiniert wird.

Mit Hilfe von Kristallstrukturen konnte in dieser Arbeit gezeigt werden, dass die basischen Stickstoffatome der hier vorgestellten stabilen Bisphosphazide als Liganden für LEWIS-acide Komplexfragmente und Akzeptoren für Wasserstoffbrückenbindungen agieren können. Der Einblick in die Koordinationschemie dieser Verbindungsklasse eröffnet somit interessante Perspektiven für den Einsatz in der Organokatalyse.

Erklärung der Eigenleistung

Das Manuskript wurde mit Ausnahme des Abschnitts *Theoretical Section* von mir verfasst. Dr. Nuri C. Abacılar gelang mit HMPN($2N_2$), P_2-HMPN($2N_2$) und APAN($2N_2$) die erstmalige Darstellung von Bisphosphaziden auf Basis von 1,8-Diazidonaphthalin,[47] wobei im Rahmen meiner Dissertation die Vervollständigung der analytischen Daten erfolgte. In der Dissertation von Abacılar wurde auch erstmals die Kristallstruktur von P_2-HMPN($2N_2$)·H_2O vorgestellt, die von Dr. Klaus Harms gelöst wurde. APAN($2N_2$), das in der Dissertation von Abacılar als das entsprechende Bisphosphazen beschrieben ist, konnte im Rahmen der eigenen Diplomarbeit durch Kristallstrukturanalyse als Bisphosphazid identifiziert werden.[52] Ebenfalls während der eigenen Diplomarbeit wurden die Verbindungen TPPN($2N_2$), TPPN($1N_2$) und P_2-TPPN($2N_2$) erstmalig synthetisiert, und es wurden die Kristallstrukturen von APAN($2N_2$), TPPN($2N_2$)·H_2O und TPPN($1N_2$) erhalten, die von Dr. Benjamin Oelkers gelöst wurden. Die Synthese und Charakterisierung der übrigen Bisphosphazide erfolgte im Rahmen dieser Dissertation, wobei einige Verbindungen in den unter meiner wissenschaftlichen Anleitung angefertigten Bachelorarbeiten von Eduard Baal (Darstellung von TPipPN($2N_2$)),[145] Donatas Gesevicius (HEPN($2N_2$) und *t*BuPyr$_2$PN($2N_2$))[146] und Felicia Weber ((*S*)-Tris(2-methoxymethylpyrrolidino)phosphin, TProN($2N_2$) und *t*BuTmg$_2$PN($2N_2$))[147] erhalten wurden. Die theoretischen Berechnungen wurden von Dr. Borislav Kovačević durchgeführt, der auch den Abschnitt *Theoretical Section* verfasste. Die Ergebnisse wurden stets eingehend mit Prof. Dr. Jörg Sundermeyer als Betreuer meiner Dissertation diskutiert.

5.4 Zwei C_2-symmetrische chelatisierende P_2-Bisphosphazen-Superbasen mit einem Binaphthylrückgrat – Synthese, strukturelle Eigenschaften und Darstellung eines kationischen Aluminiumalkylkomplexes

Chemical Communications **2014**, *50*, 4319-4321

Two C_2-Symmetric Chelating P_2-Bisphosphazene Superbases Connected *via* a Binaphthyl Backbone – Synthesis, Structural Features and Preparation of a Cationic Alkyl Aluminum Complex

Julius F. Kögel, Nis-Julian Kneusels, Jörg Sundermeyer

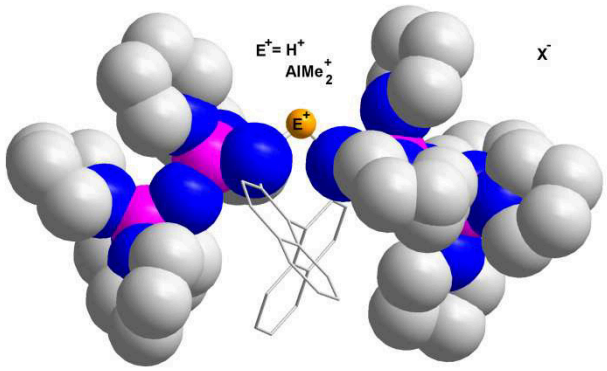

Die zwei chelatisierenden Superbasen Binap-P_2NMe_2 und Binap-P_2Pyr wurden durch Verknüpfung zweier dimethylamino- und pyrrolidinosubstituierter P_2-Phosphazene über ein axial chirales Binaphthylgerüst erhalten und als freie Basen und in ihrer protonierten Form charakterisiert. Die Synthese erfolgte über eine KIRSANOV-Reaktion zwischen (*S*)-(–)-1,1'-Binaphthyl-2,2'-diamin und den entsprechenden Bromophosphoniumbromidvorläufern. In NMR-Titrationsexperimenten wurden pK_{BH}^{+}-Werte auf der Acetonitril-Skala von 29.3 für Binap-P_2NMe_2 und 30.8 die Binap-P_2Pyr erhalten, wodurch die Basizität dieser chiralen Bisphosphazide die der weit verbreiteten chiralen Guanidine um mehrere Größenordnungen übersteigt. Die Kristallstruktur von Binap-P_2NMe_2 zeigt im Gegensatz zu klassischen Protonenschwämmen keine Wechselwirkung der beiden Basizitätszentren, was auf die höhere Flexibilität der hier gezeigten Verbindungen zurückzuführen ist. Die hohe Basizität sowie die Kopplung des aciden Protons zu zwei Phosphoratomen deuten jedoch darauf hin, dass es nach Protonierung zu einer Chelatisierung des Protons kommt. Ein seltenes Beispiel für einen Metallkomplex einer SCHWESINGER-Base konnte durch Umsetzung von Binap-P_2Pyr mit Trimethylaluminium erhalten werden, was zur Bildung eines chiralen kationischen Aluminiumkomplexes mit einem Tetramethylaluminatgegenion führte.

Die hohe Basizität der hier dargestellten Verbindungen stellt eine Anwendung im Bereich der asymmetrischen BRØNSTED-Basen-Katalyse in Aussicht, wenn die Basizität einfacher chiraler Amine oder Guanidine nicht ausreichend ist.

Erklärung der Eigenleistung

Das Verfassen des Manuskriptes und die wissenschaftlichen Arbeiten im Zusammenhang mit der vorliegenden Publikation wurden im Rahmen dieser Dissertation von mir durchgeführt. Ein Teil der synthetischen Arbeiten erfolgte unter meiner Betreuung an meinem Arbeitsplatz durch Nis-Julian Kneusels während eines Vertiefungsprojektes als Teil seines Masterstudiums. Das zuvor unpublizierte Elektrophil $(Me_2N)_3P{=}N\text{-}P(NMe_2)_2Br_2$ wurde in Anlehnung an eine bekannte Vorschrift von Dr. Nuri C. Abacılar[47] aus dem bekannten Nukleophil $(Me_2N)_3P{=}N\text{-}P(NMe_2)_2$ synthetisiert. Es fand stets ein reger wissenschaftlicher Austausch mit meinem Promotionsbetreuer Prof. Dr. Jörg Sundermeyer statt.

5.5 Die neue NH-Säure $HN(C_6F_5)(C(CF_3)_3)$ und ihre kristallinen und flüchtigen Alkalimetall- und Erdalkalimetallsalze

Inorganic Chemistry **2014**, *53*, 3839-3846.

The New NH-Acid $HN(C_6F_5)(C(CF_3)_3)$ and its Crystalline and Volatile Alkaline and Earth Alkaline Metal Salts

Julius F. Kögel, Lars H. Finger, Nicolas Frank, Jörg Sundermeyer

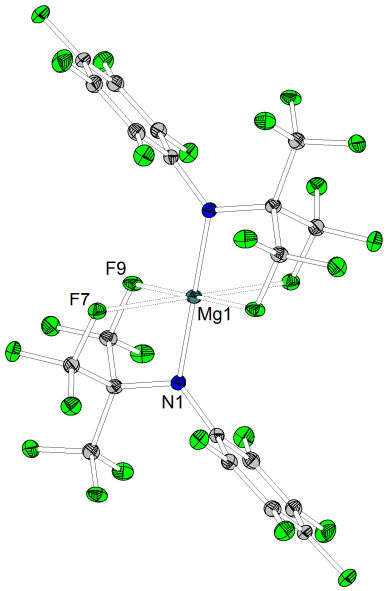

Durch Übertragung einer CF_3-Gruppe auf das Imin $C_6F_5N{=}C(CF_3)_2$ unter Verwendung des RUPPERT-Reagenzes konnte ein unsymmetrisch substituiertes Amin mit einer hohen BRØNSTED-Acidität dargestellt werden, das neben einem Pentafluorphenylsubstituenten als zweite elektronenziehende Gruppe einen perfluorierten *tert*-Butylrest aufweist. Die NH-Säure $HN(C_6F_5)(C(CF_3)_3)$ wurde mit Bis(trimethylsilyl)amiden der Alkali- und Erdalkalimetalle sowie mit Dibutylmagnesium umgesetzt, sodass eine Serie von sieben Koordinationsverbindungen erhalten wurde. Unter diesen wurde für $LiN(C_6F_5)(C(CF_3)_3)$ und $Mg[N(C_6F_5)(C(CF_3)_3)]_2$ eine unerwartet hohe thermische Stabilität und Flüchtigkeit beobachtet, die die Bildung zur Röntgenstrukturanalyse geeigneter Einkristalle durch Sublimation ermöglichte. Die röntgenkristallographische Charakterisierung gelang zudem für das Natrium-, Kalium- und Cäsiumsalz des $HN(C_6F_5)(C(CF_3)_3)$, wobei interessante strukturelle Merkmale beobachtet werden: Während die Alkalimetallsalze komplizierte Netzwerke aufweisen, die durch eine Vielzahl von Metall-Fluor-Kontakten dominiert werden, wird für $Mg[N(C_6F_5)(C(CF_3)_3)]_2$ eine oktaedrische Koordination des Metallzentrums durch zwei Stickstoffdonoren und vier organisch gebundene Fluoratome beobachtet.

Auf Grund seiner schwachen Elektronendonoreigenschaften könnten sich $HN(C_6F_5)(C(CF_3)_3)$ oder seine Alkalimetallsalze als interessante Ausgangsverbindungen zur Generierung stark LEWIS-acider Metallzentren erweisen. Von Interesse ist auch das entsprechende schwach koordinierende Anion $[N(C_6F_5)(C(CF_3)_3)]^-$, das Anwendung in ionischen Flüssigkeiten oder Lithiumbatterien finden könnte.

Erklärung der Eigenleistung

Das Verfassen des Manuskriptes sowie die wissenschaftlichen Arbeiten im Zusammenhang mit der vorliegenden Publikation wurden im Rahmen dieser Dissertation von mir durchgeführt. Ein Teil der synthetischen Arbeiten erfolgte durch Nicolas Frank während eines Vertiefungsprojektes als Teil seines Masterstudiums unter meiner Betreuung. Lars H. Finger führte die *Valence Bond*-Analysen durch und leistete Unterstützung beim Verfeinern der Kristallstrukturen. Prof. Dr. Jörg Sundermeyer stand mir stets als Ideengeber und wissenschaftlicher Diskussionspartner zur Seite.

5.6 Fluor- und Perfluoralkylsulfonylpentafluoranilide: Synthese und Charakterisierung neuer NH-Säuren für schwach koordinierende Anionen und ihre Acidität in der Gasphase und in Lösung

Manuskript in Vorbereitung

Fluoro- and Perfluoralkylsulfonyl-pentafluoroanilides: Synthesis and Characterization of New NH-Acids for Weakly Coordinating Anions and their Gas Phase and Solution Acidities

Julius F. Kögel, Thomas Linder, Fabian G. Schröder, Jörg Sundermeyer, Sascha K. Goll, Daniel Himmel, Ingo Krossing, Karl Kütt, Jaan Saame, Ivo Leito

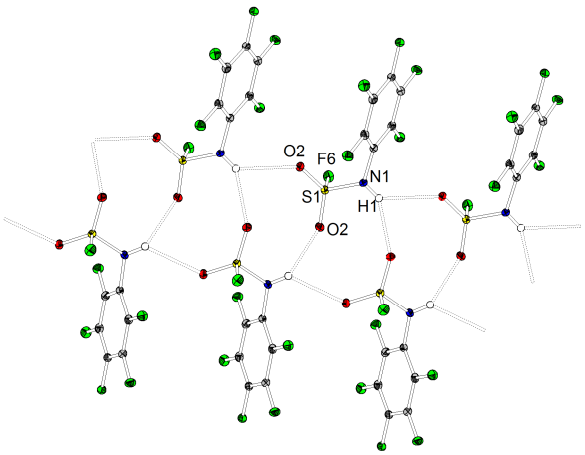

Die unsymmetrisch substituierten NH-aciden Amide $HN(C_6F_5)(SO_2X)$ (X = F, CF_3, C_4F_9, C_8F_{17}) stellen Hybride aus den literaturbekannten Verbindungen Decafluordiphenylamin ($HN(C_6F_5)_2$) und Bis(trifluormethylsulfonyl)imid ($HN(SO_2CF_3)_2$) bzw. davon abgeleiteten Derivaten dar, von denen besonders das schwach koordinierende Anion des $HN(SO_2CF_3)_2$ große Bedeutung in ionischen Flüssigkeiten und elektrochemischen Anwendungen erlangt hat. Zur Darstellung von $HN(C_6F_5)(SO_2CF_3)$, $HN(C_6F_5)(SO_2C_4F_9)$ und $HN(C_6F_5)(SO_2C_8F_{17})$ wurde *in situ* deprotoniertes Pentafluoranilin mit den entsprechenden Perfluoralkylsulfonylanhydriden bzw. -fluoriden umgesetzt, wobei die zunächst entstehenden Natriumsalze mit starken Mineralsäuren protoniert wurden. $HN(C_6F_5)(SO_2F)$ wurde durch einen Chlor-Fluor-Austausch am literaturbekannten $HN(C_6F_5)(SO_2Cl)$ mit Kaliumfluorid in Anwesenheit von [18]-Krone-6 synthetisiert. Alle beschriebenen NH-Säuren konnten röntgenkristallographisch charakterisiert werden und es wurde hierbei die Ausbildung ausgedehnter Wasserstoffbrückennetzwerke beobachtet. Des Weiteren sind die Kristallstrukturen von $LiN(C_6F_5)(SO_2C_4F_9)$ und dem Hydrat des $HN(C_6F_5)(SO_2CF_3)$ beschrieben. Gasphasen-Aciditäten wurden mit Hilfe theoretischer Berechnungen für die unsymmetrisch substituierten NH-Säuren sowie für $HN(SO_2CF_3)_2$ und $HN(C_6F_5)_2$ ermittelt. Die Hybride weisen erwartungsgemäß Aciditäten auf, die zwischen den Werten der symmetrischen Verbindungen liegen. Die ermittelten Aciditäten in der Gasphase dienten als Grundlage zur Berechnung von pK_S-Werten in Acetonitril und DMSO auf Basis

zweier theoretischer Modelle, die sich hinsichtlich der Strukturbestimmung der solvatisierten Spezies unterscheiden. Die theoretisch ermittelten pK_S-Werte in Acetonitril zeigten für $HN(C_6F_5)_2$, $HN(C_6F_5)(SO_2CF_3)$ und $HN(C_6F_5)(SO_2C_4F_9)$ eine gute Übereinstimmung mit den experimentell bestimmten Werten. Eine um mehr als sieben Größenordnungen zu niedrige Acidität wurde jedoch für $HN(SO_2CF_3)_2$ in DMSO berechnet, da während der Strukturoptimierung der NH-Säure bereits eine teilweise Protonierung des Lösungsmittels auftritt. Somit wurde an Stelle des pK_S-Wertes von $HN(SO_2CF_3)_2$ die Dissoziation des Kontaktionenpaars $Me_2SO\text{-}H^{+\cdots}N(SO_2CF_3)_2^-$ betrachtet.
Die unsymmetrisch substituierten NH-Säuren, deren Synthese, strukturelle Eigenschaften und Aciditäten in der vorliegenden Arbeit präsentiert wurden, könnten Anwendung als Liganden in LEWIS-aciden Metallkomplexen finden. Zudem sind ihre korrespondierenden schwach koordinierenden Anionen als Komponenten in ionischen Flüssigkeiten oder elektrochemischen Anwendungen von Interesse.

Erklärung der Eigenleistung

Die Abschnitte des Manuskripts *Synthesis*, *Structural Characterization* und *Experimental Details* wurden von mir verfasst. Die Abschnitte *Abstract* und *Introduction* entstanden in Zusammenarbeit mit den übrigen Autoren. Im Rahmen dieser Dissertation wurden die Kristallstrukturen von $HN(C_6F_5)(SO_2C_4F_9)$ und $HN(C_6F_5)(SO_2C_8F_{17})$ erhalten, wobei Fabian G. Schröder Unterstützung beim Verfeinern der Strukturen leistete. Zudem erfolgte die Darstellung der Verbindungen $HN(C_6F_5)(SO_2F)$ und $HN(C_6F_5)(SO_2N(SO_2F)(C_6F_5))$ sowie deren röntgenkristallographische Charakterisierung während der von mir an meinem Arbeitsplatz betreuten Bachelorarbeit von Martin Scott.[148] $HN(C_6F_5)(SO_2C_8F_{17})$ wurde parallel zu eigenen Studien auch in der Bachelorarbeit von Johannes Moldrickx bearbeitet.[149] Die Darstellung der bereits publizierten Verbindungen $HN(C_6F_5)(SO_2CF_3)$ und $HN(C_6F_5)(SO_2C_4F_9)$ erfolgte im Rahmen der Doktorarbeit von Dr. Thomas Linder.[126] Aus Arbeiten von Linder stammen zudem die Kristallstrukturen von $HN(C_6F_5)(SO_2CF_3)$, $HN(C_6F_5)(SO_2CF_3)\cdot H_2O$ und $LiN(C_6F_5)(SO_2C_4F_9)\cdot 2THF$. In meiner Dissertation erfolgte die Vervollständigung der analytischen Daten der bereits bekannten Verbindungen sowie eine Überarbeitung der Kristallstrukturen von Linder. Die theoretischen Rechnungen erfolgten durch Dr. Sascha K. Goll und Dr. Daniel Himmel aus der Arbeitsgruppe von Prof. Dr. Ingo Krossing an der Albert-Ludwigs-Universität in Freiburg. In der Arbeitsgruppe Krossing wurde auch der Teil des Manuskripts verfasst, in dem die Grundlagen und Ergebnisse dieser Rechnungen diskutiert werden. Die Titrationsexperimente zur Bestimmung der Aciditäten in Acetonitril wurden von Karl Kütt und Jan Saame aus der Arbeitsgruppe von Prof. Dr. Ivo Leito an der Universität Tartu durchgeführt. In der Arbeitsgruppe Leito entstand auch der entsprechende Abschnitt im Manuskript. Prof. Dr. Jörg Sundermeyer agierte als Betreuer meiner Dissertation stets als wichtiger Ideengeber und Diskussionspartner.

5.7 Die neue LEWIS-Supersäure $Al[N(C_6F_5)_2]_3$ und das höhere Homologe $Ga[N(C_6F_5)_2]_3$ – Strukturelle Eigenschaften, Darstellung von LEWIS-Säure-Base-Addukten und at-Komplexen und theoretische Untersuchung der Fluoridionenaffinität in der Gasphase

Manuskript in Vorbereitung

The New LEWIS Superacid $Al[N(C_6F_5)_2]_3$ and its Higher Homolog $Ga[N(C_6F_5)_2]_3$ – Structural Features, Preparation of Lewis Acid-Base Adducts and Metallates and Theoretical Investigation of the Fluoride Ion Affinity in the Gas Phase

Julius F. Kögel, Denis Sorokon, Alexander Khvorost, Martin Scott, Klaus Harms, Daniel Himmel, Ingo Krossing, Jörg Sundermeyer

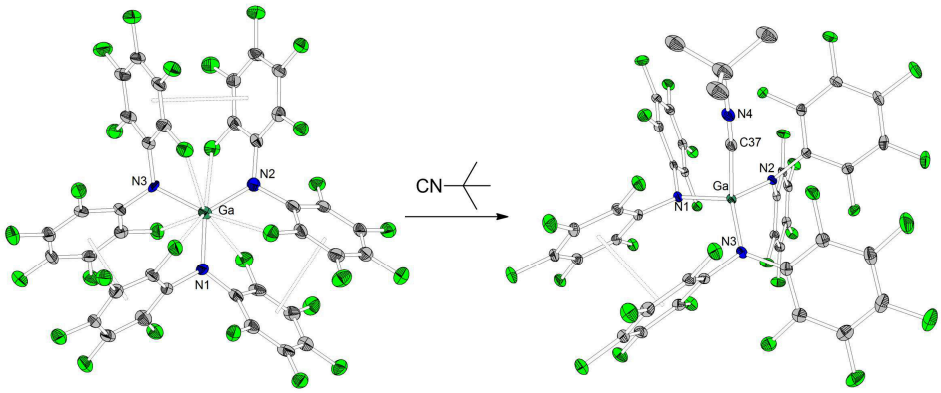

Die Umsetzungen von $LiN(C_6F_5)_2$ mit Aluminium- bzw. Galliumtrichlorid lieferten in Salzeliminierungsreaktionen die beiden Metallkomplexe $Al[N(C_6F_5)_2]_3$ und $Ga[N(C_6F_5)_2]_3$, die auf Grund der schlechten Elektronendonoreigenschaften des Decafluordiphenylamid-Liganden eine extrem hohe LEWIS-Acidität aufweisen. Die Stabilisierung der stark LEWIS-aciden Metallzentren erfolgt durch Ausbildung von Metall-Fluor-Kontakten, wobei im Falle der Aluminiumverbindung zwei extrem kurze Aluminium-Fluor-Abstände beobachtet werden, während das Galliumzentrum durch sechs Gallium-Fluor-Kontakte zu den *ortho*-Fluoratomen der C_6F_5-Einheiten stabilisiert wird. Die LEWIS-Acidität der beiden Metallkomplexe wurde zunächst durch die Ausbildung von LEWIS-Säure-Base-Addukten mit neutralen Elektronenpaardonatoren wie Ethern, Nitrilen, Isonitrilen und Phosphinen nachgewiesen. Hierbei wurde eine Pyramidalisierung der Koordinationsgeometrie sowie das Aufbrechen der Metall-Fluor-Kontakte beobachtet. Des Weiteren wurden die beiden at-Komplexe $[Cs(Tol)_3]^+[FAl[N(C_6F_5)_2]_3]^-$ und $[AsPh_4]^+[ClGa[N(C_6F_5)_2]_3]^-$ dargestellt, die jeweils interessante schwach koordinierende Anionen enthalten. Die hohe LEWIS-Acidität von $Al[N(C_6F_5)_2]_3$ wurde zudem durch Reaktionen mit Tritylfluorid ($FCPh_3$), $AgSbF_6$ oder $[CPh_4]^+[BF_4]^-$ belegt. Um qualitative

Informationen über die LEWIS-Acidität von $Al[N(C_6F_5)_2]_3$ und $Ga[N(C_6F_5)_2]_3$ zu erhalten, wurden Konkurrenzexperimente zur Chloridionenaffinität in Dichlormethan durchgeführt. In Übereinstimmung mit theoretischen Berechnungen zeigte $Al[N(C_6F_5)_2]_3$ eine höhere Chloridionenaffinität im Vergleich zu $Ga[N(C_6F_5)_2]_3$, wobei beide LEWIS-Säuren zur Abspaltung eines Chloridions aus dem Borat $[ClB(C_6F_5)_3]^-$ in der Lage waren.
Die im Rahmen dieser Arbeit untersuchten Metallkomplexe könnten Anwendung in der LEWIS-Säure-Katalyse finden und die beschriebenen schwach koordinierenden Anionen könnten die Stabilisierung hochreaktiver Kationen ermöglichen.

Erklärung der Eigenleistung

Im Rahmen der vorliegenden Dissertation wurde das Manuskript von mir verfasst und alle wissenschaftlichen Arbeiten im Zusammenhang mit $Ga[N(C_6F_5)_2]_3$ und seinen Verbindungen und die Konkurrenzexperimente zur Bestimmung der qualitativen Chloridionenaffinität in Dichlormethan wurden von mir durchgeführt. Die erstmalige Darstellung von $Ga[N(C_6F_5)_2]_3$ erfolgte durch Martin Scott unter meiner Betreuung. $Al[N(C_6F_5)_2]_3$ wurde erstmals von Alexander Khvorost synthetisiert und strukturell charakterisiert.[124] Denis A. Sorokin optimierte seine Synthese und stellte die entsprechenden LEWIS-Säure-Base-Addukte und den at-Komplex $[Cs(Tol)_3]^+[FAl[N(C_6F_5)_2]_3]^-$ dar.[125] Die Kristallstrukturen von $Al[N(C_6F_5)_2]_3$ und seinen Verbindungen wurden erstmalig von Dr. Klaus Harms gelöst und im Rahmen dieses Publikationsentwurfes von mir überarbeitet. Harms verfeinerte zudem das fehlgeordnete Lösungsmittelmolekül in der Kristallstruktur von $Ga[N(C_6F_5)_2]_3 \cdot PMe_3$. Die von Dr. Daniel Himmel in der Arbeitsgruppe von Prof. Ingo Krossing durchgeführten theoretischen Berechnungen zur Fluoridionenaffinität in der Gasphase sind im vorliegenden Manuskript noch nicht enthalten. Die Konzepte und Ergebnisse wurden stets mit dem Betreuer meiner Dissertation Prof. Dr. Jörg Sundermeyer diskutiert.

6. Literatur

[1] a) Brønsted, J. N. *Recl. Trav. Chim. Pays-Bas* **1923**, *42*, 718-728; b) Lowry, T. M. *Chem. Ind.* **1923**, *42*, 43-47.

[2] a) Ovaska, T. V. *n*-Butyllithium. In *e-EROS Encyclopedia of Reagents for Organic Synthesis*, John Wiley & Sons, Ltd., 2001; b) Ovaska, T. V.; Wittel, B.; Snieckus, V. *s*-Butyllithium; in *e-EROS Encyclopedia of Reagents for Organic Synthesis*, John Wiley & Sons, Ltd., 2007; c) Bailey, W. F.; Wachter-Jurcsak, N. *t*-Butyllithium; in *e-EROS Encyclopedia of Reagents for Organic Synthesis*, John Wiley & Sons, Ltd., 2009; d) Caubère, P. *Chem. Rev.* **1993**, *93*, 2317-2334.

[3] Ziegler, K.; Colonius, H. *Liebigs Ann. Chem.* **1930**, *479*, 135-149.

[4] a) Xu, W.; Mohan, R.; Morrissey, M. M. *Tetrahedron Lett.* **1997**, *38*, 7337-7340; b) Xu, W.; Mohan, R.; Morrissey, M. M. *Bioorg. Med. Chem. Lett.* **1998**, *8*, 1089-1092; c) Baxendale, I. R.; Lee, A.-L.; Ley, S. V. *Synlett* **2001**, *9*, 1482-1484; d) Chiara, J. L.; Encinas, L.; Díaz, B. *Tetrahedron Lett.* **2005**, *46*, 2445-2448.

[5] Tundo, P.; Anastas, P.; Black, D. S.; Breen, J.; Collins, T.; Memoli, S.; Miyamoto, J.; Polyakoff, M.; Tumas, W. *Pure Appl. Chem.* **2000**, *72*, 1207-1228.

[6] Ishikawa, T. *Superbases for Organic Synthesis: Guanidines, Amidines and Phosphazenes and Related Organocatalysts*; John Wiley & Sons, Ltd.: Chichester, UK, 2009.

[7] Kaljurand, I.; Rodima, T.; Leito, I.; Koppel, I. A.; Schwesinger, R. *J. Org. Chem.* **2000**, *65*, 6202-6208.

[8] a) Riedel, E. *Anorganische Chemie*, 6. Auflage, de Gruyter, Berlin, 2004, S. 321; b) Soovaeli, L.; Rodima, T.; Kaljurand, I.; Kuett, A.; Koppel, I. A.; Leito, I. *Org. Biomol. Chem.* **2006**, *4*, 2100-2105.

[9] a) Rodima, T.; Kaljurand, I.; Pihl, A.; Maeemets, V.; Leito, I.; Koppel, I. A. *J. Org. Chem.* **2002**, *67*, 1873-1881; b) Kaljurand, I.; Rodima, T.; Pihl, A.; Maeemets, V.; Leito, I.; Koppel, I. A.; Mishima, M. *J. Org. Chem.* **2003**, *68*, 9988-9993 c) Kolomeitsev, A. A.; Koppel, I. A.; Rodima, T.; Barten, J.; Lork, E.; Röschenthaler, G.-V.; Kaljurand, I.; Kütt, A.; Koppel, I.; Mäemets, V.; Leito, I. *J. Am. Chem. Soc.* **2005**, *127*, 17656-17666.

[10] Bordwell, F. G. *Acc. Chem. Res.* **1988**, *21*, 456-463.

[11] Kaljurand, I.; Kuett, A.; Soovaeli, L.; Rodima, T.; Maeemets, V.; Leito, I.; Koppel, I. A. *J. Org. Chem.* **2005**, *70*, 1019-1028.

[12] Raab, V.; Gauchenova, E.; Merkoulov, A.; Harms, K.; Sundermeyer, J.; Kovačević, B.; Maksić, Z. B. *J. Am. Chem. Soc.* **2005**, *127*, 15738-15743.

[13] Lias, S. G.; Liebman, J. F.; Levin, R. D. *J. Phys. Chem. Ref. Data* **1984**, *13*, 695-808.

[14] a) Kaljurand, I.; Koppel, I. A.; Kuett, A.; Room, E.-I.; Rodima, T.; Koppel, I.; Mishima, M.; Leito, I. *J. Phys Chem. A* **2007**, *111*, 1245-1250; b) Decouzon, M.; Gal, J. F.; Maria, P. C.; Raczynska, E. D. *Rapid Commun. Mass Spectrom.* **1993**, *7*, 599-602.

[15] a) Kovačević, B.; Maksić, Z. B. *Org. Lett.* **2001**, *3*, 588-597; b) Glasovac, Z.; Eckert-Maksić, M.; Maksić, Z. B. *New J. Chem.* **2009**, *33*, 588-597;

[16] Raab, V.; Kipke, J.; Gschwind, R. M.; Sundermeyer, J. *Chem. Eur. J.* **2002**, *8*, 1682-1693.

[17] Schwesinger, R.; Schlemper, H. *Angew. Chem.* **1987**, *99*, 1210-1212; *Angew. Chem., Int. Ed. Engl.* **1987**, *26*, 1165-1167.

[18] Abacılar, N. C.; Raab, V.; Gaoutchenova, E.; Garrelts, U.; Harms, K.; Sundermeyer, J. The Chemistry of Superbasic Guanidines. In *Activating Unreactive Substrates, The Role of Secondary Interactions*; Bolm, C.; Hahn, F. E., Eds.; Wiley-VCH: Weinheim, 2009; pp 17-37.

[19] Schwesinger, R.; Willaredt, J.; Schlemper, H.; Keller, M.; Schmitt, D.; Fritz, H. *Chem. Ber.* **1994**, *127*, 2435-2454.

[20] a) Schmidt, H.; Lensink, C.; Xi, S. K.; Verkade, J. G. *Z. anorg. allg. Chem*. **1989**, *578*, 75-80; b) Tang, J.; Dopke, J.; Verkade, J. G. *J. Am. Chem. Soc.* **1993**, *115*, 5015-5020; c) Laramay, M. A. H.; Verkade, J. G. *J. Am. Chem. Soc.* **1990**, *112,* 9422-9423.

[21] a) Schwesinger, R.; Schlemper, H.; Hasenfratz, C.; Willaredt, J.; Dambacher, T.; Breuer, T.; Ottaway, C.; Fletschinger, M.; Boele, J.; Fritz, H.; Putzas, D.; Rotter, H.W.; Brodwell, F. G.; Satish, A. V.; Ji, G.; Peters, E.; Peters, K.; von Schnering, H. G.; Walz, L. *Liebigs Ann*. *Chem.* **1996**, 1055-1081; b) Schwesinger, R.; Hasenfratz, C.; Schlemper, H.; Walz, L.; Peters, E.-M.; Peters, K.; von Schnering, H. G. *Angew. Chem.* **1993**, *105*, 1420-1422; *Angew. Chem., Int. Ed. Engl.* **1993**, *32*, 1361-1363.

[22] Issleib, K.; Lischewski, M. *Synth. React. Inorg. Met.-Org. Chem.* **1973**, *3*, 255-266.

[23] Bowman, P. S.; Steele, W. R. S.; Winterman, D. R.; Alder, R. W. *Chem. Commun.* **1968**, 723-724.

[24] Brown, H. C. et al.. In *Determination of Organic Structures by Physical Methods*; Braude, E. A.; Nachod, F. C., Eds.; Academic Press, New York, 1955.

[25] Benoit, R. L.; Lefebvre; D. Fréchette, M. *Can. J. Chem.* **1987**, *65*, 996-1001.

[26] a) Cox, C.; Wack, H.; Lectka, T. *Angew. Chem.* **1999**, *111*, 864-867; *Angew. Chem. Int. Ed.* **1999**, *38*, 798-800; b) Kovačević, B.; Maksić, Z.B.; Vianelloa, R.; Primorac, M. *New J. Chem.* **2002**, *26*, 1329-1334; c) Pozharskii, A. F.; Ryabtsova, O. V. Ozeryanskii, V. A.; Degtyarev, A. V.; Starikova, Z. A.; Sobczykc, L.; Filarowskic, A. *Tetrahedron Lett.* **2005**, *46*, 3973-3976; d) Ozeryanskii, V. A.; Pozharskii, A. F.; Bienko, A. J.; Sawka-Dobrowolska, W.; Sobczyk, L. *J. Phys. Chem. A* **2005**, *109*, 1637-1642; e) Parkin, A.; Wozniak, K.; Wilson, C. C. *Cryst. Growth Des.* **2007**, *7*, 1393-1398; f) Degtyarev A. V.; Ryabtsova O. V.; Pozharskii A. F.; Ozeryanskii V. A.; Starikova, Z. A.; Sobczyk, L.; Filarowski, A. *Tetrahedron* **2008**, *64*, 6209-6214; g) Del Benea, J. E.; Alkortab, I.; Elguerob, J. *Magn. Reson. Chem.* **2008**, *46*, 457-463; h) Pozharskii, A. F.; Degtyarev, A. V.; Ozeryanskii, V. A.; Ryabtsova, O. V.; Starikova, Z. A.; Borodkin, G. S. *J. Org. Chem.* **2010**, *75*, 4706-4715; i) Pietrzak, M.; Wehling, J. P.; Kong, S.; Tolstoy, P. M.; Shenderovich, I. G.; Lopez, C.; Claramunt, R. M.;Elguero, J.; Denisov, G. S.; Limbach, H. *Chem. Eur. J.* **2010**, *16*, 1679-1690; j) DeBlase, A. F.; Bloom, S.; Lectka, T.; Jordan, K. D.; McCoy, A. B.; Johnson, M. A. *J. Chem. Phys.* **2013**, *139*, 024301/1-024301/9.

[27] Staab, H. A.; Saupe, T. *Angew. Chem.* **1988**, *100*, 895-909; *Angew. Chem., Int. Ed. Engl.* **1988**, *27*, 865-879.

[28] Ozeryanskii, V. A.; Shevchuk, D. A.; Pozharskii, A. F.; Kazheva, O. N.; Chekhlov, A. N.; Dyachenko, O. A. *J. Mol. Struct.* **2008**, *892*, 63-68.

[29] Alder, R. W.; Bryce, M. R.; Goode, N. C.; Miller, N.; Owen, J. *J. Chem. Soc., Perkin Trans. 1* **1981**, *11*, 2840-2847.

[30] a) Hibbert, F.; Simpson, G. R. *J. Chem. Soc., Perkin Trans. 2* **1987**, 243-246; b) Alder, R. W.; Goode, N. C.; Miller, N.; Hibbert, F.; Hunte, K. P. P.; Robbins, H. K. *J. Chem. Soc., Chem. Commun.* **1978**, 89-90; c) Pozharskii, A. F.; Ryabtsova, O. V.; Ozeryanskii, V. A.; Degtyarev, A. V.; Kazheva, O. N.; Alexandrov, G. G.; Dyachenko O. A. *J. Org. Chem.* **2003**, *68*, 10109-10122; d) Degtyarev, A. V.; Pozharskii, A. F. *Chem. Heterocycl. Compd.* **2008**, *44*, 1138-1145; e) Ozeryanskii, V. A.; Sorokin, V. I.; Pozharskii, A. F. *Russ. Chem.*

Bull. **2004**, *53*, 404-414; f) Filatova, E. A.; Pozharskii, A. F.; Gulevskaya, A. V.; Vistorobskii, N. V.; Ozeryanskii, V. A. *Synlett* **2013,** *24*, 2515-2518.

[31] Staab, H. A.; Saupe, T.; Krieger, C. *Angew. Chem* **1983**, *95*, 748-749; *Angew. Chem., Int. Ed. Engl.* **1983**, *22,* 731-732.

[32] Staab, H. A.; Höne, M.; Krieger, C. *Tetrahedron Lett.* **1988**, *29*, 1905-1908.

[33] Saupe, T.; Krieger, C.; Staab, H. A. *Angew. Chem.* **1986**, *98*, 460-462; *Angew. Chem., Int. Ed. Engl.* **1986**, *25*, 451-453.

[34] Staab, H. A.; Krieger, C.; Hone, M. *Tetrahedron Lett.* **1988**, *29*, 5629-5632.

[35] Staab, H. A.; Zirnstein, M. A.; Krieger, C. *Angew. Chem.* **1989**, *101*, 73-75; *Angew. Chem., Int. Ed. Engl.* **1989**, *28*, 86-88.

[36] Zirnstein, M. A.; Staab, H. A. *Angew. Chem.* **1987**, *99*, 460-461; *Angew. Chem., Int. Ed. Engl.* **1987**, *26*, 460-461.

[37] Zachova, H.; Man, S.; Taraba, J.; Potacek, M. *Tetrahedron* **2009**, *65*, 792-797; b) Galeta, J.; Potáček, M. *J. Org. Chem.* **2012**, *77*, 1010-1017.

[38] a) Despotović, I.; Kovačević, B.; Maksić, Z. B. *Org. Lett.* **2007**, *9*, 4709-4712; b) Bachrach, S. M.; Wilbanks, C. C. *J. Org. Chem.* **2010**, *75*, 2651-2660; c) Uchida, N.; Kuwabara, J.; Taketoshi, A.; Kanbara, T. *J. Org. Chem.* **2012**, *77*, 10631-10637.

[39] Alder, R. W. *Chem. Rev.* **1989**, *89*, 1215-1223.

[40] Llamas-Saiz, A. L.; Foces-Foces, C.; Elguero, J. *J. Mol. Struct.* **1994**, *328*, 297-323.

[41] a) Pozharskii, A. F. *Russ. Chem. Rev.* **1998**, *67*, 1-24; b) Pozharskii, A. F.; Ozeryanskii, V. A.; Filatova, E. A. *Chem. Heterocycl. Compd.* **2012**, *48*, 200-219.

[42] Nagasawa, K. Related Organocatalysts (1): A Proton Sponge. In *Superbases for Organic Synthesis: Guanidines, Amidines and Phosphazenes and Related Organocatalysts*; Ishikawa, T., Hrsg.; John Wiley & Sons, Ltd.: Chichester, UK, 2009; pp 251-271.

[43] Chambron, J.; Meyer, M. *Chem. Soc. Rev.* **2009**, *38*, 1663-1673.

[44] Maksić, Z. B.; Kovačević, B.; Vianello, R. *Chem. Rev.* **2012**, *112*, 5240-5270.

[45] Im vorangegangenen Abschnitt sind die pK_{BH}^{+}-Werte in unterschiedlichen Lösungsmitteln angegeben, was die Vergleichbarkeit der Basizität erschwert. Bei Übertragung der Werte in DMSO, Wasser oder entsprechenden Gemischen auf die Acetonitril-Skala kann näherungsweise davon ausgegangen werden, dass sie nur um wenige Größenordnungen vom pK_{BH}^{+}-Wert des DMANs abweichen.

[46] Raab, V.; Harms, K.; Sundermeyer, J.; Kovačević, B.; Maksić, Z. B. *J. Org. Chem.* **2003**, *68*, 8790-8797.

[47] Abacılar, N. C. *Dissertation*, Philipps-Universität Marburg, **2009**.

[48] Schwesinger, R.; Schlemper, H. *Angew. Chem.* **1987**, *99*, 1212-1214; *Angew. Chem., Int. Ed. Engl.* **1987**, *26*, 1165-1167.

[49] Belding, L.; Dudding, T. *Chem. Eur. J.* **2014**, *20*, 1032-1037

[50] Kovačević, B.; Maksić, Z. B. *Tetrahedron Letr.* **2006**, *47*, 2553-2555.

[51] a) Llamas-Saiz, A. L.; Foces-Foces, C.; Molina, P.; Alajarin, M.; Vidal, A.; Claramunt, R. M.; Elguero, J. *J. Chem. Soc., Perkin Trans.* 2 **1991**, 1025-1031; b) Llamas-Saiz, A. L.; Foces-Foces, C. ; Elguero, J.; Molina, P.; Alajarin, M.; Vidal, A. *J. Chem. Soc., Perkin Trans. 2,* **1991**, 1667-1676; c) Llamas-Saiz, A. L.; Foces-Foces, C.; Elguero, J.; Molina, P.; Alajarin, M.; Vidal, A. *J. Chem. Soc., Perkin Trans. 2* **1991**, 2033-2040; d) Laynez, J.;

Menendez, M.; Velasco, S.; Luis, J.; Llamas-Saiz, A. L.; Foces-Foces, C.; Elguero, J.; Molina, P.; Alajarin, M.; Vidal, A. *J. Chem. Soc., Perkin Trans. 2* **1993**, 709-713.

[52] Kögel, J. F. *Diplomarbeit*, Philipps-Universität Marburg, **2010**.

[53] a) Kirsanov, A. V. *Izv. Akad. Nauk SSSR, Otd. Khim. Nauk* **1950**, 426; b) Rodima, T.; Mäemets, V.; Koppel, I. *J. Chem. Soc*., *Perkin Trans. 1* **2000**, 2637-2644.

[54] Xiong, Y.; Yao, S.; Inoue, S.; Berkefeld, A.; Driess, M. *Chem. Commun*. **2012**, *48*, 12198-12200; b) Xiong, Y.; Yao, S.; Inoue, S.; Irran, E.; Driess, M. *Angew. Chem.* **2012**, *124*, 10221-10224; *Angew. Chem. Int. Ed.* **2012**, *51*, 10074-10077.

[55] Staudinger, H.; Meyer, J. *Helv. Chim. Acta* **1919**, *2*, 635-646.

[56] Bebbington, M. W. P.; Bourissou, D. *Coord. Chem. Rev*. **2009**, *253*, 1248-1261.

[57] Naka, H.; Kanase, N.; Ueno, M.; Kondo, Y. *Chem. Eur. J.* **2008**, *14*, 5267-5274.

[58] Koppel, I. A.; Schwesinger, R.; Breuer, T.; Burk, P.; Herodes, K.; Koppel, I.; Leito, I.; Mishima, M. *J. Phys. Chem. A* **2001**, *105*, 9575-9586.

[59] Es sind an dieser Stelle die durch eine semi-empirische Methode ermittelten Werte angegeben. Die entsprechenden durch eine *ab initio*-Methode berechneten Werte liegen deutlich darüber ($(Me_2N)_3P{=}NH$: 256.3 kcal/mol, $(Me_2N)_3P{=}CH_2$: 274.5 kcal/mol).

[60] Margetić, D. Mitteilung vom 3.12.2012.

[61] Engelhardt, L. M.; Papasergio, R. I.; Raston, C. L.; Salem, G.; Whitaker, C. R.; White, A. H. *J. Chem. Soc., Dalton Trans.* **1987**, *7*, 1647-1653.

[62] Clark, A. J.; Al-Faiyz, Y. S. S.; Patel, D.; Broadhurst, M. J. *Tetrahedron Lett.* **2001**, *42*, 2007-2009.

[63] Bensa, D.; Brunel, J.-M.; Buono, G.; Rodriguez, J. *Synlett* **2001**, *5*, 715-717.

[64] Kobayashi, K.; Ueno, M .; Kondo, Y. *Chem. Commun.* **2006**, 3128-3130.

[65] Alonso, D. A.; Carmen, N.; Varea, M. *Tetrahedron Lett.* **2004**, *45*, 573-577.

[66] a) Solladié-Cavallo, A.; Liptaj, T.; Schmitt, M.; Solgadi, A. *Tetrahedron Lett.* **2002**, *43*, 415-418; b) Fruchart, J.-S.; Gras-Masse, H.; Melnyk O. *Tetrahedron Lett.* **2002**, *43*, 9153-9155.

[67] Solladié-Cavallo, A.; Roje, M.; Welter, R.; Šunjić, V. *J. Org. Chem.* **2004**, *69*, 1409-1412.

[68] Boileau, S.; Illy, N. *Prog. Polym. Sci.* **2011**, *36*, 1132-1151.

[69] a) Zhang, L.; Nederberg, F.; Messman, J. M.; Pratt, R. C.; Hedrick, J. L.; Wade, C. G. *J. Am. Chem. Soc.* **2007**, *129*, 12610-12611; b) Zhang, L.; Nederberg, F.; Pratt, R. C.; Waymouth, R. M.; Hedrick, J. L.; Wade, C. G. *Macromolecules* **2007**, *40*, 4154-4158; c) Helou, M.; Miserque, O.; Brusson, J.-M.; Carpentier, J.-F.; Guillaume, S. M. *Chem. Eur. J.* **2010**, *16*, 13805-13813; d) Jaffredo, C. G.; Carpentier, J.-F.; Guillaume, S. M. *Macromol. Rapid Commun.* **2012**, *33*, 1938-1944.

[70] a) Esswein, B.; Möller, M. *Angew. Chem.* **1996**, *108*, 623-625; *Angew. Chem., Int. Ed. Engl.* **1996**, *35*, 623-625; b) Misaka, H.; Sakai, R.; Satoh, T.; Kakuchi, T. *Macromolecules* **2011**, *44*, 9099-9107; Misaka, H.; Tamura, E.; c) Zhao, J.; Schlaad, H. *Macromolecules* **2011**, *44*, 5861-5864; d) Makiguchi, K.; Kamoshida, K.; Sakai, R.; Satoh, T.; Kakuchi, T. *J. Polym. Sci., Part A: Polym. Chem.* **2012**, *50*, 1941-1952.

[71] a) Illy, N.; Boileau, S.; Penelle, J.; Barbier, V. *Macromol. Rapid Commun.* **2009**, *30*, 1731-1735; b) Illy, N.; Boileau, S.; Buchmann, W.; Penelle, J.; Barbier, V. *Macromolecules* **2010**, *43*, 8782-8789.

[72] a) Molenberg, A.; Möller, M. *Macromol. Rapid Commun.* **1995**, *16*, 449-453; b) Hupfield, P. C.; Taylor, R. G. *J. Inorg. Organomet. Polym.* **1999**, *9*, 17-34.

[73] a) Pietzonka, T.; Seebach, D. *Angew. Chem.* **1993**, *105*, 741-742; *Angew. Chem., Int. Ed. Engl.* **1993**, *32*, 716-717; b) Kakuchi, T.; Chen, Y.; Kitakado, J.; Mori, K.; Fuchise, K.; Satoh, T. *Macromolecules* **2011**, *44*, 4641-4647; c) Chen, Y.; Fuchise, K.; Narumi, A.; Kawaguchi, S.; Satoh, T.; Kakuchi, T. *Macromolecules* **2011**, *44*, 9091-9098.

[74] Farrer, N. J.; Vikse, K. L.; McDonald, R.; McIndoe, J. S. *Eur. J. Inorg. Chem.* **2012**, 733-740.

[75] a) Shroff, R.; Svatoš, A. *Anal. Chem.* **2009**, *81*, 7954-7959; b) Shroff, R.; Svatoš, A. *Rapid Commun. Mass Spectrom.* **2009**, *23*, 2380-2382; c) Zhang, S.; Yao, Z.-P. *Anal. Chim. Acta* **2012**, *711*, 77-82; d) Calvano, C. D.; Zambonin, C. G.; Palmisano, F. *Rapid Commun. Mass Spectrom.* **2011**, *25*, 1757-1764; e) Cao, D.; Wang, Z.; Han, C.; Cui, L.; Hu, M.; Wu, J.; Liu, Y.; Cai, Y.; Wang, H.; Kang, Y. *Talanta* **2011**, *85*, 345-352; f) Calvano, C. D.; Monopoli, A.; Ditaranto, N.; Palmisano, F. *Anal. Chim. Acta* **2013**, *789*, 56-63.

[76] a) Fache, F.; Schulz, E.; Tommasino, M. L.; Lemaire, M. *Chem. Rev.* **2000**, *100*, 2159-2231; b) France, S.; Guerin, D. J.; Miller, S. J.; Lectka, T. *Chem. Rev.* **2003**, *103*, 2985-3012; c) Seayad, J.; List, B. *Org. Biomol. Chem.* **2005**, *3*, 719-724; Pellissier, H. *Tetrahedron* **2007**, *63*, 9267-9331; d) Xu, L.-W.; Luo, J.; Lu, Y. *Chem.Commun.* **2009**, 1807-1821; e) Kano, T.; Maruoka, *K. Bull. Chem. Soc. Jpn.* **2010**, *83*, 1421-1438.

[77] Regan, A. C. *J. Chem. Soc., Perkin Trans. 1* **1999**, *4*, 357-373.

[78] Bhuniya, D.; DattaGupta, A.; Singh, V. K. *J. Org. Chem.* **1996**, *61*, 6108-6113.

[79] Ishikawa, T. Guanidines in Organic Synthesis. In *Superbases for Organic Synthesis: Guanidines, Amidines and Phosphazenes and Related Organocatalysts*; Ishikawa, T., Hrsg.; John Wiley & Sons, Ltd.: Chichester, UK, 2009; pp 93-144.

[80] a) Ishikawa, T.; Kumamoto, T. *Synthesis* **2006**, *5*, 737-752; b) Leow, D.; Tan, C.-H. *Synlett* **2010**, *11*, 1589-1605.

[81] a) Isobe, T.; Fukuda, K.; Araki, Y.; Ishikawa, T. *Chem. Commun.* **2001**, 243-244; b) Ishikawa, T.; Isobe, T. *Chem. Eur. J.* **2002**, *8*, 552-557.

[82] Castiglia, A.; El Sehrawi, H.; Orbegozo, T.; Spitzner, D.; Claasen, B.; Frey, W.; Kantlehner, W.; Jäger, V. *Z. Naturforsch.* **2012**, *67b,* 337-346.

[83] a) Clews, J.; Curtis, A. D. M.; Malkin, H. *Tetrahedron* **2000**, *56*, 8735-8746; b) Dauwe, C.; Buddrus, J. *Synthesis* **1995**, 171-172.

[84] Alder, R. W. *J. Am. Chem. Soc.* **2005**, *127*, 7924-7931.

[85] Singh, A.; Chakraborty, S.; Ganguly, B. *Eur. J. Org. Chem.* **2006**, 4938-4942.

[86] a) Mazaleyrat, J.-P.; Wright, K. *Tetrahedron Lett.* **2008**, *49*, 4537-4541; b) Brancatelli, G.; Drommi, D.; Femino, G.; Saporita, M.; Bottari, G.; Faraone, F. *New J. Chem.* **2010**, *34*, 2853-2860.

[87] a) Liu, X.; Ilankumaran, P.; Guzei, I. A.; Verkade, J. G. *J. Org. Chem.* **2000**, *65*, 701-706; b) You, J. S.; Wroblewski, A. E.; Verkade, J. G. *Tetrahedron* **2004**, *60*, 7877-7883; c) Ishihara, K.; Karumi, Y.; Kondo, S.; Yamamoto, H. *J. Org. Chem.* **1998**, *63*, 5692-5695.

[88] Brunel, J. M.; Legrand, O.; Reymond, S.; Buono, G. *J. Am. Chem. Soc.* **1999**, *121*, 5807-5808.

[89] Alajarín, M.; López-Leonardo, C.; Berná, J. *Tetrahedron* **2006**, *62*, 6190-6202.

[90] Köhn, U.; Schulz, M.; Schramm, A.; Günther, W.; Görls, H.; Schenk, S.; Anders, E. *Eur. J. Org. Chem.* **2006**, *18*, 4128-4134.

[91] Ilankumaran, P.; Zhang, G.; Verkade, J. G. *Heteroatom Chem.* **2000**, *11*, 251-253.

[92] Maronna, A.; Bindewald, E.; Kaifer,E.; Wadepohl, H.; Himmel, H.-J. *Eur. J. Inorg. Chem.* **2011**, *8*, 1302-1314.

[93] a) Takeda, T.; Terada, M. *J. Am. Chem. Soc.* **2013**, *135*, 15306-15309; b) Terada, M.; Goto, K.; Oishi, M.; Takeda, T.; Kwon, E.; Kondoh, A. *Synlett* **2013**, *24*, 2531-2534.

[94] Vij, A.; Kirchmeier, R. L.; Shreeve, J. M.; Verma, R. D. *Coord. Chem. Rev.* **1997**, *158*, 413-432.

[95] a) Foropoulos, J.; DesMarteau, D. D. *Inorg. Chem.* **1984**, *23*, 3720-3723; b) DesMarteau, D. D.; Witz, M. *J. Fluorine Chem.* **1991**, *52*, 7-12.

[96] a) MacFarlane, D. R.; Meakin, P.; Sun, J.; Amini, N.; Forsyth, M. *J. Phys. Chem. B* **1999**, *103*, 4164-4170; b) Jin, H.; O'Hare, B.; Dong, J.; Arzhantsev, S.; Baker, G. A.; Wishart, J. F.; Benesi, A. J.; Maroncelli, M. *J. Phys. Chem. B* **2008**, *112*, 81-92.

[97] a) Noda, A.; Susan, M. A. B. H.; Kudo, K.; Mitsushima, S.; Hayamizu, K.; Watanabe, M. *J. Phys. Chem. B* **2003**, *107*, 4024-4033; b) Huddleston, J. G.; Visser, A. E.; Reichert, W. M.; Willauer, H. D.; Broker, G. A.; Rogers, R. D. *Green Chem.* **2001**, *3*, 156-164.

[98] Mateus, N. M. M.; Branco, L. C.; Lourenco, N. M. T.; Afonso, C. A. M. *Green Chem.* **2003**, *5*, 347-352.

[99] Del Sesto, R. E.; Corley, C.; Robertson, A.; Wilkes, J. S. *J. Organomet. Chem.* **2005**, *690*, 2536-2542.

[100] a) Welton, T. *Chem. Rev.* **1999,** *99,* 2071-2083; b) Sheldon, R. *Chem. Commun.* **2001**, 2399-2407; c) Earle, M. J.; Seddon, K. R. *Pure Appl. Chem.* **2000**, *72*, 1391-1398; d) Plechkova, N. V.; Seddon, K. R. *Chem. Soc. Rev.* **2008**, *37*, 123-150.

[101] Karadas, F.; Atilhan, M.; Aparicio, S. *Energy Fuels* **2010**, *24*, 5817-5828.

[102] a) MacFarlane, D. R.; Huang, J.; Forsyth, M. *Nature* **1999**, *402*, 792-794; b) Sakaebe, H.; Matsumoto, H. *Electrochem. Commun.* **2003**, *5*, 594-598; c) Endres, F. *Z. Phys. Chem.* **2004**, *218*, 255-283.

[103] a) KoppeI, I. A.; Taft, R. W.; Anvia, F.; Zbu, S.-Z.; Hu, L.-Q.; Sung, K.-S.; DesMarteau, D. D.; Yagupolskii, L. M.; Yagupolskii, Y. L.; Ignat'ev, N. V.; Kondratenko, N. V.; Volkonskii, A. Y.; Vlasov, V. M.; Notario, R.; Maria, P-C. *J. Am. Chem. Soc.* **1994**, *116*, 3047-3057; b) Leito, I.; Raamat, E.; Kütt, A.; Saame, J.; Kipper, K.; Koppel, I. A.; Koppel, I.; Zhang, M.; Mishima, M.; Yagupolskii, L. M.; Garlyauskayte, R. Y.; Filatov, A. A. *J. Phys. Chem. A* **2009,** *113,* 8421-8424; c) Kütt, A.; Rodima, T.; Saame, J.; Raamat, E.; Mäemets, V.; Kaljurand, I.; Koppel, I. A.; Garlyauskayte, R. Y.; Yagupolskii, Y. L.; Yagupolskii, L. M.; Bernhardt, E.; Willner, H.; Leito, I. *J. Org. Chem.* **2011**, *76*, 391-395; d) Trummal, A.; Rummel, A.; Lippmaa, E.; Koppel, I.; Koppel, I. A. *J. Phys. Chem. A* **2011**, *115*, 6641-6645.

[104] Die Gasphasen-Acidität entspricht der freien Gibbs-Energie der Reaktion HA → H^+ + A^- und trägt stets ein positives Vorzeichen. Eine Verbindung ist somit umso acider, je niedrigerer ihre Gasphasen-Acidität ist.

[105] Lias, S. G.; Bartmess, J. E.; Liebman, J. F.; Holmes, J. L.; Levin, R. D.; Mallard, G. W. *J. Phys. Chem. Ref. Data* **1988**, *17*, Suppl. 1, 861 pp..

[106] Viggiano, A. A.; Henchman, M. J.; Dale, F.; Deakyne, C. A,; Paulson, J. F. *J. Am. Chem. Soc.* ***1*992**, *114*, 4299-4306.

[107] Stoyanov, E. S.; Kim, K.-C.; Reed, C. A. *J. Phys. Chem. A* **2004**, *108*, 9310-9315.

[108] Takasu, K. *Synlett* **2009**, 1905-1914.

[109] Wabnitz, T. C.; Spencer, J. B. *Org. Lett.* **2003**, *5*, 2141-2144.

[110] Ryu, D. H.; Corey, E. J. *J. Am. Chem. Soc.* **2003**, *125*, 6388-6390.

[111] Zhang, L.; Kozmin, S. A. *J. Am. Chem. Soc.* **2004**, *126*, 10204-10205.

[112] Cheon, C. H.; Yamamoto, H. *Chem. Commun.* **2011**, *47*, 3043-3056.

[113] a) Antoniotti, S.; Dalla, V.; Duñach, E. *Angew. Chem.* **2010**, *122*, 8032-8060; *Ang. Chem. Int. Ed.* **2010**, *49*, 7860-7888; b) Gal, J.-F.; Iacobucci, C.; Monfardini, I.; Massi, L.; Duñach, E.; Olivero, S. *J. Phys. Org. Chem.* **2013**, *26*, 87-97.

[114] a) Brooke, G. M.; Burdon, J.; Stacey, M. ; Tatlow, J. C. *J. Chem. Soc.* **1960**, 1768-1771; b) Koppang, R. *Acta Chem. Scand.* **1971**, *25*, 3067-3071.

[115] a) Sundermeyer, J.; Linder, T. *PCT Int. Appl.* **2007**, WO 2007131498 A2 20071122; b) Linder, T.; Sundermeyer, J. *Chem. Commun.* **2009**, 2914-2916.

[116] a) Sundermeyer, J.; Roling, B.; Linder, T.; Froemling, T.; Huber, B. *Eur. Pat. Appl.* **2011**, EP 2314572 A1 20110427; b) Sundermeyer, J.; Roling, B.; Linder, T.; Huber, B.; Froemling, T. *PCT Int. Appl.* **2011**, WO 2011048152 A1 20110428; c) Huber, B.; Linder, T.; Hormann, K.; Frömling, T.; Sundermeyer, J.; Roling, B. *Z. Phys. Chem.* **2012**, *212*, 377-390.

[117] a) Plenio, H. *Chem. Rev.* **1997**, *97*, 3363-3384; b) Plenio, H. *ChemBioChem* **2004**, *5*, 650-655.

[118] Khvorost, A.; Shutov, P. L.; Harms, K.; Lorberth, J.; Sundermeyer, J.; Karlov, S. S.; Zaitseva, G. S. *Z. Anorg. Allg. Chem.* **2004**, *630*, 885-889.

[119] Yao, S.; Zhang, X.; Xiong, Y.; Schwarz, H.; Driess, M. *Organometallics* **2010**, *29*, 5353-5357.

[120] Click, D. R.; Scott, B. L.; Watkin, J. G. *Chem. Commun.* **1999**, 633-634.

[121] Giesbrecht, G. R.; Gordon, J. C.; Clark, D. L.; Hijar, C. A.; Scott, B. L.; Watkin, J. G. *Polyhedron* **2003**, *22*, 153-163.

[122] Peryshkov, D. V.; Schrock, R. R. *Organometallics* **2012**, *31*, 7278-7286.

[123] Yin, H.; Lewis, A. J.; Carroll, P.; Schelter, E. J. *Inorg. Chem.* **2013**, *52*, 8234-8243.

[124] Khvorost, A. *Dissertation*, Philipps-Universität Marburg, **2003**.

[125] Sorokin, D. A. *Dissertation*, Philipps-Universität Marburg, **2006**.

[126] Linder, T. *Dissertation*, Philipps-Universität Marburg, **2008**.

[127] Mallouk, T. E.; Rosenthal, G. L.; Müller, G.; Brusasco, R.; Bartlett, N. *Inorg. Chem.* **1984**, *23*, 3167-3173.

[128] Müller, L. O.; Himmel, D.; Stauffer, J.; Steinfeld, G.; Slattery, J.; Santiso-Quiñones, G.; Brecht, V.; Krossing, I. *Angew. Chem.* **2008**, *120*, 7772-7776; *Angew. Chem. Int. Ed.* **2008**, *47*, 7659-7663.

[129] Kraft, A.; Trapp, N.; Himmel, D.; Böhrer, H.; Schlüter, P.; Scherer, H.; Krossing, I. *Chem. Eur. J.* **2012**, *18*, 9371-9380.

[130] Timoshkin, A. Y.; Morokuma, K. *Phys. Chem. Chem. Phys.* **2012**, *14*, 14911-14916.

[131] Mück, L. A.; Timoshkin, A. Y.; Frenking, G. *Inorg. Chem.* **2012**, *51*, 640-646.

[132] Krossing, I.; Raabe, I. *Angew. Chem.* **2004**, *116*, 2116-2142; *Angew. Chem. Int. Ed.* **2004**, *43*, 2066-2090.

[133] Bihlmeier, A.; Gonsior, M.; Raabe, I.; Trapp, N.; Krossing, I. *Chem. Eur. J.* **2004**, *10*, 5041-5051.

[134] Li, J.; Schenk, C.; Winter, F.; Scherer, H.; Trapp, N.; Higelin, A.; Keller, S.; Pöttgen, R.; Krossing, I.; Jones, C. *Angew. Chem.* **2012**, *124*, 9695-9699 ; *Angew. Chem. Int. Ed.* **2012**, *51*, 9557-9561.

[135] a) Santiso-Quiñones, G.; Reisinger, A.; Slattery, J.; Krossing, I. *Chem. Commun.* **2007**, 5046-5048; b) Krossing, I.; Reisinger, A. *Angew. Chem.* **2003**, *115*, 5903-5906; *Angew. Chem. Int. Ed.* **2003**, *42*, 5725-5728; c) Reisinger, A.; Trapp, T.; Knapp, C.; Himmel, D.; Breher, F.; Rüegger, H.; Krossing, I. *Chem. Eur. J.* **2009**, *15*, 9505-9520; d) Schaefer, J.; Himmel, D.; Krossing, I. *Eur. J. Inorg. Chem.* **2013**, 2712-2717.

[136] Budanow, A.; Sinke, T.; Tillmann, J.; Bolte, M.; Wagner, M.; Lerner, H.-W. *Organometallics* **2012**, *31*, 7298-7301.

[137] Slattery, J. M.; Higelin, A.; Bayer, T.; Krossing, I. *Angew. Chem.* **2010**, *122*, 3297-3301; *Angew. Chem. Int. Ed.* **2010**, *49*, 3228-3231.

[138] Higelin, A.; Sachs, U.; Keller, S.; Krossing, I. *Chem. Eur. J.* **2012**, *18*, 10029-10034.

[139] Lehner, A. J.; Trapp, N.; Scherer, H.; Krossing, I. *Dalton Trans.* **2011**, *40*, 1448-1452.

[140] Krossing, I.; Brands, H.; Feuerhake, R.; Koenig, S. *J. Fluorine Chem.* **2001**, *112*, 83-90.

[141] Chen, X.; Ma, B.; Wang, X.; Yao, S.; Ni, L.; Zhou, Z.; Li, Y.; Huang, W.; Ma, J.; Zuo, J.; Wang, X. *Chem. Eur. J.* **2012**, *18*, 11828-11836.

[142] Gonsior, M.; Krossing, I. *Dalton Trans.* **2005**, *7*, 1203-1213.

[143] Köchner, T.; Trapp, N.; Engesser, T. A.; Lehner, A. J.; Röhr, C.; Riedel, S.; Knapp, C.; Scherer, H.; Krossing, I. *Angew. Chem.* **2011**, *124*, 11449-11452; *Angew. Chem. Int. Ed.* **2011**, *50*, 11253-11256.

[144] Kraft, A.; Beck, J.; Steinfeld, G.; Scherer, H.; Himmel, D.; Krossing, I. *Organometallics* **2012**, *31*, 7485-7491.

[145] Baal, E. *Bachelorarbeit*, Philipps-Universität Marburg, **2011**.

[146] Gesevicius, D. *Bachelorarbeit*, Philipps-Universität Marburg, **2012**.

[147] Weber, F. *Bachelorarbeit*, Philipps-Universität Marburg, **2012**.

[148] Scott, M. *Bachelorarbeit*, Philipps-Universität Marburg, **2012**.

[149] Moldrickx, J. *Bachelorarbeit*, Philipps-Universität Marburg, **2012**.

Anhang mit Manuskripten

Die sieben Manuskripte sind analog zur Reihenfolge im Abschnitt *Kumulativer Teil* angefügt. Die vier bereits online erschienenen Publikationen sind in ihrer Originalform dargestellt, wobei hierfür jeweils die Erlaubnis des Verlages eingeholt wurde. Publikation 2 wurde von der Zeitschrift *Chemistry - A European Journal* zur Veröffentlichung akzeptiert, ist jedoch noch nicht online erschienen. Im Anhang befindet sich die nach Begutachtung der Referees erneut eingereichte Version des Manuskripts im Templat der Zeitschrift. Das endgültige Layout der Publikation wird sich vermutlich von dem gezeigten unterscheiden. Die Manuskripte 6 und 7 sind noch nicht zu Veröffentlichung eingereicht.

1) „A New Synthetic Pathway to the Second and Third Generation of Superbasic Bisphosphazene Proton Sponges: The Run for the Best Chelating Ligand for a Proton“ Reprinted with permission from „Kögel, J. F.; Oelkers, B.; Kovačević, B.; Sundermeyer, J. *J. Am. Chem. Soc.* **2013**, *135*, 17768-17774.“ Copyright © 2013, American Chemical Society.

2) „Superbasic Alkyl-Substituted Bisphosphazene Proton Sponges - Synthesis, Structural Features, Thermodynamic and Kinetic Basicity, Nucleophilicity and Coordination Chemistry“ Reproduced from „Kögel, J. F.; Xie, X.; Baal, E.; Gesevicius, D.; Oelkers, B.; Kovačević, B.; Sundermeyer, J.; *Chem. Eur. J.* **2014**, *20*, 7670-7685.“ Copyright © 2014, John Wiley and Sons. License Number: 3414281011502

3) „Constrained Geometry Bisphosphazides derived from 1,8-Diazidonaphthalene – Synthesis, Spectroscopic Characteristics, Structural Features and Theoretical Investigations“ Reproduced from „Kögel, J. F.; Abacılar, N. C.; Weber, F.; Oelkers, B.; Harms, K.; Kovačević, B.; Sundermeyer, J. *Chem. Eur. J.* **2014**, *20*, 5994-6009.“ Copyright © 2014, John Wiley and Sons. License Number: 3360871023063

4) „Two C_2-Symmetric Chelating P_2-Bisphosphazene Superbases Connected *via* a Binaphthyl Backbone – Synthesis, Structural Features and Preparation of a Cationic Alkyl Aluminum Complex“ Reproduced from „Kögel, J. F.; Kneusels, N.-J.; Sundermeyer, J. *Chem. Commun.* **2014**, *50*, 4319-4321.“ with permission from The Royal Society of Chemistry.

5) „The New NH-Acid $HN(C_6F_5)(C(CF_3)_3)$ and its Crystalline and Volatile Alkaline and Earth Alkaline Metal Salts“ Reprinted with permission from „Kögel, J. F.; Finger, L. H.; Frank, N.; Sundermeyer, J. *Inorg. Chem.* **2014**, *53*, 3839-3846.“ Copyright © 2014, American Chemical Society.

6) „Fluoro- and Perfluoralkylsulfonyl-pentafluoroanilides: Synthesis and Characterization of New NH-Acids for Weakly Coordinating Anions and their Gas Phase and Solution Acidities“

7) „The New Lewis Superacid $Al[N(C_6F_5)_2]_3$ and its Higher Homolog $Ga[N(C_6F_5)_2]_3$ – Structural Features, Preparation of Lewis Acid-Base Adducts and Metallates and Theoretical Investigation of the Fluoride Ion Affinity in the Gas Phase“

JACS
JOURNAL OF THE AMERICAN CHEMICAL SOCIETY

Article

pubs.acs.org/JACS

A New Synthetic Pathway to the Second and Third Generation of Superbasic Bisphosphazene Proton Sponges: The Run for the Best Chelating Ligand for a Proton

Julius F. Kögel,[†] Benjamin Oelkers,[†] Borislav Kovačević,[‡] and Jörg Sundermeyer*[,†]

[†]Fachbereich Chemie, Philipps-Universität Marburg Hans-Meerwein-Straße, 35032 Marburg, Germany

[‡]Quantum Chemistry Group, Rudjer Bošković Institute, Bijenička c. 54, 10000 Zagreb-HR, Croatia

Supporting Information

ABSTRACT: We present the up to now strongest chelating neutral pincer ligand for the simplest electrophile of chemistry, the proton. Two novel bisphosphazene proton sponges, 1,8-bis(trispyrrolidinophosphazenyl)naphthalene (TPPN) and its higher homologue P_2-TPPN, were obtained via a Staudinger reaction and investigated concerning their structural features and basic properties by experimental and computational means. They exhibit experimental pK_{BH^+} values in acetonitrile of 32.3 and 42.1, respectively, exceeding the existing basicitiy record for proton sponges by more than 10 orders of magnitude. We show that Schwesinger's concept of homologization of phosphazene bases and Alder's concept of proton chelation in a constrained geometry regime of basic centers can be combined in the design of highly basic nonionic superbases of pincer type.

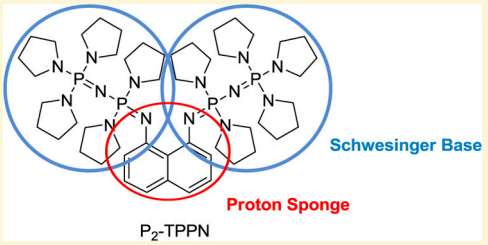

INTRODUCTION

Alder discovered the phenomenon of proton sponges in 1968, noticing the unexpectedly high basicity of 1,8-bis(dimethylamino)naphthalene (DMAN).[1] Such strong nonionic organic bases possess two basic nitrogen centers able to act as a chelate ligand for a proton which commonly is ligated in an asymmetric hydrogen bond N−H···N. The superior basicity compared to nonchelating bases can be due to the unfavorable situation in the proton sponge's free base form: the proximity of two nitrogen atoms leads to a repulsion of their lone pairs and distortion of the naphthalene backbone. Protonation is accompanied by strain relief and the formation of a favorable intramolecular hydrogen bridge. Proton sponges typically show a very low kinetic basicity which can be due to the hydrophobic shielding of the two basicity centers hindering another base from approaching this captured proton array. They have found various applications, such as as bases in organic synthesis,[2,3] as model compounds to study [N−H···N] hydrogen bridges,[4−7] as components of frustrated Lewis pairs for the activation of molecular hydrogen[8] or as a matrix in MALDI mass spectrometry.[9] Since Alder's discovery, the phenomenon of proton sponges has fascinated synthetically and theoretically oriented chemists and has been summarized in several reviews.[10−15] Classical DMAN has been modified in manifold ways to investigate the effects on basicity and chemical properties. Apart from the variation of the aromatic skeleton or the substituents at the basicity centers, superbases have been created by hybridizing the class of proton sponges with superbasic building blocks like guanidines,[16−19] amidines,[20] or phosphazenes (Figure 1).[21−25] Two representatives of the latter class with PPh_3 and PPh_2Me moieties were studied in their protonated forms but showed only moderate pK_{BH^+} values because of the electron-withdrawing effect of the aryl groups (15.6 in water for the triphenylphosphane-substituted compound). A tributyl-substituted analogue recently reported by Dries was not investigated for its basic features.[25] A vinamidine proton sponge reported by Schwesinger exhibits the highest pK_{BH^+} value for proton sponges so far (30.94 in MeCN).[20] It was suggested to use the term superbase for a neutral organic base exhibiting a gas phase basicity higher than 1000 kJ/mol

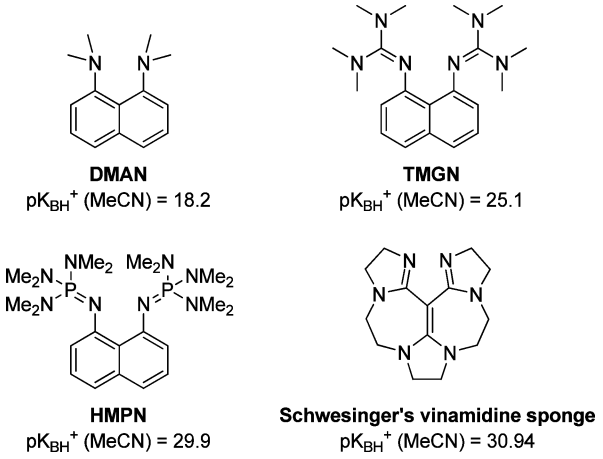

Figure 1. Alder's DMAN and three hybrid proton sponges bearing guanidine, phosphazene, or amidine moieties.

Received: June 13, 2013
Published: October 21, 2013

   dx.doi.org/10.1021/ja409760z | J. Am. Chem. Soc. 2013, 135, 17768−17774

Scheme 1. Synthesis of TPPN and P_2-TPPN via a Staudinger Reaction

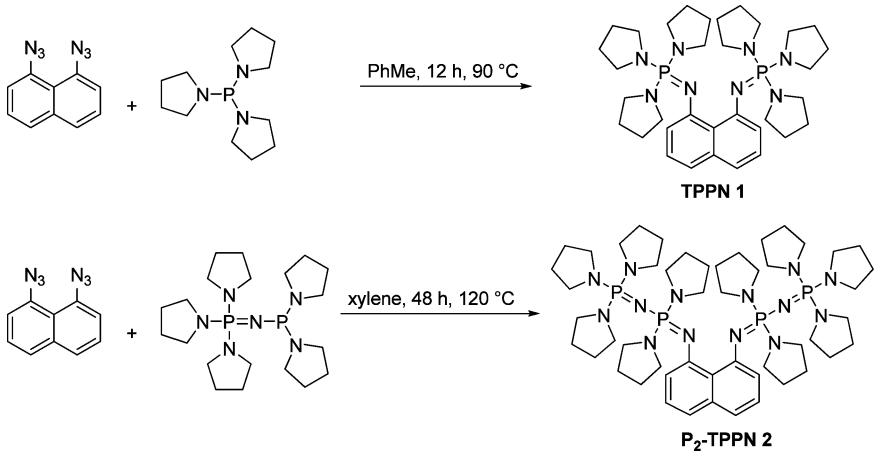

and a pK_{BH}^+ value (MeCN) higher than 25.[8] In this respect, the amidine DBU would not be a superbase, but pentamethylguanidine would mark the edge of superbasicity.

In 2005, we reported on the synthesis of the first superbasic bisphosphazene proton sponge 1,8-bis(hexamethyltriaminophosphazenyl)naphthalene (HMPN).[26] Adding the chelating effect of proton sponges to a classical phosphazene base led to a tremendous increase in basicity: by chelation, proton affinity in the gas phase rises from 250.5 kcal/mol for monodentate (dma)P_1-1-Naph (dma = NMe_2) to 274.1 kcal/mol for HMPN. As expected, an analogous rise is observed for the corresponding pK_{BH}^+ values which increase by more than 8 orders of magnitude from 21.25 for (dma)P_1-Ph[27] (pK_{BH}^+ has not been reported for the naphthalene derivative; it is 19.5 at a rough estimate)[28−30] to 29.9 for HMPN.

Aware of the fact that substituting the dimethylamino groups of a Schwesinger base for pyrrolidine moieties leads to a further growth of basicity, we identified 1,8-bis(tris(pyrrolidino)-phosphazenyl)naphthalene (**1**, TPPN) as a promising target compound whose pK_{BH}^+ could break the basicity record for proton sponges. Going deeper into Schwesinger's concept of phosphazene bases provoked us to perform a so-called homologization step: the formal insertion of further PN units into TPPN could lead to P_2-TPPN (**2**)—a compound with a pK_{BH}^+ value close to those of the strongest nonionic superbases known.

RESULTS

Since the scope of the Kirsanov route, which was used for the synthesis of HMPN, turned out to be limited due to the proximity of the basicity centers and sterically demanding only slightly electrophilic phosphonium synthons, a Staudinger reaction between 1,8-diazidonaphthalene and the corresponding phosphane was chosen as the key step for the synthesis of the new pincer ligands TPPN and P_2-TPPN (Scheme 1). Literature-known $P(pyr)_3$ (pyr = $N(CH_2)_4$)[31] was the reactant in the case of TPPN, and it could be converted to the homologous P_2 phosphane $(pyr)_3P{=}N{-}P(pyr)_2$ in a three-step procedure similar to the synthesis reported for the corresponding dimethylamino-substituted analogue.[32] The Staudinger reaction initially led to the formation of stable bisphosphazides [Ar−N═N−N═PR_3] that lost molecular nitrogen upon heating in toluene or xylene to give the desired bisphosphazene proton sponges.[33] Due to the greater steric demand and the stronger electron-donating nature of the P_2 bisphosphazide, a higher kinetic barrier for nitrogen abstraction was expected for the formation of P_2-TPPN. Thus, a higher temperature and a longer reaction time are required for bisphosphazene formation than in the case of TPPN. TPPN and P_2-TPPN were obtained in their protonated form by reaction with $HN(SO_2CF_3)_2$. The "acidic" protons exhibit chemical shifts of δ_H = 15.02 ppm for TPPN·$HN(SO_2CF_3)_2$ and 15.14 ppm in the case of P_2-TPPN·$HN(SO_2CF_3)_2$ in CD_3CN.

The molecular structures of the two bisphosphazene proton sponges in their free base forms are presented in Figures 2−4. They reveal the typical features of proton sponges: they exhibit long and nearly equal N−N distances (TPPN = 276.6(3) pm, P_2-TPPN = 276.3(2) pm) and a significant distortion of the naphthalene backbone (average twist: TPPN = 8.2(2)°, P_2-TPPN = 6.3(2)°) which can both be due to the repulsion of the nitrogen atoms' lone pairs. The two basicity centers are located slightly above and below the naphthalene plane because of the sterically demanding substituents. The molecular structures of TPPN and P_2-TPPN reveal considerable shorter nonbonding distances between the basicity centers than found in their parent compound HMPN (282.2(3) pm).[26] This indicates a higher energy content for TPPN in its initial free base form and is enforced by the sterically demanding pyrrolidine groups. Comparison with other proton sponges shows that the N−N distance is slightly shorter than in DMAN (279.2(3) pm)[34] and longer than observed for TMGN (271.7(4) pm)[16] or quino[7,8-*h*]quinoline (272.7(2) pm).[35]

Protonation is accompanied by a considerable shortening of the N···N distances from 276.6(3) to 260.0(6) and 262.5(5) pm in the two independent TPPN·$HN(SO_2CF_3)_2$ molecules found in the elementary cell and from 276.3(2) to 257.0(4) pm in the case of P_2-TPPN·$HN(SO_2CF_3)_2$. Similar or slightly shorter values for the corresponding nonbonding distance between the two basic nitrogen atoms have been reported for the monoprotonated forms of DMAN (between 255.3(5) and 265.4(2) pm),[12] HMPN (256.8(3) pm),[26] TMGN (259.3(5) pm),[16] or Schwesinger's vinamidine sponge (254.1(5) pm).[20] The acidic protons could be located on the Fourier map, revealing a hydrogen bond that is nonlinear; angle N11−H1−N12 in TPPN·$HN(SO_2CF_3)_2$ 141(2)°, in P_2-TPPN·$HN(SO_2CF_3)_2$ 146(4)° with unsymmetric NH distances: *d*(N11−H1) in TPPN·$HN(SO_2CF_3)_2$ 85(3) pm,[36] in P_2-TPPN·$HN(SO_2CF_3)_2$ 81(4) pm) (Figure 5).

dx.doi.org/10.1021/ja409760z | J. Am. Chem. Soc. 2013, 135, 17768−17774

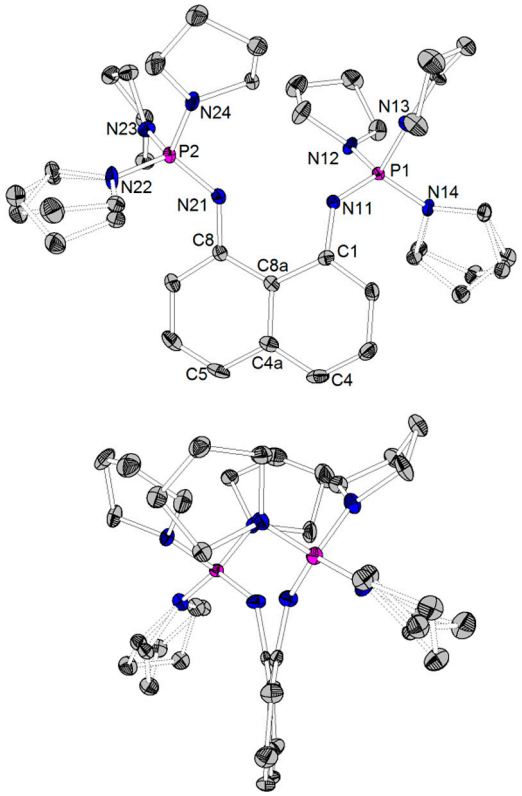

Figure 2. Molecular structure of TPPN (ellipsoids with 50% probability). Hydrogen atoms and the acetonitrile molecules are omitted for clarity. Selected bond lengths (pm) and angles (deg): N11···N12 276.6(3), N11–P1 155.0(2), P1–N12 165.1(2), P1–N13 164.2(2), P1–N14 165.0(2), N21–P2 155.3(2), P2–N22 164.4(2), P2–N23 164.1(2), P2–N24 163.7(2), C1–C8a–C4a–C5 −172.0(2), C8–C8a–C4a–C4 −171.7(2).

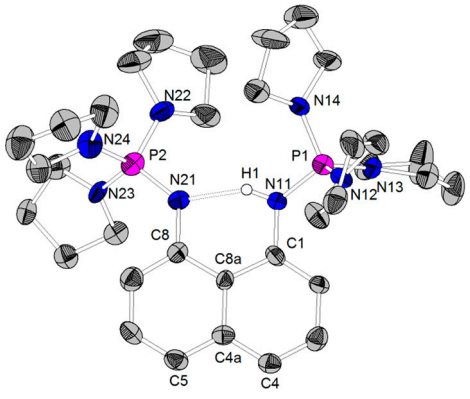

Figure 3. Molecular structure of TPPN·HN$(SO_2CF_3)_2$. Only one of two independent molecules in the asymmetric unit is shown. Carbon-bonded hydrogen atoms and the anion are omitted for clarity. Selected bond lengths (pm) and angles (deg): N11···N12 260.0(6), N11–H1 85(3), N21–H1 188(3), N11–P1 158.7(4), P1–N12 161.1(4), P1–N13 162.7(4), P1–N14 164.3(4), N21–P2 159.7(4), P2–N22 163.1(4), P2–N23 163.6(4), P2–N24 162.5(4), N11–H1–N21 141(2), C1–C8a–C4a–C5 174.3(4), C8–C8a–C4a–C4 175.6(4).

Relaxation of the naphthalene skeletons can be observed to some extent, but the aromatic backbones still exhibit a considerable distortion: average twist in TPPN·HN$(SO_2CF_3)_2$ is 5.1(4)°/2.6(4)°, and in P_2-TPPN·HN$(SO_2CF_3)_2$ it is

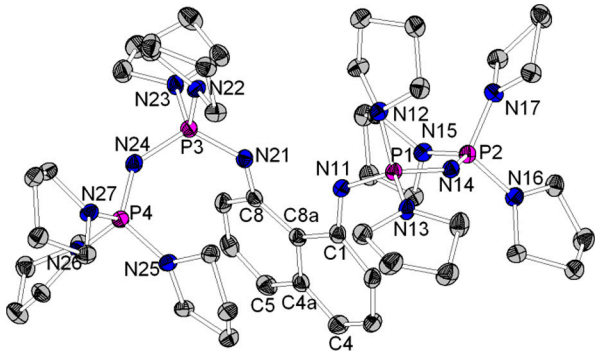

Figure 4. Molecular structure of P_2-TPPN (ellipsoids with 50% probability). Hydrogen atoms are omitted for clarity. Selected bond lengths (pm) and angles (deg): N11···N12 276.3(2), N11–P1 156.7(2), P1–N12 167.7(2), P1–N13 166.2(2), P1–N14 161.3(2), N14–P2 156.5(2), P2–N15 164.6(2), P2–N16 163.4(2), P2–N17 164.5(2), C1–C8a–C4a–C5 −173.7(2).

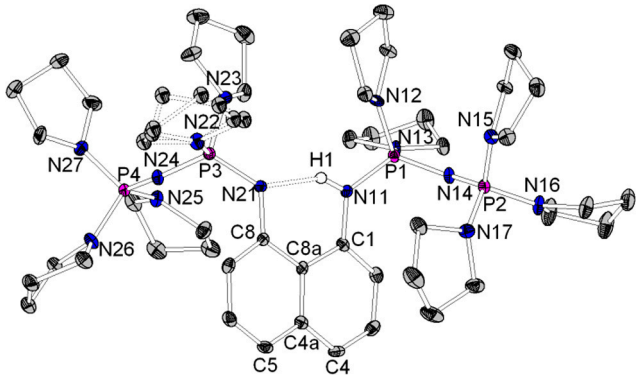

Figure 5. Molecular structure of P_2-TPPN·HN$(SO_2CF_3)_2$ (ellipsoids with 50% probability. Carbon-bonded hydrogen atoms and the anion are omitted for clarity. Selected bond lengths (pm) and angles (deg): N11···N12 257.0(4), N11–H1 81(4), N21–H1 185(4), N11–P1 162.3(3), P1–N12 164.4(2), P1–N13 163.3(2), P1–N14 158.6(2), N14–P2 156.3(2), N21–P3 161.0(2), P3–N22 163.8(2), P3–N23 166.3(2), P3–N24 158.4(2), N24–P4 155.4(2), N11–H1–N21 146(4), C1–C8a–C4a–C5 175.5(3), C8–C8a–C4a–C4 173.3(2).

5.6(3)°. Deviation from planarity can be explained by the bulky pyrrolidine substituents.

The pK_{BH}^+ values were determined via NMR titration experiments versus bases with a similar basicity. Compound (dma)P_2-*t*Bu (pK_{BH}^+ (MeCN) = 33.5)[37] was used in acetonitrile in the case of TPPN and P_2-TPPN competing with (dma)P_4-*t*Bu (pK_{BH}^+ (MeCN) = 42.7)[37] for protons in THF.[38] The titration experiments revealed pK_{BH}^+ values of 32.3 for TPPN and 42.1 for P_2-TPPN on the acetonitrile scale. For the evaluation of the effect of proton chelation on the basicity of P_2-TPPN, the "one-armed" analogue (pyr)P_2-1-Naph was synthesized via a Kirsanov reaction between 1-naphthylamine and the corresponding bromophosphonium bromide. NMR titration experiments revealed a pK_{BH}^+ value of around 26 on the acetonitrile scale.[39−41]

As already observed for HMPN, both TPPN and P_2-TPPN exhibit a very low kinetic basicity which was investigated via proton self-exchange experiments. Even at 100 °C, no coalescence but two separated sets of signals for the proton sponges in their free base form and their protonated form were observed in the ^1H and ^{31}P NMR spectra when dissolving both species in C_6D_5Br. TPPN turned out to be hydrolytically stable

dx.doi.org/10.1021/ja409760z | J. Am. Chem. Soc. 2013, 135, 17768−17774

and even remains intact after 24 h in 2 M aqueous NaOH at 70 °C.

THEORETICAL SECTION

The calculations were carried out utilizing the Gaussian 03[42] program package. The B3LYP/6-31G(d) method was used to obtain the most stable conformers in the gas phase. The frequency analysis was done at the same level of theory to confirm whether the structure is a minimum or a transition state on the potential energy surface. The structure optimizations were done without any symmetry constraints. However, the most stable conformer in both proton sponges (TPPN and P_2-TPPN) exhibits nearly C_2 symmetry. It turned out that in both sponges C_2 symmetry is lost upon protonation since the proton is attached to only one basic substituent. The C_2-symmetric protonated structure with the proton in the middle between the two basicity centers represents a first-order saddle point with one imaginary frequency that corresponds to the transfer of the proton between the two nitrogen atoms in both sponges. The energy barriers for the proton transfer calculated at the B3LYP/6-311+G(2df,p)//B3LYP/6-31G(d) + ZPVE(B3LYP/6-31G(d) level for TPPN and P_2-TPPN are 0.8 and 1.5 kcal mol^{-1}, respectively, indicating that both molecules can be classified as a sponge with localized proton motion.[43]

The gas phase proton affinities (PA) of TPPN and P_2-TPPN together with their monosubstituted analogues were calculated at the B3LYP/6-311+G(2df,p)//B3LYP/6-31G(d) level taking into account the thermal corrections estimated by the B3LYP/6-31G(d) method. They are presented in Table 1. The PA of P_2-TPPN is 298.0 kcal mol^{-1}, which is only 2 kcal mol^{-1} below the suggested threshold for hyperbasicity.[44] It is interesting that P_2-TPPN exhibits a slightly higher PA than the (dma)P_4-*t*Bu base (297.5 kcal mol^{-1}, calculated at the same level of theory).[45] The proton affinity of TPPN is 283.2 kcal mol^{-1}, thus being higher by 9.1 kcal mol^{-1} than the PA of its dimethylamino-substituted analogue HMPN (PA = 274.1 kcal mol^{-1}).[26] From where does this increase in the basicity of TPPN compared to HMPN come? Let us first consider the difference in the basicity of the basic substituents in TPPN and HMPN. The proton affinity of the $(pyr)_3P{=}NH$ moiety is 262.9 kcal mol^{-1}, which is by 6.0 kcal mol^{-1} higher than the PA of the $(dma)_3P{=}NH$ counterpart. To quantify the influence of the destabilization energy (E_d) in the neutral base and the energy of the intramolecular hydrogen bond (E_{IMHB}) in the conjugate acid, homodesmotic reactions were used analogously to the procedure applied in our previous paper[26] (see Supporting Information Figure S1). It appears that the destabilization energy due to a strain in neutral TPPN is 16.2 kcal mol^{-1}, which is 2.1 kcal mol^{-1} more than that calculated for HMPN. This finding supports the conclusion based on the experimental data for the distance between the basicity centers N(11) and N(21) that TPPN has a higher energy content in its initial base form than HMPN. However, the increase in energy is not substantial. The stabilization energy of the IMHB in TPPN's conjugate acid equals −9.9 kcal mol^{-1}, being 0.4 kcal mol^{-1} larger than in HMPN. The overall effect of the strain relief and the IMHB stabilization contributes to the PA of TPPN by 26.1 kcal mol^{-1}, which is by 2.5 kcal mol^{-1} larger than in HMPN where this contribution is 23.6 kcal mol^{-1}. It should be emphasized that the contribution from the strain relief and the formation of the IMHB corresponds to the difference between the PA of the proton sponge and its monosubstituted (one-armed) analogue, and it can be considered as a contribution from the chelating effect. To conclude, the higher PA of TPPN relative to HMPN is primarily caused by the higher basicity of $Pyr_3P{=}NH$ compared to the $(dma)_3P{=}NH$ fragment, whereas the contribution from the chelating effect is less pronounced. Now we will consider the proton affinity of P_2-TPPN, which is by 23.9 kcal mol^{-1} higher than the PA of HMPN and do the same type of analysis of energy contributions to the PA. The $(pyr)_3P{=}N{-}P(pyr)_2{=}NH$ moiety has a PA of 279.7 kcal mol^{-1}. This is by 22.8 kcal mol^{-1} higher than the PA of the $(dma)_3P{=}NH$ counterpart. Analysis by homodesmotic reactions reveals that the strain energy in neutral P_2-TPPN is 18.3 kcal mol^{-1}, whereas the energy of the IMHB stabilization in the conjugate acid equals −9.5 kcal mol^{-1}. Increase in strain energy is 2.1 kcal mol^{-1} compared to TPPN and 4.2 kcal mol^{-1} compared to HMPN. Consequently, P_2-TPPN has the highest energy content in its initial base form in this series. The stabilization due to the IMHB is exactly the same as in HMPN. The overall effect of strain relief and IMHB stabilization contributes to the PA of P_2-TPPN by 27.8 kcal mol^{-1}, which is by 4.2 kcal mol^{-1} higher than in HMPN. Therefore, the primary contribution to the PA of P_2-TPPN compared HMPN is the much higher proton affinity of $(pyr)_3P{=}N{-}P(pyr)_2{=}NH$ relative to the $(dma)_3P{=}NH$ fragment.

Theoretical calculations of the pK_{BH}^+ values in acetonitrile were performed using the isodensity polarized continuum model (IPCM; the procedure is described elsewhere).[45] The pK_{BH}^+ values for TPPN and P_2-TPPN, together with their monosubstituted (one-armed) analogues, are presented in Table 1. Most of them are in reasonable agreement with the experimental data with discrepancies being smaller than 0.7 pK_{BH}^+ units. P_2-TPPN is an exception: the difference between the experimental and the theoretical value is 1.9 units. Thus, the resultant disagreement deserves some rationalization. The gas phase PA of P_2-TPPN is by only 0.5 kcal mol^{-1} higher than in Schwesinger's (dma)P_4-*t*Bu superbase. However, the solvation effect should be less pronounced in P_2-TPPN due to the chelating effect (the proton is less exposed to the solvent molecules in P_2-TPPN than in (dma)P_4-*t*Bu). Consequently, the protonated form of P_2-TPPN is less stabilized by the solvent compared to protonated (dma)P_4-*t*Bu. That would lead to a lower pK_{BH}^+ for P_2-TPPN versus (dma)P_4-*t*Bu in acetonitrile. The same effect is observed for HMPN: it has a very similar gas phase PA as (dma)P_2-*t*Bu. However, the pK_{BH}^+ of HMPN is lower than the pK_{BH}^+ of (dma)P_2-*t*Bu by 4 units.[26] The experimental pK_{BH}^+ of P_2-TPPN is indeed lower than

Table 1. Theoretically Obtained Gas Phase Proton Affinities and pK_a Values of Proton Sponges, Their Monosubstituted Analogues and Corresponding Basic Fragments

molecule	PA	pK_{BH}^+
HMPN	274.1[26]	29.1[26]
TPPN	283.2	33.0
P_2-TPPN	298.0	40.2
(dma)P_1-1-Naph	250.5[26]	
(pyr)P_1-1-Naph	257.1	21.3
(pyr)P_2-1-Naph	270.2	26.4
$(dma)_3P{=}NH$	256.9[46]	25.7
$(pyr)_3P{=}NH$	263.0	26.9
$(pyr)_3P{=}NP(pyr)_2{=}NH$	279.7	32.8

dx.doi.org/10.1021/ja409760z | J. Am. Chem. Soc. 2013, 135, 17768−17774

Scheme 2. Stepwise Basicity Enhancement Finally Leading to P2-TPPN

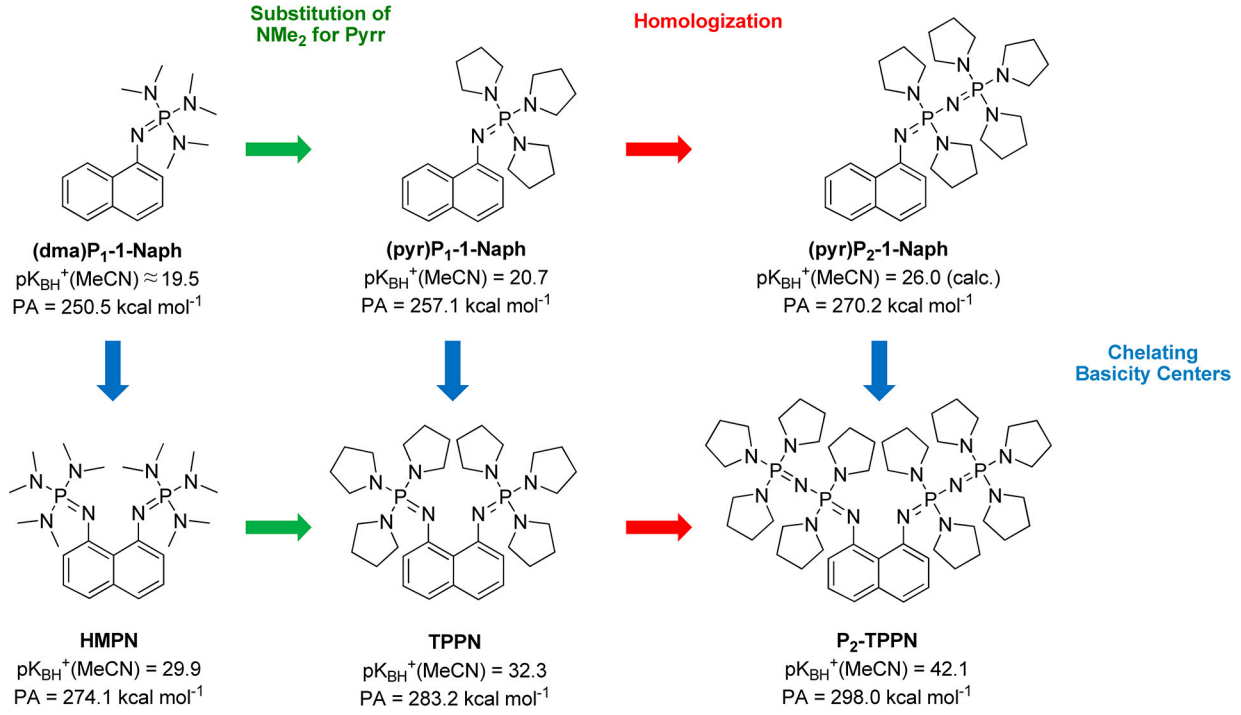

reported for (dma)P_4-*t*Bu, but the difference is only 0.7 units. Since the theoretical pK_{BH}^+ value for P_2-TPPN is by ~3 units smaller than the theoretical pK_{BH}^+ value for (dma)P_4-*t*Bu, it would be plausible to assume that the theoretical value is more realistic. However, it should be emphasized that the theoretical procedure for calculating the pK_{BH}^+ is based on the fitting between the experimental pK_{BH}^+ and theoretically obtained basicities in the corresponding solvent,[45] and there is a lack of experimental data for compounds with pK_{BH}^+ values in acetonitrile close to or above 40. Consequently, theoretically calculated values in that area of the basicity scale could be less accurate. Regardless of taking into account the theoretical or the experimental data, the estimated pK_{BH}^+ value above 40 makes P_2-TPPN by far the most basic proton sponge synthesized so far.

■ CONCLUSION AND OUTLOOK

Scheme 2 helps to rationalize the particular steps of designing P_2-TPPN and carves out the effects of its attributes on its pK_{BH}^+ value and its proton affinity in the gas phase starting from the simple Schwesinger base (dma)P_1-1-Naph: the substitution of dimethylamino groups for more basic pyrrolidine moieties only brings a minor basicity increase by about 1 order of magnitude in the case of the classical Schwesinger base (dma)P_1-1-Naph and a bit more than 2 orders of magnitude for the corresponding bisphosphazene HMPN. Comparison of the two proton sponges reported herein with classical nonchelating Schwesinger bases highlights the dramatic effect of both homologization and chelation: these two modifications each cause an increase in the pK_{BH}^+ value by more than 10 orders of magnitude. Proton chelation by a second phosphazene increases the pK_{BH}^+ value substantially by nearly 12 orders of magnitude in the case of (pyr)P_1-1-Naph. The influence of two interacting basicity centers becomes even more extreme when it comes to the higher homologue (pyr)P_2-1-Naph, which upon chelation is boosted to a pK_{BH}^+ value 16 orders of magnitude higher. Finally, it is worth mentioning that this pincer effect is much more pronounced in compounds in which the positive charge occurring after protonation is stabilized by means of negative hyperconjugation than in systems relying on conjugative effects. The bisguanidinyl proton sponge TMGN (Figure 1, pK_{BH}^+ (MeCN) = 25.1) is only by less than 5 orders of magnitude more basic than its one-armed analogue (pK_{BH}^+ (MeCN) (calcd) = 20.5).[46]

As a result, connecting two Schwesinger P_1 bases via a 1,8-disubstituted naphthalene backbone yields a bisphosphazene proton sponge with a basicity in the dimension of a classical P_2 base. The forced interaction of two P_2 bases even leads to a compound as basic as a Schwesinger P_4 base and catapults the basicity record of proton sponges into a new dimension: P_2-TPPN is by more than 10 orders of magnitude more basic than the hitherto most basic sponge. It is anticipated that in the future the strongest neutral organic bases will be gained by a combination of kinetic aspects of proton chelation with thermodynamic aspects of the intrinsic superbasicity of the chelating centers, thus overcoming the limits of higher generation monodentate phosphazene bases. We hope that the Staudinger reaction will give rise to more representatives of the class of bisphosphazene proton sponges with outstanding basic properties and to the investigation of their interesting nitrogen-rich bisphosphazide precursors.

■ EXPERIMENTAL SECTION

All reactions were carried out under inert atmosphere using standard Schlenk techniques. Moisture- and air-sensitive substances were stored in a conventional nitrogen-flushed glovebox. Solvents were purified according to literature procedures and kept under an inert atmosphere. 1,8-Diaminonaphthalene (Acros) was purified by recrystallization from toluene followed by sublimation and converted to 1,8-diazidonaphthalene via its diazonium salt.[47] Tris(pyrrolidino)phosphane was accessible by adding phosphorus trichloride to a solution of pyrrolidine in THF.[31] $HN(SO_2CF_3)_2$ was synthesized by protonation of the corresponding lithium salt.[48] The Schwesinger base P_2-*t*Bu used for

dx.doi.org/10.1021/ja409760z | J. Am. Chem. Soc. 2013, 135, 17768−17774

NMR titration experiments was purchased as 2 M solution in THF (Aldrich) and protonated with $HN(SO_2CF_3)_2$ in THF.

Spectra were recorded on the following spectrometers: NMR (Bruker ARX300, Bruker DRX400, Bruker DRX500); IR (ATR-FT-IR); MS (LTQ-FT or QStarPulsar i (finnigan)); elemental analysis (CHN-Rapid (Heraeus)).

Atoms are labeled from 1 to 8a in the naphthalene moiety and from 9 on in the alkyl groups. Labeling is described in detail in the Supporting Information.

1,8-Bis(trispyrrolidinophosphazenyl)naphthalene (TPPN, 1). Tris(pyrrolidino)phosphane (263 mg, 1.09 mmol) in toluene (10 mL) was added dropwise to a solution of 1,8-diazidonaphthalene (111 mg, 0.53 mmol) in the same solvent (10 mL). After 12 h of stirring at 90 °C, the light green solution had changed its color to brown and was evaporated to dryness. The brown residue was extracted with boiling hexane, and crystallization at −30 °C overnight yielded TPPN as a beige crystalline solid. Yield: 221 mg, 0.36 mmol, 68%. ^{1}H NMR (400.0 MHz, CD_3CN, 25 °C): δ = 6.85 (t, 2H, $^3J_{H-H}$ = 7.7 Hz, H(3,6)), 6.69 (d, 2H, $^3J_{H-H}$ = 7.7 Hz, H(4,5)), 6.34 (d, 2H, $^3J_{H-H}$ = 7.7 Hz, H(2,7)), 3.20 (m, 24H, H(9)), 1.76 (m, 24H, H(10)). $^{13}C\{^1H\}$ NMR (100.0 MHz, CD_3CN, 25 °C): δ = 153.2 (d, $^2J_{P-C}$ = 6.8 Hz, C(1,8)), 140.3 (t, $^3J_{P-C}$ = 12.7 Hz, C(4a)), 128.9 (C(8a)), 126.6 (C(3,6)), 117.2 (d, $^3J_{P-C}$ = 10.6 Hz, C(2,7)), 116.1 (C(4,5)), 48.3 (d, $^2J_{P-C}$ = 4.5 Hz, C(9)), 27.9 (d, $^3J_{P-C}$ = 8.2 Hz, C(10)). $^{31}P\{^1H\}$ NMR (121.5 MHz, CD_3CN, 25 °C): δ = 2.5. IR (cm^{-1}): $\tilde{\nu}$ = 3039 (w), 2957 (m), 2858 (m), 1544 (s), 1430 (s), 1383 (m), 1341 (m), 1290 (m), 1239 (w), 1195 (m), 1125 (s), 1065 (s), 1005 (s), 912 (w), 870 (w), 814 (m), 778 (w), 748 (s), 636 (w), 563 (s), 487 (m), 443 (w). MS (ESI, CH_3CN): $C_{34}H_{55}N_8P_2$ requires m/z 637.4019, accurate mass found 637.4025. MS (ESI, CH_3CN): m/z (%) = 637 (100) $[MH]^+$, 566 (3), 497 (3), 381 (1), 256 (1). Anal. Calcd (%) for $C_{34}H_{54}N_8P_2$ (636.79): C, 64.13; H, 8.55; N, 17.60. Found: C, 64.16; H, 8.42; N, 17.57.

Protonation of TPPN with $HN(SO_2CF_3)_2$ (1·$HN(SO_2CF_3)_2$). A solution of $HN(SO_2CF_3)_2$ (22 mg, 0.079 mmol) in THF (5 mL) was added dropwise to a solution of TPPN (50 mg, 0.079 mmol) in THF (5 mL). The pale blue solution was stirred for 1 h and evaporated to dryness. The gray residue was washed with hexane (20 mL) and dried in vacuo to give TPPN·$HN(SO_2CF_3)_2$ as a gray solid. Yield: 65 mg, 0.071 mmol, 90%. ^{1}H NMR (300.1 MHz, CD_3CN, 25 °C): δ = 15.02 (t, 1H, $^2J_{P-H}$ = 4.9 Hz, −NH), 7.17 (m, 4H, H(3,4,5,6)), 6.66 (t, 2H, $^3J_{H-H}$ = 4.0 Hz, H(2,7)), 3.26−3.21 (m, 24H, H(9)), 1.88−1.83 (m, 24H, H(10)). $^{13}C\{^1H\}$ NMR (100.6 MHz, THF-d_8, 25 °C): δ =144.2 (C(1,8)), 137.8 (C4a), 126.3 (CH_{Ar}), 120.9 (t, $^3J_{P-C}$ = 13.8 Hz, C(8a)) 120.8 (q, $^1J_{F-C}$ = 322.4 Hz, $-CF_3$), 120.1 (CH_{Ar}), 113.9 (d, $^3J_{P-C}$ = 7.2 Hz, C(2,7)), 48.0 (d, $^2J_{P-C}$ = 4.6 Hz, C(9)), 26.9 (d, $^3J_{P-C}$ = 8.2 Hz, C(10)). $^{19}F\{^1H\}$ NMR (282.4 MHz, CD_3CN, 25 °C): −81.0. $^{31}P\{^1H\}$ NMR (121.5 MHz, CD_3CN, 25 °C): δ = 18.1. IR (cm^{-1}): $\tilde{\nu}$ = 2966 (m), 2870 (m), 1608 (w), 1573 (m), 1513 (w), 1458 (w), 1410 (w), 1354 (w), 1335 (m), 1300 (m), 1259 (w), 1173 (s), 1129 (w), 1073 (s), 1050 (s), 1013 (s), 970 (w), 915 (w), 871 (w), 818 (m), 787 (w), 762 (m), 738 (w), 699 (w), 653 (w), 614 (m), 568 (m), 509 (m), 483 (w), 449 (w). MS (ESI, CH_3CN): $C_{34}H_{55}N_8P_2$ requires m/z 637.4019, accurate mass found 637.3995. MS (ESI, CH_3CN): m/z (%) = 637 (100) $[M]^+$. Anal. Calcd (%) for $C_{36}H_{55}F_6N_9O_4P_2S_2$ (917.32): C, 47.10; H, 6.04; N, 13.73; S, 6.99. Found: C, 47.04; H, 6.07; N, 13.88; S, 6.98.

1,8-Bis[tris(pyrrolidino)phosphazenylbis(pyrrolidino)-phosphazenyl]naphthalene (P_2-TPPN, 2). A solution of [tris-(pyrrolidino)phosphazenyl]bis(pyrrolidino)phosphane (629 mg, 1.475 mmol) in xylene (15 mL) was added dropwise to a solution of 1,8-diazidonaphthalene (148 mg, 0.702 mmol) in xylene (15 mL). The purple reaction mixture changed color to green and was stirred for 48 h at 120 °C. After evaporation of the solvent in vacuo, the green residue was washed twice with pentane (30 mL). P_2-TPPN (**2**) was obtained as a green solid. Yield: 383 mg, 0.380 mmol, 54%. ^{1}H NMR (400.0 MHz, THF-d_8, 25 °C): δ = 6.66 (t, 2H, $^3J_{H-H}$ = 7.6 Hz, H(3,6)), 6.43 (d, 2H, $^3J_{H-H}$ = 7.6 Hz, H(4,5)), 6.30 (d, 2H, $^3J_{H-H}$ = 7.6 Hz, H(2,7)), 3.40 (m, 8H, H(9)), 3.20 (m, 8H, H(9)), 2.97 (m, 24H, H(11)), 1.73 (m, 16H, H(10)), 1.55 (m, 24H, H(12)). $^{13}C\{^1H\}$ NMR (100.6 MHz, THF-d_8, 25 °C): δ = 155.0 (C(1,8)), 139.7 (C(4a)), 129.9 (t, $^3J_{C-P}$ = 23.8 Hz, C(8a)), 124.9 (C(3,6)), 114.9 (d, $^3J_{C-P}$ = 16.1 Hz, C(2,7)), 112.9 (C(4,5)), 47.7 (d, $^2J_{C-P}$ = 4.3 Hz, C(9)), 47.2 (d, $^2J_{C-P}$ = 4.7 Hz, C(11)), 27.4 (d, $^3J_{C-P}$ = 9.0 Hz, C(10)), 27.0 (d, $^3J_{C-P}$ = 8.4 Hz, C(10)). $^{31}P\{^1H\}$ NMR (121.5 MHz, THF-d_8, 25 °C): δ = 1.5 (d, $^2J_{P-P}$ = 41.7 Hz), 5.0 (d, $^2J_{P-P}$ = 41.7 Hz). MS (ESI, CH_3CN): $C_{50}H_{86}N_{14}P_4$ requires m/z 1007.6189, accurate mass found 1007.6183. MS (ESI, CH_3CN): m/z (%) = 1007 (100) $[M]^+$, 796 (23), 441 (8), 356 (28). Anal. Calcd (%) for $C_{50}H_{86}N_{14}P_4$ (1007.21): C, 59.62; H, 8.61; N, 19.47. Found: C, 59.32; H, 8.57; N, 19.48.

Protonation of P_2-TPPN with $HN(SO_2CF_3)_2$ (2·$HN(SO_2CF_3)_2$). A solution of $HN(SO_2CF_3)_2$ (28 mg, 0.099 mmol) in THF (10 mL) was added dropwise to a solution of P_2-TPPN (**2**) (100 mg, 0.099 mmol) in THF (10 mL) at 0 °C. The reaction mixture changed color from green to violet and was stirred at room temperature overnight. After evaporation of the solvent in vacuo, the residue was washed twice with diethylether (15 mL). P_2-TPPN·$HN(SO_2CF_3)_2$ was obtained as a pale violet solid. Yield: 79 mg, 0.061 mmol, 62%. ^{1}H NMR (300.1 MHz, CD_3CN, 25 °C): δ = 15.14 (br m, 1H, −NH), 7.05 (t, 2H, $^3J_{H-H}$ = 7.8 Hz, H(3,6)), 6.95 (d, 2H, $^3J_{H-H}$ = 7.8 Hz, H(4,5)), 6.67 (d, 2H, $^3J_{H-H}$ = 7.8 Hz, H(2,7)), 3.30 (br s, 8H, H(9)), 3.17 (br s, 8H, H(9)), 2.90 (br s, 24 H, H(11)), 1.85 (br s, 16H, H(10)), 1.55 (br s, 24H, H(12)). $^{13}C\{^1H\}$ NMR (125.8 MHz, CD_3CN, 25 °C): δ = 147.5 (C(1,8)), 137.6 (C(4a)), 126.3 (CH_{Ar}), 121.6 (t, $^3J_{P-C}$ = 13.3 Hz, C(8a)), 120.9 (q, $^1J_{F-C}$ = 320.7 Hz, CF_3), 117.7 (CH_{Ar}), 113.1 (d, $^3J_{P-C}$ = 9.5 Hz, C(2,7)), 47.3 (d, $^2J_{P-C}$ = 5.0 Hz, C(9, 11)), 27.1 (d, $^3J_{P-C}$ = 9.4 Hz, C(10)), 26.7 (d, $^3J_{P-C}$ = 8.7 Hz, C(12)). $^{31}P\{^1H\}$ NMR (121.5 MHz, CD_3CN, 25 °C): δ = 2.0 (d, $^2J_{P-P}$ = 53.7 Hz), −0.6 (d, $^2J_{P-P}$ = 53.7 Hz). $C_{50}H_{86}N_{14}P_4$ requires m/z 1007.6183, accurate mass found 1007.6153. MS (ESI, CH_3CN): m/z (%) = 1007 (100) $[M]^+$. Anal. Calcd (%) for $C_{52}H_{87}F_6N_{15}O_4P_4S_2$ (1288.36): C, 48.48; H, 6.81; N, 16.31; S, 4.98. Found: C, 47.92; H, 6.74; N, 15.90; S, 4.91.

■ ASSOCIATED CONTENT

Ⓢ Supporting Information

Synthetic procedures, crystallographic and computational data, and NMR titration experiments. This material is available free of charge via the Internet at http://pubs.acs.org.

■ AUTHOR INFORMATION

Corresponding Author

jsu@staff.uni-marburg.de

Notes

The authors declare no competing financial interest.

■ ACKNOWLEDGMENTS

We thank Fabian Schröder and Lars Finger for their valuable support with crystal structure refinement. Financial support by the Fonds der Chemischen Industrie (doctoral scholarship for J.K.) is gratefully acknowledged.

■ DEDICATION

This paper is dedicated to the memory of Prof. Zvonimir B. Maksić who recently passed away.

■ REFERENCES

(1) Bowman, P. S.; Steele, W. R. S.; Winterman, D. R.; Alder, R. W. *Chem. Commun.* **1968**, 723−724.

(2) Nagasawa, K. Related Organocatalysts (1): A Proton Sponge. In *Superbases for Organic Synthesis: Guanidines, Amidines and Phosphazenes and Related Organocatalysts*; Ishikawa, T., Ed.; John Wiley & Sons, Ltd.: Chichester, UK, 2009; pp 251−271 and references cited therein.

(3) Denmark, S. E.; Beutner, G. L. *Angew. Chem.* **2008**, *120*, 1584−1663; *Angew. Chem,. Int. Ed.* **2008**, *47*, 1560−1638.

(4) Kovačević, B.; Maksić, Z. B.; Vianello, R.; Primorac, M. *New J. Chem.* **2002**, *26*, 1329−1334.
(5) Bachrach, S. M. *Org. Lett.* **2012**, *14*, 5598−5061.
(6) Pietrzak, M.; Wehling, J. P.; Kong, S.; Tolstoy, P. M.; Shenderovich, I. G.; Lopez, C.; Claramunt, R. M.; Elguero, J.; Denisov, G. S.; Limbach, H. *Chem.—Eur. J.* **2010**, *16*, 1679−1690.
(7) Ozeryanskii, V. A.; Pozharskii, A. F.; Bienko, A. J.; Sawka-Dobrowolska, W.; Sobczyk, L. *J. Phys. Chem. A* **2005**, *109*, 1637−1642.
(8) Abacılar, N. C.; Raab, V.; Gaoutchenova, E.; Garrelts, U.; Harms, K.; Sundermeyer, J. In *The Chemistry of Superbasic Guanidines in Activating Unreactive Substrates, The Role of Secondary Interactions*; Bolm, C., Hahn, F. E., Eds.; Wiley-VCH: Weinheim, Germany, 2009; pp 17−37.
(9) Zhang, S.; Yao, Z.-P. *Anal. Chim. Acta* **2012**, *711*, 77−82.
(10) Staab, H. A.; Saupe, T. *Angew. Chem.* **1988**, *100*, 895−909; *Angew. Chem., Int. Ed. Engl.* **1988**, *27*, 865−879.
(11) Alder, R. W. *Chem. Rev.* **1989**, *89*, 1215−1223.
(12) Lamas-Saiz, A. L.; Foces-Foces, C.; Elguero, J. *J. Mol. Struct.* **1994**, *328*, 297−323.
(13) Pozharskii, A. F. *Russ. Chem. Rev.* **1998**, *67*, 1−24.
(14) Chambron, J.; Meyer, M. *Chem. Soc. Rev.* **2009**, *38*, 1663−1673.
(15) Pozharskii, A. F.; Ozeryanskii, V. A.; Filatova, E. A. *Chem. Heterocycl. Compd.* **2012**, *48*, 200−219.
(16) Raab, V.; Kipke, J.; Gschwind, R. M.; Sundermeyer, J. *Chem.—Eur. J.* **2002**, *8*, 1682−1693.
(17) Raab, V.; Harms, K.; Sundermeyer, J.; Kovačević, B.; Maksić, Z. B. *J. Org. Chem.* **2003**, *68*, 8790−8797.
(18) Peters, A.; Kaifer, E.; Himmel, H.-J. *Eur. J. Org. Chem.* **2008**, 5907−5914.
(19) Wiesner, S.; Ziesak, A.; Reinmuth, M.; Walter, P.; Kaifer, E.; Wadepohl, H.; Himmel, H.-J. *Eur. J. Inorg. Chem.* **2013**, *52*, 163−171.
(20) Schwesinger, R.; Schlemper, H. *Angew. Chem.* **1987**, *99*, 1212−1214; *Angew. Chem., Int. Ed. Engl.* **1987**, *26*, 1212−1214.
(21) Llamas-Saiz, A. L.; Foces-Foces, C.; Molina, P.; Alajarin, M.; Vidal, A.; Claramunt, R. M.; Elguero, J. *J. Chem. Soc., Perkin Trans. 2* **1991**, *7*, 1025−1031.
(22) Llamas-Saiz, A. L.; Foces-Foces, C.; Elguero, J.; Molina, P.; Alajarin, M.; Vidal, A. *J. Chem. Soc., Perkin Trans. 2* **1991**, *11*, 1667−1676.
(23) Llamas-Saiz, A. L.; Foces-Foces, C.; Elguero, J.; Molina, P.; Alajarin, M.; Vidal, A. *J. Chem. Soc., Perkin Trans. 2* **1991**, *12*, 2033−2040.
(24) Laynez, J.; Menendez, M.; Saiz Velasco, J. L.; Llamas-Saiz, A. L.; Foces-Foces, C.; Elguero, J.; Molina, P.; Alajarin, M.; Vidal, A. *J. Chem. Soc., Perkin Trans. 2* **1993**, *4*, 709−713.
(25) Xiong, Y.; Yao, S.; Inoue, S.; Irran, E.; Driess, M. *Angew. Chem.* **2012**, *124*, 10221−10224; *Angew. Chem., Int. Ed.* **2012**, *51*, 10074−10077.
(26) Raab, V.; Gauchenova, E.; Merkoulov, A.; Harms, K.; Sundermeyer, J.; Kovačević, B.; Maksić, Z. B. *J. Am. Chem. Soc.* **2005**, *127*, 15738−15743.
(27) Sooväli, L.; Rodima, T.; Kaljurand, I.; Kütt, A.; Koppel, I. A.; Leito, I. *Org. Biomol. Chem.* **2006**, *4*, 2100−2105.
(28) The pK_{BH^+} value of (dma)P_1-1-Naph in MeCN was roughly estimated by subtracting the difference of the pK_{BH^+} values of (pyr)P_1-1-Naph (pK_{BH^+} (MeCN) = 20.61, ref 29) and (pyr)P_1-Ph (pK_{BH^+} (MeCN) = 22.34, ref 30) from the pK_{BH^+} of (dma)P_1-Ph (pK_{BH^+} (MeCN) = 21.25, ref 29).
(29) Kaljurand, I.; Kütt, A.; Sooväli, L.; Rodima, T.; Mäemets, V.; Leito, I.; Koppel, I. A. *J. Org. Chem.* **2005**, *70*, 1019−1028.
(30) Sooväli, L.; Rodima, T.; Kaljurand, I.; Kütt, A.; Koppel, I. A.; Leito, I. *Org. Biomol. Chem.* **2006**, *4*, 2100−2105.
(31) Dellinger, D. J.; Sheehan, D. M.; Christensen, N. K.; Lindberg, J. G.; Caruthers, M. H. *J. Am. Chem. Soc.* **2003**, *125*, 940−950.
(32) Marchenko, A. P.; Koidan, G. N.; Pinchuk, A. M.; Kursanov, A. V. *Zh. Obshch. Khim.* **1983**, *54*, 1774−1782.
(33) These stable bisphosphazides could be isolated and will be discussed in a publication that is currently in preparation.
(34) Einspahr, H.; Robert, J. B.; Marsh, R. E.; Roberts, J. D. *Acta Crystallogr., Sect. B* **1973**, *29*, 1611−1617.
(35) Zirnstein, M. A.; Staab, H. A. *Angew. Chem.* **1987**, *99*, 460−461; *Angew. Chem., Int. Ed. Engl.* **1987**, *26*, 460−461.
(36) In the case of TPPN·HN$(SO_2CF_3)_2$, the NH distance was restrained at 85 pm using the DFIX command.
(37) Schwesinger, R.; Schlemper, H.; Hasenfratz, C.; Willaredt, J.; Dambacher, T.; Breuer, T.; Ottaway, C.; Fletschinger, M.; Boele, J.; Fritz, H.; Putzas, D.; Rotter, H. W.; Brodwell, F. G.; Satish, A. V.; Ji, G.; Peters, E.; Peters, K.; von Schnering, H. G.; Walz, L. *Liebigs Ann. Chem.* **1996**, *7*, 1055−1081.
(38) Switching from acetonitrile to THF was necessary because of P_2-TPPN's high basicity. Schwesinger also used THF for pK_{BH^+} determination for P_3 bases and their higher homologues. We assumed linearity between the basicity scales in acetonitrile and THF in all cases.
(39) NMR titration experiments were performed in THF since (pyr)P_2-1-Naph is insoluble in acetonitrile. (pyr)P_2-1-Naph is able to partly deprotonate TMGN (pK_{BH^+} (MeCN) = 25.1, ref 16), but no deprotonation of (dma)P_1-^{t}Bu·HPF_6 (pK_{BH^+} (MeCN) = 26.88, ref 40) is observed. A pK_{BH^+} value around 26 on the acetonitrile scale is in good accordance with the value found for (pyr)P_2-Ph (pK_{BH^+} (MeCN) = 27.55, ref 41) that should be a bit more basic than its naphthalene analogue. A more exact experimental determination of the pK_{BH^+} value was prevented by signal overlay and signal broadening because of proton exchange processes. A pK_{BH^+} of 26.0 was determined computationally (vide infra).
(40) Schwesinger, R.; Willaredt, J.; Schlemper, H.; Keller, M.; Schmitt, D.; Fritz, H. *Chem. Ber.* **1994**, *127*, 2435−2454.
(41) Eckert-Maksic, M.; Glasovac, Z.; Trošelj, P.; Kütt, A.; Rodima, T.; Koppel, I.; Koppel, I. A. *Eur. J. Org. Chem.* **2008**, 5176−5184.
(42) Frisch, M. J.; et al. *Gaussian 03*, revision E.01; Gaussian Inc.:Wallingford, CT, 2004.
(43) Horbatenko, Y.; Vyboishchikov, S. F. *ChemPhysChem* **2011**, *12*, 1118−1129.
(44) Maksić, Z. B.; Kovačević, B.; Vianello, R. *Chem. Rev.* **2012**, *112*, 5240−5270.
(45) Kovačević, B.; Baric, D.; Maksić, Z. B. *New J. Chem.* **2004**, *28*, 284−288.
(46) Kovačević, B.; Maksić, Z. B. *Chem.—Eur. J.* **2002**, *8*, 1694−1702.
(47) Hoffmann, R. W.; Guhn, G.; Preiss, M. *J. Chem. Soc. C* **1969**, *5*, 769−772.
(48) Desmateau, D. D.; Witz, M. *J. Fluorine Chem.* **1991**, *52*, 7−12.

ChemPubSoc Europe

DOI: 10.1002/chem.201402226

CHEMISTRY A European Journal Full Paper

Phosphazenes

Superbasic Alkyl-Substituted Bisphosphazene Proton Sponges: Synthesis, Structural Features, Thermodynamic and Kinetic Basicity, Nucleophilicity and Coordination Chemistry

Julius F. Kögel,[a] Xiulan Xie,[a] Eduard Baal,[a] Donatas Gesevičius,[a] Benjamin Oelkers,[a] Borislav Kovačević,[b] and Jörg Sundermeyer*[a]

Dedicated to Professor Helmut Werner, Würzburg, on the occasion of his 80th birthday

Abstract: Herein we describe an easily accessible class of superbasic proton sponges based on the 1,8-bisphosphazenylnaphthalene (PN) proton pincer motif and P-alkyl substituents ranging from methyl (TMPN) to *n*-butyl (TBPN), isopropyl (TiPrPN) and cyclopentyl (TcyPPN). These neutral bases with a pK_{BH}^{+} value (MeCN) of ~30 were accessible via a Kirsanov condensation using commercially available 1,8-diaminonaphthalene, and in case of TMPN and TBPN, simple one-pot procedures starting from trisalkylphosphanes can be performed. Furthermore, the known pyrrolidinyl-substituted superbase TPPN previously synthesized via a Staudinger reaction could also be prepared by the Kirsanov strategy allowing its preparation in a larger scale. The four alkyl-substituted proton sponges were structurally characterized in their protonated form; molecular XRD structures were also obtained for unprotonated TiPrPN and TcyPPN. Moreover, we present a detailed description of spectroscopic features of chelating bisphosphazenes including TPPN and its hyperbasic homologue P_2-TPPN on which we reported recently. The four alkyl-substituted superbases were investigated with respect to their basic features by computational means and by NMR titration experiments revealing unexpectedly high experimental pK_{BH}^{+} values in acetonitrile between 29.3 for TMPN and 30.9 for TBPN. Besides their thermodynamic basicity, we exemplarily studied the kinetic basicity of TMPN and TPPN by means of NMR-spectroscopic methods. Furthermore, the competing nucleophilic versus basic properties were examined by reacting the proton sponges with ethyl iodide. Insight into the coordination chemistry of chelating superbases was provided by reacting TMPN with trimethylaluminum and trimethylgallium to give cationic complexes of Group XIII metal alkyls that were structurally characterized.

Introduction

The first proton sponge was discovered in the late 1960s by Alder, who noticed the unexpectedly high basicity of 1,8-bis(dimethylamino)naphthalene (DMAN).[1] DMAN exhibits a pK_{BH}^{+} value of 12.34 in water and surprisingly outnumbers the corresponding values of other aromatic amines such as *N*,*N*-dimethylaniline ($pK_{BH}^{+}(H_2O) = 5.06$)[2] or the non-alkylated analog 1,8-diaminonaphthalene ($pK_{BH}^{+}(H_2O) = 4.61$)[1] by more than seven orders of magnitude. Successive methylation of the latter compound lead to an abrupt rise in basicity after introduction of the fourth alkyl group. This phenomenon originates from the spatial proximity of the two basicity centers in *peri*-position and the repulsion of their lone pairs leading to the unfavorable distortion of the naphthalene backbone in the proton sponge's free base form. The situation changes after protonation: An intramolecular hydrogen bridge is formed allowing relaxation of the aromatic spacer. The term proton sponge can be referred to the low kinetic basicity of most representatives of this class. The hydrophobic shielding of the basicity centers provided by DMAN's alkyl groups causes a very low proton self-exchange rate which limits the proton sponges' potential to act as bases in catalytic applications.

Naphthalene-based proton sponges, in particular the commercially available 1,8-dimethylamino and tetramethy-guanidino derivatives, DMAN and TMGN, have found various applications as versatile nonionic bases in organic synthesis.[3–8] Furthermore, they are interesting model compounds for the experimental and theoretical investigation of proton exchange barriers and the geometry of [N-H···N] hydrogen bonds that play an important role in biological systems.[9] The combination of proton sponges with strong Lewis acids leads to frustrated Lewis pairs which are able to activate molecular hydrogen by heterolytic cleavage.[10] Guanidinyl-substituted proton sponges

[a] J. F. Kögel, Dr. X. Xie, E. Baal, D. Gesevičius, Dr. B. Oelkers, Prof. Dr. J. Sundermeyer
Fachbereich Chemie
Philipps-Universität Marburg
Hans-Meerwein-Straße, 35032 Marburg (Germany)
Fax: (+49) 642128-25711
E-mail: jsu@staff.uni-marburg.de

[b] Dr. B. Kovačević
Quantum Chemistry Group
Rudjer Bošković Institute
Bijenička c. 54, 10000 Zagreb (Croatia)

Supporting information for this article is available on the WWW under http://dx.doi.org/10.1002/chem.201402226.

can act as chelate ligands for main group and transition metals.[11] For DMAN various additional applications are known such as the use as a matrix in MALDI mass spectrometry,[12] as a solid-phase extractor for perfluoroalkyl sulfonates after immobilization on silica particles,[13] as a membrane in fuel cells[14] or as an antioxidant in lubricants.[15]

Having understood the nature of DMAN's high basicity, a large number of synthetic chemists have been engaged in the modification of Alder's classical proton sponge to further enhance its pK_{BH^+} value. One strategy is the attachment of electron-donating substituents to the naphthalene backbone. The so-called buttressing effect describes the substitution of the 2- and 7-position by preferably electron-rich and bulky groups further destabilizing the unprotonated proton sponge by enforcing an even stronger repulsion of the nitrogen atoms' lone pairs.[16] Another possible modification of naphthalene-based proton sponges is the variation of the substituents at the basicity centers. Besides the replacement of DMAN's methyl groups by numerous different alkyl substituents,[17–19] the nitrogen atoms have been integrated in an aromatic system as for instance shown in Staab's quino[7,8*h*]quinoline.[20] This structure motive was recently further modified by Shaffer et al.[21] Apart from varying the substituents of DMAN, several proton-chelating compounds with backbones other than naphthalene have been synthesized. The interaction of two basicity centers has also been achieved by aromatic spacers such as fluorene,[22] heterofluorene,[23] phenantrene,[24] biphenyl[25] or helicene[26] moieties. Potáček et al. reported on the preparation of caged proton sponges with a non-aromatic skeleton.[27] Recently, the basicity of macrocyclic amino compounds with interacting basicity centers was studied theoretically and experimentally.[28] Examples for literature known proton sponges are shown in Figure 1.

Whereas modifications at DMAN's aromatic backbone or the replacement of the methyl groups at the basicity centers by other alkyl substituents only lead to minor increases in the pK_{BH^+} value, an enormous basicity enhancement can be achieved by combining Alder's concept of interacting basicity centers with other building blocks with a high intrinsic basicity. A naphthalene-based proton sponge bearing two cyclopropeniminyl moieties was reported by Belding and Dudding quite recently.[29] The—for a long time—most basic proton sponge (pK_{BH^+}(MeCN) = 31.94) was a vinamidine compound reported by Schwesinger et al. bearing two interacting amidine units and exhibiting a high kinetic basicity.[30] Further proton sponges with a high proton self-exchange rate calling for application as proton transfer catalysts have been prepared in our group by connecting two guanidinyl moieties via a 1,8-disubstituted naphthalene skeleton.[31] Among them is the commercially available 1,8-bis(tetramethyl-guanidinyl)naphthalene (TMGN) (Figure 2). Such compounds have been further investigated by Himmel et al. concerning their coordination chemistry and electrochemical behavior.[11c—e] The combination of Alder's proton sponges with Schwesinger's concept of superbasic phosphazene bases[32] was achieved in 1,8-bis(hexamethyltriaminophosphazenyl)naphthalene (HMPN) which shows a pK_{BH^+} value of 29.9 in acetonitrile.[33] Recently, we have reported on the preparation of the two bisphosphazene proton sponges TPPN and its higher homologue P_2-TPPN via a Staudinger reaction.[34] The latter compound is the most basic representative of the class of proton sponges with a pK_{BH^+} value of 42.1 on the acetonitrile scale. Synthetic and computational efforts in the area of proton sponges and superbases in general have been summarized in several review articles by Staab, Alder, Llamas–Saiz, Maksić, Pozharskii, Chambron and Ishikawa.[3,35]

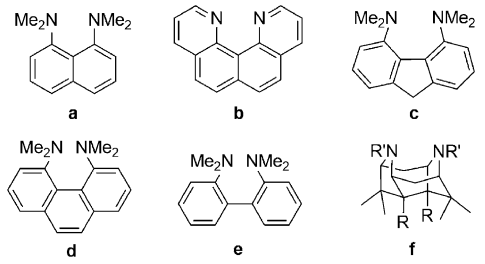

Figure 1. Alder's proton sponge DMAN (a) [1]and aromatic sponges with quino[7,8-*h*]quinoline (b),[20] fluorene (c),[22] phenantrene (d)[24] and biphenyl (e)[25] backbones as well as a proton sponge with a non-aromatic skeleton.[27]

Naphthalene-based bisphosphazene proton sponges with alkyl or aryl substituents at the phosphorus atoms that are the main topic of this publication were reported by Llamas–Saiz et al. in the early 1990s for the first time. Two representatives bearing PPh_3 and PPh_2Me moieties were characterized in their protonated forms, but exhibited only a moderate pK_{BH^+} value of 15.6 in water in case of the triphenylphosphane-substituted species due to the electron-withdrawing effect of the aryl substituents.[36] 1,8-Bis[tributylphosphazenyl]naphthalene (TBPN) that is also treated herein first appeared in literature in 2008, but apparently its protonated form was obtained and mistaken for the free base.[37] A preliminary communication on the syn-

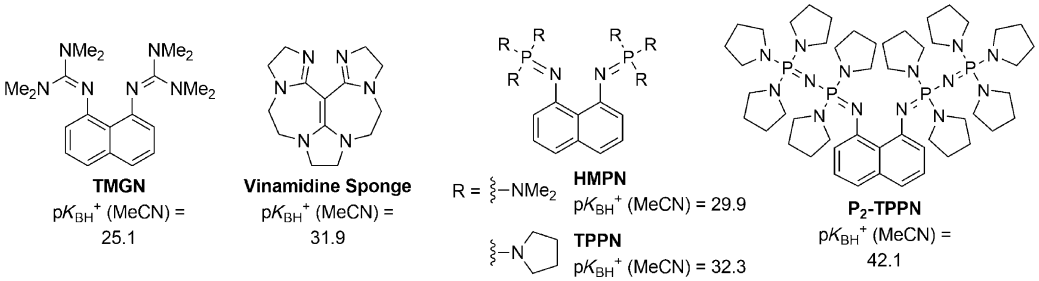

Figure 2. Hybrid superbases with guanidine,[31a] amidine[30] and phosphazene moieties.[33,34]

thesis and properties of TBPN and other members of this class of superbases appeared in 2011.[38] Recently, Driess et al. published the synthesis of TBPN using it for the stabilization of silyliumylidene $[ClSi:]^+$ and the silathionium $[ClSi{=}S]^+$ cations.[39]

Results and Discussion

Synthesis

The Staudinger[40] and the Kirsanov reaction[41] are the two most prominent synthetic tools for the formation of phosphorus nitrogen double or zwitterionic bonds of phosphazenes. Recently, we reported the synthesis of TPPN and P_2-TPPN via a Staudinger reaction,[34] but the general synthetic use of this procedure is not only limited by the surprisingly high stability of the initially formed bisphosphazides,[42] but also by the application of 1,8-diazidonaphthalene which is difficult to synthesize and can only be obtained in small quantities. In contrast, the Kirsanov reaction makes use of cheap commercially available 1,8-diaminonaphthalene. However, the scope of this strategy turned out to be limited by the spatial proximity of the two amino groups in 1,8-diaminonaphthalene: Whereas the Kirsanov reaction proceeds readily for simple aromatic amines such as aniline,[43] the synthesis of HMPN required extensive optimization of the reaction conditions and the proton sponge was only obtained in a moderate yield of 43%. Another drawback of the Kirsanov reaction is that the desired superbase is obtained in its protonated form and the free base has to be liberated in another reaction step. This can be difficult not only due to the high thermodynamic basicity, but especially because of the hydrophobic shielding of the acidic proton that is caught in a stable N-H···N hydrogen bridge. Hence, the Kirsanov reaction turned out to be unsuitable for most amino-substituted phosphorous compounds in the course of our investigations, but it was successful for the synthesis of the four alkyl-substituted bisphosphazene proton sponges presented herein.

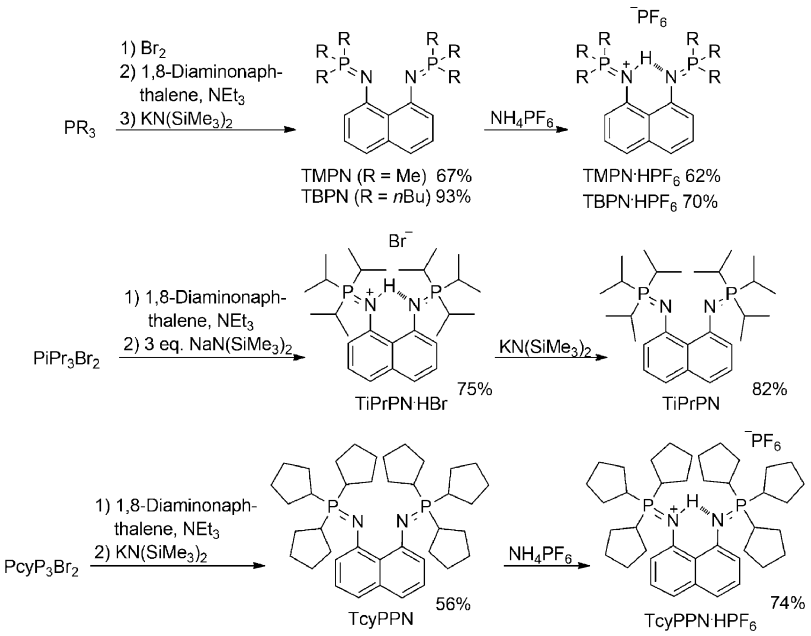

Scheme 1. Preparation of TMPN, TBPN; TiPrPN and TcyPPN via the Kirsanov reaction.

The preparation of TMPN and TBPN (Scheme 1) proceeded readily in simple one-pot procedures starting from the corresponding phosphanes which were oxidized in situ by bromine in an aromatic solvent. Subsequently, a solution of 1,8-diaminonaphthalene and triethylamine was added at room temperature and the heterogeneous reaction mixtures were stirred upon heating. Triethylamine acted as an auxiliary base quenching liberated hydrogen bromide, but of course it is not basic enough to deprotonate the HBr salts of the proton sponges. The free bases of TMPN and TBPN were liberated by addition of $KN(SiMe_3)_2$. Their protonated forms were prepared in separate steps by reaction with NH_4PF_6.

Attempts to obtain TiPrPN via a one-pot procedure resulted in incomplete conversion and the formation of several side products which were detected via ^{31}P NMR spectroscopy of the reaction mixture. The more complicated synthesis can be referred to the higher steric demand of the secondary isopropyl groups compared to methyl or *n*-butyl substituents. Thus, we decided to split the three reaction steps. $[iPr_3PBr]^+Br^-$ was isolated and reacted with 1,8-diaminonaphthalene in presence of the auxiliary base triethylamine. ^{31}P NMR spectroscopic monitoring of the reaction progress still revealed the formation of side products. Finally, isolation of TiPrPN·HBr was achieved by adding three equivalents of $NaN(SiMe_3)_2$ deprotonating the less basic byproducts, but not the superbasic proton sponge and allowing separation due to the different solubility properties. The deprotonation of TiPrPN·HBr was performed in a separate step by $KN(SiMe_3)_2$ in toluene (Scheme 1). The synthesis of TcyPPN also started from the corresponding bromophosphonium bromide $[cyP_3PBr]^+Br^-$ ($cyP = -CH(CH_2)_4$), but deprotonation was achieved in situ by $KN(SiMe_3)_2$ (Scheme 1).

TPPN that was formerly accessible via a Staudinger reaction[34] could also be synthesized by the Kirsanov reaction allowing its preparation in large scale (Scheme 2).[44] Bromination of tris(pyrrolidinyl)phosphane and reaction with 1,8-diaminonaphthalene were performed in one-pot fashion yielding the proton sponge's hydrobromide. Deprotonation turned out to be difficult and in many cases mixtures of the free base and the hydrobromide were obtained. Among the tested bases such as metal hydrides, amides or organometallic compounds, the best deprotonation conditions were observed using $KN(SiMe_3)_2$ in hexane at 60 °C which yielded TPPN in 64%.

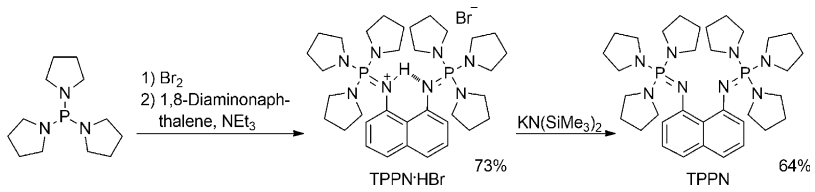

Scheme 2. Preparation of TPPN·HBr via the Kirsanov reaction and deprotonation by $KN(SiMe_3)_2$.

Spectroscopic Properties

^{31}P and ^{1}H NMR chemical shifts of the bisphosphazene proton sponges described herein are summarized in Table 1. Protonation led to a low-field shift of about 16 ppm for the ^{31}P NMR signals of the amino-substituted sponges HMPN and TPPN and more than 28 ppm in case of the alkyl-substituted species. The ^{1}H NMR signals of the aromatic protons are shifted towards the high field and their order is changed while those of the acidic protons in the protonated compounds exhibit considerable low-field shifts as described earlier for proton sponges. Thus, for the amino-substituted bisphosphazenes ^{1}H signals near 15 ppm were reported whereas for the alkyl-substituted sponges the ^{1}H resonance position varied from 13.32 ppm for TcyPPN·HBr to 15.84 ppm for TMPN·HPF_6. The acidic protons of TiPrPN·HBr ($\delta_{NH}=14.05$ ppm) and TcyPPN·HPF_6 ($\delta_{NH}=13.32$ ppm) are considerably shifted towards the high field compared to the other two alkyl-substituted bisphosphazenes studied herein. This high-field shift is accompanied by the observation that TiPrPN and TcyPPN show longer N···N distances (2.634(4) and 2.641(3) Å) in their protonated forms than found for TMPN (2.57(1) Å) and TBPN (2.594(4) Å) (see below). Even higher values for the chemical shifts of the acidic protons were observed by Llamaz–Saiz et al. for the hydrobromides of two bisphosphazene sponges bearing PPh_3 ($\delta_{NH}=16.42$ ppm, $^{2}J(P,H)=4.8$ Hz) and PPh_2Me ($\delta_{NH}=16.64$ ppm) moieties.[36b] The acidic proton in the hydrochloride of Alder's DMAN exhibits a value of 18.6 ppm in $[D_3]$MeCN.[35e] The effect of intramolecular hydrogen bonding on the proton NMR chemical shift of the acidic proton can be observed when comparing the corresponding value of P_2-TPPN (15.14 ppm) with that of the monosubstituted Schwesinger base (Pyr)P_2-1-Naph (7.07 ppm).[34] Furthermore, the ^{1}H NMR signals for the NHs appeared as triplets due to couplings with both phosphorus atoms which was verified by $^{1}H\{^{31}P\}$ experiments on TPPN and P_2-TPPN samples. The simultaneous coupling of the acidic proton with both phosphorous atoms emphasizes the existence of a low-barrier hydrogen bond. The reaction of TPPN with two equivalents of $HN(SO_2CF_3)_2$ yielded the bisprotonated sponge leading to a further low-field shift in the ^{31}P NMR spectrum ($\delta_{31P}=25.0$ ppm). The acidic protons exhibit a doublet with coupling to only one phosphorus atom ($^{2}J(P,H)=6.5$ Hz) and a chemical shift of 7.65 ppm in the proton NMR spectrum. A similar behavior of the chemical shift is observed in the case of TMGN·HPF_6 ($\delta_{NH}=14.28$ ppm) and the bisprotonated salt $[TMGN\text{-}2H]^{2+}[PF_6]^{-}[BF_4]^{-}$ ($\delta_{NH}=7.84$ ppm).[31a]

Table 1. NMR chemical shifts [ppm] of bisphosphazene proton sponges.

Base	δ_{31P} (free base)	δ_{31P} (protonated form)	$\Delta\delta_{31P}$	δ_{1H} (NH)
TMPN	1.4[a]	29.5[b,d]	28.1	15.84[b]
TBPN	12.8[a]	41.4[b,d]	28.6	15.60[b]
TiPrPN	25.6[b]	54.3[b,e]	28.7	14.05[b]
TcyPPN	21.1[a]	52.8[b,d]	31.7	13.32[b]
HMPN[33]	17.8[b]	33.9[b,d]	16.1	15.0[b]
TPPN[34]	2.5[b]	18.1[b,f]	15.6	15.02[b]
P_2-TPPN[34]	3.2, −3.6[c]	3.7, 1.4[c,f]	–	15.14[b]

[a] in C_6D_6. [b] in $[D_3]$MeCN. [c] in $[D_8]$THF. [d] HPF_6 salt. [e] HBr salt. [f] $HN(SO_2CF_3)_2$ salt.

Structural Features

The structural features of the hydrobromide salt of the four alkyl-substituted bisphosphazene proton sponges, TMPN·HBr (Figure 3),[45] TBPN·HBr (Figure 4),[46] TiPrPN·HBr (Figure 5) and TcyPPN·HBr (Figure 6), were investigated. The nitrogen-bound hydrogen atoms could be located on the Fourier map and were refined isotropically. The molecular structures reveal an unsymmetrical nonlinear hydrogen bridge with the proton preferentially bound to one of the two basic nitrogen atoms. The crystallographic N–H distances range from 0.86(2) Å for TcyPPN·HBr to 0.96(7) Å for TMPN·Br whereas values for *d*(N···H) between 1.77(4) Å for TBPN·HBr and 1.95(7) Å in case of TMPN·HBr were found. Although the accuracy of the bonding and non-bonding N–H distances is intrinsically low, it was observed that the hydrogen bonding is by trend even more unsymmetrical in case of the amino-substituted proton sponges HMPN and P_2-TPPN (*d*(N–H): 0.88(3) Å for HMPN and 0.81(4) Å for P_2-TPPN).[33,34,47] The acidic protons are located in the naphthalene plane showing N-H-N angles of 120(6)° for TMPN·HBr, 146(4)° for TBPN·HBr, 147(4)° for TiPrPN·HBr and 149(2)° for TcyPPN·HBr (the unusual low value observed for TMPN·HBr seems doubtful due to the comparatively low quality of its molecular structure XRD analysis). Furthermore, the acidic protons are located in the naphthalene plane in case of TBPN·HBr, TiPrPN·HBr and TcyPPN·HBr while it stands out of that plane in TMPN·HBr. HMPN·HPF_6 (150(3)°), TPPN·$HN(SO_2CF_3)_2$ (141(2)°) and P_2-TPPN·$HN(SO_2CF_3)_2$ (146(4)°) exhibit similar N–H–N angles to their alkyl-substituted analogs if TMPN·HBr is neglected. The formation of a linear hydrogen bridge is prevented by the short distance between the basicity centers and their lone-pair orientation. An interaction between the acidic proton and the bromide anion is observed in none of the cases. As expected, the double bond between the nitrogen and the phosphorus atom is longer on the side of the protonated nitrogen. The non-bonding distances of the two basicity centers in the protonated alkyl sponges are shorter in case of primary alkyl substituents at the phosphorous atom than for the more bulky isopropyl- and cyclopentyl-substituted deriva-

tives (TMPN·HBr: 2.57(1) Å, TBPN·HBr: 2.594(4) Å, TiPrPN·HBr: 2.634(4) Å, TcyPPN·HBr: 2.641(3) Å). The corresponding values of the amino-substituted analogues range from 2.568(3) Å for HMPN·HPF_6 to 2.600(6) Å for TPPN·$HN(SO_2CF_3)_2$. The remaining literature-known protonated bisphosphazene proton sponges show distances of 2.584(4) and 2.606(4) Å in case of the PPh_3-substituted compound and of 2.534(6) and 2.533(6) Å for the sterically less hindered sponge bearing PPh_2Me moieties.[36b] In theory, protonation leads to a relaxation of the naphthalene backbone. Naphthalene distortion is reflected by the deviation of the average of the torsion angels C1-C8a-C4a-C5 and C8-C8a-C4a-C4 from 180°. The hydrobromides of the alkyl-substituted sponges only show minor distortion which increases with the steric demand of the substituents (TMPN·HBr 1.2(9)°, TBPN·HBr 2.3(3)°, TiPrPN·HBr 3.1(3)°, TcyPPN·HBr 3.7(2)). For TPPN·$HN(SO_2CF_3)_2$ (5.1(4)°) and P_2-TPPN·$HN(SO_2CF_3)_2$ (5.6(3)°) considerably stronger distortions are observed.

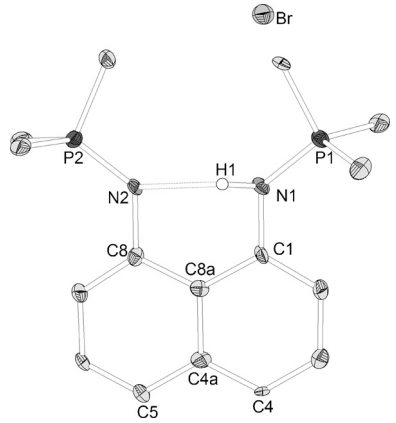

Figure 3. Molecular structure of TMPN·HBr (ellipsoids with 30% probability). Carbon-bonded hydrogen atoms and 1/2 NH_4Br are omitted for clarity. Selected bond lengths [Å] and angles [°]: N1···N11 2.57(1), N1—P1 1.630(8), N2—P2 1.574(7), N1—H1 0.96(7), N2···H1 1.95(7); N1-H1-N2 121(6), C8-C8A-C4A-C4 −179.0(9), C1-C8A-C4A-C5 −178.7(8).[65]

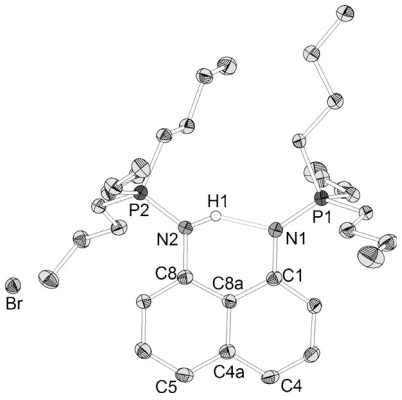

Figure 4. Molecular structure of TBPN·HBr (ellipsoids with 30% probability). Carbon-bonded hydrogen atoms and one THF molecule are omitted for clarity. Selected bond lengths [Å] and angles [°]: N1···N11 2.594(4), N1—P1 1.599(3), N2—P2 1.634(3), N1···H1 1.77(4), N2—H1 0.94(5); N1-H1-N2 146(4), C4-C4A-C8A-C8 178.1(3), C5-C4A-C8A-C1 177.3(3).[65]

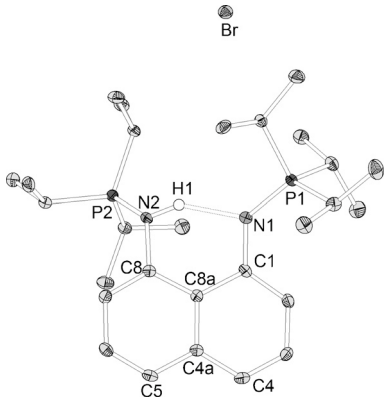

Figure 5. Molecular structure of TiPrPN·HBr (ellipsoids with 30% probability). Carbon-bonded hydrogen atoms are omitted for clarity. Selected bond lengths [Å] and angles [°]: N1···N11 2.634(4), N1—P1 1.602(2), N2—P2 1.647(2), N1···H1 1.81(4), N2—H1 0.93(3); N1-H1-N2 147(4), C4-C4A-C8A-C8 177.4(3), C5-C4A-C8A-C1 176.4(2).[65]

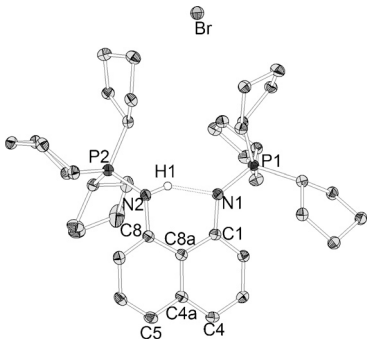

Figure 6. Molecular structure of TcyPPN·HBr (ellipsoids with 30% probability). Carbon-bonded hydrogen atoms are omitted for clarity. Selected bond lengths [Å] and angles [°]: N1···N11 2.641(3), N1—P1 1.600(2), N2—P2 1.648(2), N1···H1 1.87(3), N2—H1 0.86(2); N1-H1-N2 149(2), C4-C4A-C8A-C8 176.4(2), C5-C4A-C8A-C1 176.3(2).

TiPrPN (Figure 7) and TcyPPN (Figure 8) could also be characterized in their initial free base forms. Comparison with the corresponding hydrobromides demonstrates the effect of protonation on the non-bonding N···N distance (reduced from 2.810(2) to 2.634(4) Å in case of TiPrPN and from 2.868(3) to 2.641(3) Å for TcyPPN) and naphthalene distortion (reduced from 7.1(2)° to 3.1(3)° in case of TiPrPN and from 8.1(2)° to 3.7(2)° for TcyPPN). The non-bonding distance of the basic nitrogen atoms in TiPrPN lies between the values observed in HMPN (2.823(2) Å) and the two pyrrolidine-substituted sponges TPPN (2.766(3) Å) and P_2-TPPN (2.763(2) Å). TcyPPN exhibits the longest N···N distance in the studied series (2.868(3) Å). Selected structural features of hydrobromides of the four alkyl-substituted bisphosphazenes' hydrobromides and the free bases TiPrPN and TcyPPN are collected in Table 2.

NMR Titration Experiments

The pK_{BH}^+ values of the four alkyl-substituted bisphosphazene proton sponges were determined by means of NMR titration experiments in acetonitrile. The alkyl sponges competed against HMPN for protons and the equilibrium concentrations

Table 2. Selected structural parameters of bisphosphazene proton sponges in their free base and their protonated forms (bond lengths [Å], angles [°]).

	N···N	N–P	Average naphthalene distortion	N–H	N···H	N–H–N
free bases						
TiPrPN	2.810(2)	1.563(2), 1.562(2)	7.1(2)	–	–	–
TcyPPN	2.868(3)	1.568(2), 1.565(2)	8.1(2)	–	–	–
HMPN[33]	2.823(2)	1.555(1)	6.1(1)	–	–	–
TPPN[34]	2.766(3)	1.550(2), 1.553(2)	8.2(2)	–	–	–
P_2-TPPN[34]	2.763(2)	1.567(2)	6.3(2)	–	–	–
protonated sponges						
TMPN·HBr	2.57(1)	1.630(8), 1.574(7)	1.2(9)	0.96(7)	1.95(7)	120(6)
TBPN·HBr	2.594(4)	1.599(3), 1.634(3)	2.3(3)	0.94(5)	1.77(4)	146(4)
TiPrPN·HBr	2.634(4)	1.602(2), 1.647(2)	3.1(3)	0.93(3)	1.81(4)	147(4)
TcyPPN·HBr	2.641(3)	1.600(2), 1.648(2)	3.7(2)	0.86(2)	1.87(3)	149(2)
HMPN·HPF_6[33]	2.568(3)	1.583(2), 1.604(2)	2.2(2)	0.88(3)	1.76(3)	150(3)
TPPN ·$HN(SO_2CF_3)_2$[34,46]	2.600(6)	1.587(4), 1.597(4)	5.1(4)	0.85(3)	1.88(3)	141(2)
P_2-TPPN ·$HN(SO_2CF_3)_2$[34]	2.570(4)	1.623(3), 1.610(2)	5.6(3)	0.81(4)	1.85(4)	146(4)

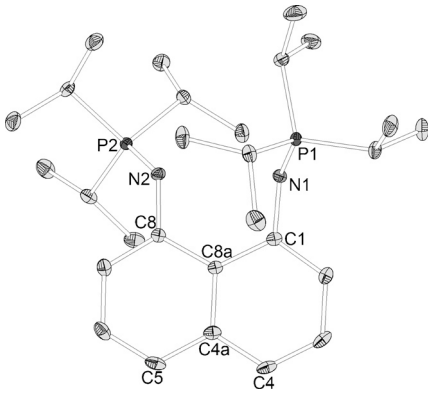

Figure 7. Molecular structure of TiPrPN (ellipsoids with 30% probability). Hydrogen atoms are omitted for clarity. Selected bond lengths [Å] and angles [°]: N1···N11 2.810(2), N1–P1 1.563(2), N2–P2 1.562(2); C1-C8A-4A-C5 172.5(2), C8-C8A-C4A-C4 173.3(2).[65]

were determined by ^{31}P NMR spectroscopy. HMPN turned out to be suitable for these kind of experiments since it exhibits a similar pK_{BH}^+ value of 29.9 in acetonitrile and a very low kinetic basicity resulting in very sharp signals in the ^{31}P NMR spectra. Signals capable of being integrated were also observed for protonated and unprotonated TBPN, TiPrPN and TcyPPN. The kinetically active TMPN and $[TMPN-H]^+$ (see below) showed very broad signals so that only the sharp peaks of HMPN were used for calculation of the equilibrium concentrations of the four species in solution. Hence, we consider the

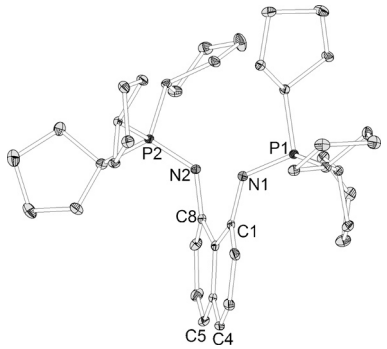

Figure 8. Molecular structure of TcyPPN (ellipsoids with 30% probability). Hydrogen atoms are omitted for clarity. Selected bond lengths [Å] and angles [°]: N1···N11 2.868(3), N1–P1 1.568(2), N2–P2 1.565(2); C5-C4A-C8A-C1 −171.3(2), C4-C4A-C8A-C8 −172.6(2).[65]

value obtained for TMPN to be less accurate since TMPN's free base shows only limited solubility in acetonitrile and even the slightest precipitation of TMPN influences the results. The obtained pK_{BH}^+ values of the alkyl-substituted sponges were cross-checked in NMR-titration experiments among themselves and in case of TBPN and TcyPPN also versus TPPN. The experiments yielded the following pK_{BH}^+ values on the acetonitrile scale: 29.3 for TMPN, 30.4 for TiPrPN, 30.5 for TcyPPN and 30.9 for TBPN. Thus, the basicity of the alkyl-substituted bisphosphazene proton sponges studied herein lies within the same order of magnitude as the basicity of the analogous dimethylamino-substituted HMPN ($pK_{BH}^+(MeCN) = 29.9$).[33] The influence of the different alkyl groups on the pK_{BH}^+ value is discussed in the theoretical section (see below). The pK_{BH}^+ values of naphthalene-based bisphosphazene proton sponges and other chelating hybrid superbases on the acetonitrile scale are presented in Figure 9.

Basic versus Nucleophilic Properties

An important characteristic of a base determining the scope of its synthetic applicability is its nucleophilicity. Since the basic lone pair of a deprotonation reagent can also react with an electrophilic position in the substrate via an S_N2 reaction, undesired side reactions can occur in case of highly nucleophilic bases. A base's nucleophilicity is mainly affected by the steric shielding of the basic site. Hence, a low nucleophilicity could be expected for bisphosphazene proton sponges due to the sterically demanding substituents at the phosphorus atoms. The reaction of a proton sponge with ethyl iodide was chosen as a benchmark to determine the nucleophilic properties in relation to the basic features. When reacting as a base, hydrogen iodide is eliminated to form ethylene in an elimination reaction whereas the ethylated proton sponge is formed from a nucleophilic substitution reaction (Scheme 3). In the latter case the proton sponge loses its rotation symmetry through C4a and C8a and the phosphorus atoms exhibit two signals in the ^{31}P NMR spectrum. Thus, the ratio of protonated to alkylated product can be easily determined by NMR spectroscopy. Furthermore, the alkylated sponge can be detected by ESI mass spectrometry.

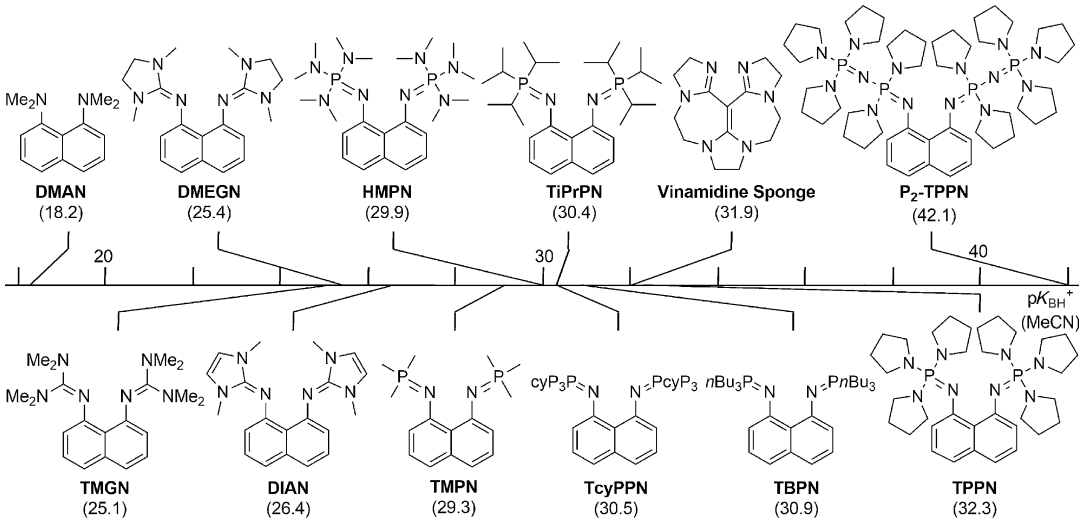

Figure 9. pK_{BH}^{+} values of hybrid proton sponges on the acetonitrile scale.

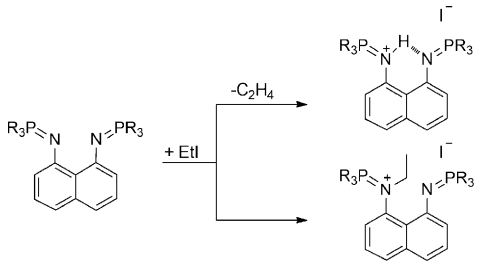

Scheme 3. Reaction of a proton sponge with ethyl iodide.

To our surprise, the alkyl-substituted sponges TMPN, TBPN and TiPrPN exclusively formed the alkylated species from a nucleophilic substitution reaction with ethyl iodide. The remaining alkyl-substituted sponge TcyPPN was reacted with ethyl iodide in THF due to its poor solubility in MeCN. The ^{31}P NMR spectrum of the reaction mixture showed a ratio of 71:29 in favor of the alkylated compound whereas the reaction is slower than observed for the other alkyl-substituted sponges in acetonitrile. A 4:1 ratio in favor of the alkylated species was reported for HMPN in the reaction with ethyl iodide in acetonitrile.[33] The same ratio is found for the related compound TPPN in acetonitrile whereas the ratio is shifted towards the alkylated species when using THF (94:6). The reaction with EtI was carried out in THF for TPPN's higher homologue P_2-TPPN due to its extremely high basicity and it exclusively showed the protonated species which can be referred to the extreme steric shielding of the basicity centers. These findings suggest that some of the applications of the investigated bisphosphazene proton sponges to organic synthesis could be limited by their unexpectedly high nucleophilicity especially in case of the alkyl-substituted compounds. The ratios of alkylation to protonation of the reaction of bisphosphazenes with ethyl iodide are displayed in Table 3 and compared with the nucleophilicity of non-chelating Schwesinger bases that show a lower nucleophilicity and with our bisphosphazene proton pincer P_2-TPPN which is the only superbase in this series revealing a perfect chemoselectivity for the HI elimination reaction. However, a further alkylation experiment showed that P_2-TPPN is readily alkylated by methyl iodide in [D_8]THF at room temperature.

Table 3. Reaction of bisphosphazene proton sponges and non-chelating Schwesinger bases with ethyl iodide.

	Solvent	*T* [°C]	Ratio Alkylation/ protonation	Alkylated species δ (^{31}P NMR) [ppm][a]
TMPN	MeCN	20	100:0	54.6, 13.7
TBPN	MeCN	20	100:0	62.6, 28.6
TiPrPN	MeCN	20	100:0	54.2, 25.5
TcyPPN	THF	20	71:29	66.3, 37.2
HMPN[33]	MeCN	20	80:20	39.1, 29.9
TPPN	MeCN	20	81:19	22.0, 14.0
TPPN	THF	20	94:6	23.4, 14.2
P_2-TPPN	MeCN	20	0:100	–
*t*Oct-$P_2(NMe_2)$[32]	Xylene	70	16:84	–
*t*Bu-$P_1(N(CH_2)_2)$[33]	MeCN	20	40:60	–

[a] The first value can be assigned to the phosphorous atom bound to the alkylated nitrogen atom.

Reactivity towards Group XIII Alkyls

The coordination behavior of DMAN[48] and proton sponges in general towards other electrophiles than protons has only been scarcely investigated. Himmel et al. have studied the coordination chemistry of guanidinyl-substituted proton sponges.[11c,49] Furthermore, palladium, platinum, rhenium, manganese and copper complexes of a sponge related to Staab's quino[7,8*h*]quinoline[20] have been reported.[50] We found that the reaction of TMPN with two equivalents of trimethylaluminum and trimethylgallium in toluene lead to the precipitation of cationic alkyl aluminum or gallium complexes [TMPN-MMe_2]$^+$ with a [MMe_4]$^-$ counteranion (Scheme 4). As observed for the protonation reaction, a low-field shift is found in the ^{31}P NMR spectra with nearly equal values of 38.5 ppm for the aluminum and 38.6 ppm for the gallium species in CD_2Cl_2. A

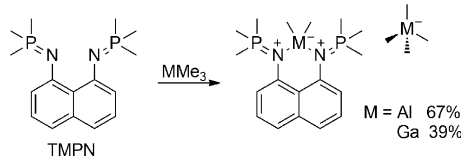

Scheme 4. Conversion of TMPN with group XIII alkyls.

similar reactivity was observed for TPPN yielding [TPPN-$AlMe_2$]$^+$[$AlCl_2Me_2$]$^-$ after reaction with $Al_2Me_4Cl_2$ (Scheme 5, ^{31}P NMR: $\delta = 26.3$ ppm). Additional experiments to obtain cationic alkyl indium or boron hydride complexes were not successful. Himmel et al. reported a comparable reaction between the tetramethylguanidinyl-substituted proton sponge TMGN with gallium trichloride. Furthermore, they obtained cationic alkylaluminum complexes by the conversion of the protonated sponge with trimethylaluminum under elimination of methane.[49a]

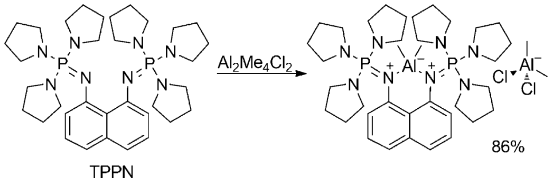

Scheme 5. Reaction of TPPN with $Al_2Me_4Cl_2$.

Recrystallization from dichloromethane/pentane yielded single crystals suitable for X-ray analysis of [TMPN-$AlMe_2$]$^+$[$AlMe_4$]$^-$ (Figure 10), [TMPN-$GaMe_2$]$^+$[$GaMe_4$]$^-$ (Figure 11) and [TPPN-$AlMe_2$]$^+$[$AlCl_2Me_2$]$^-$ (Figure 12). The two structures involving TMPN exhibit equal cell constants revealing a disorder which includes the whole [TMPN-MMe_2]$^+$ cation. In case of M = Ga only the disordered gallium atom could be located on the Fourier map while the corresponding aluminum compound allowed localization of the disordered Al atom and a fragment of the ligand backbone. The only partly resolved disorders are responsible for the comparably low quality of the structures. Whereas the acidic protons in the examined protonated bisphosphazene sponges are located in the naphthalene plane, the larger aluminum and gallium atoms are displaced outside of this plane. The metal atoms show nearly equal bond lengths to both nitrogen atoms in contrast to the observed unsymmetrical hydrogen bonds in the protonated species. The effect of the coordination of a [MMe_2]$^+$ fragment on the distortion of the naphthalene skeleton is contradictory. Relaxation is observed in case of [TMPN-$AlMe_2$]$^+$[$AlMe_4$]$^-$ (average distortion: 1.4(5)°), but the molecular structures of [TMPN-$GaMe_2$]$^+$[$GaMe_4$]$^-$ (5.7(9)°) and [TPPN-$AlMe_2$]$^+$[$AlCl_2Me_2$]$^-$ (7.8(4)°) still reveal considerable distortion. The structural features of [TPPN-$AlMe_2$]$^+$[$AlCl_2Me_2$]$^-$ can be compared to those of TPPN's free base form: Interestingly, the aluminum complex exhibits a longer non-bonding distance of the two basic nitrogen atoms than the free base (2.808(8) compared to 2.766(3) Å in TPPN). The large metal alkyl fragments do not fit into the cavity of the proton sponges so that the two nitrogen atoms have to spread away from each other to allow coordination to aluminum or gallium. This is also demonstrated by the unfavorable, nearly rectangular N–M–N angles ([TPPN-$AlMe_2$]$^+$[$AlCl_2Me_2$]$^-$: 94.1(1)°, [TMPN-$AlMe_2$]$^+$[$AlMe_4$]$^-$: 91.4(2)°, [TMPN-$GaMe_2$]$^+$[$GaMe_4$]$^-$: 87.4(3)°). Selected structural features of the three metal complexes are collected in Table 4.

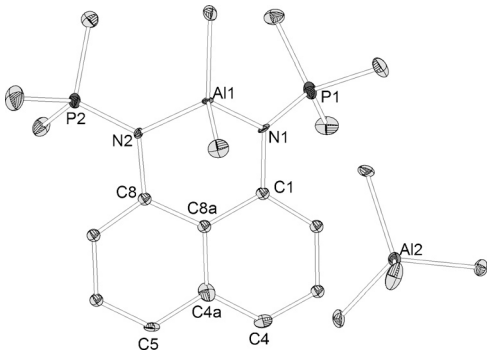

Figure 10. Molecular structure of [TMPN-$AlMe_2$]$^+$[$AlMe_4$]$^-$ (ellipsoids with 30% probability). Hydrogen atoms are omitted for clarity. Selected bond lengths [Å] and angles [°]: N1···N11 2.749(6), N1—P1 1.588(5), N2—P2 1.599(5), N1—Al1 1.917(5), N2—Al1 1.925(5); N1-Al1-N2 91.4(2), C5-C4A-C8A-C1 −177.8(5), C4-C4A-C8A-C8 179.4(5).[65]

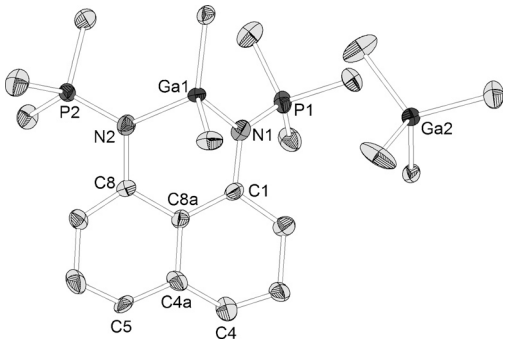

Figure 11. Molecular structure of [TMPN-$GaMe_2$]$^+$[$GaMe_4$]$^-$ (ellipsoids with 30% probability). Hydrogen atoms are omitted for clarity. Selected bond lengths [Å] and angles [°]: N1···N11 2.74(1), N1—P1 1.551(8), N2—P2 1.602(7), N1—Ga1 1.990(7), N2—Ga1 1.979(7); N1-Ga1-N2 87.4(3), C5-C4A-C8A-C1 −172.7(9), C4-C4A-C8A-C8: 175.9(9).[65]

Table 4. Selected structural parameters of cationic Group XIII metal complexes of bisphosphazene proton sponges (bond lengths [Å], angles [°]).

	N···N	N–P	Average naphthalene distortion	N–M	N–M–N
[TMPN-$AlMe_2$]$^+$[$AlMe_4$]$^-$	2.749(6)	1.588(5), 1.599(5)	1.4(5)	1.917(5), 1.925(5)	91.4(2)
[TMPN-$GaMe_2$]$^+$[$GaMe_4$]$^-$	2.74(1)	1.551(8), 1.602(7)	5.7(9)	1.990(7), 1.979(7)	87.4(3)
[TPPN-$AlMe_2$]$^+$[$AlMe_2Cl_2$]$^-$	2.808(8)	1.624(3), 1.636(3)	7.8(4)	1.897(3), 1.939(4)	94.1(1)

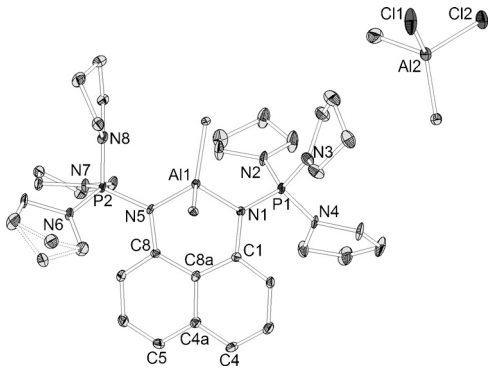

Figure 12. Molecular structure of $[TPPN\text{-}AlMe_2]^+[AlCl_2Me_2]^-$ (ellipsoids with 30% probability). Hydrogen atoms are omitted for clarity. A disorder observed for the anion is not displayed. Selected bond lengths [Å] and angles [°]: N1···N11 2.808(8), N1—P1 1.624(3), N5—P2 1.636(3), N1—Al1 1.897(3), N5—Al1 1.939(4); N1-Al1-N5 94.11(14), C5-C4A-C8A-C1 −172.4(3), C4-C4A-C8A-C8 −172.1(4).[65]

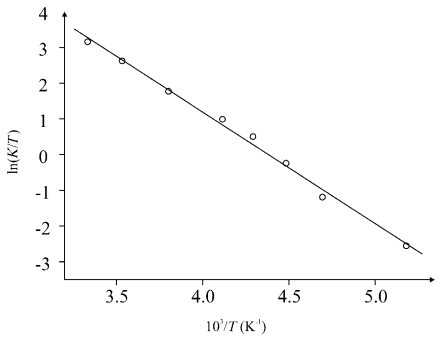

Figure 13. Eyring plot of the methyl groups of TMPN with $TMPNH^+$ (0.45:0.55) in $[D_8]$THF.

Kinetic Basicity

The kinetic basicity is expressed by the proton self-exchange rate and is usually very low for proton sponges due to the steric shielding of the acidic proton by bulky hydrophobic substituents (see above). We exemplarily investigated the kinetic basicity of the two bisphosphazene proton sponges TMPN and TPPN and determined self-exchange rates k as well as the corresponding free activation energies $\Delta G^{\neq}$ at different temperatures. Generally, a solution of the proton sponge's free base form in $[D_8]$THF was combined with a solution of the protonated sponge in the same solvent. Preliminary experiments indicated that the proton self-exchange processes for TMPN and TPPN take place on different time scales and thus different NMR spectroscopic techniques are required for the investigation of kinetic processes.

Line-shape analysis is usually used to quantitatively study exchange processes when the spectra of all three regions of the exchange processes, these are, slow exchange, intermediate (where the coalescence point sits) and fast exchange, are obtainable. The comparably high kinetic activity of TMPN allowed the application of this technique using a Bruker DRX 500 spectrometer at temperatures ranging from 193 to 300 K. In the following only the dynamic behavior of the ^{1}H NMR signals of the methyl groups will be discussed. Only one signal is observed for the two species' methyl groups at 300 K. The decrease in temperature results in the broadening of the signal until coalescence is reached at 243 K. At 193 K two separated sharp doublets were observed at 2.006 ppm (^3J(P,H) = 14 Hz) and 1.565 ppm (^3J(P,H) = 13 Hz) for the methyl groups of $TMPN{\cdot}H^+$ and TMPN, respectively. At a resonance frequency of 500 MHz, this corresponds to a frequency difference of 220 Hz between the two exchanging sites. Furthermore, from the signal intensities at 193 K a molar ratio of 0.45:0.55 was determined for $TMPN/TMPN{\cdot}H^+$ in the sample used.

Line-shape analysis of the variable temperature ^{1}H NMR spectra was done using the program DNMR within the Bruker program package Topspin 3.2 (Figure S1.1). Results of the line-shape analysis are a set of the exchange rates k and simulated spectra. By linear fitting of $\ln(k/T)$ versus $(1/T)$ via an Eyring plot one obtains the free energy, enthalpy and entropy of activation (Figure 13).

The results of the quantitative dynamic study on the proton self-exchange between TMPN and $TMPN{\cdot}H^+$ in THF on the ^{1}H NMR signals of the methyl groups are summarized in Table 5. Furthermore, a corresponding activation enthalpy of 26.6 kJ mol^{-1} and an activation entropy of −83.8 J mol^{-1} K^{-1} were determined. The detailed procedure is explained in the Supporting Information.

Table 5. Proton self-exchange of TMPN and $TMPN{\cdot}HN(SO_2CF_3)_2$ in $[D_8]$THF.

T [K]	Exchange rate k [s^{-1}]	Free energy $\Delta G^{\neq}$ [kJ mol^{-1}]
193	13	42
213	64	44
223	173	45
233	385	45
243	660	46
263	1545	48
283	3890	50
300	7050	51

The considerably lower kinetic basicity of TPPN did not allow the application of line shape analysis since the corresponding coalescence temperature lies far above the boiling point of THF. Therefore, exchange spectroscopy (EXSY) was used which is appropriate for the study of slow chemical exchange whereby no coalescence can be observed.[51]

The ^{31}P,^{31}P EXSY experiments were run on a mixture of TPPN and $TPPN{\cdot}HN(SO_2CF_3)_2$ in $[D_8]$THF using a standard pulse sequence at a Bruker AV III 500 spectrometer.[52] The spectral width for the 2D EXSY was 40 ppm with a relaxation delay of 15 s. The mixing time was 50 ms at 300 K and 10 ms at 323 and 333 K. Since the experiment is extremely time-consuming, the kinetic basicity of TPPN was studied at only three different temperatures. A free activation energy for proton self-exchange of 66 kJ mol^{-1} was observed at 300 K. The activation enthalpy is 35 kJ mol^{-1} and an activation entropy of −102 J mol^{-1} K was determined. The EXSY results for the TPPN and $TPPN{\cdot}H^+$ self-exchange in $[D_8]$THF are summarized in

Table S1.12 and the corresponding Eyring plot is shown in Figure S1.2. The detailed procedure is explained in the Supporting Information.

Up to now, the only free activation energy for proton self-exchange determined for proton sponges has been 59.3 kJ mol^{-1} for TMGN with a coalescence temperature at 300 K for ^{1}H NMR spectra observed in [D$_3$]MeCN on a 500 MHz resonance frequency. The corresponding value for DMAN was estimated to be more than 66 kJ mol^{-1} in [D$_3$]MeCN because the coalescence temperature was above the boiling point of the solvent.[33a] Thus, $\Delta G^{\neq}$ for TPPN lies between the values of TMGN and DMAN. The comparatively little steric shielding of the basicity centers by TMPN's methyl groups results in a comparably low free activation energy of 51 kJ mol^{-1} for this bisphosphazene sponge. Thus, TMPN is a kinetically active representative of the compound class of proton sponges.

Theoretical Section

The gas-phase proton affinities (PA) and gas-phase basicities (GB) of the proton sponges TMPN, TiPrPN, TBPN and TcyPPN, together with their monosubstituted analogues, are calculated at B3LYP/6-311 + G(2df,p)//B3LYP/6-31G(d) level, taking into account the thermal corrections estimated by the B3LYP/6-31G(d) method. They are presented in Table 6. All calculations were done utilizing the Gaussian03 program package.[53] The proton affinities of the alkyl-substituted bisphosphazene proton sponges range from 271.8 kcal mol^{-1} (1137.2 kJ mol^{-1}) (TMPN) to 279.0 kcal mol^{-1} (1167.3 kJ mol^{-1}) (TcypPN), thus being slightly lower/higher than the PA of Schwesinger's *t*Bu-P$_2$ phosphazene (PA = 274.4 kcal mol^{-1} (1148.1 kJ mol^{-1})).[54] Generally, there are two main contributions that determine the proton affinities of the proton sponges: 1) the intrinsic basicity of the basic fragments that undergo protonation and 2) the proton chelating effect.[34] The contribution to the PA due to the chelating effect is a consequence of: a) the destabilization in the neutral base induced mainly by a strong repulsion of unshared electron pairs that diminishes after protonation and b) the formation of an intramolecular hydrogen bond (IMHB) in the protonated form. The chelating effect can be expressed as a difference in the PA of the monosubstituted analogue of the proton sponge and the proton sponge itself. For TMPN, TiPrPN, TBPN and TcyPPN, the chelating effect contributes to the PA by 25.8 (107.9), 24.7 (103.3), 26.7 (111.7) and 26.1 kcal mol^{-1} (109.2 kJ mol^{-1}), respectively. Interestingly, this contribution is very similar for all four proton sponges, the biggest difference being 2.0 kcal mol^{-1} (8.4 kJ mol^{-1}). This is an interesting finding since it would be expected that, due to a higher strain in the neutral base, the bulkier P(cyP)$_3$ substituent would lead to a higher value for the chelating effect in TcyPPN than the relatively small PMe$_3$ substituent should do in TMPN. To quantify the influence of the destabilization energy (E_d) in the neutral base and the stabilization energy (E_s) in the conjugate acid, homodesmotic reactions were used analogously to the procedure applied in our previous papers.[33,34] It appears that the destabilization energy is indeed the largest in TcyPPN, being 13.8 (57.7), 14.7 (61.5), 14.3 (59.8) and 18.7 kcal mol^{-1} (78.2 kJ mol^{-1}) for TMPN, TiPrPN, TBPN and TcyPPN, respectively. However, the stabilization energy in the conjugated acid is 11.9 (49.8), 10.3 (43.1), 12.4 (51.9) and 7.4 kcal mol^{-1} (31.0 kJ mol^{-1}), correspondingly. Since the chelating effect is the sum of E_d and E_s, it appears that the much higher E_d in TcyPPN is partially compensated by a lower E_s value. The main contribution to the E_s energy in conjugated acids of proton sponges is the stabilization due to the formation of the intramolecular hydrogen bond. Since it is not likely that the hydrogen bond in TcyPPN is much weaker than in the other three sponges, the lower stabilization energy could be explained only by 'lingering' strain (a part of the strain still exists in the conjugated acid).[55]

Table 6. Theoretically obtained gas phase proton affinities (PA) and gas-phase basicities (GB) in [kcal mol^{-1}] and [kJ mol^{-1}] (in parentheses) together with pK_{BH^+} values in acetonitrile of bisphosphazene proton sponges, their monophosphazene analogues and the corresponding basic fragments.

Base	PA	GB	pK_{BH^+}(MeCN)
TMPN	271.8 (1137.2)	262.7 (1099.1)	29.7
TiPrPN	275.1 (1151.0)	267.9 (1120.9)	30.9
TBPN	278.8 (1166.5)	269.5 (1127.6)	30.0
TcypPN	279.0 (1167.3)	271.1 (1134.3)	32.2
Me$_3$P=NNaph	246.0 (1029.3)	238.5 (997.9)	19.2
*i*Pr$_3$P=NNaph	250.4 (1047.7)	242.6 (1015.0)	19.1
*n*Bu$_3$P=NNaph	252.1 (1054.8)	243.9 (1020.5)	19.1
(cyP)$_3$P=NNaph	252.9 (1058.1)	244.4 (1022.6)	19.1
Me$_3$P=NH	249.4 (1043.5)	242.1 (1012.9)	25.6
*i*Pr$_3$P=NH	254.5 (1064.8)	247.5 (1035.5)	24.5
*n*Bu$_3$P=NH	257.4 (1077.0)	250.6 (1048.5)	24.8
(cyP)$_3$P=NH	259.9 (1087.4)	252.4 (1056.0)	25.6

Since the spread between the PA of the lowest basic proton sponge TMPN and the most basic one TcyPPN is 7.2 kcal mol^{-1} (30.1 kJ mol^{-1}), and the energy of chelating effect for all four sponges is very similar, the main contribution to the difference in PA should then be the difference in proton affinity of the basic fragments. The perusal of the PA for fragments R$_3$P=NNaph reveals that the PA increases along the series in a similar manner to the four proton sponges. The increase in PA of the basic fragments when going from methyl to cyclopentyl can be attributed to an increase in the electron donor ability of the larger alkyl groups attached to the phosphorus atom.

Therefore, it may be concluded that the increase in the PA values of proton sponges when going from TMPN to TcyPPN is a consequence of the higher basicity of the basic substituents whereas the chelating effect plays a minor role.

Let us compare now the basicities of TcyPPN and the recently synthesized TPPN (PA = 283.2 kcal mol^{-1} (1194.9 kJ mol^{-1})).[34] TcypPN has a lower PA than TPPN by 4.2 kcal mol^{-1} (17.6 kJ mol^{-1}). In the former, cyclopentyl groups are attached to a phosphorus atom, whereas the latter possess pyrrolidinyl groups instead. Both substituents have approximately the same steric demand which results in exactly the same chelating energy of 26.1 kcal mol^{-1} (109.2 kJ mol^{-1}). However, the PA of the ((CH$_2$)$_4$N)$_3$P=NH is by 3.2 kcal mol^{-1} (13.4 kJ mol^{-1}) higher than the PA of the (cyP)$_3$P=NH as a result of a stronger electron

donating ability of the dialkylamino group. Like among the alkyl-substituted bisphosphazenes, the main reason for a difference in basicities of TcyPPN and TPPN is a difference in the basicity of their basic fragments.

Theoretical calculations of the pK_{BH}^+ values in acetonitrile were performed using the isodensity polarized continuum model (IPCM); the detailed procedure is described elsewhere.[54] The pK_{BH}^+ values for the alkyl-substituted bisphosphazene proton sponges, together with their monosubstituted analogues, are presented in Table 6. Most of them are in reasonable agreement with the experimental data–discrepancies are smaller than 1 unit for TMPN, TiPrPN and TBPN. However, the theoretical value for TcyPPN is by 1.7 units higher than the experimental one. The estimated average absolute error for the applied theoretical model is ± 0.4 units for phosphazene superbases.[54] The discrepancy of 1.7 units is far beyond that value. However, the experimental pK_{BH}^+ value of TcyPPN is very similar to the pK_{BH}^+ value of TBPN. Since both sponges have a very similar gas phase PA, the experimental pK_{BH}^+ seems to be more realistic. The error in the theoretical pK_{BH}^+ probably arises from the inaccuracy in the solvation energy calculation or from the approximation that the most stable conformer in the gas phase is at the same time the most stable conformer in solution (conformational analysis is not performed in solution).

Conclusion and Outlook

The class of superbasic bisphosphazene proton sponges was extended by four alkyl-substituted representatives that populate the scale of pK_{BH}^+ values in acetonitrile in the region around 30. The dramatic effect of proton chelation on the basicity was rationalized by means of X-ray crystallographic data and computational studies underlining the great potential of combining superbasicity concepts for the design of new powerful nonionic bases. Not only their remarkable basic properties but also their easy and upscalable synthesis routes via a Kirsanov reaction as the key step could make the alkyl-substituted bisphosphazenes interesting organocatalysts in base-mediated reactions. Future experiments will have to show if their high nucleophilicity limits their applicability in organic synthesis. Furthermore, NMR spectroscopic studies on the kinetic basicity of TMPN and TPPN gave valuable information about their potential to act as bases in catalytic processes and in the future we would like to use the established methods for the determination of the kinetic activity to other superbases. Eventually, we provided first insight into the coordination behavior of TMPN and TPPN and thereby presented rare examples of metal complexes of proton sponges. We expect that such chelating superbases will exhibit a rich coordination chemistry as superdonors towards highly electrophilic and coordinatively unsaturated metal centers.

Experimental Section

All reactions were carried out under inert atmosphere using standard Schlenk techniques. Moisture and air sensitive substances were stored in a conventional nitrogen-flushed glovebox. Solvents were purified according to literature procedures and kept under an inert atmosphere. Trimethylphosphane[56] and triisopropylphosphane[57] were prepared according to literature-known procedures. Tricyclopentylphosphane and tributylphosphane were acquired by purchase whereas the latter was purified by condensation prior to use. 1,8-Diaminonaphthalene (Acros) was purified by recrystallization from toluene followed by sublimation. Tris(pyrrolidinyl)phosphane was prepared via a condensation reaction from PCl_3.[58] The oxidation of phosphanes by bromine was performed on the basis of literature-known protocols in benzene.[59] $NaN(SiMe_3)_2$[60] and $KN(SiMe_3)_2$[61] were prepared by deprotonation of $HN(SiMe_3)_2$ by $NaNH_2$ or KH, respectively.

Spectra were recorded on the following spectrometers: NMR: ^1H and ^{31}P spectra were recorded on a Bruker AVANCE 300 spectrometer installed with an automatic sample changer; standard ^1H–^1H and ^1H–^{13}C 2D spectra, the ^{31}P decoupled spectra $^1H\{^{31}P\}$, and $^{13}C\{^{31}P\}$, as well as low temperature ^1H spectra were recorded on a Bruker DRX 500 spectrometer installed with an inverse triple-resonance probe; ^{31}P–^{31}P EXSY spectra at variable temperatures were taken on a Bruker AVANCE 500 spectrometer with a BBFO probe. Mixing times of 10 and 50 ms were used, and spectra were collected with 4096 points in the F_2 dimension, 128 increments in the F_1 dimension, 16 transients for each increment, and a relaxation delay of 15 s. Typical experiment time was about 9 h per spectrum; IR: ATR-FT-IR; MS: LTQ-FT or QStarPulsar i (Finnigan); elemental analysis: CHN-Rapid (Heraeus).

1,8-Bis(tributylphosphazenyl)naphthalene (TBPN): Bromine (3.90 g, 24.40 mmol, 2.0 equiv) was added dropwise to a solution of tributylphosphane (4.94 g, 24.40 mmol, 2.0 equiv) in chlorobenzene (200 mL) at 0 °C. A yellow solid precipitated and the suspension was stirred for 1.5 h at 0 °C and additional 1.5 h at room temperature. A solution of 1,8-diaminonaphthalene (1.93 g, 12.19 mmol, 1.0 equiv) and triethylamine (4.94 g, 48.79 mmol, 4.0 equiv) in chlorobenzene (25 mL) was added dropwise at 0 °C and the reaction mixture was stirred for 2 h at room temperature and additional 16 h at 80 °C. The hot suspension was filtered over celite and a solution of $KN(SiMe_3)_2$ (2.43 g, 12.19 mmol, 1.0 equiv) in toluene (30 mL) was added dropwise at 0 °C. The reaction mixture was stirred overnight and separated from precipitated KBr via filtration over celite. The filtrate was evaporated to dryness in vacuo and pentane (100 mL) was added to the oily residue. The suspension was filtered over celite and the solvent was removed in vacuo from the filtrate to yield TBPN (6.10 g, 93%). The spectroscopic and analytic data are in accord with the literature ^1H NMR (300 MHz, [D_6]benzene, 25 °C, TMS): $\delta = 7.42$ (dt, $^3J(H,H) = 8.0$ Hz, $^4J(H,H) = 1.8$ Hz, 2H, H(4,5)), 7.33 (t, $^3J(H,H) = 7.6$ Hz, 2H, H(3,6)), 6.80–6.76 (m, 2H, H(2,7)), 1.73–1.63 (m, 12H, H(9)), 1.50–1.38 (m, 12H, H(10)), 1.24 (sext, $^3J(H,H) = 7.2$ Hz, 12H, H(11)), 0.82 ppm (t, $^3J(H,H) = 7.3$ Hz, 18H, H(12)); ^{13}C NMR (76 MHz, [D_6]benzene, 25 °C, TMS): $\delta = 153.0$ (C(1,8)), 139.3 (C(4a)), 131.3 (t, $^3J(P,C) = 12.1$ Hz, C(8a)), 125.4 (C(3,6)), 119.0 (d, $^3J(P,C) = 11.7$ Hz, C(2,7)), 118.5 (C(4,5)), 27.0 (d, $^1J(P,C) = 62.8$ Hz, C(9)), 24.9 (C(10)), 24.8 (d, $^3J(P,C) = 8.9$ Hz, C(11)), 13.9 ppm (C(12)); ^{31}P NMR (101.3 MHz, [D_6]benzene, 25 °C, 85% H_3PO_4): $\delta = 12.8$ ppm; IR: $\tilde{\nu} = 485, 549, 636, 719, 746, 777, 815, 899, 936, 967, 1002, 1053, 1091, 1122, 1184, 1208, 1285, 1336, 1376, 1428, 1500, 1544, 1590, 2869, 2928, 2955, 3040$ cm^{-1}; ESI-MS (MeCN): *m/z* (%): 560 (100) $[M]^+$; HRMS (ESI): *m/z* calcd for $C_{34}H_{61}N_2P_2^+$: 559.4310 [M+H^+]; found: 559.4290.

TBPN·HPF$_6$: A solution of NH_4PF_6 (0.384 g, 2.355 mmol, 1.0 equiv) in THF (20 mL) was added dropwise to a solution of TBPN (1.316 g, 2.355 mmol, 1.0 equiv) in THF (20 mL) at 0 °C. After stirring the reaction mixture for 2 h at room temperature, all volatiles were re-

moved in vacuo and the oily residue was triturated three times with diethyl ether (20 mL). TBPN·HPF_6 (1.170 g, 70%) was obtained as a beige solid.[62] ^{1}H NMR (300 MHz, [D_3]MeCN, 25 °C, TMS): δ = 15.64 (t, ^3J(P,H) = 3.3 Hz, 1H, NH), 7.22–7.15 (m, 4H, H(3,4,5,6)), 6.63–6.60 (m, 2H, H(2,7)), 2.25–2.16 (m, 12H, H(9)), 1.57–1.36 (m, 24H, H(10,11)), 0.88 ppm (t, ^3J(H,H) = 7.1 Hz, 18H, H(12)); ^{13}C NMR (100.6 MHz, [D_3]MeCN, 25 °C, TMS): δ = 145.8 (d, ^2J(P,C) = 2.8 Hz, C(1,8)), 138.1 (C(4a)), 127.2 (C(4,5)), 120.7 (t, ^3J(P,C) = 11.1 Hz, C(8a)), 120.6 (C(3,6)), 113.0 (d, ^3J(P,C) = 8.7 Hz, C(2,7)), 24.3 (d, ^3J(P,C) = 15.4 Hz, C(11)), 24.0 (d, ^2J(P,C) = 3.5 Hz, C(10)), 23.0 (d, ^1J(P,C) = 60.0 Hz, C(9)), 13.7 ppm (C(12)); ^{31}P NMR (121.5 MHz, [D_3]MeCN, 25 °C, 85% H_3PO_4): δ = 41.4 (s, -PBu_3), −145.4 ppm (sept, ^1J(P,F) = 706.3 Hz, PF_6^-); IR: $\tilde{\nu}$ = 417, 486, 556, 640, 714, 757, 833, 876, 908, 930, 970, 1052, 1079, 1127, 1185, 1234, 1290, 1333, 1381, 1455, 1509, 1572, 2871, 2931, 2957 cm^{-1}; ESI-MS (MeCN): *m/z* (%): 560 (100) $[M]^+$, 359 (4) $[C_{22}H_{36}N_2P]^+$; HRMS (ESI): *m/z* calcd for $C_{34}H_{61}N_2P_2^+$: 559.4304 $[M]^+$; found: 559.4296; (−)-ESI-MS (MeCN): *m/z* (%): 145 (100) $[PF_6]^-$; HRMS ((−)-ESI): *m/z* calcd for PF_6^-: 144.9647 $[M]^-$; found: 144.9648; elemental analysis calcd (%) for $C_{34}H_{61}F_6N_2P_3$: C 57.94, H 8.72, N 3.97; found: C 57.58, H 8.97, N 4.04.

1,8-Bis(trimethylphosphazenyl)naphthalene (TMPN): Bromine (3.09 g, 19.32 mmol, 2.1 equiv) was added slowly to a solution of trimethylphosphane (1.47 g, 19.32 mmol, 2.1 equiv) in benzene (100 mL) at 0 °C. An orange solid precipitated and the suspension was stirred for 30 min at 0 °C and additional 2 h at room temperature. A solution of 1,8-diaminonaphthalene (1.45 g, 9.20 mmol, 1.0 equiv) and triethylamine (3.90 g, 38.64 mmol, 4.2 equiv) in toluene (20 mL) was added dropwise and the black reaction mixture was stirred for 1 h at room temperature and additional 16 h at 70 °C. The suspension was cooled to room temperature and a solution of $KN(SiMe_3)_2$ (7.34 g, 36.80 mmol, 4.0 equiv) in toluene (40 mL) was added dropwise. The reaction mixture was stirred for 2 h at room temperature and precipitated potassium bromide was separated by filtration over celite. The solid was extracted twice with toluene (20 mL). The toluene phases were combined with the filtrate and evaporated to dryness in vacuo. The residue was suspended in hexane (40 mL) and the solid was separated by filtration, washed twice with hexane (20 mL) and dried in vacuo. TMPN (1.87 g, 67%) was obtained as a dark brown solid. ^{1}H NMR (400 MHz, [D_3]MeCN, 25 °C, TMS): δ = 6.97 (t, ^3J(H,H) = 7.6 Hz, 2H, H(3,6)), 6.92 (dt, ^3J(H,H) = 8.0 Hz, ^4J(H,H) = 1.6 Hz, 2H, H(4,5)), 6.34 (ddd, ^3J(H,H) = 7.1 Hz, J = 3.2 Hz,[63] ^4J(H,H) = 1.5 Hz, 2H, H(2,7)), 1.52 ppm (d, ^2J(P,H) = 12.5 Hz, 18H, H(9)); ^{13}C NMR (101 MHz, [D_3]MeCN, 25 °C, TMS): δ = 153.0 (d, ^2J(P,C) = 3.5 Hz, C(1,8)), 139.9 (C(4a)), 129.9 (t, ^3J(P,C) = 7.8 Hz, C(8a)), 126.2 (C(3,6)), 118.0 (d, ^3J(P,C) = 14.6 Hz, C(2,7)), 117.8 (C(4,5)), 16.7 ppm (d, ^1J(P,C) = 69.9 Hz, C(9)); ^{31}P NMR (101 MHz, [D_6]benzene, 25 °C, 85% H_3PO_4): δ = 1.4 ppm; IR: $\tilde{\nu}$ = 480, 510, 551, 640, 665, 720, 742, 775, 813, 832, 852, 917, 931, 979, 1003, 1054, 1119, 1186, 1281, 1344, 1380, 1429, 1500, 1538, 2906, 2974, 3034 cm^{-1}; ESI-MS (MeCN): *m/z* (%): 307(40) $[M]^+$, 233 (100) $[M-PMe_3]^+$; HRMS (ESI): *m/z* calcd for $C_{16}H_{25}N_2P_2^+$: 307.1493 $[M]^+$; found: 307.1487; elemental analysis calcd (%) for $C_{16}H_{24}N_2P_2$: C 62.73, H 7.90, N 9.15; found: C 61.96, H 7.90, N 9.21.

TMPN·HPF_6: A solution of NH_4PF_6 (160 mg, 0.979 mmol, 1.0 equiv) in THF (10 mL) was added dropwise to a solution of TMPN (300 mg, 0.979 mmol, 1.0 equiv) in THF (20 mL). A white solid precipitated and the suspension was stirred for 1 h at room temperature. The reaction mixture was concentrated in vacuo to about 10 mL and the precipitate was collected by filtration. The solid was washed twice with diethyl ether (20 mL) and dried in vacuo. TMPN·HPF_6 (275 mg, 62%) was obtained as a white solid. ^{1}H NMR (300 MHz, [D_3]MeCN, 25 °C, TMS): δ = 15.84 (br s, 1H, NH), 7.20–7.19 (m, 4H, H(3,4,5,6)), 6.58–6.55 (m, 2H, H(2,7)), 1.93 ppm (d, ^2J(P,H) = 13.5 Hz, 18H, H(9)); ^{13}C NMR (126 MHz, [D_3]MeCN, 25 °C, TMS): δ = 145.7 (C(1,8)), 138.3 (C(4a)), 127.2 (C(4,5)), 120.4 (t, ^3J(P,C) = 12.1 Hz, C(8a)), 120.3 (C(3,6)), 112.3 (d, ^3J(P,C) = 10.7 Hz, C(2,7)), 13.5 ppm (d, ^1J(P,C) = 66.9 Hz, C(9)); ^{31}P NMR (122 MHz, [D_3]MeCN, 25 °C, 85% H_3PO_4): δ = 29.5 (s, -PMe_3), −145.5 ppm (sept, ^1J(P,F) = 706.3 Hz, PF_6^-); IR: $\tilde{\nu}$ = 486, 555, 632, 664, 685, 762, 820, 876, 960, 1051, 1083, 1133, 1294, 1326, 1409, 1458, 1512, 1573, 1609, 2871, 2931, 2958 cm^{-1}; ESI-MS (MeCN): *m/z* (%): 307 (100) $[M]^+$; HRMS (ESI): *m/z* calcd for $C_{16}H_{25}N_2P_2^+$: 307.1487 $[M]^+$; found: 307.1482; (−)-ESI-MS (MeCN): *m/z* (%): 145 (100) $[PF_6]^-$; HRMS ((−)-ESI): *m/z* calcd for PF_6^-: 144.9647 $[M]^-$; found: 144.9646; elemental analysis calcd (%) for $C_{16}H_{25}F_6N_2P_3$: C 42.29, H 5.57, N 6.19; found: C 42.11, H 5.55, N 6.41.

1,8-Bis(triisopropylphosphazenyl)naphthalene hydrobromide (TiPrPN·HBr): A solution of 1,8-diaminonaphthalene (297 mg, 1.87 mmol, 1.0 equiv) and triethylamine (759 mg, 7.50 mmol, 4.0 eq) in chlorobenzene (20 mL) was added dropwise to a suspension of triisopropylbromophosphoniumbromide (1200 mg, 3.75 mmol, 2.0 equiv) in chlorobenzene (40 mL). The grey reaction mixture changed color to light brown and was stirred for 1 h at 90 °C. A solution of $NaN(SiMe_3)_2$ (1031 mg, 5.63 mmol, 3.0 equiv) in chlorobenzene (20 mL) was added at room temperature and the reaction mixture was stirred for 2 h at 90 °C. The hot solution was filtered over celite and the filtrate was evaporated to dryness in vacuo. The oily residue was washed with hexane to give a powdery raw product which was washed with THF. The remaining solid was dried in vacuo to give TiPrPN·HBr (780 mg, 1.40 mmol, 75%) as a beige solid. Single crystals suitable for structure determination were obtained by layering a saturated solution of TiPrPN·HBr in acetonitrile with diethyl ether. ^{1}H NMR (300 MHz, [D_3]MeCN, 25 °C, TMS): δ = 14.05 (br s,s 1H, NH), 7.30 (d, ^3J(H,H) = 8.2 Hz, 2H, H(4,5)), 7.21 (t, ^3J(H,H) = 7.8 Hz, 2H, H(3,6)), 6.78 (d, ^3J(H,H) = 7.4 Hz, 2H, H(2,7)), 2.84 (dsept, ^3J(H,H) = 7.3 Hz, ^2J(P,H) = 12.0 Hz, 6H, H(9)), 1.30 ppm (dd, ^3J(H,H) = 7.3 Hz, ^3J(P,H) = 15.6 Hz, 36H, H(10)); ^{13}C NMR (126 MHz, [D_3]MeCN, 25 °C, TMS): δ = 145.3 (d, ^2J(P,C) = 4.0 Hz, C(1,8)), 137.7 (C(4a)), 127.0 (C(4,5)), 123.4 (t, ^3J(P,C) = 9.1 Hz, C(8a)), 121.5 (C(3,6)), 116.1 (d, ^3J(P,C) = 4.8 Hz, C(2,7)), 25.5 (d, ^1J(P,C) = 54.4 Hz, C(9)), 17.1 ppm (d, ^2J(P,C) = 2.5 Hz, C(10)); ^{31}P NMR (122 MHz, [D_3]MeCN, 25 °C, 85% H_3PO_4): δ = 54.3 ppm; IR: $\tilde{\nu}$ = 423, 479, 494, 539, 567, 660, 693, 728, 755, 819, 884, 941, 993, 1054, 1095, 1126, 1180, 1246, 1288, 1334, 1375, 1426, 1455, 1544, 1569, 2869, 2930, 2958, 3037 cm^{-1}; ESI-MS (MeCN): *m/z* (%): 476 (100) $[M]^+$; HRMS (ESI): *m/z* calcd for $C_{28}H_{49}N_2P_2^+$: 475.3365 $[M]^+$; found: 475.3368.

TiPrPN: A solution of $KN(SiMe_3)_2$ (54 mg, 0.271 mmol, 1.0 equiv) in toluene (10 mL) was added dropwise to a solution of TiPrPN·HBr (150 mg, 0.271 mmol, 1.0 equiv) in toluene (20 mL) at 0 °C. The reaction mixture was stirred for 2 h at 90 °C and filtered over celite. The filtrate was evaporated to dryness in vacuo and the remaining residue was washed with hexane to give TiPrPN as a beige solid (105 mg, 0.221 mmol, 82%). Single crystals suitable for structure determination were obtained by slowly cooling a hot saturated solution of TiPrPN in hexane to −30 °C. ^{1}H NMR (300 MHz, [D_3]MeCN, 25 °C, TMS): δ = 6.84 (t, ^3J(H,H) = 7.6 Hz, 2H, H(3,6)), 6.76 (d, ^3J(H,H) = 7.9 Hz, 2H, H(4,5)), 6.35 (dd, ^3J(H,H) = 7.3 Hz, ^4J(H,H) = 1.7 Hz, 2H, H(2,7)), 2.50 (dsept, ^3J(H,H) = 7.3 Hz, ^2J(P,H) = 11.7 Hz, 6H, H(9)), 1.22 ppm (dd, ^3J(H,H) = 7.3 Hz, ^3J(P,H) = 14.0 Hz, 36H, H(10)); ^{13}C NMR (126 MHz, [D_3]MeCN, 25 °C, TMS): δ = 154.7 (C(1,8)), 139.5 (C(4a)), 131.0 (C(8a)), 125.6 (C(3,6)), 124.4 (C(8a)), 117.3 (d, ^3J(P,C) = 8.6 Hz, C(2,7)), 116.3 (C(4,5)), 26.8 (d, ^1J(P,C) = 58.6 Hz, C(9)), 18.0 ppm (d, ^2J(P,C) = 2.6 Hz, C(10)); ^{31}P NMR (121.5 MHz, [D_3]MeCN,

25 °C, 85% H_3PO_4): $\delta = 25.6$ ppm; IR: $\tilde{\nu} = 424$, 480, 494, 536, 567, 624, 635, 660, 693, 739, 754, 772, 818, 845, 883, 929, 992, 1023, 1053, 1096, 1127, 1181, 1245, 1287, 1337, 1375, 1427, 1495, 1544, 1588, 2869, 2897, 2928, 2957, 3037 cm^{-1}; ESI-MS (MeCN): *m/z* (%): 475 (100) $[M]^+$; HRMS (ESI): *m/z* calcd for $C_{28}H_{49}N_2P_2^+$: 475.3365 $[M]^+$; found: 475.3362; elemental analysis calcd (%) for $C_{28}H_{48}N_2P_2$: C 70.85, H 5.90, N 10.19; found: C 70.88, H 6.19, N 10.36.

1,8-Bis(tricyclopentylphosphazenyl)naphthalene (TcyPPN): A solution of 1,8-diaminonaphthalene (167 mg, 1.059 mmol, 1.0 equiv) und triethylamine (429 mg, 4.236 mmol, 4.0 equiv) in chlorobenzene (10 mL) was added dropwise to a suspension of tricyclopentylbromophosphoniumbromide (843 mg, 2.117 mmol, 2.0 equiv) in chlorobenzene (30 mL). The reaction mixture was stirred for 2 h at room temperature and for additional 2 h at 80 °C. A solution of KN($SiMe_3$)$_2$ (845 mg, 4.236 mmol, 4.0 equiv) in chlorobenzene (10 mL) was added dropwise and the reaction mixture was stirred for 2 h at room temperature. The suspension was filtered over celite and the filtrate was evaporated to dryness in vacuo. The residue was extracted several times with boiling hexane (30 mL) and TcyPPN recrystallized when allowing the solution to reach room temperature. The supernatant was decanted and drying in vacuo yielded TcyPPN (373 mg, 0.591 mmol, 56%) as white crystals. ^{1}H NMR (300 MHz, [D_6]benzene, 25 °C, TMS): $\delta = 7.39$ (d, ^3J(H,H) = 8.1 Hz, 2H, H(4,5)), 7.29 (t, ^3J(H,H) = 7.5 Hz, 2H, H(3,6)), 6.83 (dd, ^3J(H,H) = 7.0 Hz, ^4J(H,H) = 2.6 Hz, 2H, H(2,7)), 2.04–1.76 (m, 18H, H(9,10)), 1.67–1.50 (m, 24H, H(10,11)), 1.67–1.50 ppm (m, 12H, H(11)); ^{13}C NMR (126 MHz, [D_6]benzene, 25 °C, TMS): $\delta = 153.9$ (C(1,8)), 138.2 (C(4a)), 133.6 (C(8a)), 124.9 (C(3,6)), 120.2 (d, ^3J(P,C) = 9.2 Hz, C(2,7)), 117.9 (C(4,5)), 38.3 (d, ^1J(P,C) = 63.6 Hz, C(9)), 28.0 (C(10)), 26.6 ppm (d, ^3J(P,C) = 9.7 Hz, C(11)); ^{31}P NMR (101 MHz, [D_6]benzene, 25 °C, 85% H_3PO_4): $\delta = 21.1$ ppm; ESI-MS (MeCN): *m/z* (%): 631 (100) $[M]^+$; HRMS (ESI): *m/z* calcd for $C_{40}H_{61}N_2P_2^+$: 631.4304 $[M]^+$; found: 631.4310; elemental analysis calcd (%) for $C_{40}H_{60}N_2P_2$: C 76.15, H 9.59, N 4.44; found: C 76.10, H 10.04, N 4.65.

TcyPPN·HPF$_6$: A solution of NH_4PF_6 (26 mg, 0.159 mmol, 1.0 equiv) in THF (6 mL) was added dropwise to a solution of TcyPPN (100 mg, 0.159 mmol, 1.0 equiv) in THF (6 mL). The precipitation of a white solid was observed after a few minutes. The suspension was stirred for 1 h at room temperature and the precipitate was separated by centrifugation and washed with pentane (15 mL). After drying in vacuo TcyPPN·HPF_6 (91 mg, 0.117 mmol, 74%) was obtained as a white solid.[64] ^{1}H NMR (300 MHz, [D_3]MeCN, 25 °C, TMS): $\delta = 13.34$ (t, ^2J(P,H) = 2.4 Hz, 1H, NH), 7.30 (d, ^3J(H,H) = 8.2 Hz, 2H, H(4,5)), 7.21 (t, ^3J(H,H) = 7.8 Hz, 2H, H(3,6)), 6.79 (d, ^3J(H,H) = 7.4 Hz, 2H, H(2,7)), 2.74–2.59 (m, 6H, H(9)), 1.79–1.60 ppm (m, 48H, H(10,11)); ^{13}C NMR (126 MHz, [D_3]MeCN, 25 °C, TMS): $\delta = 145.2$ (dd, ^2J(P,C) = 4.9 Hz, ^4J(P,C) = 1.5 Hz, C(1,8)), 137.2 (C(4a)), 126.9 (C(4,5)), 125.1 (t, ^3J(P,C) = 8.3 Hz, C(8a)), 121.5 (C(3,6)), 117.4 (d, ^3J(P,C) = 5.6 Hz, C(2,7)), 36.5 (d, ^1J(P,C) = 59.4 Hz, C(9)), 28.4 (C(10)), 26.5 ppm (d, ^3J(P,C) = 10.6 Hz, C(11)); ^{31}P NMR (101 MHz, [D_3]MeCN, 25 °C, 85% H_3PO_4): $\delta = 52.8$, −142.9 ppm (sept, ^1J(P,F) = 705.8 Hz, PF_6^-); ESI-MS (MeCN): *m/z* (%): 631 (100) $[M]^+$; HRMS (ESI): *m/z* calcd for $C_{40}H_{61}N_2P_2^+$: 631.4304 $[M]^+$; found: 631.4294; (−)-ESI-MS (MeCN): *m/z* (%): 145 (100) $[PF_6]^-$; HRMS ((−)-ESI): *m/z* calcd for PF_6^-: 144.9647 $[M]^-$; found: 144.9648; elemental analysis calcd (%) for $C_{40}H_{61}F_6N_2P_3$: C 61.84, H 7.91, N 3.61; found: C 61.57, H 7.99, N 3.88.

1,8-Bis(trispyrrolidinophosphazenyl)naphthalene hydrobromide (TPPN·HBr): Bromine (7.04 g, 44.04 mmol, 2.1 equiv) was added dropwise to a solution of trispyrrolidylphosphane (10.63 g, 44.04 mmol, 2.1 equiv) in benzene (200 mL) at 0 °C. Precipitation of trispyrrolidylbromophosphonium bromide was observed and the suspension was stirred for 1 h at 0 °C and for 1.5 h at room temperature. A solution of 1,8-diaminonaphthalene (3.32 g, 20.98 mmol, 1.0 equiv) and triethylamine (9.16 g, 83.89 mmol, 4.0 equiv) in benzene (50 mL) was added dropwise. The reaction mixture changed color to dark red and was stirred for 3 d at 80 °C. The hot suspension was filtered over celite and the filtrate was evaporated to dryness in vacuo. The residue was suspended in THF (100 mL) and separated from the red supernatant by filtration. The solid was washed three times with THF (25 mL) and dried in vacuo. TPPN·HBr (10.94 g, 73%) was obtained as a grey solid. ^{1}H NMR (300 MHz, [D_3]MeCN, 25 °C, TMS): $\delta = 15.02$ (br s, 1H, NH), 7.18–7.17 (m, 4H, H(2,3,4,5,6)), 6.66 (t, ^3J(H,H) = 4.4 Hz, 2H, H(2,7)), 3.26–3.21 (m, 24H, H(9)), 1.88–1.83 ppm (m, 24H, H(10)); ^{13}C NMR (76 MHz, [D_3]MeCN, 25 °C, TMS): $\delta = 144.2$ (C(1,8)), 137.7 (C(4a)), 126.9 (C(3,6)), 120.6 (t, ^3J(P,C) = 13.6 Hz, C(8a)), 120.0 (C(4,5)), 114.0 (t, ^3J(P,C) = 7.3 Hz, C(2,7)), 48.0 (d, ^2J(P,C) = 4.7 Hz, C(9)), 26.9 ppm (d, ^3J(P,C) = 8.2 Hz, C(10)); ^{31}P NMR (122 MHz, [D_3]MeCN, 25 °C, 85% H_3PO_4): $\delta = 18.1$ ppm; IR: $\tilde{\nu} = 448$, 484, 520, 548, 558, 573, 629, 650, 699, 758, 817, 872, 897, 910, 929, 954, 968, 1012, 1071, 1212, 1247, 1288, 1319, 1360, 1403, 1453, 1513, 1569, 1612, 2868, 2948, 3043 cm^{-1}; ESI-MS (MeCN): *m/z* (%): 638 (100) $[M]^+$; HRMS (ESI): *m/z* calcd for $C_{34}H_{55}N_8P_2^+$: 637.4019 $[M]^+$; found: 637.4012; elemental analysis calcd (%) for $C_{34}H_{55}BrN_8P_2$: C 56.90, H 7.72, N 15.61; found: C 55.41, H 7.69, N 15.75.

Deprotonation of TPPN·HBr: TPPN·HBr (1.500 g, 2.090 mmol, 1.0 equiv) and KN($SiMe_3$)$_2$ (0.417 g, 2.090 mmol, 1.0 equiv) were suspended in hexane (200 mL) and stirred for 24 h at 60 °C. The hot reaction mixture was filtered over celite and the filtrate was concentrated in vacuo to about 20 mL. TPPN was recrystallized at −30 °C and dried in vacuo. It was obtained as a beige solid (0.846 g, 64%). ^{1}H NMR (400 MHz, [D_3]MeCN, 25 °C, TMS): $\delta = 6.85$ (t, 2H, ^3J(H,H) = 7.7 Hz, H(3,6)), 6.69 (d, 2H, ^3J(H,H) = 7.7 Hz, H(4,5)), 6.34 (d, 2H, ^3J(H,H) = 7.7 Hz, H(2,7)), 3.23–3.19 (m, 24H, H(9)), 1.78–1.75 ppm (m, 24H, H(10)); ^{13}C NMR (101 MHz, [D_3]MeCN, 25 °C, TMS): $\delta = 153.2$ (d, ^2J(P,C) = 6.8 Hz, C(1,8)), 140.3 (t, ^3J(P,C) = 12.7 Hz, C(8a)), 128.9 (C(4a)), 126.6 (C(3,6)), 117.2 (d, ^3J(P,C) = 10.6 Hz, C(2,7)), 116.1 (C(4,5)), 48.3 (d, ^2J(P,C) = 4.5 Hz, C(9)), 27.9 ppm (d, ^3J(P,C) = 8.2 Hz, C(10)); ^{31}P NMR (122 MHz, [D_3]MeCN, 25 °C, 85% H_3PO_4): $\delta = 2.5$ ppm; IR: $\tilde{\nu} = 443$, 487, 563, 636, 748, 778, 814, 870, 912, 1005, 1065, 1125, 1195, 1239, 1290, 1341, 1383, 1430, 1544, 2858, 2957, 3039 cm^{-1}; ESI-MS (MeCN): *m/z* (%): 637 (100) $[MH]^+$, 566 (3) $[M-C_4H_8N]^+$, 497 (3) $[M-(C_4H_8N)_2]^+$, 381 (1) $[M-C_{12}H_{24}N_4P]^+$, 256 (1) $[MH^+-C_{12}H_{24}N_4P-(C_4H_8N)_2]^+$; HRMS (ESI): *m/z* calcd for $C_{34}H_{55}N_8P_2^+$: 637.4025 $[MH]^+$; found: 637.4019; elemental analysis calcd (%) for $C_{34}H_{54}N_8P_2$: C 64.13, H 8.55, N 17.60; found: C 64.16, H 8.42, N 17.57.

Bisprotonation of TPPN with HN(SO_2CF_3)$_2$: A solution of HN(SO_2CF_3)$_2$ (88 mg, 0.314 mmol, 2.0 equiv) in THF (5 mL) was added dropwise to a solution of TPPN (100 mg, 0.157 mmol, 1.0 equiv) in THF (10 mL). The reaction mixture turned to pale violet and was stirred for 1 h at room temperature. The solvent was removed in vacuo and the residue was washed with pentane (15 mL). It was dried in vacuo to obtain TPPN·2HN(SO_2CF_3)$_2$ (116 mg, 0.097 mmol, 62%) as a brown solid. ^{1}H NMR (300 MHz, [D_3]MeCN, 25 °C, TMS): $\delta = 7.85$ (d, ^3J(H,H) = 8.3 Hz, 2H, H(4,5)), 7.65 (d, ^2J(P,H) = 6.5 Hz, 2H, NH), 7.55 (t, ^3J(H,H) = 7.9 Hz, 2H, H(3,6)), 7.29 (d, ^3J(H,H) = 7.5 Hz, 2H, H(2,7)), 3.12 (dt, ^3J(H,H) = 6.7 Hz, ^3J(P,H) = 3.2 Hz, 24H, H(9)), 1.82–1.78 ppm (m, 24H, H(10)); ^{13}C NMR (101 MHz, [D_3]MeCN, 25 °C, TMS): $\delta = 137.7$ (C(4a)), 132.7 (C(1,8)), 128.0 (C(4,5)), 127.7 (C(2,7)), 124.2 (t, ^3J(P,C) = 6.0 Hz, C(8a)), 123.6 (d, ^3J(P,C) = 4.4 Hz, C(2,7)), 120.9 (quart, ^1J(C,F) = 320.8 Hz, CF_3), 48.6 (d, ^2J(P,C) = 4.9 Hz, C(9)), 26.7 ppm (d, ^3J(P,C) = 8.6 Hz, C(10)); ^{31}P NMR (101 MHz, [D_3]MeCN, 25 °C, 85% H_3PO_4): $\delta = 25.0$ ppm; ESI-MS (MeCN): *m/z* (%): 638 (100) $[M]^+$; HRMS (ESI): *m/z* calcd for $C_{34}H_{55}N_8P_2^+$:

637.4019 $[M]^+$; found: 637.4016; (−)-ESI-MS (MeCN): *m/z* (%): 280 (100) $[M]^-$; HRMS ((−)-ESI): *m/z* calcd for $C_2F_6NO_4S_2^-$: 279.9178 $[M]^-$; found: 279.9178.

Reaction of TPPN with dimethylaluminum chloride: A solution of dimethylaluminum chloride (29 mg, 0.314 mmol, 2.0 equiv) in toluene (0.8 mL) was added dropwise to a solution of TPPN (100 mg, 0.157 mmol, 1.0 equiv) in toluene (10 mL). The formation of a colorless precipitate was observed and the reaction mixture was stirred for 1 h at room temperature. The precipitate was separated by filtration and washed with pentane (20 mL). After drying in vacuo $[TPPN\text{-}AlMe_2][AlMe_2Cl_2]^-$ (111 mg, 86%) was obtained as a colorless solid. Single crystals suitable for structure determination were obtained by layering a saturated solution of $[TPPN\text{-}AlMe_2][AlMe_2Cl_2]^-$ in dichloromethane with pentane. ^{1}H NMR (300 MHz, CD_2Cl_2, 25 °C, TMS): δ = 7.44 (d, ^3J(H,H) = 8.2 Hz, 2H, H(4,5)), 7.29 (t, ^3J(H,H) = 7.8 Hz, 2H, H(3,6)), 7.02 (dt, ^3J(H,H) = 8.0 Hz, ^4J(H,H) = 1.5 Hz, 2H, H(2,7)), 3.12–3.07 (m, 24H, H(9)), 1.85–1.81 (m, 24H, H(10)), −0.80 (s, 6H, AlCH_3), −0.81 ppm (s, 6H, AlCH_3); ^{31}P NMR (101 MHz, CD_2Cl_2, 25 °C, 85% H_3PO_4): δ = 26.3 ppm; ESI-MS (CH_2Cl_2): *m/z* (%): 694 (100) $[M]^+$, 638 (20) $[M-AlMe_2]^+$; HRMS (ESI): *m/z* calcd for $C_{36}H_{60}AlN_8P_2^+$: 693.4226 $[M]^+$; found: 693.4223; elemental analysis calcd (%) for $C_{22}H_{42}Al_2N_2P_2$: C 55.54, H 8.09, N 13.64; found: C 55.00, H 7.79, N 13.85.

Reaction of TMPN with trimethylaluminum: A solution of trimethylaluminium (47 mg, 0.653 mmol, 2.0 equiv) in toluene (5 mL) was added dropwise to a solution of TMPN (100 mg, 0.326 mmol, 1.0 equiv) in toluene (10 mL). A white solid precipitated and the suspension was stirred for 3 h at room temperature. The precipitate was collected by filtration, washed with pentane (15 mL) and dried in vacuo. $[TMPN\text{-}AlMe_2]^+[AlMe_4]^-$ (99 mg, 67%) was obtained as a beige solid. Single crystals suitable for structure determination were obtained by layering a saturated solution of $[TMPN\text{-}AlMe_2]^+[AlMe_4]^-$ in dichloromethane with hexane. ^{1}H NMR (400 MHz, CD_2Cl_2, 25 °C, TMS): δ = 7.59 (d, ^3J(H,H) = 8.3 Hz, 2H, H(4,5)), 7.39 (t, 2H, ^3J(H,H) = 7.9 Hz, H(3,6)), 6.88 (d, ^3J(H,H) = 7.5 Hz, 2H, H(2,7)), 1.98 (d, ^2J(P,H) = 12.5 Hz, 18H, H(9)), −0.86 (s, 6H, H(10)), −1.20 - −1.27 ppm (m, 12H, H(11)); ^{13}C NMR (101 MHz, CD_2Cl_2, 25 °C, TMS): δ = 141.3 (d, ^2J(P,C) = 4.6 Hz, C(1,8)), 137.4 (C(4a)), 126.5 (t, ^3J(P,C) = 8.6 Hz, C(8a)), 126.1 (C(3,6)), 125.2 (C(4,5)), 121.0 (d, ^3J(P,C) = 10.0 Hz, C(2,7)), 16.7 (d, ^1J(P,C) = 67.1 Hz, C(9)), −4.6 (sext, ^1J(Al,C) = 70.5 Hz, C(11)), −6.2 ppm (C(10)); ^{31}P NMR (101 MHz, CD_2Cl_2): δ = 38.5 ppm; ESI-MS (MeCN): *m/z* (%): 307 (100) $[M-AlMe_2]^+$; HRMS (ESI): *m/z* calcd for $C_{16}H_{25}N_2P_2^+$: 307.1487 $[M-AlMe_2]^+$; found: 307.1485.

Reaction of TMPN with trimethylgallium: A solution of trimethylgallium (75 mg, 0.653 mmol, 2.0 equiv) in toluene (5 mL) was added dropwise to a solution of TMPN (100 mg, 0.326 mmol, 1.0 equiv) in toluene (10 mL). A brown solid precipitated and the suspension was stirred for 6 h at room temperature. All volatiles were removed in vacuo and the brown residue was recrystallized from dichloromethane/hexane (2:1). The precipitate was collected by filtration, washed twice with hexane (15 mL) and dried in vacuo. $[TMPN\text{-}GaMe_2]^+[GaMe_4]^-$ (68 mg, 39%) was obtained as brown needles. Single crystals suitable for structure determination were obtained by layering a saturated solution of $[TMPN\text{-}GaMe_2]^+[GaMe_4]^-$ in dichloromethane with hexane. ^{1}H NMR (400 MHz, CD_2Cl_2, 25 °C, TMS): δ = 7.55 (d, ^3J(H,H) = 7.2 Hz, 2H, H(4,5)), 7.34 (t, 2H, ^3J(H,H) = 6.9 Hz, H(3,6)), 6.83 (d, ^3J(H,H) = 7.5 Hz, 2H, H(2,7)), 1.84 (d, ^2J(P,H) = 12.3 Hz, 18H, H(9)), −0.42 ppm (s, 6H, H(10)), −0.90 (s, 12H, H(11)); ^{13}C NMR (101 MHz, CD_2Cl_2, 25 °C, TMS): δ = 142.9 (C(1,8)), 137.7 (C(4a)), 126.4 (t, ^3J(P,C) = 10.0 Hz, C(8a)), 125.8 (C(3,6)), 125.0 (C(4,5)), 121.1 (d, ^3J(P,C) = 9.8 Hz, C(2,7)), 16.7 (d, ^1J(P,C) = 67.1 Hz, C(9)), −3.1 (C(11)), −3.4 ppm (C(10)); ^{31}P NMR (101 MHz, CD_2Cl_2, 25 °C, 85% H_3PO_4): δ = 38.6 ppm; ESI-MS (MeCN): *m/z* (%): 307 (100) $[M-GaMe_2]^+$; HRMS (ESI): *m/z* calcd for $C_{16}H_{25}N_2P_2^+$: 307.1487 $[MH^+\text{-}GaMe_2]^+$; found: 307.1485; elemental analysis calcd (%) for $C_{22}H_{42}Ga_2N_2P_2$: C 49.30, H 7.90, N 5.23; found: C 48.56, H 7.96, N 5.34.

Acknowledgements

We thank Dr. Klaus Harms, Lars Finger, and Fabian Schröder for their valuable support with crystal structure refinement. Financial support by the Fonds der Chemischen Industrie (doctoral scholarship for J.K.) is gratefully acknowledged. B.K. gratefully acknowledges support of the Computing Center of the University of Zagreb (SRCE) for granting computational time on ISABELLA cluster. X.X. acknowledges the Deutsche Forschungsgemeinschaft for funding the Bruker NMR Spectrometers

Keywords: ab initio calculations · basicity · N ligands · phosphazenes

[1] P. S. Bowman, W. R. S. Steele, D. R. Winterman, R. W. Alder, *Chem. Commun. (London)* **1968**, 723–724.
[2] H. C. Brown, D. H. McDaniel, O. Häflinger in *Determination of Organic Structures by Physical Methods* (Eds.: E. A. Braude, F. C. Nachod), Academic Press, New York, **1955**, pp. 567–662.
[3] T. Ishikawa, *Superbases for organic synthesis: guanidines, amidines and phosphazenes and related organocatalysts* (Ed.: T. Ishikawa), Wiley, **2009**, pp. 251–271 and references therein.
[4] J. E. Richman, *Tetrahedron Lett.* **2010**, *51*, 2793–2796.
[5] D. A. Evans, A. M. Ratz, B. E. Huff, G. S. Sheppard, *Tetrahedron Lett.* **1994**, *35*, 7171–7172.
[6] S. Kanemasa, Y. Oderatoshi, E. Wada, *J. Am. Chem. Soc.* **1999**, *121*, 8675–8676.
[7] F. Tur, J. M. Saá, *Org. Lett.* **2007**, *9*, 5079–5082.
[8] D. Kiely, P. J. Guiry, *J. Organomet. Chem.* **2003**, *687*, 545–561.
[9] a) B. Kovačević, Z. B. Maksić, R. Vianelloa, M. Primorac, *New J. Chem.* **2002**, *26*, 1329–1334; b) A. F. Pozharskii, A. V. Degtyarev, V. A. Ozeryanskii, O. V. Ryabtsova, Z. A. Starikova, G. S. Borodkin, *J. Org. Chem.* **2010**, *75*, 4706–4715; c) A. Parkin, K. Wozniak, C. C. Wilson, *Cryst. Growth Des.* **2007**, *7*, 1393–1398; d) A. V. Degtyarev, O. V. Ryabtsova, A. F. Pozharskii, V. A. Ozeryanskii, Z. A. Starikova, L. Sobczyk, A. Filarowski, *Tetrahedron* **2008**, *64*, 6209–6214; e) C. Cox, H. Wack, T. Lectka, *Angew. Chem.* **1999**, *111*, 864–867; *Angew. Chem. Int. Ed.* **1999**, *38*, 798–800; f) V. A. Ozeryanskii, A. F. Pozharskii, A. J. Bienko, W. Sawka-Dobrowolska, L. Sobczyk, *J. Phys. Chem. A* **2005**, *109*, 1637–1642; g) J. E. Del Benea, I. Alkortab, J. Elguerob, *Magn. Reson. Chem.* **2008**, *46*, 457–463; h) A. F. Pozharskii, O. V. Ryabtsova, V. A. Ozeryanskii, A. V. Degtyarev, Z. A. Starikova, L. Sobczykc, A. Filarowskic, *Tetrahedron Lett.* **2005**, *46*, 3973–3976; i) S. M. Bachrach, *Org. Lett.* **2012**, *14*, 5598–5601; j) M. Pietrzak, J. P. Wehling, S. Kong, P. M. Tolstoy, I. G. Shenderovich, C. Lopez, R. M. Claramunt, J. Elguero, G. S. Denisov, H. Limbach, *Chem. Eur. J.* **2010**, *16*, 1679–1690; k) V. A. Ozeryanskii, A. F. Pozharskii, *Tetrahedron* **2013**, *69*, 2107–2112; l) M. T. Scerba, C. M. Leavitt, M. E. Diener, A. F. DeBlase, T. L. Guasco, M. A. Siegler, N. Bair, M. A. Johnson, T. Lectka, *J. Org. Chem.* **2011**, *76*, 7975–7984.
[10] N. C. Abacilar, V. Raab, E. Gaoutchenova, U. Garrelts, K. Harms, J. Sundermeyer, *The Chemistry of Superbasic Guanidines in Activating Unreactive Substrates, The Role of Secondary Interactions* (Eds.: C. Bolm, F. E. Hahn), Wiley-VCH, Weinheim, **2009**, pp. 17–37.
[11] a) T. Yamasaki, N. Ozaki, Y. Saika, K. Ohta, K. Goboh, F. Nakamura, M. Hashimoto, S. Okeya, *Chem. Lett.* **2004**, *33*, 928–929; b) G. Villaverde, A. Arnanz, M. Iglesias, A. Monge, F. Sanchez, N. Snejko, *Dalton Trans.* **2011**, *40*, 9589–9600; c) U. Wild, O. Hübner, A. Maronna, M. Enders, E. Kaifer, H. Wadepohl, H. Himmel, *Eur. J. Inorg. Chem.* **2008**, 4440–4447; d) V. Vitske, C. König, O. Hübner, E. Kaifer, H. Himmel, *Eur. J. Inorg. Chem.*

2010, 115 – 126; e) S. Wiesner, A. Ziesak, M. Reinmuth, P. Walter, E. Kaifer, H. Wadepohl, H. Himmel, *Eur. J. Inorg. Chem.* **2013**, 163 – 171.

[12] a) R. Shroff, A. Svatoš, *Anal. Chem.* **2009**, *81*, 7954 – 7959; b) R. Shroff, A. Svatoš, *Rapid Commun. Mass Spectrom.* **2009**, *23*, 2380 – 2382; c) S. Zhang, Z.-P. Yao, *Anal. Chim. Acta* **2012**, *711*, 77 – 82; d) C. D. Calvano, C. G. Zambonin, F. Palmisano, *Rapid Commun. Mass Spectrom.* **2011**, *25*, 1757 – 1764; e) D. Cao, Z. Wang, C. Han, L. Cui, M. Hu, J. Wu, Y. Liu, Y. Cai, H. Wang, Y. Kang, *Talanta* **2011**, *85*, 345 – 352; f) C. D. Calvano, A. Monopoli, N. Ditaranto, F. Palmisano, *Anal. Chim. Acta* **2013**, *798*, 56 – 63.

[13] D. Cao, M. Hu, C. Han, J. Yu, L. Cui, Y. Liu, H. Wang, Y. Cai, Y. Kang, Y. Zhou, *Analyst* **2012**, *137*, 2218 – 2225.

[14] Y. Zou, PhD Thesis, Universität Stuttgart (Germany), **2001**.

[15] R. E. Cherpeck, C. Y. Chan, G. Bhalla (Chevron Oronite Company), CA 2646839, **2008**.

[16] a) R. W. Alder, N. C. Goode, N. Miller, F. Hibbert, K. P. P. Hunte, H. J. Robbins, *J. Chem. Soc. Chem. Commun.* **1978**, *3*, 89 – 90; b) R. W. Alder, M. R. Bryce, N. C. Goode, N. Miller, J. Owen, *J. Chem. Soc. Perkin Trans. 1* **1981**, 2840 – 2847; c) F. Hibbert, K. P. P. Hunte, *J. Chem. Soc. Perkin Trans. 2* **1983**, 1895 – 1890; d) A. F. Pozharskii, O. V. Ryabtsova, V. A. Ozeryanskii, A. V. Degtyarev, O. N. Kazheva, G. G. Alexandrov, O. A. Dyachenko, *J. Org. Chem.* **2003**, *68*, 10109 – 10122; e) A. V. Degtyarev, A. F. Pozharskii, *Chem. Heterocycl. Compd.* **2008**, *44*, 1138 – 1145; f) E. A. Filatova, A. F. Pozharskii, A. V. Gulevskaya, N. V. Vistorobskii, V. A. Ozeryanskii, *Synlett* **2013**, *24*, 2515 – 2518.

[17] F. J. Hibbert, *Chem. Soc. Perkin Trans. 2* **1974**, 1862 – 1866.

[18] A. Awwal, F. J. Hibbert, *Chem. Soc. Perkin Trans. 2* **1977**, 1589 – 1592.

[19] F. Hibbert, G. R. Simpson, *J. Chem. Soc. Perkin Trans. 2* **1987**, 613 – 615.

[20] M. A. Zirnstein, H. A. Staab, *Angew. Chem.* **1987**, *99*, 460 – 461; *Angew. Chem. Int. Ed. Engl.* **1987**, *26*, 460 – 461.

[21] K. J. Shaffer, D. C. Parr, M. Wenzel, G. J. Rowlands, P. G. Plieger, *Eur. J. Org. Chem.* **2012**, 6967 – 6975.

[22] H. A. Staab, T. Saupe, C. Krieger, *Angew. Chem.* **1983**, *95*, 748 – 749; *Angew. Chem. Int. Ed. Engl.* **1983**, *22*, 731 – 732.

[23] H. A. Staab, M. Höne, C. Krieger, *Tetrahedron Lett.* **1988**, *29*, 1905 – 1908.

[24] T. Saupe, C. Krieger, H. A. Staab, *Angew. Chem.* **1986**, *98*, 460 – 462; *Angew. Chem. Int. Ed. Engl.* **1986**, *25*, 451 – 453.

[25] H. A. Staab, C. Krieger, M. Hone, *Tetrahedron Lett.* **1988**, *29*, 5629 – 5632.

[26] H. A. Staab, M. A. Zirnstein, C. Krieger, *Angew. Chem.* **1989**, *101*, 73 – 75; *Angew. Chem. Int. Ed. Engl.* **1989**, *28*, 86 – 88.

[27] H. Zachova, S. Man, J. Taraba, M. Potacek, *Tetrahedron* **2009**, *65*, 792 – 797; b) J. Galeta, M. Potáček, *J. Org. Chem.* **2012**, *77*, 1010 – 1017.

[28] a) I. Despotović, B. Kovačević, Z. B. Maksić, *Org. Lett.* **2007**, *9*, 4709 – 4712; b) S. M. Bachrach, C. C. Wilbanks, *J. Org. Chem.* **2010**, *75*, 2651 – 2660; c) N. Uchida, J. Kuwabara, A. Taketoshi, T. Kanbara, *J. Org. Chem.* **2012**, *77*, 10631 – 10637.

[29] L. Belding, T. Dudding, *Chem. Eur. J.* **2014**, *20*, 1032 – 1037.

[30] R. Schwesinger, H. Schlemper, *Angew. Chem.* **1987**, *99*, 1210 – 1212; *Angew. Chem. Int. Ed. Engl.* **1987**, *26*, 1165 – 1167.

[31] a) V. Raab, J. Kipke, R. M. Gschwind, J. Sundermeyer, *Chem. Eur. J.* **2002**, *8*, 1682 – 1693; b) V. Raab, K. Harms, J. Sundermeyer, B. Kovačević, Z. B. Maksić, *J. Org. Chem.* **2003**, *68*, 8790 – 8797.

[32] R. Schwesinger, H. Schlemper, C. Hasenfratz, J. Willaredt, T. Dambacher, T. Breuer, C. Ottaway, M. Fletschinger, J. Boele, H. Fritz, D. Putzas, H. W. Rotter, F. G. Brodwell, A. V. Satish, G. Ji, E. Peters, K. Peters, H. G. von Schnering, L. Walz, *Liebigs Ann.* **1996**, *7*, 1055 – 1081 and references therein.

[33] V. Raab, E. Gauchenova, A. Merkoulov, K. Harms, J. Sundermeyer, B. Kovačević, Z. B. Maksić, *J. Am. Chem. Soc.* **2005**, *127*, 15738 – 15743.

[34] J. F. Kögel, B. Oelkers, B. Kovačević, J. Sundermeyer, *J. Am. Chem. Soc.* **2013**, *135*, 17768 – 17774.

[35] a) H. A. Staab, T. Saupe, *Angew. Chem.* **1988**, *100*, 895 – 909; *Angew. Chem. Int. Ed. Engl.* **1988**, *27*, 865 – 879; b) R. W. Alder, *Chem. Rev.* **1989**, *89*, 1215 – 1223; c) A. L. Llamas-Saiz, C. Foces-Foces, J. Elguero, *J. Mol. Struct.* **1994**, *328*, 297 – 323; d) Z. B. Maksić, B. Kovačević, R. Vianello, *Chem. Rev.* **2012**, *112*, 5240 – 5270; e) A. F. Pozharskii, *Russ. Chem. Rev.* **1998**, *67*, 1 – 24; f) A. F. Pozharskii, V. A. Ozeryanskii, E. A. Filatova, *Chem. Heterocycl. Compd.* **2012**, *48*, 200 – 219; g) J. Chambron, M. Meyer, *Chem. Soc. Rev.* **2009**, *38*, 1663 – 1673.

[36] a) A. L. Llamas-Saiz, C. Foces-Foces, P. Molina, M. Alajarin, A. Vidal, R. M. Claramunt, J. Elguero, *J. Chem. Soc. Perkin Trans. 2* **1991**, 1025 – 1031; b) A. L. Llamas-Saiz, C. Foces-Foces, J. Elguero, P. Molina, M. Alajarin, A. Vidal, *J. Chem. Soc. Perkin Trans. 2* **1991**, 1667 – 1676; c) A. L. Llamas-Saiz, C. Foces-Foces, J. Elguero, P. Molina, M. Alajarin, A. Vidal, *J. Chem. Soc. Perkin Trans. 2* **1991**, 2033 – 2040; d) J. Laynez, M. Menendez, S. Velasco, J. Luis, A. L. Llamas-Saiz, C. Foces-Foces, J. Elguero, P. Molina, M. Alajarin, A. Vidal, *J. Chem. Soc. Perkin Trans. 2* **1993**, 709 – 713.

[37] H. G. Alt, K. J. Schneider, E. Funk, *Jord. J. Chem.* **2008**, *3*, 367 – 379.

[38] TBPN has been known in our group since 2011 (E. Baal, bachelor thesis, Philipps-Universität Marburg (Germany), **2011**) and was presented at the ESOR XIII (J. F. Kögel, B. Oelkers, B. Kovačević, Z. B. Maksić, J. Sundermeyer, "New Superbasic Bisphosphazene Proton Sponges", 13th European Symposium on Organic Reactivity (ESOR XIII), Tartu, 11.–16.09.2011).

[39] a) Y. Xiong, S. Yao, S. Inoue, A. Berkefeld, M. Driess, *Chem. Commun.* **2012**, *48*, 12198 – 12200; b) Y. Xiong, S. Yao, S. Inoue, E. Irran, M. Driess, *Angew. Chem.* **2012**, *124*, 10221 – 10224; *Angew. Chem.* **2012**, *124*, 10221 – 10224; *Angew. Chem. Int. Ed. Angew. Chem. Int. Ed. Engl.* **2012**, *51*, 10074 – 10077.

[40] H. Staudinger, J. Meyer, *Helv. Chim. Acta* **1919**, *2*, 635 – 646.

[41] a) A. V. Kirsanov, *Izv. Akad. Nauk SSSR, Otd. Khim. Nauk* **1950**, 426; b) G. I. Derkach, I. N. Zhmurova, A. V. Kirsanov, V. I. Shevchenko, A. S. Shtepanek, *Phosphazo Compounds* **1965**, Naukova Dumka, Kiew.

[42] J. F. Kögel, N. C. Abacılar, F. Weber, B. Oelkers, K. Harms, B. Kovačević, J. Sundermeyer, *Chem. Eur. J.* **2014**, manuscript accepted, 201304498.

[43] T. Rodima, V. Mäemets, I. Koppel, *J. Chem. Soc. Perkin Trans. 1* **2000**, 2637 – 2644.

[44] We prepared up to 10.94 g TPPN·HBr from the described procedure. In principle, further upscaling should be possible.

[45] The crystal structure of TMPN·HBr contained half a unit of NH_4Br per unit of TMPN·HBr. The structure was prepared from the protonation reaction of crude TMPN with NH_4PF_6. The used TMPN contained traces of TMPN·HBr leading to crystallization of the hydrobromide instead of the HPF_6 salt. It was verified by bromide analysis that the bulk of TMPN·HPF_6 was free of bromide.

[46] The molecular structure of TBPN·HBr has already been published in the Supporting Information of ref. [39b]. The synthesis of TBPN·HBr is described in the Supporting Information.

[47] *d*(NH) was restrained at 0.85 Å in case of TPPN·$HN(SO_2CF_3)_2$ and therefore is not discussed herein.

[48] See ref. [11a].

[49] a) M. Reinmuth, U. Wild, D. Rudolf, E. Kaifer, M. Enders, H. Wadepohl, H.-J. Himmel, *Eur. J. Inorg. Chem.* **2009**, 4795 – 4808; b) P. Roquette, A. Maronna, A. Peters, E. Kaifer, H.-J. Himmel, C. Hauf, V. Herz, E.-W. Scheidt, W. Scherer, *Chem. Eur. J.* **2010**, *16*, 1336 – 1350; c) A. Maronna, E. Bindewald, E. Kaifer, H. Wadepohl, H.-J. Himmel, *Eur. J. Inorg. Chem.* **2011**, 1302 – 1314; d) V. Vitske, P. Roquette, S. Leingang, C. Adam, E. Kaifer, H. Wadepohl, H.-J. Himmel, *Eur. J. Inorg. Chem.* **2011**, 1593 – 1604.

[50] a) H.-U. Wüstefeld, W. C. Kaska, F. Schüth, G. D. Stuckly, X. Bu, B. Krebs, *Angew. Chem.* **2001**, *113*, 3280 – 3282; *Angew. Chem. Int. Ed.* **2001**, *40*, 3182 – 3184; b) H.-U. Wuestefeld, W. C. Kaska, G. D. Stucky, F. Schueth, B. Krebs, PCT Int. Appl., WO 2002059134 A1 20020801, **2002;** c) K. J. Shaffer, M. Wenzel, P. G. Plieger, *Polyhedron* **2013**, *52*, 1399 – 1402.

[51] a) R. R. Ernst, G. Bodenhausen, A. Wokaun, *Principles of Nuclear Magnetic Resonance in One and Two Dimensions*, Oxford University Press, London/New York, **1987**; b) C. L. Perrin, T. J. Dwyer, *Chem. Rev.* **1990**, *90*, 935 – 967.

[52] S. Berger, S. Braun, *200 and More NMR Experiments, a Practical Course*, Wiley-VCH, Weinheim, **2004**.

[53] Gaussian 03, Revision E.01, M. J. Frisch, G. W. Trucks, H. B. Schlegel, G. E. Scuseria, M. A. Robb, J. R. Cheeseman, J. A. Montgomery, Jr., T. Vreven, K. N. Kudin, J. C. Burant, J. M. Millam, S. S. Iyengar, J. Tomasi, V. Barone, B. Mennucci, M. Cossi, G. Scalmani, N. Rega, G. A. Petersson, H. Nakatsuji, M. Hada, M. Ehara, K. Toyota, R. Fukuda, J. Hasegawa, M. Ishida, T. Nakajima, Y. Honda, O. Kitao, H. Nakai, M. Klene, X. Li, J. E. Knox, H. P. Hratchian, J. B. Cross, V. Bakken, C. Adamo, J. Jaramillo, R. Gomperts, R. E. Stratmann, O. Yazyev, A. J. Austin, R. Cammi, C. Pomelli, J. W. Ochterski, P. Y. Ayala, K. Morokuma, G. A. Voth, P. Salvador, J. J. Dannenberg, V. G. Zakrzewski, S. Dapprich, A. D. Daniels, M. C. Strain, O. Farkas, D. K. Malick, A. D. Rabuck, K. Raghavachari, J. B. Foresman, J. V. Ortiz, Q. Cui, A. G. Baboul, S. Clifford, J. Cioslowski, B. B. Stefanov, G. Liu, A. Liashenko, P. Piskorz, I. Komaromi, R. L. Martin, D. J. Fox, T. Keith, M A. Al-

Laham, C. Y. Peng, A. Nanayakkara, M. Challacombe, P. M. W. Gill, B. Johnson, W. Chen, M. W. Wong, C. Gonzalez, J. A. Pople, Gaussian, Inc., Wallingford CT, **2004**.
[54] B. Kovačević, D. Barić, Z. B. Maksić, *New J. Chem.* **2004**, *28*, 284 – 288.
[55] S. T. Howard, *J. Am. Chem. Soc.* **2000**, *122*, 8238 – 8244.
[56] V. C. Gibson, C. E. Graimann, P. M. Hare, M. L. H. Green, J. A. Bandy, P. D. Grebenik, K. Prout, *J. Chem. Soc. Dalton Trans.* **1985**, 2025 – 2035.
[57] W. C. Davies, *J. Chem. Soc.* **1933**, 1043 – 1044.
[58] D. J. Dellinger, D. M. Sheehan, N. K. Christensen, J. G. Lindberg, M. H. Caruthers, *J. Am. Chem. Soc.* **2003**, *125*, 940 – 950.
[59] R. Bartsch, O. Stelzer, R. Schmutzler, *Z. Naturforsch. B* **1981**, *36*, 1349 – 1355.
[60] G. Brauer, *Handbuch der Präparativen Anorganischen Chemie, 3. Auflage*, Ferdinand Enke Verlag, Stuttgart, **1975**, pp. 712 – 713.
[61] J. Ahman, P. Somfai, *Synth. Commun.* **1995**, *25*, 2301 – 2303.
[62] Single crystals suitable for structure determination of protonated TBPN were obtained by layering a saturated solution of TBPN·HBr in THF with hexane. The preparation of the hydrobromide is described in the Supporting Information.
[63] The origin of this coupling constant could not be identified.
[64] Single crystals suitable for structure determination of protonated TcyPPN were obtained by diffusion of pentane into a saturated solution of TcyPPN·HBr in chlorobenzene. The preparation of the hydrobromide is described in the Supporting Information.
[65] CCDC-997546 (TMPN·HBr), -997546 (TBPN·HBr), -997548 (TiPrPN·HBr), -997550 (TcyPPN·HBr), -997549 (TiPrPN), -997551 (TcyPPN), -997553 ($[TMPN\text{-}AlMe_2]^+[AlMe_4]^-$), -997554 ($[TMPN\text{-}GaMe_2]^+[GaMe_4]^-$), and -997552 ($[TPPN\text{-}AlMe_2]^+[AlCl_2Me_2]^-$), contain the supplementary crystallographic data for this paper. These data can be obtained free of charge from The Cambridge Crystallographic Data Centre via www.ccdc.cam.ac.uk/data_request/cif.

Received: February 17, 2014
Published online on May 5, 2014

ChemPubSoc Europe

DOI: 10.1002/chem.201304498

CHEMISTRY
A European Journal
Full Paper

Organocatalysis

Constrained-Geometry Bisphosphazides Derived from 1,8-Diazidonaphthalene: Synthesis, Spectroscopic Characteristics, Structural Features, and Theoretical Investigations

Julius F. Kögel,[a] Nuri C. Abacılar,[a] Felicia Weber,[a] Benjamin Oelkers,[a] Klaus Harms,[a] Borislav Kovačević,[b] and Jörg Sundermeyer*[a]

Abstract: Investigations on the Staudinger reaction between 1,8-diazidonaphthalene and phosphorous(III) building blocks, a key step in the synthesis of superbasic bisphosphazene proton sponges, yielded a set of bisphosphazides with a constrained geometry 1,8-disubstituted naphthalene backbone. This compound class has attracted our interest not only due to their surprisingly high stability, but in particular because of their theoretically predicted basicity in the range of their bisphosphazene analogues that can be referred to the constrained geometry interaction of two highly basic nitrogen atoms. Eleven new bisphosphazides bearing simple P-amino groups as well as P-guanidino substituents, azaphosphatrane moieties, P_2 building blocks, or chiral P-amino substituents derived from L-proline are presented. They were studied concerning their spectroscopic properties and partly also their chromophoric and structural features. In the case of the pyrrolidino-substituted TPPN($2N_2$) (TPPN = 1,8-bis(trispyrrolidinophosphazenyl)naphthalene), the stepwise nitrogen elimination is investigated theoretically and experimentally, which led to the isolation and structural characterization of TPPN($1N_2$) bearing a phosphazide and a phosphazene functionality in one molecule. Attempts to protonate the obtained bisphosphazides and to prove the computationally predicted pK_{BH}^{+} values through NMR titration reactions resulted in their decay, which again was rationalized by theoretical calculations. Altogether we present the so far most extensive spectroscopic, structural and theoretical investigation of constrained geometry bisphosphazides and their Brønsted and Lewis basic properties.

Introduction

Since its discovery in 1919, the Staudinger reaction has been a useful tool for synthetic chemists.[1] It describes the conversion of an organic azide with a phosphane to a phosphazene under elimination of molecular nitrogen and oxidation of the phosphorous atom. Subsequent hydrolysis leads to a phosphine oxide and a primary amine. Thus, the Staudinger reaction and the related Staudinger ligation have become valuable methods, especially on a laboratory scale, making them part of countless synthetic sequences.[2]

The first step of the Staudinger reaction is the formation of a phosphazide or Staudinger adduct, which can exhibit an *s-cis* or *s-trans* conformation (Scheme 1). The state of equilibrium between the two conformers depends on the steric and electronic properties of the substituents at the phosphorous atom

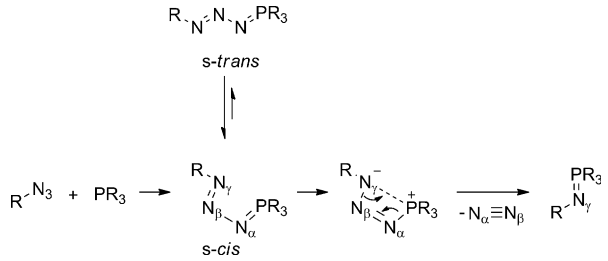

Scheme 1. Mechanism of the Staudinger reaction.

and the γ-nitrogen atom. In most cases the *s-cis* conformer is more stable, allowing the interaction between the phosphorous atom and the γ-nitrogen atom and irreversible elimination of molecular nitrogen through a four-membered-ring transition state. The mechanism of the Staudinger reaction has been the subject of various theoretical investigations that revealed additional reaction profiles according to the substituents and reaction conditions.[3]

[a] J. F. Kögel, N. C. Abacılar, F. Weber, Dr. B. Oelkers, Dr. K. Harms, Prof. Dr. J. Sundermeyer
Fachbereich Chemie
Philipps-Universität Marburg
Hans-Meerwein-Strasse
35032 Marburg (Germany)
Fax: (+49) 642128-25711
E-mail: jsu@staff.uni-marburg.de

[b] Dr. B. Kovačević
Quantum Chemistry Group
Rudjer Bošković Institute
Bijenička c. 54, HR-10000 Zagreb (Croatia)

Supporting information for this article is available on the WWW under http://dx.doi.org/10.1002/chem.201304498.

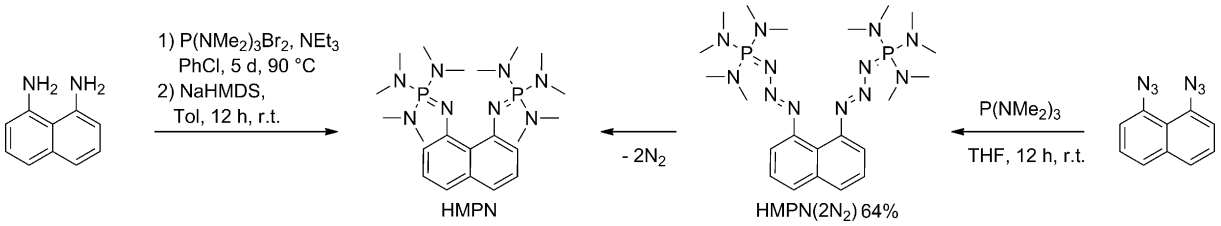

Scheme 2. Synthesis of HMPN through a Kirsanov reaction and a Staudinger reaction with the bisphosphazide intermediate HMPN($2N_2$).

Phosphazides, the initially formed intermediates of the Staudinger reaction, were originally considered to be unstable and have only been studied for about three decades now. In most cases nitrogen elimination is prevented by making the *s-trans* conformer energetically more favorable compared with the reactive *s-cis* conformation. This is achieved by electron-donating groups at the phosphorous atom and electron-withdrawing groups at the γ-nitrogen atom that reduce the opposite partial charges at these atoms and therefore hamper their interaction in a four-membered cycle. Furthermore, the *s-cis* conformation can be destabilized by sterically demanding substituents. Other strategies are the incorporation of the phosphazide into a cyclic[4] or macrocyclic[5] system, or its coordination to metal atoms like boron,[6] zirconium,[7] molybdenum,[8] tungsten,[9] iron,[10] ruthenium,[11] cerium,[12] or lutetium[13] in which different coordination modes have been found. In a few cases, open-chain phosphazides in an *s-cis* conformation with $-CH_2CN$,[14] adamantyl,[15] or *ortho-closo*-dicarbadodecaboranyl[16] substituents at the γ-nitrogen atom were observed. Verkade et al. stabilized phosphazides by incorporating the phosphorous atom into an azaphosphatrane cage allowing transannular interactions between the phosphorous atom and the apical nitrogen atom.[17] This structural motif was also incorporated into a dendrimer able to catalyze Michael additions, nitroaldol reactions, or aryl isocyanate trimerizations.[18] Furthermore, immobilization on a Merrifield resin yielded an organocatalyst for 1,4-Michael addition reactions.[19] Recently, stable phosphazides were obtained in connection with the synthesis of Schwesinger P_1-bases through a Staudinger reaction.[20] The field of stable phosphazides was extensively reviewed by Bebbington and Bourissou in 2009.[21]

Generally, the focus of our research lies on the synthesis of bisphosphazene proton sponges—neutral organic superbases combining the concept of interacting basicity centers[22] with Schwesinger's phosphazene bases.[23] In the course of our synthetic efforts we have discovered the first superbasic bisphosphazene proton sponge 1,8-bis(hexamethyltriaminophosphazenyl)naphthalene (HMPN), which was obtained through a Kirsanov reaction between 1,8-diaminonaphthalene and the corresponding bromophosphonium bromide (Scheme 2).[24] Whereas Kirsanov reactions are known to proceed readily for sterically unhindered systems like aniline, only a moderate yield of 43% was obtained in case of HMPN, which can be referred to the spacial proximity of the amino groups in the *peri*-position and the sterically demanding phosphazene moieties. So far the Kirsanov reaction has not been successful for amino-substituted bromophosphonium bromides bearing substituents other than sterically undemanding dimethylamino or pyrrolidino groups in our case.

Because prior art condensation reactions did not allow for extension of the scope of these superbasic proton pincers, we chose the Staudinger reaction for preparing high-energy molecules (chelating superbases), from even higher-energy molecules such as 1,8-diazidonaphthalene (Scheme 2). This strategy led to a more basic descendant of HMPN, 1,8-bis(trispyrrolidinophosphazenyl)naphthalene (TPPN), and its higher homologue P_2-TPPN (Scheme 3).[25] The reactions provided access to initially formed bisphosphazides, which turned out to be unexpectedly stable.

Four stable chiral C_2-symmetric bisphosphazides with two interacting γ-nitrogen atoms (Figure 1 f) have already been reported by Naka et al. who used them as catalysts for the conjugate addition of nucleophilic enols to enones.[26] In the context of Naka's work, the bisphosphazides were employed as Brønsted bases as well as Lewis bases forming 1:1 complexes with lithium salts. This and our own study motivated us to extend the field of rigid constrained geometry bisphosphazides and to strive for insight into their structural features, basic properties, and donor capability towards Lewis acids.

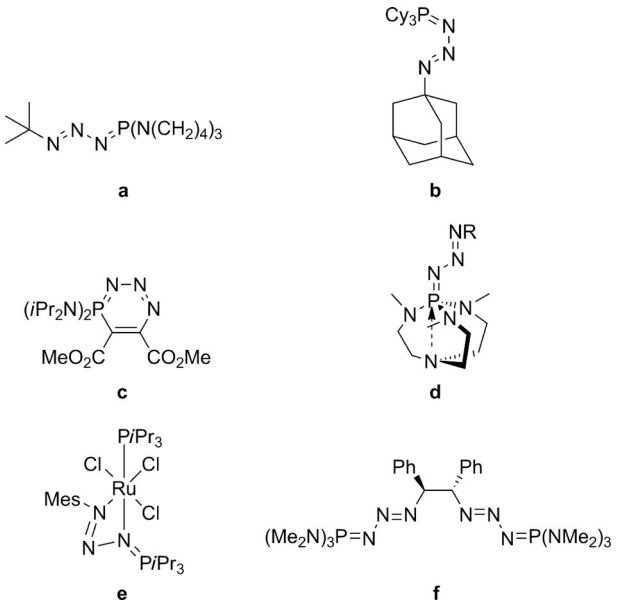

Figure 1. Examples of phosphazides in the *s-trans*[20] (**a**) and *s-cis* (**b**)[15] conformations, stabilization of phosphazides by cyclization (**c**),[8a] incorporation into an azaphosphatrane cage (**d**),[17] or coordination of a metal atom (**e**),[11] and a chiral bisphosphazide able to act as an organocatalyst (**f**).[26]

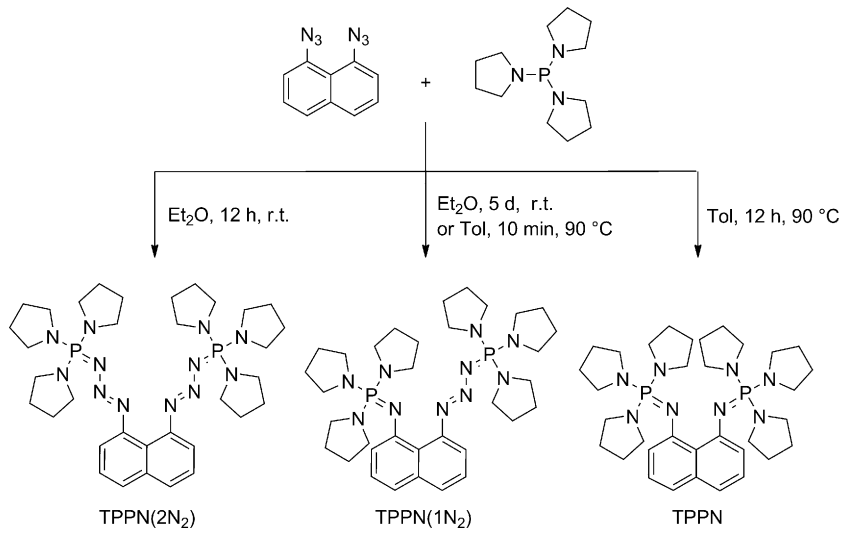

Scheme 3. Variation of the reaction conditions to selectively obtain TPPN($2N_2$), TPPN($1N_2$), or TPPN.

Results and Discussion

General synthesis

In a general procedure, 1,8-diazidonaphthalene was reacted with a phosphorus(III) precursor in an aprotic solvent such as diethyl ether, THF, or toluene at ambient temperature. After a short time, the reaction mixture changed color from deep violet (due to the diazido compound) to green and the reaction progress was monitored by ^{31}P NMR spectroscopy. Oxidation of the phosphorous(III) amide by the azide is accompanied by a strong high-field shift in all cases. Elimination of molecular nitrogen was achieved at high temperatures in aromatic solvents for HMPN($2N_2$), TPPN($2N_2$), and P_2-TPPN($2N_2$). All other bisphosphazides did not lose N_2 under the applied conditions (see below).

Spectroscopic properties

When entering the field of synthesizing bisphosphazene proton sponges by using a Staudinger reaction, at first the stability of the bisphosphazides was underestimated. Initially, it was difficult to distinguish bisphosphazides from bisphosphazenes only by ^{1}H, ^{13}C, or ^{31}P NMR spectroscopic methods without X-ray crystallographic information.

In some cases mass spectrometry also proved unsuitable, because molecular nitrogen was eliminated from the bisphosphazides under electrospray ionization (ESI) and atmospheric pressure chemical ionization (APCI) conditions and thus revealed only signals of the corresponding bisphosphazenes. In the course of our investigations, several criteria could be carved out for differentiation by comparing HMPN, TPPN, and P_2-TPPN with their corresponding bisphosphazides: Elimination of two equivalents of molecular nitrogen from the bisphosphazides is accompanied by a high-field shift in the ^{31}P NMR spectrum by about 25 ppm in case of HMPN and TPPN (HMPN($2N_2$): $\delta = 43.2$; HMPN: 17.8;[24] TPPN($2N_2$): 29.2; TPPN: 2.5 ppm[25]). Similar shifts compared to the dimethylamino-substituted compounds were observed by Kroshevsky and Verkade for Ph–N=N–N=P(NMe_2)$_3$ ($\delta = 42.8$ ppm) and Ph–N=P(NMe_2)$_3$ ($\delta = 19.5$ ppm).[27]

Furthermore, the aromatic protons show a considerable low-field shift in case of the bisphosophazides and also the signal order deviates in the proton NMR spectra. In contrast to the bisphosphazenes, no coupling of aromatic carbon atoms with the phosphorous atoms can be detected for C(1,8), C(2,7), and C(8a) in the ^{13}C NMR spectra of the bisphosphazides. As expected, elemental analyses show different nitrogen contents. Finally, the bisphosphazides could be identified by their characteristic green color, supposedly originating from the P=N–N=N–Ar π-system and ranging from a light green, in the case of APAN($2N_2$) or P_2-TPPN($2N_2$), to a very dark tone for TAzPN($2N_2$), whereas TPPN and HMPN reveal a beige color (only P_2-TPPN shows a greenish shade).

In the case of TPPN it was possible to isolate the mixed compound TPPN($1N_2$) bearing a phosphazide and a phosphazene moiety in one molecule by stirring TPPN($2N_2$) for five days in diethyl ether at room temperature or ten minutes in toluene at 90 °C (Scheme 3). As expected, TPPN($1N_2$) shows two different ^{31}P NMR signals with chemical shifts similar to the ones found for the related homofunctional compounds TPPN and TPPN($2N_2$) ($\delta = 28.7$ and 5.7 ppm). The course of the reaction of TPPN($2N_2$) to TPPN at 90 °C in toluene was observed by ^{31}P NMR spectroscopic analysis of the reaction mixture (Figure 2). Whereas the elimination of the first equivalent of molecular nitrogen was already completed after 10 min, formation of TPPN from the intermediate TPPN($1N_2$) took another 12 h, indicating that the kinetic barrier for the second nitrogen

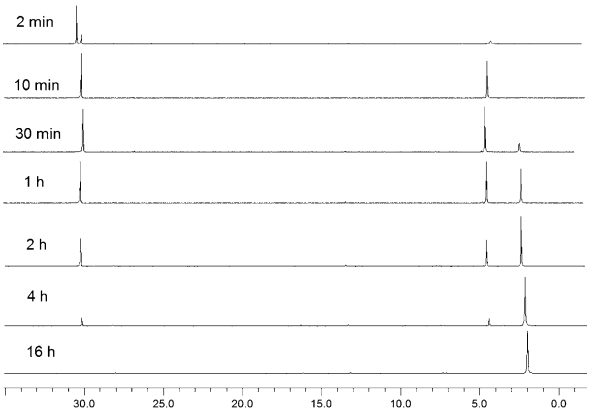

Figure 2. Visualization of the reaction from TPPN($2N_2$) through TPPN($1N_2$) to TPPN by using ^{31}P NMR spectroscopy (samples taken from the reaction mixture at 90 °C in toluene).

elimination is significantly higher. This observation is in good accordance with theoretical calculations (see below) and can be explained by an increased steric hindrance at the naphthalene backbone impeding the formation of the *s-cis* conformation necessary for nitrogen elimination.

Bisphosphazides with other amino substituents

To extend the structural variety in the area of stable bisphosphazides and explore their thermal stability, the dimethylamino groups of HMPN($2N_2$) were replaced by diethylamino substituents, and instead of the pyrrolidine moieties of TPPN($2N_2$), the larger heterocycles piperidine and azepane were introduced (Figure 3). The desired bisphosphazides could be obtained readily by the known procedure and exhibited the typical characteristics of that compound class showing chemical shifts of $\delta = 41.4$ (HEPN($2N_2$)), 35.4 (TPipPN($2N_2$)), and 39.3 ppm (TAzPN($2N_2$)) in the phosphorous NMR spectra. Whereas HMPN($2N_2$) and TPPN($2N_2$) smoothly eliminate molecular nitrogen in toluene heated at reflux, already the small structural variation provided by diethylamino, piperidyl, or azepanyl substituents prevented the reaction to the desired bisphosphazene proton sponges even at higher temperatures like 130 °C in xylene.

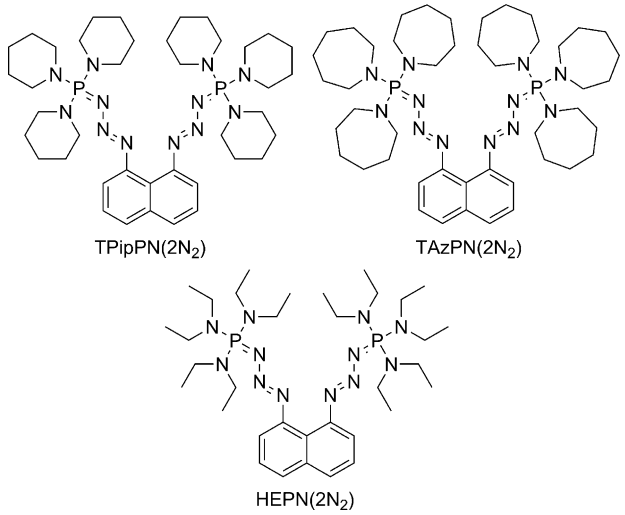

Figure 3. Bisphosphazides bearing diethylamino, piperidyl, and azepanyl moieties.

Higher homologues of bisphosphazides

According to Schwesinger's concept of phosphazene bases and theoretical calculations, a so-called homologization, the replacement of amino substituents by further phosphazene moieties leads to a dramatic increase in the pK_{BH^+} value by several orders of magnitude. Hence, the phosphorous(III) precursors for the synthesis of P_2-HMPN and P_2-TPPN through a Staudinger reaction were prepared by using a three-step procedure starting from $P(NMe_2)_3$ and $P(N(CH_2)_4)_3$, respectively (Scheme 4).[25,28] Synthesis of the bisphosphazides P_2-HMPN($2N_2$) and P_2-TPPN($2N_2$) proceeded readily at room temperature, but the desired bisphosphazene proton sponge could only be obtained in case of P_2-TPPN. Due to the higher steric demand and the stronger electron-donating nature of the P_2 moiety compared with the pyrrolidino groups in TPPN($2N_2$), higher temperature and a longer reaction time are required for nitrogen elimination from the higher homologue: Whereas TPPN is prepared in toluene at 90 °C overnight, P_2-TPPN is synthesized in xylene at 120 °C after 48 h (Figure 4). Again nitrogen elimination is accompanied by a high-field shift in the ^{31}P NMR spectrum (P_2-TPPN($2N_2$): $\delta = 19.7$, 9.5 ppm; P_2-TPPN: $\delta = 1.5$, 5.0 ppm[25]). The mixed intermediate P_2-TPPN($1N_2$) with a phosphazide and a phosphazene unit was observed in the reaction mixture by using ^{31}P NMR spectroscopy (Figure 5), but not isolated in that case. Due to the weaker electron-donating nature of the dime-

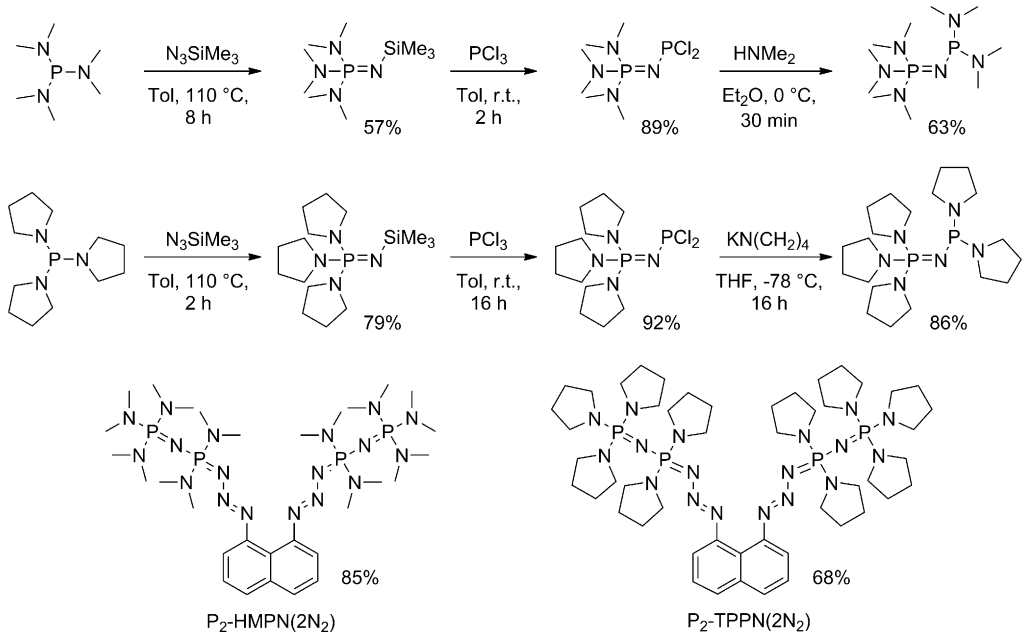

Scheme 4. Higher homologues of HMPN($2N_2$) and TPPN($2N_2$) and the synthesis of their precursors.

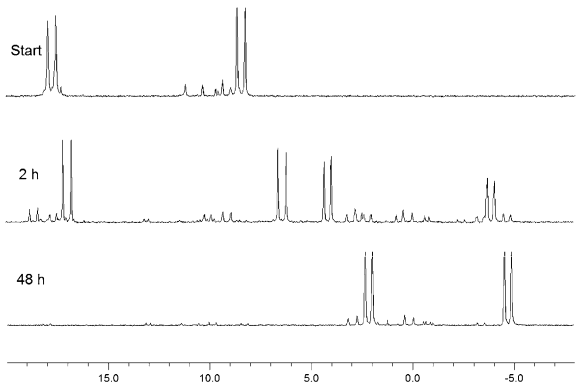

Figure 4. Visualization of the reaction from P_2-TPPN($2N_2$) through P_2-TPPN($1N_2$) to P_2-TPPN by using ^{31}P NMR spectroscopy (samples taken from the reaction mixture at 120 °C in xylene).

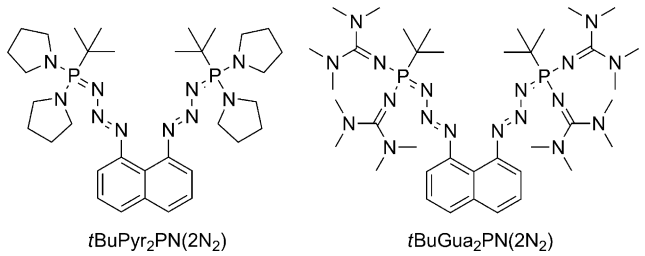

Figure 5. Bisphosphazides carrying *tert*-butyl substituents.

thylamino groups compared with the pyrrolidino moieties, the signals of P_2-HMPN($2N_2$) in the ^{31}P NMR spectrum are observed further in the low-field region ($\delta = 24.0$ and 19.4 ppm). Both bisphosphazides show ^2J(P,P) coupling (P_2-HMPN($2N_2$): 51.7 Hz, P_2-TPPN($2N_2$): 48.0 Hz). Suchlike higher homologues of phosphazides have already been reported in patent literature and were used in the conversion of a ketone with a trimethylsilyl-substituted alkyne to tertiary silyl ethers.[29]

tert-Butyl-substituted bisphosphazides

It has been described in the literature that the replacement of one amino group in a trisamino-substituted phosphorous(III) compound by an alkyl group leads to a higher basicity. Only two of the amino groups can act as electron donors, whereas the third amino substituent has an electron-withdrawing effect due to the high electronegativity of the nitrogen atom (concept of "special nitrogen").[30] Thus, a basicity enhancement was expected for TPPN after replacing one pyrrolidine moiety by a *tert*-butyl group. Reaction of *tert*-butylbispyrrolidinophosphane with 1,8-diazidonaphthalene yielded the corresponding bisphosphazide (^{31}P NMR: $\delta = 48.9$ ppm, Figure 5), which did not eliminate molecular nitrogen even at high temperatures. Theoretical calculations have identified guanidino-substituted bisphosphazene proton sponges as promising target compounds because they incorporate three superbasic features in one molecule.[31] As trisguanidino-substituted phosphanes are not described in the literature and could not be prepared from condensation or transamination reactions,[32] the known compound *tert*-butylbis(tetramethylguanidino)phosphane[33] was chosen as a precursor for the Staudinger reaction and gave the first phosphazide containing guanidino substituents at the phosphorous atom (^{31}P NMR: $\delta = 24.6$ ppm, Figure 5). Both bisphosphazides bearing *tert*-butyl groups were investigated by means of X-ray diffraction analysis (see below).

A bisphosphazide with azaphosphatrane moieties

In connection with our attempts to combine different superbasic features in one molecule, we intended to make use of the high intrinsic basicity of Verkade's azaphosphatrane cages that should be connected through an 1,8-disubstituted naphthalene backbone. As described above, proazaphosphatranes have already shown to react readily with phenyl, benzyl, or alkyl azides to form stable phosphazides.[17] The light-green bisphosphazide APAN($2N_2$) was obtained easily from the treatment of proazaphosphatrane with 1,8-diazidonaphthalene in THF (Figure 6). The ^{31}P NMR chemical shift of the resulting compound ($\delta = 36.4$ ppm) is in good accordance with the shift

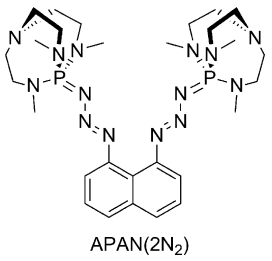

Figure 6. APAN($2N_2$) carrying two azaphosphatrane cages.

of $PhN_3P(NCH_3(CH_2)_2)_3N$ ($\delta = 38.1$ ppm).[17a] The structure could be identified by XRD measurements. High-resolution mass spectrometry did not reveal the bisphosphazide, but only the bisphosphazene was observed as pseudo-molecular ion under ESI and APCI conditions. However, attempts to eliminate molecular nitrogen at temperatures up to 120 °C have not been selective so far.

A bisphosphazide with chiral substituents

Having noticed the synthetic limitations of the Staudinger reaction for the synthesis of highly constrained bisphosphazene proton sponges, a chiral phosphane precursor derived from L-proline was obtained to probe the synthesis of a chiral version of the superbase TPPN. The carboxylic group of L-proline was converted into a methoxy group in a simple four-step procedure and treated with phosphorous trichloride in the presence of triethylamine in THF to form (*S*)-tris(2-methoxymethylpyrrolidino)phosphane. It reveals a chemical shift of $\delta =$ 102.9 ppm in the ^{31}P NMR spectrum in [D_6]benzene, which is similar to the related trispyrrolidinophosphane ($\delta = 103.1$ ppm).

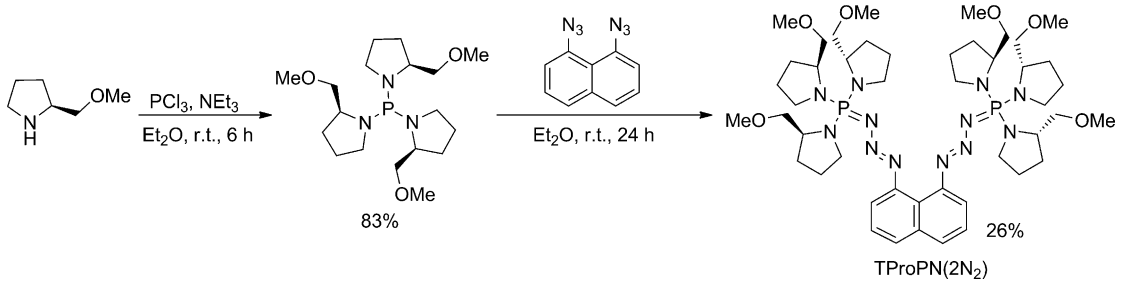

Scheme 5. Synthesis of TProPN($2N_2$) and its chiral phosphane precursor.

Treatment with 1,8-diazidonaphthalene yielded the corresponding chiral bisphosphazide TProPN($2N_2$) with a chemical shift of $\delta = 31.0$ ppm in the ^{31}P NMR spectrum (Scheme 5). It was expected that the similarity of the substituents to pyrrolidine would allow elimination of molecular nitrogen at high temperatures, but the reaction turned out to be very unselective. Compared with the chiral bisphosphazide **f** (Figure 1), TProPN($2N_2$) has a more rigid backbone and six stereocenters. Due to these constraints, it is a good candidate for organocatalytic studies.

For all bisphosphazides, various reaction conditions were applied to lower the kinetic barrier for the elimination of molecular nitrogen. Besides stirring the compounds in high-boiling solvents of different polarity, like toluene, xylene, chlorobenzene, 1,2-dichlorobenzene, di-*n*-butyl ether, DMSO, or DME at high temperatures, they were also exposed to UV radiation. Furthermore, the reducing agent C_8K was added to solutions of the bisphosphazides to achieve a single-electron transfer into an antibonding orbital, or the Lewis acid aluminum trichloride was used, which should coordinate to the nitrogen atoms leading to a conformation change allowing N_2 elimination. In all cases, highly unselective reactions to unidentified products were observed through ^{31}P NMR spectroscopy and highly selective stepwise nitrogen elimination could only be achieved for HMPN($2N_2$), TPPN($2N_2$), and P_2-TPPN($2N_2$).

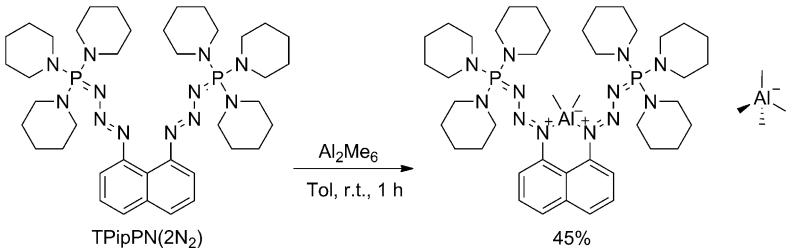

Scheme 6. Reaction of TPipPN($2N_2$) with trimethylaluminum.

Reactivity towards Brønsted and Lewis acids

Attempts to protonate TPPN($2N_2$) with $HN(SO_2CF_3)_2$ or NH_4PF_6 in THF resulted in the decomposition of the bisphosphazide to several unidentified species leading to a large number of signals in the ^{31}P NMR spectrum. Crystals grown directly from the reaction mixture revealed the protonated Schwesinger P_1-base $((CH_2)_4N)_3P{=}NH{\cdot}HPF_6$ as one degradation product. We consider the formation of highly reactive aryne species as possible intermediates in the course of degradation of bisphosphazides after protonation, which is supported by theoretical calculations (see below) and would explain the numerous degradation products. NMR titration experiments in [D_3]MeCN showed, that TPPN($2N_2$) is unable to deprotonate HMPN·HPF_6 (pK_{BH}^+ (MeCN) = 29.9),[24] $Pyr_3P{=}NtBu{\cdot}HPF_6$ (pK_{BH}^+ (MeCN) = 28.42),[34] and $(Me_2N)_3P{=}NtBu{\cdot}HPF_6$ (pK_{BH}^+ (MeCN) = 26.98),[34] which suggests a considerably lower pK_{BH}^+ value than calculated, but since protonation of TPPN($2N_2$) results in its decay, the experimental determination of the pK_{BH}^+ values of the bisphosphazides was not possible. A similar behavior towards Brønsted acids was also observed for the other bisphosphazides described herein.

Whereas reactions of bisphosphazides with Brønsted acids were not possible without decomposition of the substrate, TPipPN($2N_2$) reacted readily with two equivalents of the Lewis acid trimethylaluminum to give a cationic alkyl aluminum complex with a tetramethyl aluminate counteranion (Scheme 6). A molecular structure of low quality was obtained revealing that the metal ion is coordinated by the two γ-nitrogen atoms (the Supporting Information, Figure S2.1). This coordination mode is also suggested by the ^{31}P NMR chemical shift, which only shows a minor difference from the free bisphosphazide, indicating coordination of the metal ion far away from the phosphorous atoms (TPipPN($2N_2$): $\delta = 35.4$ ppm, [TPipPN($2N_2$)–$AlMe_2]^+[AlMe_4]^-$: $\delta = 32.9$ ppm). The cation [TPipPN($2N_2$)–$AlMe_2]^+$ was also detected in the ESI mass spectrum. A similar reaction of our guanidino-substituted proton sponge TMGN with gallium trichloride was reported by Himmel.[35]

Structural features

Molecular structures could be obtained of TPPN($2N_2$) (Figure 7), TPPN($1N_2$) (Figure 8), HEPN($2N_2$) (Figure 9), P_2-HMPN($2N_2$) (Figure 10), *t*BuPyr$_2$PN($2N_2$) (Figure 11), *t*BuGua$_2$PN($2N_2$) (Figure 12), and APAN($2N_2$) (Figure 13). In the case of

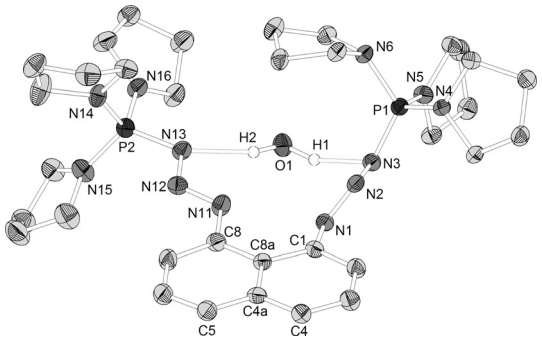

Figure 7. Molecular structure of TPPN($2N_2$)·H_2O (ellipsoids with 30% probability). Hydrogen atoms are omitted for clarity. Selected bond lengths [Å] and angles [°]: d(N1-N11): 2.695(3), d(N1-N2): 1.286(3), d(N2-N3): 1.377(3), d(N3-P1): 1.611(2), d(P1-N4): 1.643(2), d(P1-N5): 1.628(2), d(P1-N6): 1.654(2), d(N11-N12): 1.273(3), d(N12-N13): 1.356(3), d(N13-P2): 1.612(2), d(P2-N14): 1.626(2), d(P2-N15): 1.627(2), d(P2-N16): 1.628(2), d(O1-N3): 2.907(3), d(O1-N13): 2.918(3), C1-C8a-C4a-C5: 178.0(2), C8-C8a-C4a-C4: 176.6(2).

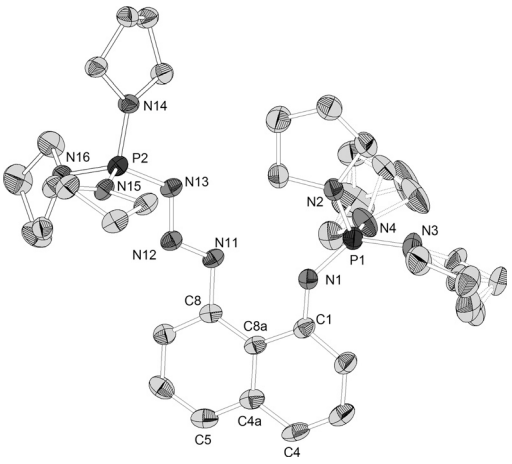

Figure 8. Molecular structure of TPPN($1N_2$) (ellipsoids with 30% probability). Hydrogen atoms are omitted for clarity. Selected bond lengths [Å] and angles [°]: d(N1-N11): 2.755(5), d(N1-P1): 1.558(4), d(P1-N2): 1.633(5), d(P1-N3): 1.655(5), d(P1-N4): 1.646(5), d(N11-N12): 1.295(5), d(N12-N13): 1.362(5), d(N13-P2): 1.621(4), d(P2-N14): 1.621(4), d(P2-N15): 1.632(3), d(P2-N16): 1.635(3), C1-C8a-C4a-C5: 176.6(4), C8-C8a-C4a-C4: 177.7(4).

TPPN($2N_2$)·H_2O, HEPN($2N_2$)·H_2O, and P_2-HMPN($2N_2$)·H_2O, traces of moisture lead to the incorporation of a water molecule forming two hydrogen bridges to the α-nitrogen atoms. The water molecule seems to fix the conformation of the bisphosphazides, allowing the compounds to form single crystals. Such interaction of host molecules with bisphosphazides is of interest to understand their role and potential as organocatalysts. Whereas a crystal structure determination of TPPN($2N_2$) displayed both phosphazide arms *anti* with respect to the naphthalene plane (the Supporting Information, Figure S2.2), the water molecule in TPPN($2N_2$)·H_2O is trapped in a *syn* conformation of the N_3PR_3 units. Interestingly, in HEPN($2N_2$)·H_2O and P_2-HMPN·H_2O, the *anti* conformation is preserved.

Selected bond lengths and angles are discussed in the following section: d(N_γ-N_β) ranges from 1.266(3) in *t*BuPyr$_2$PN($2N_2$) to 1.310(6) Å in P_2-HMPN·H_2O, whereas d(N_β-N_α) ranges from 1.319(6) to 1.386(6) Å. Interestingly, the last two values were

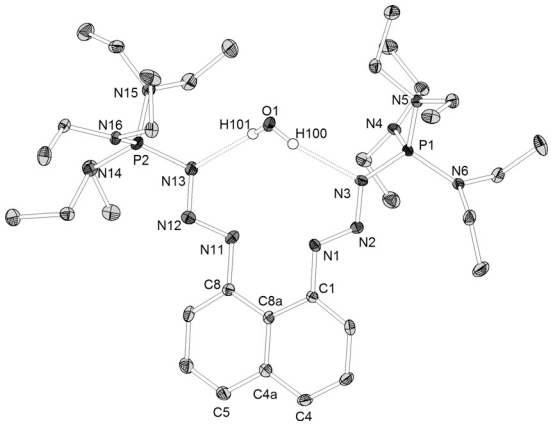

Figure 9. Molecular structure of HEPN($2N_2$)·H_2O (ellipsoids with 30% probability). Carbon-bonded hydrogen atoms are omitted for clarity. Selected bond lengths [Å] and angles [°]: d(N1-N11): 2.697(3), d(N1-N2): 1.282(3), d(N2-N3): 1.351(3), d(N3-P1): 1.624(2), d(N4-P1): 1.643(2), d(N5-P1): 1.636(2), d(N6-P1): 1.646(2), d(N11-N12): 1.306(3), d(N12-N13): 1.346(3), d(N13-P2): 1.630(2), d(N14-P2): 1.662(2), d(N15-P2): 1.638(2), d(N16-P2): 1.654(2), d(O1-N3): 2.932(3), d(O1-N13): 2.945(4), C4-C4A-C8A-C8: 177.1(2), C5-C4A-C8A-C1: 179.6(2).

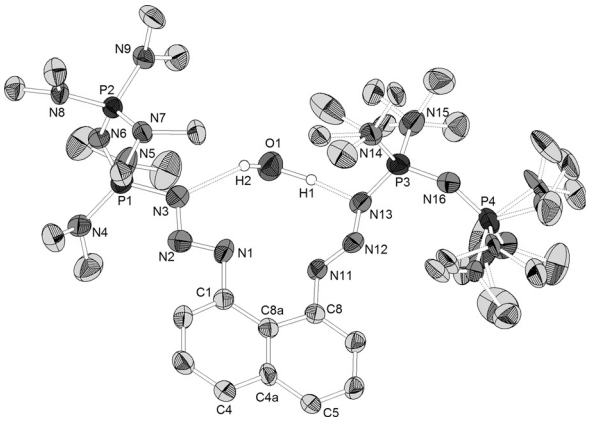

Figure 10. Molecular structure of P_2-HMPN·H_2O (ellipsoids with 30% probability). Carbon-bonded hydrogen atoms are omitted for clarity. Selected bond lengths [Å] and angles [°]: d(N1-N11): 2.704(7), d(N1-N2): 1.310(6), d(N2-N3): 1.319(6), d(N3-P1): 1.630(6), d(P1-N6): 1.578(5), d(N6-P2): 1.558(5), d(N11-N12): 1.284(6), d(N12-N13): 1.386(6), d(N13-P3): 1.628(5), d(P3-N16): 1.586(5), d(N16-P4): 1.517(5), d(O1-N13): 2.971(8), d(O1-N3): 2.874(8), C1-C8a-C4a-C5: −178.4(5), C8-C8a-C4a-C4: 178.0(5).

both observed for P_2-HMPN·H_2O showing large discrepancies for the corresponding values in the two "arms" of the molecule. It has to be mentioned that the resolution of the molecular structure of P_2-HMPN·H_2O is comparatively low due to disorders and low crystal quality. d(N_α-P) exhibits values from 1.611(2) in TPPN($2N_2$)·H_2O to 1.658(3) Å in *t*BuGua$_2$PN($2N_2$). The shorter bond length of d(N_γ-N_β) compared with d(N_β-N_α) emphasizes the dominance of the resonance structure free of partial charges (Scheme 7). It is noticeable that the longest N_α—P

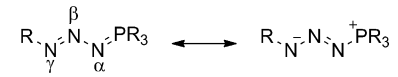

Scheme 7. Resonance structures of phosphazides.

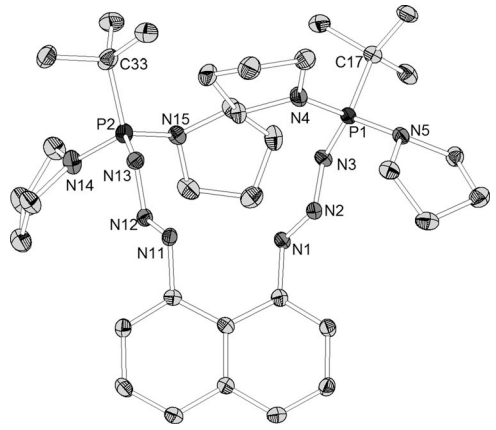

Figure 11. Molecular structure of *t*BuPyr$_2$PN(2N$_2$) (ellipsoids with 30% probability). Hydrogen atoms are omitted for clarity. Selected bond lengths [Å] and angles [°]: d(N1-N11): 2.710(3), d(N1-N2): 1.266(3), d(N2-N3): 1.375(3), d(N3-P1): 1.615(2), d(N4-P1): 1.642(2), d(N5-P1): 1.661(2), d(P1-C17): 1.845(3), d(N11-N12): 1.272(3), d(N12-N13): 1.368(3), d(N13-P2): 1.613(2), d(N14-P2): 1.635(2), d(N15-P2): 1.651(2), d(P2-C33): 1.827(3), C5-C4A-C8A-C1: −176.9(2), C4-C4A-C8A-C8: −177.4(2).

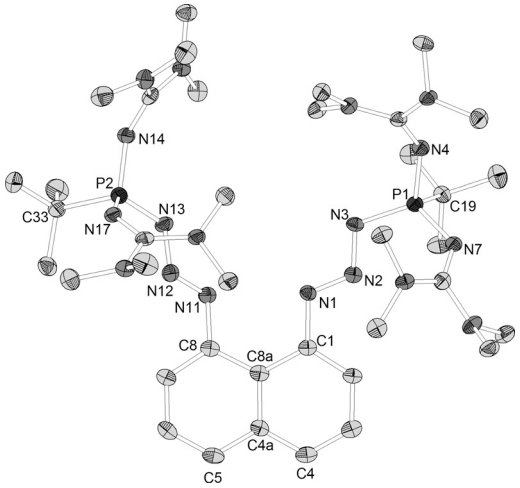

Figure 12. Molecular structure of *t*BuGua$_2$PN(2N$_2$) (ellipsoids with 30% probability). Hydrogen atoms and two acetonitrile molecules are omitted for clarity. Selected bond lengths [Å] and angles [°]: d(N1-N11): 2.720(3), d(N1-N2): 1.280(3), d(N2-N3): 1.346(3), d(N3-P1): 1.655(3), d(N4-P1): 1.599(2), d(N7-P1): 1.640(3), d(P1-C19): 1.847(3), d(N11-N12): 1.298(3), d(N12-N13): 1.357(4), d(N13-P2): 1.658(3), d(N14-P2): 1.595(3), d(N17-P2): 1.634(3), d(P2-C33): 1.829(3), C4-C4A-C8A-C8: 177.0(3), C5-C4A-C8A-C1: 174.0(3).

bond is found in *t*BuGua$_2$PN(2N$_2$), which can be referred to the strongly electron-donating guanidino moieties weakening the P–N$_\alpha$ bond. This is reflected by the resonance structures shown in Scheme 8. Metal-free open-chain phosphazides in *s-trans* conformation such as $Ph_3C–N=N–N=P(NMe_2)_3$ (d(N$_\gamma$-

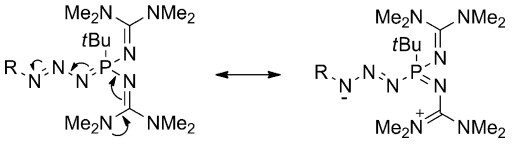

Scheme 8. Resonance structures of TGua$_2$*t*BuPN(2N$_2$).

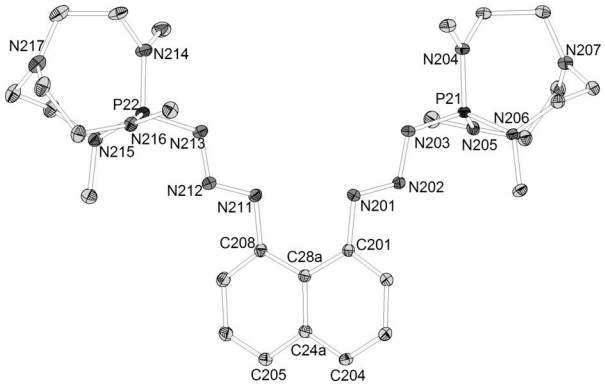

Figure 13. Molecular structure APAN(2N$_2$) (ellipsoids with 30% probability). Hydrogen atoms and acetonitrile molecules are omitted for clarity. Only one of the tree APAN(2N$_2$) molecules in the asymmetric unit is shown. Selected bond lengths [Å] and angles [°]: d(N201-N211): 2.785(2), d(N201-N202): 1.281(2), d(N202-N203): 1.356(2), d(N203-P21): 1.619(1), d(N211-N212): 1.283(2), d(N212-N213): 1.348(2), d(N213-P22): 1.620(1), d(P21-N207): 3.082(1), d(P22-N217): 3.091(2), C201-C28A-C24A-C205: −175.2(1), C208-C28A-C24A-C204: −176.4(1).

N$_\beta$) = 1.261(2), d(N$_\beta$-N$_\alpha$) = 1.376(2), d(N$_\alpha$-P) = 1.620(2) Å),[36] $OH(CH_2)_3N=N–N=P(NMe_2)_3$ (d(N$_\gamma$-N$_\beta$) = 1.256(2), d(N$_\beta$-N$_\alpha$) = 1.375(2), d(N$_\alpha$-P) = 1.615(1) Å),[37] or Ar–N=N–N=PPh$_3$ (Ar = 2-carboxyphenyl, d(N$_\gamma$-N$_\beta$) = 1.279, d(N$_\beta$-N$_\alpha$) = 1.328, d(N$_\alpha$-P) = 1.651 Å) show similar N$_\alpha$–P bond lengths and reveal a shorter nitrogen–nitrogen distance between N$_\gamma$ and N$_\beta$. A different situation is observed for Ar–N=N–N=P(N(CH$_2$)$_4$O)$_3$ (Ar = 2,4,6-trinitrophenyl; d(N$_\gamma$-N$_\beta$) = 1.315, d(N$_\beta$-N$_\alpha$) = 1.298, d(N$_\alpha$-P) = 1.637 Å)[38] in which the strongly electron-withdrawing aryl group stabilizes a negative partial charge at N$_\gamma$.[39]

Considering APAN(2N$_2$) with its azaphosphatrane moieties, an interesting feature is the distance between the phosphorous atom and the apical nitrogen atom since the oxidation of the proazaphosphatrane leads to a contraction of the phosphatrane cage allowing electron donation from the apical nitrogen atom to the phosphorous atom. These distances range from 3.054(2) to 3.091(2) Å in APAN(2N$_2$) (when neglecting the distance of one highly disordered cage with 3.112(2) Å). Verkade et al. reported similar distances for $PhCH_2N_3P(N\textit{i}Bu(CH_2)_2)_3N$ (3.120 Å), $PhCH_2N_3P(NCH_3(CH_2)_2)_3N$ (3.072 Å),[40] and a trisphosphazide derived from *cis*-1,3,5-triazidocyclohexane (between 3.061(2) and 3.155(1) Å).[17d] Furthermore, it should be mentioned that the phosphazide moieties in two of the three independent molecules found in asymmetric unit of APAN(2N$_2$) are located at the same side of the naphthalene backbone, whereas they are located on different sides of the aromatic skeleton in the third APAN(2N$_2$) molecule (Figure 14). This is probably a consequence of packing effects and demonstrates a small energy gap between the *syn* and *anti* forms.

Comparison of the bisphosphazides with their bisphosphazene analogues reveals a considerably longer P=N distance for phosphazenes ranging from 1.550(2) in TPPN to 1.567(2) Å in P$_2$-TPPN (Table 1). The effect of negative hyperconjugation shortening the P=N bond is stronger in phosphazenes than in bisphosphazides. TPPN(1N$_2$) demonstrates the difference of the P=N bond lengths in one molecule (phosphazide unit:

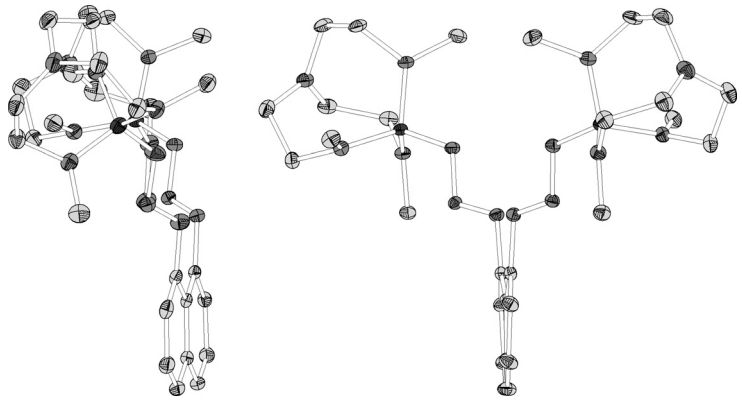

Figure 14. Two of the three independent APAN($2N_2$) molecules in the asymmetric unit in *syn* (left) and *anti* conformation (right).

1.621(4), phosphazene unit: 1.558(4) Å). By trend, the distance of the two interacting γ-nitrogen atoms is shorter in the bisphospazides ranging from 2.695(3) in TPPN($2N_2$)·H_2O to 2.785(2) Å in APAN($2N_2$) (HMPN: 2.823(2), TPPN: 2.766(3), P_2-TPPN: 2.763(2) Å), which can be explained by the stronger repulsion of the more electron-rich nitrogen centers in the bisphosphazene proton sponges. A clear distinction between bisphosphazides and bisphosphazenes can be made when considering the second important structural features of proton sponges: The average distortion of the naphthalene backbone is smaller in case of the bisphosphazides and ranges from 1.5(1) in APAN($2N_2$) to 4.5(3)° found in *t*BuGua$_2$PN($2N_2$) (HMPN: 6.1(1), TPPN: 8.2(2), P_2-TPPN: 6.3(2)°). The bulky PR_3 units, which are jointly responsible for the naphthalene distortion, are kept further away from the aromatic skeleton by the N_3 spacers in bisphosphazides.

Table 1. Structural features of bisphosphazides and comparison with the bisphosphazenes TPPN, P_2-TPPN, and HMPN (bond lengths in [Å] and angles in [°]).

Compound	d(N-N)	$d(N_\gamma\text{-}N_\beta)$	$d(N_\beta\text{-}N_\alpha)$	$d(N_\alpha\text{-}P)$	Average distortion[a]
TPPN($2N_2$)·H_2O	2.695(3)	1.286(3), 1.273(3)	1.377(3), 1.356(3)	1.611(2), 1.612(2)	2.7(2)
TPPN($1N_2$)	2.755(5)	1.295(5)	1.362(5)	1.558(4), 1.621(4)[b]	2.9(4)
TPPN[25]	2.766(3)	–	–	1.550(2), 1.553(2)	8.2(2)
P_2-TPPN[25]	2.763(2)	–	–	1.567(2)	6.3(2)
HMPN[24]	2.823(2)	–	–	1.555(1)	6.1(1)
P_2-HMPN($2N_2$)·H_2O	2.704(7)	1.310(6), 1.284(6)	1.319(6), 1.386(6)	1.630(6), 1.628(5)	1.8(5)
HEPN($2N_2$)·H_2O	2.697(3)	1.282(3), 1.306(3)	1.351(3), 1.346(3)	1.624(2), 1.630(2)	1.7(2)
APAN($2N_2$)	2.723(2)	1.292(2)	1.328(2)	1.624(2)	1.5(1)
	2.785(2)	1.281(2)	1.353(2)	1.621(1)	4.2(1),
	2.731(2)	1.281(2)	1.356(2)	1.619(1)	2.4(1)
		1.283(2)	1.348(2)	1.620(1)	
		1.281(2)	1.358(2)	1.625(1)	
		1.288(2)	1.335(2)	1.614(1)	
*t*BuPyr$_2$PN($2N_2$)	2.710(3)	1.266(3), 1.272(3)	1.375(3), 1.368(3)	1.615(2), 1.613(2)	2.9(2)
*t*BuGua$_2$PN($2N_2$)	2.720(3)	1.280(3), 1.298(3)	1.346(3), 1.357(4)	1.655(3), 1.658(3)	4.5(3)

[a] Average difference of the torsion angles C1-C8a-C4a-C5 and C8-C8a-C4-C4 from 180°. [b] Longer distance observed for the bisphosphazide moiety.

Theoretical Section

The Staudinger reaction

The first computational studies of the Staudinger reaction were carried out simultaneously by the groups of Rzepa[3b] and Grützmacher.[3a] Grützmacher et al. applied a high level ab initio CCSD(T)/6-31G(d,p)//MP2/6-31G(d) method, whereas Rzepa and co-workers utilized density functional theory (DFT) at the B3LYP/6-311G(d,p) level to investigate the reaction mechanism on the simplest model system ($PH_3 + HN_3$). They found that the primary product formed in this reaction is a phosphazide ($H_3P{=}N{-}N{=}NH$), which exists as both the *trans* and *cis* isomer. The *cis* isomer relatively easily decomposes into $H_3P{=}NH$ and N_2. The generally accepted mechanism of the Staudinger reaction is presented in Scheme 1. Later, Tian and Wang[3c] reported a DFT study of the Staudinger reaction with phosphanes and azides substituted with various alkyl and aryl groups.[3]

Herein, we present a mechanistic study of the reaction of 1,8-diazidonaphthalene with two molecules of tris(pyrrolidino)-phosphane giving a bisphosphazene to offer a suitable explanation for the experimental facts described previously in this work. The total reaction is divided into three parts: 1) Treatment of a phosphane with an azide giving the bisphosphazide TPPN($2N_2$); 2) conversion of TPPN($2N_2$) into TPPN($1N_2$), and 3) conversion of TPPN($1N_2$) into TPPN as presented in the Scheme 9a–c, respectively. The relative free-energy profiles obtained by the BMK/6-311+G(3df,2p)//B3LYP/6-31G(d) model (denoted hereafter as M(I)) are shown in the Scheme 10a–c. The attack of tris(pyrrolidino)-phosphane on 1,8-diazidonaphthalene (Scheme 9a) occurs from the *cis* direction. The energy barrier of 22 kcal mol^{-1} for a *cis* attack is lower by 19.9 kcal mol^{-1} than the energy barrier for a *trans* attack (the latter is not presented in Scheme 10). This is compatible with the findings of Tian and Wang,[3c] who found that the *cis* transition state in unsubstituted phosphane and azide has a lower energy than the *trans* transition state by 25 kcal mol^{-1}.

The *cis* intermediate (int1-*cis*) can easily isomerize to a more stable *trans* intermediate (int1-*trans*), thus giving the opportu-

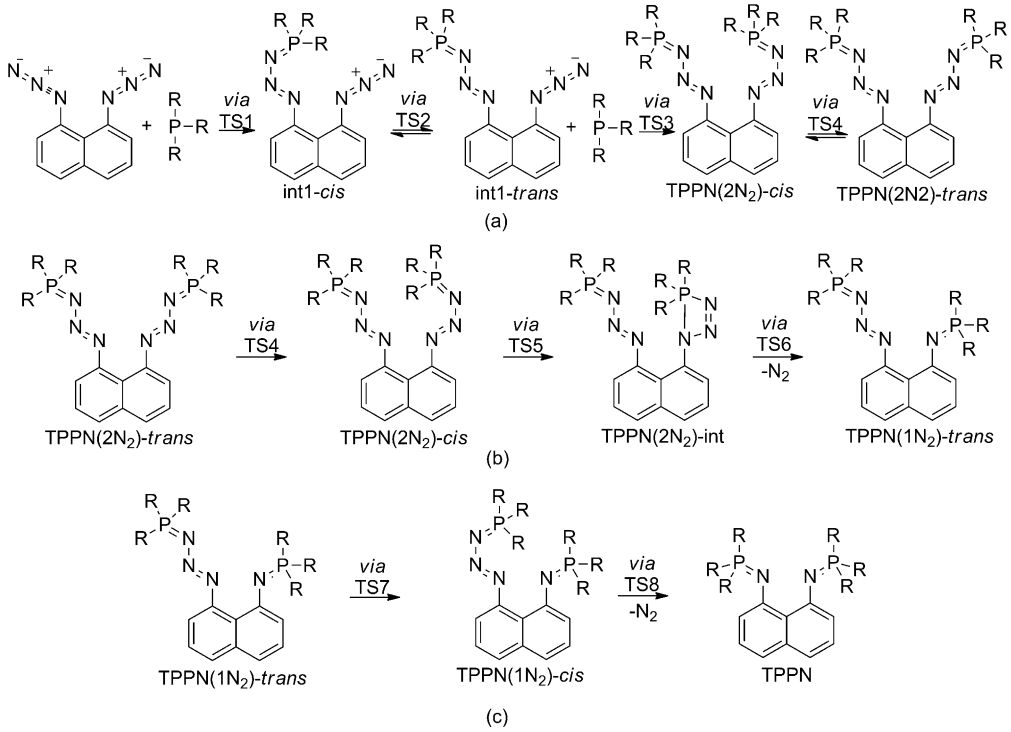

Scheme 9. Schematic representation of the Staudinger reaction pathway: (a) from phosphane and azide to TPPN($2N_2$), (b) from TPPN($2N_2$) to TPPN($1N_2$) and (c) from TPPN($1N_2$) to TPPN. (R = $N(CH_2)_4$).

nity to a second molecule of phosphane for *cis* attack on the remaining azido group. The isomerization of int1-*cis* to int1-*trans* proceeds via the transition state TS2 and requires an activation energy of 4.8 kcal mol^{-1}. Int1-*trans* reacts with a second molecule of phosphane giving the TPPN($2N_2$)-*cis* phosphazide that can easily isomerize to a more stable TPPN($2N_2$)-*trans* isomer. However, according to the accepted mechanism, elimination of an N_2 molecule from a phosphazide occurs exclusively from the *cis* isomer.[1,2] *Cis–trans* isomerization in bisphosphazides is associated with a relatively low barrier. For the simplest PH_3–N–N–NH system, Grützmacher et al. calculated a barrier of 14.6 kcal mol^{-1} with the CCSD(T) approach, whereas Wang et al., using the B3LYP/6-31G(d) method, obtained a lower value of 7 kcal mol^{-1}. Our calculations on TPPN($2N_2$) and TPPN($1N_2$) give isomerization barriers of 8.2 and 7.6 kcal mol^{-1}, respectively. Interestingly, in both cases the *cis* isomer is less stable than the *trans* isomer, specifically by 2.3 kcal mol^{-1} in TPPN($2N_2$), and 5.5 kcal mol^{-1} in TPPN($1N_2$). On the contrary, the *cis* isomer is more stable than the *trans* isomer by 8.2 kcal mol^{-1} in the unsubstituted phosphazide PH_3–N–N–NH.[3a]

Once the system has reached the *cis* phosphazide isomer, elimination of N_2 generally occurs through a two-step process.[1,2] The first step is the intramolecular nucleophilic attack of the γ-nitrogen atom at the positively charged phosphorus atom leading to a metastable four-membered triazaphosphete intermediate TPPN($2N_2$)-int. This metastable intermediate is observed on the potential energy surface for conversion of TPPN($2N_2$) into TPPN($1N_2$) (Scheme 9b), though its energy is well-above the TPPN($2N_2$) reactant (23.8 kcal mol^{-1}). The activation energy for its formation is 29.3 kcal mol^{-1}. However, the triazaphosphete intermediate does not exist on a potential energy surface (PES) for conversion of TPPN($1N_2$) into TPPN (Scheme 9c). The nonexistence of this intermediate is presumably due to the steric repulsion of bulky $(C_4H_8N)_3P$ groups that are closer to each other in the TPPN($1N_2$)-*cis* than in the TPPN($2N_2$)-*cis* intermediate. The formation of the four-membered triazaphosphete ring brings the bulky groups even nearer. Consequently, the destabilizing steric effect overcomes the relatively low stability of the triazaphosphete intermediate. In the subsequent step of the process (depicted in Scheme 9b) the triazaphosphete intermediate eliminates N_2 through the transition state TS6 with an activation energy of 25.7 kcal mol^{-1}. TPPN($1N_2$)-*cis* directly eliminates N_2 through the transition state TS8 with an activation energy of 37.3 kcal mol^{-1}. It follows that the barrier for N_2 elimination from the *cis*-TPPN($1N_2$) phosphazide is higher than from the *cis*-TPPN($2N_2$) counterpart, which is in accordance with the experimental findings.

Inspection of Scheme 10 reveals the existence of a deep well on the free-energy profile corresponding to TPPN($2N_2$) and TPPN($1N_2$). This fact can explain their relative stability. On the potential energy surface for the reaction of the unsubstituted phosphane and the azide, phosphazide ($H_3P{=}N{-}N{=}NH$) is an intermediate that lies 20.4 kcal mol^{-1} above the reactant.[3a] Only 8 kcal mol^{-1} more energy is needed for the elimination of an N_2 molecule. On the other hand, the energy of TPPN($2N_2$) is 19.6 kcal mol^{-1} below the reactants, and subsequent elimination of N_2 is energetically very demanding, which makes TPPN($2N_2$) a stable intermediate on the potential energy surface.

To find out why some of the phosphazides studied in this work do not react by elimination of N_2 to give the corresponding phosphazene, we calculated a free-energy profile (the Supporting Information, Scheme S3.2) for APAN($2N_2$), a compound that also exhibits such behavior. Apparently, the energy barriers responsible for N_2 elimination (TS5a, TS6a) are very similar to those of TPPN($2N_2$), namely, 29.7 and 28.6 kcal mol^{-1}. Only the barrier for the elimination of a second molecule of N_2 (TS8a) is higher (41.9 kcal mol^{-1}) than in TPPN($1N_2$) (37.3 kcal mol^{-1}). It seems that the inability of APAN($2N_2$) to eliminate N_2 does not originate in an increase of energy required for it. There is a possibility that some side reaction takes place in APAN($2N_2$) rather than in TPPN(2N2). However, this issue remains unclear.

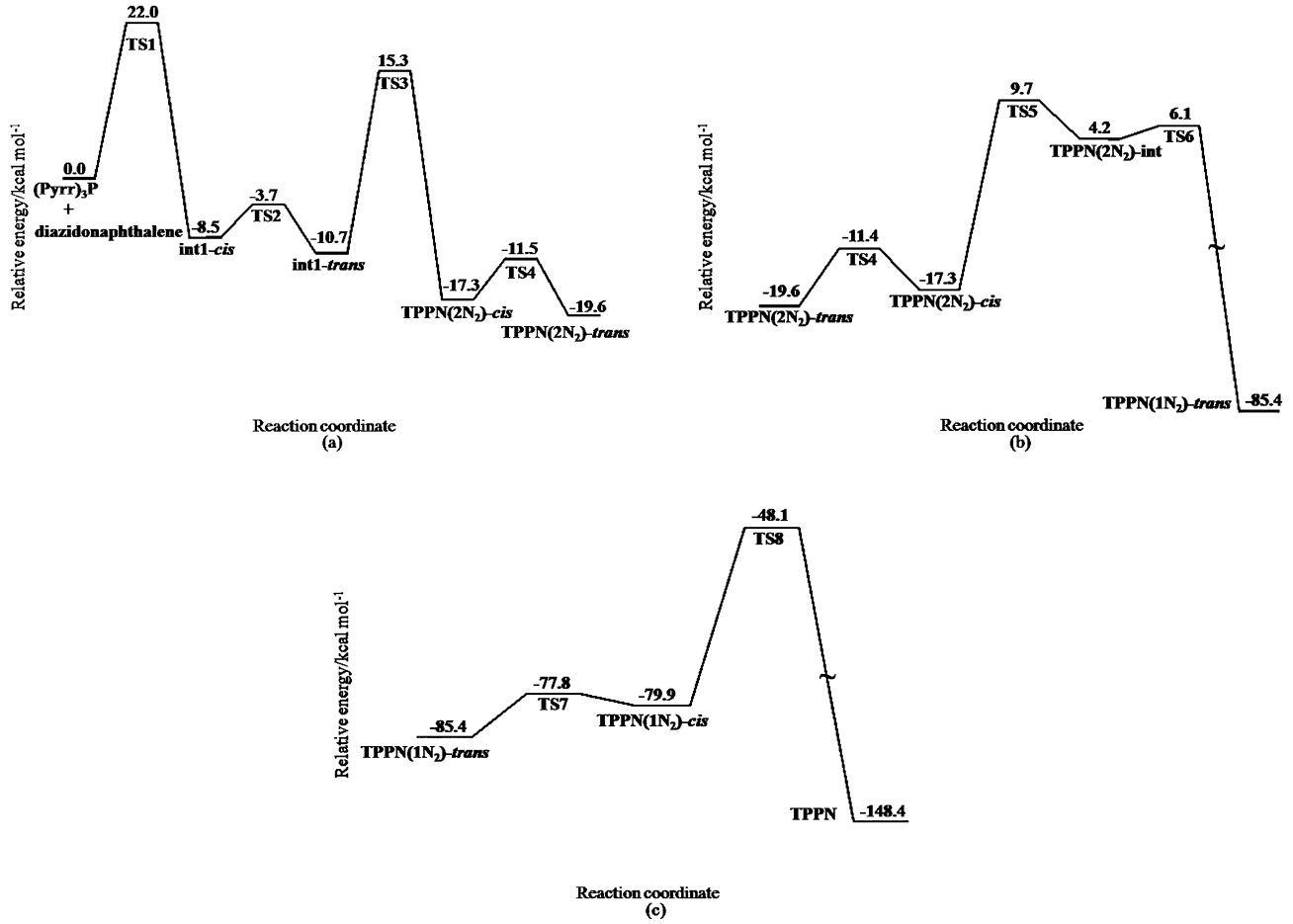

Scheme 10. (a) Relative free-energy profile (in kcal mol^{-1}) for the conversion of: (a) phosphane and azide into TPPN($2N_2$), (b) TPPN($2N_2$) into TPPN($1N_2$) and (c) TPPN($1N_2$) into TPPN.

Gas-phase structure and basicity of TPPN($2N_2$)

The X-ray analysis of crystals of TPPN($2N_2$) obtained from moist ether reveals the incorporation of one water molecule between the phosphazide moieties (Figure 7), which are located on the same side of the naphthalene plane (*syn* conformation). In contrast to the crystal structure, the calculations in the gas phase demonstrate that the *anti* conformation of water-containing TPPN($2N_2$) bisphosphazide is more stable. Geometry optimization starting from the crystal structure exhibited a spontaneous change of the conformation from *syn* to *anti*. The most stable conformer of water-free TPPN($2N_2$) in the gas phase also takes an *anti* conformation. It would appear that the *syn* conformation in the crystals is probably caused by the presence of a water molecule and crystal forces. Interestingly, TPPN($2N_2$) has a substantial affinity towards a water molecule. The enthalpy of binding of a single water molecule in the gas phase calculated by model M(I) is 10.8 kcal mol^{-1}.

Gas-phase proton affinities are calculated by using the B3LYP/6-311+G(2df,p)//B3LYP/6-31G* model. TPPN($2N_2$) has two basic nitrogen atoms, N1 and N3. Protonation at N1 leads to a PA of 281.9 kcal mol^{-1}, whereas the N3 position is less basic by 13.2 kcal mol^{-1} (PA = 268.7 kcal mol^{-1}). The lower PA of N3 is primarily a consequence of the lack of a chelating effect. Gas-phase PAs reveal that TPPN($2N_2$) is only slightly less basic than TPPN (PA = 283.2 kcal mol^{-1}). The pK_{BH^+} values in acetonitrile are calculated by a procedure described elsewhere.[41] The calculated pK_{BH^+} value of TPPN($2N_2$) in acetonitrile is 30.0 which is about 3 units less than observed for TPPN. However, experimental findings reveal that TPPN($2N_2$) is unable to deprotonate even $(Me_2N)_3P{=}NtBu$ (whose pK_{BH^+} value in MeCN is 26.98),[34] suggesting a considerably lower pK_{BH^+} value than calculated. Additionally, protonation resulted in the decomposition of the bisphosphazide. These findings deserve some rationalization.

Decomposition of TPPN($2N_2$) can be explained only by protonation at nitrogen N3. In this case, the N2–N3 bond becomes long and weak and may, therefore, easily break. However, the basicity is higher when TPPN($2N_2$) is protonated at the N1 position as presented above. Therefore, we suppose that the N3 position is kinetically more accessible than the N1 position. This can be clarified by inspecting the 3D structure of TPPN($2N_2$), in which it is evident that the N3 nitrogen is more exposed to the solvent than N1. If TPPN($2N_2$) is protonated at the N3 position, two main processes can take place: migration of the proton to the more stable N1 position or decay of TPPN($2N_2$) with breaking of the N2–N3 bond, as presented in Scheme 11 a and b, respectively.

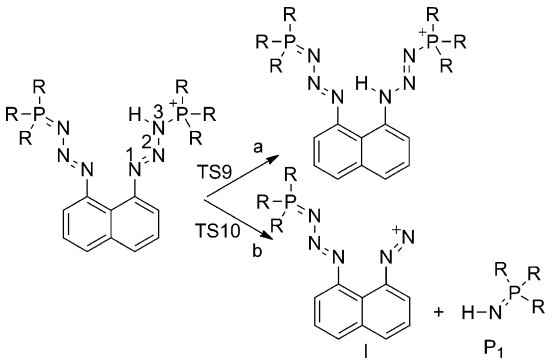

Scheme 11. Schematic representation of (a) proton transfer and (b) decay of protonated TPPN($2N_2$).

The barriers for proton transfer (TS9) and N2–N3 bond-breaking (TS10) are calculated by using the M(I) model. It appears that the proton transfer is kinetically more demanding with an activation barrier of 31.3 kcal mol^{-1}, whereas the barrier for N2–N3 bond-breaking is only 23.2 kcal mol^{-1}. The products of decay, namely the neutral P1 phosphazene base and the intermediate (I), lie 9.2 kcal mol^{-1} above TPPN($2N_2$) on a free-energy profile. After decay, the phosphazene base P1 can react with intermediate (I) in such a way as presented in Scheme 12, in which a highly reactive aryne species is produced. The energy barrier (TS11) for that process is 19.7 kcal mol^{-1}, whereas the products of the reaction are 6.6 kcal mol^{-1} below the reactant level. Alternatively, intermediate (I) could eliminate an N_2 molecule with the formation of intermediate (II). Although this reaction is more exergonic than the previous one, it is kinetically less preferred. The energy of TS12 is 27.0 kcal mol^{-1}. Consequently, it is plausible to assume that the aryne can be obtained as an intermediate in a process of decay of protonated TPPN($2N_2$), which would then explain the experimentally observed diversity of decay products.[42]

Basicity of TPPN($1N_2$)

Calculations show that TPPN($1N_2$) takes an *anti* conformation, which is in accordance with the molecular structure. This compound possesses three positions for which high proton affinities are expected. Two of them are the nitrogen atoms (N_α and N_γ) of the phosphazide moiety and the third one is the nitrogen atom on the phosphazene fragment (N1). Calculation reveals that the phosphazene nitrogen is the most basic site with a PA of 283.2 kcal mol^{-1}. The N_α and N_γ positions on the phosphazide fragment give PAs of 281.9 and 264.5 kcal mol^{-1}, respectively. Hence, the proton affinity of the N_α position of the phosphazide moiety is only slightly lower than the basicity of the phosphazene fragment. The calculated pK_{BH^+} value of this base in acetonitrile is 31.3.

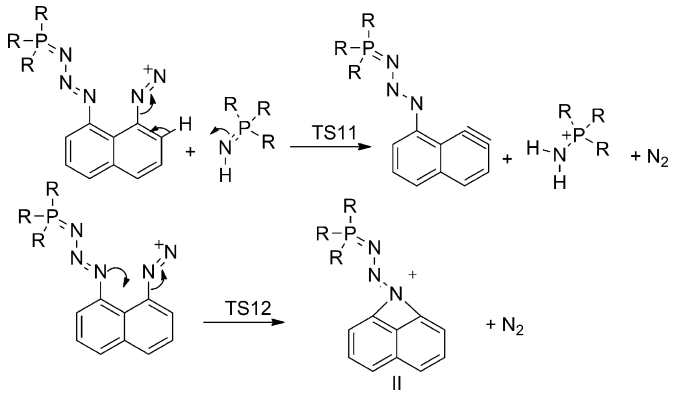

Scheme 12. Possible decay mechanism after protonation of TPPN($2N_2$) followed by N2–N3 bond-breaking.

UV/Vis Spectra and excited singlet-state calculations of TPPN and TPPN($2N_2$)

As described above, all studied bisphosphazides possess a green color, whereas the phosphazenes exhibit a beige tone in case of HMPN and TPPN. To explain the color difference we have measured and calculated the UV/Vis spectra of TPPN($2N_2$) and TPPN in THF. The calculations of molecular spectra are performed by using TD-DFT approach with B3LYP/6-311+G(2df,p)//B3LYP/6-31G(d) model and the spectra are presented in Figure 15. The calculated excitation energy of the lowest excited state in TPPN corresponds to a wavelength of 365 nm, whereas the spectrum of TPPN($2N_2$) reveals a very weak absorption at 405.6 nm and a strong absorption at 400.6 nm. In the TPPN molecule the lowest excitation corresponds to a transfer of an electron from the HOMO to the LUMO orbital. In TPPN($2N_2$) absorption at 405.6 nm corresponds to a transfer of an electron from HOMO-1 to LUMO, whereas absorption at 400.6 nm corresponds to a HOMO–LUMO transfer. HOMO and LUMO orbitals in both compounds have a π symmetry (the

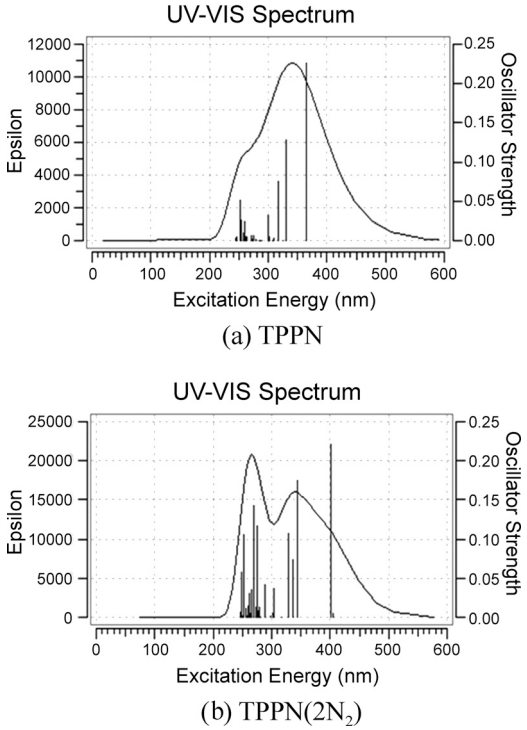

Figure 15. Calculated UV/Vis spectra of (a) TPPN and (b) TPPN($2N_2$).

Supporting Information, Figure S3.1), so the strong excitations at high wavelengths correspond to the $\pi \rightarrow \pi^*$ transitions. Shifting of absorption lines towards higher wavelengths observed in TPPN($2N_2$) is typical for conjugated systems due to a lower HOMO–LUMO energy gap. TPPN absorbs mostly in the UV region and the highest wavelength of absorption at 365 nm is just at the border to the visible part of the spectrum. Consequently it is almost colorless. On the other hand, absorption of TPPN($2N_2$) is shifted towards the visible part of the spectrum. A wavelength around 400 nm corresponds to a violet color. Absorption of violet color results in the complementary green color of TPPN($2N_2$) in solution. The calculated UV/Vis spectra are in relatively good agreement with the measured ones (the Supporting Information, Figures S1.1 and S1.2).

Conclusion

We have extended the class of stable open-chain phosphazides by a set of eleven bisphosphazides with a rigid constrained geometry 1,8-naphthalene backbone. The substrates that were reacted with 1,8-diazidonaphthalene in a Staudinger reaction ranged from simple phosphanes with acyclic or cyclic amino substituents to more sophisticated systems like proazaphosphatranes, P_2-moieties, or compounds bearing guanidino units or chiral groups derived from L-proline. The obtained Staudinger adducts were studied by experimental and theoretical means with respect to their spectroscopic characteristics and in part also their thermal stability, as well as their basic and chromophoric properties. Crystal structures gave insight into the interaction of the two phosphazide moieties and revealed the coordination of a water molecule through hydrogen bonding in three cases, which is a valuable finding to understand the role of bisphosphazides in organocatalysis.

However, only the three bisphosphazene proton sponges HMPN, TPPN, and P_2-TPPN could be obtained through a Staudinger reaction due to the unexpectedly high stability of the initially formed bisphosphazides. For all other bisphosphazides described herein, a selective elimination of molecular nitrogen could neither be achieved at high temperatures, UV radiation, nor by the use of additives such as aluminum trichloride or C_8K. The energy profile of the reaction between 1,8-diazidonaphthalene and tris(pyrrolidino)phosphane through TPPN($2N_2$) and TPPN($1N_2$) to TPPN was studied by computational means and the course of the reaction could be followed by using ^{31}P NMR spectroscopy, which finally allowed the isolation and structural characterization of TPPN($1N_2$) bearing a phosphazene and a phosphazide moiety in one molecule. Theoretical calculations predicting a high basicity for TPPN($2N_2$) could not be verified experimentally because protonation resulted in the decomposition of the bisphosphazide to unidentified products. A decay mechanism through an aryne species was investigated computationally. Furthermore, TPipPN($2N_2$) was successfully treated with the Lewis acid trimethylaluminum, which resulted in a cationic alkylaluminum species with a tetramethyl aluminate counteranion. The presentation of a rigid chiral bisphosphazide with six centers of chirality and the findings concerning the specific interaction mode of neutral bisphosphazides with cationic Lewis acids ($AlMe_2^+$) or neutral molecules (H_2O) will inspire further investigations with this interesting class of bifunctional molecules.

Experimental Section

General methods

Reactions were carried out under inert atmosphere using standard Schlenk techniques. Moisture and air sensitive substances were stored in a conventional nitrogen-flushed glovebox. Solvents were purified according to literature procedures and kept under an inert atmosphere. 1,8-diaminonaphthalene (ACROS) was purified by recrystallization from toluene followed by sublimation and converted to 1,8-diazidonaphthalene through its diazonium salt.[43] Tris(amino)phosphanes were prepared through condensation[44] or transamination reactions.[45] The P_2 precursors for the syntheses of P_2-HMPN($2N_2$) and P_2-TPPN($2N_2$) were prepared in a three-step procedure from the corresponding phosphanes.[28,25] The precursors for *t*BuPyr$_2$PN($2N_2$) and *t*BuGua$_2$PN($2N_2$) were obtained from the reaction of PCl_2tBu with pyrrolidine or tetramethylguanidine, respectively.[30b,33] (*S*)-2-(methoxymethyl)pyrrolidine is accessible through a four-step procedure starting from L-proline.[46] The proazaphosphatrane used for the synthesis of APAN($2N_2$) was obtained from the reaction of $PCl(NMe_2)_2$ with $N((CH_2)_2NHMe)_3$, followed by deprotonation with potassium *tert*-butoxide.[17a]

Spectra were recorded on the following spectrometers: NMR: Bruker ARX300, Bruker DRX400, Bruker DRX500; IR: ATR-FTIR; MS: LTQ-FT or QStarPulsar i (Finnigan); elemental analysis: CHN-Rapid (Heraeus).

Atoms are labeled from 1 to 8a in the naphthalene moiety and from 9 for the remaining carbon atoms. The exact numbering is shown in the Supporting Information.

Syntheses

Synthesis of HMPN($2N_2$): HMPN($2N_2$) is given as a representative example for the synthesis of bisphosphazides (the detailed procedures are described in the Supporting Information). A solution of tris(dimethylamino)phosphane (126 mg, 0.772 mmol, 2.25 equiv) in THF (7.5 mL) was added drop-wise to a solution of 1,8-diazidonaphthalene (72 mg, 0.343 mmol, 1.0 equiv) in THF (7.5 mL). The reaction mixture changed color from violet to deep green and was stirred for 3 h at room temperature. All volatiles were removed in vacuo and the remaining residue was washed twice with pentane (15 mL). After drying in vacuo, 1,8-bis-(hexamethyltriaminophosphazidyl)naphthalene (118 mg, 64%) was obtained as a dark-green solid. ^{1}H NMR (300 MHz, [D$_3$]MeCN, 25 °C, TMS): $\delta = 7.71$ (dd, ^3J(H,H) = 8.2 Hz, ^4J(H,H) = 1.1 Hz, 2H, H(2,7)), 7.45 (t, ^3J(H,H) = 7.7 Hz, 2H, H(3,6)), 7.00 (t, ^3J(H,H) = 7.3 Hz, ^4J(H,H) = 0.9 Hz, 2H, H(4,5)), 2.83 ppm (d, ^3J(P,H) = 9.1 Hz, 36H, H(9)); ^{13}C NMR (76 MHz, [D$_3$]MeCN, 25 °C, TMS): $\delta = 153.4$ (C(1,8)), 137.4 (C(8a)), 127.3 (C(3,6)), 126.2 (C(2,7)), 125.1 (C(4a)), 116.3 (C(4,5)), 48.4 ppm (d, ^2J(P,C) = 2.3 Hz, C(9)); ^{31}P NMR (101 MHz, [D$_3$]MeCN, 25 °C, 85% H_3PO_4): $\delta = 43.2$ ppm; ESI-MS (MeCN): *m/z* (%): 537 (100) $[M]^+$, 509 (16) $[M-N_2]^+$, 359 (69) $[M-C_6H_{18}N_4P]^+$, 331 (92) $[M-C_6H_{18}N_6P]^+$, 179 (52) $[(Me_2N)_3P{=}NH_2]^+$; HRMS (ESI): *m/z* calcd for $C_{22}H_{43}N_{12}P_2^+$: 537.3203 [M+H$^+$]; found: 537.3201.[47]

P_2-HMPN($2N_2$): Yield: 85%. ^{1}H NMR (300 MHz, [D$_3$]MeCN, 25 °C, TMS): $\delta = 7.47$ (d, ^3J(H,H) = 7.5 Hz, 2H, H(2,7)), 7.25 (t, ^3J(H,H) = 7.5 Hz, 2H, H(3,6)), 6.97 (d, ^3J(H,H) = 7.5 Hz, 2H, H(4,5)), 2.69 (d, ^3J(P,H) = 9.6 Hz, 24H, H(9)), 2.60 ppm (d, ^3J(P,H) = 10.2 Hz, 36H, H(10)); ^{13}C NMR (101 MHz, [D$_3$]MeCN, 25 °C, TMS): $\delta = 153.7$ (C(1,8)),

137.2 (C(8a)), 126.1 (C(3,6)), 124.9 (C(4a)), 124.3 (C(2,7)), 115.2 (C(4,5)), 37.9 (d, ^2J(P,C) = 1.9 Hz, C(9)), 37.5 ppm (d, ^2J(P,C) = 4.5 Hz, C(10)); ^{31}P NMR (122 MHz, [D$_3$]MeCN, 25 °C, 85% H_3PO_4): δ = 24.0 (d, ^2J(P,P) = 51.7 Hz, -P(NMe$_2$)$_2$), 19.4 ppm (d, ^2J(P,P) = 51.7 Hz, -P(NMe$_2$)$_3$); IR: $\tilde{\nu}$ = 445, 491, 537, 591, 623, 654, 685, 739, 807, 824, 850, 949, 969, 1064, 1106, 1128, 1185, 1248, 1281, 1328, 1385, 1454, 1559, 2796, 2839, 2871, 2994, 3044 cm^{-1}; HRMS (ESI): *m/z* calcd for $C_{30}H_{67}N_{18}P_4^+$: 825.4561 [*M*+H$^+$]; found: 825.4560.

TPPN(2 N$_2$): Yield: 75%. ^{1}H NMR (300 MHz, [D$_3$]MeCN, 25 °C, TMS): δ = 7.57 (dd, ^3J(H,H) = 7.4 Hz, ^4J(H,H) = 1.0 Hz, 2H, H(2,7)), 7.32 (t, ^3J(H,H) = 7.4 Hz, 2H, H(3,6)), 6.87 (dd, ^3J(H,H) = 7.4 Hz, ^4J(H,H) = 1.0 Hz, 2H, H(4,5)), 3.29–3.23 (m, 24H, H(9)), 1.84–1.80 ppm (m, 24H, H(10)); ^{13}C NMR (76 MHz, [D$_3$]MeCN, 25 °C, TMS): δ = 152.9 (C(1,8)), 136.8 (C(8a)), 126.6 (C(3,6)), 125.2 (C(2,7)), 124.6 (C(C4a), 115.4 (C(4,5)), 47.9 (d, ^2J(P,C) = 2.7 Hz, C(9)), 27.0 ppm (d, ^3J(P,C) = 7.1 Hz, C(10)); ^{31}P NMR (122 MHz, [D$_3$]MeCN, 25 °C, 85% H_3PO_4): δ = 29.2 ppm; IR: $\tilde{\nu}$ = 474, 508, 535, 563, 599, 629, 651, 675, 760, 815, 832, 871, 912, 967, 1008, 1065, 1172, 1204, 1292, 1345, 1417, 1563, 2861, 2956, 3043 cm^{-1}; APCI-MS (MeCN): *m/z* (%):665 (35) [*M*−N$_2$]$^+$, 637 (100) [*M*−2N$_2$]$^+$, 381 (52) [*M*−C$_{12}$H$_{24}$N$_6$P−2N$_2$]$^+$, 257 (44) [C$_{12}$H$_{24}$N$_3$OP]$^+$, 242 (42) [C$_{12}$H$_{25}$N$_3$P]$^+$; HRMS (APCI): *m/z* calcd for $C_{34}H_{55}N_{10}P_2^+$: 665.4086 [*M*H$^+$−N$_2$]; found: 665.4083; elemental analysis calcd (%) for $C_{34}H_{54}N_{12}P_2$: C 58.94, H 7.68, N 24.26; found: C 58.33, H 7.80, N 24.27.

TPPN(1 N$_2$): A solution of tris(pyrrolidino)phosphane (262 mg, 1.086 mmol, 2.1 equiv) in toluene (5 mL) was added drop-wise to a solution of 1,8-diazidonaphthalene (109 mg, 0.517 mmol, 1.0 equiv) in toluene (10 mL). The reaction mixture changed color from violet to deep green and was stirred for 10 min at room temperature and 10 min at 90 °C. All volatiles were removed in vacuo and the remaining greasy residue was washed with pentane (15 mL). After drying in vacuo, 1-[tris(pyrrolidino)phosphazidyl]-8-[tris(pyrrolidino)phosphazenyl]naphthalene (210 mg, 61%) was obtained as a deep-green solid. ^{1}H NMR (400 MHz, [D$_6$]benzene, 25 °C, TMS): δ = 7.68 (dd, 1H, ^3J(H,H) = 8.1 Hz, ^4J(H,H) = 1.1 Hz, H(2)), 7.43 (t, 1H, ^3J(H,H) = 7.7 Hz, H(6)), 7.39 (t, 1H, ^3J(H,H) = 7.7 Hz, H(3)), 7.35 (d, 1H, ^3J(H,H) = 7.9 Hz, H(5)), 7.10 (dd, 1H, ^3J(H,H) = 7.2 Hz, ^4J(H,H) = 1.2 Hz, H(4)), 7.04 (dt, 1H, ^3J(H,H) = 7.5 Hz, ^4J(H,H) = 1.5 Hz, H(7)), 3.39–3.35 (m, 12H, H(9)), 3.15–3.11 (m, 12H, H(11)), 1.65–1.62 (m, 12H, H(10)), 1.51–1.48 ppm (m, 12H, H(12)); ^{13}C NMR (101 MHz, [D$_6$]benzene, 25 °C, TMS): δ = 155.3 (C(1)), 151.3 (d, ^2J(P,C) = 4.4 Hz, C(8)), 138.4 (d, ^3J(P,C) = 2.3 Hz, C(8a)), 127.2 (C(4a)), 126.4 (C(6)), 125.8 (C(2)), 125.0 (C(3)), 117.2 (d, ^3J(P,C) = 9.5 Hz, C(7)), 116.0 (C(5)), 114.7 (C(4)), 47.3 (d, ^2J(P,C) = 3.6 Hz, C(9)), 47.2 (d, ^2J(P,C) = 2.7 Hz, C(11)), 26.8 (d, ^3J(P,C) = 7.5 Hz, C(10)), 26.5 ppm (d, ^3J(P,C) = 6.8 Hz, C(12)); ^{31}P NMR (122 MHz, [D$_3$]MeCN, 25 °C, 85% H_3PO_4): δ = 28.7 (CN$_3$P), 5.7 ppm (CNP); IR: $\tilde{\nu}$ = 467, 520, 556, 575, 597, 648, 704, 761, 782, 804, 870, 913, 936, 1004, 1063, 1162, 1199, 1235, 1259, 1315, 1346, 1373, 1395, 1448, 1550, 2859, 2957, 3042 cm^{-1}; ESI-MS (MeCN): *m/z* (%): 665 (8) [*M*]$^+$, 637 (34) [*M*−N$_2$]$^+$, 381 (100) [*M*−N$_3$P(NC$_4$H$_8$)$_3$]$^+$, 312 (9) [*M*−N$_3$P(NC$_4$H$_8$)$_3$−NC$_4$H$_8$]$^+$, 257 (68) [H$_2$NP(NC$_4$H$_8$)$_3$]$^+$, 242 (28) [HP(NC$_4$H$_8$)$_3$]$^+$; HRMS (ESI): *m/z* calcd for $C_{34}H_{55}N_{10}P_2^+$: 665.4086 [*M*+H$^+$]; found: 665.4081; elemental analysis calcd (%) for $C_{34}H_{54}N_{10}P_2$: C 61.43, H 8.19, N 21.07; found: C 60.98, H 8.31, N 20.79.

P$_2$-TPPN(2 N$_2$): Yield: 68%. ^{1}H NMR (400 MHz, [D$_6$]benzene, 25 °C, TMS): δ = 7.66 (dd, ^3J(H,H) = 8.0 Hz, 2H, ^4J(H,H) = 1.3 Hz, H(2,7)), 7.47 (t, ^3J(H,H) = 7.6 Hz, 2H, H(3,6)), 7.39 (d, ^3J(H,H) = 7.3 Hz, 2H, H(4,5)), 3.61–3.44 (m, 8H, H(9)), 3.19–3.13 (m, 12H, H(11)), 1.80–1.75 (m, 8H, H(10)), 1.63–1.58 ppm (m, 8H, H(12)); ^{13}C NMR (126 MHz, [D$_6$]benzene, 25 °C, TMS): δ = 155.1 (C(1,8)), 136.9 (C(8a)), 125.5 (C(3,6)), 125.2 (C(4a)), 123.7 (C(2,7)), 115.7 (C(4,5)), 47.7 (d, ^2J(P,C) = 3.0 Hz, C(9)), 47.2 (d, ^2J(P,C) = 4.8 Hz, C(11)), 27.0 (d, ^3J(P,C) = 8.0 Hz, C(10)), 26.7 ppm (d, ^3J(P,C) = 8.1 Hz, C(12)); ^{31}P NMR (101 MHz, [D$_6$]benzene, 25 °C, 85% H_3PO_4): δ = 19.7 (d, ^2J(P,P) = 48.0 Hz, P(Pyrr)$_2$), 9.5 ppm (d, ^2J(P,P) = 48.0 Hz, P(Pyrr)$_3$); IR: $\tilde{\nu}$ = 427, 495, 538, 567, 590, 635, 656, 693, 755, 819, 881, 943, 976, 1007, 1054, 1125, 1199, 1259, 1288, 1336, 1427, 1448, 1544, 2865, 2928, 2957, 3037 cm^{-1}; ESI-MS (MeCN): *m/z* (%): 1063 (12) [*M*]$^+$, 610 (5) [*M*−C$_{20}$H$_{40}$N$_8$P$_2$]$^+$, 566 (6) [*M*−C$_{20}$H$_{41}$N$_{11}$P$_2$]$^+$, 442 (23) [*M*−C$_{30}$H$_{46}$N$_{11}$P$_2$]$^+$, 356 (100) [*M*−C$_{30}$H$_{46}$N$_{12}$P$_2$−C$_4$H$_8$N]$^+$; HRMS (ESI): *m/z* calcd for $C_{50}H_{87}N_{18}P_4^+$: 1063.6312 [*M*+H$^+$]; found: 1063.6335.

HEPN(2 N$_2$): Yield: 35%. ^{1}H NMR (400 MHz, [D$_3$]MeCN, 25 °C, TMS): δ = 7.56 (d, ^3J(H,H) = 7.4 Hz, 2H, H(2,7)), 7.31 (t, ^3J(H,H) = 7.7 Hz, 2H, H(3,6)), 6.98 (d, ^3J(H,H) = 7.3 Hz, 2H, H(4,5)), 3.18 (dq, ^3J(P,H) = 9.7 Hz, ^3J(H,H) = 7.1 Hz, 24H, H(9)), 1.11 ppm (t, ^3J(H,H) = 7.1 Hz, 36H, H(10)); ^{13}C NMR (101 MHz, [D$_3$]MeCN, 25 °C, TMS): δ = 152.9 (C(1,8)), 137.0 (C(8a)), 126.5 (C(3,6)), 125.3 (C(2,7)), 124.8 (C(4a)), 115.4 (C(4,5)), 40.4 (^2J(P,C) = 2.9 Hz, C(9)), 14.1 ppm (^3J(P,C) = 2.3 Hz, C(10)); ^{31}P NMR (122 MHz, [D$_3$]MeCN, 25 °C, 85% H_3PO_4): δ = 41.4 ppm; ESI-MS (MeCN): *m/z* (%): 705 (100) [*M*]$^+$; HRMS (ESI): *m/z* calcd for $C_{34}H_{67}N_{12}P_2^+$: 705.5081 [*M*+H$^+$]; found: 705.5071.

TPipPN(2 N$_2$): Yield: 77%. ^{1}H NMR (500 MHz, [D$_3$]MeCN, 25 °C, TMS): δ = 7.59 (dd, ^3J(H,H) = 8.2 Hz, ^4J(H,H) = 0.9 Hz, 2H, H(2,7)), 7.34 (t, ^3J(H,H) = 7.7 Hz, 2H, H(3,6)), 6.96 (d, ^3J(H,H) = 7.2 Hz, 2H, H(4,5)), 3.17–3.14 (m, 24H, H(9)), 1.60- 1.56 (m, 12H, H(11)), 1.54–1.49 ppm (m, 24H, H(10)); ^{13}C NMR (126 MHz, [D$_3$]MeCN, 25 °C, TMS): δ = 152.8 (C(1,8)), 136.9 (C(8a)), 126.6 (C(3,6)), 125.4 (C(2,7)), 124.5 (C(4a)), 115.5 (C(4,5)), 47.0 (C(9)), 27.0 (d, ^3J(P,C) = 4.6 Hz, C(10)), 25.4 ppm (C(11)); ^{31}P NMR (122 MHz, [D$_3$]MeCN, 25 °C, 85% H_3PO_4): δ = 35.4 ppm; IR: $\tilde{\nu}$ = 464, 540, 564, 592, 615, 651, 666, 684, 723, 743, 764, 815, 835, 853, 943, 987, 1055, 1113, 1141, 1162, 1209, 1277, 1338, 1375, 1428, 1540, 2845, 2923, 3039 cm^{-1}; ESI-MS (MeCN): *m/z* (%): 777 (100) [*M*]$^+$; HRMS (ESI): *m/z* calcd for $C_{40}H_{67}N_{12}P_2^+$: 777.5087 [*M*+H$^+$]; found: 777.5098; elemental analysis calcd (%) for $C_{40}H_{66}N_{12}P_2$: C 61.83, H 8.56, N 21.63; found: C 61.48, H 8.69, N 20.99.

TAzPN(2 N$_2$): Yield: 40%. ^{1}H NMR (400 MHz, [D$_3$]MeCN, 25 °C, TMS): δ = 7.57 (dd, ^3J(H,H) = 8.1 Hz, ^4J(H,H) = 1.0 Hz, 2H, H(2,7)), 7.32 (t, ^3J(H,H) = 7.8 Hz, 2H, H(3,6)), 7.06 Hz (d, ^3J(H,H) = 7.3 Hz, 2H, H(4,5)), 3.24 (dt, ^3J(H,H) = 5.6 Hz, ^3J(P,H) = 8.0 Hz, 12H, H(9)), 1.69–1.65 (m, 24H, H(10)), 1.62–1.59 ppm (m, 24H, H(11)); ^{13}C NMR (101 MHz, [D$_3$]MeCN, 25 °C, TMS): δ = 152.6 (C(1,8)), 137.1 (C(8a)), 126.4 (C(3,6)), 125.3 (C(2,7)), 124.8 (C(4a)), 115.1 (C(4,5)), 49.6 (d, ^2J(P,C) = 1.7 Hz, C(9)), 30.9 (d, ^3J(P,C) = 3.7 Hz, C(10)), 27.5 ppm (C(11)); ^{31}P NMR (122 MHz, [D$_3$]MeCN, 25 °C, 85% H_3PO_4): δ = 39.3 ppm; ESI-MS (MeCN): *m/z* (%): 862 (100) [*M*]$^+$, 521 (24) [*M*−C$_{18}$H$_{36}$N$_4$P]$^+$, 325 (9) [*M*−C$_{28}$H$_{23}$N$_9$P]$^+$; HRMS (ESI): *m/z* calcd for $C_{46}H_{79}N_{12}P_2^+$: 861.6020 [*M*+H$^+$]; found: 861.6009.

***t*BuPyr$_2$PN(2 N$_2$)**: Yield: 67%. ^{1}H NMR (500 MHz, [D$_3$]MeCN, 25 °C, TMS): δ = 7.58 (dd, ^3J(H,H) = 8.2 Hz, ^4J(H,H) = 1.1 Hz, 2H, H(2,7)), 7.33 (t, 2H, ^3J(H,H) = 7.3 Hz, H(3,6)), 6.86 (dd, ^3J(H,H) = 7.3 Hz, ^4J(H,H) = 1.0 Hz, 2H, H(4,5)), 3.38–3.23 (m, 16H, H(9)), 1.86–1.75 (m, 16H, H(10)), 1.33 ppm (d, ^3J(P,H) = 14.7 Hz, 18H, H(12)); ^{13}C NMR (126 MHz, [D$_3$]MeCN, 25 °C, TMS): δ = 152.9 (C(1,8), 136.8 (C(8a)), 126.7 (C(3,6)), 125.4 (C(2,7)), 124.4 (C(4a)), 115.4 (C(4,5)), 49.2 (d, ^2J(P,C) = 1.1 Hz, C(9)), 35.7 (d, ^1J(P,C) = 108.4 Hz, C(11)), 27.2 (d, ^3J(P,C) = 1.2 Hz, C(10)), 26.9 ppm (d, ^2J(P,C) = 6.1 Hz, C(12)); ^{31}P NMR (122 MHz, CD$_3$CN, 25 °C, 85% H_3PO_4): δ = 48.9 ppm (s); IR: $\tilde{\nu}$ = 417, 487, 518, 541, 567, 594, 620, 640, 662, 727, 765, 817, 874, 961, 1003, 1058, 1105, 1161, 1175, 1197, 1294, 1349, 1391, 1415, 1457, 1474, 1563, 2862, 2963, 3045 cm^{-1}; ESI-MS (MeCN): *m/z* (%): 667 (100) [*M*]$^+$; HRMS (ESI): *m/z* calcd for $C_{34}H_{57}N_{10}P_2^+$: 667.4237 [*M*+H$^+$]; found: 667.4231; elemental analysis calcd (%) for $C_{34}H_{56}N_{10}P_2$: C 61.24, H 8.46, N 21.01; found: C 60.95, H 8.53, N 20.84.

***t*BuTmg$_2$PN(2 N$_2$)**: Yield: 38%. ^{1}H NMR (300 MHz, [D$_3$]MeCN, 25 °C, TMS): δ = 7.38 (d, ^3J(H,H) = 7.8 Hz, 2H, H(2,7)), 7.19 (t, ^3J(H,H) = 7.7 Hz, 2H, H(3,6)), 6.92 (d, ^3J(H,H) = 7.8 Hz, 2H, H(4,5)), 2.80 (s, 48H, H(10)), 1.27 ppm (d, ^3J(P,H) = 15.0 Hz, 18H, H(12)); ^{13}C NMR (101 MHz, [D$_6$]benzene, 25 °C, TMS): δ = 161.7 (C(9)), 154.9 (C(1,8)), 137.0 (C(8a)), 125.7 (C(3,6)), 125.2 (C(4a)), 123.5 (C(2,7)), 115.7 (C(4,5)), 40.4 (C(10)), 35.0 ppm (d, ^1J(P,C) = 133.3 Hz, C(11)), 26.8 (C(12)); ^{31}P NMR (101 MHz, [D$_6$]benzene, 25 °C, 85% H$_3$PO$_4$): δ = 24.6 ppm; IR: $\tilde{\nu}$ = 467, 518, 578, 638, 761, 795, 823, 880, 905, 951, 1012, 1059, 1128, 1173, 1206, 1226, 1333, 1372, 1419, 1471, 1500, 1540, 1599, 2869 cm^{-1}; ESI-MS (MeCN): *m/z* (%): 843 (75) $[M]^+$, 333 (99) $[C_{14}H_{33}N_6OP]^+$; HRMS (ESI): *m/z* calcd for $C_{38}H_{73}N_{18}P_2^+$: 843.5738 $[M+H^+]$; found: 843.5738.

APAN(2 N$_2$): Yield: 56%. ^{1}H NMR (400 MHz, [D$_3$]MeCN, 25 °C, TMS): δ = 7.58 (dd, 2H, ^3J(H,H) = 7.8 Hz, ^4J(H,H) = 0.9 Hz, H(2,7)), 7.32 (t, 2H, ^3J(H,H) = 7.8 Hz, H(3,6)), 6.89 (d, 2H, ^3J(H,H) = 7.8 Hz, H(4,5)), 2.99–2.93 (m, 12H, H(9)), 2.84–2.81 (m, 12H, H(10)) 2.78 ppm (d, 18H, ^3J(P,H) = 7.9 Hz, H(11)); ^{13}C NMR (100 MHz, [D$_3$]MeCN, 25 °C, TMS): δ = 153.2 (C(1,8)), 136.8 (C(8a)), 126.5 (C(3,6)), 125.2 (C(2,7)), 124.6 (C(4a)), 115.9 (C(4,5)), 52.2 (C(9)), 50.2 (C(10)), 35.8 ppm (d, ^2J(P,C) = 3.3 Hz, C(11)); ^{31}P NMR (121 MHz, [D$_3$]MeCN, 25 °C, 85% H$_3$PO$_4$): δ = 36.4 ppm; IR: $\tilde{\nu}$ = 411, 466, 480, 508, 539, 569, 597, 624, 645, 654, 693, 722, 756, 765, 786, 815, 864, 901, 946, 985, 1009, 1045, 1110, 1128, 1155, 1172, 1199, 1221, 1289, 1329, 1377, 1426, 1450, 1544, 2812, 2869, 2895, 2926, 2956, 3036 cm^{-1}; APCI-MS (MeCN): *m/z* (%): 587.4 (100) $[M-(N_2)_2]^+$; HRMS (APCI): *m/z* calcd for $C_{28}H_{48}N_{10}P_2$: 587.3617 $[MH-(N_2)_2]^+$; found: 587.3618; elemental analysis calcd (%) for $C_{28}H_{48}N_{14}P_2$: C 52.32, H 7.53, N 30.51; found: C 52.03, H 8.00, N 30.13.

Tris(2-methoxymethylpyrrolidino)phosphane: A solution of (*S*)-2-(methoxymethyl)pyrrolidine (2.29 g, 19.90 mol, 3.5 equiv) in diethyl ether (50 mL) was added drop-wise to a solution of phosphorous trichloride (0.78 g, 5.69 mmol, 1.0 equiv) and triethylamine (2.01 g, 19.91 mmol, 3.5 equiv) in diethyl ether (100 mL) at 0 °C. The reaction mixture was stirred for 6 h at room temperature and precipitated triethylammonium chloride was separated by filtration over Celite. The solid was extracted three times with diethyl ether (20 mL) and the combined organic phases were evaporated to dryness under reduced pressure. The remaining oily residue was distilled to give tris(2-methoxymethylpyrrolidiyl)phosphane (1.75 g, 83%) as a colorless oil. B.p.: 180 °C at 4.2×10^{-1} mbar; $[\alpha]_D^{20}$ = +78.2 (*c* = 3.25, toluene); ^{1}H NMR (300 MHz, [D$_6$]benzene, 25 °C, TMS): δ = 3.82–3.71 (m, 1H, H(2)), 3.43 (dd, ^3J(H,H) = 8.9 Hz, ^2J(H,H) = 4.5 Hz, 1H, H(6)), 3.34–3.25 (m, 1H, H(5)), 3.18–3.12 (m, 1H, H(6)) 3.16 (s, 3H, H(7)), 2.97–2.90 (m, 1H, H(5)), 1.95–1.78 (m, 2H, H(3)), 1.76–1.59 ppm (m, 2H, H(4)); ^{13}C NMR (76 MHz, [D$_6$]benzene, 25 °C, TMS): δ = 77.3 (d, ^3J(P,C) = 4.8 Hz, C(6)), 59.8 (d, ^2J(P,C) = 30.8 Hz, C(2)), 58.6 (C(7)), 47.0 (C(5)), 29.5 (d, ^3J(P,C) = 4.9 Hz, C(3)), 25.6 ppm (C(4)); ^{31}P NMR (122 MHz, [D$_6$]benzene, 25 °C, 85% H$_3$PO$_4$): δ = 102.9 ppm; ESI-MS (C$_6$H$_6$): *m/z* (%): 390.3 (100) $[M+OH]^+$, 116.1 (50) $[M-P(C_6H_{12}ON)_2]^+$; HRMS (ESI): *m/z* calcd for $C_{18}H_{37}N_3O_3P^+$: 374.2567 $[M+H^+]$; found: 374.2569.

TProPN(2 N$_2$): Yield: 26%. $[\alpha]_D^{20}$ = +2.91 (*c* = 0.78 in toluene); ^{1}H NMR (500 MHz, [D$_3$]MeCN, 25 °C, TMS): δ = 7.61 (d, 2H, ^3J(H,H) = 8.8 Hz, H(2,7)), 7.34 (t, 2H, ^3J(H,H) = 7.8 Hz, H(3,6)), 6.99 (d, 2H, ^3J(H,H) = 7.3 Hz, H(4,5)), 3.91–3.86 (m, 6H, H(9)), 3.52–3.47 (m, 6H, H(12)), 3.44 (dd, ^3J(H,H) = 9.2 Hz, ^2J(H,H) = 4.1 Hz, 6H, H(13)), 3.28 (dd, ^3J(H,H) = 9.1 Hz, ^2J(H,H) = 7.9 Hz, 6H, H(13)), 3.23 (s, 18H, H(14)), 3.18–3.12 (m, 6H, H(12)), 1.91–1.85 (m, 12H, H(10)), 1.83–1.79 ppm (m, 12H, H(11)); ^{13}C NMR (126 MHz, [D$_3$]MeCN, 25 °C, TMS): δ = 152.5 (C(1,8)), 136.8 (C(8a)), 126.3 (C(3,6)), 125.6 (C(2,7)), 124.5 (C(4a)), 115.7 (C(4,5)), 75.7 (C(13)), 58.9 (C(14)), 58.5 (d, ^2J(P,C) = 2.9 Hz, C(9)), 47.9 (C(12)), 29.3 (d, ^3J(P,C) = 5.5 Hz, C(10)), 25.1 ppm (d, ^3J(P,C) = 5.7 Hz, C(11)); ^{31}P NMR (122 MHz, [D$_3$]MeCN, 25 °C, 85% H$_3$PO$_4$): δ = 31.0 ppm; IR: $\tilde{\nu}$ = 453, 479, 518, 540, 576, 632, 659, 677, 771, 819, 894, 959, 989, 1060, 1128, 1174, 1198, 1228, 1247, 1290, 1332, 1352, 1401, 1460, 1564, 2808, 2823, 2872, 2963 cm^{-1}; ESI-MS (MeCN): *m/z* (%): 957 (35) $[M]^+$, 389 (100) $[HOP(C_6H_{12}NO)_3]^+$; HRMS (ESI): *m/z* calcd for $C_{46}H_{79}N_{12}O_6P_2^+$: 957.5715 $[M+H^+]$; found: 957.5707.

[TPipPN(2 N$_2$)-AlMe$_2$]$^+$[AlMe$_4$]$^-$: A solution of trimethylaluminum (14 mg, 0.193 mmol, 1.0 equiv) in toluene (5 mL) was added drop-wise to a solution of TPipPN(2N$_2$) (75 mg, 0.097 mmol, 1.0 equiv) in toluene (10 mL). A precipitate formed and the suspension was stirred for 1 h at room temperature. All volatiles were removed in vacuo and the residue was recrystallized from THF/hexane (1:2) and dried in vacuo. [TPipPN(2N$_2$)−AlMe$_2$]$^+$[AlMe$_4$]$^-$ (40 mg, 45%) was obtained as a deep-green solid. ^{1}H NMR (400 MHz, [D$_3$]MeCN, 25 °C, TMS): δ = 8.08 (d, ^3J(H,H) = 7.8 Hz, 2H, H(2,7)), 7.77 (d, ^3J(H,H) = 8.1 Hz, 2H, H(4,5)), 7.51 (t, ^3J(H,H) = 8.0 Hz, 2H, H(3,6)), 3.18–3.15 (m, 24H, H(9)), 1.63–1.62 (m, 12H, H(11)), 1.56–1.55 (m, 24H, H(10)), −0.72 (s, 6H, H(12)), −0.97–1.38 ppm (m, 12H, H(13)); ^{13}C NMR (101 MHz, [D$_3$]MeCN, 25 °C, TMS): δ = 142.3 (C(1,8)), 137.4 (C(4a)), 127.5 (C(4,5)), 127.4 (C(3,6)), 118.9 (C(8a)), 113.5 (C(2,7)), 46.7 (C(9)), 26.7 (d, ^3J(P,C) = 4.0 Hz, C(10)), 24.8 (C(11)), −7.9 ppm (C(12)) (the signal of C(13) is very broad and cannot be identified clearly); ^{31}P NMR (101 MHz, [D$_3$]MeCN, 25 °C, 85% H$_3$PO$_4$): δ = 32.9 ppm; ESI-MS (MeCN): *m/z* (%): 777 (100) $[M-AlMe_2]^+$, 451 (10) $[M-AlMe_2-C_{15}H_{30}N_6P]^+$, 283 (6) $[M-AlMe_2-C_{25}H_{36}N_9P]^+$; HRMS (ESI): *m/z* calcd for $C_{42}H_{72}AlN_{12}P_2^+$: 833.5288 $[M]^+$; found: 833.5301.

Acknowledgements

We thank Fabian Schröder and Lars Finger for their valuable support with crystal structure refinement. Financial support by the Fonds der Chemischen Industrie is gratefully acknowledged (Ph.D. scholarship for J.K.). B.K. gratefully acknowledges support of the Computing Center of the University of Zagreb (SRCE) for granting computational time on ISABELLA cluster.

Keywords: ab initio calculations · basicity · ligands · phosphazenes · reaction mechanisms

[1] H. Staudinger, J. Meyer, *Helv. Chim. Acta* **1919**, *2*, 635–646.

[2] a) Y. G. Gololobov, I. N. Zhmurova, L. F. Kasukhin, *Tetrahedron* **1981**, *37*, 437–472; b) Y. G. Gololobov, L. F. Kasukhin, *Tetrahedron* **1992**, *48*, 1353–1406; c) M. Köhn, R. Breinbauer, *Angew. Chem.* **2004**, *116*, 3168–3178; *Angew. Chem. Int. Ed.* **2004**, *43*, 3106–3116; d) S. Bräse, C. Gil, K. Knepper, V. Zimmermann, *Angew. Chem.* **2005**, *117*, 5320–5374; *Angew. Chem. Int. Ed.* **2005**, *44*, 5188–5240.

[3] a) C. Widauer, H. Grützmacher, I. Shevchenko, V. Gramlich, *Eur. J. Inorg. Chem.* **1999**, *10*, 1659–1664; b) M. Alajarin, C. Conesa, H. S. Rzepa, *J. Chem. Soc. Perkin Trans. 2* **1999**, *2*, 1811–1814; c) W. Q. Tian, Y. A. Wang, *J. Org. Chem.* **2004**, *69*, 4299–4308; d) W. Q. Tian, Y. A. Wang, *J. Chem. Theory Comput.* **2005**, *1*, 353–362.

[4] K. Bieger, J. Tejeda, R. Réau, F. Dahan, G. Bertrand, *J. Am. Chem. Soc.* **1994**, *116*, 8087–8094.

[5] a) M. Alajarín, P. Molina, A. López-Lázaro, C. Foces-Foces, *Angew. Chem.* **1997**, *109*, 147–150; *Angew. Chem. Int. Ed. Engl.* **1997**, *36*, 67–70; b) M. Alajarín, A. Vidal, C. López-Leonardo, J. Berná, M. C. Ramírez de Arellano, *Tetrahedron Lett.* **1998**, *39*, 7807–7810; c) M. Alajarín, A. López-Lázaro, A. Vidal, J. Berná, *Chem. Eur. J.* **1998**, *4*, 2558–2570.

[6] M. W. P. Bebbington, S. Bontemps, G. Bouhadir, D. Bourissou, *Angew. Chem.* **2007**, *119*, 3397–3400; *Angew. Chem. Int. Ed.* **2007**, *46*, 3333–3336.

[7] V. Cadierno, M. Zablocka, B. Donnadieu, A. Igau, J.-P. Majoral, A. Skowronska, *Chem. Eur. J.* **2000**, *6*, 345 – 352.
[8] a) K. Bieger, G. Bouhadir, R. Réau, F. Dahan, G. Bertrand, *J. Am. Chem. Soc.* **1996**, *118*, 1038 – 1044; b) G. C. Fortman, B. Captain, C. D. Hoff, *Organometallics* **2009**, *28*, 3587 – 3590.
[9] G. L. Hillhouse, G. V. Goeden, B. L. Haymore, *Inorg. Chem.* **1982**, *21*, 2064 – 2071.
[10] L. LePichon, D. W. Stephan, *Inorg. Chem.* **2001**, *40*, 3827 – 3829.
[11] A. A. Danopoulos, R. S. Hay-Motherwell, G. Wilkinson, S. M. Cafferkey, T. K. N. Sweet, M. B. Hursthouse, *J. Chem. Soc. Dalton Trans.* **1997**, *18*, 3177 – 3184.
[12] E. M. Broderick, P. S. Thuy-Boun, N. Guo, C. S. Vogel, J. Sutter, J. T. Miller, K. Meyer, P. L. Diaconescu, *Inorg. Chem.* **2011**, *50*, 2870 – 2877.
[13] B. Liua, D. Cui, *Dalton Trans.* **2009**, *3*, 550 – 556.
[14] F. Palacios, D. Aparicio, J. García, *Tetrahedron* **1996**, *52*, 9609 – 9628.
[15] G. C. Fortman, B. Captain, C. D. Hoff, *Inorg. Chem.* **2009**, *48*, 1808 – 1810.
[16] R. D. Kennedy, *Chem. Commun.* **2010**, *46*, 4782 – 4784.
[17] a) H. Schmidt, C. Lensink, S. K. Xi, J. G. Verkade, *Z. anorg. allg. Chem.* **1989**, *578*, 75 – 80; b) J. Tang, J. Dopke, J. G. Verkade, *J. Am. Chem. Soc.* **1993**, *115*, 5015 – 5020; c) N. Thirupathi, X. Liu, J. G. Verkade, *Inorg. Chem.* **2003**, *42*, 389 – 397; d) X. Liu, N. Thirupathi, I. A. Guzei, J. G. Verkade, *Inorg. Chem.* **2004**, *43*, 7431 – 7440.
[18] A. Sarkar, P. Ilankumaran, P. Kisanga, J. G. Verkade, *Adv. Synth. Catal.* **2004**, *346*, 1093 – 1096.
[19] C. Reddy, V. Reddy, J. G. Verkade, *J. Org. Chem.* **2007**, *72*, 3093 – 3096.
[20] A. V. Alexandrova, T. Mašek, S. M. Polyakova, I. Císařová, J. Saame, I. Leito, I. M. Lyapkalo, *Eur. J. Org. Chem.* **2013**, *9*, 1811 – 1823.
[21] M. W. P. Bebbington, D. Bourissou, *Coord. Chem. Rev.* **2009**, *253*, 1248 – 1261.
[22] a) P. S. Bowman, W. R. S. Steele, D. R. Winterman, R. W. Alder, *Chem. Commun. (London)* **1968**, *13*, 723 – 724; b) H. A. Staab, T. Saupe, *Angew. Chem.* **1988**, *100*, 895 – 909; *Angew. Chem. Int. Ed. Engl.* **1988**, *27*, 865 – 879; c) R. W. Alder, *Chem. Rev.* **1989**, *89*, 1215 – 1223; d) A. L. Llamas-Saiz, C. Foces-Foces, J. Elguero, *J. Mol. Struct.* **1994**, *328*, 297 – 323; e) Z. B. Maksić, B. Kovačević, R. Vianello, *Chem. Rev.* **2012**, *112*, 5240 – 5270; f) A. F. Pozharskii, *Russ. Chem. Rev.* **1998**, *67*, 1 – 24; g) J. Chambron, M. Meyer, *Chem. Soc. Rev.* **2009**, *38*, 1663 – 1673; h) K. Nagasawa, *Related Organocatalysts (1): A Proton Sponge in Superbases for organic synthesis: guanidines, amidines and phosphazenes and related organocatalysts* (Ed.: T. Ishikawa), John Wiley & Sons, Ltd., Chichester, UK, **2009**; pp. 251 – 271 and references cited therein.
[23] R. Schwesinger, H. Schlemper, C. Hasenfratz, J. Willaredt, T. Dambacher, T. Breuer, C. Ottaway, M. Fletschinger, J. Boele, H. Fritz, D. Putzas, H. W. Rotter, F. G. Brodwell, A. V. Satish, G. Ji, E. Peters, K. Peters, H. G. von Schnering, L. Walz, *Liebigs Ann. Chem.* **1996**, *7*, 1055 – 1081.
[24] V. Raab, E. Gauchenova, A. Merkoulov, K. Harms, J. Sundermeyer, B. Kovačević, Z. B. Maksić, *J. Am. Chem. Soc.* **2005**, *127*, 15738 – 15743.
[25] J. F. Kögel, B. Oelkers, B. Kovačević, J. Sundermeyer, *J. Am. Chem. Soc.* **2013**, *135*, 17768 – 17774.
[26] H. Naka, N. Kanase, M. Ueno, Y. Kondo, *Chem. Eur. J.* **2008**, *14*, 5267 – 5274.
[27] R. D. Kroshefsky, J. G. Verkade, *Inorg. Chem.* **1975**, *14*, 3090 – 3095.
[28] A. P. Marchenko, G. N. Koidan, A. M. Pinchuk, A. V. Kursanov, *Zh. Obshch. Khim.* **1983**, *53*, 1774 – 1782.
[29] Y. Kondo, H. Naka, T. Shimo, (Jpn. Kokai Tokkyo Koho), JP 2010030941, **2010**.
[30] a) M. L. Clarke, D. J. Cole-Hamilton, A. M. Z. Slawin, J. D. Woollins, *Chem. Commun.* **2000**, 2065 – 2066; b) M. L. Clarke, G. L. Holliday, A. M. Z. Slawin, J. D. Woollins, *J. Chem. Soc. Dalton Trans.* **2002**, *6*, 1093 – 1103.
[31] B. Kovačević, Z. B. Maksić, *Tetrahedron Lett.* **2006**, *47*, 2553 – 2555.
[32] a) J. Münchenberg, H. Thönnessen, P. G. Jones, R. Schmutzler, *Phosphorus Sulfur Silicon Relat. Elem.* **1997**, *123*, 57 – 74; b) M. Freytag, V. Plack, P. G. Jones, R. Schmutzler, *Z. Naturforsch.* **2004**, *59b*, 499 – 502.
[33] J. Münchenberg, O. Böge, A. K. Fischer, P. G. Jones, R. Schmutzler, *Phosphorus Sulfur Silicon Relat. Elem.* **1994**, *86*, 102 – 121.
[34] I. Kaljurand, A. Kütt, L. Sooväli, T. Rodima, V. Mäemets, I. Leito, I. A. Koppel, *J. Org. Chem.* **2005**, *70*, 1019 – 1028.
[35] M. Reinmuth, U. Wild, D. Rudolf, E. Kaifer, M. Enders, H. Wadepohl, H.-J. Himmel, *Eur. J. Inorg. Chem.* **2009**, *32*, 4795 – 4808.
[36] J. R. Goerlich, M. Farkens, A. Fischer, P. G. Jones, R. Schmutzler, *Z. anorg. allg. Chem.* **1994**, *620*, 707 – 715.
[37] C. G. Chidester, J. Szmuszkovicz, D. J. Duchamp, L. G. Laurian, J. P. Freeman, *Acta Crystallogr.* **1988**, *C44*, 1080 – 1083.
[38] A. N. Chernega, M. Y. Antipin, Y. T. Struchkov, M. P. Ponomarchuk, L. F. Kasukhin, V. P. Kukhar, *Zh. Obshch. Khim.* **1989**, *59*, 1256 – 1261.
[39] A. N. Chernega, M. Y. Antipin, Y. T. Struchkov, I. E. Boldeskul, M. P. Ponomarchuk, L. F. Kasukhin, V. P. Kukhar, *Zh. Obshch. Khim.* **1984**, *54*, 1979 – 1985.
[40] C. R. V. Reddy, B. M. Fetterly, J. G. Verkade, *Energy Fuels* **2007**, *21*, 2466 – 2472.
[41] B. Kovačević, D. Baric, Z. B. Maksić, *New J. Chem.* **2004**, *28*, 284 – 288.
[42] An analogous intramolecular process could be taken into consideration to explain the decay of the bisphosphazides at high temperatures leading to various unidentified products. A possible mechanism is presented in the Supporting Information (Scheme S3.3). However, this mechanism has not been examined computationally.
[43] R. W. Hoffmann, G. Guhn, M. Preiss, *J. Chem. Soc. C* **1969**, *5*, 769 – 772.
[44] D. J. Dellinger, D. M. Sheehan, N. K. Christensen, J. G. Lindberg, M. H. Caruthers, *J. Am. Chem. Soc.* **2003**, *125*, 940 – 950.
[45] L. A. Hussain, A. J. Elias, M. N. S. Rao, *Tetrahedron Lett.* **1988**, *29*, 5983 – 5986.
[46] a) T. Widianti, Y. Hiraga, S. Kojima, M. Abe, *Tetrahedron: Asymmetry* **2010**, *21*, 1861 – 1868; b) D. Seebach, H.-O. Kalinowski, B. Bastani, G. Crass, H. Daum, H. Dörr, N. P. DuPreez, V. Ehrig, W. Langer, C. Nüssler, H.-A. Oei, M. Schmidt, *Helv. Chim. Acta* **1977**, *60*, 301 – 325.
[47] Elemental analyses show values for carbon and nitrogen that are too low in most cases, although NMR-spectroscopically pure samples or single crystals were measured. We refer the deviations from the calculated values to the hygroscopic properties and moisture sensitivity of the compounds as well as the presence of silicon grease in some samples. Hence, ^{1}H, ^{13}C, and ^{31}P NMR spectra are shown in the Supporting Information.

Received: November 17, 2013
Published online on March 28, 2014

ChemComm

COMMUNICATION

View Article Online
View Journal | View Issue

Cite this: *Chem. Commun.*, 2014, 50, 4319

Received 28th January 2014,
Accepted 26th February 2014

DOI: 10.1039/c4cc00773e

www.rsc.org/chemcomm

Two C_2-symmetric chelating P_2-bisphosphazene superbases connected *via* a binaphthyl backbone – synthesis, structural features and preparation of a cationic alkyl aluminum complex†

Julius F. Kögel, Nis-Julian Kneusels and Jörg Sundermeyer*

Two P_2-phosphazenyl groups were linked *via* a C_2-symmetric binaphthyl backbone resulting in two novel chiral superbases with dimethylamino and pyrrolidino substituents. We investigated their basic properties and coordination chemistry towards a cationic alkyl aluminum fragment. The outstanding basicity of the chiral tetrasphosphazenes presented herein leads to interesting perspectives for application in asymmetric Brønsted base catalysis.

Chiral amines play a very important role in asymmetric catalysis – especially with regard to extensive scientific activities in the field of organocatalysis during the past decade.[1] However, due to their low basicity the role of chiral amines in enantioselective reactions in which they act as Brønsted-bases is strongly limited to comparably acidic substrates. Thus, chiral representatives of all classes of organic superbases such as amidines,[2] guanidines,[3] azaphosphatranes,[4] proton sponges[5] or phosphazenes[6] have been prepared and investigated with respect to their applicability to asymmetric synthesis.[7] This renaissance of well-established concepts of superbasicity becomes manifest in a cluster on superbases published in *Synlett* quite recently.[8] So far, the class of chiral guanidines is the most advanced with respect to its structural variety and utilization in enantioselective reactions. The area has already been the subject of review articles by Ishikawa and Tan.[9] Chiral guanidines were applied to asymmetric Michael addition, silylation, nucleophilic epoxidation and TMS cyanation reactions.[3a,b] Taking into consideration that the pK_{BH}^+ values of organic superbases range from 25 to about 45 on the acetonitrile scale, it must be stated that chiral guanidines presented to date only populate the very low end of the basicity scale (pentamethylguanidine: pK_{BH}^+ (MeCN) = 25.00[10]). Extension of the synthetic scope of chiral superbases requires the design of compounds with higher pK_{BH}^+ values by making use of the high intrinsic basicity of phosphazenes with multiple PN units or the combination of several superbasic features in one molecule. In this context Terada *et al.* recently published helically chiral spirocyclic P_3 phosphazenes and a series of highly basic chiral guanidinophosphazenes that were used in enantioselective amination reactions of ketones.[11] Raab[12] and Himmel *et al.*[13] linked two guanidinyl moieties *via* a C_2-symmetric binaphthyl backbone allowing the formation of an energetically favorable [N–H···N] hydrogen bond after protonation. Since we have thoroughly studied the basicity-enhancing effect of proton chelation,[14] we were interested to combine this proton pincer ligand concept with a chiral binaphthyl skeleton to achieve a unique interaction of two amino-substituted Schwesinger-P_2 bases in a chiral environment. A related bis(monophosphazene) with two PPh_3 units was prepared by Reetz *et al.* in 1998, but the electron-withdrawing triphenylphosphonio substituents were not able to grant a high basicity or even superbasicity with a pK_{BH}^+ value (MeCN) > 25.00.[15]

We chose a Kirsanov condensation to achieve the linkage between two P_2 fragments and the aromatic diamine. The required bromophosphonium bromide precursors **1** and **2** were prepared by the bromination of the literature known P(III) compounds that were accessible *via* three-step procedures from tris(dimethylamino) phosphane and tris(pyrrolidino)phosphane.[14b,17,18] The reaction of (*S*)-(–)-1,1′-binaphthyl-2,2′-diamine with the bromophosphonium bromides in the presence of the auxiliary base triethylamine and subsequent deprotonation with metal bis(trimethylsilyl)amides gave the two chiral tetraphosphazenes **3** and **4**. They were characterized *via* ^1H, ^{13}C and ^{31}P spectroscopy, ESI mass spectrometry, elemental analysis and in the case of the dimethylamino-substituted species also X-ray crystallographic analysis (Fig. 1). The two independent molecules found in the asymmetric unit reveal a large distance of 3.98(1) and 4.10(1) Å between the two basicity centers. Unlike in proton sponges, their N-centered lone pairs avoid each other by suitable torsion of the two naphthalene moieties around the axial carbon–carbon bond. Hence, no steric strain in the

Philipps-Universität Marburg, Fachbereich Chemie, Hans-Meerwein-Straße, 35032 Marburg, Germany. E-mail: jsu@staff.uni-marburg.de; Fax: +49 (0)642128-25711

† Electronic supplementary information (ESI) available: Detailed synthetic procedures and analytical data. CCDC 977138–9771340. For ESI and crystallographic data in CIF or other electronic format see DOI: 10.1039/c4cc00773e

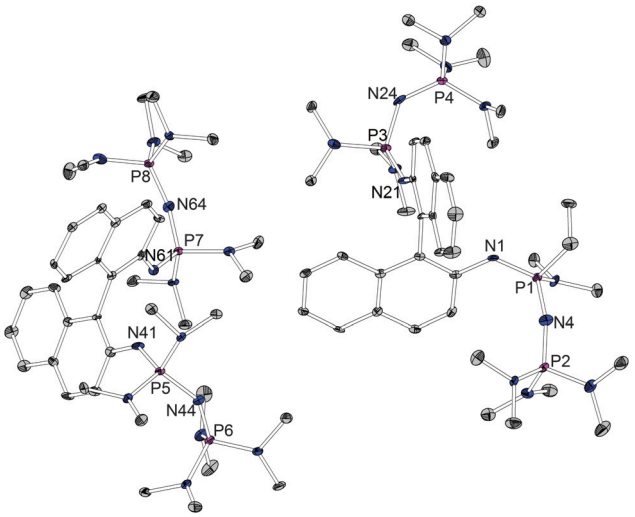

Fig. 1 Molecular structure of **3** (ellipsoids with 30% probability). Hydrogen atoms are omitted for clarity. Selected bond lengths/Å and angles/°: *d*(N1···N21) 3.98(1), *d*(N1–P1) 1.567(6), *d*(P1–N4) 1.593(7), *d*(N4–P2) 1.536(7), *d*(N21–P3) 1.561(6), *d*(P3–N24) 1.627(7), *d*(N24–P4) 1.545(7), *d*(N41···N61) 4.10(1), *d*(N41–P5) 1.557(6), *d*(P5–N44) 1.609(6), *d*(N44–P6) 1.549(6), *d*(N61–P7) 1.542(7), *d*(P7–N64) 1.596(6), *d*(N64–P8) 1.539(7).[16]

aromatic backbones or repulsion of the lone pairs of the nitrogen atoms destabilizing the free base form of tetraphosphazene is observed.

Protonation of the two tetraphosphazenes was studied with *p*-toluenesulfonic acid. It is accompanied by a low-field shift of the signals in the ^{31}P NMR spectrum and an increase in the ^{2}J(P,P) coupling constants. In the case of the pyrrolidino-substituted species, the acidic proton exhibits a triplet with a ^{2}J(P,H) coupling constant of 7.4 Hz indicating interaction with two phosphorous atoms and thus the formation of an intramolecular [N–H···N] hydrogen bond.

The pK_{BH^+} values were determined *via* NMR titration experiments *versus* bisphosphazene proton sponges.[20] As expected, **4** exhibits a higher pK_{BH^+} value of 30.8 on the acetonitrile scale than its dimethylamino-substituted counterpart **3** which shows a pK_{BH^+} value of 29.3. These results also suggest the energetically favorable chelation of the acidic proton since the basicity of **4** exceeds the pK_{BH^+} value of the non-chelating naphthalene-substituted P_2 Schwesinger base (pyr)P_2-1-Naph (pK_{BH^+} (MeCN) (calc.) = 26.0)[14b] by nearly five orders of magnitude. For Terada's chiral guanidinophosphazenes pK_{BH^+} values (THF) close to 26.8 were estimated.[11]

The coordination behavior of proton sponges[21] or other chelating superbases towards electrophiles other than protons has attracted considerable scientific interest.[13,22] However, whereas metal complexes of macrocyclic phosphazenes have been reported,[23] the coordination chemistry of classical open chain Schwesinger superbases is widely unexplored.[24] We were interested to demonstrate the use of the title compounds not only as a base but also as a chiral donor ligand towards Lewis acids of catalytic interest. The reaction of **4** with two equivalents of trimethylaluminum resulted in the asymmetric dissociation and formation of [**4**-AlMe$_2$]$^+$[AlMe$_4$]$^-$ (Scheme 1) which could be investigated concerning its structural features (Fig. 2). An angle of 69.3(9)° is observed between the two naphthalene planes. The cationic fragment [AlMe$_2$]$^+$ is chelated by the two basic nitrogen atoms showing an N–Al–N angle of 98.3(2)° and a non-bonding N···N distance of 2.931(6) Å.

In the state of the art the concept of Schwesinger polyphosphazene superbases has not been extended to chelating chiral representatives, favorably with a rigid backbone. Furthermore,

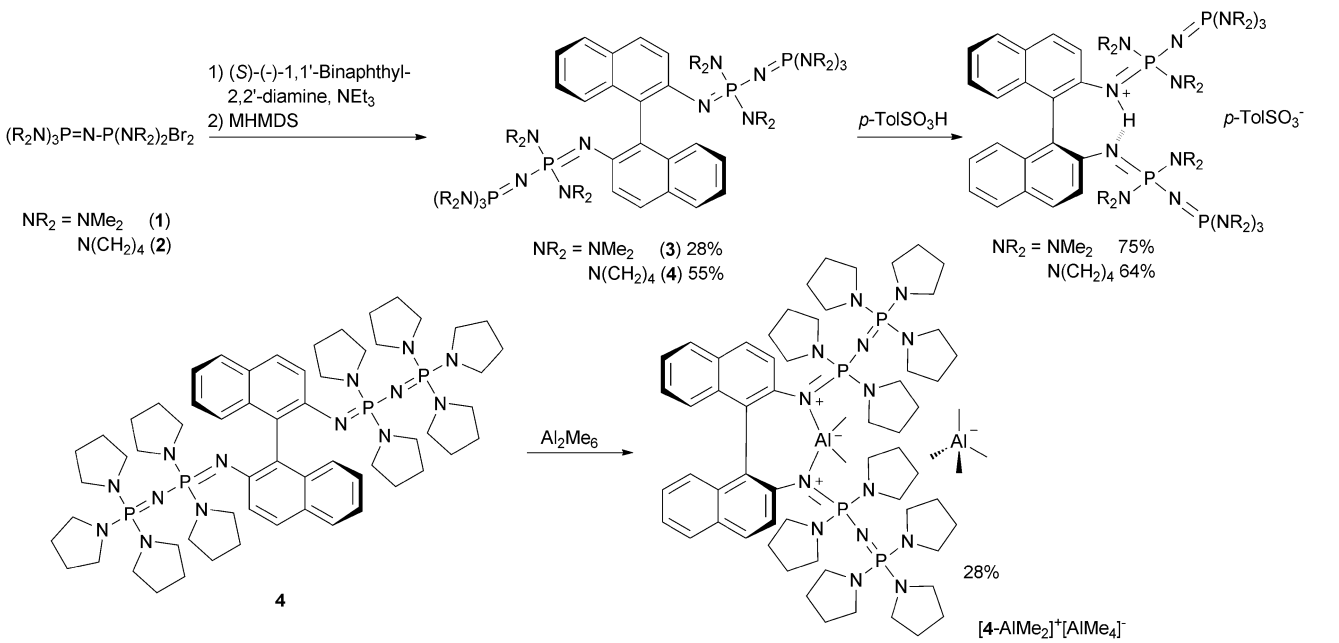

Scheme 1 Preparation of the chiral tetraphosphazenes **3** and **4** *via* a Kirsanov reaction, protonation with *para*-toluenesulfonic acid and reaction of **4** with trimethylaluminum.

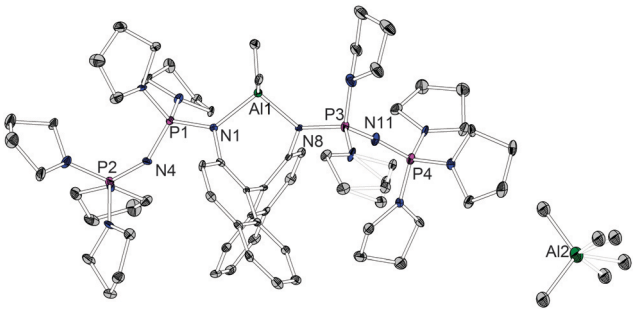

Fig. 2 Molecular structure of [**4**-$AlMe_2$]$^+$[$AlMe_4$]$^-$ (ellipsoids with 30% probability). The disorder in the [$AlMe_4$]$^-$ anion is not displayed. Hydrogen atoms are omitted for clarity. Selected bond lengths/Å and angles/°: *d*(N1–Al1) 1.938(5), *d*(N1–P1) 1.633(5), *d*(P1–N4) 1.582(5), *d*(N4–P2) 1.558(4), *d*(N8–Al1) 1.938(5), *d*(N8–P3), *d*(P3–N11) 1.576(5), *d*(N11–P4) 1.548(5), N1–Al1–N8 98.3(2).[19]

Schwesinger polyphosphazene bases have not been used as superstrong chelating neutral donor ligands in coordination chemistry and catalysis. In this respect the chiral tetraphosphazenes communicated herein add valuable perspectives to the highly topical field of chiral superbases with expected applications as enantioselective organocatalysts with an extraordinarily high Brønsted-basicity and as chiral superdonor ligands for cationic metal complexes of catalytic interest.

We thank Fabian Schröder and Lars Finger for their valuable support with crystal structure refinement. Financial support by the Fonds der Chemischen Industrie (doctoral scholarship for J.K.) is gratefully acknowledged.

Notes and references

1 (*a*) F. Fache, E. Schulz, M. L. Tommasino and M. Lemaire, *Chem. Rev.*, 2000, **100**, 2159; (*b*) S. France, D. J. Guerin, S. J. Miller and T. Lectka, *Chem. Rev.*, 2003, **103**, 2985; (*c*) J. Seayad and B. List, *Org. Biomol. Chem.*, 2005, **3**, 719; (*d*) H. Pellissier, *Tetrahedron*, 2007, **63**, 9267; (*e*) L.-W. Xu, J. Luo and Y. Lu, *Chem. Commun.*, 2009, 1807; (*f*) T. Kano and K. Maruoka, *Bull. Chem. Soc. Jpn.*, 2010, **83**, 1421.
2 (*a*) J. Clews, A. D. M. Curtis and H. Malkin, *Tetrahedron*, 2000, **56**, 8735; (*b*) C. Dauwe and J. Buddrus, *Synthesis*, 1995, 171.
3 (*a*) T. Isobe, K. Fukuda, Y. Araki and T. Ishikawa, *Chem. Commun.*, 2001, 243; (*b*) T. Ishikawa and T. Isobe, *Chem.–Eur. J.*, 2002, **8**, 552; (*c*) A. Castiglia, H. El Sehrawi, T. Orbegozo, D. Spitzner, B. Claasen, W. Frey, W. Kantlehner and V. Jäger, *Z. Naturforsch., B: J. Chem. Sci.*, 2012, **67**, 337.
4 (*a*) X. Liu, P. Ilankumaran, I. A. Guzei and J. G. Verkade, *J. Org. Chem.*, 2000, **65**, 701; (*b*) J. S. You, A. E. Wroblewski and J. G. Verkade, *Tetrahedron*, 2004, **60**, 7877; (*c*) K. Ishihara, Y. Karumi, S. Kondo and H. Yamamoto, *J. Org. Chem.*, 1998, **63**, 5692.
5 (*a*) R. W. Alder, *J. Am. Chem. Soc.*, 2005, **127**, 7924; (*b*) A. Singh, S. Chakraborty and B. Ganguly, *Eur. J. Org. Chem.*, 2006, 4938; (*c*) J.-P. Mazaleyrat and K. Wright, *Tetrahedron Lett.*, 2008, **49**, 4537; (*d*) G. Brancatelli, D. Drommi, G. Femino, M. Saporita, G. Bottari and F. Faraone, *New J. Chem.*, 2010, **34**, 2853.
6 (*a*) J. M. Brunel, O. Legrand, S. Reymond and G. Buono, *J. Am. Chem. Soc.*, 1999, **121**, 5807; (*b*) M. Alajarín, C. López-Leonardo and J. Berná, *Tetrahedron*, 2006, **62**, 6190; (*c*) U. Köhn, M. Schulz, A. Schramm, W. Günther, H. Görls, S. Schenk and E. Anders, *Eur. J. Org. Chem.*, 2006, 4128.
7 T. Ishikawa, in *Superbases for Organic Synthesis: Guanidines, Amidines and Phosphazenes and Related Organocatalysts*, ed. T. Ishikawa, John Wiley & Sons Ltd., Chichester, UK, 2009.
8 T. Ishikawa and L. M. Harwood, *Synlett*, 2013, 2507.
9 (*a*) T. Ishikawa and T. Kumamoto, *Synthesis*, 2006, 737–752; (*b*) D. Leow and C.-H. Tan, *Synlett*, 2010, 1589.
10 (*a*) R. Schwesinger, J. Willaredt, H. Schlemper, M. Keller, D. Schmitt and H. Fritz, *Chem. Ber.*, 1994, **127**, 2435. The preparation of non-chiral guanidines with considerably higher pK_{BH}^+ values was achieved recently: (*b*) R. A. Kunetskiy, S. M. Polyakova, J. Vavřík, I. Císařová, J. Saame, E. R. Nerut, I. Koppel, I. A. Koppel, A. Kütt, I. Leito and I. M. Lyapkalo, *Chem.–Eur. J.*, 2012, **18**, 3621–3630; (*c*) K. Vazdar, R. Kunetskiy, J. Saame, K. Kaupmees, I. Leito and U. Jahn, *Angew. Chem.*, 2014, **126**, 1459–1462 (*Angew. Chem., Int. Ed.*, 2014, **53**, 1435–1438). Those examples could serve as blueprints for powerful chiral superbases.
11 (*a*) M. Terada, K. Goto, M. Oishi, T. Takeda, E. Kwon and A. Kondoh, *Synlett*, 2013, 2531; (*b*) T. Takeda and M. Terada, *J. Am. Chem. Soc.*, 2013, **135**, 15306.
12 V. Raab, Peralkyl Guanidines in Copper Catalysed Oxidative Transformations and Novel Proton Sponges, Dissertation Marburg 2001, Klaus Bielefeld Verlag 2002, ISBN 3-89833-053-2.
13 A. Maronna, E. Bindewald, E. Kaifer, H. Wadepohl and H.-J. Himmel, *Eur. J. Inorg. Chem.*, 2011, 1302.
14 (*a*) V. Raab, E. Gauchenova, A. Merkoulov, K. Harms, J. Sundermeyer, B. Kovačević and Z. B. Maksić, *J. Am. Chem. Soc.*, 2005, **127**, 15738; (*b*) J. F. Kögel, B. Oelkers, B. Kovaĉević and J. Sundermeyer, *J. Am. Chem. Soc.*, 2013, **135**, 17768.
15 M. T. Reetz, E. Bohres and R. Goddard, *Chem. Commun.*, 1998, 935.
16 **3** crystallizes in the triclinic space group *P*1 with the unit cell constants a = 10.5097(10) Å, b = 13.3588(14) Å, c = 16.9068(17) Å, α = 87.901(4)°, β = 89.867(4)° and γ = 82.976(4)°. Detailed crystal data and experimental conditions are given in the ESI†.
17 A. P. Marchenko, G. N. Koidan, A. M. Pinchuk and A. V. Kirsanov, *Zh. Obshch. Khim.*, 1983, **54**, 1774.
18 A molecular structure of **1** is presented in the ESI† (Fig. S1).
19 [**4**-$AlMe_2$]$^+$[$AlMe_4$]$^-$ crystallizes in the monoclinic space group *P*1211 with the unit cell constants a = 10.751(3) Å, b = 33.100(7) Å, c = 10.900(3) Å, $\alpha = \gamma$ = 90° and β = 116.309(13)°.
20 NMR titration experiments were performed in THF due to the low solubility of the free base forms in acetonitrile. **4** competed with HMPN and TPPN for protons while an unpublished *iso*-propyl-substituted bisphosphazene proton sponge with a pK_{BH}^+ value of 30.4 in acetonitrile was used in the case of **3**. A linear correlation between the THF and the acetonitrile scale can be assumed by approximation. The procedure is described in ref. 14*a*.
21 (*a*) H.-U. Wüstefeld, W. C. Kaska, F. Schüth, G. D. Stuckly, X. Bu and B. Krebs, *Angew. Chem.*, 2001, **113**, 3280 (*Angew. Chem., Int. Ed.*, 2001, **40**, 3182); (*b*) H.-U. Wuestefeld, W. C. Kaska, G. D. Stucky, F. Schueth and B. Krebs, *PCT Int. Appl.*, WO 2002059134 A1 20020801, 2002.
22 (*a*) T. Yamasaki, N. Ozaki, Y. Saika, K. Ohta, K. Goboh, F. Nakamura, M. Hashimoto and S. Okeye, *Chem. Lett.*, 2004, **33**, 928; (*b*) P. Roquette, A. Maronna, A. Peters, E. Kaifer, H.-J. Himmel, C. Hauf, V. Herz, E.-W. Scheidt and W. Scherer, *Chem.–Eur. J.*, 2010, **16**, 1336; (*c*) A. Maronna, E. Bindewald, E. Kaifer, H. Wadepohl and H.-J. Himmel, *Eur. J. Inorg. Chem.*, 2011, 1302.
23 (*a*) W. C. Marsh, N. L. Paddock, C. J. Stewart and J. Trotter, *Chem. Commun.*, 1970, 1190; (*b*) J. P. O'Brien, R. W. Allen and H. R. Allcock, *Inorg. Chem.*, 1979, **18**, 2230.
24 M. Sauthier, J. Forniés-Cámer, L. Toupet and R. Réau, *Organometallics*, 2000, **19**, 553.

Inorganic Chemistry

Article

pubs.acs.org/IC

The New NH-Acid $HN(C_6F_5)(C(CF_3)_3)$ and Its Crystalline and Volatile Alkaline and Earth Alkaline Metal Salts

Julius F. Kögel, Lars H. Finger, Nicolas Frank, and Jörg Sundermeyer*

Fachbereich Chemie, Philipps-Universität Marburg, Hans-Meerwein-Straße, 35043 Marburg, Germany

Supporting Information

ABSTRACT: Herein we report on the new NH-acid *N*-(2,3,4,5,6-pentafluorophenyl)-*N*-nonafluoro-*tert*-butylamine, $HN(C_6F_5)(C(CF_3)_3)$, bearing two different sterically demanding and strongly electron-withdrawing perfluorinated amine substituents. The title compound and seven of its alkaline and alkaline earth metal salts were synthesized and investigated concerning their thermal, spectroscopic, and structural properties. The Li, Na, K, Cs, and Mg salts were investigated by single-crystal XRD analysis. The molecular structures reveal interesting motifs such as manifold fluorine metal secondary interactions. The lithium and magnesium compounds exhibit a remarkable thermal stability and an unexpectedly high volatility. We believe that this report will provoke investigations to apply the corresponding anion in ionic liquids, in lithium electrolytes, and as a weakly electron-donating ligand in the preparation of highly Lewis-acidic main group, rare earth, or transition metal complexes.

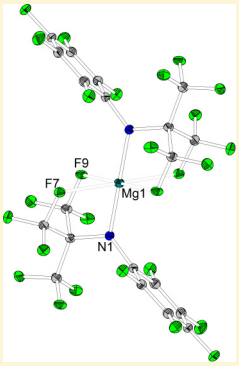

INTRODUCTION

Highly Brønsted acidic amines or imides HNRR′ with two electron-withdrawing perfluorinated alkyl, aryl, or acid functionalities, so-called NH-acids, have attracted considerable scientific interest during the last decades. In particular, the most prominent representative bis(trifluoromethylsulfonyl) imide, $HN(SO_2CF_3)_2$,[1] has found widespread use: Its corresponding anion has been used as a component of ionic liquids[2] or electrochemical devices[3] due to its weakly coordinating nature. Exhibiting a higher acidity in the gas phase than hydrogen iodide, $HN(SO_2CF_3)_2$ has been the subject of manifold experimental and theoretical investigations on its acidic behavior.[4] The extraordinary acidity allows the use of bis(trifluoromethylsulfonyl)imide as a Brønsted acid catalyst in imine amidation reactions,[5] hetero-Michael additions,[6] and enantioselective Diels−Alder[7] or cyclization reactions of siloxyalkynes with arenes and alkenes.[8] Furthermore, various metal complexes of $HN(SO_2CF_3)_2$ have been applied to reactions catalyzed by Lewis acids, which was recently reviewed by Antoniotti et al.[9] The weakly donating property of the corresponding anion was used to design copper and silver complexes $[M(L)N(SO_2CF_3)_2]$ with high binding affinity toward arenes and olefins L.[10]

Although being less acidic than $HN(SO_2CF_3)_2$ by several orders of magnitude, bis(pentafluorophenyl)amine first reported by Brooke et al. has also been a subject of research.[11] Metal amido complexes of $HN(C_6F_5)_2$ show interesting metal fluorine interactions in many cases since this ligand offers only aromatic fluorine atoms as possible donors besides the nitrogen atom. For example, this has been observed for the lithium salts $LiN(C_6F_5)_2{\cdot}Et_2O$ and $LiN(C_6F_5)_2{\cdot}THF$[12] and the neodymium complex (η^6-toluene)$Nd[N(C_6F_5)_2]_3$.[13] Recently Yin et al. reported the preparation of the homoleptic cerium and lanthanum complexes stabilized by M···F interactions.[14] $[N(C_6F_5)_2]^-$ is also found as a ligand for the transition metals titanium, zirconium, vanadium, iron, cobalt,[15] and tungsten.[16]

The two unsymmetrical hybrids of bis(perfluoroalkylsulfonyl)imide and bis(pentafluorophenyl)amine, $HN(C_6F_5)(SO_2CF_3)$ and $HN(C_6F_5)(SO_2C_4F_9)$, have also been applied to the preparation of imidazolium- and phosphonium-based ionic liquids in the same way as their parent compound $HN(C_6F_5)_2$.[17] Furthermore, their corresponding lithium salts were studied as electrolytes in lithium ion batteries.[18]

Perfluorinated alcohols, in particular those with a sterically demanding nonafluor-*tert*-butyl group, have been used by Krossing et al. to prepare the Lewis superacidic aluminum complex $Al(OC(CF_3)_3)_3$.[19] Corresponding perfluorinated secondary amines and their complexes containing the electron-withdrawing $C(CF_3)_3$ group have not been thoroughly investigated so far. Therefore we set out to synthesize one example of such an acidic amine, in particular the title compound $HN(C_6F_5)(C(CF_3)_3)$ and its basic group 1 and 2 amido metal coordination compounds. It is expected that the two different sterically demanding N-substituents are competing in their specific secondary C−F···M interactions next to the primary N−M interaction. Other points of interest of such metal perfluoramides are their thermal stability, their solubility in organic solvents, and their ability to form crystalline perfluoramido metal Lewis acids.

SYNTHESES

The synthesis of *N*-(2,3,4,5,6-pentafluorophenyl)-*N*-nonafluoro-*tert*-butylamine, $HN(C_6F_5)(C(CF_3)_3)$, starts with the

Received: January 22, 2014
Published: March 17, 2014

   dx.doi.org/10.1021/ic5001717 | *Inorg. Chem.* 2014, 53, 3839−3846

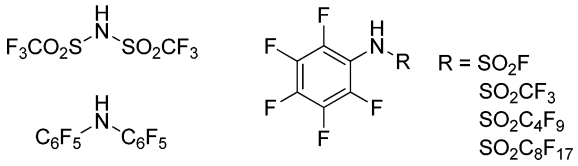

Figure 1. Examples of symmetric and unsymmetric NH-acids.

reaction of pentafluoroaniline with hexafluoroacetone followed by the addition of phosphoryl chloride, giving *N*-pentafluorophenyl-2-iminohexafluoropropane with a yield of up to 87%.[20] The transfer of a trifluoromethyl group to the imine carbon atom is achieved by trifluoromethyltrimethylsilane, the so-called Ruppert's reagent,[21] in the presence of 1.2 equivalents of cesium fluoride in THF following a protocol by Petrov used for other derivatives.[22] In our case, the cesium salt was isolated and extensively dried to remove traces of THF. Protonation with 10% aqueous hydrochloric acid yielded pure $HN(C_6F_5)(C(CF_3)_3)$ as a colorless oil (Scheme 1).

The lithium, sodium, and potassium salts were obtained by deprotonation of $HN(C_6F_5)(C(CF_3)_3)$ with the corresponding bis(trimethylsilyl)amides in hexane or toluene. $Ca[N(C_6F_5)(C(CF_3)_3)]_2$ and $Ba[N(C_6F_5)(C(CF_3)_3)]_2$ were prepared in an analogous manner, whereas the corresponding magnesium salt was obtained from the reaction of the NH-acid with di-*n*-butylmagnesium.

SPECTROSCOPIC AND ACIDIC PROPERTIES

All compounds described herein were analyzed by ^1H, ^{13}C, and ^{19}F NMR spectroscopy, IR spectroscopy, and elemental analysis. The proton NMR spectrum of $HN(C_6F_5)(C(CF_3)_3)$ shows a singlet, whereas its chemical shift is strongly solvent dependent, as it has already been observed for related NH-acids. The ^{13}C NMR signals of carbon atoms carrying fluorine atoms show large $^1J_{FC}$ coupling constants between 251.3 and 292.2 Hz. For most compounds studied herein, only the $^1J_{FC}$ coupling constant can be determined, whereas $^2J_{FC}$ and $^3J_{FC}$ coupling constants remain unresolved. A triplet with a chemical shift of −69.6 ppm in benzene-d_6 and a coupling constant of 7.1 Hz is observed for the CF_3 groups in the ^{19}F NMR spectrum of $HN(C_6F_5)(C(CF_3)_3)$, which can be referred to a coupling through space with the aromatic *ortho*-fluorine atoms. The IR spectrum shows an absorption band for the NH stretch vibration at 3406 cm^{-1} ($HN(C_6F_5)_2$: 3423 cm^{-1},[11b] $HN(C(CF_3)_3)_2$: 3454 cm^{-1}).[22] Furthermore, the molecular ion peak of $[N(C_6F_5)(C(CF_3)_3)]^-$ was detected in the (−)-ESI mass spectrum.

All of the reported complexes are slightly soluble in toluene, the solvent that was mainly used for the metalation of the perfluorinated amine title compound. This underlines a certain molecular nature of the complexes. Their latent ionic character is manifested in strongly donating solvents such as DMSO-d_6: Independently of the cation, the ^{13}C and ^{19}F NMR spectra exhibit nearly identical chemical shifts and the ^{13}C NMR signals

Scheme 2. Preparation of Alkaline and Earth Alkaline Metal Salts of $HN(C_6F_5)(C(CF_3)_3)$

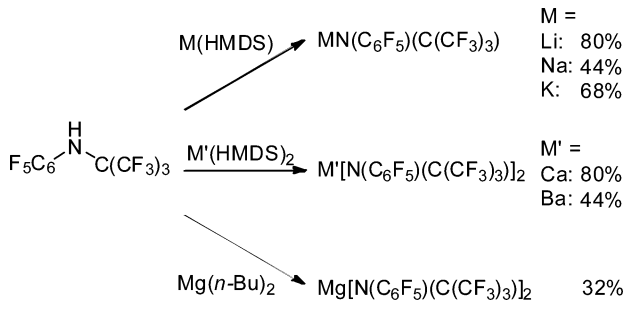

show almost equal $^1J_{CF}$ coupling constants, suggesting that a complete dissociation into solvated cations $[M(dmso)_x]^{+/2+}$ and anions $[N(C_6F_5)(C(CF_3)_3)(dmso)_y]^-$ is occurring. The ^{19}F NMR signals for the anion solvated in DMSO-d_6 show a considerable high-field shift compared to the solvated NH-acid that is especially distinct for the *para*-fluorine atoms (e.g., −185.0 ppm in the case of $Li(dmso)_xN(C_6F_5)(C(CF_3)_3)$ compared to −153.0 ppm for the NH-acid).

A qualitative competition experiment versus bis(pentafluorophenyl)amine (gas phase acidity: 316.5 kcal/mol)[4a] in DMSO solution was performed to estimate the acidity of $HN(C_6F_5)(C(CF_3)_3)$ and the electron-withdrawing character of the perfluorinated *tert*-butyl group.

The observation that $HN(C_6F_5)_2$ fully protonates $LiN(C_6F_5)(C(CF_3)_3)$ (1:1 molar ratio) suggests that the symmetric NH-acid is more acidic in DMSO than $HN(C_6F_5)(C(CF_3)_3)$ by at least 1 order of magnitude.[23] Furthermore, we could show that the strong acid $HN(SO_2CF_3)_2$ (gas phase acidity: 286.5 kcal/mol)[4b] is not able to protonate the amine $HN(C_6F_5)(C(CF_3)_3)$ in DMSO to form an ammonium salt.

STRUCTURAL FEATURES

The molecular structures of the lithium, sodium, and potassium salts (Figures 2−5) display dinuclear molecular complexes: Two metal atoms are bridged by the nitrogen atoms of two $[N(C_6F_5)(C(CF_3)_3)]^-$ moieties (d(Li−N) 2.08(1) and 2.10(1) Å; d(Na−N) 2.477(2) and 2.442(2) Å; d(K−N) 2.822(1) and 2.904(1) Å). As expected, the nonbonding N···N distances within the dimers increase when advancing from the small lithium ion (3.234(8) Å) to the larger sodium (3.481(2) Å) and potassium (3.744(1) Å) ions. Furthermore, the small size of the lithium atom results in a small Li−N−Li angle of 78.7(5)° and a large N−Li−N angle of 101.3(5)°, whereas the corresponding values invert with increasing size of the metal ion (Na−N−Na 89.58(5)°; N−Na−N 90.42(5)°; K−N−K 98.36(3)°; N−K−N 81.64(3)°). In addition to the coordination of the metal atoms by nitrogen donors, the formation of several metal fluorine contacts is observed (illustrated as dashed lines in Figures 2−8). The lithium salt shows three particularly short Li···F distances between 2.02(1) and 2.12(1) Å and three additional

Scheme 1. Preparation of $HN(C_6F_5)(C(CF_3)_3)$ Starting from Pentafluorononaniline

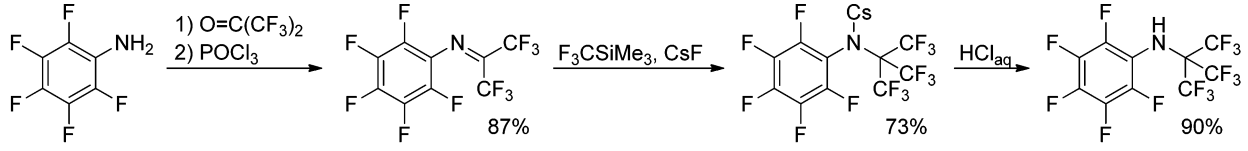

dx.doi.org/10.1021/ic5001717 | Inorg. Chem. 2014, 53, 3839−3846

Table 1. Crystal Data and Experimental Conditions

	$LiN(C_6F_5)(C_4F_9)$	$NaN(C_6F_5)(C_4F_9)$	$KN(C_6F_5)(C_4F_9)$	$CsN(C_6F_5)(C_4F_9)$	$Mg[N(C_6F_5)(C_4F_9)]_2$
empirical formula	$C_{10}F_{14}LiN$	$C_{10}F_{14}NaN$	$C_{10}F_{14}KN$	$C_{10}F_{14}CsN$, C_7H_8	$C_{20}F_{28}MgN_2$
mol weight [g mol^{-1}]	407.05	423.10	439.21	625.15	824.53
cryst habit	colorless block	colorless needle	colorless plate	colorless plate	colorless block
cryst size [mm^3]	0.11 × 0.10 × 0.10	0.35 × 0.11 × 0.10	0.25 × 0.23 × 0.07	0.32 × 0.10 × 0.07	0.26 × 0.22 × 0.16
cryst system	orthorhombic	triclinic	monoclinic	monoclinic	triclinic
space group	*Pccn*	$P\bar{1}$	*C*2/*c*	*P*121/*m*1	$P\bar{1}$
a [Å]	18.685(3)	6.9421(5)	15.9930(5)	10.0049(9)	6.785(5)
b [Å]	10.6119(12)	9.8740(6)	13.9077(6)	20.860(2)	10.022(5)
c [Å]	12.2994(16)	10.4269(6)	11.7967(4)	10.3310(10)	10.497(4)
α [deg]	90	64.0980(17)	90	90	61.91(3)
β [deg]	90	75.0294(19)	95.485(3)	112.852(3)	85.492(11)
γ [deg]	90	74.6100(20)	90	90	74.112(5)
volume [Å^3]	2438.8(6)	611.46(7)	2611.88(16)	1986.8(3)	604.6(6)
Z	8	2	8	4	1
density [g cm^{-3}]	2.217	2.298	2.234	2.090	2.265
T [K]	100(2)	100(2)	100(2)	100(2)	100(2)
absorp coeff [mm^{-1}]	0.281	0.318	0.584	1.997	0.310
θ range [deg]	2.2 to 25.0	2.2 to 26.2	1.9 to 26.8	2.2 to 27.2	2.2 to 26.0
index ranges	$-22 \le h \le 19, -12 \le k \le 11, -14 \le l \le 12$	$-8 \le h \le 8, -12 \le k \le 12, -12 \le l \le 11$	$-20 \le h \le 20, -17 \le k \le 17, -14 \le l \le 14$	$-12 \le h \le 12, -26 \le k \le 26, -13 \le l \le 13$	$-8 \le h \le 8, -12 \le k \le 12, -12 \le l \le 12$
reflns collected	6827	12 094	17 992	31 732	5614
indep reflns	2162 [*R*(int) = 0.1524]	2457 [*R*(int) = 0.0596]	2775 [*R*(int) = 0.0409]	4535 [*R*(int) = 0.0406]	2368 [*R*(int) = 0.0849]
absorp corr	multiscan	multiscan	multiscan	multiscan	multiscan
max. and min. transmn	0.9719 and 0.9673	0.969 and 0.959	0.9645 and 0.8222	0.7455 and 0.6153	1.2918 and 0.6145
data/restraints/params	2162/2/205	2457/0/235	2775/0/235	4535/6/314	2368/0/232
goodness-of-fit on F^2	0.488	1.059	1.029	1.203	0.981
final *R* indices [$I > 2\sigma(I)$]	R1 = 0.0417	R1 = 0.0350	R1 = 0.0214	R1 = 0.0235	R1 = 0.0460
R indices (all data)	wR2 = 0.0727	wR2 = 0.0956	wR2 = 0.0537	wR2 = 0.0704	wR2 = 0.1217
larg diff peak/hole [e Å^{-3}]	0.34/−0.29	0.54/−0.35	0.36/−0.26	0.72/−0.47	0.57/−0.51
treatment of H atoms				constr	

Li···F contacts exhibiting lengths between 2.94(1) and 3.14(1) Å, which are only slightly below the sum of the van der Waals radii of lithium and fluorine.[24] The bigger sodium ion allows the coordination of eight fluorine atoms and shows a broad range of Na···F distances from 2.336(2) to 3.348(1) Å. The potassium is coordinated by seven fluorine atoms with K···F distances between 2.7255(8) and 2.9939(8) Å. Plenio, who reviewed the field of interactions between metals and organically bound fluorine atoms, reported a maximum between 2.45 and 2.75 Å in the distribution of Na···F distances and between 2.85 and 3.05 Å in the case of K···F contacts.[25] Thus, most of the corresponding values observed for $KN(C_6F_5)(C(CF_3)_3)$ are comparably short, which can be referred to the fact that the ligand exhibits only one nitrogen donor atom beside the fluorine atoms. The crystal structures of $LiN(C_6F_5)(C(CF_3)_3)$, $NaN(C_6F_5)(C(CF_3)_3)$, and $KN(C_6F_5)(C(CF_3)_3)$ reveal the interaction of neighboring dimers *via* M···F contacts. The fact that single crystals of $LiN(C_6F_5)(C(CF_3)_3)$ were obtained *via* sublimation at 120 °C and 1.3×10^{-3} mbar is in accord with only weak Li···F contacts between the dimers. Furthermore, this unexpected behavior proves the remarkable thermal stability of $LiN(C_6F_5)(C(CF_3)_3)$ with respect to LiF elimination. We could show that $LiN(C_6F_5)_2$ readily eliminates lithium fluoride during attempts to sublime it.[18] A high volatility is known for fluorinated alkoxides that are used for chemical vapor deposition[26] and for alkaline metal bistrimethylsilylamides, but it is unique for lithium (and magnesium, see below) amides with perfluorinated ligands.

In the case of the sodium salt the formation of two-dimensional chains can be observed in the crystal structure (Figure 4), whereas the lithium and the potassium salts form complicated three-dimensional networks. Dimeric substructures revealing metal fluorine contacts were also found for $LiN(C_6F_5)_2{\cdot}Et_2O$ (*d*(Li−N) between 2.09(1) and 2.12(1) Å, *d*(Li···Li) 2.67(1) Å, N−Li−N 100.7(4)° and 101.4(4)°, Li−N−Li 78.4(4)° and 79.1(4)°) and $LiN(C_6F_5)_2{\cdot}THF$ (*d*(Li−N) between 2.080(6) and 2.178(6) Å, *d*(Li···Li) 2.675(8) Å, N−Li−N 103.2(3)° and 99.2(3)°, Li−N−Li 79.2(2)° and 77.8(2)°), which exhibit similar N−Li and Li···Li distances as well as N−Li−N and Li−N−Li angles to the lithium salt discussed herein.[12] The shortest Li···F contact observed in these structures is longer than in the solvent-free lithium salt discussed herein ($LiN(C_6F_5)_2{\cdot}Et_2O$: 2.196(9) Å, $LiN(C_6F_5)_2{\cdot}THF$: 2.098(6) Å).

The crystal structure of (η^6-toluene)$CsN(C_6F_5)(C(CF_3)_3)$ (Figure 6) also reveals nitrogen-bridged dimers, but addition-

dx.doi.org/10.1021/ic5001717 | *Inorg. Chem.* 2014, 53, 3839−3846

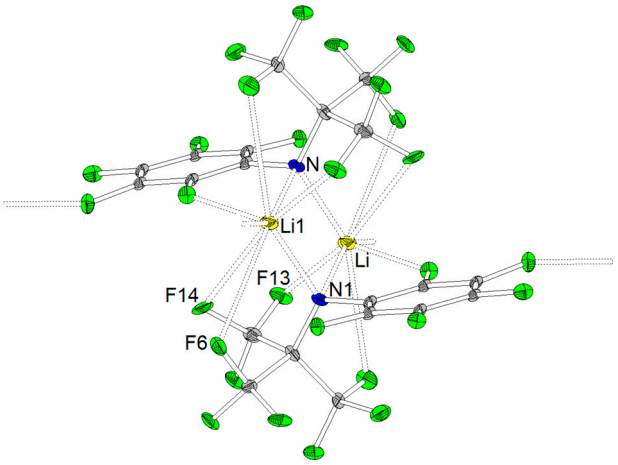

Figure 2. Molecular structure of $LiN(C_6F_5)(C(CF_3)_3)$ (ellipsoids with 30% probability). Selected bond lengths (Å) and angles (deg): Li1–N1 2.10(1), Li1–N(1–*x*, –*y*, 1–*z*) 2.08(1), Li1···F1(1–*x*, –*y*, 1–*z*) 2.02(1), Li1···F2(*x*, 0.5–*y*, –0.5+*z*) 2.06(1), Li1···F6 3.10(1), Li1···F11(1–*x*, –*y*, 1–*z*) 3.14(1), Li1···F13(1–*x*, –*y*, 1–*z*) 2.12(1), Li1···F14 2.94(1), Li1···Li(1–*x*, –*y*, 1–*z*) 2.65(2), Li1–N1–Li1(1–*x*, –*y*, 1–*z*) 98.36(3).

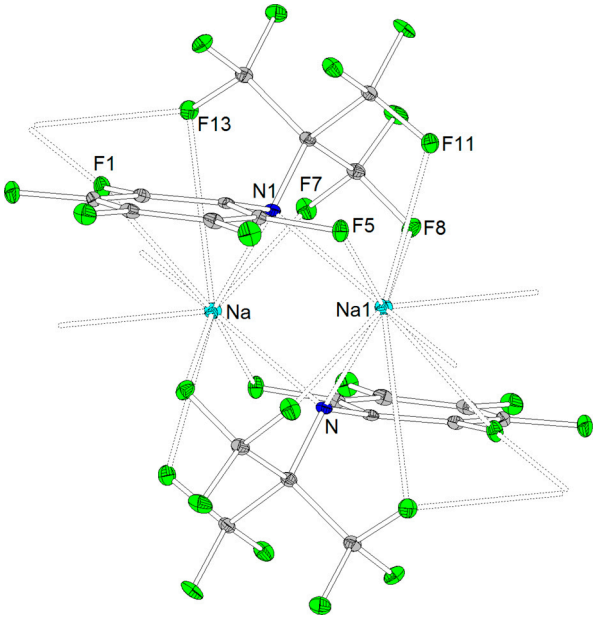

Figure 3. Molecular structure of $NaN(C_6F_5)(C(CF_3)_3)$ (ellipsoids with 30% probability). Selected bond lengths (Å) and angles (deg): Na1–N1 2.477(2), Na1–N(1–*x*, –*y*, 1–*z*) 2.442(2), Na1···F1(1+*x*, *y*, *z*) 2.336(2), Na1···F1(1–*x*, –*y*, 1–*z*) 3.117(1), Na1···F5 2.483(2), Na1···F7(1–*x*, –*y*, 1–*z*) 2.558(1), Na1···F8 2.420(1), Na1···F11 2.804(1), Na1···F13(1+*x*, *y*, *z*) 2.688(1), Na1···F13(1–*x*, –*y*, 1–*z*) 3.348(1), Na1···Na(1–*x*, –*y*, 1–*z*) 3.466(1), Na1–N1–Na1(1–*x*, –*y*, 1–*z*) 89.58(5).

ally contains a toluene molecule showing η^6-coordination to two cesium atoms, which emphasizes the soft Lewis-acidic character of this metal center (distance between Cs and the center of toluene: 3.4092(4) Å). The Cs···C_{Ar} distances are between 3.625(2) and 3.739(2) Å and thus lie within the range from 3.3 to 3.8 Å that was reported for cesium arene interactions.[27] The toluene ligands link two vicinal dimers in each case (Figure 7). Each cesium atom shows interactions with three $[N(C_6F_5)(C(CF_3)_3)]^-$ units. Two of these provide their

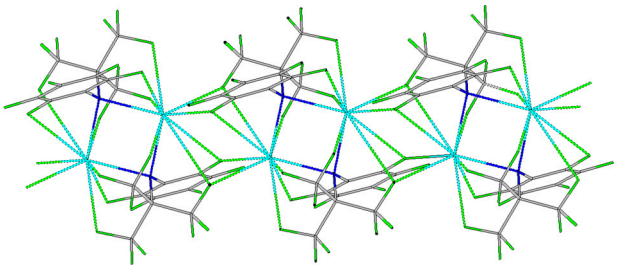

Figure 4. Two-dimensional chains observed in the crystal structure of $NaN(C_6F_5)(C(CF_3)_3)$.

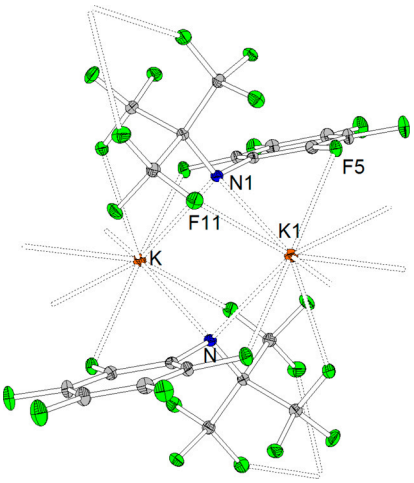

Figure 5. Molecular structure of $KN(C_6F_5)(C(CF_3)_3)$ (ellipsoids with 30% probability). Selected bond lengths (Å) and angles (deg): K1–N1 2.904(1), K1–N(1.5–*x*, 0.5–*y*, 2–*z*) 2.822(1), K1···F1(1.5–*x*, 0.5–*y*, 2–*z*) 2.8259(9), K1···F4(2–*x*, y, 2.5–*z*) 2.9939(8), K1···F5 2.7978(7), K1···F7(1.5–*x*, 0.5–*y*, 2–*z*) 2.7633(8), K1···F9 (x, 1–*y*, 0.5+*z*) 2.9865(9), K1···F11 2.7255(8), K1···F12(x, 1–*y*, 0.5+*z*) 2.9865(9), K1···K(1.5–*x*, 0.5–*y*, 2–*z*) 4.3337(4), K1–N1–K1(1.5–*x*, 0.5–*y*, 2–*z*) 78.7(5).

nitrogen atoms, two fluorine atoms belonging to CF_3 groups, and one aromatic fluorine atom as donor atoms. The third $[N(C_6F_5)(C(CF_3)_3)]^-$ moiety coordinates with one *meta*- and the *para*-fluorine atom of a C_6F_5 moiety to the metal center. The distances between the cesium atom and coordinating fluorine atoms range from 3.054(1) to 3.653(2) Å. Plenio reported a maximum in the distribution between 3.20 and 3.40 Å for weakly bonding Cs···F contacts.[25] The M–N–M (96.07(5)°) and the N–M–N angles (83.93(5)°) in (η^6-toluene)$CsN(C_6F_5)(C(CF_3)_3)$ are similar to the corresponding values found in the potassium salt (98.36(3)° and 81.64(3)°). As expected, the cesium salt shows the largest M–N bond lengths (3.212(2) and 3.330(2) Å) and nonbonding N···N distance (4.375(2) Å) among the structures studied herein.

A different coordination mode is found for the magnesium compound (Figure 8) in which a distorted octahedron formed by two $[N(C_6F_5)(C(CF_3)_3)]^-$ moieties is observed, whereas the asymmetric unit contains only half of the octahedron. Neighboring octahedra interact via π-stacking of C_6F_5 moieties. The fact that single crystals of $Mg[N(C_6F_5)(C(CF_3)_3)]_2$ were obtained by sublimation at 115 °C and atmospheric pressure suggests comparably weak intermolecular interactions and a remarkable thermal stability. The magnesium atom is coordinated by two nitrogen atoms *trans* to each other (*d*(Mg–N) 1.981(2) and 1.981(2) Å) and four fluorine

dx.doi.org/10.1021/ic5001717 | *Inorg. Chem.* 2014, 53, 3839–3846

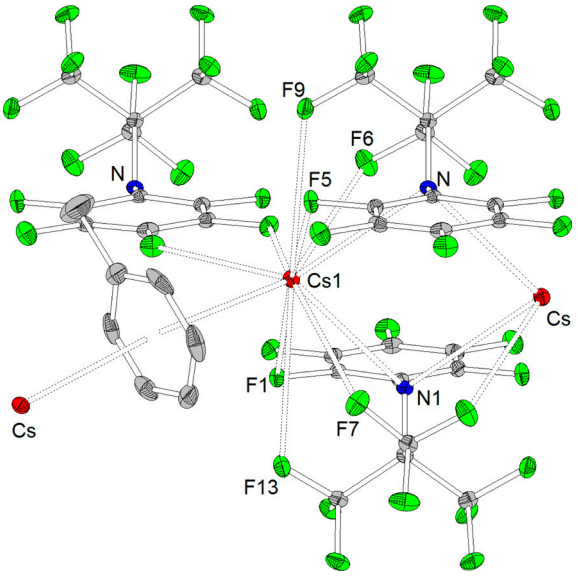

Figure 6. Molecular structure of (η^6-toluene)CsN(C_6F_5)($C(CF_3)_3$) (ellipsoids with 30% probability). Cs···F contacts are shown only for Cs1. Selected bond lengths (Å) and angles (deg): Cs1−N1 3.212(2), Cs1−N1(1−*x*, 1−*y*, 1−*z*) 3.330(2), Cs1···F1 3.082(2), Cs1···F2(2−*x*, 1−*x*, 1−*z*) 3.454(2), Cs1···F3(2−*x*, 1−*x*, 1−*z*) 3.303(2), Cs1···F5(1−*x*, 1−*y*, 1−*z*) 3.054(1), Cs1···F6 3.079(2), Cs1···F7 3.140(2), Cs1···F9 3.356(2), Cs1···F13 3.653(2), Cs1···Cs1(1−*x*, 1−*y*, 1−*z*) 4.8648(4), Cs1−N1−Cs1(1−*x*, 1−*y*, 1−*z*) 96.07(5).

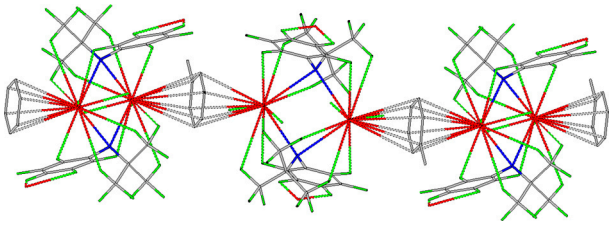

Figure 7. Connection of dimers by η^6-coordinated toluene molecules in (η^6-toluene)CsN(C_6F_5)($C(CF_3)_3$).

atoms that are part of *tert*-butyl moieties (*d*(Mg···F) 2.186(2) and 2.223(1) Å). It seems that the harder cation Mg^{2+} favors the interaction with sp^3 C−F donors of the *tert*-butyl moiety, while the softer alkali cations M^+ are much less specific in their competitive sp^2 C−F vs sp^3 C−F interaction and in their coordinative configuration. The linear N−Mg−N axis is tilted toward the plane formed by the four coordinating fluorine atoms by 15.57(5)°. The F−Mg−F angle of fluorine atoms belonging to the same $[N(C_6F_5)(C(CF_3)_3)]^-$ unit is 72.14(5)°, whereas this value is 107.86(5)° for fluorine atoms of different $[N(C_6F_5)(C(CF_3)_3)]^-$ moieties. The C−F distances involving coordinating fluorine atoms (1.388(3) and 1.385(3) Å) are considerably longer compared to noncoordinating fluorine atoms bound to aliphatic carbon atoms (ranging from 1.313(3) to 1.333(3) Å). Whereas literature-known alkaline earth metal complexes of $HNPh_2$ such as $(thf)_2Mg(NPh_2)_2$, $(dme)_2Ca(NPh_2)_2$, $(thf)_4Sr(NPh_2)_2$, and $(thf)_4Ba(NPh_2)_2$ reveal the coordination of ether molecules to the metal center,[28] the magnesium complex reported herein is a rare example of a solvent-free group II metal amide coordinated only by organically bound fluorine atoms in addition to two nitrogen donors. The two diphenylamide ligands and the two THF molecules in $(thf)_2Mg(NPh_2)_2$ form a distorted tetrahedron

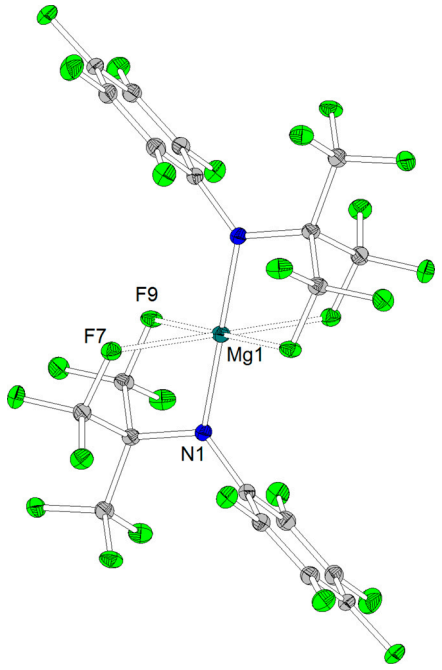

Figure 8. Molecular structure of $Mg[N(C_6F_5)(C(CF_3)_3)]_2$ (ellipsoids with 30% probability). Selected bond lengths (Å) and angles (deg): Mg1−N1 1.981(2), Mg1···F7 2.186(2), Mg1···F9 2.223(1), N1−Mg−N1 180, F9−Mg1−F7 72.14(5).

and a longer Mg−N distance of 2.013(3) Å than found for $Mg[N(C_6F_5)(C(CF_3)_3)]_2$. Similar Mg···F distances of 2.200(2) and 2.199(3) Å to the magnesium complex studied herein were found in a literature-known magnesium amide with a cyclam ligand.[29] An octahedral coordination of a magnesium atom involving Mg···F contacts was also observed for the homoleptic magnesium complex of $HN(C_6F_5)((CH_2)_2NMe_2)$ showing Mg···F distances of 2.431(3) Å.[30]

Generally, we notice a trend that more fluorine atoms belonging to CF_3 groups than to aromatic fluorine atoms are involved in M···F contacts.[31] This can be explained by the higher flexibility of the aliphatically bound fluorine atoms due to rotation around the N−C_{tert} and the C_{tert}−C bonds, allowing a less constrained alignment of the fluorine lone pairs to the metal center. However, we have to be aware that some of the longer M···F contacts originate from the inevitable vicinity of the metal cations and fluorine atoms caused by the extremely bulky perfluorinated ligands or packing effects rather than solely from an energetically favorable interaction. Thus, the higher number of M···F contacts involving CF_3 groups might also be a result of the higher number of aliphatic compared to aromatic fluorine atoms.

■ CONCLUSION AND OUTLOOK

We have presented the synthesis of a new secondary amine with strongly electron-withdrawing and sterically demanding perfluorinated phenyl and *tert*-butyl substituents. *N*-(2,3,4,5,6-Pentafluorophenyl)-*N*-nonafluoro-*tert*-butylamine, $HN(C_6F_5)(C(CF_3)_3)$, was obtained *via* a CF_3-group transfer reaction from trifluoromethyltrimethylsilane to the corresponding imine precursor. This NH-acid was fully characterized and used for the synthesis of the alkaline metal salts of lithium, sodium, potassium, and cesium. In addition, the homoleptic complexes of the earth alkaline metals magnesium, calcium, and barium were prepared. We observed a rather unusual volatility for the

dx.doi.org/10.1021/ic5001717 | *Inorg. Chem.* 2014, 53, 3839−3846

Table 2. Selected Structural Features of the Crystal Structures of $LiN(C_6F_5)(C(CF_3)_3)$, $KN(C_6F_5)(C(CF_3)_3)$, $CsN(C_6F_5)(C(CF_3)_3)$, and $Mg[N(C_6F_5)(C(CF_3)_3)]_2$[a]

	N−M	M···F contacts	coordinating $[N(C_6F_5)(C(CF_3)_3)]^-$ units	CN	M···F_{Ar}	M···F_{Al}	N···N	N−M−N	M−N−M
$LiN(C_6F_5)(C(CF_3)_3)$	2.08(1)	6	3	8		2.12(1)	3.234(8)	101.3(5)	78.7(5)
					2.02(1)	2.94(1)			
	2.10(1)				2.06(1)	3.10(1)			
						3.14(1)			
$NaN(C_6F_5)(C(CF_3)_3)$	2.442(2)	8	3	10		2.420(1)	3.481(2)	90.42(5)	89.58(5)
					2.336(2)	2.558(1)			
	2.477(2)				2.483(2)	2.688(1)			
					3.117(1)	2.804(1)			
						3.348(1)			
$KN(C_6F_5)(C(CF_3)_3)$	2.822(1)	7	4	9		2.7255(8)	3.744(1)	81.64(3)	98.36(3)
					2.7978(7)	2.7633(8)			
					2.8259(9)	2.7930(8)			
	2.904(1)				2.9939(8)	2.8831(8)			
						2.9865(9)			
$CsN(C_6F_5)(C(CF_3)_3)$	3.212(2)	8	3	10	3.054(1)	3.079(2)	4.375(2)	83.93(5)	96.07(5)
					3.082(1)	3.140(2)			
	3.330(2)				3.303(2)	3.356(2)			
					3.454(2)	3.653(2)			
$Mg[N(C_6F_5)(C(CF_3)_3)]_2$	1.981(2)	4	2	6		2.186(2)	3.962(3)	180.0	
						2.186(1)			
	1.981(2)					2.223(1)			
						2.223(1)			

[a]Bond lengths in Å, angles in deg, CN = coordination number, F_{Ar} = aromatic fluorine atoms, F_{Al} = fluorine atoms of CF_3 groups.

lithium and the magnesium salts, which reveal certain covalent character. This was used to grow single crystals via sublimation. Molecular structures of the lithium, sodium, potassium, cesium, and magnesium salts reveal interesting coordination motifs with manifold labile metal fluorine contacts. Due to its low basicity, we anticipate that the anion $[N(C_6F_5)(C(CF_3)_3)]^-$ is a promising rather weakly coordinating ligand for the generation of highly Lewis-acidic main group, rare earth, or transition metal complexes. The alkaline metal salts reported herein could serve as starting materials for the synthesis of such Lewis superacids via salt elimination reactions, or they could prove to be valuable precursors for the preparation of highly hydrophobic electrolyte systems.

EXPERIMENTAL SECTION

Reactions were carried out under an inert atmosphere using standard Schlenk techniques. Moisture- and air-sensitive substances were stored in a conventional nitrogen-flushed glovebox. Solvents were purified according to literature procedures and kept under an inert atmosphere. *N*-Pentafluorophenyl-2-iminohexafluoropropane was prepared as described above.[20] The metal precursors $LiN(SiMe_3)_2$,[32] $NaN(SiMe_3)_2$,[32] $KN(SiMe_3)_2$,[33] $Ca[N(SiMe_3)_2]_2$,[34] and $Ba[N(SiMe_3)_2]_2(THF)$[35] were synthesized according to literature procedures. Spectra were recorded on the following spectrometers. NMR: Bruker ARX300, Bruker DRX400, Bruker DRX500. IR: ATR-FT-IR. MS: LTQ-FT or QStarPulsar i (Finnigan). Elemental analysis: CHN-Rapid (Heraeus).

Synthesis of $CsN(C_6F_5)(C(CF_3)_3)$. A mixture of *N*-pentafluorophenylbis(trifluoromethyl)methyleneimine (5.37 g, 16.23 mmol, 1.0 equiv) and trifluoromethyltrimethylsilane (2.54 g, 17.85 mmol 1.1 equiv) was added dropwise to a suspension of cesium fluoride (2.98 g, 19.47 mmol, 1.2 equiv) in 40 mL of THF over 30 min. The reaction mixture changed color to yellow and turned red after stirring overnight. The suspension was filtered over Celite, and the filtrate was evaporated to dryness *in vacuo*. The red residue was washed with 40 mL of hexane, and the remaining solid was excessively dried *in vacuo* to remove traces of THF and obtain $CsN(C_6F_5)(C(CF_3)_3)$ (6.34 g, 11.89 mmol, 73%) as a red solid. Single crystals suitable for structure determination were obtained by slowly cooling a saturated solution of $CsN(C_6F_5)(C(CF_3)_3)$ in toluene from 90 °C to −30 °C. ^{13}C NMR (101 MHz, DMSO-d_6): δ 142.7 (d, $^1J_{FC}$ = 231.2 Hz, *o*-C_{Ar}), 137.6 (dm, $^1J_{FC}$ = 239.4 Hz, *m*-C_{Ar}), 133.2 (t, $^2J_{FC}$ = 12.1 Hz, *ipso*-C_{Ar}), 128.1 (dt, $^1J_{FC}$ = 231.5 Hz, $^2J_{FC}$ = 14.5 Hz, *p*-C_{Ar}), 123.0 (q, $^1J_{FC}$ = 297.0 Hz, $-CF_3$), 76.1 ppm (dec, $^2J_{FC}$ = 25.4 Hz, $C(CF_3)_3$). ^{19}F NMR (282 MHz, DMSO-d_6): δ −68.8 (t, $^{ts}J_{FF}$ = 9.7 Hz, 9F, $-CF_3$), −156.7 (br s, 2F, *o*-F_{Ar}), −170.1 (t, $^3J_{FF}$ = 21.7 Hz, 2F, *m*-F_{Ar}), −184.1 ppm (br s, 1F, *p*-F_{Ar}). IR: $\tilde{\nu}$ 1615 (w), 1507 (m), 1481 (m), 1412 (m), 1279 (m), 1234 (s), 1214 (s), 1190 (s), 1112 (w), 1072 (s), 1025 (w), 972 (s), 930 (s), 771 (w), 756 (w), 721 (s), 673 (m), 582 (w), 556 (w), 537 (w), 497 (w), 449 cm^{-1} (w). (−)-ESI-MS (MeCN): *m*/*z* (%) 400 (32) $[M]^-$, 219 (100) $[M - C_6F_5N]^-$, 180 (8) $[M - C_4F_9]^-$, 167 (18) $[M - C_4F_9N]^-$. HRMS ((−)-ESI): *m*/*z* calcd for $C_{10}F_{14}N^-$ 399.9813 $[M]^-$; found 399.9817. Anal. Calcd (%) for $C_{10}CsF_{14}N$ (533.00): C 22.53, H 0.00, N 2.63. Found: C 22.29, H 0.19, N 2.78.

Synthesis of $HN(C_6F_5)(C(CF_3)_3)$. A suspension of $CsN(C_6F_5)(C(CF_3)_3)$ (1000 mg, 1.876 mmol) in 50 mL of dichloromethane was extracted with 40 mL of hydrochloric acid (10%). The aqueous phase was additionally extracted twice with 75 mL of dichloromethane, and the combined organic phases were dried over $MgSO_4$. The solvent was removed at the rotary evaporator, and the remaining oily residue was distilled at 74 °C and 57 mbar to give $HN(C_6F_5)(C(CF_3)_3)$ (675 mg 1.687 mmol, 90%) as a colorless oil, which was stored under an inert atmosphere. ^1H NMR (300 MHz, benzene-d_6): δ 2.58 ppm (s, 1H, NH). ^{13}C NMR (101 MHz, benzene-d_6): δ 146.4 (dm, $^1J_{FC}$ = 251.3 Hz, C_{Ar}), 141.3 (dm, $^1J_{FC}$ = 256.1 Hz, *p*-C_{Ar}), 137.7 (dm, $^1J_{FC}$ = 251.3 Hz, C_{Ar}), 121.0 (q, $^1J_{FC}$ = 292.2 Hz, $-CF_3$), 113.8 (t, $^2J_{FC}$ = 14.8 Hz, *ipso*-C_{Ar}), 69.0 ppm (dec, $^2J_{FC}$ = 28.4 Hz, $C(CF_3)_3$). ^{19}F NMR (282 MHz, benzene-d_6): δ −69.6 (t, $^{ts}J_{FF}$ = 7.1 Hz, 9F, $-CF_3$), −143.2 to −143.3 (m, 2F, F_{Ar}), −153.0 (t, $^3J_{FF}$ = 22.2 Hz, 1F, *p*-F_{Ar}), −162.9 ppm (t, $^3J_{FF}$ = 19.6 Hz, 2F, F_{Ar}). IR: $\tilde{\tilde{\nu}}$ 3406 (w, ν(N−H)), 1522 (s), 1243 (s), 1114 (m), 1018 (s), 989 (s), 959 (s), 757 (w), 726 (s), 686 (w), 667 (m), 540 (m), 473 cm^{-1} (w). (−)-ESI-MS (MeCN): *m*/*z* (%) 400 (2) $[M]^-$, 167 (8) $[C_6F_5]^-$. HRMS ((−)-ESI): *m*/*z* calcd for $C_{10}F_{14}N^-$ 399.9813 $[M]^-$; found 399.9815. Anal. Calcd (%) for

dx.doi.org/10.1021/ic5001717 | Inorg. Chem. 2014, 53, 3839−3846

$C_{10}HF_{14}N$ (401.10): C 29.94, H 0.25, N 3.49. Found: C 30.55, H 0.39, N 4.03.

Synthesis of $LiN(C_6F_5)(C(CF_3)_3)$. A solution of LiHMDS (1.137 g, 6.79 mmol, 1.0 equiv) in 30 mL of hexane was added dropwise to a solution of $HN(C_6F_5)(C(CF_3)_3)$ (2.727 g, 6.79 mmol, 1.0 equiv) in 30 mL of hexane. A colorless solid precipitated, and the reaction mixture was stirred for 2 h at room temperature. The precipitate was separated by centrifugation and washed twice with 20 mL of pentane. It was dried *in vacuo* to give $LiN(C_6F_5)(C(CF_3)_3)$ (2.222 g, 5.45 mmol, 80%) as a white solid. Single crystals suitable for structure determination were obtained by sublimation of $LiN(C_6F_5)(C(CF_3)_3)$ at 120 °C and 6.3×10^{-3} mbar. ^{13}C NMR (101 MHz, DMSO-d_6): δ 142.5 (dm, $^1J_{FC}$ = 230.9 Hz, *o*-C_{Ar}), 137.5 (dm, $^1J_{FC}$ = 239.0 Hz, *m*-C_{Ar}), 133.5 (t, $^2J_{FC}$ = 13.0 Hz, *ipso*-C_{Ar}), 127.7 (dm, $^1J_{FC}$ = 230.7 Hz, *p*-C_{Ar}), 123.0 (q, $^1J_{FC}$ = 297.1 Hz, $-CF_3$), 76.2 ppm (dec, $^2J_{FC}$ = 25.3 Hz, $C(CF_3)_3$). ^{19}F NMR (376 MHz, DMSO-d_6): δ −69.0 (t, $^{ts}J_{FF}$ = 10.6 Hz, 9F, $-CF_3$), −157.1 to −157.3 (m, 2F, *o*-F_{Ar}), −170.5 (t, $^3J_{FF}$ = 23.3 Hz, 2F, *m*-F_{Ar}), −185.0 ppm (tt, $^3J_{FF}$ = 24.1 Hz, $^4J_{FF}$ = 11.6 Hz, 1F, *p*-F_{Ar}). IR: $\tilde{\nu}$ 1516 (m), 1490 (m), 1427 (w), 1285 (w), 1250 (m), 1228 (m), 1196 (m), 1165 (m), 1125 (w), 1074 (s), 991 (s), 972 (s), 948 (s), 874 (w), 793 (w), 758 (w), 723 (m), 685 (m), 668 (w), 631 (w), 599 (w), 563 (w), 538 (w), 516 (m), 483 (w), 467 (w), 446 cm^{-1} (w). (−)-ESI-MS (MeCN): *m*/*z* (%) 400 (8) $[M]^-$, 167 (100) $[C_6F_5]^-$. HRMS ((−)-ESI): *m*/*z* calcd for $C_{10}F_{14}N^-$ 399.9813 $[M]^-$; found 399.9811. Anal. Calcd (%) for $C_{10}LiF_{14}N$ (407.03): C 29.51, H 0.00, N 3.44. Found: C 29.15, H 0.00, N 3.74.

Synthesis of $NaN(C_6F_5)(C(CF_3)_3)$. A solution of NaHMDS (104 mg, 0.567 mmol, 1.0 equiv) in 10 mL of toluene was added dropwise to a solution of $HN(C_6F_5)(C(CF_3)_3)$ (226 mg, 0.567 mmol, 1.0 equiv) in 10 mL of toluene. A gray solid precipitated, and the reaction mixture was stirred overnight at room temperature. The precipitate was separated by centrifugation and washed twice with 10 mL of hexane. It was dried *in vacuo* to give $NaN(C_6F_5)(C(CF_3)_3)$ (106 mg, 0.251 mmol, 44%) as a light gray solid. Single crystals suitable for structure determination were obtained by the slow diffusion of a solution of $HN(C_6F_5)(C(CF_3)_3)$ in pentane into a solution of NaHMDS in toluene. ^{13}C NMR (101 MHz, DMSO-d_6): δ 142.5 (dt, $^1J_{FC}$ = 231.2 Hz, $^2J_{FC}$ = 8.4 Hz, *o*-C_{Ar}), 137.6 (dm, $^1J_{FC}$ = 239.4 Hz, *m*-C_{Ar}), 133.6 (t, $^2J_{FC}$ = 13.2 Hz, *ipso*-C_{Ar}), 127.8 (dtt, $^1J_{FC}$ = 230.9 Hz, $^2J_{FC}$ = 14.7 Hz, $^3J_{FC}$ = 4.8 Hz, *p*-C_{Ar}), 123.1 (q, $^1J_{FC}$ = 297.0 Hz, CF_3), 76.2 ppm (dec, $^2J_{FC}$ = 25.4 Hz, $C(CF_3)_3$). ^{19}F NMR (282 MHz, DMSO-d_6): δ −69.3 (t, $^{ts}J_{FF}$ = 10.3 Hz, 9F, $-CF_3$), −157.5 to −157.8 (m, 2F, *o*-F_{Ar}), −170.9 (t, $^3J_{FF}$ = 23.0 Hz, 2F, *m*-F_{Ar}), −185.4 ppm (tt, $^3J_{FF}$ = 24.2 Hz, $^4J_{FF}$ = 11.9 Hz, 1F, *p*-F_{Ar}). IR: $\tilde{\nu}$ 1516 (m), 1480 (m), 1420 (w), 1180 (br), 1076 (m), 965 (s), 934 (s), 774, (w), 721 (m), 668 (w), 538 cm^{-1} (w). (−)-ESI-MS (MeCN): *m*/*z* (%): 219 (10) $[C_4F_9]^-$, 167 (25) $[C_6F_5]^-$. HRMS ((−)-ESI): *m*/*z* calcd for $C_{10}F_{14}N^-$ 399.9813 $[M]^-$; found 399.9813. Anal. Calcd (%) for $C_{10}NaF_{14}N$ (423.08): C 28.39, H 0.00, N 3.31. Found: C 28.59, H 0.29, N 3.46.

Synthesis of $KN(C_6F_5)(C(CF_3)_3)$. A solution of KHMDS (644 mg, 3.22 mmol, 1.0 equiv) in 20 mL of toluene was added dropwise to a solution of $HN(C_6F_5)(C(CF_3)_3)$ (1292 mg, 3.22 mmol, 1.0 equiv) in 15 mL of hexane. A colorless solid precipitated, and the reaction mixture was stirred for 2 h at room temperature. The precipitate was separated by centrifugation and washed twice with 20 mL of hexane. It was dried *in vacuo* to give $KN(C_6F_5)(C(CF_3)_3)$ (956 mg, 2.18 mmol, 68%) as a white solid. Single crystals suitable for structure determination were obtained by layering a saturated solution of $KN(C_6F_5)(C(CF_3)_3)$ in toluene with hexane. ^{13}C NMR (63 MHz, DMSO-d_6): δ 142.5 (dt, $^1J_{FC}$ = 231.3 Hz, $^2J_{FC}$ = 8.9 Hz, *o*-C_{Ar}), 137.6 (dm, $^1J_{FC}$ = 239.3 Hz, *m*-C_{Ar}), 133.6 (t, $^2J_{FC}$ = 12.6 Hz, *ipso*-C_{Ar}), 127.8 (dtt, $^1J_{FC}$ = 230.9 Hz, $^2J_{FC}$ = 14.6 Hz, $^3J_{FC}$ = 4.8 Hz, *p*-C_{Ar}), 123.1 (q, $^1J_{FC}$ = 297.1 Hz, $-CF_3$), 76.2 ppm (dec, $^2J_{FC}$ = 25.4 Hz, $C(CF_3)_3$). ^{19}F NMR (376 MHz, DMSO-d_6): δ −69.0 (t, $^{ts}J_{FF}$ = 9.9 Hz, 9F, $-CF_3$), −157.1 to −157.3 (m, 2F, *o*-F_{Ar}), −170.5 (t, $^3J_{FF}$ = 23.3 Hz, 2F, *m*-F_{Ar}), −185.5 ppm (tt, $^3J_{FF}$ = 24.1 Hz, $^4J_{FF}$ = 11.6 Hz, 1F, *p*-F_{Ar}). IR: $\tilde{\nu}$ 1642 (w), 1496 (s), 1465 (s), 1341 (m), 1256 (w), 1120 (w), 1018 (s), 997 (s), 972 (s), 817 (w), 729 (w), 708 (m), 645 (m), 564 (m), 477 cm^{-1} (w). Anal. Calcd (%) for $C_{10}KF_{14}N$ (439.19): C 27.35, H 0.00, N 3.19. Found: C 27.21, H 0.14, N 3.39.

Synthesis of $Mg[N(C_6F_5)(C(CF_3)_3)]_2$. A solution of di-*n*-butylmagnesium (1 mol/L in heptane, 0.722 mL, 0.722 mmol, 1.0 equiv) was added dropwise to a solution of $HN(C_6F_5)(C(CF_3)_3)$ (401 mg, 1.444 mmol, 2.0 equiv) in 20 mL of toluene. A gray solid precipitated, and the reaction mixture was stirred overnight at room temperature. The precipitate was separated by centrifugation and washed with 15 mL of hexane. It was dried *in vacuo* to give $Mg[N(C_6F_5)(C(CF_3)_3)]_2$ (192 mg, 0.233 mmol, 32%) as a light gray solid. Single crystals suitable for structure determination were obtained by sublimation of $Mg[N(C_6F_5)(C(CF_3)_3)]_2$ at 117 °C and 1 mbar. ^{13}C NMR (101 MHz, DMSO-d_6): δ 142.7 (d, $^1J_{FC}$ = 231.4 Hz, *o*-C_{Ar}), 137.5 (dm, $^1J_{FC}$ = 240.4 Hz, *m*-C_{Ar}), 132.9 (t, $^2J_{FC}$ = 12.9 Hz, *ipso*-C_{Ar}), 128.3 (dt, $^1J_{FC}$ = 232.1 Hz, $^2J_{FC}$ = 14.1 Hz, *p*-C_{Ar}), 123.0 (q, $^1J_{FC}$ = 296.9 Hz, $-CF_3$), 75.9 ppm (dec, $^2J_{FC}$ = 25.4 Hz, $C(CF_3)_3$). ^{19}F NMR (282 MHz, DMSO-d_6): δ −68.8 (t, $^{ts}J_{FF}$ = 10.5 Hz, 18F, $-CF_3$), −156.9 to −157.2 (m, 4F, *o*-F_{Ar}), −170.3 (t, $^3J_{FF}$ = 23.1 Hz, 4F, *m*-F_{Ar}), −184.8 ppm (tt, $^3J_{FF}$ = 23.9 Hz, $^4J_{FF}$ = 11.8 Hz, 2F, *p*-F_{Ar}). IR: $\tilde{\nu}$ 1513 (m), 1495 (w), 1260 (br), 1181 (m), 1083 (s), 984 (s), 932 (s), 730 (m), 532 (w), 433 cm^{-1} (w), Anal. Calcd (%) for $C_{20}F_{28}MgN_2$ (824.49): C 29.13, H 0.00, N 3.40. Found: C 29.32, H 0.32, N 3.46.

Synthesis of $Ca[N(C_6F_5)(C(CF_3)_3)]_2$. A solution of $HN(C_6F_5)(C(CF_3)_3)$ (470 mg, 1.170 mmol, 2.0 equiv) in 15 mL of toluene was added dropwise to a solution of $Ca(HMDS)_2$ (211 mg, 0.585 mmol, 1.0 equiv) in 15 mL of toluene. A brown solid precipitated, and the reaction mixture was stirred overnight at room temperature. The precipitate was separated by centrifugation and washed twice with 15 mL of hexane. It was dried *in vacuo* to give $Ca[N(C_6F_5)(C(CF_3)_3)]_2$ (300 mg, 0.373 mmol, 64%) as a beige solid. ^{13}C NMR (101 MHz, DMSO-d_6): δ 142.5 (d, $^1J_{FC}$ = 231.3 Hz, *o*-C_{Ar}), 137.6 (dm, $^1J_{FC}$ = 239.1 Hz, *m*-C_{Ar}), 133.6 (t, $^2J_{FC}$ = 14.2 Hz, *ipso*-C_{Ar}), 127.7 (dm, $^1J_{FC}$ = 230.9 Hz, *p*-C_{Ar}), 123.0 (q, $^1J_{FC}$ = 297.3 Hz, $-CF_3$), 76.0 ppm (dec, $^2J_{FC}$ = 24.9 Hz, $C(CF_3)_3$). ^{19}F NMR (282 MHz, DMSO-d_6): δ −68.8 (t, $^{ts}J_{FF}$ = 10.3 Hz, 18F, $-CF_3$), −156.9 to −157.1 (m, 4F, *o*-F_{Ar}), −170.3 (t, $^3J_{FF}$ = 22.9 Hz, 4F, *m*-F_{Ar}), −184.6 ppm (s, 2F, *p*-F_{Ar}). IR: $\tilde{\nu}$ 1517 (m), 1482 (m), 1421 (w), 1224 (br), 1076 (s), 974 (s), 941 (s), 816 (s), 758 (s), 561 cm^{-1} (w). Anal. Calcd (%) for $C_{20}F_{28}CaN_2$ (840.26): C 28.59, H 0.00, N 3.33. Found: C 28.38, H 0.22, N 3.56.

Synthesis of $Ba[N(C_6F_5)(C(CF_3)_3)]_2 \cdot THF$. A solution of $HN(C_6F_5)(C(CF_3)_3)$ (190 mg, 0.474 mmol, 2.0 equiv) in 10 mL of toluene was added dropwise to a solution of $Ba(HMDS)_2 \cdot THF$ (126 mg, 0.237 mmol, 1.0 equiv) in 10 mL of toluene. The reaction mixture was stirred overnight at room temperature, and all volatiles were removed *in vacuo*. The remaining residue was washed twice with 15 mL of hexane. It was dried *in vacuo* to give $Ba[N(C_6F_5)(C(CF_3)_3)]_2 \cdot THF$ (110 mg, 0.109 mmol, 46%) as a light brown solid. ^1H NMR (300.1 MHz, DMSO-d_6): δ 3.60 (br s, 4H, OCH_2), 1.76 ppm (br s, 4H, OCH_2CH_2). ^{13}C NMR (125.8 MHz, DMSO-d_6): δ 142.5 (dt, $^1J_{FC}$ = 231.0 Hz, $^2J_{FC}$ = 7.7 Hz, *o*-C_{Ar}), 137.5 (dm, $^1J_{FC}$ = 238.8 Hz, *m*-C_{Ar}), 133.5 (t, $^2J_{FC}$ = 13.8 Hz, *ipso*-C_{Ar}), 127.7 (dtt, $^1J_{FC}$ = 231.2 Hz, $^2J_{FC}$ = 14.7 Hz, $^3J_{FC}$ = 4.7 Hz, *p*-C_{Ar}), 123.0 (q, $^1J_{FC}$ = 297.2 Hz, $-CF_3$), 76.2 (dec, $^2J_{FC}$ = 25.5 Hz, $C(CF_3)_3$), 66.9 (OCH_2), 25.0 ppm (OCH_2CH_2). ^{19}F NMR (282.4 MHz, DMSO-d_6): δ -69.6 (t, $^{ts}J_{FF}$ = 10.4 Hz, 18F, $-CF_3$), −157.7 to −158.0 (m, 4F, *o*-F_{Ar}), −171.1 (t, $^3J_{FF}$ = 23.0 Hz, 4F, *m*-F_{Ar}), −185.6 ppm (tt, $^3J_{FF}$ = 23.9 Hz, $^4J_{FF}$ = 11.8 Hz, 2F, *p*-F_{Ar}). IR: $\tilde{\nu}$ 1508 (m), 1483 (m), 1440 (w), 1200 (br), 1076 (s), 982 (s), 935 (s), 873 (m), 804 (m), 719 (m), 665 (w), 538 cm^{-1} (w). Anal. Calcd (%) for $C_{24}H_8BaF_{28}N_2O$ (1009.62): C 28.55, H 0.80, N 2.77. Found: C 27.93, H 1.64, N 2.21.

■ ASSOCIATED CONTENT

Ⓢ Supporting Information

Supporting Information contains the bond valence analyses of the Mg−N and Mg···F interactions. This material is available free of charge via the Internet at http://pubs.acs.org.

dx.doi.org/10.1021/ic5001717 | *Inorg. Chem.* 2014, 53, 3839−3846

AUTHOR INFORMATION

Corresponding Author

*E-mail: jsu@staff.uni-marburg.de.

Notes

The authors declare no competing financial interest.

ACKNOWLEDGMENTS

We thank Fonds der Chemischen Industrie (doctoral scholarship for J.F.K. and L.H.F.) for support of this work. We thank Dr. Klaus Harms and Fabian Schröder for their valuable support with crystal structure refinement. We thank Felicia Weber for her synthetic contribution.

REFERENCES

(1) (a) Foropoulos, J.; DesMarteau, D. D. *Inorg. Chem.* **1984**, *23*, 3720−3723. (b) DesMarteau, D. D.; Witz, M. *J. Fluorine Chem.* **1991**, *52*, 7−12. (c) Rey, I.; Johansson, P.; Lindgren, J.; Lassègues, J. C.; Grondin, J.; Servant, L. *J. Phys. Chem. A* **1998**, *102*, 3249−3258.

(2) (a) Tokuda, H.; Hayamizu, K.; Ishii, K.; Susan, Md. A. B. H.; Watanabe, M. *J. Phys. Chem. B* **2004**, *108*, 16593−16600. (b) Fujii, K.; Fujimori, T.; Takamuku, T.; Kanzaki, R.; Umebayashi, Y.; Ishiguro, S. *J. Phys. Chem. B* **2006**, *110*, 8179−8183. (c) Williams, D. B.; Stoll, M. E.; Scott, B. L.; Costa, D. A.; Oldham, W. J. *Chem. Commun.* **2005**, *11*, 1438−1440. (d) Jin, H.; O'Hare, B.; Dong, J.; Arzhantsev, S.; Baker, G. A.; Wishart, J. F.; Benesi, A. J.; Maroncelli, M. *J. Phys. Chem. B* **2008**, *112*, 81−92.

(3) (a) MacFarlane, D. R.; Huang, J.; Forsyth, M. *Nature* **1999**, *402*, 792−794. (b) Howlett, P. C.; MacFarlane, D. R.; Hollenkamp, A. F. *Electrochem. Solid-State Lett.* **2004**, *7*, A97−A101. (c) Matsumoto, H.; Sakaebe, H.; Tatsumi, K.; Kikuta, M.; Ishiko, E.; Kono, M. *J. Power Sources* **2006**, *160*, 1308−1313. (d) Borgel, V.; Markevicha, E.; Aurbacha, D.; Semraub, G.; Schmidt, M. *J. Power Sources* **2009**, *189*, 331−336.

(4) (a) KoppeI, I. A.; Taft, R. W.; Anvia, F.; Zbu, S.-Z.; Hu, L.-Q.; Sung, K.-S.; DesMarteau, D. D.; Yagupolskii, L. M.; Yagupolskii, Y. L.; Ignat'ev, N. V.; Kondratenko, N. V.; Volkonskii, A. Y.; Vlasov, V. M.; Notario, R.; Maria, P.-C. *J. Am. Chem. Soc.* **1994**, *116*, 3047−3057. (b) Leito, I.; Raamat, E.; Kütt, A.; Saame, J.; Kipper, K.; Koppel, I. A.; Koppel, I.; Zhang, M.; Mishima, M.; Yagupolskii, L. M.; Garlyauskayte, R. Y.; Filatov, A. A. *J. Phys. Chem. A* **2009**, *113*, 8421−8424. (c) Kütt, A.; Rodima, T.; Saame, J.; Raamat, E.; Mäemets, V.; Kaljurand, I.; Koppel, I. A.; Garlyauskayte, R. Y.; Yagupolskii, Y. L.; Yagupolskii, L. M.; Bernhardt, E.; Willner, H.; Leito, I. *J. Org. Chem.* **2011**, *76*, 391−395.

(5) Rowland, G. B.; Zhang, H.; Rowland, E. B.; Chennamadhavuni, S.; Wang, Y.; Antilla, J. C. *J. Am. Chem. Soc.* **2005**, *127*, 15696−15697.

(6) Wabnitz, T. C.; Spencer, J. B. *Org. Lett.* **2003**, *5*, 2141−2144.

(7) Ryu, D. H.; Corey, E. J. *J. Am. Chem. Soc.* **2003**, *125*, 6388−6390.

(8) Zhang, L.; Kozmin, S. A. *J. Am. Chem. Soc.* **2004**, *126*, 10204−10205.

(9) Antoniotti, S.; Dalla, V.; Dunach, E. *Angew. Chem.* **2010**, *122*, 8032−8060; *Ang. Chem., Int. Ed.* **2010**, *49*, 7860−7888 and references therein.

(10) Stricker, M.; Oelkers, B.; Rosenau, C. P.; Sundermeyer, J. *Chem.—Eur. J.* **2013**, *19*, 1042−1057.

(11) (a) Brooke, G. M.; Burdon, J.; Stacey, M.; Tatlow, J. C. *J. Chem. Soc.* **1960**, 1768−1771. (b) Koppang, R. *Acta Chem. Scand.* **1971**, *25*, 3067−3071.

(12) Khvorost, A.; Shutov, P. L.; Harms, K.; Lorberth, J.; Sundermeyer, J.; Karlov, S. S.; Zaitseva, G. S. *Z. Anorg. Allg. Chem.* **2004**, *630*, 885−889.

(13) Click, D. R.; Scott, B. L.; Watkin, J. G. *Chem. Commun.* **1999**, 633−634.

(14) Yin, H.; Lewis, A. J.; Carroll, P.; Schelter, E. J. *Inorg. Chem.* **2013**, *52*, 8234−8243.

(15) Giesbrecht, G. R.; Gordon, J. C.; Clark, D. L.; Hijar, C. A.; Scott, B. L.; Watkin, J. G. *Polyhedron* **2003**, *22*, 153−163.

(16) Peryshkov, D. V.; Schrock, R. R. *Organometallics* **2012**, *31*, 7278−7286.

(17) Linder, T.; Sundermeyer, J. *Chem. Commun.* **2009**, *20*, 2914−2916.

(18) (a) Sundermeyer, J.; Roling, B.; Linder, T.; Froemling, T.; Huber, B. *Eur. Pat. Appl.* EP 2314572 A1, 20110427, 2011. (b) Sundermeyer, J.; Roling, B.; Linder, T.; Huber, B.; Froemling, T. *PCT Int. Appl.* WO 2011048152 A1, 20110428, 2011. (c) Huber, B.; Linder, T.; Hormann, K.; Frömling, T.; Sundermeyer, J.; Roling, B. *Z. Phys. Chem.* **2012**, *212*, 377−390.

(19) (a) Müller, L. O.; Himmel, D.; Stauffer, J.; Steinfeld, G.; Slattery, J.; Santiso-Quiñones, G.; Brecht, V.; Krossing, I. *Angew. Chem.* **2008**, *120*, 7772−7776; *Angew. Chem., Int. Ed.* **2008**, *47*, 7659−7663. (b) Kraft, A.; Trapp, N.; Himmel, D.; Böhrer, H.; Schlüter, P.; Scherer, H.; Krossing, I. *Chem.—Eur. J.* **2012**, *18*, 9371−9380.

(20) Petrov, V. A.; DesMarteau, D. D. *J. Fluorine Chem.* **1996**, *77*, 175−181.

(21) Singh, R. P.; Shreeve, J. M. *Tetrahedron* **2000**, *56*, 7613−7632.

(22) Petrov, V. A. *Tetrahedron Lett.* **2000**, *41*, 6959−6963.

(23) The exact pK_a value in acetonitrile solution was determined in the group of Ivo Leito and will probably be published soon as a part of an acidity ladder.

(24) We are aware that the use of the sum of the van der Waals radii as the upper limit for a M···F interaction is problematic since we deal with metal ions. This issue is addressed in a review on M···F contacts by Plenio (ref 25).

(25) (a) Plenio, H. *Chem. Rev.* **1997**, *97*, 3363−3384. (b) Plenio, H. *ChemBioChem* **2004**, *5*, 650−655.

(26) (a) Samuels, J. A.; Chiang, W.-C.; Yu, C.-P.; Apen, E.; Smith, D. C.; Baxter, D. V.; Caulton, K. G. *Chem. Mater.* **1994**, *6*, 1684−1692. (b) Chou, T.-Y.; Chi, Y.; Huang, S.-F.; Liu, C.-S.; Carty, A. J.; Scoles, L.; Udachin, K. A. *Inorg. Chem.* **2003**, *42*, 6041−6049. (c) Matthews, J. S.; Rees, W. S., Jr. *Adv. Inorg. Chem.* **2000**, *50*, 173−192. (d) Liu, Y.-H.; Cheng, Y.-C.; Tung, Y.-L.; Chi, Y.; Chen, Y.-L.; Liu, C.-S.; Peng, S.-M.; Lee, G.-H. *J. Mater. Chem.* **2003**, *13*, 135−142.

(27) (a) Smith, J. D. *Adv. Organomet. Chem.* **1998**, *43*, 267−348. (b) Eaborn, C.; Hitchcock, P. B.; Smith, J. D.; Zhang, S. *Organometallics* **2000**, *19*, 1190−1193.

(28) Gärtner, M.; Fischer, R.; Langer, J.; Görls, H.; Walther, D.; Westerhausen, M. *Inorg. Chem.* **2007**, *46*, 5118−5124.

(29) Alves, L. G.; Martins, A. M.; Duarte, M. T. *J. Mol. Stuct.* **2012**, *1026*, 168−173.

(30) Deacon, G. B.; Junk, P. C.; Kelly, R. P. *Aust. J. Chem.* **2013**, *66*, 1288−1296.

(31) Bond valence analyses were performed for the M···F interactions in the crystal structures reported herein. The results are in accordance with the corresponding M···F distances and are presented as Supporting Information. (a) Brese, N. E.; O'Keeffe, M. *Acta Crystallogr.* **1991**, *B47*, 192−197. (b) Brown, I. D. *The Chemical Bond in Inorganic Chemistry: The Bond Valence Model*; Oxford University Press, 2002.

(32) Brauer, G. *Handbuch der Präparativen Anorganischen Chemie*; Ferdinand Enke Verlag: Stuttgart, 1975; pp 712−713.

(33) Aahman, J.; Somfai, P. *Synth. Commun.* **1995**, *25*, 2301−2303.

(34) Brady, E. D.; Hanusa, T. P.; Pink, M.; Young, V. G. *Inorg. Chem.* **2000**, *39*, 6028−6037.

(35) Vaartstra, B. A.; Huffman, J. C.; Streib, W. E.; Caulton, K. G. *Inorg. Chem.* **1991**, *30*, 121−125.

Fluoro- and Perfluoralkylsulfonyl-pentafluoroanilides: Synthesis and Characterization of New NH-Acids for Weakly Coordinating Anions and their Gas Phase and Solution Acidities

Julius F. Kögel,[1] Thomas Linder,[1] Fabian G. Schröder,[1] Jörg Sundermeyer,[1,*] Sascha K. Goll,[2] Daniel Himmel,[2] Ingo Krossing,[2,*] Karl Kütt,[3] Jaan Saame,[3] Ivo Leito[3,*]

[1]*Fachbereich Chemie der Philipps-Universität, Hans-Meerwein Straße, 35043 Marburg, e-mail: jsu@staff.uni-marburg.de*

[2]*Institut für Anorganische und Analytische Chemie, Freiburger Materialforschungszentrum (FMF) and Freiburg Institute for Advanced Studies (FRIAS), Section Soft Matter Science, Universität Freiburg, Albertstr. 19, 79104 Freiburg, Germany.*

[3]*University of Tartu, Institute of Chemistry, 14a Ravilastr, 50411 Tartu, Estonia.*

Abstract

The title compounds $HN(C_6F_5)(SO_2X)$ (X = F, CF_3, C_4F_9, C_8F_{17}) are a class of amides having two different strongly electron-withdrawing substituents attached to a nitrogen atom. They are NH-acids, the unsymmetrical hybrids of the well-known symmetrical bissulfonylimides and bispentafluorophenylamine. The syntheses and the structures of the perfluoroanilides, their solvates and some selected lithium salts give rise to a structural variety beyond the symmetrical parent compounds. The acidities of these novel NH-acids were investigated experimentally and quantum-chemically and we report here the gas phase acidities (GAs) as well as the pK_a values of a representative subset of these compounds in acetonitrile (MeCN) and DMSO solution. In quantum chemical investigations with the vertical and relaxed *COSMO* Cluster Continuum models (*vCCC*/*rCCC*), we encountered the unusual situation that the DMSO solvated acid Me_2SO--H-$N(SO_2CF_3)_2$ optimized in the gas phase (*vCCC* model), dissociated to Me_2SO-H^+--$N(SO_2CF_3)_2^-$ during structural relaxation and full optimization with the solvation model turned on (*rCCC* model). This proton transfer underlines the extremely high acidity of $HN(SO_2CF_3)_2$. The importance of this effect was studied for all acids in DMSO and MeCN solution. Usually this effect is less pronounced in MeCN and of higher importance in the more basic solvent DMSO. Nevertheless, the neglect of the structural relaxation upon solvation causes typical changes in the computational pK_a values of 1 to 4 orders of magnitude (4 to 20 kJ mol^{-1}). Our results provide evidence that the experimental DMSO pK_a value of

$HN(SO_2CF_3)_2$ should be rather interpreted as the pK_a of a $Me_2SO\text{-}H^+\text{--}N(SO_2CF_3)_2^-$ contact ion pair.

1. Introduction

Bis(trifluormethanesulfonyl)imide $HN(SO_2CF_3)_2$ (or shorter $HNTf_2$) was first described by *DesMarteau* in 1984.[1,2] Since then it has attracted most scientific interest among the NH-acidic compounds. Its extraordinary Brønsted acidity is caused by the two strongly electron-withdrawing triflyl (CF_3SO_2–, Tf–) moieties and has been examined in various theoretical and experimental works.[3-6] It provides applications in numerous Brønsted acid-catalyzed reactions like Diels-Alder reactions,[7] hetero-Michael additions,[8] cyclizations of siloxyalkynes with arenes and alkenes[9] or imine amidation reactions.[10] Due to its weakly coordinating nature the corresponding anion $[NTf_2]^-$ is widely used in imidazolium-,[11,12] pyrrolidinium-,[13,14] guanidinium-[15] or phosphonium-based[16] ionic liquids with low melting points which can serve as reaction media[17] or components of electrochemical devices.[18-21] Furthermore, $[NTf_2]^-$ can act as a ligand generating extremely electron-poor and therefore highly Lewis acidic metal centers that have been successfully tested in Lewis acid-catalyzed reactions.[22] Other applications of its metal complexes include the field of materials for gas absorption[23] or luminescent lanthanide complexes.[24-27] The related fluorosulfonylimide $HN(SO_2F)_2$ has also been a prominent subject of theoretical and electrochemical investigations.[28-30] Though being less acidic by more than ten orders of magnitude than both sulfonylimides, decafluorodiphenylamine $HN(C_6F_5)_2$ is another popular representative of the nitrogen acid family.[31,32] So far research has focused on its use as a weakly basic and sterically demanding amido ligand for transitions metals,[33-35] lanthanides[36] and main group metals.[37,38] The sterically demanding aryl substituents provide a shielding of the Lewis acidic metal centers and chelating coordination of the *ortho*-fluorine atoms can lead to an increase in the coordination number through secondary metal-fluorine contacts. Additionally, ionic liquids with the rather naked amide anion $[N(C_6F_5)_2]^-$ have been prepared and structurally characterized.[39]

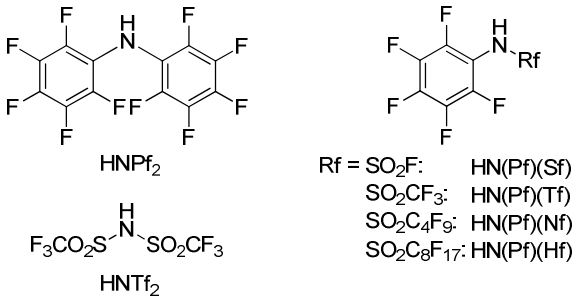

Figure 1. Symmetric and asymmetric NH-acids treated in this work.

This report is dedicated to the hybrids of both classes of NH-acids, namely $HN(C_6F_5)(SO_2Rf)$ (Rf = F, CF_3, C_4F_9, C_8F_{17}). For easier notation, the following abbreviations are used: C_6F_5 = Pf, SO_2F = Sf, SO_2CF_3 = Tf, $SO_2C_4F_9$ = Nf and $SO_2C_8F_{17}$ = Hf (Figure 1). The syntheses of these molecules are reported, their molecular structures as pure acid, as solvate or as lithium salts are presented and pK_a values in MeCN were experimentally determined. Additionally, the Gibbs solvation energies and pK_a values in MeCN and DMSO were also calculated with the high-level *vCCC / rCCC* models. Unusually the DMSO solvated $HNTf_2$ acid dissociated upon optimization in the solvent, and neglect of this effect led to a by 10 orders of magnitude erroneous pK_a value. Therefore, the importance of accounting for possible dissociation of the acid upon solvation during computations was studied for an exemplarily chosen set of systems in DMSO and MeCN. It should be noted that these investigations would have been impossible without the experimental input.

2. Results and Discussion

2.1 Synthesis and characterization of fluoro- and perfluoroalkylsulfonyl-pentafluoroanilides

2.1.1 Synthesis

Herein, we report on the full account of an optimized synthetic procedure to HN(Pf)(Tf) which in preliminary communications has been used as an anion-generating acid for various highly lipophilic ionic liquids[39] and thermally stable as well as electrochemically suitable lithium electrolyte systems.[41,42] The reaction of C_6F_5NHNa generated *in situ* from pentafluoroaniline and $NaN(SiMe_3)_2$ with $(CF_3SO_2)_2O$ gives the sodium salt NaN(Pf)(Tf) and one equivalent of sodium triflate.

If only one equivalent of the base $NaN(SiMe_3)_2$ instead of two is applied in this synthesis, the acidic product HN(Pf)(Tf) is quenching the nucleophile C_6F_5NHNa and as a result, the yield does not exceed the theoretical maximum of 50%. After protonation of this salt mixture with sulfuric acid followed by sublimation, the pure nitrogen acid is obtained as colorless solid. It is slightly hygroscopic and fuming in the air. The higher homologues with nonafluorobutyl and heptadecafluorooctyl chains, HN(Pf)(Nf) and HN(Pf)(Hf), are generated in analogous procedures using the sulfonylfluorides $C_4F_9SO_2F$ and $C_8F_{17}SO_2F$ as S-electrophiles. In case of HN(Pf)(Hf), protonation of the corresponding sodium salt is preferably carried out with *meta*-phosphoric acid prepared from mixing H_3PO_4 (85%) and P_4O_{10}. The less volatile the NH-acid, the more difficult is its isolation via distillation or sublimation free from traces of H_2SO_4 if 100% sulfuric acid is used as protonating agent. In general, we can recommend the use of *meta*-phosphoric acid as non-volatile protonation reagent superior to sulfuric acid to yield purest NH-acids, such as the known $HNTf_2$, from corresponding lithium or sodium salts. Conversion of pentafluoroaniline with chlorosulfuric acid and subsequent reaction with phosphorous pentachloride yields $HN(C_6F_5)(SO_2Cl)$.[43] The chlorine-fluorine exchange is now achieved by potassium fluoride in acetonitrile in the presence of 0.1 equivalents of 18-crown-6 followed by protonation of the generated potassium salt with hydrochloric acid in diethyl ether yielding HN(Pf)(Sf). The experimental procedures are shown in Scheme 1.

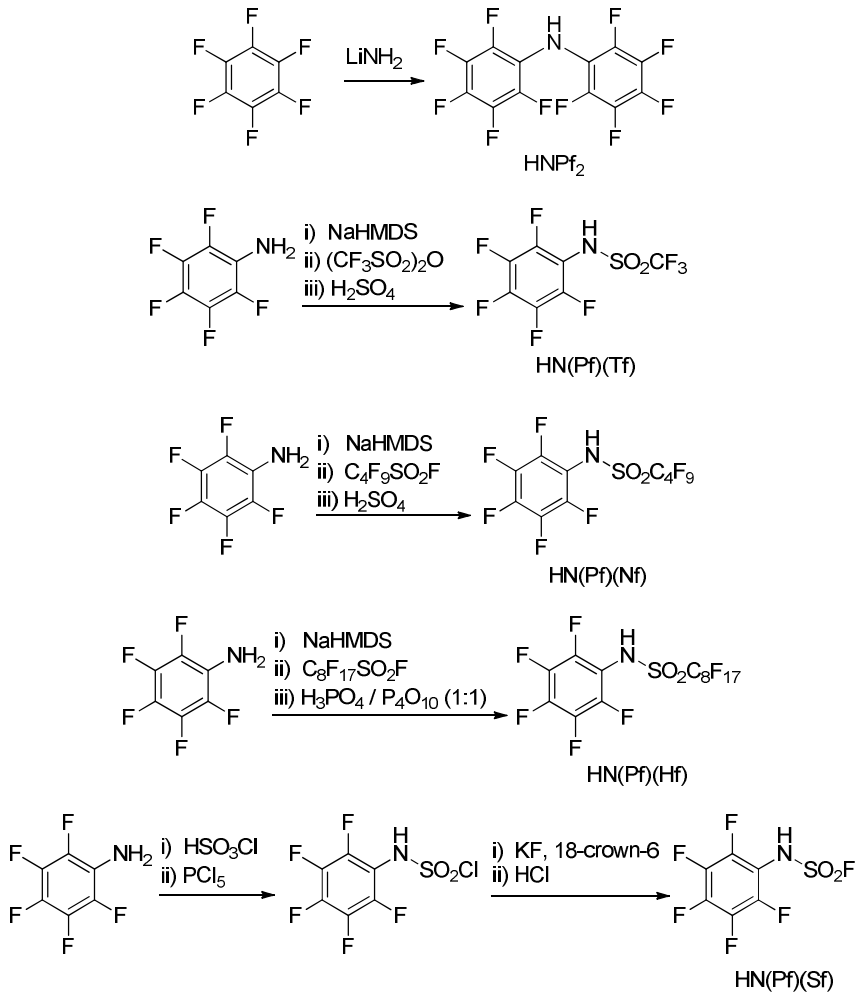

Scheme 1. Syntheses of pentafluorophenyl-substituted NH-acids.

For the chemical shifts of the nitrogen acids' acidic protons, a strong solvent dependency is observed in the proton NMR spectra. In the ^{13}C NMR spectra, carbon-fluorine coupling is found with typical ^{1}J(C,F)- and ^{2}J(C,F)-coupling constants. The ^{19}F NMR spectra show characteristic chemical shifts for the C_6F_5 moieties and the aliphatic fluorine atoms. The sulfur-bound fluorine atom in HN(Pf)(Sf) exhibits a considerable low-field shift of 54.2 ppm (471 MHz, C_6D_6, 25 °C). Furthermore, it seems worth mentioning that the CF_3 group in HN(Pf)(Tf) shows a coupling through space with the *ortho*-fluorine atoms of the C_6F_5 group with a coupling constant of 5.8 Hz.

Huber *et al.* reported the preparation of $LiNPf_2$, LiN(Pf)(Tf) and LiN(Pf)(Nf), which show interesting electrochemical properties and are discussed as components in lithium batteries.[44] LiN(Pf)(Hf) was prepared in an analogous procedure by the deprotonation of the corresponding NH-acid with $LiN(SiMe_3)_2$. In case of HN(Pf)(Sf), deprotonation experiments led to a nucleophilic attack of the nitrogen atom at the

SO_2F moiety of another molecule under formation of lithium fluoride, which can be referred to the lability of the S-F bond (Scheme 2). The resulting product was characterized *via* (–)-ESI HRMS and XRD analysis (Figure 2).

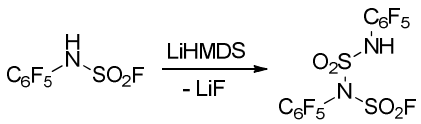

Scheme 2. Reaction of HN(Pf)(Sf) with $LiN(SiMe_3)_2$.

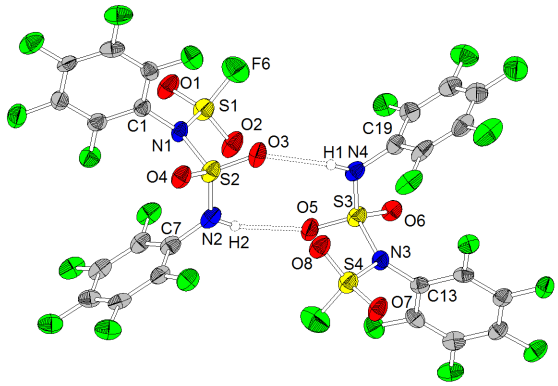

Figure 2. Molecular structure of the dimeric product obtained from the reaction between HN(Pf)(Sf) and $LiN(SiMe_3)_2$ (ellipsoids with 30% propability).

2.1.2 Structural Characterization

In the following section the molecular structures of the four novel NH-acids are described and light is shed on their intermolecular interactions, which are dominated by NHO-hydrogen bonds as well as π-contacts and T-shaped interactions of aromatic groups. Furthermore, molecular structures of the hydrate of HN(Pf)(Tf) and the lithium salt LiN(Pf)(Nf) are presented. Selected bond lengths and angles are summarized in Table 1.

Table 1. Selected bond lengths /pm and angles /° found in the molecular structures discussed herein.

	C-N	N-H	O-H	N-S	S-O	S-O	C-N-S
HN(Pf)(Sf)	141.8(2)	83(2)[1]	227(3)[2] 241(2)[2]	159.5(2)	140.8(1)[3]	141.3(1)[3]	120.5(1)
HN(Pf)(Tf)	142.1(4)	82(4)	210(4)	159.6(3)	141.6(3)	142.6(2)[3]	123.2(2)
HN(Pf)(Nf)	142.0(4) 142.2(4)	82(2)[1] 84(2)[1]	217(2) 206(2)	160.5(3) 160.3(3)	141.3(2) 140.9(2)	142.6(2)[3] 142.3(2)[3]	125.5(2) 123.3(2)
HN(Pf)(Hf) · C_7H_8	143.3(5)	86(5)	205(5)	161.5(6)	141.6(4)	143.6(4)[3]	120.9(3)
HN(Pf)(Tf) · H_2O	142.0(4) 143.0(4)	185(4) 195(4)	108(4)[4] 109(4)[4]	153.0(3) 154.8(3)	142.7(3)[3] 144.6(3)[3]	143.5(3)[3] 143.4(2)[3]	120.3(2) 119.0(2)
LiN(Pf)(Nf) · 2THF	139.5(4)	-	-	152.2(3)	143.7(3)	145.0(3)	121.0(2)

[1]N-H bond lengths set during refinement by DFIX command. [2]Nitrogen atom acts as hydrogen bond donor for the oxygen atoms of two neighboring molecules. [3]Oxygen atom acting as hydrogen bond acceptor. [4]O5-H1 and O6-H4.

The nitrogen acids reported herein exhibit similar values concerning equivalent bond lengths and angles. C-N distances range from 141.8(2) pm (HN(Pf)(Sf)) to 143.3(5) pm (HN(Pf)(Hf)) and are slightly longer than in the symmetrical $HNPf_2$ (139.7(3) pm).[45] The N-S distances lie between 159.5(2) pm (HN(Pf)(Sf)) and 161.5(6) pm (HN(Pf)(Hf)) and are shorter than observed for the classical acid $HNTf_2$ (N-S 164.4(1) pm).[46] The S-C bond lengths (184.0(3) pm) in $HNTf_2$ are similar to the ones observed for HN(Pf)(Tf) (183.4(4) pm), HN(Pf)(Nf) (184.8(3) pm), HN(Pf)(Hf) (183.4(7) pm). The same is true for the S-O distances (140.1(2) pm and 141.7(2) pm in $HNTf_2$). As expected, oxygen atoms acting as hydrogen bond acceptors show slightly longer S-O bond lengths (e.g. 142.6(2) pm in HN(Pf)(Tf)) than oxygen atoms that are not involved in hydrogen bridges (e.g. 141.6(3) pm in HN(Pf)(Tf)).

HN(Pf)(Sf): Single crystals of HN(Pf)(Sf) were obtained by sublimation at 65 °C and $1.8 \cdot 10^{-2}$ mbar. The low steric demand of the SO_2F moiety allows the nitrogen atom to act as a hydrogen bridge donor for two oxygen atoms of two vicinal molecules (Figures 3 and 4). Thus, double strands held together by hydrogen bridges and π-interactions of the C_6F_5 moieties are formed. The N-S and the S-F bonds (N1-S1 159.5(2) pm, S1-F6 156.1(1) pm) exhibit similar lengths as observed for $HN(C_6H_5)(Sf)$ (N-S 158.7(3) pm, S-F 156.14(19) pm).[47] The symmetrical $HN(Sf)_2$ shows a longer N-S distance (162.7(3) pm) and a shorter S-F bond (153.3(2) pm).[29]

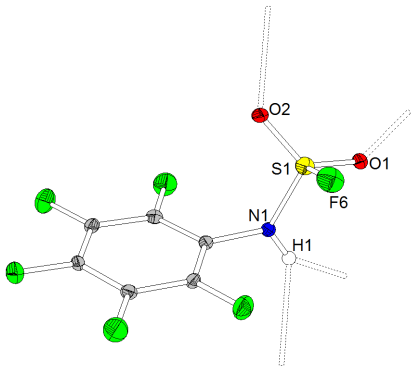

Figure 3. Molecular structure of HN(Pf)(Sf) (ellipsoids with 30% propability). Selected bond lengths /pm and angles /°: C6-N1 141.8(2), N1-S1 159.5(2), S1-O1 140.8(1), S1-O2 141.3(1), S1-F6 156.1(1), C6-N1-S1 120.5(1), O1-S1-O2 123.4(7).

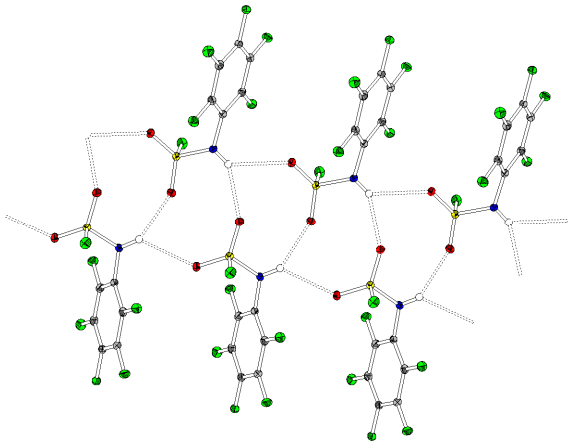

Figure 4. Double strands observed in the solid state structure of HN(Pf)(Sf).

HN(Pf)(Tf): Single crystals of HN(Pf)(Tf) were obtained by slow sublimation. In contrast to HN(Pf)(Sf), no double strands, but only one-dimensional chains connected *via* NHO-hydrogen bonds are observed (Figures 5 and 6). Within a chain, the aromatic rings of two neighboring molecules always lie on opposite sides of the chain so that the C_6F_5 moieties are each vicinal to two CF_3 groups. Vicinal chains are linked *via* T-shaped interactions of pentafluorophenyl groups in a staircase-like manner.

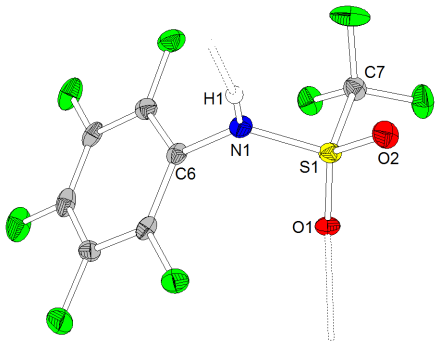

Figure 5. Molecular structure of HN(Pf)(Tf) (ellipsoids with 30% propability). Selected bond lengths /pm and angles /°: C6-N1 142.1(4), N1-S1 159.6(3), S1-O1 142.6(2), S1-O2 141.6(3), S1-C7 183.4(4), C6-N1-S1 123.2(2), O1-S1-O2 122.9(1).

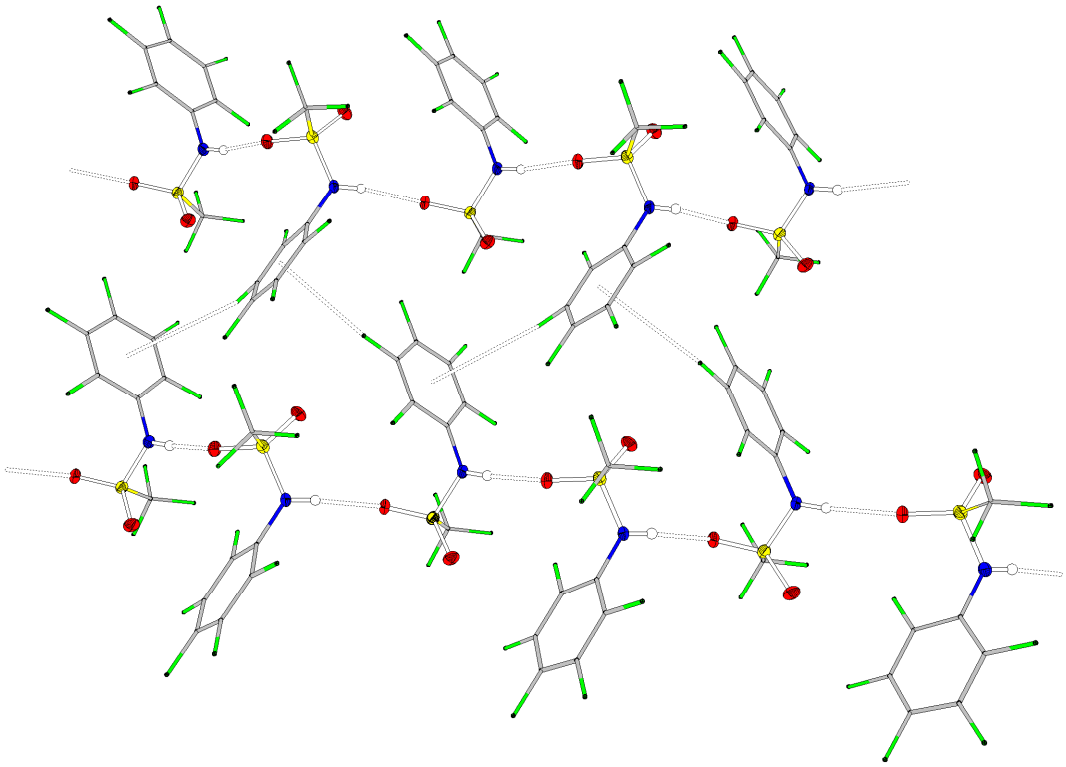

Figure 6. Interactions of one-dimensional HN(Pf)(Tf) chains *via* T-shaped interactions of C_6F_5 moieties.

HN(Pf)(Nf): Single crystals of HN(Pf)(Nf) were obtained by sublimation at 50 °C and $5 \cdot 10^{-2}$ mbar. The hydrogen bond network is similar to the one observed for HN(Pf)(Tf) (Figures 7 and 8). T-shaped interactions between the aromatic rings are observed within the one-dimensional chains.

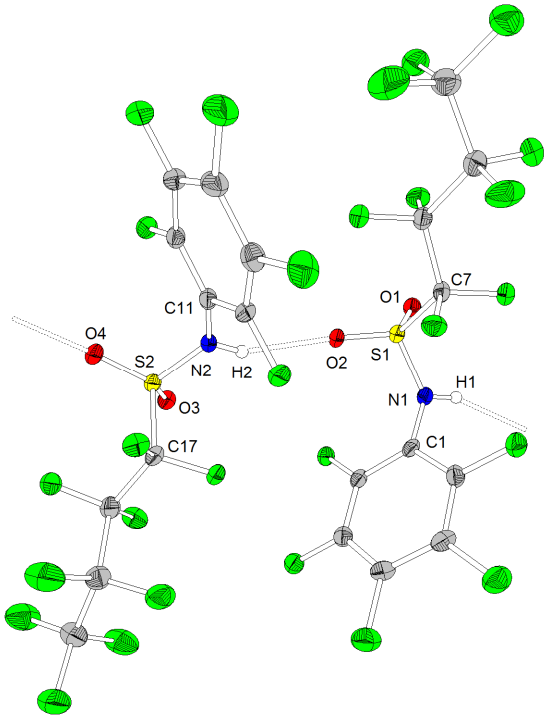

Figure 7. Molecular structure of HN(Pf)(Nf) (ellipsoids with 30% propability). Selected bond lengths /pm and angles /°: C1-N1 142.0(4), N1-S1 160.5(3), S1-O1 141.3(2), S1-O2 142.6(2), S1-C7 184.8(3), C6-N1-S1 125.5(2), O1-S1-O2 122.8(1), C11-N2 142.2(4), N2-S2 160.3(3), S2-O3 140.9(2), S2-O4 142.3(2), S2-C17 184.8(3), C11-N2-S2 123.3(2), O3-S2-O4 123.2(1).

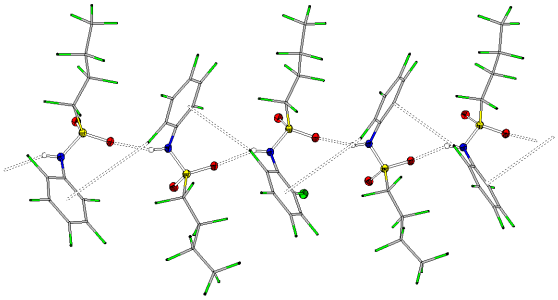

Figure 8. T-shaped interactions between vicinal C_6F_5 moieties within one-dimensional HN(Pf)(Nf) chains.

HN(Pf)(Hf)·C_7H_8: HN(Pf)(Hf)·C_7H_8 was crystallized as colorless needles by cooling a saturated solution in toluene slowly to –30 °C. Hydrogen bridges are formed between the nitrogen atom and an oxygen atom of a neighboring HN(Pf)(Hf) molecule (Figures 9 and 10). On every side of the chain aromatic rings and alkyl groups are alternating, which allows van der Waals interactions between the C_8F_{17} tails of every second

molecule. The asymmetric unit contains one disordered toluene molecule showing π-interactions with a C_6F_5 moiety (angle between C_6F_5 plane and toluene plane: 6.1(2)°; distances of centroids: 368.54(4) pm and 373.46(4) pm).

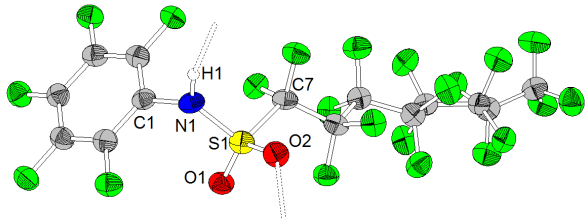

Figure 9. Molecular structure of HN(Pf)(Hf)·C_7H_8 (ellipsoids with 30% propability, toluene omitted for clarity). Selected bond lengths /pm and angles /°: C1-N1 143.3(5), N1-S1 161.5(6), S1-O1 141.6(4), S1-O2 143.6(4), S1-C7 183.4(7), C6-N1-S1 120.9(3), O1-S1-O2 122.9(2).

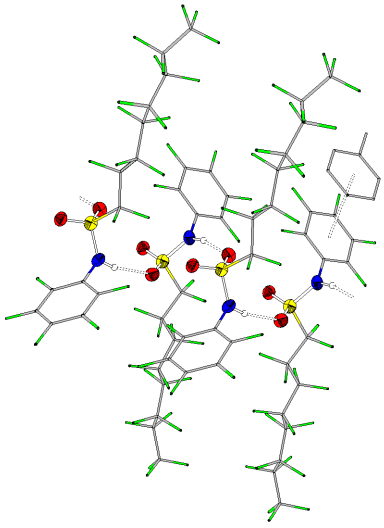

Figure 10. One-dimensional chains observed in the solid state structure of HN(Pf)(Hf)·C_7H_8. π-stacking between the toluene molecule and a C_6F_5 ring is observed.

HN(Pf)(Tf)·H_2O: The crystal structure points out that the acidity of the reported compounds is sufficient to protonate water (Figure 11). As observed for the lithium salt of HN(Pf)(Nf), the N-S distance in HN(Pf)(Tf)·H_2O (153.0(3) pm and 154.8(3) pm) is significantly shortened in comparison to the free acid (159.6(3) pm). This emphasizes the delocalization of the negative charge over the oxygen atoms. The water molecules are involved in a complex network of hydrogen bridges. Furthermore, π-contacts between C_6F_5 rings play a role in intermolecular interaction (distance between centroids: 402.8(8) pm, angle between planes of the phenyl rings: 23.4(1)°).

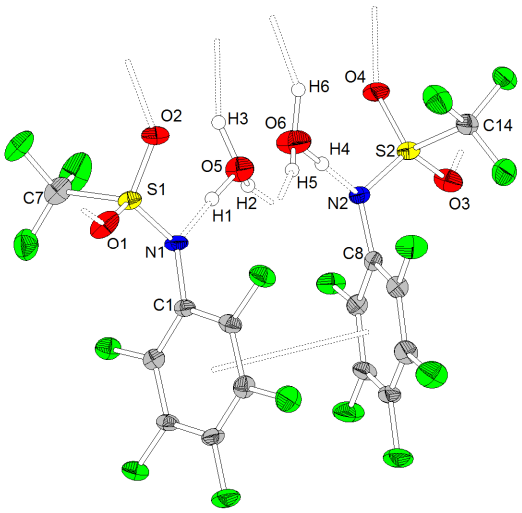

Figure 11. Molecular structure of HN(Pf)(Tf)·H_2O (ellipsoids with 30% propability). Selected bond lengths /pm and angles /°: C1-N1 142.0(4), N1-S1 153.0(3), S1-O1 142.7(3), S1-O2 144.6(3), S1-C7 183.7(4), C6-N1-S1 120.3(2), O1-S1-O2 117.3(2), C8-N2 143.0(4), N2-S2 154.8(3), S2-O3 143.5(3), S2-O4 143.4(2), S2-C14 183.2(3), C8-N2-S2 119.0(2), O3-S2-O4 117.8(1).

LiN(Pf)(Nf)·2THF: Single crystals of LiN(Pf)(Nf)·2THF were obtained from a solution of LiN(Pf)(Nf) in THF revealing a lithium atom coordinated in a distorted tetrahedral fashion by two THF molecules and the oxygen atoms of two neighboring N(Pf)(Nf) moieties (Figures 12 and 13). One-dimensional chains with the sequence Li-O-S-O with bond angles around the lithium atom ranging from 103.1(3)° to 126.0(3)° and Li-O distances between 191.6(7) pm and 195.5(7) pm are formed. Neighboring molecules point their C_4F_9 groups to the same side of the chain allowing van der Waals interactions. Coordination of the lithium atom by nitrogen atoms or short contacts between the lithium atom and aromatic fluorine atoms are not observed. The N-S distance in the lithium salt (152.2(3) pm) is significantly shorter than in the free acid (160.5(3) pm and 160.3(3) pm) emphasizing a stronger double bond character. In contrast to the linear chains observed for LiN(Pf)(Nf)·2THF, the related lithium salt $LiNPf_2$·THF forms dimers exhibiting short contacts between the lithium atom and two *ortho*-fluorine atoms of vicinal C_6F_5 groups.[37]

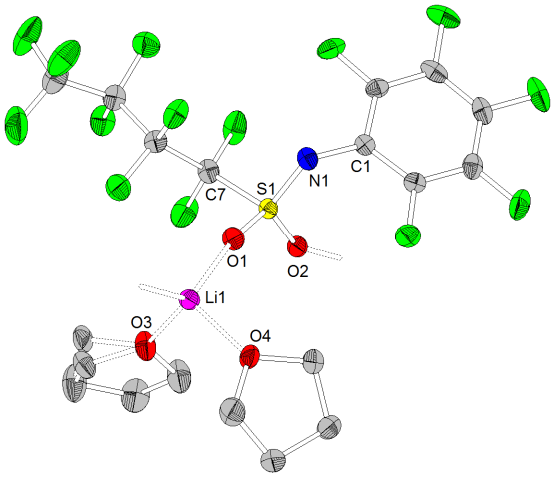

Figure 12. Molecular structure of LiN(Pf)(Nf)·2THF (ellipsoids with 30% propability, hydrogen atoms omitted for clarity). Selected bond lengths /pm and angles /°:C1-N1 139.5(4), N1-S1 152.2(3), S1-O1 143.7(3), S1-O2 145.0(3), S1-C7 185.9(4), Li1-O1 191.6(7), Li1-O2 195.5(7), Li1-O3 192.3(5), Li1-O4 192.7(8), C6-N1-S1 121.0(2), O1-S1-O2 116.0(1), O1-Li1-O2 126.0(3), O1-Li1-O3 105.6(3), O1-Li1-O4 105.8(3), O2-Li1-O3 107.4(3), O2-Li1-O4 106.8(3), O3-Li1-O4 103.1(3).

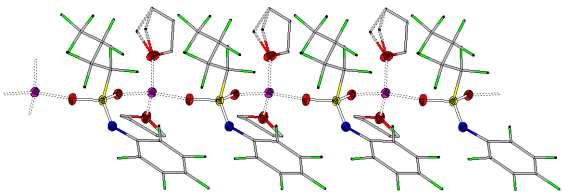

Figure 13. One-dimensional chains formed by LiN(Pf)(Nf)·2THF (including the disorder of one THF molecule).

2.2 Investigation of the Acidity of the NH-Acids

In the following we analyze the acidity of the new acids in comparison to the known symmetric $HNTf_2$ and $HNPf_2$ acids on experimental and computational grounds.

2.2.1 Background to the Acidity Measures

Gas Phase Acidities GA: The gas phase acidity (GA) of an acid H-A is given by its *Gibbs* energy of dissociation ($\Delta_r G^o$) or the gas-phase basicity (GB) of the conjugated base [equation (1)] and strong acids have low GA values. A large collection of GA /

GB values exists in the literature[3,48-67] that have been obtained by experimental techniques like FT-ICR-MS and / or quantum chemical procedures.

$$\text{H-A} \xrightarrow[\substack{= GA(H\text{-}A)\\ = GB(A^-)}]{\Delta_r G^\circ} H^+ + A^- \qquad (1)$$

In this work, we calculated the GA values of the acids $HNPf_2$, HN(Pf)(Tf), HN(Pf)(Nf) and HN(Pf)(Sf) using isodesmic proton exchange reactions based on an initially at the high-level $G3_{mod}$ calculated[40] GA value of $HNTf_2$.

Calculated pK_a Values: In solution the pK_a value serves as a measure for the acidity of an acid in a given medium. As specified in some recent reviews,[68-71] tremendous effort has been made to predict pK_a values computationally, mainly in aqueous solution. Some exemplarily selected examples are given here.[72-75] In our work we focused on calculating pK_a values in DMSO and MeCN solution.[66,76-101] As a standard for the *ab initio* pK_a calculations, combinations of high quality GA calculations or experimental values with continuum solvent models[102-104] were applied. To improve the obtained results, solvent molecules have to be taken into account explicitly for the dissociation of the acid, for example in the cluster-continuum model[73,105] or the implicit-explicit solvent approach.[74] In this work we employed the recently introduced *rCCC* model[40] coupled with the anchor points[40] of the newly established unified pH scale[106] to predict the pK_a values of the four investigated acids in DMSO and MeCN solution.

2.2.2 Experimental pK_a-Values in MeCN

The UV-Vis spectrophotometric titration method used in this work was described in detail.[107] For each investigated compound, the relative acidity and basicity were measured against at least two (mostly three) different reference compounds with known pK_a values in MeCN.[5,107] To determine the relative acidity of two compounds, a mixture of two different acids was titrated with UV-Vis radiation non-absorbing acidic (solution of triflic acid in MeCN) and basic (solution of phosphazene *t*Bu-N=P(pyrr)$_3$ in MeCN) titrants to obtain several spectra of solutions containing both

neutral and anionic forms of the two acids in different proportions. Both of the acids were also titrated separately to obtain the spectra of the neutral and anionic forms of the pure compounds. From the titration data, the relative acidity of the acids – the difference between their pK_a values (ΔpK_a values) – was calculated.[107] All the compounds investigated in this work have different spectra of protonated and deprotonated forms in the UV region and calculation methods using only spectral data obtained from the titration of pure compounds and mixture were used to obtain ΔpK_a values. From each titration experiment of the mixture of two compounds, the ΔpK_a value was determined as the mean of 8–20 values. Concentrations of the measured compounds were mostly in the order of $n \cdot 10^{-5}$ M to $n \cdot 10^{-4}$ M, while concentrations of acidic and basic titrants were in the $n \cdot 10^{-3}$ M range.

From the ΔpK_a values of measurements carried out in this work and from the absolute pK_a values assigned to the reference compounds in previous works,[5,107] the absolute pK_a values of the investigated compounds were obtained as presented in Table 2.

Table 2. Results of pK_a measurements in MeCN.

Acid (A)	Reference acid (Ra)[a]		ΔpK_a	pK_a (A)	Assigned pK_a (A)
	Identity	pK_a (Ra)			
$HNPf_2$	$(4\text{-Me-}C_6F_4)_2CHCN$	22.80	–1.17	23.97	23.97
	9-COOMe-Fluorene	23.53	–0.44	23.97	
	Fluoradene	23.90	–0.06	23.96	
HN(Pf)(Tf)	Picricacid	11.00	–0.41	11.41	11.43
	$4\text{-H-}C_6F_4CH(CN)_2$	12.98	1.52	11.46	
	$(4NC_5F_4)_2CHCN$	13.46	1.89	11.57	
HN(Pf)(Nf)	$4\text{-H-}C_6F_4CH(CN)_2$	12.98	1.81	11.17	11.22
	Picricacid	11.00	–0.21	11.21	
	$C_6(CF_3)_4CH(CN)_2$	10.45	–0.78	11.23	
HN(Pf)(Hf)	Picricacid	11.00	–0.21	11.21	11.22
	$C_6(CF_3)_4CH(CN)_2$	10.45	–0.79	11.24	
	$4\text{-H-}C_6F_5CH(CN)_2$	12.98	1.65	11.33	

[a] pK_a values of the reference acids are from refs 106 and http://dx.doi.org/10.1021/jo702513w.

2.2.3 Computational Analysis:

Methodology to calculate pK_a values in MeCN/DMSO: Similar to the scheme introduced to determine anchor points[40] for the *Gibbs* solvation energies of the proton *inter alia* in DMSO and MeCN, the pK_a values of an acid H-A in DMSO and MeCN solution may be calculated using the following *Born-Fajans-Haber* cycle (*BFHC 1*) (Scheme 2) (for energy and pK_a values see Table 4 below):

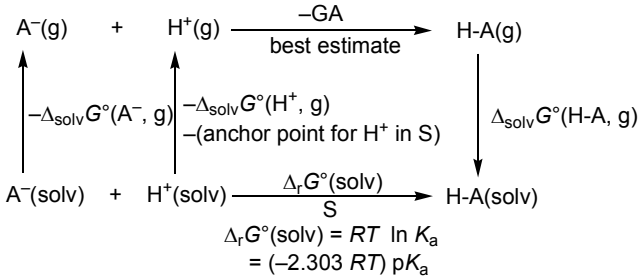

Scheme 2. *BFHC 1* for the calculation of the pK_a value of an acid H-A in a solvent S.

With the known[40] anchor points $\Delta_{solv}G°$ (H^+, g→S) (–1119.6 kJ mol^{-1} for DMSO and –1056.3 kJ mol^{-1} for MeCN), we only had to evaluate the GA values (chapter 2.2.3.2, Table 4) as well as the *Gibbs* solvation energies of the anions A^- and the corresponding acids H-A (Table 4, *BFHC*s in chapter 4 of the SI). Here we also had to take into account a possible further coordination of solvent molecules to the acids H-A as well as the corresponding anions A^-. For H-A or for A^- this can be done according to the following *BFHC 2* and a subsequent evaluation of their *Gibbs* solvation energies with the *Gibbs* solvation energies calculated for the isolated H-A or A^- monomers.

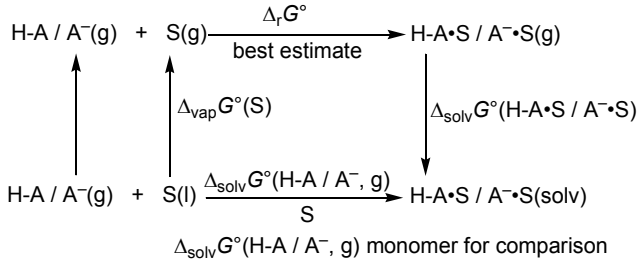

Scheme 3. *BFHC 2* for the calculation of *Gibbs* solvation energy of an anion A^- or an acid H-A, each coordinated to a solvent molecule S.

For the above *BFHC 2* (Scheme 3) we extracted the *Gibbs* vaporization energies $\Delta_{vap}G°$(S) (17.7 kJ mol^{-1} for DMSO and 5.3 kJ mol^{-1} for MeCN) from experimental vapor pressures (8×10^{-4} bar for DMSO[108] and 0.118 bar for MeCN[109]). The *Gibbs*

gas phase reaction energies for the coordination of the solvent S to H-A / A^- and the *Gibbs* solvation energies of the aggregates H-A•S / A^-•S were calculated (see below, cf. S-Tables 2/3, *BFHC*s in chapter 4, E.S.I.).

Assessment of the GA values: To calculate GAs with good accuracy, we recently established the modified G3 method ($G3_{mod}$),[40] which unfortunately is too "expensive" for the larger of the here investigated acids: We barely managed to calculate the GA of $HNTf_2$ with this method. Therefore, after an extensive method validation with experimental literature GA values (1198.7 kJ mol^{-1} for $HNTf_2$[59] and 1324.2 kJ mol^{-1} for $HNPf_2$[3]) as benchmark (chapter 1,E.S.I.), we applied isodesmic reactions as a "cheaper" alternative to obtain reliable GAs for the acids HN(Pf)(Tf), HN(Pf)(Sf) and $HNPf_2$ ($G3MP2_{mod}$ → $G3_{mod}$, see S-Figure 1 in the SI). For the largest system HN(Pf)(Nf) we had to use the isodesmic approximation twice (M1 → $G3MP2_{mod}$ → $G3_{mod}$ with M1 = MP2(FC)/aug-cc-pVTZ//B3LYP/aug-cc-pVTZ, see S-Figure 1,E.S.I.), an approach we call isodesmic squared (isodesmic^2).

From the results collected in S-Table 1 (E.S.I.), we estimate an error bar of around 5-8 kJ mol^{-1} for the GA values obtained through the isodesmic respectively isodesmic^2 approach and calculated "best estimates" of the GA from the most acidic $HNTf_2$ (1197.7 kJ mol^{-1}) over HN(Pf)(Nf) (1251.3 kJ mol^{-1}), HN(Pf)(Tf) (1260.3 kJ mol^{-1}) and HN(Pf)(Sf) (1273.5 kJ mol^{-1}) to the least acidic $HNPf_2$ (1328.7 kJ mol^{-1}) with our selected reference methods (collected in Table 4 below).

Gibbs energies of the gas phase reaction of H-A / A^- with MeCN or DMSO: For the determination of the *Gibbs* gas phase reaction energies of the coordination of the solvent S to H-A / A^- we employed the isodesmic^2 approach (for H-A = $HNPf_2$, HN(Pf)(Tf), HN(Pf)(Nf), HN(Pf)(Sf) respectively A^- = $N(Pf)(Tf)^-$, $N(Pf)(Nf)^-$) or the isodesmic method for H-A = $HNTf_2$ and A^- = NTf_2^-, NPf_2^-. In the special case of A^- = $N(Pf)(Sf)^-$ we used a directly calculated $G3MP2_{mod}$ value for the coordination of MeCN and an isodesmic^2 value for the coordination of DMSO (cf. S-Tables 2/3, explanations and *BFHC*s in chapter 2-4, E.S.I.).

Gibbs solvation energies of the acid-solvent aggregates H-A•S and the anion-solvent aggregates A^-•S: We calculated *Gibbs* solvation energies with COSMO@BP86/def-TZVP for the solvents[110] MeCN (with ε_r = 36.64) and DMSO (ε_r = 46.7) and compared the values of the recently established vertical or relaxed *COSMO* Cluster Continuum models (*vCCC* / *rCCC*).[40] Vertical and relaxed *CCC* differ in the inclusion of solvation: with the *vCCC* model only a single point is done on the gas phase structure, while in the *rCCC* the gas phase structure is optimized with *COSMO*@BP86/def-TZVP in C_1 symmetry.

Ionization of $HNTf_2$•DMSO: We discovered an amazingly large decrease of the *Gibbs* solvation energy of $HNTf_2$•DMSO in DMSO, when changing from the *vCCC* to the *rCCC* model ($\Delta_{solv}G°(rCCC) - \Delta_{solv}G°(vCCC)$ = –54.5 kJ mol^{-1}). This would be commensurate to an increase of –54.5/–5.71 = 9.5 pK_a units upon changing from vertical to relaxed structures (ΔpK_a = 1 corresponds to RT ln 0.1 = –5.71 kJ mol^{-1} at 298.15 K)[40,106] – neglecting the small energy differences between the *vCCC* and the *rCCC* model at other parts of the *BFHC*s. Looking at the respective structures reveals a hitherto to our knowledge not encountered phenomenon: The DMSO adduct of $HNTf_2$ ionizes during optimization with *COSMO*@BP86/def-TZVP yielding a contact ion pair with transfer of the proton from N to O. Thus, *d*(N-H) is elongated from 110.0 pm with the *vCCC* to 157.9 pm (*rCCC*); *d*(H-O) is shortened from 151.7 pm (*vCCC*) to 104.9 pm (*rCCC*) (Figure 14).

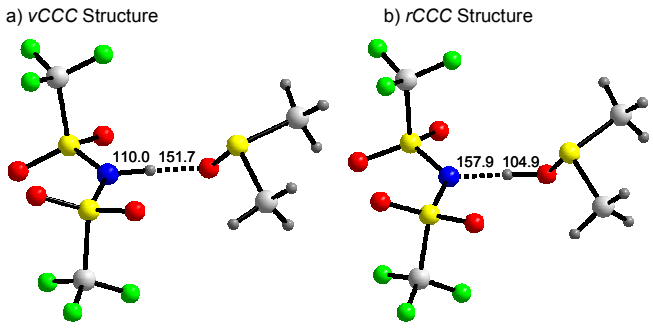

Figure 14. Calculated structures of the DMSO-solvates of the $HNTf_2$ acid optimized in the gas phase (*vCCC* model, a, left) and in DMSO solution (*rCCC model*, b, right). Distances in pm. One notes the transfer of the proton from the N to the O-(DMSO) atom upon inclusion of solvation.

To exclude that the phenomenon can be assigned solely to an influence of the functional or the basis set, we also employed *COSMO*@B3LYP/aug-cc-pVTZ. The

observed effect is even larger here with an energy decrease of –68.1 kJ mol^{-1} from *vCCC* to *rCCC*, a corresponding elongation of *d*(N-H) from 106.9 pm (*vCCC*) to 170.0 pm (*rCCC*) and a shortening of *d*(H-O) from 158.5 pm (*vCCC*) to 100.9 pm (*rCCC*). To eliminate also the possibility of a *COSMO* artifact, we transferred the *vCCC* and *rCCC* methodology to the PCM model by performing a PCM@BP86/TZVP single point in DMSO based on the BP86/def-TZVP optimized gas-phase structure of $HNTf_2$•DMSO and a PCM@BP86/TZVP full optimization in DMSO. The obtained results confirm our previous studies accompanied by an energy decrease during optimization of –41.9 kJ mol^{-1} and an optimized structure with 154.7 pm for *d*(N-H) and 106.1 pm for *d*(H-O). Thus, the magnitude of the effect is similar to *COSMO*.

Investigation of the other solvates H-A•S: We then decided to systematically examine the behavior of the MeCN and DMSO adducts of all the investigated acids upon optimization with *COSMO* (see Table 3 below). For the adducts of the more basic DMSO solvent we found a more pronounced trend towards "ionization" during optimization that led to a larger decrease of the *Gibbs* solvation energies from the *vCCC* to the *rCCC* model, and from $HNPf_2$ over HN(Pf)(Tf), HN(Pf)(Nf) and HN(Pf)(Sf) to $HNTf_2$. This order also corresponds to increased acidity according to the GA values of the respective acids with HN(Pf)(Sf) as an anomaly.

Some words of caution have to be mentioned: Apart from $HNTf_2$•DMSO the developing ionization does not lead to real contact ion pairs. But there are significant energetic and structural changes. For HN(Pf)(Sf)•DMSO the change of the N-H / H-O bonds from *vCCC* to *rCCC* amounts to +4.4 / –15.5 pm and the change of the *Gibbs* solvation energy value to –20.0 kJ mol^{-1}. Similar values were calculated for HN(Pf)(Nf)•DMSO (N-H / H-O change: +3.6 / –13.5 pm; energy change: –15.0 kJ mol^{-1}) and HN(Pf)(Tf)•DMSO (+3.2 / –11.8 pm and–12.9 kJ mol^{-1}). The smallest alterations showed the DMSO adduct of the weakest acid $HNPf_2$ (+1.0 / –6.4 pm and –4.2 kJ mol^{-1}). For the adducts of the other acids and the much less basic solvent MeCN the "ionization" effect is only marginal. Here overall small elongations of the (acid)N-H bond and a small decrease of the *Gibbs* solvation energy values, but a relatively large shortening of the H--NCMe bond were observed (from –4.6 pm at $HNPf_2$•MeCN to –12.1 pm at $HNTf_2$•MeCN). The structural and energetic changes are collected in Table 3.

Table 3. Bond lengths of the hydrogen bond of the acid-solvent adducts optimized in the gas phase (*vCCC* model) and in solution (*rCCC* model). Changes of the *Gibbs* solvation energies from *vCCC* to *rCCC*.

Investigated species	(acid)**N-H** bond		**H-N**CMe bond		*vCCC*→ *rCCC*
MeCN adducts	***vCCC*** **[pm]**	***rCCC*** **[pm]**	***vCCC*** **[pm]**	***rCCC*** **[pm]**	$\Delta(\Delta_{solv}G°)$ **[kJ mol^{-1}]**
$HNTf_2$•MeCN	105.2	107.2	181.9	169.8	–4.6
$HNPf_2$•MeCN	103.1	103.5	198.8	194.2	–0.6
HN(Pf)(Tf)•MeCN	104.0	105.0	190.3	181.3	–4.6
HN(Pf)(Nf)•MeCN	103.8	105.0	191.2	181.7	–4.5
HN(Pf)(Sf)•MeCN	104.2	105.5	188.6	178.8	–5.6
	(acid)**N-H** bond		**H-O**(DMSO) bond		*vCCC*→ *rCCC*
DMSO adducts	***vCCC*** **[pm]**	***rCCC*** **[pm]**	***vCCC*** **[pm]**	***rCCC*** **[pm]**	$\Delta(\Delta_{solv}G°)$ **[kJ mol^{-1}]**
$HNTf_2$•DMSO	110.0	157.9	151.7	104.9	**–54.5**
$HNPf_2$•DMSO	104.4	105.4	176.3	169.9	–4.2
HN(Pf)(Tf)•DMSO	106.7	109.9	163.1	151.3	–12.9
HN(Pf)(Nf)•DMSO	106.9	110.5	162.8	149.3	–15.0
HN(Pf)(Sf)•DMSO	106.9	111.3	162.8	147.3	–20.0

Investigation of the A^-•S Solvates: When assessing the *Gibbs* solvation energies of the anion-solvent aggregates A^-•S, we did not discover any explicit contact ion pair formation comparable to $HNTf_2$•DMSO switching from the *vCCC* to the *rCCC* model, so we did not investigate the corresponding structures in detail. Nevertheless, the slight structural relaxation in the *rCCC* model is accompanied by changes of the *Gibbs* solvation energies that were in this case larger for the MeCN- than for the DMSO-adducts (up to –17.2 kJ mol^{-1} for $N(Pf)(Tf)^-$•MeCN; *BFHC*s, chapter 4, E.S.I.).

2.3 Discussion of the gas phase and solution acidity of the investigated acids

Our measured and calculated (*rCCC*) pK_a values are collected in Table 4. The calculated values differ at most by 3.1 units from the experimental values. This is within our estimated error bar of 20 kJ mol^{-1} respectively 20 / 5.71 = 3.5 pK_a units, mainly due to the residual error of the (*rCCC*) *Gibbs* solvation energies. *vCCC* values

dramatically lack structural relaxation in their solvation *Gibbs* energy and are only given for comparison in Table 4 but should not be used. The trends of the pK_a values in MeCN and DMSO show a similar sequence like the GA values, but for HN(Pf)(Tf), HN(Pf)(Nf) and HN(Pf)(Sf) (GA scatters over a range of 22.2 kJmol^{-1} respectively 22.2 / 5.71 = 3.9 pK_a units) nearly the same *rCCC* pK_a values in DMSO occur due to variations in *Gibbs* solvation energies of HN(Pf)(Tf) / (Pf)(Tf)$^-$ respectively of the corresponding solvent aggregates (see Scheme 2) compared to HN(Pf)(Nf) / (Pf)(Nf)$^-$ and / or HN(Pf)(Sf) / (Pf)(Sf)$^-$. Thus, the weakest asymmetric acid in the gas phase– HN(Pf)(Sf)– is in MeCN the most acidic of the three mixed acids HN(Pf)(Tf), HN(Pf)(Nf) and HN(Pf)(Sf) according to the calculations.

Table 4. pK_a values based on the *rCCC* model (bold type, *vCCC* values in bracketed italics only for comparison) of the five investigated acids in MeCN and DMSO as well as GA values [in kJ mol^{-1}] and all *rCCC Gibbs* solvation energies [in kJ mol^{-1}] (known anchor points for H^+, respectively, received from Scheme 2 for H-A, A^-) needed to calculate these pK_a values using Scheme1. Experimental pK_a and GA values, if available.

Acidity	**$HNTf_2$**	**$HNPf_2$**	**HN(Pf)(Tf)**	**HN(Pf)(Nf)**	**HN(Pf)(Sf)**
GA (exp.)	1198.7[59]	1324.2[3]			
GA (best estimate)	1197.7	1328.7	1260.3	1251.3	1273.5
a) Solvation with MeCN					
$\Delta_{solv}G°(H^+, g)$ (*rCCC*)	–1056.3	–1056.3	–1056.3	–1056.3	–1056.3
$\Delta_{solv}G°$(H-A, g) (*rCCC*)	–60.2	–35.6	–63.3	–63.6	–56.6
$\Delta_{solv}G°(A^-, g)$ (*rCCC*)	–216.9	–174.0	–211.8	–202.7	–223.9
pK_aMeCN (*rCCC*)	**–2.7**	**23.5**	**9.7**	**9.8**	**8.7**
pK_aMeCN (exp.)	**0.3[5]**	**23.97**	**11.43**	**11.22**	**–**
[pK_aMeCN (vCCC)]	*[0.5]*	*[26.1]*	*[13.2]*	*[13.1]*	*[11.9]*
b) Solvation with DMSO					
$\Delta_{solv}G°(H^+, g)$ (*rCCC*)	–1119.6	–1119.6	–1119.6	–1119.6	–1119.6
$\Delta_{solv}G°$(H-A, g) (*rCCC*)	–130.0	–54.2	–76.8	–78.6	–80.1
$\Delta_{solv}G°(A^-, g)$ (*rCCC*)	–214.3	–180.6	–209.8	–201.1	–224.9
pK_a DMSO (*rCCC*)	**–1.1**	**14.5**	**1.3**	**1.6**	**1.6**
pK_a DMSO (exp.)	**2.0[111,112]**	**12.6[113]**	**-**	**-**	**-**
[pK_a DMSO (vCCC)]	*[–8.8]*	*[15.7]*	*[1.0]*	*[0.9]*	*[0.3]*

For $HNTf_2$ a significant anomaly appeared, mainly due to the effect of contact ion pair formation in DMSO: The *rCCC* pK_a value in MeCN is lower than in DMSO due to the increase of 7.7 pK_a units[114] from the *vCCC* to the *rCCC* value in DMSO. The reason is that in the course of *rCCC* geometry optimization proton transfer occurs within the species $Me_2SO\cdots HNTf_2$ to give $Me_2SO\text{-}H^+\cdots NTf_2^-$. Using the latter species as the neutral acidic form leads to grossly underestimated acidity (overestimated pK_a value),

because our initial state is not the neutral $HNTf_2$ molecule any more but an ion pair, in which $HNTf_2$ is in fact already deprotonated. In other words, the *rCCC* pK_a value in DMSO is rather the dissociation constant of the contact ion pair than the acidity constant of $HNTf_2$.

This is also supported by observing the *rCCC* acidity change in the hypothetical row of transformations $HNPf_2$ → HN(Pf)(Tf) → $HNTf_2$. In MeCN, the pK_a changes corresponding to the two steps are around –14 and –12 pK_a units, respectively. In DMSO, however, –13 and –2.4. Given the generally very good correlation between pK_a values in MeCN and DMSO, it is difficult to see why the trends in this row of changes should be so different between the two solvents.

Interestingly, the *rCCC* pK_a of $HNTf_2$ in DMSO is in agreement with the experimentally determined acidity. There is, however, strong reason to believe that the experimental pK_a value of $HNTf_2$ in DMSO of 2.0 is several orders of magnitude too high for the pK_a of "molecular" $HNTf_2$. This value has been obtained using potentiometric titration and the actual presence of the molecule $HNTf_2$ in solution was not monitored in any way. The dangers of pK_a determination of strong acids in DMSO whereby the protonated form of the acid is actually not monitored in the solution have been discussed in a recent paper (http://dx.doi.org/10.1002/anie.201303605).

Thus, we conclude it was actually the $Me_2SO\text{-}H^+\cdots NTf_2^-$ contact ion pair that was titrated.

Such a contact ion pair formation in DMSO solution may also explain observations by Kütt *et al.*.[115] When they plotted pK_a values in MeCN against pK_a values in DMSO, there were two significant outliers, namely the strong acids 4-Me-$C_6H_4SO_3H$ and $C_6H_5CH(SO_2CF_3)_2$ with deviations of –4.6 respectively –6.4 pK_a units in MeCN.

The *vCCC* pK_a value of $HNTf_2$, however, fits very well with the above discussed trend of acidity change from $HNPf_2$ to $HNTf_2$. Indeed this *vCCC* pK_a can be interpreted as the pK_a of a "$HNTf_2$ molecule in DMSO". But as this exists only in silico, but not in real DMSO, also its pK_a is a hypothetical one.

Overall we found a much lower range of acidities in DMSO compared to MeCN. Similar to the difference of the absolute acidities at equal pH in MeCN and DMSO of 11.1 pH_{abs} units ($\Delta(\Delta_{solv}G°(H^+$ in S): –1056.3 + 1119.6 = 63.3 kJ mol^{-1}; in logarithmic

units: 63.3/5.71 = 11.1pH_{abs} units), the difference between the pK_a values in MeCN and DMSO at the *rCCC* level is 9.0 for $HNPf_2$, it decreases over HN(Pf)(Tf) (8.4), HN(Pf)(Nf) (8.2) and HN(Pf)(Sf) (7.1) to $HNTf_2$ (–1.6, with full formation of a contact ion pair in DMSO). This is mainly attributed to the increase of contact ion pair formation in DMSO. Our computations and the above reasoning provide strong evidence that the anomalously high experimental DMSO pK_a value of Tf_2NH (and possibly other strong acids, such as TfOH) is in fact the dissociation constant of a contact ion pair.

3. Conclusion/Outlook:

We described a family of perfluorinated sulfonylanilides with a tunable acidity and lipophilicity depending on the length of the perfluoroalkyl chain. Due to the asymmetric nature of their anions, their anion polarizabilities and ligand properties differ from those of the parent symmetric NH-acids $HNTf_2$ and $HNPf_2$. This opens new perspectives in the design of thermally stable Lewis acids with weakly coordinating anions or thermally stable lithium electrolytes and ionic liquids with tunable anion properties.

The gas phase and solution acidities of these NH-acids were determined experimentally in MeCN, and computationally in the gas phase, in MeCN and DMSO solution. Experimental and calculated values generally agree well, with the exception of the interesting $HNTf_2$ / DMSO case: Here we encounter the transition from molecular to medium acidity when changing from the vertical *vCCC* to the relaxed *rCCC* model. That means with the vertical model, including the gas phase structure of the DMSO adduct of $HNTf_2$, we still describe the – attenuated – acidity of the molecular acid $HNTf_2$. If we allow structural relaxation during the optimization of the solvated adduct, a proton transfer occurs and now in the *rCCC* model, we describe the molecular acidity of protonated DMSO solvated by the NTf_2^- anion. This proton transfer signals that $HNTf_2$ in DMSO medium is a strong acid that allows to protonate the solvent. However, it implies that our *rCCC* calculated pK_a value of $HNTf_2$ in DMSO is not the pK_a of $HNTf_2$ but that of H-$DMSO^+[NTf_2]^-$ in DMSO.

4. Experimental Details

All reactions were carried out under inert atmosphere using standard Schlenk techniques. Moisture and air sensitive substances were stored in a conventional nitrogen-flushed glovebox. Solvents were purified according to literature procedures and kept under an inert atmosphere. Pentafluoroaniline (CHEMPUR), triflic acid anhydride (CHEMPUR), nonafluorobutylsulfonylfluoride (ALDRICH) and heptadecaoctylsulfonylfluoride (CHEMPUR) were purchased from commercial sources. Sodium bis(trimethylsilyl)amide,[116] lithium bis(trimethylsilyl)amide[116] and $HN(C_6F_5)(SO_2Cl)$[43] were prepared according to literature procedures.

Spectra were recorded on the following spectrometers: NMR: BRUKER ARX300, BRUKER DRX400, BRUKER DRX500; IR: ATR-FT-IR; MS: LTQ-FT or QStarPulsari (FINNIGAN); elemental analysis: CHN-Rapid (HERAEUS).

Synthesis of HN(Pf)(Tf): A solution of 2,3,4,5,6-pentafluoroaniline (8.86 g, 48.34 mmol) in diethylether (20 mL) was added to a solution of sodium bis(trimethylsilyl)amide (17.75 g, 96.80 mmol) in diethylether (100 mL) at -78 °C. The resulting solution was brought to 0 °C and stirred at this temperature for 2 h. The reaction mixture was cooled again to -78 °C and a precooled solution of (8.14 mL, 48.34 mmol) triflic acid anhydride in diethylether (50 mL) was added slowly to the reaction mixture *via* a cannula. The reaction mixture was slowly brought to room temperature and stirred for 12 h. All volatiles were removed *in vacuo* at 50 °C. The colorless residue was suspended in $CFCl_3$ (100 mL) and the suspension was cooled to 0 °C. Then concentrated sulphuric acid (15 mL) was added and the mixture was refluxed for two additional hours. The phases were separated by decantation and the fluorous phase was stored at -30 °C which lead to the formation of colorless crystals. The precipitate was separated from the solution, dried *in vacuo*and finally sublimed (90 °C, $1.0 \cdot 10^{-2}$ mbar). This gave HN(Pf)(Tf) (10.45 g, 69%) as a white solid.

M.p. 56 °C; ^{1}H NMR (300 MHz, [D_6]DMSO, 25 °C, TMS): δ=12.33 ppm (s, 1H, NH); ^{13}C NMR (101 MHz, $CDCl_3$, 25 °C, TMS): δ=146.6-143.8 (m, ^1J(C,F) = 252.3 Hz, CF_{Ar}), 144.1-141.1 (m, ^1J(C,F) = 265.4 Hz, CF_{Ar}), 139.3-136.5 (m, ^1J(C,F) = 254.4 Hz, CF_{Ar}), 119.3 (q, ^1J(C,F) = 321.3 Hz, CF_3), 108.2 ppm (t, ^2J(C,F) = 17.1 Hz, *ipso*-C); ^{19}F NMR (346 MHz, $CDCl_3$, 25 °C, $CFCl_3$): δ=-77.0 (t, ^{ts}J(F,F) = 5.8 Hz, 3F, CF_3), -142.9 (d, ^3J(F,F) = 22.6 Hz, 2F, *o*-F), -149.7 (t, ^3J(F,F) = 21.4 Hz, 1F, *p*-F),

-160.1 ppm (t, ^{3}J(F,F) = 18.6 Hz 2F, *m*-F); IR (Nujol): $\tilde{\nu}$=631 (m), 681 (w), 895 (s), 986 (s), 1047 (s), 1119 (s), 1140 (w), 1159 (w), 1180 (s), 1205 (s), 1287 (s), 1317 (m), 1502 (m), 1520 (m), 1649 (w), 3219 cm^{-1} (br, N-H); MS (70 eV): m/z (%): 315 (8) [M^{+}], 182 (92) [$HNC_6F_5^{+}$], 155 (51) [$C_5F_5^{+}$], 69 (100) [CF_3^{+}]; elemental analysis calcd. (%) for $C_7HF_8NO_2S$: C 26.68, H 0.32, N 4.44; found: C 26.21, H 0.57, N 4.37.

Synthesis of HN(Pf)(Nf): A solution of 2,3,4,5,6-pentafluoroaniline (8.56 g, 46.77 mmol) in diethylether (20 mL) was added to a solution of sodium bis(trimethylsilyl)amide (17.15 g, 93.53 mmol) in diethylether (100 mL) at -78 °C. The resulting solution was brought to 0 °C and stirred at this temperature for 2 h. The reaction mixture was cooled again to -78 °C and a precooled solution of nonafluorobutylsulfonylfluoride (8.40 mL, 46.77 mmol) in diethylether (50 mL) was added slowly to the reaction mixture *via* a cannula. The reaction mixture was slowly brought to room temperature and stirred for 12 h. All volatiles were removed *in vacuo* at 50 °C. The colorless residue was suspended in $CFCl_3$ (100 mL) and the suspension was cooled to 0 °C. Then concentrated sulphuric acid (15 mL) was added and the mixture was refluxed for two additional hours. The phases were separated by decantation and the fluorous phase was evaporated to dryness *in vacuo*. The residue was sublimed (100 °C, $1.0 \cdot 10^{-2}$ mbar) to yield HN(Pf)(Nf) (18.18 g, 84%) as a white solid.

M.p. 73 °C; ^{1}H NMR (300 MHz, [D_6]DMSO, 25 °C, TMS): δ=13.24 ppm (s, 1H, NH); ^{13}C NMR (101 MHz, $CDCl_3$, 25 °C, TMS): δ=146.5-143.7 (m, ^{1}J(C,F) = 255.2 Hz, CF_{Ar}), 144.1-141.3 (m, ^{1}J(C,F) = 261.1 Hz, CF_{Ar}), 139.4-136.5 (m, ^{1}J(C,F) = 254.3 Hz, CF_{Ar}), 117.1 (tq, ^{1}J(C,F) = 288.4 Hz, ^{2}J(C,F) = 32.9 Hz, CF_3), 114.9 (tt, ^{1}J(C,F) = 300.4 Hz, ^{2}J(C,F) = 35.5 Hz, -CF_2-), 110.2 (tt, ^{1}J(C,F) = 270.0 Hz, ^{2}J(C,F) = 31.6 Hz, -CF_2-), 108.5 (t, ^{2}J(C,F) = 14.9 Hz, *ipso*-C), 108.3 ppm (tt, ^{1}J(C,F) = 270.5 Hz, ^{2}J(C,F) = 33.1 Hz, -CF_2-); ^{19}F NMR (376 MHz, $CDCl_3$, 25 °C, $CFCl_3$): δ=-81.1 (t, ^{3}J(F,F) = 9.8 Hz, 3F, CF_3), -111.6 – -111.4 (m, 2F, -CF_2-CF_3), -121.1 (br s, 2F, -CF_2-), -126.2 – -126.4 (m, 2F, -SO_2-CF_2), -142.7 – -142.9 (m, 2F, *o*-F), -150.1 (t, ^{3}J(F,F) = 21.4 Hz, 1F, *p*-F), -160.5 – -160.7 ppm (m, 2F, *m*-F); IR (Nujol): $\tilde{\nu}$=625 (m), 650 (m), 681 (w), 700 (w), 735 (m), 833 (w), 893 (s), 991 (s), 1053 (m), 1136 (s), 1209 (s), 1518 (m), 1629 (w), 3270 cm^{-1} (br, N-H); MS (70 eV): m/z (%): 465 (8) [M^{+}], 232 (8) [M^{2+}], 182 (100) [$HNC_6F_5^{+}$], 155 (30) [$C_5F_5^{+}$], 69 (52) [CF_3^{+}]; elemental

analysis calcd. (%) for $C_{11}HF_{14}NO_2S$: C 25.82, H 0.22, N 3.01; found: C 25.62, H 0.28, N 3.17.

Synthesis of HN(Pf)(Hf): A solution of 2,3,4,5,6-pentafluoroaniline (4.47 g, 24.4 mmol) in diethylether (20 mL) was added to a solution of sodium bis(trimethylsilyl)amide (4.47 g, 24.4 mmol) in diethylether (50 mL) at -78 °C. The resulting solution was brought to 0 °C and stirred at this temperature for 2 h. The reaction mixture was cooled again to -78 °C and a precooled solution of heptadecaoctylsulfonylfluoride (6.6 mL, 24.4 mmol) in diethylether (25 mL) was added slowly. The reaction mixture was brought to room temperature overnight and all volatiles were removed *in vacuo*. The brown residue was treated with a mixture of metaphosphoric acid and phosphorous pentoxide (1:1 (m/m)) (6 mL) and sublimed from the viscous mixture (140 °C, $1.0 \cdot 10^{-2}$ mbar) to yield HN(Pf)(Hf) (7.17 g, 43%) as an off-white solid.
M.p. 90 °C; ^{1}H NMR(400 MHz, [D_6]DMSO, 25 °C, TMS): δ=14.16 ppm (s, 1H, NH); ^{13}C NMR (101 MHz, C_6D_6, 25 °C, TMS): δ=145.0 (pd, ^1J(C,F) = 254.9 Hz, CF_{Ar}), 142.2 (pd, ^1J(C,F) = 251.5 Hz, *p*-C_{Ar}), 137.7 (pd, ^1J(C,F) = 251.2 Hz, CF_{Ar}), 117.5 (qt, ^1J(C,F) = 288.5 Hz, ^2J(C,F) = 32.9 Hz, CF_3), 115.4 (tt, ^1J(C,F) = 300.4 Hz, ^2J(C,F) = 35.2 Hz, SO_2CF_2), 114.5-107.9 ppm (m, CF_2 + *ipso*-C_{Ar}); ^{19}F NMR (376 MHz, [D_6]DMSO, 25 °C, $CFCl_3$): δ=-79.6 – -79.4 (m, 3F, CF_3), -113.2 – -112.9 (m, 2F, CF_2), -119.1 (br s, 2F, CF_2), -121.1 – -120.6 (m, 6F, CF_2), -121.7 (br s, 2F, CF_2), -125.1 – -124.9 (m, 2F, CF_2), -148.8 – -148.6 (m, 2F, *o*-F_{Ar}), -165.9 – -165.6 (m, 2F, *m*-F_{Ar}), -166.6 – -166.2 ppm (m, 1F, *p*-F); IR: $\tilde{\nu}$=444 (m), 481 (m), 516 (m), 549 (m), 601 (m), 618 (m), 657 (w), 694 (w), 738 (w), 747 (w), 852 (w), 888 (w), 992 (s), 1038 (m), 1125 (m), 1149 (s), 1187 (m), 1215 (m), 1370 (m), 1434 (m), 1516 (s), 3233 cm^{-1} (w, N-H); (–)-ESI-MS (CH_2Cl_2): m/z (%): 664 (100) [M-H^+], 181 (23) [M-$SO_2C_8F_{17}$]; HRMS ((–)-ESI (CH_2Cl_2)): m/z calcd. for $C_{14}F_{22}NO_2S^-$ 663.9304 [M-H^+]; found: 663.9293; elemental analysis calcd. (%) for $C_{14}HF_{22}NO_2S$: C 25.28, H 0.15, N 2.11, S 4.82; found: C 25.12, H 0.22, N 2.35, S 4.97.

Synthesis of LiN(Pf)(Hf): A solution of lithium bis(trimethylsilyl)amide (75 mg, 0.451 mmol) in toluene (5 mL) was added dropwise to a solution of HN(C_6F_5)($SO_2C_8F_{17}$) (300 mg, 0.451 mmol) in toluene (10 mL). Immediately a white solid precipitated. After stirring the suspension for 2 h at room temperature the

precipitate was separated by centrifugation, washed twice with hexane (15 mL) and dried *in vacuo*. LiN(Pf)(Hf) (258 mg, 85%) was obtained as an off-white solid.
^{13}C NMR (101 MHz, [D$_6$]DMSO, 25 °C, TMS): δ=142.9 (pd, ^1J(C,F) = 240.1 Hz, CF_{Ar}), 136.9 (pd, ^1J(C,F) = 244.1 Hz, CF_{Ar}), 134.8 (pd, ^1J(C,F) = 241.6 Hz, *p*-C_{Ar}), 123.4 (t, ^2J(C,F) = 15.2 Hz, *ipso*-C_{Ar}), 116.5 (qt, ^1J(C,F) = 288.4 Hz, ^2J(C,F) = 33.3 Hz, CF_3), 115.0 (tt, ^1J(C,F) = 293.6 Hz, ^2J(C,F) = 32.8 Hz, SO_2CF_2), 109.6 (tt, ^1J(C,F) = 239.9 Hz, ^2J(C,F) = 31.4 Hz, CF_2) 113.9-106.9 ppm (m, CF_2); ^{19}F NMR (376 MHz, [D$_6$]DMSO, 25 °C, $CFCl_3$): δ=-80.0 (t, ^3J(F,F) = 9.7 Hz, 3F, -CF_3), -113.5 (s, 2F, -CF_2-), -119.4 (s, -CF_2-), -121.2 – -121.4 (m, 6F, -CF_2-), -122.1 (s, 2F, -CF_2-) -125.4 (br s, 2F, -CF_2-), -149.4 (d, ^3J(F,F) = 24.7 Hz, 2F, *o*-F), -166.6 (t, ^3J(F,F) = 21.6 Hz , 2F, *m*-F), -168.1 ppm (t, ^3J(F,F) = 22.7 Hz , 1F, *p*-F); IR: $\tilde{\nu}$=415 (w), 527 (m), 552 (m), 602 (w), 631 (m), 660 (w), 680 (w), 708 (w), 745 (w), 815 (w), 850 (w), 898 (m), 985 (s), 1061 (m), 1140 (s), 1199 (s), 1274 (m), 1320 (w), 1369 (w), 1465 (w), 1502 (m), 1521 (m), 1654 (w), 2979 cm^{-1} (w); (–)-ESI-MS (MeCN): m/z (%): 664 (100) [M]; HRMS ((–)-ESI (MeCN)): m/z calcd. for $C_{14}F_{22}NO_2S^-$ 663.9304 [M$^-$]; found: 663.9295; elemental analysis calcd. (%) for $C_{14}F_{22}LiNO_2S$: C 25.05, H 0.00, N 2.09, S 4.78; found: C 25.81, H 0.48, N 2.56, S 4.32.

Synthesis of HN(Pf)(Sf): A mixture of H-N-(2,3,4,5,6-pentafluorophenyl)-sulfamoylchloride (1.34 g, 4.75 mmol), dried potassium fluoride (1.38 g, 23.7 mmol) and 18-crown-6 (0.126 g, 0.475 mmol) were suspended in acetonitrile (40 mL). After 30 min the reaction mixture changed color to orange and it was stirred for 3 d at room temperature. The green suspension was filtered and all volatiles were removed from the filtrate *in vacuo*. The green residue was dissolved in diethyl ether (30 mL). Hydrogen chloride was passed through the solution for five minutes resulting in a color change to red. Precipitated potassium chloride was separated by filtration and diethyl ether was removed from the filtrate *in vacuo*. The residue was sublimed (65 °C, 1.8·10^{-2} mbar) to yield HN(Pf)(Sf) (0.901 g, 72%) as a white crystalline solid.
M.p. 35 °C; ^{1}H NMR (300 MHz, C_6D_6, 25 °C, TMS): δ=4.92 ppm (s, 1H, NH); ^{13}C NMR (126 MHz, C_6D_6, 25 °C, TMS): δ=144.7 (d, ^1J(C,F) = 254.2 Hz, CF_{Ar}), 141.8 (d, ^1J(C,F) = 256.8 Hz, CF_{Ar}), 137.8 (d, ^1J(C,F) = 252.1 Hz, CF_{Ar}), 109.2 ppm (d, ^2J(C,F) = 14.9 Hz, *ipso*-C); ^{19}F NMR (471 MHz, C_6D_6, 25 °C, $CFCl_3$): δ=54.2 (m, 1F, -SO_2F), -145.0 (m, 2F, *o*-F), -150.7 (t, ^3J(F,F) = 22.9 Hz, 1F, *p*-F), -160.9 ppm (t, ^3J(F,F) = 21.4 Hz, 2F, *m*-F); IR: $\tilde{\nu}$=411 (m), 456 (m), 495 (m), 533 (m), 562 (s), 584 (w), 621

(m), 768 (s), 804 (s), 929 (m), 986 (s), 1037 (m), 1074 (m), 1164 (w), 1214 (s), 1319 (m), 1355 (w), 1462 (s), 1514 (s), 1652 (w), 3305 cm^{-1} (m, N-H); (–)-ESI-MS (MeCN): m/z (%): 264 (100) [M-H^+], 249 (25) [M-H^+-O]; HRMS ((–)-ESI (MeCN)): m/z calcd. for $C_6F_6NO_2S^-$ 263.9559 [M-H^+]; found: 263.9559; elemental analysis calcd. (%) for $C_6HF_6NO_2S$: C 27.18, H 0.38, N 5.28, S 12.09; found: C 27.25, H 0.40, N 5.47, S 12.49.

X-ray structure analysis: IPDS I and IPDS II (Stoe) diffractometers were used for data collection by the x-ray department at the Philipps-Universität Marburg (*Dr. K. Harms*, *G. Geiseler*, *M. Marsch*, and *R. Riedel*). Data collection, reduction and cell refinement was performed with Stoe IPDS Software. Structures were solved with SIR92,[117] SIR97[118] or SIR2004[119] and refined with SHELXL-97[120] Absorption correction was performed with semi-empirical methods within WinGX (multi-scan[121] or gaussian[122]).

Carbon-bonded hydrogen atoms were calculated in their idealized positions and refined with fixed isotropic thermal parameters. Hydrogen atoms connected to heteroatoms were located on the *Fourier* map and refined isotropically. In case of HN(Pf)(Nf), HN(Pf)(Sf) and HN(Pf)(SO_2N(Pf)(Sf)), NH distances were restrained at 87 pm using the DFIX command. All molecular structures were illustrated with Diamond 3[123] using thermal ellipsoids at the 30% probability level for all non-hydrogen atoms and fixed radii for heteroatom-bonded hydrogen atoms. Carbon-bonded hydrogen atoms are omitted for clarity.

Crystal data and experimental conditions are listed in the supporting information. Selected bonding and non-bonding distances and angles with standard deviations in parentheses are collected in Table 1. The corresponding CIF files providing full information concerning the molecular structures and experimental conditions are deposited at the Cambridge Crystallographic Data Center.

5. Computational Details

The program *TURBOMOLE*[124,125] was used for DFT and MP2 calculations. By default, vibrational, rotational and translational as well as entropical corrections to thermochemistry were calculated with BP86[126-128]/def-TZVP[129] using the *FREEH* tool

(unscaled[130]). For this the vibrational frequencies were determined analytically with the *AOFORCE*[131,132] module. We ensured that all structures are true minima and show no imaginary frequencies. For obtaining absolute energies, we applied the optimized structures gained from the B3LYP[126,133,134] hybrid functional in combination with augmented correlation-consistent triple-zeta basis sets of *Dunning* et al.[135,136] (aug-cc-pVTZ). We then calculated a MP2(FC[137])/aug-cc-pVTZ single point on the B3LYP/aug-cc-pVTZ geometry and called the method "M1". When available, we used the RI approximation for DFT[138-140] and MP2.[141,142]As an alternative[143] we applied the RIJK[144] approach for B3LYP/aug-cc-pVTZ.For our extensive model validation (see SI) we applied various combinations of density functionals and MP2(FC) with different basis sets, in addition to the methods mentioned above including the hybrid-functional PBE0[145-147] and the basis sets def2-TZVPP[148], def2-QZVPP[148] and aug-cc-pVQZ.[135,136]

We also used the *Gaussian* packages[149,150] to calculate the compound approaches G3[151] and G3MP2.[152] Our recently introduced modified G3 ($G3_{mod}$)[40] served as reference method for model validation (besides the experimental values) by means of the GA values of the investigated acids and for the isodesmic calculations. Thus we improved G3MP2 analogously to $G3_{mod}$ by using thermochemical corrections at the BP86/def-TZVP level. The definition of the $G3MP2_{mod}$*Gibbs* energies at standard conditions follows equation (2):

$G°(G3MP2_{mod})$ = G3MP2(0K) – ZPE(G3MP2) + FreeH energy + RT – T• FreeH entropy

As described in section 2.2 above *Gibbs* solvation energies were calculated with *COSMO*[153,154] as implemented in *TURBOMOLE* at the BP86/def-TZVP level of theory. We employed default *COSMO* options as well as default optimized *COSMO* radii. For control purposes we also applied *COSMO* at the B3LYP/aug-cc-pVTZ level and PCM[155,156] as implemented in *Gaussian03* at the BP86/TZVP level. By default all *Gibbs* solvation energy calculations were performed in C_1 symmetry and *Gaussian03* reference values were adopted for the dielectricity constants. Note: The value yielded from *COSMO* respectively *PCM* reflects a transfer from a 1 M ideal gas (24.79 bar at 298.15 K) to a 1 M ideal solution. To obtain the *Gibbs* standard solvation energy $\Delta_{solv}G°$ (transfer from an ideal gas at 1 bar to a 1 M ideal solution), we therefore had to add RTln 24.79 = 7.96 kJ mol^{-1}.[40]

6. Acknowledgement

This work was supported by the University of Freiburg, the DFG and the ERC in the Advanced Grant UniChem.

7. References

(1) Foropoulos Jr., J.; DesMarteau, D. D. *Inorg. Chem.***1984**, *23*, 3720.
(2) DesMarteau, D. D.; Witz, M. *J. Fluorine Chem.***1991**, *52*, 7.
(3) Koppel, I. A.; Taft, R. W.; Anvia, F.; Zhu, S.-Z.; Hu, L.-Q.; Sung, K.-S.; DesMarteau, D. D.; Yagupolskii, L. M.; Yagupolskii, Y. L.; Ignat'ev, N. V.; Kondratenko, N. V.; Volkonskii, A. Y.; Vlasov, V. M.; Notario, R.; Maria, P.-C. *J. Am. Chem. Soc.***1994**, *116*, 3047.
(4) Burk, P.; Koppel, I. A.; Koppel, I.; Yagupolskii, L. M.; Taft, R. W. *J. Comput. Chem.***1996**, *17*, 30.
(5) Kütt, A.; Rodima, T.; Saame, J.; Raamat, E.; Mäemets, V.; Kaljurand, I.; Koppel, I. A.; Garlyauskayte, R. Y.; Yagupolskii, Y. L.; Yagupolskii, L. M.; Bernhardt, E.; Willner, H.; Leito, I. *J. Org. Chem.***2011**, *76*, 391.
(6) Rey, I.; Johansson, P.; Lindgren, J.; Lassègues, J. C.; Grondin, J.; Servant, L. *J. Phys. Chem. A***1998**, *102*, 3249.
(7) Ryu, D. H.; Corey, E. J. *J. Am. Chem. Soc.***2003**, *125*, 6388.
(8) Wabnitz, T. C.; Spencer, J. B. *Org. Lett.***2003**, *5*, 2141.
(9) Zhang, L.; Kozmin, S. A. *J. Am. Chem. Soc.***2004**, *126*, 10204.
(10) Rowland, G. B.; Zhang, H.; Rowland, E. B.; Chennamadhavuni, S.; Wang, Y.; Antilla, J. C. *J. Am. Chem. Soc.***2005**, *127*, 15696.
(11) Noda, A.; Susan, M. A. B. H.; Kudo, K.; Mitsushima, S.; Hayamizu, K.; Watanabe, M. *J. Phys. Chem. B***2003**, *107*, 4024.
(12) Huddleston, J. G.; Visser, A. E.; Reichert, W. M.; Willauer, H. D.; Broker, G. A.; Rogers, R. D. *Green Chem.***2001**, *3*, 156.
(13) MacFarlane, D. R.; Meakin, P.; Sun, J.; Amini, N.; Forsyth, M. *J. Phys. Chem. B***1999**, *103*, 4164.
(14) Jin, H.; O'Hare, B.; Dong, J.; Arzhantsev, S.; Baker, G. A.; Wishart, J. F.; Benesi, A. J.; Maroncelli, M. *J. Phys. Chem. B***2008**, *112*, 81.
(15) Mateus, N. M. M.; Branco, L. C.; Lourenço, N. M. T.; Afonso, C. A. M. *Green Chem.***2003**, *5*, 347.
(16) Del Sesto, R. E.; Corley, C.; Robertson, A.; Wilkes, J. S. *J. Organomet. Chem.***2005**, *690*, 2536.
(17) Lozano, P.; Bernal, J. M.; Piamtongkam, R.; Fetzer, D.; Vaultier, M. *ChemSusChem***2010**, *3*, 1359.
(18) Matsumoto, H.; Sakaebe, H.; Tatsumi, K.; Kikuta, M.; Ishiko, E.; Kono, M. *J. Power Sources***2006**, *160*, 1308.
(19) Borgel, V.; Markevich, E.; Aurbach, D.; Semrau, G.; Schmidt, M. *J. Power Sources***2009**, *189*, 331.
(20) Howlett, P. C.; MacFarlane, D. R.; Hollenkamp, A. F. *Electrochem. Solid-State Lett.***2004**, *7*, A97.
(21) Frömling, T.; Kunze, M.; Schönhoff, M.; Sundermeyer, J.; Roling, B. *J. Phys. Chem. B***2008**, *112*, 12985.
(22) Antoniotti, S.; Dalla, V.; Duñach, E. *Angew. Chem.***2010**, *122*, 8032.
(23) Stricker, M.; Linder, T.; Oelkers, B.; Sundermeyer, J. *Green Chem.***2010**, *12*, 1589.
(24) Mudring, A. V. *ACS Symp. Ser.***2007**, *975*, 172.

(25) Mudring, A.-V.; Babai, A.; Arenz, S.; Giernoth, R.; Binnemans, K.; Driesen, K.; Nockemann, P. *J. Alloys Compd.***2006**, *418*, 204.
(26) Arenz, S.; Babai, A.; Binnemans, K.; Driesen, K.; Giernoth, R.; Mudring, A.-V.; Nockemann, P. *Chem. Phys. Lett.***2005**, *402*, 75.
(27) Tang, S.; Babai, A.; Mudring, A. V. *Angew. Chem., Int. Ed.***2008**, *47*, 7631.
(28) Vij, A.; Kirchmeier, R. L.; Shreeve, J. M.; Verma, R. D. *Coord. Chem. Rev.***1997**, *158*, 413.
(29) Krumm, B.; Vij, A.; Kirchmeier, R. L.; Shreeve, J. M. *Inorg. Chem.***1998**, *37*, 6295.
(30) Guerfi, A.; Duchesne, S.; Kobayashi, Y.; Vijh, A.; Zaghib, K. *J. Power Sources***2008**, *175*, 866.
(31) Brooke, G. M.; Burdon, J.; Stacey, M.; Tatlow, J. C. *J. Chem. Soc.***1960**, 1768.
(32) Koppang, R. *Acta Chem. Scand.***1971**, *25*, 3067.
(33) Giesbrecht, G. R.; Gordon, J. C.; Clark, D. L.; Hijar, C. A.; Scott, B. L.; Watkin, J. G. *Polyhedron***2003**, *22*, 153.
(34) Shutov, P. L.; Karlov, S. S.; Harms, K.; Zabalov, M. V.; Sundermeyer, J.; Lorberth, J.; Zaitseva, G. S. *Eur. J. Inorg. Chem.***2007**, *2007*, 5684.
(35) Shutov, P. L.; Karlov, S. S.; Harms, K.; Sundermeyer, J.; Lorberth, J.; Zaitseva, G. S. *J. Fluorine Chem.***2009**, *130*, 1017.
(36) Click, D. R.; Scott, B. L.; Watkin, J. G. *Chem. Commun. (Cambridge, U. K.)***1999**, 633.
(37) Khvorost, A.; Shutov, P. L.; Harms, K.; Lorberth, J.; Sundermeyer, J.; Karlov, S. S.; Zaitseva, G. S. *Z. Anorg. Allg. Chem.***2004**, *630*, 885.
(38) Shutov, P. L.; Karlov, S. S.; Harms, K.; Tyurin, D. A.; Sundermeyer, J.; Lorberth, J.; Zaitseva, G. S. *Eur. J. Inorg. Chem.***2004**, *2004*, 2498.
(39) Linder, T.; Sundermeyer, J. *Chem. Commun. (Cambridge, U. K.)***2009**, 2914.
(40) Himmel, D.; Goll, S. K.; Leito, I.; Krossing, I. *Chem. Eur. J.***2011**, *17*, 5808.
(41) Sundermeyer, J. R., B.; Linder, T.; Froemling, T.; Huber, B. 2011; Vol. EP 2314572 A1 20110427.
(42) Sundermeyer, J. R., B.; Linder, T.; Huber, B.; Froemling, T. 2011; Vol. PCT Int. Appl. WO 2011048152 A1 20110428.
(43) Jäger, U.; Sundermeyer, W.; Pritzkow, H. *Chem. Ber.***1987**, *120*, 1191.
(44) Huber, B.; Linder, T.; Hormann, K.; Frömling, T.; Sundermeyer, J.; Roling, B. *Z. Phys. Chem.***2012**, *226*, 377.
(45) Grzegorczyk, M.; Gdaniec, M. *Acta Cryst. C***2006**, *62*, o419.
(46) Haas, A.; Klare, C.; Betz, P.; Bruckmann, J.; Krüger, C.; Tsay, Y.-H.; Aubke, F. *Inorg. Chem.***1996**, *35*, 1918.
(47) Ochiai, M.; Okada, T.; Tada, N.; Yoshimura, A.; Miyamoto, K.; Shiro, M. *J. Am. Chem. Soc.***2009**, *131*, 8392.
(48) Koppel, I. A.; Anvia, F.; Taft, R. W. *J. Phys. Org. Chem.***1994**, *7*, 717.
(49) Bouchoux, G.; Gal, J.-F.; Maria, P. C.; Szulejko, J. E.; McMahon, T. B.; Tortajada, J.; Luna, A.; Yàñez, M.; Mó, O. *J. Phys. Chem. A***1998**, *102*, 9183.
(50) Burk, P.; Koppel, I. A.; Rummel, A.; Trummal, A. *J. Phys. Chem. A***2000**, *104*, 1602.
(51) Koppel, I. A.; Burk, P.; Koppel, I.; Leito, I.; Sonoda, T.; Mishima, M. *J. Am. Chem. Soc.***2000**, *122*, 5114.
(52) Koppel, I. A.; Koppel, J.; Leito, I.; Koppel, I.; Mishima, M.; Yagupolskii, L. M. *J. Chem. Soc., Perkin Trans. 2***2001**, 229.
(53) Koppel, I. A.; Schwesinger, R.; Breuer, T.; Burk, P.; Herodes, K.; Koppel, I.; Leito, I.; Mishima, M. *J. Phys. Chem. A***2001**, *105*, 9575.
(54) Kolomeitsev, A. A.; Koppel, I. A.; Rodima, T.; Barten, J.; Lork, E.; Röschenthaler, G.-V.; Kaljurand, I.; Kütt, A.; Koppel, I.; Mäemets, V.; Leito, I. *J. Am. Chem. Soc.***2005**, *127*, 17656.
(55) Jones, C. M.; Bernier, M.; Carson, E.; Colyer, K. E.; Metz, R.; Pawlow, A.; Wischow, E. D.; Webb, I.; Andriole, E. J.; Poutsma, J. C. *Int. J. Mass Spectrom.***2007**, *267*, 54.

(56) Kaljurand, I.; Koppel, I. A.; Kütt, A.; Rõõm, E.-I.; Rodima, T.; Koppel, I.; Mishima, M.; Leito, I. *J. Phys. Chem. A***2007**, *111*, 1245.
(57) Hurtado, M.; Yánez, M.; Herrero, R.; Guerrero, A.; Dávalos, J. Z.; Abboud, J.-L. M.; Khater, B.; Guillemin, J.-C. *Chem. Eur. J.***2009**, *15*, 4622.
(58) Kütt, A.; Koppel, I.; Koppel, I. A.; Leito, I. *ChemPhysChem***2009**, *10*, 499.
(59) Leito, I.; Raamat, E.; Kütt, A.; Saame, J.; Kipper, K.; Koppel, I. A.; Koppel, I.; Zhang, M.; Mishima, M.; Yagupolskii, L. M.; Garlyauskayte, R. Y.; Filatov, A. A. *J. Phys. Chem. A***2009**, *113*, 8421.
(60) Meyer, M. M.; Wang, X.-B.; Reed, C. A.; Wang, L.-S.; Kass, S. R. *J. Am. Chem. Soc.***2009**, *131*, 18050.
(61) Namazian, M.; Coote, M. L. *J. Fluorine Chem.***2009**, *130*, 621.
(62) Leito, I.; Koppel, I. A.; Burk, P.; Tamp, S.; Kutsar, M.; Mishima, M.; Abboud, J.-L. M.; Davalos, J. Z.; Herrero, R.; Notario, R. *J. Phys. Chem. A***2010**, *114*, 10694.
(63) Meyer, M. M.; Kass, S. R. *J. Phys. Chem. A***2010**, *114*, 4086.
(64) Rayne, S.; Forest, K. *Theor. Chem. Acc.***2010**, *127*, 697.
(65) Rayne, S.; Forest, K. *J. Mol. Struct.: THEOCHEM***2010**, *956*, 83.
(66) Lipping, L.; Kütt, A.; Kaupmees, K.; Koppel, I.; Burk, P.; Leito, I.; Koppel, I. A. *J. Phys. Chem. A***2011**, *115*, 10335.
(67) Kunetskiy, R. A.; Polyakova, S. M.; Vavřík, J.; Císařová, I.; Saame, J.; Nerut, E. R.; Koppel, I.; Koppel, I. A.; Kütt, A.; Leito, I.; Lyapkalo, I. M. *Chem. Eur. J.***2012**, *18*, 3621.
(68) Lee, A. C.; Crippen, G. M. *J. Chem. Inf. Model.***2009**, *49*, 2013.
(69) Ho, J.; Coote, M. L. *Theor. Chem. Acc.***2010**, *125*, 3.
(70) Ho, J.; Coote, M. L. *WIREs Comput. Mol. Sci.***2011**, *1*, 649.
(71) Zevatskii, Y. E.; Samoilov, D. V. *Russ. J. Org. Chem.***2011**, *47*, 1445.
(72) Liptak, M. D.; Shields, G. C. *J. Am. Chem. Soc.***2001**, *123*, 7314.
(73) Pliego, J. R., Jr.; Riveros, J. M. *J. Phys. Chem. A***2002**, *106*, 7434.
(74) Kelly, C. P.; Cramer, C. J.; Truhlar, D. G. *J. Phys. Chem. A***2006**, *110*, 2493.
(75) Bryantsev, V. S.; Diallo, M. S.; Goddard, W. A., III *J. Phys. Chem. A***2007**, *111*, 4422.
(76) Kovačević, B.; Maksić, Z. B. *Org. Lett.***2001**, *3*, 1523.
(77) Chipman, D. M. *J. Phys. Chem. A***2002**, *106*, 7413.
(78) Almerindo, G. I.; Tondo, D. W.; Pliego, J. R., Jr. *J. Phys. Chem. A***2004**, *108*, 166.
(79) Fu, Y.; Liu, L.; Li, R.-Q.; Liu, R.; Guo, Q.-X. *J. Am. Chem. Soc.***2004**, *126*, 814.
(80) Magill, A. M.; Cavell, K. J.; Yates, B. F. *J. Am. Chem. Soc.***2004**, *126*, 8717.
(81) Fu, Y.; Liu, L.; Yu, H.-Z.; Wang, Y.-M.; Guo, Q.-X. *J. Am. Chem. Soc.***2005**, *127*, 7227.
(82) Vianello, R.; Maksić, Z. B. *Tetrahedron Lett.***2005**, *46*, 3711.
(83) Vianello, R.; Maksić, Z. B. *Mol. Phys.***2005**, *103*, 209.
(84) Villamena, F. A.; Merle, J. K.; Hadad, C. M.; Zweier, J. L. *J. Phys. Chem. A***2005**, *109*, 6083.
(85) Fu, Y.; Liu, L.; Wang, Y.-M.; Li, J.-N.; Yu, T.-Q.; Guo, Q.-X. *J. Phys. Chem. A***2006**, *110*, 5874.
(86) Holland, J. P.; Green, J. C.; Dilworth, J. R. *Dalton Trans.***2006**, 783.
(87) Li, J.-N.; Liu, L.; Fu, Y.; Guo, Q.-X. *Tetrahedron***2006**, *62*, 4453.
(88) Qi, X.-J.; Liu, L.; Fu, Y.; Guo, Q.-X. *Organometallics***2006**, *25*, 5879.
(89) Qi, X.-J.; Fu, Y.; Liu, L.; Guo, Q.-X. *Organometallics***2007**, *26*, 4197.
(90) Shen, K.; Fu, Y.; Li, J.-N.; Liu, L.; Guo, Q.-X. *Tetrahedron***2007**, *63*, 1568.
(91) Yu, A.; Liu, Y.; Li, Z.; Cheng, J.-P. *J. Phys. Chem. A***2007**, *111*, 9978.
(92) Ding, F.; Smith, J. M.; Wang, H. *J. Org. Chem.***2009**, *74*, 2679.
(93) Eckert, F.; Leito, I.; Kaljurand, I.; Kütt, A.; Klamt, A.; Diedenhofen, M. *J. Comput. Chem.***2009**, *30*, 799.
(94) Fu, Y.; Wang, H.-J.; Chong, S.-S.; Guo, Q.-X.; Liu, L. *J. Org. Chem.***2009**, *74*, 810.
(95) Glasovac, Z.; Eckert-Maksić, M.; Maksić, Z. B. *New J. Chem.***2009**, *33*, 588.

(96) Trummal, A.; Rummel, A.; Lippmaa, E.; Burk, P.; Koppel, I. A. *J. Phys. Chem. A***2009**, *113*, 6206.
(97) Huang, X.-Y.; Wang, H.-J.; Shi, J. *J. Phys. Chem. A***2010**, *114*, 1068.
(98) Uudsemaa, M.; Kanger, T.; Lopp, M.; Tamm, T. *Chem. Phys. Lett.***2010**, *485*, 83.
(99) Vianello, R.; Maksić, Z. B. *J. Org. Chem.***2010**, *75*, 7670.
(100) Zhu, X.-Q.; Wang, C.-H.; Liang, H. *J. Org. Chem.***2010**, *75*, 7240.
(101) Solis, B. H.; Hammes-Schiffer, S. *Inorg. Chem. (Washington, DC, U. S.)***2011**, *50*, 11252.
(102) Tomasi, J. *Theor. Chem. Acc.***2004**, *112*, 184.
(103) Tomasi, J.; Mennucci, B.; Cammi, R. *Chem. Rev. (Washington, DC, U. S.)***2005**, *105*, 2999.
(104) Ho, J.; Klamt, A.; Coote, M. L. *J. Phys. Chem. A***2010**, *114*, 13442.
(105) Pliego, J. R., Jr.; Riveros, J. M. *J. Phys. Chem. A***2001**, *105*, 7241.
(106) Himmel, D.; Goll, S. K.; Leito, I.; Krossing, I. *Angew. Chem., Int. Ed.***2010**, *49*, 6885.
(107) Kütt, A.; Leito, I.; Kaljurand, I.; Sooväli, L.; Vlasov, V. M.; Yagupolskii, L. M.; Koppel, I. A. *J. Org. Chem.***2006**, *71*, 2829.
(108) Original data taken from T. B. Douglas, J. Am. Chem. Soc. 1948, 70, 2001; reworked by NIST Chemistry WebBook, NIST Standard Reference Database Number 69, http://webbook.nist.gov.
(109) Original data taken from W. E. Putnam, D. M. McEachern Jr., J. E. Kilpatrick, J. Chem. Phys. 1965, 42, 749; reworked by NIST Chemistry WebBook, NIST Standard Reference Database Number 69, http://webbook.nist.gov.
(110) Gaussian03 reference values were adopted for the dielectricity constants.
(111) Koppel, I.; Koppel, J.; Leito, I.; Pihl, V.; Grehn, L.; Ragnarsson, U. *J. Chem. Res., Synop.***1994**, 212.
(112) Koppel, I.; Koppel, J.; Maria, P.-C.; Gal, J.-F.; Notario, R.; Vlasov, V. M.; Taft, R. W. *Int. J. Mass Spectrom. Ion Processes***1998**, *175*, 61.
(113) Vlasov, V. M.; Terekhova, M. I.; Petrov, E. S.; Shatenshtein, A. I.; Yakobson, G. G. *Zh. Org. Khim.***1981**, *17*, 2025.
(114) Note: As mentioned above the contact ion pair formation of $HNTf_2$•DMSO in DMSO during optimization yields an increase of 9.5 pKa units, but there are energy differences between the vCCC and the rCCC model at other parts of the BFHCs too.
(115) Kuett, A.; Leito, I.; Kaljurand, I.; Soovaeli, L.; Vlasov, V. M.; Yagupolskii, L. M.; Koppel, I. A. *J. Org. Chem.***2006**, *71*, 2829.
(116) Brauer, G.; Ferdinand Enke Verlag: Stuttgart, 1975, p 712.
(117) Altomare, A.; Cascarano, G.; Giacovazzo, C.; Guagliardi, A. *J. Appl. Crystallogr.***1993**, *26*, 343.
(118) Altomare, A.; Burla, M. C.; Camalli, M.; Cascarano, G. L.; Giacovazzo, C.; Guagliardi, A.; Moliterni, A. G. G.; Polidori, G.; Spagna, R. *J. Appl. Crystallogr.***1999**, *32*, 115.
(119) Burla, M. C.; Caliandro, R.; Camalli, M.; Carrozzini, B.; Cascarano, G. L.; De Caro, L.; Giacovazzo, C.; Polidori, G.; Spagna, R. *J. Appl. Crystallogr.***2005**, *38*, 381.
(120) Sheldrick, G. *Acta Cryst. A***2008**, *64*, 112.
(121) Blessing, R. H. *Acta Cryst. A***1995**, *51*, 33.
(122) Coppens, P.; Ahmed, F. R., Hall, S. R., Huber, P. C., Eds. Munksgaard, Copenhagen, 1970, p 225.
(123) Brandenburg, K.; Putz, H.; v3.2i ed.; Crystal Impact GbR: Bonn, Germany, 2012.
(124) Ahlrichs, R.; Bär, M.; Häser, M.; Horn, H.; Kölmel, C. *Chem. Phys. Lett.***1989**, *162*, 165.
(125) Treutler, O.; Ahlrichs, R. *J. Chem. Phys.***1995**, *102*, 346.
(126) Becke, A. D. *Phys. Rev. A***1988**, *38*, 3098.
(127) Perdew, J. P. *Phys. Rev. B***1986**, *33*, 8822.
(128) Perdew, J. P. *Phys. Rev. B***1986**, *34*, 7406.
(129) Schaefer, A.; Horn, H.; Ahlrichs, R. *J. Chem. Phys.***1992**, *97*, 2571.

(130) Coincidentally for BP86/def-TZVP frequencies the scaling factor is very close to unity.
(131) Deglmann, P.; Furche, F. *J. Chem. Phys.***2002**, *117*, 9535.
(132) Deglmann, P.; Furche, F.; Ahlrichs, R. *Chem. Phys. Lett.***2002**, *362*, 511.
(133) Becke, A. D. *J. Chem. Phys.***1993**, *98*, 5648.
(134) Lee, C.; Yang, W.; Parr, R. G. *Phys. Rev. B***1988**, *37*, 785.
(135) Dunning, T. H., Jr. *J. Chem. Phys.***1989**, *90*, 1007.
(136) Kendall, R. A.; Dunning, T. H., Jr.; Harrison, R. J. *J. Chem. Phys.***1992**, *96*, 6796.
(137) The core orbitals were retained frozen, only the valence shell orbitals were considered.
(138) Eichkorn, K.; Treutler, O.; Öhm, H.; Häser, M.; Ahlrichs, R. *Chem. Phys. Lett.***1995**, *240*, 283.
(139) Eichkorn, K.; Treutler, O.; Öhm, H.; Häser, M.; Ahlrichs, R. *Chem. Phys. Lett.***1995**, *242*, 652.
(140) Eichkorn, K.; Weigend, F.; Treutler, O.; Ahlrichs, R. *Theor. Chem. Acc.***1997**, *97*, 119.
(141) Weigend, F.; Häser, M. *Theor. Chem. Acc.***1997**, *97*, 331.
(142) Weigend, F.; Häser, M.; Patzelt, H.; Ahlrichs, R. *Chem. Phys. Lett.***1998**, *294*, 143.
(143) For B3LYP/aug-cc-pVTZ currently no RI approximation for sulfur is available. So we first performed the calculations without any auxiliary basis sets for the respective geometry optimizations. Later we switched to the computationally less “expensive” RIJK approximation, which is available for sulfur too, to calculate the anion-solvent adducts as well as the isodesmic model systems of the anions and their solvent adducts. The RIJK approximation was also used for all B3LYP/aug-cc-pVTZ calculations regarding the acidity of HN(Pf)(Sf). We performed control accounts with RIJK versus without RIJK for the anions of the weakest and the strongest acid (NPf_2^- respectively NTf_2^-) as well as for MeCN and DMSO. We found deviations (see SI) up to 0.2 kJ mol–1 for the energies of the optimized B3LYP/aug-cc-pVTZ structures and up to 0.1 kJ mol–1 for the (RI-)MP2(FC)/aug-cc-pVTZ single points based on this geometries as employed in our M1 method. We decided to neglect the latter.
(144) Weigend, F. *Phys. Chem. Chem. Phys.***2002**, *4*, 4285.
(145) Perdew, J. P.; Burke, K.; Ernzerhof, M. *Phys. Rev. Lett.***1996**, *77*, 3865.
(146) Perdew, J. P.; Burke, K.; Ernzerhof, M. *Phys. Rev. Lett.***1997**, *78*, 1396.
(147) Adamo, C.; Barone, V. *J. Chem. Phys.***1999**, *110*, 6158.
(148) Weigend, F.; Ahlrichs, R. *Phys. Chem. Chem. Phys.***2005**, *7*, 3297.
(149) Gaussian 03, Revision D.02, M. J. Frisch, G. W. Trucks, H. B. Schlegel, G. E. Scuseria, M. A. Robb, J. R. Cheeseman, J. J. A. Montgomery, T. Vreven, K. N. Kudin, J. C. Burant, J. M. Millam, S. S. Iyengar, J. Tomasi, V. Barone, B. Mennucci, M. Cossi, G. Scalmani, N. Rega, G. A. Petersson, H. Nakatsuji, M. Hada, M. Ehara, K. Toyota, R. Fukuda, J. Hasegawa, M. Ishida, T. Nakajima, Y. Honda, O. Kitao, H. Nakai, M. Klene, X. Li, J. E. Knox, H. P. Hratchian, J. B. Cross, V. Bakken, C. Adamo, J. Jaramillo, R. Gomperts, R. E. Stratmann, O. Yazyev, A. J. Austin, R. Cammi, C. Pomelli, J. W. Ochterski, P. Y. Ayala, K. Morokuma, G. A. Voth, P. Salvador, J. J. Dannenberg, V. G. Zakrzewski, S. Dapprich, A. D. Daniels, M. C. Strain, O. Farkas, D. K. Malick, A. D. Rabuck, K. Raghavachari, J. B. Foresman, J. V. Ortiz, Q. Cui, A. G. Baboul, S. Clifford, J. Cioslowski, B. B. Stefanov, G. Liu, A. Liashenko, P. Piskorz, I. Komaromi, R. L. Martin, D. J. Fox, T. Keith, M. A. Al-Laham, C. Y. Peng, A. Nanayakkara, M. Challacombe, P. M. W. Gill, B. Johnson, W. Chen, M. W. Wong, C. Gonzalez, and J. A. Pople, Gaussian, Inc., Wallingford CT, 2004.
(150) Gaussian 09, Revision B.01, M. J. Frisch, G. W. Trucks, H. B. Schlegel, G. E. Scuseria, M. A. Robb, J. R. Cheeseman, G. Scalmani, V. Barone, B. Mennucci, G. A. Petersson, H. Nakatsuji, M. Caricato, X. Li, H. P. Hratchian, A. F. Izmaylov, J. Bloino, G. Zheng, J. L. Sonnenberg, M. Hada, M. Ehara, K. Toyota, R. Fukuda, J. Hasegawa, M. Ishida, T. Nakajima, Y. Honda, O. Kitao, H. Nakai, T. Vreven, J. J. A. Montgomery, J. E. Peralta, F. Ogliaro, M. Bearpark, J. J. Heyd, E. Brothers, K. N. Kudin, V. N. Staroverov, T. Keith, R.

Kobayashi, J. Normand, K. Raghavachari, A. Rendell, J. C. Burant, S. S. Iyengar, J. Tomasi, M. Cossi, N. Rega, J. M. Millam, M. Klene, J. E. Knox, J. B. Cross, V. Bakken, C. Adamo, J. Jaramillo, R. Gomperts, R. E. Stratmann, O. Yazyev, A. J. Austin, R. Cammi, C. Pomelli, J. W. Ochterski, R. L. Martin, K. Morokuma, V. G. Zakrzewski, G. A. Voth, P. Salvador, J. J. Dannenberg, S. Dapprich, A. D. Daniels, O. Farkas, J. B. Foresman, J. V. Ortiz, J. Cioslowski, D. J. Fox, Gaussian, Inc., Wallingford CT, 2010.

(151) Curtiss, L. A.; Raghavachari, K.; Redfern, P. C.; Rassolov, V.; Pople, J. A. *J. Chem. Phys.***1998**, *109*, 7764.

(152) Curtiss, L. A.; Redfern, P. C.; Raghavachari, K.; Rassolov, V.; Pople, J. A. *J. Chem. Phys.***1999**, *110*, 4703.

(153) Klamt, A.; Schüürmann, G. *J. Chem. Soc., Perkin Trans. 2***1993**, 799.

(154) Schäfer, A.; Klamt, A.; Sattel, D.; Lohrenz, J. C. W.; Eckert, F. *Phys. Chem. Chem. Phys.***2000**, *2*, 2187.

(155) Miertus, S.; Scrocco, E.; Tomasi, J. *Chem. Phys.***1981**, *55*, 117.

(156) Cossi, M.; Scalmani, G.; Rega, N.; Barone, V. *J. Chem. Phys.***2002**, *117*, 43.

The New Lewis Superacid $Al[N(C_6F_5)_2]_3$ and its Higher Homolog $Ga[N(C_6F_5)_2]_3$ - Structural Features, Preparation of Lewis Acid-Base Adducts and Metallates and Theoretical Investigation of the Fluoride Ion Affinity in the Gas Phase

Julius F. Kögel, Denis A. Sorokin, Alexander Khvorost, Martin Scott, Klaus Harms, Daniel Himmel, Ingo Krossing, Jörg Sundermeyer*

Abstract: Herein we present the synthesis of the two Lewis acids $Al[N(C_6F_5)_2]_3$ and $Ga[N(C_6F_5)_2]_3$ *via* salt elimination reactions. The metal complexes were characterized by NMR-spectroscopic methods and x-ray diffraction analysis revealing the stabilization of the highly Lewis acidic metal centers by secondary metal-fluorine contacts. The Lewis acidic properties of $Al[N(C_6F_5)_2]_3$ and $Ga[N(C_6F_5)_2]_3$ are demonstrated by reactions with Lewis basic solvent molecules like acetonitrile or THF resulting in the formation of Lewis acid-base adducts accompanied by crucial structural changes. Furthermore, we prepared the two metallates $[Cs(Tol)_3]^+[FAl(N(C_6F_5)_2)_3]^-$ and $[AsPh_4]^+[ClGa(N(C_6F_5)_2)_3]^-$ containing interesting weakly coordinating anions. The reaction of $Al[N(C_6F_5)_2]_3$ with trityl fluoride yielded $[CPh_3]^+[FAl(N(C_6F_5)_2)_3]^-$ which could find application in the activation of metallocene polymerization catalysts. The qualitative Lewis acidity of $Al[N(C_6F_5)_2]_3$ and $Ga[N(C_6F_5)_2]_3$ was investigated by means of competition experiments for chloride ions in solution. DFT calculations yielded fluoride ion affinities in the gas phase (FIA) of 515 kJ/mol for $Al[N(C_6F_5)_2]_3$ and 466 kJ/mol for $Ga[N(C_6F_5)_2]_3$. Thus, $Al[N(C_6F_5)_2]_3$ can be considered a Lewis superacid with a fluoride affinity higher than SbF_5 whereas the FIA of the corresponding gallium complex is slightly below the threshold to Lewis superacidity.

Introduction

Lewis acidic compounds play an important role in synthetic chemistry and have been successfully applied to Diels-Alder reactions,[1] rearrangements,[2] conjugate additions[3] or Friedel-Crafts reactions[4] to name only a few examples. Thus, Lewis acid catalysis has been the subject of various review articles[5] and the scientific acitivity in the field of Lewis acids was additionally kindled by the development of frustrated Lewis pair chemistry by Stephan since 2006.[6]

The importance of Lewis acids as valuable synthetic tools has evoked a fundamental interest in the phenomenon of Lewis acidity and its underlying principles. In this context, Krossing *et al*. introduced the fluoride ion affinity in the gas phase (FIA) as the benchmark for the quantification of Lewis acidity on the basis of works published by Bartlett *et al.*.[7,8] By definition, SbF_5 as the strongest conventional molecular Lewis acid with an FIA of 489 kJ/mol marks the threshold to Lewis superacidity. Krossing *et al.* reported on the preparation of the fluorobenzene adduct of the homoleptic aluminum complex $Al[OC(CF_3)_3]_3$ (FIA: 505 kJ/mol in case of the PhF adduct and 537 kJ/mol for the corresponding adduct free form) and highlighted important requirements for the design of Lewis superacids: The

generation of an extremely electron-poor metal center can be achieved by ligands with weak donor properties that usually contain strongly electron-withdrawing substituents like perfluorinated alkyl groups. In case of $Al[OC(CF_3)_3]_3$, the aluminum center is stabilized by the formation of two hemilabile aluminum-fluorine interactions masking the high Lewis acidity of the metal center. These metal-fluorine contacts break up in the presence of a Lewis base. The incorporation of additional O- or N-donor atoms in the ligand backbone instead of the carbon-bonded fluorine atoms would allow the formation of stable chelates which drastically reduce the Lewis acidic properties of the metal complex. Furthermore, sufficient bulkiness of the ligand moieties should prevent oligomerization which would have an reducing effect on the Lewis acidity and hamper the theoretical determination of the FIA. Such decrease in Lewis acidity due to aggregation is observed for aluminum triiodide and aluminum tribromide that reach the demanded FIA for Lewis superacidity in their monomeric forms in the gas phase (AlI_3: 499 kJ/mol $AlBr_3$: 494 kJ/mol),[8] but show dramatically lower values in condensed phase (AlI_3: 393 kJ/mol $AlBr_3$: 393 kJ/mol).[8] Eventually, the ligand regime has to provide inertness towards intramolecular or intermolecular degradation processes like the abstraction of fluorine atoms from the ligand backbone.

Beside $Al[OC(CF_3)_3]_3$, the related $Al[O(C_6F_{10}(C_6F_5))]_3$ (530 kJ/mol)[9] also meets the criterion for Lewis superacidity. Whereas common boranes like the widely used $B(C_6F_5)_3$ (444 kJ/mol) show FIAs below the threshold to Lewis superacidity, only the chelating 1,2-$[(C_6F_5)_2B]_2C_6F_4$ (510 kJ/mol) exhibits an FIA higher than that of SbF_5.[10]

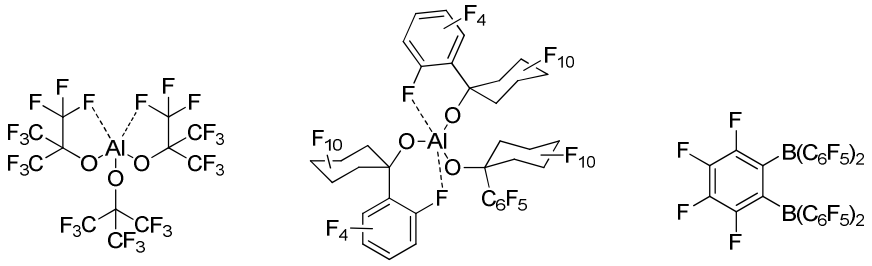

Figure 1. Examples for Lewis superacids and their calculated FIAs.

The design of highly Lewis acidic metal complexes has also been the subject of theoretical works.[11] Frenking *et al.* reported on the enhancement of the Lewis acidity of B, Al and Ga compounds with adamantyl substituents by pyramidalization of the coordination geometry.[12]

The research in the field of strong Lewis acids goes hand in hand with the investigation of the corresponding weakly coordinating anions (WCAs) derived from the reaction of a Lewis acid with an Lewis basic anion. The metal center is shielded by the hydrophobic and sterically demanding perfluorinated ligand regime granting delocalization of the negative charge. Thus, WCAs allow the stabilization of highly reactive cationic species like the carbocations $[CCl_3]^+$ and $[CBr_3]^+$,[13] the tritylium cation,[14] a radical cation of benzidine,[15] a stable $[AsBr_4]^+$ cation[16] or a $[Ag_2Se_{12}]^+$ cage.[17] In this context, especially $Ag^+[Al(OC(CF_3)_3)_4]^-$ has emerged as a versatile reagent for the abstraction of

chloride ions from neutral precursors to generate reactive cations stabilized by the WCA $[Al(OC(CF_3)_3)_4]^-$.[18] Such reactions yielded stabilized amido-substituted germanium(II) and tin(II) monocations,[19] homoleptic ethylene complexes of the coinage metals,[20] the tBu_3Si^+ source $[tBu_3Si\text{-}Ga\text{-}SitBu_3]^+$,[21] gallium(I) arene complexes[22] or univalent gallium and indium phosphane complexes.[23]

Aluminum and gallium are proper metals for the generation of strong Lewis acids due to the small size and the high charge of their M^{3+} cations. The principle for the preparation of Lewis acidic aluminum or gallium compounds is to find a negatively charged ligand with weak donor character leaving a high positive partial charge on the metal center. This can be achieved by delocalizing the ligand's negative charge over perfluorinated electron-withdrawing groups. As described above, it has been demonstrated that perfluorinated alkoxo ligands are able to form Lewis superacidic aluminum complexes. This article is concerned with the question: Can certain metal amides also be Lewis superacids and display a higher fluoride affinity than SbF_5? In this context, we identified bis(pentafluorophenyl)amide $[N(C_6F_5)_2]^-$ as a promising ligand for the preparation of strong Lewis acids.[24] $HN(C_6F_5)_2$ can be easily prepared in large scale[25] and its two strongly electron-withdrawing pentafluorophenyl substituents should provide complexes with good solubility in nonpolar solvents and sufficient sterical shielding of the metal center. Furthermore, the NH-acid is known for its ability to form hemilabile metal-fluorine contacts *via* its *ortho*-fluorine atoms stabilizing the metal center and leading to interesting coordination modes. It has already been incorporated into complexes of lithium,[26] the f-block metals neodymium,[27] cerium, lanthanum[28] and uranium[29] and the d-block metals titanium, zirconium, vanadium, iron, cobalt[30] and tungsten.[31]

Discussion

Preparation: $Al[N(C_6F_5)_2]_3$ and $Ga[N(C_6F_5)_2]_3$ were both prepared *via* reactions of $LiN(C_6F_5)_2$ with the corresponding metal trichloride in hot toluene leading to the precipitation of lithium chloride (Scheme 1). $Al[N(C_6F_5)_2]_3$ was first isolated from an alkane elimination reaction between trimethylaluminum and $HN(C_6F_5)_2$ in toluene at 105 °C, but this route only yielded traces of the desired product. The ^{19}F NMR spectra of $Al[N(C_6F_5)_2]_3$ (δ = -153.1, -158.6 and -161.1 ppm) and $Ga[N(C_6F_5)_2]_3$ (δ = -151.8, -158.1 and -161.4 ppm) in $[D_6]$benzene reveal three signals with similar chemical shifts in a 2:1:2 ratio for the three aromatic fluorine atoms. As expected, especially the aluminum compound turned out to be extremely moisture-sensitive.

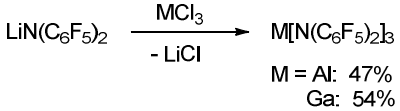

Scheme 1. Preparation of $Al[N(C_6F_5)_2]_3$ and $Ga[N(C_6F_5)_2]_3$ *via* salt elimination reactions.

Structural features of the free Lewis acids: A trigonal planar AlN_3 coordination geometry is found for $Al[N(C_6F_5)_2]_3$ with Al-N1 1.843(2) Å, Al-N2 1.840(2) Å and Al-N3 1.805(2) Å (Figure 2). The metal center is further stabilized by two axial aluminum-fluorine contacts with Al···F distances of

2.084(1) and 2.060(1) Å and an F12-Al-F24 angle of 164.93(6)°. The incorporation of the two *ortho*-fluorine atoms in Al···F contacts leads to an elongation of the corresponding C-F bonds (1.3897(2) and 1.3867(1) Å compared to 1.3459(2) and 1.3480(2) Å found for the two other C-F_{ortho} bond lengths in the corresponding C_6F_5 rings). Similar to the κ-N_3F_2 configuration experimentally verified for this aluminum trisamide, a κ-O_3F_2 configuration with longer Al···F contacts (2.143 and 2.155 Å) was proposed for the alkoxido superacid $Al[OC(CF_3)_3]_3$ on the basis of DFT calculations.[8]

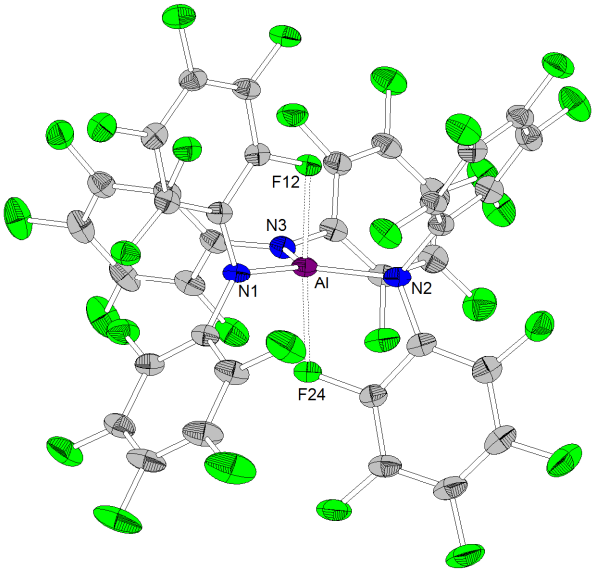

Figure 2. Molecular structure of $Al[N(C_6F_5)_2]_3$ (ellipsoids with 30% probability). Selected bond lengths /Å and angles /°: Al-N1 1.843(2), Al-N2 1.840(2), Al-N3 1.805(2), Al···F12 2.084(1), Al···F24 2.060(1), N1-Al-N2 123.7(1), N2-Al-N3 116.2(1), N3-Al-N1 120.09(9), F24-Al-F12 164.93(6).

As observed for the corresponding aluminum complex, the molecular structure of $Ga[N(C_6F_5)_2]_3$ (Figure 3) reveals a trigonal planar GaN_3 coordination geometry with Ga-N bond lenghts of 1.826(5), 1.798(5) and 1.848(5) Å. These values are shorter than found in the molecular structure of $Al[N(C_6F_5)_2]_3$. In addition to the three nitrogen donors, the gallium atom is coordinated by six *ortho*-fluorine atoms with gallium-fluorine distances ranging from 2.914(4) to 3.102(4) Å. The complex is further stabilized by π-stacking interactions between the pentafluorophenyl rings of neighboring $N(C_6F_5)_2$ moieties (distances of the rings' centroids: 3.5192(3), 3.7848(4) and 3.5463(3) Å). Similar coordination modes were observed for the homoleptic lanthanum and cerium complexes of $HN(C_6F_5)_2$ recently reported by Yin *et al.*.[28] $La[N(C_6F_5)_2]_3$ and $Ce[N(C_6F_5)_2]_3$ show longer N-M bond lengths (La-N between 2.410(2) and 2.512(2) Å, Ce-N between 2.406(3) and 2.430(2) Å), but shorter M···F contacts (La···F between 2.6695(17) and 2.8942(16) Å, Ce···F between 2.6764(16) and 2.7064(17) Å) compared to $Ga[N(C_6F_5)_2]_3$. According to a review article on interactions between metal atoms and organically bound fluorine atoms by Plenio, this kind of coordination mode is one of the two recurrent structure motives for gallium complexes with fluorinated ligands.[32] The coordination of a gallium

center by six fluorine atoms incorporated in the organic ligand backbone was also observed in case of tris(2,4,6-tris(trifluoromethyl)phenyl)gallium exhibiting Ga···F distances between 2.683 and 2.821 Å.[33]

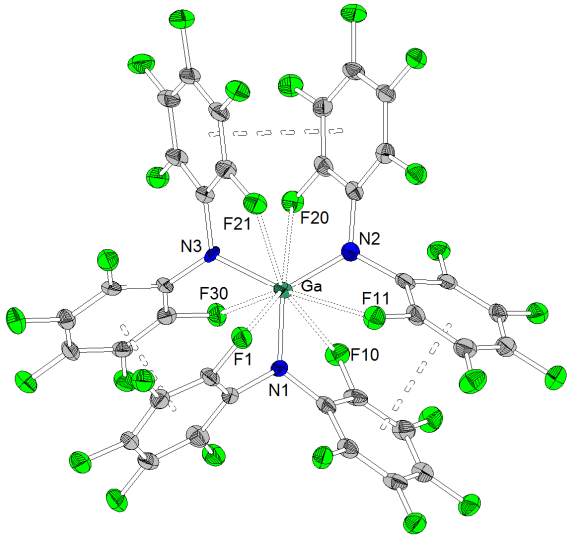

Figure 3. Molecular structure of $Ga[N(C_6F_5)_2]_3$ (ellipsoids with 30% probability). Selected bond lengths /Å and angles /°: Ga-N1 1.826(5), Ga-N2 1.798(5), Ga-N3 1.848(5), Ga···F1 3.032(4), Ga···F10 2.981(4), Ga···F11 3.096(4), Ga···F20 2.994(4), Ga···F21 3.102(4), Ga···F30 2.914(4), N1-Ga-N2 122.8(2), N2-Ga-N3 123.0(2), N3-Ga-N1 114.3(2).

Theoretical fluoride ion affinity of $Al[N(C_6F_5)_2]_3$ and $Ga[N(C_6F_5)_2]_3$: *This section will be added by Dr. Daniel Himmel and Prof. Ingo Krossing.*

Qualitative chloride ion affinity in dichloromethane: To evaluate the Lewis acidity of $Al[N(C_6F_5)_2]_3$ and $Ga[N(C_6F_5)_2]_3$ in solution, their chloride ion affinity in dichloromethane was studied in qualitative competition experiments *via* ^{19}F NMR spectroscopy. Both compounds turned out to be able to abstract a chloride ion from $[AsPh_4]^+[ClB(C_6F_5)_3]^-$. The addition of one equivalent of tetraphenylarsonium chloride to a 1:1 mixture of $Al[N(C_6F_5)_2]_3$ and $Ga[N(C_6F_5)_2]_3$ resulted in the formation of $[AsPh_4]^+[ClAl(N(C_6F_5)_2)_3]^-$ identifying the aluminum complex the stronger Lewis acid under the applied conditions (Scheme 2). Thus, the experimental results for the chloride ion affinity follow the trend of the fluoride ion affinity predicted by theoretical calculations. The isolation and structural features of $[AsPh_4]^+[ClGa(N(C_6F_5)_2)_3]^-$ are discussed later.

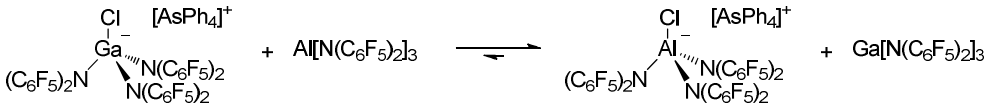

Scheme 2. Qualitative competition experiments for the determination of the chloride ion affinity of $Al[N(C_6F_5)_2]_3$ and $Ga[N(C_6F_5)_2]_3$.

Structural features of Lewis acid-base adducts: We crystallized Lewis acid-base adducts by reacting $Al[N(C_6F_5)_2]_3$ and $Ga[N(C_6F_5)_2]_3$ with Lewis basic donor molecules like ethers, nitriles, isonitriles or phosphanes to investigate the influence of adduct formation on the structural features. Molecular structures of $Al[N(C_6F_5)_2]_3{\cdot}NCMe$ (Figure 4), $Al[N(C_6F_5)_2]_3{\cdot}CN\textit{t}Bu$ (Figure 5), $Ga[N(C_6F_5)_2]_3{\cdot}NCMe$ (Figure 6), $Ga[N(C_6F_5)_2]_3{\cdot}CN\textit{t}Bu$ (Figure 7), $Ga[N(C_6F_5)_2]_3{\cdot}THF$ (Figure 8) and $Ga[N(C_6F_5)_2]_3{\cdot}PMe_3$ (Figure 9) were obtained. All crystal structures reveal the pyramidalization of the coordination sphere around the metal atoms. The two adducts of $Al[N(C_6F_5)_2]_3$ show similar M-N distances (between 1.838(2) and 1.844(2) Å for $Al[N(C_6F_5)_2]_3{\cdot}NCMe$ and between 1.835(2) and 1.841(2) Å for $Al[N(C_6F_5)_2]_3{\cdot}CN\textit{t}Bu$) to the free Lewis acid whereas adduct formation leads to a considerable elongation of the M-N bonds in case of $Ga[N(C_6F_5)_2]_3$ (e.g. Ga-N is 1.929(2) Å for $Ga[N(C_6F_5)_2]_3{\cdot}PMe_3$ and between 1.889(2) and 1.901(2) Å for $Ga[N(C_6F_5)_2]_3{\cdot}THF$). The presence of a better donor molecule results in the breakup of the hemilabile metal-fluorine contacts. However, metal-fluorine distances slightly below the sum of the van-der-Waals radii of the corresponding metal and fluorine remain, but most of them are considerable longer than observed in the free lewis acids.[34,35] They can probably be referred to the high sterical demand of the three $[N(C_6F_5)_2]^-$ moieties rather than to energetically favorable interactions stabilizing the metal center. Thus, short M···F distances are inevitably enforced by the crowded coordination sphere. As observed for adduct-free $Ga[N(C_6F_5)_2]_3$, the molecular structure of $Ga[N(C_6F_5)_2]_3{\cdot}PMe_3$ reveals three π-stacking interactions between neighboring pentafluorophenyl groups (distances of the rings' centroids: 3.4462(1) Å). Only one of such interactions per $M[N(C_6F_5)_2]_3$ unit is observed for the other three structurally characterized Lewis acid-base adducts of $Ga[N(C_6F_5)_2]_3$. The distance between the metal atoms and the donor molecules and the M-N distances are summarized in Table 1.

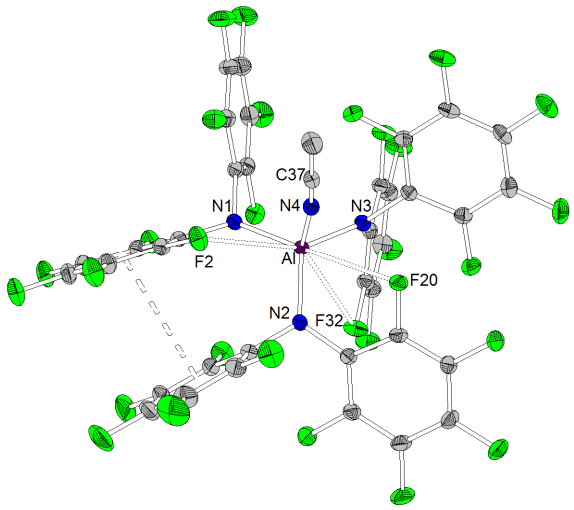

Figure 4. Molecular structure of $Al[N(C_6F_5)_2]_3{\cdot}NCMe$ (ellipsoids with 30% probability, one toluene molecule omitted for clarity). Selected bond lengths /Å and angles /°: Al-N1 1.838(2), Al-N2 1.844(2), Al-N3 1.839(2), Al···F2 3.148(2), Al···F20 2.948(2), Al···F32 3.230(2), Al-N4 1.940(2), C37-N4 1.138(3), N1-Al-N2 113.63(8), N2-Al-N3 117.23(8), N3-Al-N1 112.45(9), N1-Al-N4 104.48(8), N2-Al-N4 106.20(9), N3-Al-N4 100.90(8).

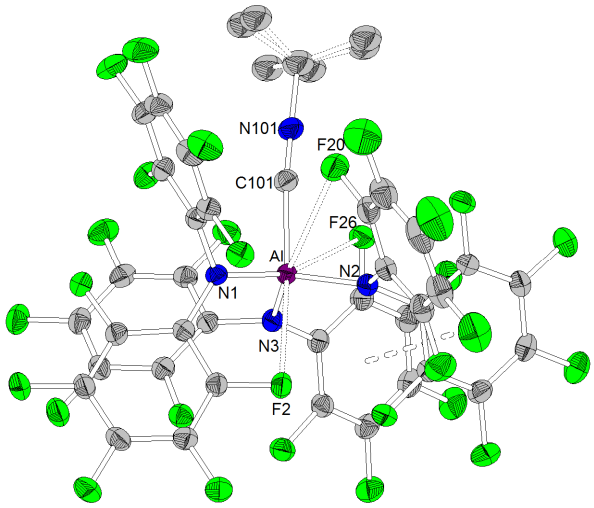

Figure 5. Molecular structure of Al[N(C_6F_5)$_2$]$_3$· CN*t*Bu (ellipsoids with 30% probability). Selected bond lengths /Å and angles /°: Al-N1 1.841(2), Al-N2 1.835(2), Al-N3 1.836(2), Al···F2 3.057(1), Al···F20 3.071(2), Al···F26 3.256(1), Al-C101 2.047(2), C101-N101 1.146(3), N1-Al-N2 118.87(7), N2-Al-N3 114.05(7), N3-Al-N1 112.37(7), N1-Al-C101 101.30(7), N2-Al-C101 104.07(8), N3-Al-C101 103.56(8).

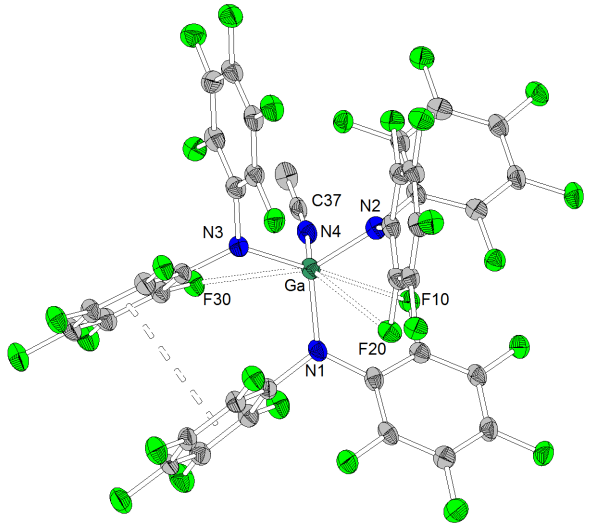

Figure 6. Molecular structure of Ga[N(C_6F_5)$_2$]$_3$·NCMe (ellipsoids with 30% probability, one toluene molecule omitted for clarity). Selected bond lengths /Å and angles /°: Ga-N1 1.885(4), Ga-N2 1.875(4), Ga-N3 1.877(4), Ga···F10 2.956(3), Ga···F20 3.209(4), Ga···F30 3.147(3), Ga-N4 2.005(5), C37-N4 1.135(7), N1-Ga-N2 118.4(2), N2-Ga-N3 112.6(2), N3-Ga-N1 114.1(2), N1-Ga-N4 105.1 (2), N2-Ga-N4 100.1(2), N3-Ga-N4 103.9(2).

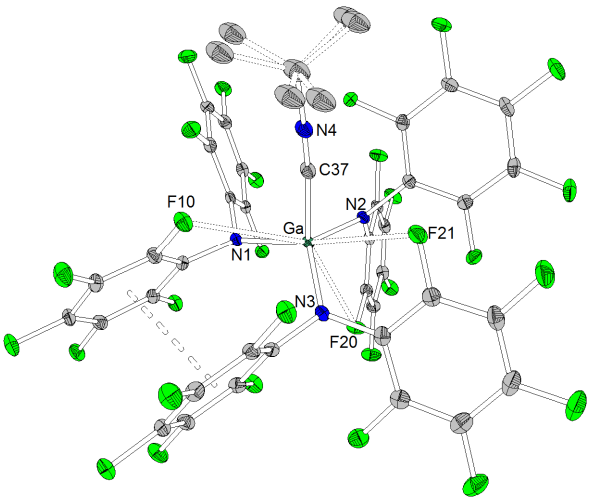

Figure 7. Molecular structure of $Ga[N(C_6F_5)_2]_3 \cdot CN\textit{t}Bu$ (ellipsoids with 30% probability). Selected bond lengths /Å and angles /°: Ga-N1 1.883(2), Ga-N2 1.885(2), Ga-N3 1.883(2), Ga···F10 3.231(1), Ga···F20 3.029(1), Ga···F21 3.037(2), Ga-C37 2.074(2), C37-N4 1.137(3), N1-Ga-N2 110.67(7), N2-Ga-N3 119.76(8), N3-Ga-N1 113.98(8), N1-Ga-C37 104.81(9), N2-Ga-C37 100.75(8), N3-Ga-C37 104.56(8).

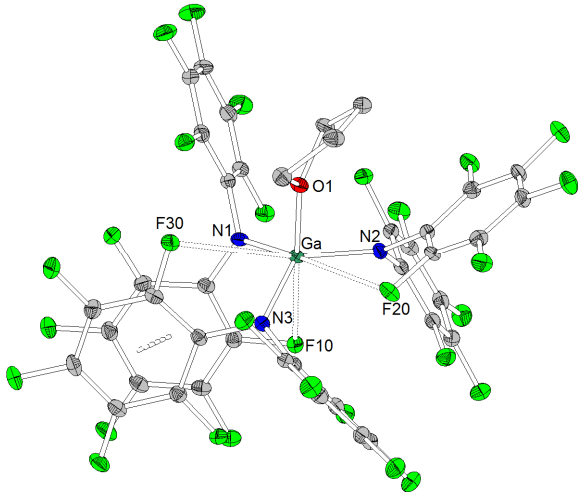

Figure 8. Molecular structure of $Ga[N(C_6F_5)_2]_3 \cdot THF$ (ellipsoids with 30% probability, one toluene molecule omitted for clarity). Selected bond lengths /Å and angles /°: Ga-N1 1.901(2), Ga-N2 1.898(2), Ga-N3 1.889(2), Ga···F10 3.053(1), Ga···F20 3.085(1), Ga···F30 3.276(1), Ga-O1 1.978(1), N1-Ga-N2 116.58(7), N2-Ga-N3 123.58(7), N3-Ga-N1 104.12(7), N1-Ga-O1 106.90(6), N2-Ga-O1 93.46(7), N3-Ga-O1 110.83(7).

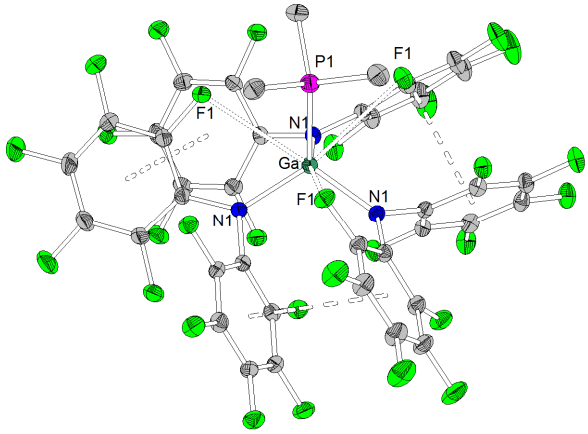

Figure 9. Molecular structure of $Ga[N(C_6F_5)_2]_3 \cdot PMe_3$ (ellipsoids with 30% probability, one toluene molecule omitted for clarity). The structure is C3v-symmetric. Selected bond lengths /Å and angles /°: Ga-N1 1.929(2), Ga···F1 2.957(2), Ga-P1 2.438(1), N1-Ga-N1(1-y, x-y, z) 109.64(7), N1-Ga-P1 109.31(7).

Table 1. M-N bond lengths and distances between the metal atom and the donor in Lewis acid-base adducts of $Al[N(C_6F_5)_2]_3$ and $Ga[N(C_6F_5)_2]_3$ and comparison to the donor-free Lewis acids.

	$Al[N(C_6F_5)_2]_3$	$Ga[N(C_6F_5)_2]_3$	$Al[N(C_6F_5)_2]_3$ ·NCMe	$Al[N(C_6F_5)_2]_3$ ·CN*t*Bu	$Ga[N(C_6F_5)_2]_3$ ·NCMe
M-N1	1.843(2)	1.826(5)	1.838(2)	1.841(2)	1.885(4)
M-N2	1.840(2)	1.798(5)	1.844(2)	1.835(2)	1.875(4)
M-N3	1.805(2)	1.848(5)	1.839(2)	1.836(2)	1.877(4)
M-Donor	-	-	1.940(2)	2.047(2)	2.005(5)

	$Ga[N(C_6F_5)_2]_3$ ·THF	$Ga[N(C_6F_5)_2]_3$ ·PMe_3	$Ga[N(C_6F_5)_2]_3$ ·CN*t*Bu
M-N1	1.901(2)	1.929(2)	1.883(2)
M-N2	1.898(2)	1.929(2)	1.885(2)
M-N3	1.889(2)	1.929(2)	1.883(2)
M-Donor	1.978(1)	2.438(1)	2.074(2)

Reactivity and experimental fluoride ion affinity of $Al[N(C_6F_5)_2]_3$: The enormous fluoride ion affinity of $Al[N(C_6F_5)_2]_3$ could also be demonstrated experimentally. The reaction of $Al[N(C_6F_5)_2]_3$ with $[PPh_4]^+[SbF_6]^-$ in toluene at 100 °C resulted in the precipitation of a mixture of $[PPh_4]^+[FAl(N(C_6F_5)_2)_3]^-$ and free $HN(C_6F_5)_2$ (Scheme 3 (a)). The ^{19}F NMR spectrum of $[PPh_4]^+[FAl(N(C_6F_5)_2)_3]^-$ exhibits signals with chemical shifts of -149.6, -166.2, -167.5 and -172.3 ppm in a 12:12:6:1 ratio. The formation of $HN(C_6F_5)_2$ can be referred to the presence of HF which is formed by the reaction of free SbF_5 with toluene or $[PPh_4]^+$. A mixture of unidentified products can be observed when reacting $Al[N(C_6F_5)_2]_3$ with $AgSbF_6$ in refluxing benzene (Scheme 3 (b)). This also indicates the abstraction of a fluoride ion from $[SbF_6]^-$ by $Al[N(C_6F_5)_2]_3$. Further proofs

for the high fluoride affinity of $Al[N(C_6F_5)_2]_3$ could be obtained when dissolving the Lewis acid in hexafluorobenzene and F_2ClCCF_2Cl. Both solutions slowly turn black at room temperature which can be referred to the abstraction of F^- from the solvent.

a) $Al[N(C_6F_5)_2]_3 + [PPh_4]^+[SbF_6]^- \xrightarrow[100\ °C,\ 5\ min]{toluene} [PPh_4]^+[FAl(N(C_6F_5)_2)_3]^- + SbF_5 \longrightarrow$ further reactions

b) $Al[N(C_6F_5)_2]_3 + AgSbF_6 \xrightarrow[reflux]{benzene} Ag^+[FAl(N(C_6F_5)_2)_3]^- + SbF_5 \longrightarrow$ further reactions

c) $Al[N(C_6F_5)_2]_3 + FCPh_3 \xrightarrow[r.t.]{toluene} [CPh_3]^+[FAl(N(C_6F_5)_2)_3]^-$

d) $Al[N(C_6F_5)_2]_3 + [CPh_3]^+[FB(C_6F_5)_3]^- \xrightarrow[80\ °C,\ 1\ min]{toluene} [CPh_3]^+[FAl(N(C_6F_5)_2)_3]^- + B(C_6F_5)_3$

e) $Al[N(C_6F_5)_2]_3 + [CPh_3]^+[BF_4]^- \xrightarrow[r.t.]{CH_2Cl_2\ /\ toluene} [CPh_3]^+[FAl(N(C_6F_5)_2)_3]^- + BF_3$

Scheme 3. Reactions proving the high Lewis acidity of $Al[N(C_6F_5)_2]_3$.

The reaction of $Al[N(C_6F_5)_2]_3$ with trityl fluoride in toluene yields $[CPh_3]^+[FAl(N(C_6F_5)_2)_3]^-$ which is stable in solution for at least three days (Scheme 3 (c)). Attempts to isolate the yellow compound resulted in its decomposition after 24 h at room temperature. *In situ* generated $[CPh_3]^+[FAl(N(C_6F_5)_2)_3]^-$ was able to abstract a methyl group from dimethyl zirconocene to give $[Cp_2ZrMe]^+[FAl(N(C_6F_5)_2)_3]^-$ as a white solid (Scheme 4 (a)). The ^{19}F NMR spectrum shows four signals with chemical shifts of -148.1, -149.4, -160.6 and -163.5 ppm in a 1:12:6:12 ratio. The aluminum bound fluorine atom is shifted to lower field compared to $[FAl(N(C_6F_5)_2)_3]^-$ (δ = -170.8 ppm). This can be referred to the coordination of the fluorine atom to the zirconium center which was also observed in a low quality crystal structure of $[Cp_2ZrMe]^+[FAl(N(C_6F_5)_2)_3]^-$. The strong $Zr^{\cdots}F$ interaction explains why $[Cp_2ZrMe]^+[FAl(N(C_6F_5)_2)_3]^-$ turned out to be inactive in ethene polymerization reactions.

a) $[CPh_3]^+[FAl(N(C_6F_5)_2)_3]^- + Cp_2ZrMe_2 \xrightarrow[-50\ °C]{toluene} [Cp_2ZrMe]^+[FAl(N(C_6F_5)_2)_3]^- + MeCPh_3$

b) $2\ [CPh_3]^+[FAl(N(C_6F_5)_2)_3]^- + n\text{-BuLi} \xrightarrow[-80\ °C]{toluene} [CPh_3]^+$ 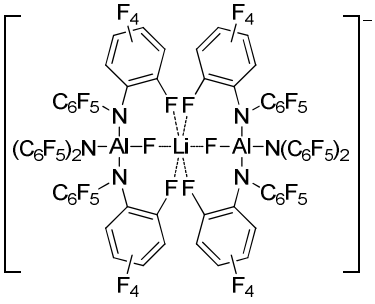 $+ Ph_3CBu$

Scheme 4. Reactions of $[CPh_3]^+[FAl(N(C_6F_5)_2)_3]^-$ with *n*-butyllithium and Cp_2ZrMe_2.

In agreement with the theoretically predicted trend of the FIA in the gas phase, $[CPh_3]^+[FAl(N(C_6F_5)_2)_3]^-$ is also formed when reacting $Al[N(C_6F_5)_2]_3$ with $[CPh_3]^+[FB(C_6F_5)_3]^-$ in toluene and with $[CPh_3]^+[BF_4]^-$ in a mixture of toluene and dichloromethane (Scheme 3 (d + e)). Orange crystals suitable for x-ray diffraction analysis were grown directly from the solution of the latter reaction and revealed the formation of $[CPh_3]^+[((C_6F_5)_2N)_3AlF\text{-}Li\text{-}FAl(N(C_6F_5)_2)_3]^-$. The

presence of lithium in the crystal structure can be referred to traces of lithium chloride or $Li^+[ClAl(N(C_6F_5)_2)_3]^-$ in the used $Al[N(C_6F_5)_2]_3$. The selective preparation of $[CPh_3]^+[((C_6F_5)_2N)_3AlF\text{-}Li\text{-}FAl(N(C_6F_5)_2)_3]^-$ could be achieved from the reaction of two equivalents of *in situ* generated $[CPh_3]^+[FAl(N(C_6F_5)_2)_3]^-$ with *n*-butyllithium (Scheme 4 (b)). A quartet with a chemical shift of -179.3 ppm and ^1J(F,Li) coupling constant of 94 Hz is observed for the fluorine atoms bound to aluminum atoms in the ^{19}F NMR spectrum. The crystal structure reveals Al-F distances of 1.714(3) and 1.710(3) Å. The lithium cation possesses a distorted octahedral coordination sphere and is coordinated by the two aluminum bound fluorine atoms and additional four *ortho*-fluorine atoms of C_6F_5 units. The Li···F distances to the aluminum-bound fluorine atoms are comparably short (1.793(9) and 1.809(9) Å) whereas the distances to the organically bound fluorine atoms range from 2.185(12) to 2.392(10) Å. The $X_3Al\text{-}F\text{-}Li\text{-}F\text{-}AlX_3$ structure motive has already been described in the literature for $[Ag(PhCH_3)_3]^+[\{((SiMe_3)_3C)_2Al_2F_5\}_2Li]^-$ (Al-F 1.688(2) Å, Li-F 1.854(6) Å),[36] $[Li(Me_3Si)_3CAlF_3(THF)]_4$ (Al-F 1.694(2) Å and 1.701(2) Å, Li-F 1.873(6) Å and 1.801(6) Å)[37] and $Li^+[(Me_3Si)_3CAlF_3]^-\cdot THF$ (mean Al-F 1.687(8) Å, mean Li-F 1.85(2) Å)).[38] In contrast to $[CPh_3]^+[((C_6F_5)_2N)_3AlF\text{-}Li\text{-}FAl(N(C_6F_5)_2)_3]^-$, all lithium atoms in these references exhibit a tetrahedral coordination sphere. The three compounds described in the literature show slightly shorter Al-F distances and longer Li-F distances than found for $[CPh_3]^+[((C_6F_5)_2N)_3AlF\text{-}Li\text{-}FAl(N(C_6F_5)_2)_3]^-$.

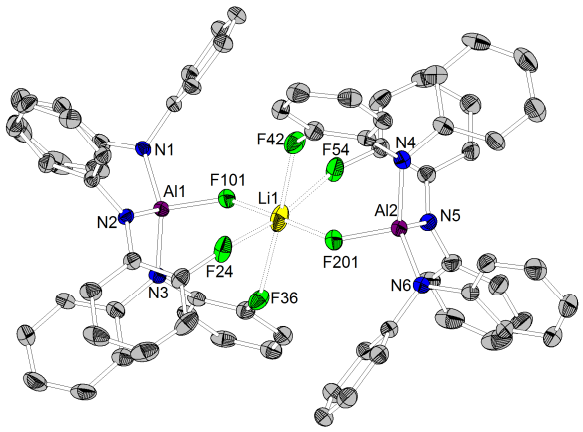

Figure 10. Molecular structure of $[CPh_3]^+[((C_6F_5)_2N)_3AlF\text{-}Li\text{-}FAl(N(C_6F_5)_2)_3]^-$ (ellipsoids with 30% probability, non-coordinating fluorine atoms, the cation and two toluene molecules omitted for clarity). Selected bond lengths /Å and angles /°: Al1-N1 1.862(3), Al1-N2 1.859(4), Al1-N3 1.857(3), Al1-F101 1.714(3), Al2-N4 1.865(4), Al2-N5 1.859(4), Al2-N6 1.861(4), Al2-F201 1.710(3), Li1···F101 1.793(9), Li1···F201 1.809(9), Li1···F24 2.185(12), Li1···F36 2.392(10), Li1···F42 2.280(10), Li1···F54 2.287(12), N1-Al1-N2 113.51(15), N2-Al1-N3 102.24(16), N1-Al1-N3 123.30(16), N1-Al1-F101 99.83(15), N2-Al1-F101 114.48(15), N3-Al1-F101 103.57(14), N4-Al2-N5 102.41(17), N5-Al2-N6 115.61(17), N4-Al2-N6 122.56(17), N4-Al2-F201 102.66(15), N5-Al2-F201 112.48(16), N6-Al2-F201 100.55(16).

Preparation of metallates: The reaction of $Al[N(C_6F_5)_2]_3$ with cesium fluoride in toluene and the reaction of $Ga[N(C_6F_5)_2]_3$ with tetraphenylarsonium chloride in dichloromethane (Scheme 5) yielded the two metallates $[Cs(Tol)_3]^+[FAl(N(C_6F_5)_2)_3]^-$ (Figure 11) and $[AsPh_4]^+[ClGa(N(C_6F_5)_2)_3]^-$ (Figure

12). The aluminum bound fluorine atom in the former compound exhibits chemical shift of -157.4 ppm in the ^{19}F NMR spectrum. Both metallates could be structurally characterized. The two weakly coordinating anions show the pyramidalization of the coordination geometry around the metal atoms. The M-N bonds are elongated in comparison to the parent compounds whereas this is more pronounced in case of the gallium compound (Al-N between 1.860(3) and 1.865(3) Å, Ga-N between 1.912(2) and 1.931(2) Å). The molecular structure of $[Cs(Tol)_3]^+[FAl(N(C_6F_5)_2)_3]^-$ reveals η^2-, η^3- and η^6-coordination of the cesium atom by three toluene molecules and the cesium atom also interacts with the fluorine atom bound to the aluminum center with a Cs···F distance of 2.878(2) Å. Furthermore, the crystal structure reveals four metal-fluorine contacts between the cesium atom and organically bound fluorine atoms (Cs···F between 3.094(2) and 3.807(3) Å).

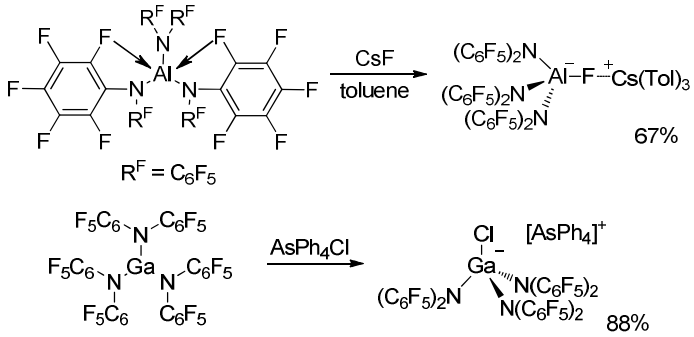

Scheme 5. Preparation of $[Cs(Tol)_3]^+[FAl(N(C_6F_5)_2)_3]^-$ and $[AsPh_4]^+[ClGa(N(C_6F_5)_2)_3]^-$.

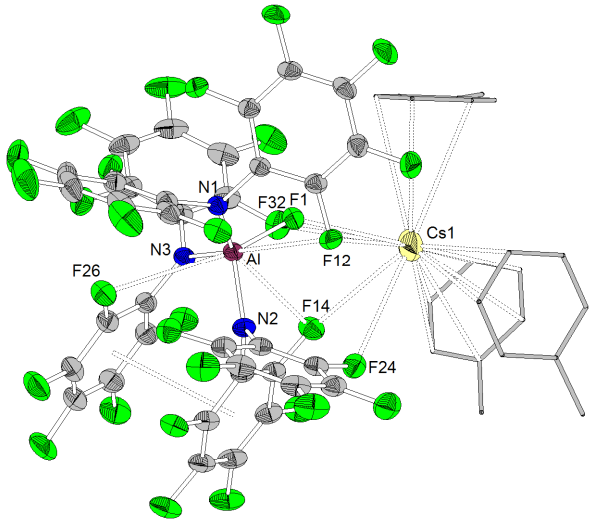

Figure 11. Molecular structure of $[Cs(Tol)_3]^+[FAl(N(C_6F_5)_2)_3]^-$ (ellipsoids with 30% probability, the three toluene molecules displayed in wireframe design). Selected bond lengths /Å and angles /°: Al-N1 1.863(3), Al-N2 1.860(3), Al-N3 1.865(3), Al-F1 1.689(2), Al···F12 3.099(3), Al···F14 3.169(3), Al···F26 3.202(3), Cs1···F1 2.878(2), Cs1···F12 3.773(2), Cs1···F14 3.094(3), Cs1···F24 3.807(3), Cs1···F32 3.692(3), N1-Al-N2 112.31(14), N2-Al-N3 102.59(14), N3-Al-N1 123.22(15), N1-Al-F1 98.64(12), N2-Al1-F1 113.94(14), N3-Al1-F1 106.43(14).

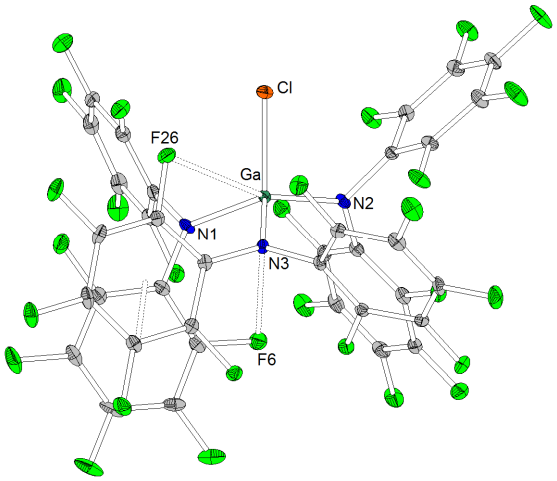

Figure 12. Molecular structure of $[AsPh_4]^+[ClGa(N(C_6F_5)_2)_3]^-$ (ellipsoids with 30% probability, the $[AsPh_4]^+$ cation and one pentane molecule are omitted for clarity). Selected bond lengths /Å and angles /°: Ga-N1 1.912(2), Ga-N2 1.912(2), Ga-N3 1.931(2), Ga···F6 3.244(2), Ga···F26 3.205(2), Ga-Cl1 2.1890(8), N1-Ga-N2 117.4(1), N2-Ga-N3 115.7(1), N3-Ga-N1 99.9(0), N1-Ga-Cl1 113.90(8), N2-Ga-Cl1 98.83(7), N3-Ga-Cl1 111.85(7).

Table 2. M-N bond lengths and distances between the metal atom and the donor atom in the ate complexes $[Cs(Tol)_3]^+[FAl(N(C_6F_5)_2)_3]^-$ and $[AsPh_4]^+[ClGa(N(C_6F_5)_2)_3]^-$.

	$[Cs(Tol)_3]^+[FAl(N(C_6F_5)_2)_3]^-$	$[AsPh_4]^+[ClGa(N(C_6F_5)_2)_3]^-$
M-N1	1.863(3)	1.912(2)
M-N2	1.860(3)	1.912(2)
M-N3	1.865(3)	1.931(2)
M-Hal	1.689(2)	2.1890(8)

Conclusion

We presented the synthesis of the two group XIII metal amides $Al[N(C_6F_5)_2]_3$ and $Ga[N(C_6F_5)_2]_3$, provided insights into their structural features and examined their Lewis acidic behavior in reactions with neutral electron donor molecules, by the preparation of metallates and in competition experiments for chloride ions. Thus, we could prove that perfluorinated amido ligands are able to generate highly Lewis acidic metal complexes with a higher fluoride ion affinity in the gas phase than SbF_5. $[N(C_6F_5)_2]^-$ possesses the ability to stabilize extremely Lewis acidic metal centers by forming hemilabile secondary metal fluorine contacts that are loosened in presence of a Lewis base. We believe that Lewis acidic aluminum and gallium amides will add new perspectives to the highly topical field of frustrated Lewis pairs that has mainly been dominated by boron-based Lewis acids so far. Furthermore, the two weakly coordinating anions presented herein, $[FAl(N(C_6F_5)_2)_3]^-$ and $[ClGa[N(C_6F_5)_2]_3]^-$, could be applied to the stabilization of highly reactive cations such as the cationic species of metallocene catalysts used for olefin polymerization.

Experimental Section

All reactions were carried out under inert atmosphere using standard Schlenk techniques. Moisture and air sensitive substances were stored in a conventional nitrogen-flushed glovebox. Solvents were purified according to literature procedures and kept under an inert atmosphere. $HN(C_6F_5)_2$ was prepared from the reaction of hexafluorobenzene with lithium amide[25b] and deprotonated with *n*-butyllithium to obtain $LiN(C_6F_5)_2$.[26] Commercially available aluminum trichloride was sublimed prior to use.

Spectra were recorded on the following spectrometers: NMR: BRUKER ARX300, BRUKER DRX400, BRUKER, DRX500; IR: ATR-FT-IR; MS: LTQ-FT or QStarPulsar i (FINNIGAN); elemental analysis: CHN-Rapid (HERAEUS).

Further syntheses and experimental details are described in the supporting information.

Preparation of $Al[N(C_6F_5)_2]_3$: A solution of *n*-butyllithium (1.6 M, 8.0 mL, 12.8 mmol, 3.1 eq.) in hexane was added dropwise over 1 min to a solution of $HN(C_6F_5)_2$ (4.48 g, 12.8 mmol, 3.1 eq.) in toluene (45 mL) at -50 °C. The formed suspension of $LiN(C_6F_5)_2$ was stirred for 20 min at -50 °C and a suspension of finely pesteled aluminum trichloride (0.55 g, 4.1 mmol) in toluene (20 mL) was added. The reaction mixture was allowed to reach room temperature and stirred for 18 h at 75 °C. The hot suspension was filtered and large colorless crystals grew from the filtrate after 12 h at room temperature. The crystals were separated from the supernatant by decantation, recrystallized from toluene, washed with pentane and dried *in vacuo* to give $Al[N(C_6F_5)_2]_3$ (2.06 g, 1.9 mmol, 47%) as a white solid. The yield strongly depends on the grain size of the used $AlCl_3$. Single crystals suitable for structure determination were obtained by layering a saturated solution in toluene with pentane at -30 °C.

M. p. 167.8 °C (decomposition); ^{13}C NMR (101 MHz, [D$_6$]benzene, 25 °C, TMS): δ=143.8 (dm, ^1J(C,F) = 240.2 Hz, *o*-C_{Ar}), 138.3 (dm, ^1J(C,F) = 255.4 Hz, *p*-C_{Ar}), 137.8 (dm, ^1J(C,F) = 241.2 Hz, *m*-C_{Ar}), 120.7 ppm (s, *ipso*-C_{Ar}); ^{19}F NMR (188.2 MHz, [D$_6$]benzene, 25 °C, $CFCl_3$): δ=-153.1 (d, ^3J(F,F) = 20 Hz, 12F, *o*-F), -158.6 (t, ^3J(F,F) =21 Hz, 6F, *p*-F), -161.1 ppm (t, ^3J(F,F) = 21 Hz, 12F, *m*-F); IR: $\tilde{\nu}$=440 (m), 453 (w), 507 (w), 619 (w), 638 (w), 683 (m), 764 (m), 802 (br m), 990 (s), 1030 (br s), 1096 (br m), 1182 (w), 1211 (m), 1507 (s), 1520 (s) cm^{-1}; elemental analysis calcd (%) for $C_{36}AlF_{30}N_3$: C 40.36, N 3.92; found: C 39.48, N 3.73.

Preparation of $[Cs(Tol)_3]^+[FAl(N(C_6F_5)_2)_3]^-$: $Al[N(C_6F_5)_2]_3$ (0.360 g, 0.33 mmol, 1.0 eq.) and cesium fluoride (0.102 g, 0.66 mmol, 2.0 eq.) were suspended in toluene (10 mL) and the reaction mixture was stirred for 20 h at 100 °C. The hot solution was filtered to separate remaining CsF and the filtrate was cooled to room temperature and set aside for crystallization. Colorless crystals formed that were

separated from the supernatant by filtration, washed with pentane and dried in the argon stream to yield $[Cs(Tol)_3]^+[FAl(N(C_6F_5)_2)_3]^-$ (0.330 g, 0.22 mmol, 67%) as a white crystalline solid.
M. p. 124.7 °C; ^{1}H NMR (200 MHz, [D$_6$]benzene, 25 °C, TMS): δ=6.98-7.17 (m, 15H, C_6H_5), 2.10 ppm (s, 9H, CH_3); ^{19}F-NMR (188 MHz, [D$_6$]benzene, 25 °C, $CFCl_3$): δ=-150.4 (br s, 12F, *o*-F), -157.4 (br s, 1F, Al-F), -164.0 (t, ^3J(F,F) = 20 Hz, 6F, *p*-F), -166.3 ppm (t, ^3J(F,F) = 22 Hz, 12F, *m*-F); elemental analysis calcd (%) for $C_{57}H_{24}AlCsF_{31}N_3$: C 45.65, H 1.61, N 2.80; found: C 44.89, H 1.68, N 2.76.

Preparation of $Ga[N(C_6F_5)_2]_3$: A solution of gallium trichloride (0.330 g, 1.878 mmol, 1.0 eq.) in toluene (10 mL) was added to a suspension of $LiN(C_6F_5)_2$ (2.000 g, 5.633 mmol, 3.0 eq.) in toluene (40 mL). The reaction mixture was stirred for 16 h at 90 °C and the hot suspension was filtered over Celite®. The filter cake was extracted twice with toluene (20 mL) and the filtrate was evaporated to dryness *in vacuo*. The white residue was washed twice with hexane (40 mL). After drying *in vacuo* $Ga[N(C_6F_5)_2]_3$ (1.120 g, 1.005 mmol, 54%) was obtained as a white solid. Single crystals suitable for structure determination were obtained by cooling a saturated solution in toluene from 90 °C to -30 °C.
^{13}C NMR (126 MHz, [D$_6$]benzene, 25 °C, TMS): δ=142.8 (dd, ^1J(C,F) = 246.5 Hz, ^2J(C,F) = 11.5 Hz, *o*-C_{Ar}), 138.9 (dt, ^1J(C,F) = 256.3 Hz, ^2J(C,F) = 13.5 Hz, *p*-C_{Ar}), 137.9 (dt, ^1J(C,F) = 256.3 Hz, ^2J(C,F) = 12.9 Hz, *m*-C_{Ar}), 120.8 ppm (t, ^2J(C,F) = 9.3 Hz, *ipso*-C_{Ar}); ^{19}F NMR (376 MHz,): δ=-151.8 (d, ^3J(F,F) = 20.6 Hz, 12F, *o*-F), -158.1 (dt, ^3J(F,F) = 21.7 Hz, ^4J(F,F) = 4.8 Hz, 6F, *p*-F), -161.4 ppm (t, ^3J(F,F) = 21.1 Hz, 12F, *m*-F); IR: $\tilde{\nu}$=410 (w), 498 (w), 573 (w), 639 (m), 669 (w), 712 (w), 725 (w), 806 (w), 837 (m), 987 (s), 1026 (s), 1140 (w), 1191 (w), 1264 (w), 1322 (w), 1369 (w), 1501 (s), 1632 (w) cm^{-1}; elemental analysis calcd (%) for $C_{36}F_{30}GaN_3$: C 38.81, H 0.00, N 3.77; found: C 38.21, H 0.66, N 3.67.

Preparation of $[AsPh_4]^+[ClGa(N(C_6F_5)_2)_3]^-$: A solution of $Ga[N(C_6F_5)_2]_3$ (200 mg, 0.180 mmol, 1.0 eq.) in dichloromethane (7.5 mL) was added to a solution of tetraphenylarsonium chloride (75 mg, 0.180 mmol, 1.0 eq.) in dichloromethane (7.5 mL). The reaction mixture was stirred for 1 h at room temperature and evaporated to dryness *in vacuo*. The remaining solid was washed with pentane (15 mL) and dried *in vacuo*. $[AsPh_4]^+[ClGa(N(C_6F_5)_2)_3]^-$ (242 mg, 0.158 mmol, 88%) was obtained as a white solid. Single crystals suitable for structure determination were obtained by layering a saturated solution in diethylether with pentane at -30 °C. ^{1}H NMR (400 MHz, CD_2Cl_2, 25 °C, TMS): δ=7.87 (t, ^3J(H,H) = 7.5 Hz, 4H, *p*-H), 7.75 (t, ^3J(H,H) = 7.8 Hz, 8H, *m*-H), 7.61 ppm (d, ^3J(H,H) = 7.5 Hz, 8H, *o*-H); ^{13}C NMR (101 MHz, CD_2Cl_2, 25 °C, TMS): δ=145.6 (dm, ^1J(C,F) = 245.2 Hz, *p*-C), 139.1 (dm, ^1J(C,F) = 247.2 Hz, CF_{Ar}), 135.4 (*p*-C_{Ph}), 133.3 (C_{Ph}), 131.7 (C_{Ph}), 126.6 (*ipso*-C), 120.8 ppm (*ipso*-C_{Ph}) (the remaining carbon atoms belonging to the C_6F_5 groups were not detected due to signal overlay); ^{19}F NMR (282 MHz, CD_2Cl_2, 25 °C, $CFCl_3$): δ=-147.7 (d, ^3J(F,F) = 18.1 Hz, 6F, F_{Ar}), -165.4 (t, ^3J(F,F) = 21.7 Hz, 3F, *p*-F), -167.0 ppm (t, ^3J(F,F) = 19.9 Hz, 6F, F_{Ar}); ESI-MS (CH_2Cl_2): *m*/*z* (%):

383 (100) $[M]^+$, HRMS (ESI): *m*/*z* calcd for $C_{24}H_{20}As^+$: 383.0775 $[M]^+$; found: 383.0774, (-)-ESI-MS (CH_2Cl_2): *m*/*z* (%): 348 (100) $[N(C_6F_5)_2]^-$, (-)-HRMS (ESI): *m*/*z* calcd for $C_{36}ClF_{30}GaN_3^-$: 1147.8563 $[M]^+$; found: 1147.8576; elemental analysis calcd (%) for $C_{60}H_{20}AsClF_{30}GaN_3$: C 47.01, H 1.32, N 2.74; found: C 47.17, H 1.79, N 2.83.

Supporting Information

The supporting information contains synthetic procedures, crystallographic and computational data. This material is available free of charge *via* the internet at:

Corresponding Author

jsu@staff.uni-marburg.de

Acknowledgement

We thank Fabian Schröder and Lars Finger for their valuable support with crystal structure refinement. Financial support by the Fonds der Chemischen Industrie (doctoral scholarship for J.K.) is gratefully acknowledged.

References

[1] a) Houk, K. N.; Strozier, R. W. *J. Am. Chem. Soc.* **1973**, *95*, 4094-4096; b) Otto, S.; Bertoncin, F.; Engberts, J. B. F. N. *J. Am. Chem. Soc.* **1996**, *118*, 7702-7707. c) Fringuelli, F.; Piermatti, O.; Pizzo, F.; Vaccaro, L. *Eur. J. Org. Chem.* **2001**, *3*, 439-455.
[2] a) Shao, L.-X.; Zhang, Y.-P.; Qi, M.-H.; Shi, M. *Org. Lett.* **2007**, *9*, 117-120; b) Zicmanis, A.; Katkevica, S.; Mekss, P. *Catal. Commun.* **2009**, *10*, 614-619
[3] a) Sibi, M. P.; Ji, J.; Wu, J. H.; Guertler, S.; Porter, N. A. *J. Am. Chem. Soc.* **1996**, *118*, 9200-9201; b) Sibi, M. P.; Shay, J. J.; Liu, M.; Jasperse, C. P. *J. Am. Chem. Soc.* **1998**, *120*, 6615-6616.
[4] Suyama, K.; Matsumoto, K.; Katsuki, T. *Heterocycles* 2009, *77*, 817-824.
[5] a) Corma, A.; Garcia, H. *Chem. Rev.* **2003**, *103*, 4307-4365; b) Kobayashi, S.; Manabe, K. *Pure Appl. Chem.* **2000**, *72*, 1373-1380; c) Antoniotti, S.; Dalla, V.; Dunach, E. *Angew. Chem.* **2010**, *122*, 8032-8060; *Ang. Chem. Int. Ed.* **2010**, *49*, 7860-7888;
[6] a) Welch, G. C.; San Juan, R. R.; Masuda, J. D.; Stephan, D. W. *Science* **2006**, *314*, 1124-1126; b) McCahill, J. S. J.; Welch, G. C.; Stephan, D. W. *Angew. Chem.* **2007**, *119*, 5056-5059: *Angew. Chem. Int. Ed.* **2007**, *46*, 4968-4971; c) Stephan, D. W. *Org. Biomol. Chem.* **2008**, *6*, 1535-1539; d) Stephan, D. W.; Erker, G. *Angew. Chem.* **2010**, *122*, 50-81; *Angew. Chem. Int Ed.* **2010**, *49*, 46-76
[7] Mallouk, T. E.; Rosenthal, G. L.; Müller, G.; Brusasco, R.; Bartlett, N. *Inorg. Chem.* **1984**, *23*, 3167-3173.
[8] Müller, L. O.; Himmel, D.; Stauffer, J.; Steinfeld, G.; Slattery, J.; Santiso-Quiñones, G.; Brecht, V.; Krossing, I. *Angew. Chem.* **2008**, *120*, 7772-7776; *Angew. Chem. Int. Ed.* **2008**, *47*, 7659-7663.
[9] Kraft, A.; Trapp, N.; Himmel, D.; Böhrer, H.; Schlüter, P.; Scherer, H.; Krossing, I. *Chem. Eur. J.* **2012**, *18*, 9371-9380.
[10] Williams, V. C.; Piers, W. E.; Clegg, W.; Elsegood, M. R. J.; Collins, S.; Marder, T. B. *J. Am. Chem. Soc.* **1999**, *121*, 3244-3245.
[11] Timoshkin, A. Y.; Morokuma, K. *Phys. Chem. Chem. Phys.* **2012**, *14*, 14911-14916.
[12] Mück, L. A.; Timoshkin, A. Y.; Frenking, G. *Inorg. Chem.* **2012**, *51*, 640-646.
[13] Lehner, A. J.; Trapp, N.; Scherer, H.; Krossing, I. *Dalton Trans.* **2011**, *40*, 1448-1452.
[14] Krossing, I.; Brands, H.; Feuerhake, R.; Koenig, S. *J. Fluorine Chem.* **2001**, *112*, 83-90.
[15] Chen, X.; Ma, B.; Wang, X.; Yao, S.; Ni, L.; Zhou, Z.; Li, Y.; Huang, W.; Ma, J.; Zuo, J.; Wang, X. *Chem. Eur. J.* **2012**, *18*, 11828-11836.
[16] Gonsior, M.; Krossing, I. *Dalton Trans.* **2005**, *7*, 1203-1213.

[17] Köchner, T.; Trapp, N.; Engesser, T. A.; Lehner, A. J.; Röhr, C.; Riedel, S.; Knapp, C.; Scherer, H.; Krossing, I. *Angew. Chem.* **2011**, *124*, 11253-11256; *Angew. Chem. Int. Ed.* **2011**, *50*, 11253-11256.
[18] Bihlmeier, A.; Gonsior, M.; Raabe, I.; Trapp, N.; Krossing, I. *Chem. Eur. J.* **2004**, *10*, 5041-5051.
[19] Li, J.; Schenk, C.; Winter, F.; Scherer, H.; Trapp, N.; Higelin, A.; Keller, S.; Pöttgen, R.; Krossing, I.; Jones, C. *Angew. Chem.* **2012**, *124*, 9695-9699; *Angew. Chem. Int. Ed.* **2012**, *51*, 9557-9561.
[20] a) Santiso-Quiñones, G.; Reisinger, A.; Slattery, J.; Krossing, I. *Chem. Commun.* **2007**, 5046-5048; b) Krossing, I.; Reisinger, A. *Angew. Chem.* **2003**, *115*, 5903–5906; *Angew. Chem. Int. Ed.* **2003**, *42*, 5725-5728; c) Reisinger, A.; Trapp, T.; Knapp, C.; Himmel, D.; Breher, F.; Rüegger, H.; Krossing, I. *Chem. Eur. J.* **2009**, *15*, 9505-9520; d) Schaefer, J.; Himmel, D.; Krossing, I. *Eur. J. Inorg. Chem.* **2013**, 2712-2717.
[21] Budanow, A.; Sinke, T.; Tillmann, J.; Bolte, M.; Wagner, M.; Lerner, H.-W. *Organometallics* **2012**, *31*, 7298-7301.
[22] Slattery, J. M.; Higelin, A.; Bayer, T.; Krossing, I. *Angew. Chem.* **2010**, *122*, 3297-3301; *Angew. Chem. Int. Ed.* **2010**, *49*, 3228-3231.
[23] Higelin, A.; Sachs, U.; Keller, S.; Krossing, I. *Chem. Eur. J.* **2012**, *18*, 10029-10034.
[24] Khvorost, A. *Dissertation*, Philipps-Universität Marburg, **2003**.
[25] a) Brooke, G. M.; Burdon, J.; Stacey, M. ; Tatlow, J. C. *J. Chem. Soc.* **1960**, 1768-1771; b) Koppang, R. *Acta Chem. Scand.* **1971**, *25*, 3067-3071.
[26] Khvorost, A.; Shutov, P. L.; Harms, K.; Lorberth, J.; Sundermeyer, J.; Karlov, S. S.; Zaitseva, G. S. *Z. Anorg. Allg. Chem.* **2004**, *630*, 885-889.
[27] Click, D. R.; Scott, B. L.; Watkin, J. G. *Chem. Commun.* **1999**, 633-634.
[28] Yin, H.; Lewis, A. J.; Carroll, P.; Schelter, E. J. *Inorg. Chem.* **2013**, *52*, 8234-8243.
[29] Yin, H.; Lewis, A. J.; Williams, U. J.; Carroll, P. J.; Schelter, E. J. *Chem. Sci.* **2013**, *4*, 798-805.
[30] Giesbrecht, G. R.; Gordon, J. C.; Clark, D. L.; Hijar, C. A.; Scott, B. L.; Watkin, J. G. *Polyhedron* **2003**, *22*, 153-163.
[31] Peryshkov, D. V.; Schrock, R. R. *Organometallics* **2012**, *31*, 7278-7286.
[32] Plenio, H. *Chem. Rev.* **1997**, *97*, 3363-3384.
[33] Schluter, R. D.; Isom, H. S.; Cowley, A. H.; Atwood, D. A.; Jones, R. A.; Olbrich, F.; Corbelin, S.; Lagow, R. J. *Organometallics* **1994**, *13*, 4058-4063.
[34] We arbitrarily chose the sum of the van der Waals as the upper limit for a metal fluorine contact radii (3.31 Å for Al and F, 3.34 Å for Ga and F according to the values reported by Mantina *et al.* (Ref. 35)). The issue of defining a proper threshold for M···F interaction is addressed by Plenio in Ref. 32.
[35] Mantina, M.; Chamberlin, A. C.; Valero, R.; Cramer, C. J.; Truhlar, D. G. *J. Phys. Chem. A* **2009**, *113*, 5806-5812.
[36] Hatop, H.; Roesky, H. W.; Labahn, T.; Röpken, C.; Sheldrick, G. M.; Bhattacharjee, M. *Organometallics* **1998**, *17*, 4326-4328.
[37] Hatop, H.; Schiefer, M.; Roesky, H. W.; Herbst-Irmer, R.; Labahn, T. *Organometallics* **2001**, *20*, 2643-2646.
[38] Avent, A. G.; Chen, W.-Y.; Eaborn, C.; Gorrell, I. B.; Hitchcock, P. B.; Smith, J. D. *Organometallics* **1996**, *15*, 4343-4345.